Modeling, Analysis, and Control for Upset Recovery-from System Theory to Unmanned Aircraft Flight

Torbjørn Cunis

Université Fédérale
Toulouse Midi-Pyrénées

THÈSE

En vue de l'obtention du

DOCTORAT DE L'UNIVERSITÉ DE TOULOUSE

Délivré par l'Institut Supérieur de l'Aéronautique et de l'Espace

---

Présentée et soutenue par

Torbjørn CUNIS

Le 27 septembre 2019

Modélisation, analyse et commande pour la récupération d'un aéronef en situation de décrochage : de la théorie des systèmes au pilote automatique

---

Ecole doctorale : **SYSTEMES**

Spécialité : **Automatique**

Unité de recherche :
ISAE-ONERA CSDV - Commande des Systèmes et Dynamique du Vol

Thèse dirigée par
Laurent BURLION et Jean-Philippe CONDOMINES

Jury

M. Mazen AL-AMIR, Rapporteur
M. Peter SEILER, Rapporteur
Mme Sophie TABOURIECH, Examinatrice
M. Mark LOWENBERG, Examinateur
M. Laurent BURLION, Directeur de thèse
M. Jean-Philippe CONDOMINES, Co-directeur de thèse

Doctoral Thesis

Modeling, Analysis, and Control for Upset Recovery

—from System Theory to Unmanned Aircraft Flight

Torbjørn Cunis

Final Version

to Sólveig.

Preface

"If – and the thing is wildly possible – the charge of writing nonsense were ever brought against the author of this brief but instructional poem, it would be based, I feel convinced, on the line,

'Then the bowsprit got mixed with the rudder sometimes.'"

—Lewis Carroll[1]

⇆

Publications

In the scope of the thesis, several publications have been conducted:

1. Torbjørn Cunis et al. (2017). "Non-linear Analysis and Control Proposal for In-flight Loss-of-control". In: *20th IFAC World Congress, preprints*. Toulouse, FR, pp. 10681–10685.

2. Torbjørn Cunis and Murat Bronz (2017). "EDURA: an Evolvable Demonstrator for Upset Recovery Approaches with a 3D-printed Launcher". In: *9th International Micro Air Vehicle Conference and Competition*. Toulouse, FR.

3. Torbjørn Cunis, Jean-Philippe Condomines, and Laurent Burlion (2017). "Full-envelope, Six-Degrees-of-Freedom Trim Analysis of Unmanned Aerial Systems based on Piece-wise Polynomial Aerodynamic Coefficients". In: *4th Workshop on Research, Education, and Development of Unmanned Aerial Systems*. Linköping, SE, pp. 108–113. DOI: 10.1109/RED-UAS.2017.8101652.

4. Torbjørn Cunis et al. (2018a). "Piece-wise Identification and Analysis of the Aerodynamic Coefficients, Trim Conditions, and Safe Sets of the Generic Transport Model". In: *AIAA Guidance, Navigation, and Control Conference*. Kissimmee, US-FL. DOI: 10.2514/6.2018-1114.

5. Torbjørn Cunis, Tobias Leth, et al. (2018). "Identification of Thrust, Lift, and Drag for Deep-stall Flight Data of a Fixed-wing Unmanned Aircraft". In: *2018 International Conference on Unmanned Aircraft Systems*. Dallas, US-TX, pp. 531–538. DOI: 10.1109/ICUAS.2018.8453340.

[1] For how (and why) bowsprit and rudder got anywhere close, refer to "The Hunting of the Snark" by Lewis Carroll.

6. Torbjørn Cunis (2018). "The `pwpfit` Toolbox for Polynomial and Piece-wise Polynomial Data Fitting". In: *18th IFAC Symposium on System Identification*. Stockholm, SE, pp. 682–687. DOI: 10.1016/j.ifacol.2018.09.204.

7. Torbjørn Cunis and Sarah Gluschitz (2018). "Talking Aviation Safety: How to make airplanes safer". In: *EuroScience Open Forum*. Toulouse, FR

8. Torbjørn Cunis and Elgiz Baskaya (2018). "Performance of Unmanned Aircrafts in the Event of Loss-of-control". In: *10th International Micro Air Vehicle Conference and Competition*. Melbourne, AU.

9. Torbjørn Cunis et al. (2018b). *Piecewise Polynomial Model of the Aerodynamic Coefficients of the Generic Transport Model and its Equations of Motion*. Tech. rep. `hal-01808649`, version 3. Toulouse, FR: ONERA – The French Aerospace Lab; French Civil Aviation School. URL: `https://archives-ouvertes.fr/hal-01808649v3`

10. Torbjørn Cunis et al. (2019). "Piecewise Polynomial Modeling for Control and Analysis of Aircraft Dynamics beyond Stall". In: *Journal of Guidance, Control, and Dynamics* 42.4, pp. 949–957. DOI: 10.2514/1.G003618.

11. Torbjørn Cunis and Anders la Cour-Harbo (2019). *Piecewise Polynomial Model of the Aerodynamic Coefficients of the* Cumulus One *Unmanned Aircraft*. Tech. rep. `hal-02280789`. Støvring, DK: Sky-Watch A/S. URL: `https://archives-ouvertes.fr/hal-02280789`

12. Torbjørn Cunis, Jean-Philippe Condomines, Laurent Burlion, and Anders la Cour-Harbo (2019). "Dynamic Stability Analysis of Aircraft Flight in Deep Stall". In: *Journal of Aircraft*. DOI: 10.2514/1.C035455.

13. Torbjørn Cunis, Dominic Liao-McPherson, et al. (2019). "Economic Model-Predictive Control Strategies for Aircraft Deep-stall Recovery with Stability Guarantees". In: *58th IEEE Conference on Decision and Control* (to be presented). Nice, FR.

14. Torbjørn Cunis, Jean-Philippe Condomines, and Laurent Burlion (2019b). "Sum-of-squares Flight Control Synthesis for Deep-stall Recovery". In: Revision under review for *Journal of Guidance, Control, and Dynamics*.

15. Torbjørn Cunis, Jean-Philippe Condomines, and Laurent Burlion (2019a). "Local stability analysis for large polynomial spline systems". In: Revision under review for *Automatica*.

Acknowledgements

The research presented here is the product of three years' work at ONERA – The French Aerospace Lab and the French Civil Aviation School (ENAC) in Toulouse. My time in France has been preceded by an eight months internship in Delft and five-and-a-half years undergraduate and graduate studies in Germany. The dissertation thus completes the education to an European scientist. To both research and the manuscript itself several people, groups, and institutions, some of them without knowing or wanting, have contributed. While providing a full list here seems infeasible, I will try and duly enumerate some:

First and foremost, this thesis wouldn't have been possible without my advisors Laurent Burlion and Jean-Philippe Condomines who initiated the research topic and whose helpful comments and critical review provided guidance for my research. On a related note, I remain thankful to ONERA and ENAC for the institutional support and funding. Thierry Le Moing, Yannick Jestin, Valérie Cassignol, and Carsten Döll provided invaluable help whenever administrative matters were to resolve. For issues of technical nature with software or hardware, I would like to thank Gautier Hattenberger and Michel Goraz, respectively, as well as Murat Bronz for his expertise in aerodynamics and aeronautics.

A collaboration with the Aalborg University as well as my visit at the University of Michigan have significantly contributed to its results. In Aalborg, I would like to thank Anders la Cours-Harbo for initiating this collaboration during the 4th RED-UAS Workshop in Linköping and eventually inviting me to Aalborg; Tobias Leth and Luminita Totu for numerous discussions; and Sky-Watch A/S, in particular Jesper Holst, for their generous support of the project. As for the visit in Michigan, I thank Ilya Kolmanovsky and Dominic Liao-McPherson for their warm welcome and providing me with their great knowledge of model-predictive control theory.

I have been very happy that my friend and favourite scientific illustrator, Sarah Gluschitz, followed my invitation to visit Toulouse in the Summer of 2018 and that ENAC agreed to fund her stay in the first place. Our joint work, which I have indeed much enjoyed, has not only led to a gorgeous poster which we presented in the 2018 EuroScience Open Forum, but also provided several figures that illustrate the content of the first two chapters (Figures 1.1, 2.1, 2.2, 2.3, and 2.4).

I was moreover lucky enough to rely at all times on the support of my friends and family, both in Toulouse and from distance. Elgiz Baskaya both was a great colleague and supportive of my work at ENAC, and also were her much appreciated dinners a reliable source of nutrition. With Jan Bolting I shared the fate of a German expatriate in Toulouse and his help dealing with administrative matters in French was a great support. I regret that I never had the chance of biking with Jim Sharples, but I enjoyed watching Tour de France and our occasional discussions of British, French, and European politics as well as languages. Gustav Lundin was always ready for a chat at ONERA and truly is a very *friendly Swede*. Jeanne Methel seemed to have been disappeared either in her wind-tunnel or climbing the Pyrénées for most of the time I remember,

but I have been the more happy meeting her when she did not. From Germany, Lisa Blochberger *née* Richter kept poking me about the progress of my thesis and also made sure of my well-being when visiting southern France in 2018. I am grateful for the continuing support of my family, foremost my parents Ursula and Roman, just as they have supported me during my studies all the time. Last but not least, Solveig Hübner was very patient and enduring with her not only always busy, and more often than good stressed, but also most of times absent boyfriend!

Finally, I would like to honour three of my almarum matrum teachers who have, indirectly and probably rather unconsciously, but influenced this work: Dirk Abel, in lieu of the initiators of the Master's programme in automation engineering in Aachen, whose lecture notes on control theory I have regularly frequented for basic definitions. Dieter Moormann's lectures provided a good mix of aircraft flight dynamics and control technique, even though I was the "fellow who already knew a thing or two about control." Last (chronologically first), the classes of Christian Glaßer in theoretical computer science have been a great example for vivid explanation of complex matters (he was later, much deservedly, promoted for excellence in teaching) and I took great aim at keeping up with his clear notation and formal rigourosity.

TC

Toulouse
Norderstedt
Ann Arbor
Oktober 2019

Contents

Chapters marked with a star (⋆) have recently been published, or are currently under review for publication, in international journals and level-A* conferences.

Chapter 1

Introduction

Airborne travel is one of safest means of passenger transportation. Modern aircraft constitute complex cyber-physical systems and it is due to scrutinising certification processes of the regularising bodies, such as the European Aviation Safety Agency, that a high standard of safe, large-scale operation is maintained. Yet, the few accidents involving civil aircraft usually claim a large number of victims and thus are highly newsworthy. Any incident has the potential to shatter public trust into the technology anew, including, to the authors very consternation, two recent accidents of a freshly redesigned airliner model of a major company. The present dissertation aims to contribute to tomorrow's aviation safety by design and evaluation of advanced flight control systems.

Motivation

Aviation authorities and manufactures jointly monitor incidents and accidents that occur in the operation of civil aircraft as well as their – potentially multiple – causes. This efforts led to the development of the ICAO[1]/CAST[2] *Common taxonomy* to classify occurrences into principal categories (Corey et al. 2008, p. 8). According to figures for the past three decades, the foremost cause of accidents leading to fatal injuries have been events of *in-flight loss-of-control* (LOC-I), with a contribution of 26 % to all fatal accidents from 1991 to 2015 (based on accumulated data of Boeing 2001, p. 19; Boeing 2008, p. 21; Boeing 2016, p. 22). Unsurprisingly, LOC-I events also constitute the single largest contributor to fatalities (*ibid.*). Data of the International Air Transport Association (IATA) for the recent years mirrors the fatality of LOC-I (Fig. 1.1; based on IATA 2015, pp. 3 and 6–7); however, the figure highlights a further paradox of aircraft accidents: counting both fatal and nonfatal accidents, the three major contributors to fatal injuries (84 %), in-flight loss of control, controlled flight into terrain, and excursion from runway or taxiway, make up less than 40 % of all accidents. In other words, the majority of accidents in civil aviation remain nonfatal. Yet albeit rare, the high fatality of LOC-I events makes it today's "highest risk to aviation safety" (IATA 2015, p. 1).

The Common taxonomy defines the category of LOC-I flight events as "extreme" deviation of the aircraft from its desired flight-path (ICAO 2013, p. 5); the US Federal Aviation Administration (FAA) maintains a similar definition (cf. also FAA 2016, Chapter 4, p. 1). The definition further notes that loss of control, contrary to the category title, is not necessary for such a deviation, and further incidences may lead to loss

[1] International Civil Aviation Organization
[2] Commercial Aviation Safety Team

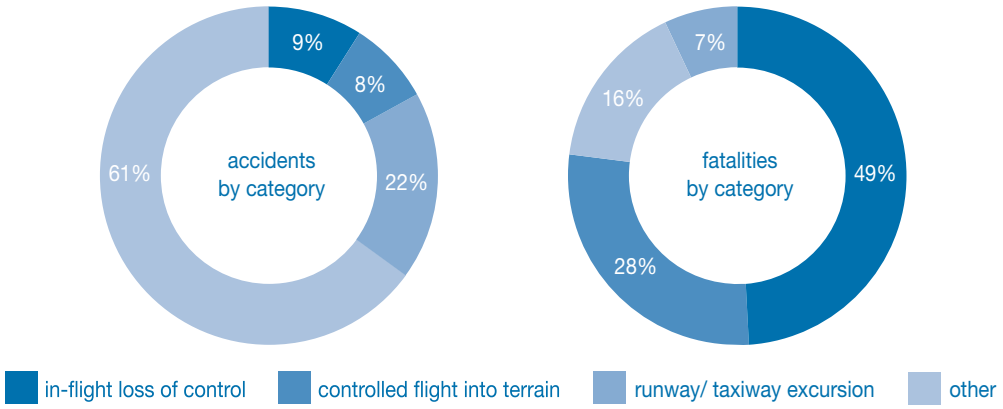

Figure 1.1: Contribution of ICAO/CAST categories to accidents and fatalities, respectively, for 2010–2014 (IATA 2015). *Commissioned illustration.*

of control. Notwithstanding, events of loss-of-control that are direct result of another, severe incident are to be assigned to the latter's category (ICAO 2013). The term "in-flight loss of control" is sometimes used synonymously to an *upset* of the aircraft, and so is the idea of upset recovery; yet, the two terms are related but not identical. However, in-flight loss of control may eventually lead to an upset, and (intentional) flight at conditions otherwise qualifying as upset increase the risk of loss-of-control (ICAO 2013, p. 5). In the late 90s, a joint project of Boeing and NASA identified distinguished sets of flight conditions, called "upset envelopes," which are supposed to constitute an event of LOC-I (Wilborn and Foster 2004, pp. 3–5). Upset flight of an aircraft is characterised by highly nonlinear behaviour of the aircraft aerodynamics, including stall, oscillatory spin, spirals, and post-stall rotations (cf. Chambers and Grafton 1977). In response to this severe threat to aviation, manufacturers, airlines, and aviation authorities have developed procedures for flight crews to avoid and tackle upset events (see Carbaugh et al. 2008; IATA 2015).

Scientific Context

The severity of LOC-I events has led to a surge of high-quality scientific publications on the detection, prevention, and recovery from aircraft upset conditions. A notable part considered flight control technologies as an assistant component of a piloted aircraft's cockpit (including Schuet, Lombaerts, Acosta, et al. 2017; Smaili et al. 2016; Stepanyan et al. 2017); these studies commonly include experiments with full-scale flight simulators and professional pilots. Other researchers have approached the aircraft upset dynamics from the perspective of system theory, applying well-established as well as recently developed analysis methods (such as Chakraborty et al. 2011c; Kwatny et al. 2013; McDonough and Kolmanovsky 2017). These approaches utilised algebraic models of the aircraft aerodynamics, i.e., polynomial, rational, or piecewise affine (to name a few) representation of the aerodynamic coefficients, which have been identified and modeled

a priori. A third major group of work studies advanced analysis and control methods combined with high-fidelity aircraft computer models (e.g., Gill et al. 2013; Engelbrecht 2016; Tekles et al. 2017). A joint work of NASA and Boeing into the development of a vehicle for aircraft upset research resulted in the widely recognised Generic Transport Model (GTM). Along with the GTM's openly available, high-fidelity model for MATLAB/Simulink comes a 2.08 m-wingspan unmanned aircraft representing a 5.5 % scaled generalised airliner (see Foster et al. 2005; Jordan et al. 2006). Despite the GTM, few designs have actually been tested in flight experiments (such as Gregory et al. 2011).

We give a detailed review of the literature on upset recovery and related work in the next chapter.

Research Objectives

Analysis and control of the aircraft flight dynamics over a large range of flight conditions is one of the most difficult problems in systems and control engineering. To describe the aircraft's translational and rotational motion relative to earth at any time, numerous independent states and inputs are required. The aerodynamic forces and moments induced by the wings, control surfaces, and the fuselage have no known algebraic relation to the aircraft's state and geometries but must be investigated in extensive wind-tunnel measurements or simulations of fluid dynamics. (cf. Brockhaus et al. 2011, pp. 31, 99–108, and 138–142). Moreover, control inputs are inherently constrained by physical limits and control effects may change significantly with the state of the aircraft.

Consequently, insights due to algebraic analysis are limited by the accuracy of the underlying model. On the other hand, nonlinearity of the aerodynamics and increasing complexity of the aircraft flight control systems call for advanced certification methods in order to ensure safe recovery, which, in turn, require algebraic models of higher order. We have chosen an approach that adopts analysis and control methods from system theory for as-accurate-as-possible aerodynamic models, in order to prove mathematically the properties of the controlled aircraft system. We further consider recovery of a vehicle without a pilot in the loop, that is, an autonomous unmanned aircraft or autonomous operation of a piloted aircraft (see ICAO 2011, p. ix, for a glossary). In following procedures for manual recovery (FAA 2016, Chapter 4, pp. 7 and 15), we will focus on upset recovery using the aircraft's control surfaces only, thus reducing the number of control inputs. We then assume the aircraft to be *recovered* if it has been brought back into its normal flight envelope (see Terminology in the next chapter) whence continuation of the flight operation, such as regaining altitude or returning to level flight, can be ensured.

Contributions

The research of this thesis has contributed both to system's theory and aeronautical control engineering. Its major contributions are:

1. to develop a new and simplified fitting method for piecewise models that accurately describe the aerodynamics over the full flight envelope, distributed in the open-source `pwpfit` toolbox;

2. to thus provide a piecewise aircraft model for the Generic Transport Model for analysis and control beyond the normal flight envelope;

3. to investigate the dynamics of a small, fixed-wing unmanned aircraft in deep-stall flight and, based on the results, identify an algebraic model suitable for analysis and control of longitudinal upset conditions;

4. to adapt and extend system theoretical analysis tools to piecewise-defined (aerodynamic) models including multivariate splines;

5. to implement a strategy for the synthesis of upset recovery control laws that guarantee stable recovery;

6. to reformulate the problem of upset recovery subject to minimal loss of altitude as receding-horizon control problem and rigorously prove its stability; and

7. to demonstrate the application of receding-horizon control for recovery from upset conditions such as oscillatory spins and spirals.

The probably greatest contribution of this thesis however are not its theoretical suggestions nor the aeronautical results, although those too are new results; it is to transfer the concepts of the wider field of system's theory to the aerospace community, to adapt theories for the needs of aerial designs, and to make their approaches available for aeronautical engineering and research.

Thesis Outline

The dissertation is divided into two parts, with the aim that both parts can be read – and understood – independently. This is also ensured by the fact the main chapters have been written as self-contained research articles. For this document, they have been partially edited and are linked together. Further introduction and technical background chapters give space for extended discussions. The following structure provide a logical order and does not necessarily reflect the temporal sequence:

Chapter 1 The present chapter has given a rather broad introduction into the topic and context of this dissertation. It was written for the thesis.

Chapter 2 The purpose of the second chapter is to introduce more specifically the challenges of upset recovery and accommodate the reader with the relevant terminology and literature. Furthermore, we define general notations and present the two aircraft used in this dissertation. The chapter was written for the thesis.

Part I is dedicated to modeling and analysis of an aircraft as nonlinear system. It emphasises the unstable and nonlinear behaviour of an aircraft outside its normal flight envelope. Throughout the first part, the aircraft is treated as open-loop system.

Chapter 3 We introduce a novel technique of piecewise-defined, polynomial modeling of the aerodynamic coefficients and discuss the necessary adaptations for nonlinear analysis tools. Chapter 3 has been published in the Journal of Guidance, Control, and Dynamics (Cunis et al. 2019).

Chapter 4 Based on the piecewise polynomial modeling of the previous chapter, we study in deep the change of dynamics during the transition from normal flight into deep-stall, both by means of nonlinear analysis and inflight measurement data. Chapter 4 is currently under review for the Journal of Aircraft (Cunis, Condomines, Burlion, and la Cour-Harbo 2019).

Chapter 5 The last chapter of Part I constitutes a stand-alone, mainly theoretical contribution that takes some of the ideas for the analysis of piecewise polynomial models and extends these to more complex systems, making the results of the dissertation available for accurate modeling techniques. Chapter 5 is currently under review for *Automatica* (Cunis, Condomines, and Burlion 2019a).

Part II considers the problem of providing (autonomous) control for an aircraft in order to restore its normal flight conditions, without exceeding its limitations, after an upset situation. Here, we revisit the major results of the first part as such as we make use of the provided models and its properties.

Chapter 6 In the first chapter of the control part, we start by extending the analysis tool of Chapters 3 and 5 for control synthesis. Thus, we are able to derive provable certificates for stable recovery from deep-stall flight conditions. This chapter is currently under review for the Journal of Guidance, Control, and Dynamics (Cunis, Condomines, and Burlion 2019b).

Chapter 7 We now consider a powerful control methodology for constrained nonlinear systems, namely variants of model predictive control, in order to recover an aircraft from deep-stall flight. In addition, we prove stability of the designed feedback. Chapter 7 has been accepted for presentation in the 58th Conference on Decision and Control (Cunis, Liao-McPherson, et al. 2019).

Chapter 8 With the last chapter of the main parts of this thesis, we further extend and demonstrate the use of model predictive control for a full, six-degrees-of-freedom aircraft model. This allows us to recover from upset situations such as spirals and oscillatory spins subject to constraints and indicates future work. This chapter has not been published yet.

Chapter 9 concludes the dissertation with a discussion of the obtained results, their interconnection, and indicated future work. We finally summarise the major findings and contributions. The last chapter, again, was written for the thesis.

Chapter 2

Upset Recovery

Over the better part of the past two decades, researchers and aeronautical engineers have directed their strength towards the reduction of accidents and fatalities related to in-flight loss-of-control events. This has led to a rich body of scientific literature – including a special issue of the Journal of Guidance, Control, and Dynamics (Lu et al. 2017) – which can be loosely subsumed under the headings *upset prediction*, *upset prevention*, and *upset recovery*. This chapter aims to introduce the reader to the terminology and literature of upset recovery and to provide a common background to understand the challenges and contributions of the subsequent study.

2.1 Terminology

Understanding the key concepts of aircraft upset recovery is imperative for the further discussion. Due to the diverse nature of the literature, some concepts are well founded in system's theory, others are directly related to aeronautical (control) engineering. Moreover, we found the literature to be not always consistent in the terms its authors used. In the following, we concisely review and, where necessary, define the most important concepts in common language.

In-flight loss-of-control (LOC-I) A deviation of the aircraft's actual flight path from the desired flight path, which is 'significant' (FAA 2016, Chapter 4, p. 1) or 'extreme' (ICAO 2013, p. 5). Also, a category of the ICAO/CAST Common taxonomy for aircraft incident reports.

Flight envelope Generally speaking, a *flight envelope* is a hyper-dimensional manifold – or sub-space – of which each dimension represents a single parameter of aircraft flight. A flight envelope may be defined by a set of conditions on some or all parameters (e.g., $\alpha_{\min} \leq \alpha \leq \alpha_{\max}$ for the angle of attack α). Besides the envelopes of Wilborn and Foster (2004) about which conditions constitute an upset, there are further envelopes worth consideration (illustrated in Fig. 2.1):

- The *structural flight envelope* or *operational envelope* comprises conditions at which the aircraft may be operated without jeopardising the structural integrity of the vehicle. For commercial aircraft, the operational envelope is specified by the manufacturer within the process of flight-worthiness certification.
- The *normal* (or "nominal") *flight envelope* is described by parameter values at which the aircraft is supposed to fly over the course of regular operation.

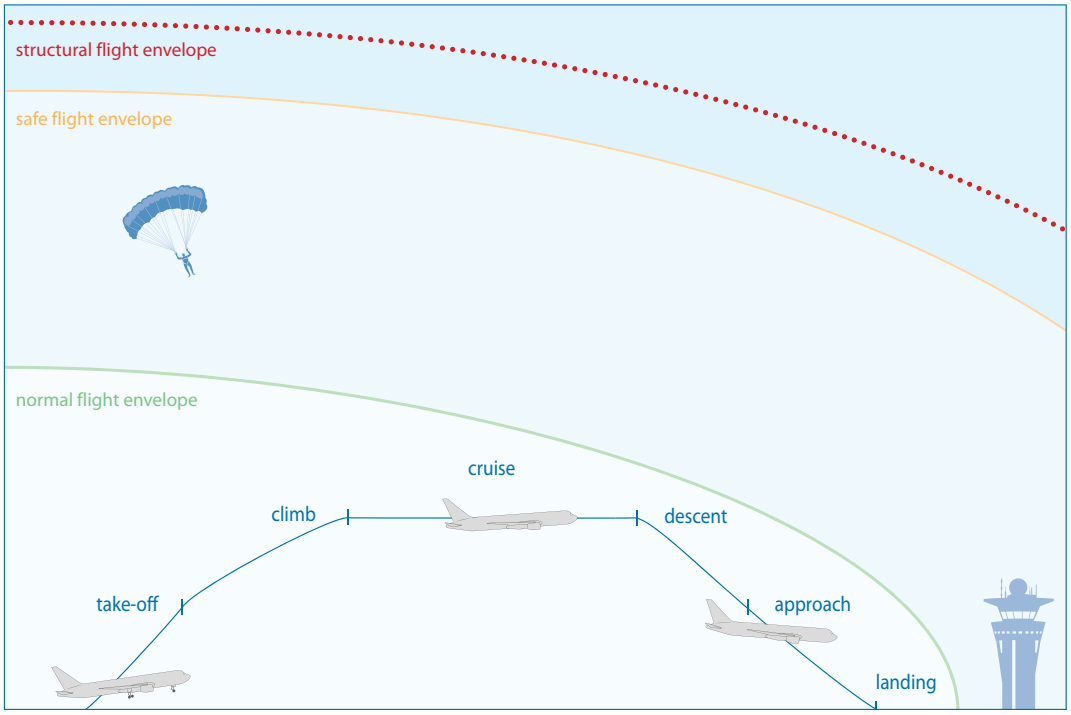

Figure 2.1: Artistic illustration of normal flight envelope, (structural) safe flight envelope, and structural flight envelope. *Commissioned illustration.* (Note: planar depiction is for illustration purposes only and does not represent the location of the aircraft. Envelopes do not necessarily share common boundaries.)

- The *safe flight envelope* is commonly defined as the maximal set such that the aircraft can, for all times, be kept within either a normal flight envelope (*nominal safe*) or the structural flight envelope (*structural safe*) by means of flight control (cf. Kwatny et al. 2013, p. 157). In other words, the safe flight envelope is the largest controlled invariant[1] (not necessarily strict) subset of the another, given envelope.

Trim (condition) An aircraft is called *in trim* if the forces and moments (lift, drag, engine thrust, weight, etc.) level out. Then, a *trim condition* is a state at which the aircraft is in trim. Almost all civil airliners are passively stable to moderate perturbations of the *normal flight* trim conditions (Brockhaus et al. 2011, p. 672).

Upset (condition) An aircraft *upset* is an event at which the aircraft (unintentionally) exceeds some parameters of normal flight (FAA 2016, Chapter 4, p. 2). Furthermore, Wilborn and Foster (2004) have tied the notion of upset to one of five *flight envelopes* commonly observed in LOC-I incidents. An *upset condition* is subsequently a state at which the aircraft is upset (that is, a state that lies within one of the upset envelopes). Often, an upset condition constitutes a stable and attractive mode of the flight dynamics (Goman et al. 1997, p. 546), such as oscillatory spin or spiral (Fig. 2.2), increasing the difficulty of upset recovery.

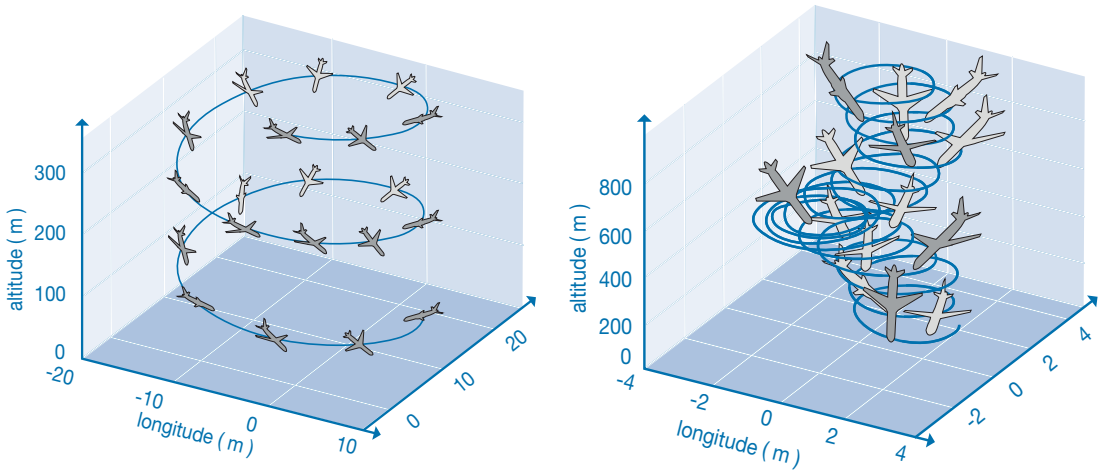

(a) Steep spiral.

(b) Period-three oscillatory spin.

Figure 2.2: Illustrations of aircraft flight paths in upset conditions (based on Gill et al. 2013, Figures 4 and 8). *Commissioned illustrations.*

Aerodynamic stall A wing generates a force that lifts the aircraft due to the fact that an incoming air flow streams around the wing (Brockhaus et al. 2011, p. 100); initially, the generated lift increases with the angle relative to the advancing air.

[1] See Blanchini 1999, p. 1749, for a mathematical definition.

However, at some point (namely the *stall angle of attack*) the air stream detaches from the wing (see Fig. 2.3 for an illustration). Subsequently, insufficient lift is generated (FAA 2016, Chapter 4, p. 5). Stall events typically occur when the aircraft's nose is pulled up too far, or horizontal or vertical gusts change the environment of the aircraft spontaneously and unanticipated.

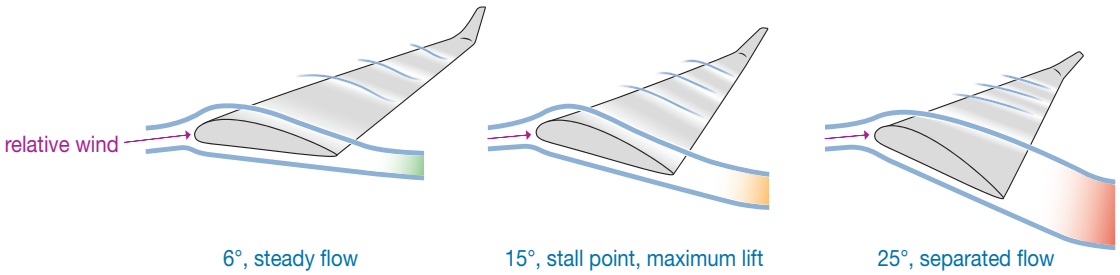

Figure 2.3: Illustration of the airflow around an aircraft wing before, at, and beyond the stall angle of attack. *Commissioned illustration.*

With this terminology in mind, we can proceed to formulate upset recovery by means of system theory. By the common definition, the aircraft is in a state of in-flight loss-of-control once it deviates, by an exceptional margin, from the initially specified flight path. An upset occurs, in addition, if the aircraft also leaves its normal flight envelope and enters one of the upset envelopes. Any control action in order to return the aircraft into the normal flight envelope must be applied within the safe flight envelope. However, the safe flight envelope, by its definition, does not guarantee that the aircraft can be recovered; only, that it can be kept within a desired envelope. In contrast to upset recovery control, upset *prevention* aims to apply control before the aircraft has left or is about to leave the normal flight envelope. LOC-I prevention, finally, could be both understood as *a*) preventing a deviation from the desired flight path in the first place, or *b*) prevention of a LOC-I *accident* as final result, paramount to upset recovery. It should be noted though that only the safe flight envelopes are derived by system theory, whereas normal, upset, and structural flight envelopes are to be specified a priori.

2.2 Literature Review

Belcastro et al. (2017), in their introduction-cum-survey for the JGCD special issue, emphasised the multifaceted nature of hazards and challenges imposed by LOC-I. As key elements for a 'holistic solution' (Belcastro et al. 2017, p. 742), they thus identified research into the development of models for aircraft dynamics in upset conditions; detection, prevention, and recovery of upset conditions by onboard systems monitoring the

aircraft in real-time; and analysis and validation methods suitable for complex control systems and nonlinear dynamics (Belcastro et al. 2017, pp. 744, 748–752, and 755).

The FAA *Airplane Flying Handbook* has since long been a reference for manual recovery of a piloted aircraft (FAA 2016, Chapter 4), with procedures for stall recovery, spin recovery, and spiral recovery. Gratton et al. (2014) evaluated different actions in response to a stall upset; in this study, initially adding thrust was found to be effective in reducing the loss of altitude during stall recovery (Gratton et al. 2014, p. 472). A major contribution for multidisciplinary research into upset recovery has been the development of the *Generic Transport Model* (GTM). Based on aerodynamic wind-tunnel test data for 3.5 % and 5.5 % scaled transport aircraft models, assessing in particular the impact of elevator, rudder, flaps, and side-slip by increasing angle-of-attack, the Generic Transport Model was developed (Foster et al. 2005) and validated against flight tests of the AirSTAR, an unmanned aircraft representing a 5.5 % scaled generic transport aircraft (Jordan et al. 2004; Jordan et al. 2006). The GTM's three-gestalt, consisting of a high-fidelity desktop simulation,[2] aerodynamic data for aircraft training simulators, and the test aircraft AirSTAR, provided background and comparability for researchers of several disciplines. The GTM's "big brother," a full-scale aircraft model of its kin, is referred to in the literature as *Transport Class Model* (TCM).

Today's literature highlights the disparity of fields and approaches contributing to upset recovery and the related issues. In the following, we will distinguish studies with pilot-in-the-loop experiments, system theoretical approaches using algebraic models, and control approaches developed on and evaluated against high-fidelity desktop simulations.

Control methodologies with pilot-in-the-loop experiments

Large aircraft simulators are commonplace in aeronautic practice. These training devices emulate the aerial flight experience mimicking an aircraft's instrumentation and handling. Its wide range of application include training and licensing of pilots as well as studies into crew behaviour under stress. Indeed, pilot-in-the-loop studies are fundamental for the evaluation of recovery schemes for commercial airliners. Cunningham et al. (2011) evaluated and compared different control laws, namely linear quadratic regulator, model-reference adaptive control, $\mathcal{L}_1$-adaptive control, and $\mathcal{H}_\infty$ control, against a piloted GTM simulator. Crespo et al. (2012) further compared different linear, outer-loop control strategies for upset recovery using piloted simulations with the GTM. In addition, Gregory et al. (2011) reported practical flights with the AirSTAR aircraft using an $\mathcal{L}_1$-adaptive control approach which was prior detailed by Xargay et al. 2010.

Nonlinear control techniques have been applied, too. Richards et al. (2017) detailed an upset recovery system for both piloted and automated vehicles which has been evaluated in a pilot-in-the-loop simulation of the GTM. Optimal recovery trajectories are computed solving linear receding-horizon (i.e., model-predictive) control problems online. Using pseudo-control hedging (compare Lombaerts et al. 2010) and nonlinear dynamic inversion, Stepanyan et al. (2016) presented upset recovery guidance algorithms under

[2]Made available as MATLAB/Simulink model in NASA (2016).

state or input constraints. The different approaches were evaluated in a piloted GTM simulation. Stepanyan et al. (2017) further proposed an adaptive approach to predict the boundary of the safe nominal envelope during flight. Applied to the GTM, the prediction system has been evaluated in a pilot-in-the-loop simulation. Moreover, Lombaerts et al. (2013) computed invariant, viable, and forward and backward-reachable sets under the presence of uncertainties.

Schuet, Lombaerts, Kaneshige, et al. (2017), too, employed fast (linear) model predictive control for guidance of the pilot in order to recover the aircraft from a stall event. Lombaerts et al. (2017) developed a guidance system for recovery from stall events based on the aircraft's total energy. The two guidance systems were later evaluated in pilot-in-the-loop simulations of the GTM (Lombaerts et al. 2018). Simulations of these and further guidance algorithms are detailed in Schuet, Lombaerts, Stepanyan, et al. (2017).

From a conceptual point of view, taking into account human-vehicle interactions, Smaili et al. (2017) details the design of upset recovery systems for civil airliner. Both autonomous and manual (guidance) operations were evaluated in piloted simulations. A visual guidance system for piloted upset recovery was presented by Richards et al. (2018). This system was tested in piloted flights of a Learjet aircraft in different upset scenarios including vehicle impairment.

Not only are recovery control and guidance procedures subjected to pilot-in-the-loop simulation, Nooij et al. (2016) evaluated the SUPRA generic aircraft model itself using the feedback of pilots with experience in post-stall flight. Smaili et al. (2016) further developed a simulation environment based on a Boeing 747 commercial airliner as well as a benchmark classification for upset recovery by modeling the 1982 accident of a B747-200F freighter in order to test and compare piloted and automated operations.

System theoretical approaches to upset recovery

Analysis and control techniques founded in system theory have produced provable results. Chakraborty et al. used a nonlinear model of an F/A-18 fighter jet to investigate the so-called "falling-leaf" upset mode, of which this aircraft model had been reported to be prone. They considered linear analysis methods such as Bode margins and robustness against uncertainties (Chakraborty et al. 2011b), but found they could not discriminate between an initial control approach and its revised version. Only with a nonlinear region-of-attraction estimation (Chakraborty et al. 2011c) they were able to show that the revised controller could actually prevent entering the falling-leaf mode.

McDonough et al. (2014) computed the set of initial conditions for which a closed-loop system trajectory satisfies its constraints for all time, so-called *recoverable set*. Under certain conditions, including a linear system and linear inequalities, the recoverable set is finite and thus computable. The authors presented the computation, scaling, and application of linear recoverable sets for flight planning under changing, environmental conditions. Subsequently, McDonough and Kolmanovsky (2017) employed recoverable sets in order to design a trim-point-to-trim-point control approach for a nominal, linear control law synthesised for each trim point. Thus, the feasibility of a sequence of trim points is guaranteed by the obtained, recoverable sets.

Allen et al. (2012) determined the controlled invariant set of the nominal flight envelope solving the Hamilton-Jacobian partial-differential equations (Lygeros 2004, p. 920). The authors further discuss restoration, that is, recovery into, and protection of the safe set by linear quadratic and sliding-mode control approaches, respectively, for the longitudinal aircraft motion. Moreover, Kwatny et al. (2013) worked out a nonlinear, full-envelope analysis of the longitudinal dynamics of the GTM. They compared normal as well as high-angle of attack trim conditions obtained by continuation analysis and argued that the trim condition at stall is, in fact, a bifurcation point; thus, controllability at stall is reduced (Kwatny et al. 2013, p. 154). Reachability, safe sets, and control under constraints are discussed and lead to a discussion of the GTM's manoeuvrability in terms of viable flight-path inclination over airspeed, which further demonstrates the effects of limited elevator deflections. Based on these results, Dongmo (2010) in his PhD thesis considered upset recovery as boundary-value problem employing nonlinear smooth regulators as well as switching controllers with underlying sliding-mode formulation.

Based on the nonlinear the F/A-18 (presented in Chakraborty et al. 2011c), Chang et al. (2016) evaluated the ability to recover from an initial upset condition to a predefined trim condition using linear controllers. A linear quadratic regulator feedback was subsequently modified in order to take into account the periodicity of the bank angle; in addition, an linear quadratic regulator (LQR) feedback law was combined with height tracking control, and then augmented for accommodation of elevator jam failures. In particular, the authors demonstrated the ability to recover the aircraft into stable level-flight trim conditions for different settings of the jammed elevator.

Recently, Zhao (2016) dedicated her PhD thesis to the design and development of a discrete-event-driven, automatic flight control system for prevention and recovery of upset events. The multi-mode, hierarchical control architecture was based on trajectory-linearisation control and bandwidth adaptation techniques and subsequently analysed applying linear robust control theory.

Control design for high-fidelity aircraft simulations

Several studies analysed, designed, and evaluated upset recovery systems using high-fidelity desktop simulations such as the GTM simulation. Sparks and Moerder (2002), as early example, employed trajectory optimisation for recovery from a high-bank upset condition with minimal loss of altitude during recovery. Trajectories with and without a rudder jam failure are compared.

Gill et al. (2013) performed a rich numerical continuation analysis of the GTM and discussed bifurcation of the eight-states aircraft model with respect to the elevator deflection. They obtained several stationary and periodic solutions (such as spirals and oscillatory spins), partially attractive, which constitute upset conditions. The authors further investigated the transition between upset conditions and concluded that, for some conditions, a sequence of disturbances or unfortunate control inputs is necessary to reach these conditions (Gill et al. 2013, p. 1839).
Based on a similar analysis, Engelbrecht et al. (2013) described a state-machine based control approach of simple linear controllers for upset recovery. The approach sequen-

tially stabilises first body rates and aerodynamic angles; then recovers the attitude; and finally reduces overspeed and recovers flight altitude. The PhD thesis of Engelbrecht 2016 constitutes one of the most comprehensive studies of upset recovery approaches using high-fidelity models of the recent years. Additionally to the state-machine based approach and bifurcation analysis as well as Monte Carlo simulations of the passive GTM aircraft, he further discusses control approaches based on Lyapunov's stability theory and dynamic programming. All approaches were simulated against the GTM high-fidelity model.
Kim et al. (2016) conducted a numerical bifurcation analysis of the nonlinear spin dynamics of an F/A-18 fighter jet and presented an optimal spin recovery approach based on reinforcement learning.

Schuet, Lombaerts, Acosta, et al. (2017) proposed an online estimation and system identification method that is employed to predict the safe flight envelope during flight, in particular under presence of disturbances or damages. The authors discussed different examples using a desktop simulator of a transport aircraft. Tekles et al. (2017) further reported the development of a flight envelope protection system for the GTM which overrides the conventional flight control system in order to ensure a safe flight condition.

Bunge and Kroo (2018) developed a control architecture for spin recovery with the objective to reduce the loss of altitude during recovery. The architecture consists of a switching control design with arrest and pull-out stages. The arrest controller is derived by optimisation over an aircraft model for high angles of attack and the control architecture is validated, with good results, against spin flight data recorded by NASA. The authors further conducted flight test using a micro air vehicle (see Bunge 2017).

Akcal et al. (2018) performed Monte-Carlo simulations with a high-fidelity F/A-18 aircraft model to study the ability of different linear and nonlinear feedback laws to recover the aircraft from high-rate upset conditions. The authors measure time and ability to recover over a range of initial angles of attack. Yildiz et al. (2019) further detailed the design of an elaborate switching-mode upset recovery control system, of which the switching conditions are computed by parameter optimisation. The synthesised control system is evaluated in Monte-Carlo simulations of the GTM and its ability to recover the aircraft is compared to the designs of Engelbrecht et al. (2013) and Richards et al. (2017). The proposed recovery scheme is further demonstrated on a high-fidelity simulation of the F-16 agile aircraft.

Further studies

Early approaches for upset recovery studied the use of engine thrust only for recovery in case of a failure of the hydraulic system. Burcham Jr et al. (1997) detailed the development and evaluation of a flight control system based on throttle-only control. Controlling both longitudinal and lateral dynamics of an MD-11 transport aircraft, both landing and upset recovery using throttle-only control has been demonstrated in flight tests. Later, Burcham Jr et al. 2009 discussed the effectiveness and feasibility of throttle-only control. Flight tests have been performed with different transport aircraft and recoverability by throttle only is evaluated for multiple flight segments. Throttle-only control is also pre-

sented for military aircraft in Urnes Sr 2012, including throttle-only landing of a NASA F-15 aircraft. Upset recovery of damaged aircraft was briefly discussed.

2.3 Challenges

Despite extensive research and many contributions, LOC-I still imposes significant challenges. This includes advances in computational methods for large-scale system application and coordinated toolchains incorporating multiple approaches (Belcastro et al. 2017, p. 767). In particular, validation and certification of flight control systems is imperative to ensure safe recovery. However, future complex systems and flight at non-nominal flight conditions call for novel verification techniques beyond Monte-Carlo simulations and robust linear control theory (Philippe 2011, p. 206). Integration of this techniques from research into practice is a tedious process (Philippe et al. 2011, p. 11) and requires a close interaction between systems theory and aeronautical engineering.

Recent years have seen an increasing participation of unmanned aircraft within the common airspace and this trend is widely expected to lead to unmanned as well as (small) passenger aircraft that operate autonomously. Indeed, these vehicles aren't any less prone to upset situations. For a remote-piloted aircraft for example, flight through heavy clouds implies an obstruction of the line-of-sight under presence of strong upwinds risks a vehicle upset upon which the pilot may only react delayed. Autonomous and unmanned aircraft which are upset do not only endanger passengers onboard as well as humans and infrastructure in the proximity, but the safety of the wider aviation system and its participating aircraft (Belcastro et al. 2017, pp. 764 and 766). In the absence of a pilot, upset prevention and recovery requires extensive decision-making processes (Marshall et al. 2018, p. 2) – a conundrum given the bespoken need for rigorous certification!

The role of autonomous and semi-autonomous operation in commercial aviation is steadily increasing and the successful integration of automatic flight control systems for military aircraft (Philippe et al. 2011, p. 12; Swihart et al. 2011, p. 10) strengthens wider acceptance. Automatic operations do not only increase the vehicles safety, but also reduce pilot's mental load (Harris 2007, p. 521; Endsley 2017, p. 16). In the view of the perils of upset situations as well as recent accidents involving malfunctioning flight control systems, unmanned aircraft can provide testbeds for experiments, demonstrations, and inflight validation, thus serving as moderators for public compliance.

Over the last years, researchers have developed several upset recovery control approaches and evaluated the proposed systems successfully with high-fidelity simulations. System-theoretic approaches have made tremendous progress for nonlinear validation and certification. However, there is a considerable disparity between the models considered in system theoretic studies and the aforementioned high-fidelity models. If nonlinear system theory and analysis is to be applied for verification of future upset recovery schemes, further research is imperative to incorporate the highly nonlinear aircraft dynamics into modeling and analysis tools. Moreover, extension towards analysis of hybrid systems is necessary for verification of multi-mode, discrete-event-driven, and switching control approaches such as Engelbrecht et al. (2013) or Yildiz et al. (2019).

2.4 Preliminaries

The main chapters of the dissertation were written as self-contained research articles, including preliminary definitions and notations. In order to avoid repetitions, we limit this section to the most fundamental concepts; some of which may have been tacitly used in the remainer.

2.4.1 Notations

We make use of the following conventions, notations, and definitions:

Mathematical notations

The set of natural numbers is denoted by $\mathbb{N}$; the set of discrete, by $\mathbb{Z}$; and the set of real, by $\mathbb{R}$. The sets of positive and non-negative (real) numbers are further denoted by $\mathbb{R}_+$ and $\mathbb{R}_{\geq 0}$, respectively. For a pair of vectors $\mathbf{a}, \mathbf{b} \in \mathbb{K}^n$, $n \in \mathbb{N}$, the scalar product is written as $\langle \mathbf{a}, \mathbf{b} \rangle = \mathbf{a}^T \mathbf{b}$. The 2-norm of a vector $\mathbf{x} \in \mathbb{K}^n$ is denoted by $\|\cdot\|_2$ and defined as $\|\mathbf{x}\|_2 = \sqrt{\langle \mathbf{x}, \mathbf{x} \rangle}$. Polynomials in a body $\mathbb{K}$ and vector $\mathbf{x} \in \mathbb{K}^n$ form the set $\mathbb{K}[\mathbf{x}]$.

We make further use of the *kappa-ell* classes $\mathcal{K}$, $\mathcal{K}_\infty$, $(\mathcal{L})$, and $\mathcal{KL}$ of continuous functions, which are defined as follows:

Definitions 2.1. Let $\alpha \colon [0, a) \to \mathbb{R}_{\geq 0}$, $\delta \colon [0, \infty) \to \mathbb{R}_{\geq 0}$, and $\beta \colon [0, a) \times [0, \infty) \to \mathbb{R}_{\geq 0}$ be continuous with $a \in \mathbb{R}_+ \cup \{\infty\}$;

- α belongs to class $\mathcal{K}$ if and only if $\alpha(\cdot)$ is strictly increasing and $\alpha(0) = 0$;
- α belongs to class $\mathcal{K}_\infty$ if and only if $a = \infty$, $\alpha \in \mathcal{K}$, and $\alpha(r) \to \infty$ for $r \to \infty$;
- δ belongs to class $\mathcal{L}$ if and only if $\delta(\cdot)$ is strictly decreasing and $\lim_{t \to \infty} \delta(t) = 0$;
- β belongs to class $\mathcal{KL}$ if and only if $\beta(\cdot, t) \in \mathcal{K}$, $\beta(r, \cdot) \in \mathcal{L}$;

with $t \in [0, \infty), r \in [0, a)$.

We will frequently use the set-builder notation

$$\mathcal{A} = \{ \mathbf{x} \in \mathbb{K}^n \,|\, \wp(\mathbf{x}) \} \tag{2.1}$$

for some $n \in \mathbb{N}$, body $\mathbb{K}$, and predicate $\wp \colon \mathbb{K}^n \to \{\bot, \top\}$; by this notation, we say that $\mathcal{A}$ is the set of all elements $\mathbf{x}$ in $\mathbb{K}^n$ such that $\wp$ holds, and $\mathcal{A} \subseteq \mathbb{K}^n$. More specifically, the predicate might be specified by a real scalar field $\mathcal{L} \colon \mathbb{K}^n \to \mathbb{R}$ and $\nu \in \mathbb{R}$, in which case we write

$$\Omega_{\mathcal{L} \leq \nu} =_{\text{def}} \{ \mathbf{x} \in \mathbb{K}^n \,|\, \mathcal{L}(\mathbf{x}) \leq \nu \}; \tag{2.2}$$

however, in Chapter 3 we use alternatively $\Omega_{\mathcal{L}} =_{\text{def}} \{ \mathbf{x} \in \mathbb{K}^n \,|\, \mathcal{L}(\mathbf{x}) = 0 \}$ (note the equality here) and in Chapter 6, we write short $\Omega_\nu = \Omega_{\mathcal{L} \leq \nu}$ if the choice of $\mathcal{L}(\cdot)$ is unambiguous.

Notations for aircraft dynamics

Variables for the notation of the aircraft state and motion follow, where possible, ISO 1151-1 (1988): Flight dynamics – Concepts, quantities and symbols – Part 1: Aircraft motion relative to the air. Vector-valued variables such as forces, moments, and velocities, are conveniently expressed in one of the following orthogonal, right-handed reference axis systems:

- *Body axis system* $(x_\mathrm{f}, y_\mathrm{f}, z_\mathrm{f})$: Originated in the aircraft's centre of gravity; x_f-axis points longitudinally towards the nose; y_f-axis points along star-board wing; z_f-axis completes the setup;
- *Air-path axis system* $(x_\mathrm{a}, y_\mathrm{a} z_\mathrm{a})$: Originated in the aircraft's centre of gravity; x_a-axis follows the aircraft's velocity vector $(\mathbf{V}_\mathrm{A})$; y_a-axis points along star-board wing but orthogonally to x_a-axis; z_a-axis completes the setup;
- *Earth-fixed axis system* $(x_\mathrm{g}, y_\mathrm{g}, z_\mathrm{g})$: Originated in an arbitrary, fixed point; x_g-axis points (geographically) north; y_g-axis points (geographically) east; z_g-axis points vertically down completing the setup.

Vector components referring to the respective axis system are indicated by subscripts ($_\mathrm{f}$, $_\mathrm{a}$, $_\mathrm{g}$); subscripts for the body axis system may be omitted.

The aircraft's *attitude* vector is defined by rotation of the earth-fixed axes into body axes using the Euler angle sequence Ψ (azimuth angle), Θ (pitch angle), and Φ (roll angle). Likewise, the air-path angles χ_A (air-path azimuth), γ_A (air-path inclination), and μ_A (air-path bank), in this order, rotate the earth-fixed axes into air-path axes. Throughout the dissertation, we neglect the presence of wind and thus may drop the subscript $(_\mathrm{A})$. The aerodynamic angles α (angle of attack) and β (side-slip angle) are finally defined, in reversed order, by rotation of the air-path axes into body axes.

We prefer to denote the aircraft control inputs by the greek letters ξ (aileron deflection), η (elevator deflection), and ζ (rudder deflection) instead of $\delta_\mathrm{a}, \delta_\mathrm{e}, \delta_\mathrm{r}$.[3] By convention, a control deflection is positive if it leads to a mathematically-negative moment with respect to the x_f, y_f, and z_f-axis, respectively.

2.4.2 Nonlinear aircraft dynamics

The nonlinear equations of motion in this thesis are derived from Newtonian laws taking the aircraft for a rigid body and a point mass. During flight, we consider the following three types of forces and moments: *aerodynamic* force $\mathbf{R}^\mathrm{A}$ and moment $\mathbf{Q}^\mathrm{A}$ due to the aircraft's motion relative to the air; *weight* force $\mathbf{R}^\mathrm{G}$ due to the earth's gravity; and *thrust* force $\mathbf{R}^\mathrm{F}$ and torque $\mathbf{Q}^\mathrm{F}$ due to the propulsion. The total of forces lead to change in the aircraft's velocity vector $\mathbf{V}_\mathrm{Af}$, in body axis obtained as

$$\dot{\mathbf{V}}_\mathrm{Af} = \frac{1}{m}\left(\mathbf{R}^\mathrm{A}_\mathrm{f} + \mathbf{R}^\mathrm{G}_\mathrm{f} + \mathbf{R}^\mathrm{F}_\mathrm{f}\right) + \boldsymbol{\omega}_\mathrm{f} \times \mathbf{V}_\mathrm{Af}, \tag{2.3}$$

[3] Or $\delta_\mathrm{l}, \delta_\mathrm{m}, \delta_\mathrm{n}$ according to ISO 1151-1.

where $\boldsymbol{\omega}_\mathrm{f}$ is the vector of body rates and m is the mass of the aircraft. Likewise, the angular velocity is subject to the moments and

$$\dot{\boldsymbol{\omega}}_\mathrm{f} = \mathbf{I}^{-1}\left(\mathbf{Q}_\mathrm{f}^\mathrm{A} + \mathbf{Q}_\mathrm{f}^\mathrm{F} - \boldsymbol{\omega}_\mathrm{f} \times \mathbf{I}\boldsymbol{\omega}_\mathrm{f}\right), \tag{2.4}$$

where $\mathbf{I}$ is the matrix of inertias with

$$\mathbf{I} = \begin{bmatrix} I_{xx} & 0 & -I_{xz} \\ 0 & I_{yy} & 0 \\ -I_{xz} & 0 & I_{zz} \end{bmatrix}$$

for a symmetric aircraft (that is, $I_{xy} = I_{yz} = 0$). Rotating the weight force into body axis, we have

$$\mathbf{R}_\mathrm{f}^\mathrm{G} = -g \begin{bmatrix} \sin\Theta \\ \sin\Phi\cos\Theta \\ \cos\Phi\sin\Theta \end{bmatrix}. \tag{2.5}$$

If we assume the engines (or propeller) to be aligned with the x_f-axis, symmetric to the x_f-y_f-plane, and shifted vertically from the centre of gravity by l_t, the induced thrust force and torque can be written as

$$\mathbf{R}_\mathrm{f}^\mathrm{F} = \begin{bmatrix} F \\ 0 \\ 0 \end{bmatrix}, \qquad \mathbf{Q}_\mathrm{f}^\mathrm{F} = \begin{bmatrix} 0 \\ l_\mathrm{t} F \\ 0 \end{bmatrix}, \tag{2.6}$$

where F is the (undirected) thrust. We further obtain the aerodynamic forces and moments as

$$\mathbf{R}_\mathrm{f}^\mathrm{A} = \frac{1}{2}\varrho S V_\mathrm{A}^2 \begin{bmatrix} C_\mathrm{X} \\ C_\mathrm{Y} \\ C_\mathrm{Z} \end{bmatrix}, \qquad \mathbf{Q}_\mathrm{f}^\mathrm{A} = \frac{1}{2}\varrho S V_\mathrm{A}^2 \begin{bmatrix} b\,C_\mathrm{l} \\ c_\mathrm{A} C_\mathrm{m} \\ b\,C_\mathrm{n} \end{bmatrix}, \tag{2.7}$$

where ϱ denotes air pressure, S the wing area, b the wing-span, c_A the mean chord, and $V_\mathrm{A} = \|\mathbf{V}_\mathrm{Af}\|$ is the airspeed.[4] The dimensionless aerodynamic coefficients $C_\mathrm{X}, C_\mathrm{Y}, C_\mathrm{Z}, C_\mathrm{l}$, $C_\mathrm{m}, C_\mathrm{n}$ in body axis are functions of angle of attack, side-slip angle, surface deflections, and body rates. For the latter, the normalised rates $\hat{\boldsymbol{\omega}}_\mathrm{f}$ are commonly used:

$$\hat{\boldsymbol{\omega}}_\mathrm{f} = \frac{1}{2V_\mathrm{A}} \begin{bmatrix} b & & \\ & c_\mathrm{A} & \\ & & b \end{bmatrix} \boldsymbol{\omega}_\mathrm{f}. \tag{2.8}$$

Finally, the body rates are converted into the nonorthogonal change of attitude

$$\begin{bmatrix} \dot{\Phi} \\ \dot{\Theta} \\ \dot{\Psi} \end{bmatrix} = \begin{bmatrix} 1 & \sin\Phi\tan\Theta & \cos\Phi\tan\Theta \\ 0 & \cos\Phi & \sin\Phi \\ 0 & \sin\Phi\sec\Theta & \cos\Phi\sec\Theta \end{bmatrix} \boldsymbol{\omega}_\mathrm{f}. \tag{2.9}$$

[4] Throughout the thesis, we use "velocity" for the vector value and "speed" for its norm.

We use the following notation for the vectors and their components:

$$\mathbf{V} = \begin{bmatrix} u \\ v \\ w \end{bmatrix}; \quad \boldsymbol{\omega} = \begin{bmatrix} p \\ q \\ r \end{bmatrix}; \quad \mathbf{R} = \begin{bmatrix} X \\ Y \\ Z \end{bmatrix}; \quad \mathbf{Q} = \begin{bmatrix} L \\ M \\ N \end{bmatrix}; \tag{2.10}$$

in accordance with ISO 1151-1.

For the aircraft's state vector, we choose the nine parameters

$$\mathbf{x}^T = \left[\begin{array}{ccc|ccc|ccc} u_\mathrm{f} & v_\mathrm{f} & w_\mathrm{f} & p & q & r & \Phi & \Theta & \Psi \end{array} \right]. \tag{2.11}$$

Note that this choice excludes position of the aircraft from being a state, as these do not affect the derivatives above.[5] On the other hand, our choice is convenient for equilibrium ($\dot{\mathbf{x}} = 0$) and trim condition are equivalent here. The azimuth, too, has no effect on the aircraft's equations of motion and can hence be dropped. However, we might want to impose the additional constraint

$$\dot{\Psi} = 0 \tag{2.12}$$

for level flight or

$$\dot{\Psi} = \dot{\chi}_\mathrm{A} \tag{2.13}$$

for a coordinated turn (see Cunis, Condomines, and Burlion 2017, pp. 109 and 111, for details). The change of position now constitutes an output of the system aircraft dynamics, namely

$$\dot{\mathbf{x}}_\mathrm{g} = \mathbf{M}_\mathrm{gf}(\Phi, \Theta, \Psi)\, \mathbf{V}_\mathrm{f}, \tag{2.14}$$

where $\mathbf{M}_\mathrm{gf}$ denotes the Euler rotation matrix from body into earth axis system under the aforementioned sequence.

We also consider the longitudinal dynamics only, assuming level flight and zero side-slip ($\Phi = \beta = 0$). In this case, the equations of motion are reduced to

$$\dot{V}_\mathrm{A} = \frac{1}{m}\left(F\cos\alpha - \frac{1}{2}\varrho S V_\mathrm{A}^2 C_\mathrm{D} - mg\sin\gamma_\mathrm{A} \right), \tag{2.15}$$

$$\dot{\gamma}_\mathrm{A} = \frac{1}{mV_\mathrm{A}}\left(F\sin\alpha + \frac{1}{2}\varrho S V_\mathrm{A}^2 C_\mathrm{L} - mg\cos\gamma_\mathrm{A} \right), \tag{2.16}$$

$$\dot{q} = \frac{1}{I_{yy}}\frac{1}{2}\varrho S c_\mathrm{A} V_\mathrm{A}^2 C_\mathrm{m}, \tag{2.17}$$

$$\dot{\Theta} = q, \tag{2.18}$$

and $\Theta = \alpha + \gamma_\mathrm{A}$. Here, the aerodynamic lift and drag coefficients $C_\mathrm{L}, C_\mathrm{D}$ are obtained from C_X and C_Z by rotation into the air-path axis system:

$$\begin{bmatrix} C_\mathrm{L} \\ C_\mathrm{D} \end{bmatrix} = \begin{bmatrix} +\sin\alpha & -\cos\alpha \\ -\cos\alpha & -\sin\alpha \end{bmatrix} \begin{bmatrix} C_\mathrm{X} \\ C_\mathrm{Z} \end{bmatrix} \tag{2.19}$$

with $Y_\mathrm{f} = L_\mathrm{f} = N_\mathrm{f} = 0$.

[5] However, simulations such as the GTM implement an atmospheric model based on the altitude.

2.4.3 Aircraft

We are going to model, analyse, and finally control the upset dynamics of two different aircraft in the course of this dissertation. The first is the already introduced *Generic Transport Model*, the result of a cooperation between Boeing and NASA in order to improve studies of upset dynamics, and sujet d'étude of numerous research papers. The second is a further fixed-wing unmanned aircraft called "Cumulus One" which is developed by a Danish start-up and that has initially been studied through a cooperation with the University of Aalborg (cf. Cunis, Leth, et al. 2018). Fig. 2.4 illustrates the two aircraft; Tab. 2.1 compares their main parameters. Unlike the GTM whose asymmetry at stall prompts a roll departure into a spiral or oscillatory spin, Cumulus One has been designed to descend in a stable deep-stall trim condition; thus, we are able to isolate and investigate separately its longitudinal dynamics.

Table 2.1: Parameters of the Generic Transport Model and Cumulus One.

		GTM	Cumulus	unit
flight mass	m	26.19	1.55	kg
wing span	b	2.09	1.66	m
mean chord	c_A	0.28	0.174	m
wing area	S	0.55	0.277	m^2
engine displacement	l_t	0.10	–	m
air density	ϱ	1.20	1.25	kg/m
gravitational constant	g	9.806 65		$\mathrm{m/s}^2$

Generic Transport Model

Widely recognised, the different instances of the GTM (Fig. 2.5) have facilitated research and comparison of upset recovery in the last years. Equipped with twin engines, the GTM is supposed to resemble a common passenger airliner in a scale of 5.5:100. Its high-fidelity simulation is openly available as MATLAB/Simulink model (NASA 2016) and gives access to a wide range of aerodynamic data. Although based on Newtonian dynamics too, the simulation goes well beyond the nonlinear equations of motion of the previous section; its many (optional) details include segmented control surfaces as well as flaps, stabilisers, and landing gear, actuator dynamics, aerodynamic coupling, shifting of the centre of gravity through fuel consumption, telecommunication delay and noise, as well as an atmospheric model. Damage cases are provided, too.

For the shifting of the centre of gravity, the aerodynamics coefficients are determined with respect to a reference $\mathbf{x}_\mathrm{cg}^\mathrm{ref}$ (in the body axis system); displacement of the centre of gravity then induces the additional torque

$$\mathbf{Q}_\mathrm{f}^\mathrm{cg} = \mathbf{R}_\mathrm{f}^\mathrm{A} \times \left(\mathbf{x}_\mathrm{cg}(t) - \mathbf{x}_\mathrm{cg}^\mathrm{ref} \right), \tag{2.20}$$

where $\mathbf{x}_\mathrm{cg}(t)$ is the position of the centre of gravity at time t with $\mathbf{x}_\mathrm{cg}(0) = \mathbf{x}_\mathrm{cg0} \neq \mathbf{x}_\mathrm{cg}^\mathrm{ref}$. In the following, we assume the centre of gravity to be fixed to $\mathbf{x}_\mathrm{cg}(\cdot) \equiv \mathbf{x}_\mathrm{cg0}$, referred

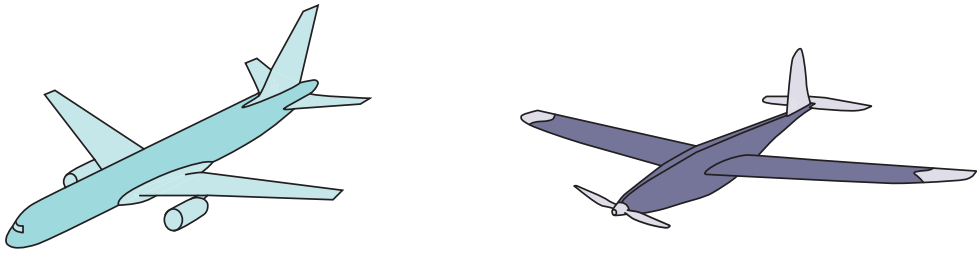

(a) Generic Transport Model. (b) Cumulus One.

Figure 2.4: Illustrations of aircraft studied in the thesis. *Commissioned illustrations.*

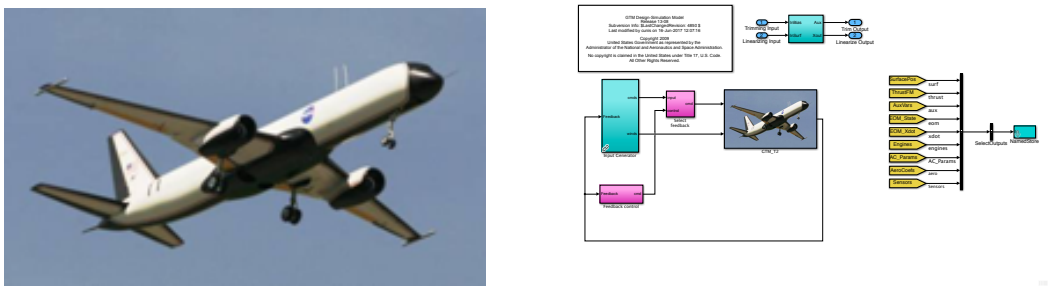

(a) AirSTAR vehicle. (b) MATLAB/Simulink model.

Figure 2.5: Real-world and digital instances of the *Generic Transport Model*.

(a) Configuration in flight. (b) Disassembled for transport.

Figure 2.6: *Cumulus One* during and between flights.

to simply as "$\mathbf{x}_{\text{cg}}$". We further consider the thrust force F to be equally distributed onto the engines and simultaneous deflections of the segments of ailerons, elevator, and rudder, respectively denoted by ξ, η, ζ.

The GTM is taken into account in Chapters 3, 5, and 8.

Cumulus One

The Danish company Sky-Watch has been developing, manufacturing, and distributing *Cumulus One* as an autonomous aircraft for agricultural mapping, surveillance, and reconnaissance. Cumulus One (Fig. 2.6) is equipped with a singe propeller located at the nose, a full-surface elevator, ailerons, and rudder. For weight reduction, there is no landing gear but the aircraft is designed to deliberately enter and descent in a deep-stall trim condition (*deep-stall landing*, cf. Cunis, Leth, et al. 2018, p. 532). Therefore, its elevator has an extended range, down to $-60°$, the rotor blades fold back when idle, and shock-absorbing foam at the belly dampens the vehicle upon impact. The wings are further placed with an upward inclination in order to enhance lateral stability.

We initially discuss the model of Cumulus One in Chapter 4 and subsequently use its longitudinal dynamics in Chapters 6 and 7.

Photograph of *Cumulus One* in deep-stall flight (Courtesy Sky-Watch A/S).

2.5 Remarks

In order to address the challenges of upset recovery and the need of combined system theoretical and aeronautical engineering, the two parts of this dissertation focus on systems theory for analysis and control, respectively, of aircraft dynamics in general, and unmanned or autonomous aircraft in particular, subject to upset conditions. Partially, the tools we will employ are rooted in bespoken upset recovery approaches; yet, we have identified and will address shortcomings of the methodologies prior for a wholesome foundation of upset recovery in theory and practice. Doing so, we will introduce the reader to further domains of aeronautical analysis and control as well as control and system theory. Each part is therefore preceded by an introduction into aeronautical applications as well as background chapters on the underlying theory. Due to the variety and ongoing research of the covered domains, however, a full literature survey exceeds the possibilities of the dissertation.

Part I

Modeling & Analysis

Modeling & Analysis

Analysis of aircraft dynamics in upset conditions provides valuable insight for upset prevention and recovery, as well as serves as entry point for control verification. Yet, confidence into an analysis result depends on the accuracy of the analysed model. Modeling the dynamics of an upset vehicle is, however, a challenging task due to the variety and nonlinearity of upset conditions.

Modeling Techniques Modeling of aircraft dynamics is commonly reduced to identification and representation of the aerodynamic coefficients in several aerodynamic conditions and surface deflections. However, one might consider further subsystems such as the actuator and engines, shifting of the centre of gravity, or flexible modes. For identification, the aircraft is often subjected to extensive wind-tunnel measurements (as for the GTM, Foster et al. 2005), flight tests (e.g., Rao et al. 2012), or, nowadays, simulations of continuous fluid dynamics (see Kuzmin 2010, for an overview). Once the aerodynamic coefficients have been measured, various methods for representation are applied depending on complexity and purpose of the model. High-fidelity simulation often rely on look-up tables and advanced techniques (Frink et al. 2017, p. 796) such as fuzzy logic (Brandon and Morelli 2016, pp. 1271–1275). Other approaches rely on neural networks (Linse and Stengel 1993, p. 1022) for identification from flight test data.

An alternative approach was demonstrated by Selig (2010), who computed a full-envelope aerodynamic model for small acrobatic airplane (ca 80 cm up to 2.5 m) by modeling component-wise lift and drag of wings, tail, fuselage, and propeller.

System theoretic approaches, on the other hand, have more specific needs for algebraic models; while bifurcation analysis has been applied to a variety of models, some techniques assume either linear dynamics (μ-analysis), polynomial-based models (sum of squares), or at least smooth derivatives (e.g., optimal control). Here, polynomial spline functions can provide continuous models of desired accuracy and smoothness (Klein and Morelli 2006, p. 54). De Visser et al. (2010) reported a fitting method for multi-variate splines, which was later extended to accommodate for aerodynamic uncertainties (Tol et al. 2016).

Analysis Methods For the purpose of certification, aircraft models are subjected to extensive Monte-Carlo simulations of the high-fidelity models. Advanced linear analysis techniques, which handle nonlinearities as uncertainties, are often applied supplementary in the neighbourhoods of nominal trim conditions (Marcos et al. 2007, p. 69). For the analysis of highly nonlinear upset dynamics, however, we focus on techniques that explicitly take into account nonlinearities.

Continuation and bifurcation analysis has been developed from mathematical theory into a state-of-the-art analysis tool for trim conditions and periodical orbits in the nonlinear aircraft dynamics. As one of the first papers applying continuation and bifurcation analysis to nonlinear aircraft dynamics, in particular for high angles-of-attack,

Caroll and Mehra (1982) focused on spin dynamics and recovery. Jahnke (1990) further analysed the nonlinear dynamics of both a generic fighter jet and the F-14 aircraft, applying a continuation method and bifurcation theory to determine equilibria and their stability for varying deflections of the control surfaces. Goman et al. (1997) reviewed bifurcation analysis of nonlinear flight dynamics including stall, deep-stall, roll-coupling, and oscillatory spins. Bifurcation analysis was applied in several recent publications that considered upset dynamics and recovery (e.g., Engelbrecht et al. 2013; Gill et al. 2013; Kwatny et al. 2013).

Recent improvements in semidefinite programming lead to the development and application of polynomial sum-of-squares techniques. Chakraborty et al. (2011a) employed sum-of-squares to estimate the region of attraction for the longitudinal motion of the GTM using polynomial models of the aerodynamic coefficients. The authors further exercised the same approach for nonlinear analysis of the F/A-18's falling-leaf mode (Chakraborty et al. 2011c). Anderson and Papachristodoulou (2012), too, computed the region of attraction as well as various robust stability and performance indicators using sum-of-squares for the longitudinal motion of the F/A-18.

Part Outline This part studies on nonlinear modeling and analysis of upset dynamics. It is organised as follows: The first of two initial technical background chapters introduces the reader to the theory of stability of nonlinear, switching, and hybrid systems including LaSalle's theory of invariant sets, which serves as foundation for the estimation of regions of attraction. The second background chapters gives details on the concepts and implementation of sum-of-squares programming and further proposes a new formulation that highlights the set-theoretic aspects. Chapter 3 then introduces the author's piecewise polynomial modeling technique as a simplified spline approach and illustrates the application of bifurcation and sum-of-squares analysis to piecewise systems. Chapter 4 further applies bifurcation theory in order to analyse and model the dynamics of Cumulus One during transition into deep-stall. Chapter 5, as interim conclusion, provides an improved algorithm that will allow to extend the results of this part to elaborate spline-based models.

Stability Concepts

The theory of system analysis, or system theory, divides the field of study into a multitude of classes of systems. Always keen to abstract and refine in order to isolate and study certain phenomena, we are aware of system definitions from general but complex to simple and specific. Fig. I.1 recalls some of these classes and their hierarchy, yet without claim of completeness. At the very bottom of the generalisation tree, linear systems benefit from a single equilibrium at the origin, which is either globally attractive or not at all, and an explicit solution (Åström and Murray 2008, pp. 132, 136–137, and 141), however they seldom provide an exact description of physical systems (Robert H. Cannon, cited in Åström and Murray 2008, p. 131) even though they are often "good enough" approximations for analysis and control design in a small neighbourhood of the equilibrium. Systems that are not linear may be characterised by multiple equilibria with local stability only, exhibit periodic solutions that are approached one side or the other, both sides, or none, and even display chaotic behaviour (Slotine and Li 1991, pp. 7–12). Classical approaches therefore apply the term *nonlinear system* often to anything that is just not linear, including systems of higher polynomial order, with saturations or exhibiting hystereses (Abel 2013, pp. 379 & 380).

As we are not going to further consider linear systems, although we will now and then retreat to linear control synthesis derived from a local linearisation, it is worth distinguishing the different kinds of nonlinear systems. *Describing functions* separate linear and nonlinear elements (Slotine and Li 1991, p. 162) and thus provide a constructive method to apply classical analysis methods to system with various nonlinear elements (Abel 2013, pp. 396–401). For the purpose of our study of aircraft dynamics however, describing functions are too vague—and at the same time, only applicable to restricted nonlinearities (Slotine and Li 1991, p. 164). On the other hand, polynomial and rational polynomial systems can represent most continuous functions, approximating irrational elements by polynomial Taylor expansion. Moreover, a piecewise definition can reduce the complexity of each subfunction without loss of overall accuracy (compare spline regression; Klein and Morelli 2006, pp. 437 & 438). Piecewise definitions are also suitable to represent saturations and other simple, nondifferentiable nonlinearities, and all together yield the class of *switching systems*, i.e., the system dynamics "switches" along well-defined surfaces. Complicated nonlinearities such as hysteresis, however, are only modeled by *hybrid systems*, where the switching of inner dynamics is more arbitrary.

In the following, we study dynamics and stability of continuous nonlinear systems, having in mind the equations of motion of our aircrafts, which we will at some points approximate by polynomial functions.

We start with trajectories as the fundamental principle of systems theory. Simply speaking, system analysis studies the behaviour of trajectories of a system, just as control theory provides techniques of trajectory manipulation. Subsequently, we encounter special types of trajectories and learn about different mathematical characterisations for stability. Introducing continuation, we see our systems change and bifurcate; in other

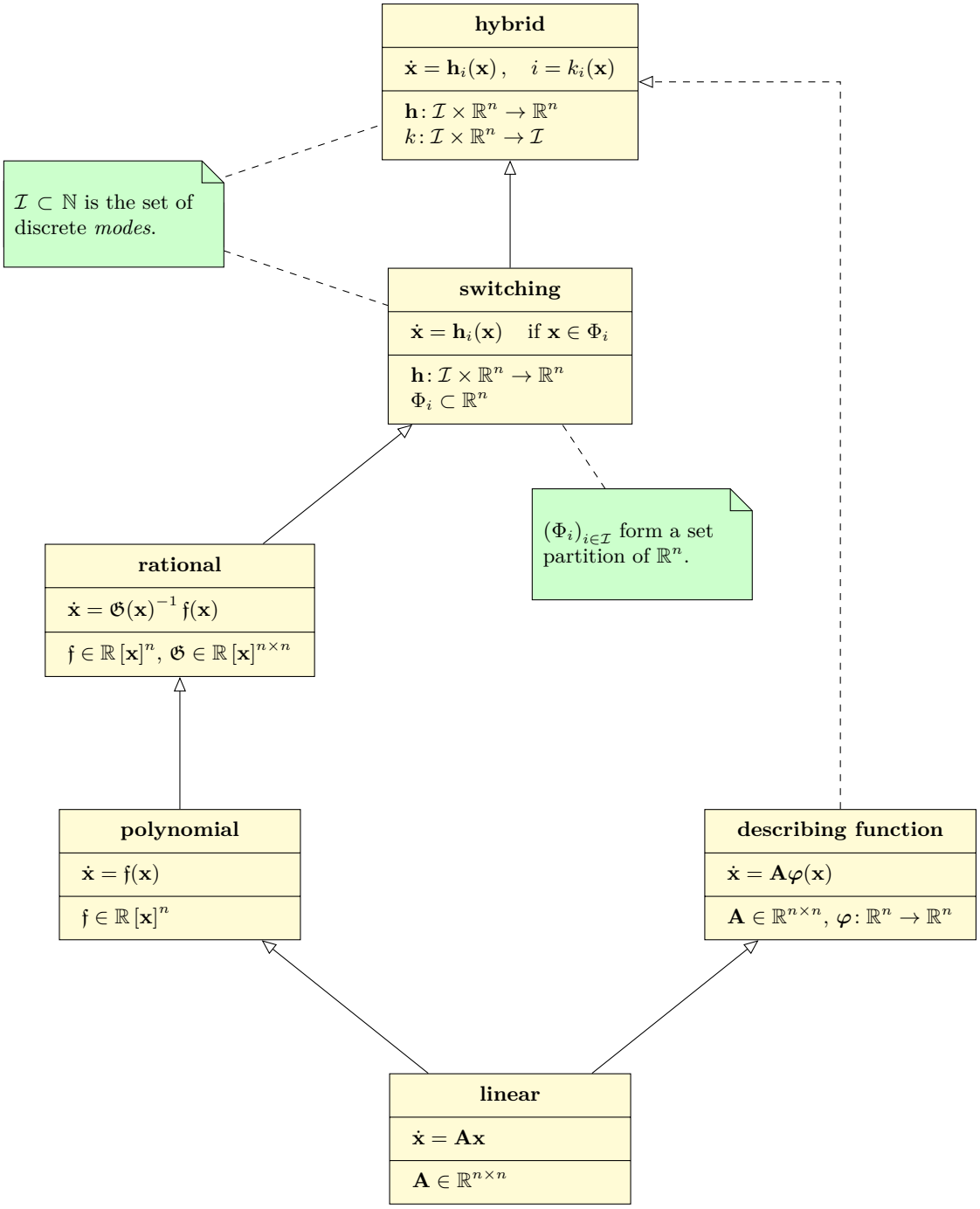

Figure I.1: Overview of linear and nonlinear system classes and their relationship (non-exhaustive).

words, we enter a world of higher dimension, similar to spacetime that has our stars born and collapsed. The final definition of attractive and invariant sets elevates our study of single trajectories to sub-spaces and quantitative rather than qualitative assessments.

Trajectories

A trajectory in the sense of system and control theory is a parametrised curve into the n-dimensional state-space,

$$\mathbf{x}\colon \mathbb{R} \longrightarrow \mathcal{X}, \tag{I.1}$$

where $\mathcal{X} \subseteq \mathbb{R}^n$, which solves the nonlinear differential equation

$$\dot{\mathbf{x}}(t) = \mathbf{f}(t, \mathbf{x}(t)) \tag{I.2}$$

with $\mathbf{f}\colon \mathbb{R} \times \mathcal{X} \to \mathbb{R}^n$. The function $\mathbf{f}$ is simply called "the system". For deterministic systems, we have that if $\mathbf{x}_1(t_0) = \mathbf{x}_2(t_0)$ for trajectories $\mathbf{x}_1, \mathbf{x}_2$ and $t_0 \geq 0$, then $\mathbf{x}_1(t) = \mathbf{x}_2(t)$ for all $t \geq t_0$—that is, two trajectories never cross. Systems that do not depend on the time directly, $\dot{\mathbf{x}} = \mathbf{f}(\mathbf{x}(t))$, are called *autonomous* or *time-invariant*. Here, the trajectories of $\mathbf{f}$ effectively form equivalence classes:

$$[\mathbf{x}(\cdot)] =_{\text{def}} \left\{ \mathbf{x}'\colon \mathbb{R} \to \mathcal{X} \,\middle|\, \exists t_0 \in \mathbb{R}\, \forall t \in \mathbb{R}. \quad \mathbf{x}'(t) = \mathbf{x}(t_0 + t) \right\}. \tag{I.3}$$

For most parts of this thesis, we consider autonomous systems. Due to determinism and autonomy, a trajectory $\mathbf{x}(\cdot)$ is sufficiently described by $\mathbf{f}$ and a starting point $\mathbf{x}_0 \in \mathcal{X}$ such that $\mathbf{x}(t_0) = \mathbf{x}_0$ for an arbitrary $t_0 \in \mathbb{R}$. If $\mathbf{f}$ is Lipschitz-continuous,[6] the solution $\mathbf{x}(\cdot)$ to the thus defined initial value problem exists and is unique (Åström and Murray 2008, pp. 97 & 98); we then say "$\mathbf{x}(\cdot)$ starts in $\mathbf{x}_0$ for t_0" and denote the *flow* of the system by $\boldsymbol{\phi}(\mathbf{x}_0, t) = \mathbf{x}(t_0 + t)$. The systems of this thesis are tacitly understood to be (locally) Lipschitz.

Ordinary differential equations

Both time-variant and invariant systems are described by *ordinary differential equations* (ODEs), that is, we consider only derivatives by time. ODEs are hardly the only type of differential equations studied in systems theory; other, such as partial differential equations with derivatives in multiple variables, give rise to systems such as the heat equation or multidimensional oscillations (e.g., Yu 2003, pp. 109–110), but are not relevant in the scope of rigid aircraft dynamics.[7] We therefore limit our study to ordinary differential equations, which are sufficiently multifaceted.

⁂

[6] Or simply "Lipschitz," namely, there is a constant $\kappa \in \mathbb{R}$ such that $\|\mathbf{f}(\mathbf{x}_1) - \mathbf{f}(\mathbf{x}_2)\|_2 \leq \kappa \|\mathbf{x}_1 - \mathbf{x}_2\|_2$ for all $\mathbf{x}_1, \mathbf{x}_2 \in \mathcal{X}$ (Åström and Murray 2008, p. 98).

[7] Notwithstanding propulsion, of course. Analysis of *flexible* aircraft is indeed based on partial differential equations.

I.1 Equilibria, Stability, and Limit Cycles

Of the numerous possible trajectories of a system, two types of solutions are noteworthy:

Stationary solutions A trajectory $\mathbf{x}^*(\cdot) = const.$ is a *stationary solution* if and only if $\mathbf{f}(\mathbf{x}^*(\cdot)) = 0$. From an interpretation of $\mathbf{f}$ as sum of multiple forces, stationary solutions are usually called "equilibria," as the forces are balanced in this point. In the aeronautical context, the term *trim condition* is common, too. We will frequently use $\mathbf{x}^*$ for both the trajectory and its stationary value.

Periodic solutions A solution $\mathbf{x}^\dagger(\cdot)$ for $\mathbf{f}$ is *periodic* if and only if there is a constant $\tau \in \mathbb{R}$ such that $\mathbf{x}^\dagger(t) = \mathbf{x}^\dagger(\tau + t)$ for all $t \in \mathbb{R}$. By determinism, we also have $\mathbf{x}^\dagger(t) = \mathbf{x}^\dagger(k\tau + t)$ for any $k \in \mathbb{Z}$, and τ is called the *period* of $\mathbf{x}^\dagger(\cdot)$.

Both stationary and periodic solutions can be *stable* in the intuitive sense that, despite a (small) variation from the original trajectory, the system does not deviate. While there are several mathematical characterisations for stability, we will only consider *Lyapunov stability* and *asymptotic stability* here, as they are also important to understand the later concepts of this chapter. A common third characterisation, *exponential stability* (cf. Slotine and Li 1991, p. 51) is not further considered. While we define both kinds of stability in terms of stationary solutions, a similar definition can be given for trajectories.

Definition I.2. A stationary solution $\mathbf{x}^*$ of the system $\mathbf{f}$ is *stable in the sense of Lyapunov* if and only if for every $\epsilon \in \mathbb{R}_+$ there is a $\delta \in \mathbb{R}_+$ such that for any $\mathbf{x}_0 \in \mathcal{X}$ with $\|\mathbf{x}_0 - \mathbf{x}^*\|_2 < \delta$ holds: if $\mathbf{x}(\cdot)$ is the trajectory starting in $\mathbf{x}_0$ for some $t_0 \in \mathbb{R}$, then $\|\mathbf{x}(t_0 + t) - \mathbf{x}^*\|_2 < \epsilon$ for all $t \geq 0$.

Stability in the sense of Lyapunov,[8] or simply Lyapunov-stability, provides the weaker characterisation for mathematical stability, since any trajectory that is close "enough" to an equilibrium is only required to *stay* sufficiently close for all times, but no further assumptions on the steady-state behaviour of the trajectories are taken. This is done by the second and stronger form of our stability characterisations.

Definition I.3. A stationary solution $\mathbf{x}^*$ of the system $\mathbf{f}$ is *asymptotically stable* if and only if it is Lyapunov stable *and* there is a $\delta \in \mathbb{R}_+$ such that for any $\mathbf{x}_0 \in \mathcal{X}$ with $\|\mathbf{x}_0 - \mathbf{x}^*\|_2 \leq \delta$ holds: a trajectory $\mathbf{x}(\cdot)$ starting in $\mathbf{x}_0$ for some $t_0 \in \mathbb{R}$ converges towards $\mathbf{x}^*$ for time ad infinitum, i.e., there exists a function $\beta \in \mathcal{KL}$ such that $\|\mathbf{x}(t_0 + t) - \mathbf{x}^*\|_2 \leq \beta(|\mathbf{x} - \mathbf{x}^*|, t)$ for all $\mathbf{x} \in \mathcal{X}$ and $t \geq 0$.

A solution that is asymptotically stable is, by definition, also Lyapunov stable. A stationary solution that is neither asymptotically nor Lyapunov-stable is *unstable*. A periodic solution that is asymptotically stable is called *limit cycle*; otherwise, it can still be approached by trajectories from either within or without, or none (Slotine and Li 1991, p. 35).

[8] Notwithstanding, Lyapunov's renown *theorem of stability* (see I.1.1) provides a condition for *asymptotic* stability.

Asymptotic stability is defined in terms of a non-singular unitary ball of radius δ around the stationary solution as $\delta > 0$. Indeed, it is easy to see that for $\delta = 0$, the requirements in Definition I.3 would hold trivially for any stationary solution. If, on the other hand, asymptotic stability is given for *any* $\delta > 0$, then $\mathbf{x}^*$ is called *globally* asymptotically stable; otherwise, *locally* (—) stable.

Stability of non-stationary trajectories

We result in equivalent definitions of stability for a non-stationary solution $\mathbf{x}'(\cdot)$ of $\mathbf{f}$ if we consider the reformulated non-autonomous system $\mathbf{f}'(t, \mathbf{e}(t))$ with

$$\begin{aligned} \mathbf{e}(t) &= \quad \mathbf{x}(t) \quad - \mathbf{x}'(t) \\ \dot{\mathbf{e}}(t) &= \mathbf{f}(\mathbf{e}(t) + \mathbf{x}'(t)) - \mathbf{f}(\mathbf{x}'(t)) \,. \end{aligned} \tag{I.4}$$

Then, $\mathbf{e}^*(\cdot) = 0$ is a stationary solution of $\mathbf{f}'$ and stability of $\mathbf{x}'(\cdot)$ can be defined in terms of $\mathbf{e}^*(\cdot)$ and $\mathbf{f}'$.

I.1.1 Criteria for local and global stability

Determining whether a given system is stable or not can be a dreary task. A simulation of several trajectories might give an indication, but would never be exhaustive and is computationally difficult for systems with numerous states. While extensive Markov simulations are in fact applied for certification of safety-critical systems such as passenger aircraft (Philippe 2011), we rather consider mathematical tools for stability:

Local stability: linearization theory

In order to proof local stability, we have to look into the vicinity of a stationary solution. From Taylor expansion, we have (Abel 2013, p. 17)

$$\frac{\mathrm{d}}{\mathrm{d}t}(\mathbf{x}^* + \delta\mathbf{x}) = \mathbf{f}(\mathbf{x}^* + \delta\mathbf{x}) = \mathbf{f}(\mathbf{x}^*) + \frac{\partial \mathbf{f}}{\partial \mathbf{x}}(\mathbf{x}^*)\,\delta\mathbf{x} + \sum_{i,j} \frac{\partial^2 \mathbf{f}}{\partial x_i\,\partial x_j}(\mathbf{x}^*)\,\delta x_i\,\delta x_j + \cdots \tag{I.5}$$

and with $\mathbf{f}(\mathbf{x}^*) = 0$,

$$\lim_{\|\delta\mathbf{x}\|_2 \to 0} \frac{\mathrm{d}}{\mathrm{d}t}\delta\mathbf{x} = \left.\frac{\partial \mathbf{f}}{\partial \mathbf{x}}\right|_{\mathbf{x}^*} \delta\mathbf{x} \tag{I.6}$$

if $\frac{\partial \mathbf{f}}{\partial \mathbf{x}}(\mathbf{x}^*) \neq 0$. The matrix $\mathbf{J}^* = \frac{\partial \mathbf{f}}{\partial \mathbf{x}}(\mathbf{x}^*)$ is called the *Jacobian matrix* of $\mathbf{x}^*$ and Eq. (I.6) is the *linearised system* for $\mathbf{f}$ (*around* $\mathbf{x}^*$), where $\mathbf{J}^*$ replaces the state matrix of a linear system. That is, a nonlinear system $\mathbf{f}$ behaves like its linearised variant in a sufficiently close to the stationary solution. As "sufficiently close" has been all that it took for stability, the linearised dynamics tell us about the stability of the nonlinear system.

↬

Without further study of linear systems' dynamics—which is beyond the purpose of this chapter—we can therefore conclude in a theorem for local stability.

Theorem I.4 (Åström and Murray 2008, p. 108)**.** *Let* $\mathbf{x}^*$ *be a stationary solution of* $\mathbf{f}$ *and* $\mathbf{J}^*$ *the Jacobian matrix of* $\mathbf{x}^*$*; if* $\mathbf{J}^* \neq 0$*, the following hold:*

1. $\mathbf{x}^*$ *is asymptotically stable if each eigenvalue of* $\mathbf{J}^*$ *has strictly negative real part;*
2. $\mathbf{x}^*$ *is unstable if any eigenvalue of* $\mathbf{J}^*$ *has strictly positive real part.*

◁

In Theorem I.4, the criterion for local asymptotic stability is also a sufficient condition for Lyapunov stability, just as Lyapunov stability is necessary for asymptotic stability.

Example I.1. Consider a nonlinear low-pass filter with exponential damping governed by the second-order differential equation

$$\ddot{\xi} = -\xi + 2\mu e^{\xi}\dot{\xi}, \tag{I.7}$$

where $\mu \in \mathbb{R}$ is some parameter. Introducing $x_1 =_{\text{def}} \xi$, $x_2 =_{\text{def}} \dot{\xi}$, we can write (I.7) equivalently as $\dot{\mathbf{x}} = \mathbf{f}(\mathbf{x})$ and the Jacobian matrix has the eigenvalues $\mu \pm \sqrt{\mu^2 - 1}$. Applying Theorem I.4, we learn that our nonlinear filter is asymptotically stable for $\mu < 0$, Lyapunov stable for $\mu \leq 0$, and unstable for $\mu > 0$. Directly solving (I.7) for $\mu = 0$, we further encounter infinitely-many periodic solutions $\xi \colon t \mapsto \zeta \cos t$ with $\zeta \in \mathbb{R}$; this is sometimes called a *meta-stable* mode.

Note that zero eigenvalues are not sufficient for Lyapunov stability; indeed, the system of $\dot{\xi} = \mu\xi^3$ is unstable if $\mu > 0$ but its eigenvalue will always be zero. That is, if $\mathbf{J}^*$ has zero eigenvalues, we cannot tell of the local behaviour from the linearised system but have to take into account the terms of higher order.

Global stability: Lyapunov function theory

Lyapunov's extensive work on the dynamics of nonlinear systems provides exact results for local and global stability without the need of linearisation. Inspired by a system's total energy, the idea behind Lyapunov's theorem is that a scalar field $\mathcal{V}(\cdot)$ decreases along each trajectory towards a global minimum in the stable equilibrium. For a trajectory $\mathbf{x}(\cdot)$, we then have $\mathcal{V}_{\mathbf{x}}(t) = \mathcal{V}(\mathbf{x}(t))$ and $\dot{\mathcal{V}}_{\mathbf{x}} = \nabla\mathcal{V} \cdot \dot{\mathbf{x}}$.

Definition I.5. A function $\mathcal{V} \colon \mathbb{R}^n \to \mathbb{R}_{\geq 0}$ is a *Lyapunov candidate-function* if and only if there exist functions $\alpha_1, \alpha_2 \in \mathcal{K}_\infty$ such that

$$\alpha_1(|\mathbf{x}|) \leq \mathcal{V}(\mathbf{x}) \leq \alpha_2(|\mathbf{x}|) \tag{I.8}$$

for all $\mathbf{x} \in \mathbb{R}^n$.

We revisit the criterion for global stability here; results for local stability will be discussed in I.3 when we are looking closer into the determination of attractive and invariant sets. The renown theorem has originally been formulated by Alexandr Lyapunov in his 1892 doctoral[9] thesis (Parks 1992, pp. 277, 280) but today can be found, in similar form and under different names, in most textbooks on nonlinear analysis and control (cf. Slotine and Li 1991, p. 59; Abel 2013, p. 409; Åström and Murray 2008, pp. 111–112).

[9]The Russian degree of a *Doktor Nauk* ("Doctor of Sciences") is considered a higher doctorate.

Theorem I.6 (Lyapunov's stability theorem)**.** *Let* $\mathbf{x}^*$ *be a stationary solution of* $\mathbf{f}$ *and* $\mathcal{V}(\cdot)$ *a Lyapunov candidate-function; if there exist a function* $\rho\colon \mathbb{R}_{\geq 0} \to \mathbb{R}_{\geq 0}$ *continuous, positive definite such that*

$$\nabla\mathcal{V}(\mathbf{x}-\mathbf{x}^*)\,\mathbf{f}(\mathbf{x}) \leq -\rho(|\mathbf{x}-\mathbf{x}^*|) \tag{I.9}$$

for all $\mathbf{x} \in \mathcal{X}$*, then* $\mathbf{x}^*$ *is globally asymptotically stable.* $\lhd$

For simplicity, the stationary solution of interest is often assumed without loss of generality to be located in the origin, i.e., $\mathbf{x}^* = 0$. If the condition in Theorem I.6 holds, $\mathcal{V}(\cdot)$ is called a *Lyapunov function* for $\mathbf{f}$ and $\mathbf{x}^*$.

The stability criterion using Lyapunov's theorem is straight-forward, yet a Lyapunov function for a given system may not be unique and it is thus often difficult to construct a suitable Lyapunov function that satisfies the condition in Theorem I.6 (Slotine and Li 1991, pp. 67 and 77). However, it can be proven that there exists a Lyapunov-function for an asymptotically stable equilibrium (Malisoff and Mazenc 2009, p. 28); in fact, different Lyapunov-functions may exist for a single stationary solution.

I.1.2 Stability of switching and hybrid systems

The analysis of systems which exhibit switching behaviour between distinguished, local dynamics is much more difficult and stability of the local dynamics does not necessarily imply stability of the switching dynamics. For example, it is well known that one can choose matrices $\mathbf{A}_1, \mathbf{A}_2 \in \mathbb{R}^{n\times n}$ and disjunct domains $\Phi_1, \Phi_2 \subset \mathbb{R}^n$ such that trajectories of the switching system

$$\dot{\mathbf{x}} = \begin{cases} \mathbf{A}_1\mathbf{x} & \text{if } \mathbf{x} \in \Phi_1 \\ \mathbf{A}_2\mathbf{x} & \text{if } \mathbf{x} \in \Phi_2 \end{cases}$$

diverge, even though both $\mathbf{A}_1$ and $\mathbf{A}_2$ have only strictly negative eigenvalues (De Schutter et al. 2009, p. 44). The study of stability, reachability, and related safety criteria for classes of switching or hybrid systems is subject of the *Theory of Hybrid Systems* (see, e.g., Grossman et al. 1993; Lunze and Lamnabhi-Lagarrigue 2009, for an overview).

$$\div$$

Indeed, if there is one function $\mathcal{V}(\cdot)$ for the switching system "$\dot{\mathbf{x}} = \mathbf{h}_i(\mathbf{x})$ if $\mathbf{x} \in \Phi_i$" with suitable $\mathbf{h}_i\colon \mathbb{R}^n \to \mathbb{R}^n$, $\Phi_i \subset \mathbb{R}^n$ such that the condition in Theorem I.6 is satisfied by $\mathcal{V}$ and for each local dynamic $\mathbf{h}_i$, then the switching dynamics are asymptotically stable, too. However, the existence of a single Lyapunov-function is not *necessary* for stability of the switching dynamics, even if one requires Eq. (I.9) to hold only within the respective Φ_i (Johansson and Rantzer 1998, pp. 555–556). In this case, stability may

still be provable using a piecewise defined Lyapunov function. We summarise the results of this section in the following theorem.[10]

Theorem I.7. *Let a switching system be defined by the local dynamics* $\mathbf{h}\colon \mathcal{I} \times \mathbb{R}^n \to \mathbb{R}^n$ *with* $\mathcal{I} \subset \mathbb{N}$ *and* $(\Phi_i)_{i\in\mathcal{I}}$ *forming a set partition of* $\mathbb{R}^n$*; let further* $\mathbf{x}^*$ *be a stationary solution of any* $\mathbf{h}_i$ *satisfying* $\mathbf{x}^* \in \Phi_i$*; if there exist a function* $\rho\colon \mathbb{R}_{\geq 0} \to \mathbb{R}_{\geq 0}$ *positive definite such that one the following conditions hold*

1. *There is a Lyapunov-candidate function* $\mathcal{V}(\cdot)$ *such that* $\nabla\mathcal{V}(\mathbf{x}-\mathbf{x}^*)\,\mathbf{h}_i(\mathbf{x}) < 0$ *for all* $\mathbf{x} \neq \mathbf{x}^*$ *and* $i \in \mathcal{I}$*;*

2. *There is a Lyapunov-candidate function* $\mathcal{V}(\cdot)$ *such that* $\nabla\mathcal{V}(\mathbf{x}-\mathbf{x}^*)\,\mathbf{h}_i(\mathbf{x}) < 0$ *for all* $\mathbf{x} \in \Phi_i - \{\mathbf{x}^*\}$ *and* $i \in \mathcal{I}$*;*

3. *There is a family of Lyapunov-candidate functions* $(\mathcal{V}_i)_{i\in\mathcal{I}}$ *such that* $\nabla\mathcal{V}_i(\mathbf{x}-\mathbf{x}^*)$ $\mathbf{h}_i(\mathbf{x}) < 0$ *for all* $\mathbf{x} \in \Phi_i - \{\mathbf{x}^*\}$ *and* $i \in \mathcal{I}$*; as well as* $\mathcal{V}_i(\mathbf{x}) = \mathcal{V}_j(\mathbf{x})$ *for all* $\mathbf{x} \in \partial\Phi_i \cap \partial\Phi_j$ *and* $i, j \in \mathcal{I}$*;*

then $\mathbf{x}^*$ *is a globally asymptotically stable equilibrium of the switching dynamics.* $\lhd$

I.2 Continuation and Bifurcation

In the previous example of the low-pass filter, we have seen how the sign of the parameter μ affected the stability of the origin. In fact, for $\mu = 0$, the system turned meta-stable and exhibited periodic solutions. The study of the change of system behaviour, in particular the existence and stability of stationary solutions, by variation of one or more parameters is called *continuation and bifurcation theory* and shall be the topic of this section.

Consider the extended nonlinear differential equation

$$\dot{\mathbf{x}}(t) = \mathbf{f}(\mathbf{x}(t)\,, \boldsymbol{\mu}) \tag{I.10}$$

for $\boldsymbol{\mu} \in \mathbb{R}^p$ constant. Here, $\boldsymbol{\mu}$ is called the *continuation parameter* and might represent physical properties of the system and its environment, constant control inputs, uncertainties, constant disturbances, and many more. A trajectory $\mathbf{x}^*(\cdot)$ is a stationary solution of $\mathbf{f}$ *for a parameter* $\boldsymbol{\mu}^* \in \mathbb{R}^p$ if and only if $\mathbf{x}^*(\cdot)$ is a stationary solution of $\mathbf{f}(\,\cdot\,, \boldsymbol{\mu} = \boldsymbol{\mu}^*)$; in this case, we might write shortly that $(\mathbf{x}^*, \boldsymbol{\mu}^*)$ is a stationary solution. Likewise, $\mathbf{x}^\dagger(\cdot)$ is periodic for $\boldsymbol{\mu}^\dagger \in \mathbb{R}^p$ if and only if it is a periodic solution of $\mathbf{f}(\,\cdot\,, \boldsymbol{\mu} = \boldsymbol{\mu}^\dagger)$.

Depending on the structure of $\mathbf{f}$, location and stability of a stationary solution $\mathbf{x}^*$ for $\boldsymbol{\mu}^*$ often change if the value of $\boldsymbol{\mu}^*$ is varied. Moreover, the system $\mathbf{f}$ may *bifurcate* for a stationary solution $(\mathbf{x}^*, \boldsymbol{\mu}^*)$, where additional stationary and periodic solutions appear, vanish, or interchange stability. A mathematical characterisation of a bifurcation point is given by (Kwatny et al. 2003, p. 68):

[10] See Branicky 1998, pp. 477–479, for a concise treatment of multiple Lyapunov functions for hybrid systems with arbitrary switching.

Definition I.8. A stationary solution $(\mathbf{x}^*, \boldsymbol{\mu}^*)$ of $\mathbf{f}$ is a *bifurcation point* if and only if there is no neighbourhood $\mathcal{M}$ of $\boldsymbol{\mu}^*$ with a unique, continuously differentiable function $\mathbf{x}\colon \mathcal{M} \to \mathcal{X}$ such that

$$\mathbf{f}(\mathbf{x}(\boldsymbol{\mu}), \boldsymbol{\mu}) = 0$$

for all $\boldsymbol{\mu} \in \mathcal{M}$.

We can state a simple, necessary condition for a bifurcation point (cf. Crawford 1991, p. 996; Chen et al. 2000, p. 516).

Lemma I.9. *Let $(\mathbf{x}^*, \boldsymbol{\mu}^*)$ be a stationary solution of $\mathbf{f}$; only if there is at least one eigenvalue λ of the Jacobian $\mathbf{J}(\mathbf{x}, \boldsymbol{\mu})$ that crosses the imaginary axis for $\boldsymbol{\mu} = \boldsymbol{\mu}^*$, i.e., $\Re\lambda(\boldsymbol{\mu}^*) = 0$, then $(\mathbf{x}^*, \boldsymbol{\mu}^*)$ is bifurcation point.* $\lhd$

This lemma is implied by the *Implicit function theorem* stating that, if $\det \mathbf{J}^* \neq 0$ for a stationary solution $(\mathbf{x}^*, \boldsymbol{\mu}^*)$, there is indeed a unique differentiable function defined on a neighbourhood $\mathcal{M}$ of $\boldsymbol{\mu}^*$ that solves the zero equation above (Crawford 1991, p. 999).

Various bifurcation types can be distinguished depending on *how* and *where* one or more eigenvalues change the stability of a given system. In the following, we will focus on bifurcations that occur in the continuation of a single parameter as well as the continuation of those bifurcations for further parameters.[11]

I.2.1 Bifurcations in one parameter

Occurrence and properties of bifurcations in a single parameter are still subject to research of the fields of applied mathematics and systems theory. For the sake of brevity, we recall only some of the more common bifurcations in continuous systems which are relevant for the study of this thesis, namely *saddle-node*, *pitchfork*, *transcritical*, and *Andronov-Hopf*-bifurcations. A brief overview of these bifurcation types is given by Tab. I.1. For further types of bifurcations such as the period-doubling bifurcation in discrete systems, refer to, e.g., Crawford 1991, p. 1005 or Kuznetsov 1998, Chapter 4.

Table I.1: Bifurcations in continuous systems and one parameter.

	States	Equilibria created	Change of stability	Periodic orbits
Saddle-node	1	2	–	–
Pitchfork	1	2	1	–
Transcritical	1	–	2	–
Andronov-Hopf	2	–	1	1

The following bifurcation types are illustrated in Fig. I.2:

[11] For bifurcations in multiple parameters, refer to Kuznetsov 1998, Chapters 8 and 9.

Saddle-node (Fig. I.2a). A simple bifurcation of one state at which a pair of equilibria of opposite stability is created; consider examplary the system

$$\dot{x} = \mu - x^2 \tag{I.11}$$

with $\mu \in \mathbb{R}$. Simple to see, the pair of equilibria $\pm\sqrt{\mu}$ exists only for $\mu > 0$ and coincides for $\mu = 0$, such that there are no equilibria for $\mu < 0$ (that is to say, branches of equilibria are "created" when μ changes from negative to positive). One of the resulting branches is stable, the other unstable. In general, the stationary solution (x^*, μ^*) is also a saddle-node bifurcation of the system f if both $\frac{\partial f}{\partial \mu}(x^*, \mu^*)$ and $\frac{\partial^2 f}{\partial x^2}(x^*, \mu^*)$ are non-zero (Crawford 1991, p. 1000). The name *saddle-node bifurcation* stems from the fact that, for more than one dimensions, an either stable or unstable equilibrium ("node") is turned into a stationary solution with both negative and positive eigenvalues ("saddle") due to the bifurcation (Crawford 1991, p. 1001).

Pitchfork (Fig. I.2b). Named after its characteristic shape, this bifurcation combines an equilibrium that changes stability with the creation of two further branches of equilibria; consider examplary

$$\dot{x} = \mu x - x^3 \tag{I.12}$$

with $\mu \in \mathbb{R}$. Here, the origin is an equilibrium for all μ but further equilibria $\pm\sqrt{\mu}$ exist only if $\mu \geq 0$. If the origin is stable for $\mu < 0$, then it is unstable for $\mu > 0$ whereas the created branches are both stable (and vice-versa). Necessary for a pitchfork bifurcation are $\frac{\partial f}{\partial \mu} = 0$, $\frac{\partial^2 f}{\partial \mu \, \partial x} \neq 0$, $\frac{\partial^2 f}{\partial x^2} = 0$, and $\frac{\partial^3 f}{\partial x^3} \neq 0$ (Crawford 1991, p. 1002).

Transcritical (Fig. I.2c). Another simple bifurcation of one state yet instead of the creation of further equilibria, two equilibria coincide and subsequently "interchange" stability. Consider the system

$$\dot{x} = \mu x - x^2 \tag{I.13}$$

with $\mu \in \mathbb{R}$. The equilibria 0 and μ converge for $\mu \to -0$ and turn unstable and stable, respectively, in $\mu = 0$. A transcritical bifurcation occurs if $\frac{\partial f}{\partial \mu} = 0$, $\frac{\partial^2 f}{\partial \mu \, \partial x} \neq 0$, yet $\frac{\partial^2 f}{\partial x^2} \neq 0$ (Crawford 1991, p. 1001).

Andronov-Hopf (Fig. I.2d; also *Hopf-bifurcation*). Requires two or more states. In an Andronov-Hopf-bifurcation, a single equilibrium changes stability as a pair of complex-conjugated eigenvalues crosses the imaginary, and a family of periodic orbits encircling the equilibrium is born. If some generecy conditions hold[12], a

[12] see Kuznetsov 1998, Theorem 3.3.

system is in the neighbourhood of the bifurcation point topologically equivalent[13] to the *Andronov-Hopf normal form* (Kuznetsov 1998, pp. 86 and 91–100)

$$\dot{\mathbf{x}} = \begin{bmatrix} \mu & -1 \\ 1 & \mu \end{bmatrix} \mathbf{x} - \|\mathbf{x}\|_2^2 \, \mathbf{x} \tag{I.14}$$

with $\mu \in \mathbb{R}$ and $\mathbf{x} \in \mathbb{R}^2$. For $\mu \geq 0$, Eq. I.14 has the periodic solutions

$$\mathbf{x}^\dagger(t) = \pm\sqrt{\mu} \begin{bmatrix} \cos t \\ \sin t \end{bmatrix}^T .$$

I.2.2 Continuation of bifurcations

In addition to secondary bifurcations that may occur for variation of further parameters (e.g., Torus or Hopf-Hopf-bifurcations, see Yu 2003, pp. 102 and following), the continuation of an initial bifurcation along auxiliary parameters often also changes the location of this bifurcation. Therefore, the continuation of a bifurcation can give important insight into the robustness of a system with respect to changes of these parameters. We want to further illustrate the relationship of a simple bifurcation and the variation of a second parameter with a small example: Consider the system

$$\dot{x} = \mu_1 - \mu_2 - x^2 \tag{I.15}$$

similar to (I.11) but with $(\mu_1, \mu_2) \in \mathbb{R}^2$. If we initially hold $\mu_2 =_{const.} 0$, analysis of the equilibrium reveals a saddle-node bifurcation for $\mu_1^* = 0$. Indeed, the saddle-node bifurcation occurs for *any* pair (μ_1^*, μ_2^*) with $\mu_1^* = \mu_2^*$. This is further illustrated in Fig. I.3. Here, μ_2 provides a lower bound such that there is a (stable) equilibrium for μ_1 and we might say that $\mu_2 = \mu_1$ constitutes a *critical* condition for the system in (I.11); that is, $|\mu_1 - \mu_2|$ serves as a measure for its robustness.

Despite the fact that this example is purely academic, it illustrates well an otherwise rather complicated relationship between bifurcations and secondary parameters. We make further use of the continuation of bifurcations in Chapter 4 in order to investigate the change of stability of an aircraft due to uncertain system parameters.

◊

[13] Functions $\mathbf{f}, \mathbf{g} \colon \mathbb{R}^n \to \mathbb{R}^n$ are *(locally) topologically equivalent* in the neighbourhoods $\mathcal{X}, \mathcal{Y} \subset \mathbb{R}^n$ of $\mathbf{x}_0, \mathbf{y}_0$ if there is a homeomorphism $\hbar \colon \mathcal{X} \to \mathcal{Y}$ such that $(\hbar \circ \mathbf{f})(\mathbf{x}) = (\mathbf{g} \circ \hbar g)(\mathbf{x})$ for all $\mathbf{x} \in \mathcal{X} \cap \mathbf{f}^{-1}(\mathcal{X})$ and $\hbar(\mathbf{x}_0) = \mathbf{y}_0$ (Kuznetsov 1998, p. 64).

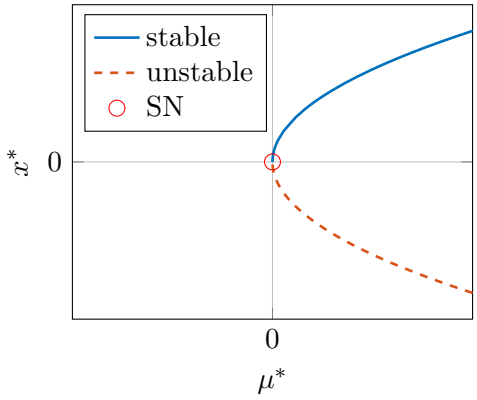

(a) Saddle-node bifurcation.

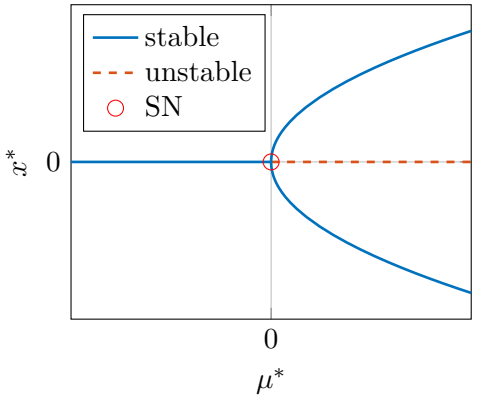

(b) Pitchfork bifurcation.

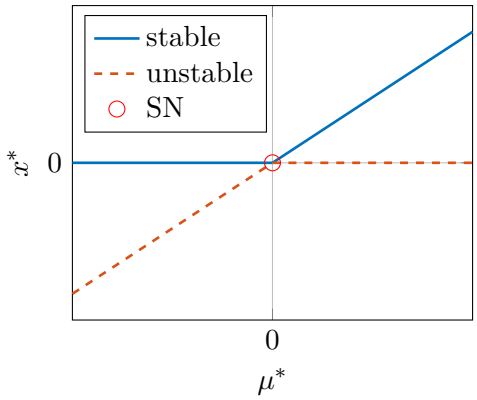

(c) Transcritical bifurcation.

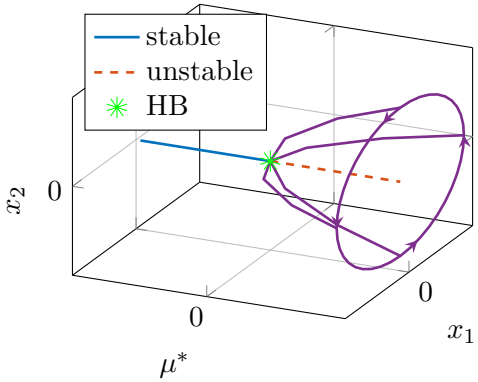

(d) Andronov-Hopf-bifurcation.

Figure I.2: Bifurcations in continuous systems and one parameter. A change of stability is denoted by SN (○), the origin of a family of periodic orbits by HB (✳).

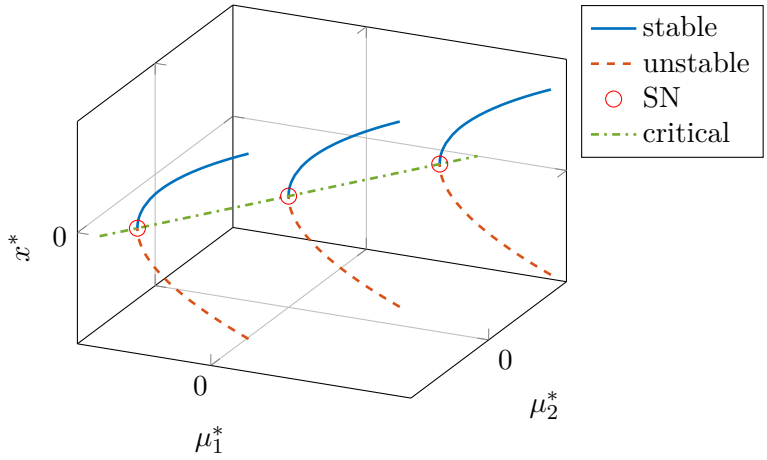

Figure I.3: Continuation of saddle-node (SN) bifurcations at (x^*, μ_1^*) along μ_2^*.

I.3 Attractors, Invariance, and the Region of Attraction

Similar to Lyapunov and asymptotic stability, we have the concepts of invariant sets and regions of attraction, respectively. While the previous sections dealt with the existence and interchange of (local) stability, in the following we are going to quantify the stable domain. Before we discuss attraction and invariance, and subsequently define the region of attraction of a stable stationary solution, we have to explain the circumstances under which a set is "larger" than another set.

A partial order on sets

The binary *subset* or inclusion operator "$\subseteq$" for any two sets $\mathcal{A}, \mathcal{B} \in \mathbb{K}$—namely, $\mathcal{A} \subseteq \mathcal{B}$ if and only if $x \in \mathcal{B}$ for each $x \in \mathcal{A}$—forms an order on $2^{\mathbb{K}}$ as it is reflexive,

$$\mathcal{A} \subseteq \mathcal{A} \tag{I.16}$$

for any $\mathcal{A} \in \mathbb{K}$; and antisymmetric,

$$\mathcal{A} \subseteq \mathcal{B} \wedge \mathcal{B} \subseteq \mathcal{A} \Longrightarrow \mathcal{A} = \mathcal{B} \tag{I.17}$$

for $\mathcal{A}, \mathcal{B} \in \mathbb{K}$. However, the inclusion is not *total*, since there are $\mathcal{A}', \mathcal{B}' \in \mathbb{K}$ with neither $\mathcal{A}' \subseteq \mathcal{B}'$ nor $\mathcal{B}' \subseteq \mathcal{A}'$. In this case, $\mathcal{A}'$ and $\mathcal{B}'$ are incomparable.

That is, if we are to say "$\mathcal{B}$ is larger than $\mathcal{A}$" as $\mathcal{A} \subseteq \mathcal{B}$, then we will soon encounter sets $\mathcal{A}', \mathcal{B}'$ that we cannot compare. Instead, we will say "Υ is the largest set of $\mathbb{K}$" if and only if—given existence—$\mathcal{A} \subseteq \Upsilon$ for all $\mathcal{A} \in \mathbb{K}$; in other words,

$$\bigcup_{\mathcal{A} \in \mathbb{K}} = \Upsilon. \tag{I.18}$$

Similar to maximum and supremum of a measurable class, the largest set Υ, if existing, may or may not be element of $\mathbb{K}$.

I.3.1 Invariant and attractive sets

For the definition of both Lyapunov and (local) asymptotic stability, we relied on unitary balls around the stationary solution. We now extend this to arbitrary shaped subsets Ω of the state-space $\mathcal{X}$.

Definition I.10. A bounded set $\Omega \subset \mathcal{X}$ is an *invariant set* of the system $\mathbf{f}$ if and only if for any $\mathbf{x}_0 \in \Omega$ holds: if $\mathbf{x}(\cdot)$ is the trajectory starting in $\mathbf{x}_0$ for some $t_0 \in \mathbb{R}$, then $\mathbf{x}(t) \in \Omega$ for all $t \geq t_0$.

A stationary solution $\mathbf{x}^*$ is stable in the sense of Lyapunov if for any $\epsilon \in \mathbb{R}_+$ there is an invariant set Ω that contains $\mathbf{x}^*$ in its interior and $\|\mathbf{x} - \mathbf{x}^*\|_2 < \epsilon$ for every $\mathbf{x} \in \Omega$.

Definition I.11. A bounded set $\Omega \subset \mathcal{X}$ is an *attractive set* of the system $\mathbf{f}$ with the stationary solution $\mathbf{x}^*$ as *attractor* if and only if for any $\mathbf{x}_0 \in \Omega$ holds: if $\mathbf{x}(\cdot)$ is the trajectory starting in $\mathbf{x}_0$ for some $t_0 \in \mathbb{R}$, then $\lim_{t\to\infty} \|\mathbf{x}(t_0 + t) - \mathbf{x}^*\|_2 = 0$.

A stationary solution $\mathbf{x}^*$ is asymptotically stable only if there is an attractive set Ω that contains its attractor $\mathbf{x}^*$ in its interior. If $\mathbf{x}^*$ is locally asymptotically stable, the largest attractive set $\mathcal{R}$ exists, in which case we call $\mathcal{R}$ the *region of attraction* of $\mathbf{x}^*$, and is invariant if bounded. For global asymptotic stability, as there is no bounded largest attractive set, the state-space effectively constitutes the region of attraction.

I.3.2 Estimating the region of attraction

Determining the region of attraction of a locally stable equilibrium is less tractable than proving its stability in the first place. Hard enough, one might be content with an estimate $\Omega_{\mathcal{R}}$.

Definition I.12. Let $\mathcal{R}$ be the region of attraction of a stationary solution $\mathbf{x}^*$ of $\mathbf{f}$; a set $\Omega_{\mathcal{R}} \subset \mathcal{R}$ is called *region of attraction estimate* if and only if it is an invariant set of $\mathbf{f}$.

In their comprehensive 1985 survey, Genesio et al. mainly distinguished three methods for the determination or estimation of a region of attraction: Zubov's equation, the theorem of La Salle, (both derived from Lyapunov's stability theory) and "non-Lyapunov" methods such as exploiting the phase plane (Genesio et al. 1985, pp. 747–749).

Non-Lyapunov: phase-plane analysis

Phase-plane analysis and other non-Lyapunov methods for region of attraction estimation are often limited to nonlinear systems with two states only (Genesio et al. 1985, p. 749). Among those techniques, one might profit from the existence of a limit cycle around the stable equilibrium as boundary of the region of attraction or study the flow of the system (see Example I.2). The presence of further, unstable stationary solutions in the neighbourhood of a stable equilibrium also limits its possible region of attraction.

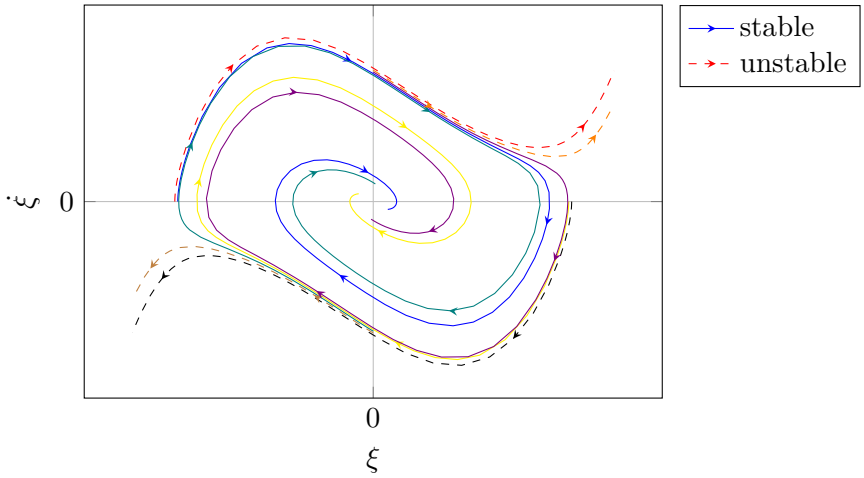

Figure I.4: Phase-plane of the Van-der-Pol oscillator with $\mu = -1$. Solid lines converge into the origin, dashed lines diverge.

Example I.2 (Van-der-Pol oscillator). A famous example for a system exhibiting periodic behaviour, named after its inventor, is given by

$$\ddot{\xi} = -\xi - \mu\left(\xi^2 - 1\right)\dot{\xi} \tag{I.19}$$

with $\mu \in \mathbb{R}$ and the stationary solution $\xi = \dot{\xi} = 0$ is unstable for $\mu > 0$. For $\mu \to +0$, the Van-der-Pol oscillator exhibits a near-circular stable limit cycle that becomes deformed for larger μ (Slotine and Li 1991, p. 161). Since the existence of a limit cycles here is independent of the sign of μ, the stationary solution and the limit cycle interchange stability for $\mu < 0$ (Fig. I.4): Trajectories that start within yet arbitrary close to the limit cycle converge towards the stationary solution, whereas trajectories starting outside will diverge. That is, the limit cycle defines the region of attraction of the origin.

Zubov's equation

Zubov (1964) initially proposed to use that if

$$\nabla\mathcal{V}\,\mathbf{f} = -\left(1 - \mathcal{V}\right)\phi \tag{I.20}$$

holds for a Lyapunov-candidate function $\mathcal{V}(\cdot)$ and positive definite[14] function $\phi(\cdot)$, then $\{\mathbf{x}\,|\,\mathcal{V}(\mathbf{x}) \leq 1\}$ is an exact characterisation of the region of attraction for the stationary solution $\mathbf{x}^* = 0$ of $\mathbf{f}$ (cited after Genesio et al. 1985, p. 748). Since an algebraic solution of Zubov's equations is usually difficult to find, his method has been further extended in order to find a suitable estimate of the region of attraction. Extensions include the

[14] A (continuous) function ϕ is said to be *positive definite* (p.d.) if and only $\phi(\cdot) > 0$ everywhere except at the origin and $\phi(0) = 0$.

under and over-approximation of the region of attraction boundary by a finite partial sum of Lyapunov-candidate functions of increasing degree. Today, this approach is known as method of *maximal Lyapunov-functions* based on the contributions of Vannelli and Vidyasagar 1985.[15]

The theorem of La Salle

La Salle's 1960 theorem provides the perhaps most widespread backend for region of attraction estimation. It is often given as follows (La Salle 1960, Theorem 1; cited after Genesio et al. 1985, p. 478):

Theorem I.13 (La Salle's basic theorem)**.** *Let the set $\Omega \subset \mathcal{X}$ contain the stationary solution $\mathbf{x}^*$ of $\mathbf{f}$ and let $\mathcal{V}(\cdot)$ be a Lyapunov-candidate function; if*

$$\nabla\mathcal{V}(\mathbf{x}-\mathbf{x}^*)\,\mathbf{f}(\mathbf{x}) \leq 0$$

for all $\mathbf{x} \in \Omega$ with $\mathbf{x} \neq \mathbf{x}^*$ and there is no trajectory $\mathbf{x}'(\cdot)$ of $\mathbf{f}$ such that $\mathbf{x}'(\mathbb{R}) \subset E = \{\mathbf{x} \,|\, \nabla\mathcal{V}(\mathbf{x}-\mathbf{x}^*)\,\mathbf{f}(\mathbf{x}) = 0\}$, then Ω is a region of attraction estimate of $\mathbf{x}^*$. $\lhd$

However, for the purpose of region of attraction estimation as provided in the following chapters, a modification of the basic theorem is more suitable. This is a modified version of La Salle's theorem (La Salle 1960, Theorem 2) for the case $E = \{\mathbf{x}^*\}$.

Theorem I.14 (La Salle's extended theorem)**.** *Let $\mathbf{x}^*$ be a stationary solution of $\mathbf{f}$, $\mathcal{V}(\cdot)$ a Lyapunov candidate-function, and $\Omega_\gamma = \{\mathbf{x} \,|\, \mathcal{V}(\mathbf{x}-\mathbf{x}^*) \leq \gamma\}$ for some $\gamma \in \mathbb{R}_+$; if*

$$\nabla\mathcal{V}(\mathbf{x}-\mathbf{x}^*)\,\mathbf{f}(\mathbf{x}) < 0$$

for all $\mathbf{x} \in \Omega_\gamma$ with $\mathbf{x} \neq \mathbf{x}^*$, then Ω_γ is a region of attraction estimate of $\mathbf{x}^*$. $\lhd$

Several publications have been dedicated to the region of attraction estimation using La Salle's extended theorem.[16] One of the most fruitful in recent days, namely the use of sum-of-squares programming in order to check the condition in Theorem I.14, is elaborately discussed in the subsequent chapter.

$\bowtie$

[15] Further reading: Rozgonyi et al. 2010; Chesi 2013; Valmorbida and Anderson 2017.
[16] Further reading: Topcu et al. 2008; Topcu et al. 2010; Khodadadi et al. 2014.

Sum of squares

For about 150 years, mathematicians have studied the problem of polynomial nonnegativity; namely, how to decide for a given polynomial $\mathfrak{f}$ in n variables ($\mathfrak{f} \in \mathbb{R}[x_1, \ldots, x_n]$) if $\mathfrak{f}(x_1, \ldots, x_n) \geq 0$ for all $x_1, \ldots, x_n \in \mathbb{R}$. It is quite obvious now, that a polynomial which is defined by a (finite) sum of squared polynomials, i.e., $\mathfrak{f} = \sum_i \mathfrak{f}_i^2$ with $\mathfrak{f}_i \in \mathbb{R}[x_1, \ldots, x_n]$, is nonnegative. This leads to the immediate question whether, in turn, *any nonnegative* polynomial can also be represented by a sum of squares. While that assertion holds for polynomials in only one variable, Hilbert had soon disproven it in general (Putinar 1993, p. 969) – even though an actual example of such a nonnegative, not-sum-of-squares polynomial was only found by Motzkin (1967). Nonnegativity remains an NP-hard problem for polynomials of 4th degree or higher (Parillo 2003, p. 295). Sum-of-squares polynomials, on the other hand, can be reduced to positive semi-definite matrices and thus solved in polynomial time.

Definition I.15. A symmetric matrix $\mathbf{M} \in \mathbb{R}^{n \times n}$ is positive semi-definite ($\mathbf{M} \succeq 0$) if and only if $\mathbf{x}^T \mathbf{M} \mathbf{x} \geq 0$ for all $\mathbf{x} \in \mathbb{R}^n$ or, equivalently, all eigenvalues of $\mathbf{M}$ are nonnegative.

We denote the set of positive semi-definite matrices by $\mathbb{S}_n$ and the set of sum-of-squares (SOS) polynomials, by $\Sigma[x_1, \ldots, x_n]$. The lemma that connects the two utilizes the *Gram matrix* form a of a SOS polynomial, $\mathfrak{z}^T \mathbf{Q} \mathfrak{z}$, where each element of the vector $\mathfrak{z}$ is a monomial in the variables $x_1, \ldots, x_n$.

Lemma I.16 (Choi et al. 1995, p. 106–108)**.** *A polynomial $\mathfrak{f} \in \mathbb{R}[\mathbf{x}]$ of degree $2k$ is sum-of-squares ($\mathfrak{f} \in \Sigma[\mathbf{x}]$) if and only if there is positive semi-definite matrix $\mathbf{Q}$ of size l ($\mathbf{Q} \in \mathbb{S}_l$) and a vector $\mathfrak{z}$ of monomials in $\mathbf{x}$ ($\mathfrak{z} \in \mathbb{B}[\mathbf{x}]^l$) of degrees k or lower such that $\mathfrak{f} = \mathfrak{z}^T \mathbf{Q} \mathfrak{z}$. Furthermore, the smallest number l' such that $\mathfrak{f} = \sum_{i=1}^{l'} \mathfrak{f}_i^2$ is equal to the rank of $\mathbf{Q}$.* $\lhd$

With advances in semi-definite programming relaxations (most notably, by Parillo 2003), sum-of-squares optimisation techniques are today one of the most powerful tools for semi-algebraic certification; that is, although the underlying semi-definite problems are solved numerically, polynomial nonnegativity (and induced properties) hold algebraically the lemma above and subsequent theorems. Despite their mathematical power, sum-of-squares programming becomes computationally infeasible for polynomials of high degree and in numerous variables; efforts to make large problems tractable include the selection of a suitable basis (e.g., via facial reduction, Permenter and Parrilo 2014), exploitation of sparsity (see, e.g., Ahmadi et al. 2017), and, most recently, alternative characterisations of polynomial nonnegativity which can be reduced to linear and second-order cone programming rather than semi-definite programming (so-called DSOS and SDSOS optimisation, Ahmadi and Majumdar 2018). Further relaxations of quadratic matrix-inequalities (as in Kheirandishfard et al. 2018) potentially lead to improvements for bilinear sum-of-squares problem, which heretofore are subject to bisection.

In this chapter, we review the foundations of sum-of-squares which have led to SOS-based techniques for the estimation of regions of attraction and related applications. We start and recall the definitions of semi-definite and sum-of-squares programs. The main result, the *Positivstellensatz* of real algebraic geometry, provides a theoretical framework for the computation of SOS certificates which prove the implication of polynomial predicates. We subsequently propose a new, general formulation that allows an interpretation as set-inclusion problems and thus eases the discussion of invariant sets and regions of attraction, as we shall finally demonstrate.

From semi-definite to sum-of-squares and quasi-convex optimisation

Semi-definite programs have been thoroughly studied. For a historical overview and several examples, refer to Vandenberghe and Boyd (1996, pp. 52–62). A semi-definite optimisation program is stated as minimising a linear function subject to a linear matrix inequality in the decision variables $\boldsymbol{\lambda} \in \mathbb{R}^n$:

$$\begin{aligned} &\text{minimise} && \mathbf{c}^T \boldsymbol{\lambda} \\ &\text{subject to} && \mathbf{F}(\boldsymbol{\lambda}) = \mathbf{F}_0 + \sum_{i=1}^{n} \mathbf{F}_i \lambda_i \succeq 0, \end{aligned} \tag{I.21}$$

where $\boldsymbol{\lambda} = (\lambda_1, \ldots, \lambda_n)$, $\mathbf{c} \in \mathbb{R}^n$, and $\mathbf{F}_0, \mathbf{F}_1, \ldots, \mathbf{F}_n \in \mathbb{R}^{n \times n}$. Eq. (I.21) is convex and can be reduced to a polynomial-time problem (Vandenberghe and Boyd 1996, p. 52). We can write equivalently

$$\begin{aligned} &\text{minimise} && \operatorname{tr}(\mathbf{C}\boldsymbol{\Lambda}) \\ &\text{subject to} && \mathbf{F}(\boldsymbol{\Lambda}) = \mathbf{A}_0 + \sum_{i=1}^{k} \mathbf{A}_i \boldsymbol{\Lambda} \succeq 0 \end{aligned} \tag{I.22}$$

with matrix decision variable $\boldsymbol{\Lambda} \in \mathbb{R}^{n \times n}$ and $\mathbf{C}, \mathbf{A}_0, \mathbf{A}_1, \ldots, \mathbf{A}_k \in \mathbb{R}^{n \times n}$. Choosing suitable monomials $\mathfrak{z}(\mathbf{x})$, Eq. (I.22) extends to the sum-of-squares optimisation problem

$$\begin{aligned} &\text{minimise} && \mathbf{c}_1^T \boldsymbol{\lambda}_1 + \cdots + \mathbf{c}_k^T \boldsymbol{\lambda}_k \\ &\text{subject to} && \mathfrak{p}_1(\boldsymbol{\lambda}_1, \mathbf{x}), \ldots, \mathfrak{p}_k(\boldsymbol{\lambda}_k, \mathbf{x}) \in \Sigma[\mathbf{x}], \end{aligned} \tag{I.23}$$

where $\mathfrak{p}_1, \ldots, \mathfrak{p}_k$ are affine in the decision variables $\boldsymbol{\lambda}_1, \ldots, \boldsymbol{\lambda}_k$. Using the Gram matrix from of Lemma I.16, we have $\mathfrak{p}_i(\boldsymbol{\lambda}_i, \mathbf{x}) = \mathfrak{z}_i^T \mathbf{Q}_i \mathfrak{z}_i$ with $\mathbf{Q}_i \in \mathbb{S}_{l_i}$ and Eq. (I.23) reduces to a semi-definite program. Unfortunately, the necessary dimension l_i increases significantly – even though still polynomially – with the number of variables or the polynomial degrees (Parillo 2003, p. 299). The formulation above highlights the fact that the decision variables of a sum-of-squares program are the polynomial *coefficients*, not the polynomials itself; however, we conveniently denote the sum-of-squares feasibility problem as

$$\begin{aligned} &\text{find} && \mathfrak{s}_1, \ldots, \mathfrak{s}_{k'} \in \Sigma[\mathbf{x}] \\ &\text{subject to} && \mathfrak{f}_0 + \sum_{i=1}^{k} \mathfrak{s}_i \mathfrak{f}_i \in \Sigma[\mathbf{x}] \end{aligned} \tag{I.24}$$

with $k' \leq k$, where $\mathfrak{s}_1, \ldots, \mathfrak{s}_k$ are of bounded degree and $\mathfrak{f}_0, \mathfrak{f}_1, \ldots, \mathfrak{f}_k \in \mathbb{R}[\mathbf{x}]$.

A bilinear sum-of-squares problem requires to solve quadratic matrix inequalities, which are NP-hard (Toker and Özbay 1995, p. 2526). Despite that, if the problem is bilinear in a scalar only, the problem remains tractable using a quasi-convex optimisation approach as described by Seiler and Balas (2010, p. 3339). There, a *generalised SOS program* is given as

$$\begin{aligned} &\text{minimise} && \mu \\ &\text{subject to} && \mathfrak{f}_0 + \mu\,\mathfrak{s}_0 + \sum_{i=1}^{k} \mathfrak{s}_i \mathfrak{f}_i \in \Sigma\,[\mathbf{x}] \\ &\text{and} && \mathfrak{s}_0, \mathfrak{s}_1, \ldots, \mathfrak{s}_{k'} \in \Sigma\,[\mathbf{x}] \end{aligned} \tag{I.25}$$

with $k' \leq k$, where $\mu \in \mathbb{R}$, $\mathfrak{s}_0, \mathfrak{s}_1, \ldots \mathfrak{s}_k$ are of bounded degree, and $\mathfrak{f}_0, \mathfrak{f}_1, \ldots, \mathfrak{f}_k \in \mathbb{R}\,[\mathbf{x}]$.

I.4 Semi-algebraic Set Inclusion

So far, we have considered sum-of-squares programming as a tool to certify global properties, namely, nonnegativity. For a local analysis such estimating as the region of attraction, we would like to assert a statement ("$\mathcal{A}$ holds") only for certain subspace ("for all $\mathbf{x}$ that satisfy $\mathcal{B}$"). If both $\mathcal{A}$ and $\mathcal{B}$ are described by polynomial inequalities, we can prove "$\mathcal{B} \Rightarrow \mathcal{A}$" by computation of SOS certificates. Recall first the duality between logical implication and set inclusion:

Lemma I.17. *Let $\mathfrak{p}, \mathfrak{q}$ be polynomials in n variables $\mathbf{x}$ ($\mathfrak{p}, \mathfrak{q} \in \mathbb{R}\,[\mathbf{x}]$); the following statements are equivalent:*

$$\forall \mathbf{x} \in \mathbb{R}^n. \quad (\mathfrak{p}(\mathbf{x}) \leq a \Rightarrow \mathfrak{q}(\mathbf{x}) \leq b)\,; \tag{α}$$

$$\{\mathbf{x} \in \mathbb{R}^n \,|\, \mathfrak{p}(\mathbf{x}) \leq a\} \subseteq \{\mathbf{x} \in \mathbb{R}^n \,|\, \mathfrak{q}(\mathbf{x}) \leq b\}\,; \tag{β}$$

$$\{\mathbf{x} \in \mathbb{R}^n \,|\, \mathfrak{p}(\mathbf{x}) \leq a\} \cap \{\mathbf{x} \in \mathbb{R}^n \,|\, \mathfrak{q}(\mathbf{x}) > b\} = \varnothing; \tag{γ}$$

for any $a, b \in \mathbb{R}$. $\lhd$

For simplicity, we introduce the notation $\Omega_{\mathfrak{p} \leq a} =_{\text{def}} \{\mathbf{x} \,|\, \mathfrak{p}(\mathbf{x}) \leq a\}$ for $\mathfrak{p} \in \mathbb{R}\,[\mathbf{x}]$ and $a \in \mathbb{R}$. Likewise, we shall write $\mathcal{O}_{\mathfrak{p}=a} =_{\text{def}} \{\mathbf{x} \,|\, \mathfrak{p}(\mathbf{x}) = a\}$. These notations, combined with the theoretical backing of the Positivstellensatz, allow us to discuss the stability concepts of the previous chapter within the framework of sum-of-squares programming.

I.4.1 Der Positivstellensatz

The Positivstellensatz as lined out in this section is a generalization of Hilbert's *Nullstellensatz* for the real numbers $\mathbb{R}$ (Parillo 2003, p. 305). It constitutes nothing less than both sufficient *and* necessary conditions for the existence of sum-of-squares certification for set inclusion. Stating the theorem, however, requires some preliminary definitions:

Definitions (*Monoid, Cone, & Ideal*)**.** Let $S = \{\mathfrak{p}_1, \ldots, \mathfrak{p}_k\}$ be a finite set ($k \in \mathbb{N}_0$) of polynomials in n variables $\mathbf{x}$; define:

- The *multiplicative monoid* as $\mathcal{M}(S) = \{\prod_{i=1}^{r} \mathfrak{p}_i \,|\, \mathfrak{p}_i \in S,\, r \in \mathbb{N}_0\}$.
- The *polynomial cone* as $\mathcal{P}(S) = \{\mathfrak{s}_0 + \sum_{i=1}^{r} \mathfrak{s}_i \mathfrak{p}_i \,|\, \mathfrak{s}_i \in \mathcal{P}(\varnothing)\,,\, \mathfrak{p}_i \in \mathcal{M}(S)\,,\, r \in \mathbb{N}_0\}$.
- The *ring ideal* as $\mathcal{I}(S) = \{\sum_{i=1}^{r} \mathfrak{t}_i \mathfrak{p}_i \,|\, \mathfrak{t}_i \in \mathbb{R}[\mathbf{x}]\,,\, \mathfrak{p}_i \in S,\, r \in \mathbb{N}_0\}$.

Note that $\mathcal{M}(\varnothing) = \{1\}$, $\mathcal{I}(\varnothing) = \{0\}$, and $\mathcal{P}(\varnothing) = \Sigma[\mathbf{x}]$. The following theorem goes back to Stengle (1974, pp. 91–92) and is cited after Parillo (2003, Theorem 4.6).

Theorem I.18 (Positivstellensatz)**.** *Let $\mathfrak{f}_1, \ldots, \mathfrak{f}_k$, $\mathfrak{g}_1, \ldots, \mathfrak{g}_m$, and $\mathfrak{h}_1, \ldots, \mathfrak{h}_r$ be polynomials in n variables $\mathbf{x}$ with $k, m, r \in \mathbb{N}_0$; the following statements are equivalent:*

1. *We have that the set*

$$\left\{ \mathbf{x} \in \mathbb{R}^n \;\middle|\; \begin{array}{ll} \mathfrak{f}_i(\mathbf{x}) \geq 0 & \text{for all } 1 \leq i \leq k \\ \mathfrak{g}_j(\mathbf{x}) \neq 0 & \text{for all } 1 \leq j \leq m \\ \mathfrak{h}_l(\mathbf{x}) = 0 & \text{for all } 1 \leq l \leq r \end{array} \right\} \tag{I.26}$$

   is empty;

2. *There are $\mathfrak{f} \in \mathcal{P}$, $\mathfrak{g} \in \mathcal{M}$, and $\mathfrak{h} \in \mathcal{I}$ such that $\mathfrak{f} + \mathfrak{g}^2 + \mathfrak{h} = 0$;*

where $\mathcal{P}$, $\mathcal{M}$, and $\mathcal{I}$ are the cone of $\{\mathfrak{f}_i\}_{1 \leq i \leq k}$, the monoid of $\{\mathfrak{g}_j\}_{1 \leq j \leq m}$, and the ideal of $\{\mathfrak{h}_l\}_{1 \leq l \leq r}$, respectively. ◁

The polynomials $\mathfrak{f}$, $\mathfrak{g}$, and $\mathfrak{h}$ in Theorem I.18 are *refutations* of the non-emptyness of Eq. (I.26). Although their existence is guaranteed by the Positivstellensatz, the computation is virtually intractable as they require highly exponential-time computations (Parillo 2003, p. 305). Therefore, one uses only its sufficient condition in practice (Topcu et al. 2008, Lemma 2):

Lemma I.19. *Let $\mathfrak{f}_0$, $\mathfrak{f}_1, \ldots, \mathfrak{f}_k$, and $\mathfrak{h}_1, \ldots, \mathfrak{h}_r$ be polynomials in n variables $\mathbf{x}$ with $k, r \in \mathbb{N}_0$; we have*

$$\{\mathbf{x} \in \mathbb{R}^n \,|\, \mathfrak{f}_1(\mathbf{x}) \geq 0, \ldots, \mathfrak{f}_k(\mathbf{x}) \geq 0,\, \mathfrak{h}_1(\mathbf{x}) = 0, \ldots, \mathfrak{h}_r(\mathbf{x}) = 0\} \subseteq \{\mathbf{x} \in \mathbb{R}^n \,|\, \mathfrak{f}_0(\mathbf{x}) \geq 0\} \tag{I.27}$$

if there are $(\mathfrak{s}_i)_i \subset \Sigma[\mathbf{x}]$ and $(\mathfrak{t}_l)_l \subset \mathbb{R}[\mathbf{x}]$ such that $\mathfrak{f}_0 - \sum_{i=1}^{k} \mathfrak{s}_i \mathfrak{f}_i + \sum_{l=1}^{r} \mathfrak{t}_l \mathfrak{h}_l \in \Sigma[\mathbf{x}]$.

Lemma I.19 can easily be seen if one replaces "$(\cdot) \in \Sigma[\mathbf{x}]$" by "$(\cdot) \geq 0$" and inserts the left-hand side of (I.27) into the last equation. However, the proof given by Tan (2006, p. 15–16) provides interesting details about the mechanisms of the Positivstellensatz as well as the necessities of sum-of-squares certification.

Proof of Lemma I.19. As $\mathcal{A} \subseteq \{\mathbf{x} \,|\, \mathfrak{f}_0(\mathbf{x}) \geq 0\}$, for any $\mathcal{A} \in 2^{\mathbb{R}}$, is equivalent to $\varnothing = \mathcal{A} \cap \{\mathbf{x} \,|\, -\mathfrak{f}_0(\mathbf{x}) \geq 0 \wedge \mathfrak{f}_0(\mathbf{x}) \neq 0\}$, Eq. (I.27) follows necessarily from the existence of $\mathfrak{f} \in \mathcal{P}(\{-\mathfrak{f}_0, \mathfrak{f}_1, \ldots, \mathfrak{f}_k\})$, $\mathfrak{g} \in \mathcal{M}(\{\mathfrak{f}_0\})$, and $\mathfrak{h} \in \mathcal{I}(\{\mathfrak{h}_1, \ldots, \mathfrak{h}_r\})$ such that $\mathfrak{f} + \mathfrak{g}^2 + \mathfrak{h} = 0$.

Thus, we may choose $\mathfrak{f}' = \mathfrak{s}_0\,(-\mathfrak{f}_0) + \sum_{i=1}^{r} \mathfrak{s}_i\,(-\mathfrak{f}_0)\,\mathfrak{f}_i$; $\mathfrak{g}' = \mathfrak{f}_0$; $\mathfrak{h}' = \sum_{l=1}^{k} \hat{\mathfrak{t}}_l \mathfrak{h}_l$; and with $\hat{\mathfrak{t}}_l = \mathfrak{f}_0 \mathfrak{t}_l$

$$-\mathfrak{f}_0 \left(\mathfrak{s}_0 - \mathfrak{f}_0 + \sum_{i=1}^{r} \mathfrak{s}_i \mathfrak{f}_i - \sum_{l=1}^{k} \mathfrak{t}_l \mathfrak{h}_l \right) = 0. \tag{I.28}$$

If $\mathfrak{f}_0$ is not the null-polynomial[17], $\mathfrak{s}_0 \in \Sigma\,[\mathbf{x}]$ and the zero multiplication property yield the desired sufficient condition. □

Recall that we must choose the degree of the sum-of-square certificates $(\mathfrak{s}_i)_i$ (and the polynomials $(\mathfrak{t}_l)_l$) a priori; comparing the coefficients in (I.28), we obtain that $\mathfrak{s}_0$ as well as the terms $(\mathfrak{s}_i \mathfrak{f}_i)_i$ and $(\mathfrak{t}_l \mathfrak{h}_l)_l$ should be of similar degree in order to ensure feasibility (Tan 2006, p. 113). However, the choice of the candidates $\mathfrak{f}', \mathfrak{g}', \mathfrak{h}'$ was restrictive – they are, in fact, the smallest possible polynomials such that the Positivstellensatz provides a meaningful condition – and other refutations involving more certificates could be chosen. Parillo gives a more general procedure yet also notes that, given knowledge of the problem structure, this results in an overparametrisation (Parillo 2003, pp. 306–307).

I.4.2 A general formulation

Theorem I.18 and Lemma I.19 give us the theoretical background to handle problems of inclusion of polynomial semi-algebraic sets rather than problems of polynomial nonnegativity. We shall now extend this methodology with a new formulation that highlights the relation of the underlying sets:

Definition I.20. Let $\mathfrak{f}_0, \mathfrak{f}_1, \ldots, \mathfrak{f}_k$, and $\mathfrak{h}_1, \ldots, \mathfrak{h}_r$ be polynomials in n variables $\mathbf{x}$ with $k, r \in \mathbb{N}_0$; we say, "$(\mathbf{s}, \mathbf{t})$ *prove* the set inclusion of Eq. (I.27)," and write

$$(\mathbf{s}, \mathbf{t}) \vdash \bigcap_{i=1}^{k} \{\mathbf{x} \in \mathbb{R}^n \,|\, \mathfrak{f}_i(\mathbf{x}) \geq 0\} \cap \bigcap_{l=1}^{r} \{\mathbf{x} \in \mathbb{R}^n \,|\, \mathfrak{h}_l(\mathbf{x}) = 0\} \subseteq_\Sigma \{\mathbf{x} \in \mathbb{R}^n \,|\, \mathfrak{f}_0(\mathbf{x}) \geq 0\} \tag{I.29}$$

if $\mathbf{s} = (\mathfrak{s}_1, \ldots, \mathfrak{s}_k) \subset \Sigma\,[\mathbf{x}]$, $\mathbf{t} = (\mathfrak{t}_1, \ldots, \mathfrak{t}_r) \subset \mathbb{R}\,[\mathbf{x}]$, and $\mathfrak{f}_0 - \sum_{i=1}^{k} \mathfrak{s}_i \mathfrak{f}_i + \sum_{l=1}^{r} \mathfrak{t}_l \mathfrak{h}_l \in \Sigma\,[\mathbf{x}]$.

With this definition, and recalling the $\Omega_{(\cdot)}$-notation from the beginning of this section, we can formulate a simple sum-of-squares certification problem based on (I.24) as

$$\begin{aligned} &\text{find} && \mathbf{s} = (\mathfrak{s}_1, \ldots, \mathfrak{s}_{k'}) \subset \Sigma\,[\mathbf{x}] \\ &\text{subject to} && \mathbf{s} \vdash \bigcap_{i=1}^{k} \Omega_{\mathfrak{f}_i \leq 0} \subseteq_\Sigma \Omega_{\mathfrak{f}_0 \leq 0}, \end{aligned} \tag{I.30}$$

where, again, $\mathfrak{s}_1, \ldots, \mathfrak{s}_k$ are of bounded degree and $\mathfrak{f}_0, \mathfrak{f}_1, \ldots, \mathfrak{f}_k \in \mathbb{R}\,[\mathbf{x}]$. We now want to extend Definition I.20 to the intuitive notion that some SOS certificates prove an algebraic set notion such as $Q_1 \cup Q_2 \subseteq \mathcal{P}_1 \cap \mathcal{P}_2$. The following properties systematise this idea.

[17] If it was, Eq. (I.27) would hold trivially.

Proposition I.21. *Let $\mathfrak{p}, \mathfrak{q}, \mathfrak{r} \in \mathbb{R}[\mathbf{x}]$; the following are sum-of-squares feasibility problems:*

1. *Solve $\mathfrak{s} \vdash \Omega_{\mathfrak{q}\leq 0} \subseteq_\Sigma \Omega_{\mathfrak{p}\leq 0}$;*
2. *Solve $\mathfrak{t} \vdash \mathcal{O}_{\mathfrak{r}=0} \subseteq_\Sigma \Omega_{\mathfrak{p}\leq 0}$;*
3. *Solve*

$$(\mathbf{s}_1, \mathbf{s}_2) \vdash Q_1 \cap Q_2 \subseteq_\Sigma \mathcal{P}_1 \tag{α}$$
$$(\mathbf{s}_1, \mathbf{s}_2) \vdash Q_1 \subseteq_\Sigma \mathcal{P}_1 \cap \mathcal{P}_2 \tag{β}$$
$$(\mathbf{s}_1, \mathbf{s}_2) \vdash Q_1 \cup Q_2 \subseteq_\Sigma \mathcal{P}_1 \tag{γ}$$

   for any $Q_1, Q_2, \mathcal{P}_1, \mathcal{P}_2 \subset \mathbb{R}^n$, if $\mathbf{s}_{1,2} \vdash Q_{1,2} \subseteq_\Sigma \mathcal{P}_1$ and $\mathbf{s}_{1,2} \vdash Q_1 \subseteq_\Sigma \mathcal{P}_{1,2}$, respectively, are SOS feasibility problems;

where the certificates are of bounded degree.

Proof. The first three statements follow directly from Definition I.20, Lemma I.19, and Eq. (I.24). Now, let $\mathbf{s}_{1,2} \vdash Q_1 \subseteq_\Sigma \mathcal{P}_{1,2}$ be feasibility problems; if they have solutions, by Lemma I.19, we have that $Q_1 \subseteq \mathcal{P}_1, \mathcal{P}_2$ and therefore, $Q_1 \subseteq \mathcal{P}_1 \cap \mathcal{P}_2$. Likewise, if $\mathbf{s}_{1,2} \vdash Q_{1,2} \subseteq_\Sigma \mathcal{P}_1$ have solutions, then $Q_1, Q_2 \subseteq \mathcal{P}_1$ and $Q_1 \cup Q_2 \subseteq \mathcal{P}_1$. □

We derive similar results for the quasi-convex sum-of-squares optimization. Here, we denote by $Q(a)$ a subset of $\mathbb{R}^n$ that is governed by a scalar $a \in \mathbb{R}$, e.g, $Q : a \mapsto \Omega_{\mathfrak{q}\leq a}$ with $\mathfrak{q} \in \mathbb{R}[\mathbf{x}]$.

Proposition I.22. *Let $p, q \in \mathbb{R}[x]$ and $I \subset \mathbb{R}$; the following are quasi-convex sum-of-squares problems:*

1. *Solve $\min_{a\in I} -a$ s. t. $\mathfrak{s} \vdash \Omega_{q\leq a} \subseteq_\Sigma \Omega_{p\leq 0}$;*
2. *Solve*

$$\min_{a\in I} -a \quad \text{s. t. } (\mathbf{s}, \mathbf{s}') \vdash Q_1(a) \cap Q' \subseteq_\Sigma \mathcal{P}_1 \tag{α}$$
$$\min_{a\in I} -a \quad \text{s. t. } (\mathbf{s}, \mathbf{s}') \vdash Q_1(a) \subseteq_\Sigma \mathcal{P}_1 \cap \mathcal{P}_2 \tag{β}$$
$$\min_{a\in I} -a \quad \text{s. t. } (\mathbf{s}_1, \mathbf{s}_2) \vdash Q_1(a) \cup Q_2(a) \subseteq_\Sigma \mathcal{P}_1 \tag{γ}$$

   for any $Q_1, Q_2 : \mathbb{R} \to 2^{\mathbb{R}^n}$, $Q', \mathcal{P}_1, \mathcal{P}_2 \subset \mathbb{R}^n$, if $\min_{a\in I} -a$ s. t. $\mathbf{s}_{1,2} \vdash Q_{1,2}(a) \subseteq_\Sigma \mathcal{P}_{1,2}$ are quasi-convex SOS problems and $\mathbf{s}' \vdash Q' \subseteq_\Sigma \mathcal{P}_{1,2}$ are SOS feasibility problems;

where the certificates are of bounded degree.

Proof. The first two statements follow directly from Definition I.20, Lemma I.19, and Eq. (I.25). Now, let $\min_{a\in I} -a$ s. t. $\mathbf{s}_{1,2} \vdash Q_1(a) \subseteq_\Sigma \mathcal{P}_{1,2}$ be quasi-convex problems with solutions $a_{1,2} \in I$; by Lemma I.19, we have that $Q_1(a_1) \subseteq \mathcal{P}_1, Q_1(a_2) \subseteq \mathcal{P}_2$, and therefore, $Q_1(\tilde{a}) \subseteq \mathcal{P}_1 \cap \mathcal{P}_2$ for $\tilde{a} = \min(a_1, a_2)$. Furthermore, if $\min_{a\in I} -a$ s. t. $\mathbf{s}_{1,2} \vdash Q_{1,2}(a) \subseteq_\Sigma \mathcal{P}_1$ have solutions $a_{1,2} \in I$, then $Q_1(a_1), Q_2(a_2) \subseteq \mathcal{P}_1$ and $Q_1(\tilde{a}) \cup Q_2(\tilde{a}) \subseteq \mathcal{P}_1$ for $\tilde{a} = \min(a_1, a_2)$. □

From here on, we will write "$\max a$" rather than "$\min -a$," as convenient.

Some concluding remarks: We might also write $\mathfrak{s} \vdash \forall \mathbf{x}.\, \mathfrak{q} \leq 0 \Rightarrow_\Sigma \mathfrak{p} \leq 0$ instead of the set-notation of Definition I.20. The special cases $(\cdot) \vdash \forall \mathbf{x}.\, \mathfrak{p} \leq 0$ and $\mathfrak{s} \vdash \nexists \mathbf{x}.\, \mathfrak{q} \leq 0$ can then be written as $(\cdot) \vdash \mathbb{R}^n \subseteq_\Sigma \Omega_{\mathfrak{p} \leq 0}$ and $\mathfrak{s} \vdash \Omega_{\mathfrak{q} \leq 0} \subseteq_\Sigma \varnothing$, respectively.

I.5 Region of Attraction Estimation

Backed by the theoretical results in real algebraic geometry of the previous section, sum-of-squares programming seems almost predestined for analysis – and certification – of stability by the theory of Lyapunov and La Salle. Notwithstanding, further applications include robustness (Chesi 2014, pp. 2815–2818), dissipativity (Ebenbauer and Allgöwer 2006, p. 1598), $\mathcal{L}_2$ gain and reachability (Anderson and Papachristodoulou 2012, pp. 1103–1106), attractive invariant set (Tan 2006, pp. 42–44), and control synthesis (Majumdar et al. 2013, pp. 4056–4058). The estimation of the region of attraction is a common application of sum-of-squares, yet it also belongs to the more difficult problems.

Global monotonicity Given a polynomial Lyapunov candidate-function $\mathfrak{V}$ and a system $\mathfrak{f}$ in the variables $\mathbf{x}$, we can check the conditions of Lyapunov's stability theorem for global stability by sum-of-squares decomposition (Parillo 2003, p. 299); namely, that the derivative $\nabla\mathfrak{V} \cdot \mathfrak{f}(\mathbf{x})$ is strictly monotonic around the equilibrium (here, without loss of generality, assumed to be the origin). As sum-of-squares are limited to semi-definiteness, we will require instead of strict negativeness,

$$\nabla\mathfrak{V} \cdot \mathfrak{f}(\mathbf{x}) + \epsilon \left\|\mathbf{x}\right\|_2^2 \leq 0 \tag{I.31}$$

with $\epsilon > 0$ small, which can be implemented as sum-of-squares feasibility problem. If $\mathfrak{V}$ is unknown but of bounded degree, we can furthermore search for a Lyapunov-function if we implement additionally $\mathfrak{V} - \epsilon\|\mathbf{x}\|_2^2 \in \Sigma\left[\mathbf{x}\right]$.

In the following, we denote the set of all $\mathbf{x} \in \mathbb{R}^n$ such that (I.31) holds by $\Omega_{\mathfrak{V},\mathfrak{f},\epsilon}$ for $\mathfrak{V} \in \mathbb{R}\left[\mathbf{x}\right]$, $\mathfrak{f} \in \mathbb{R}\left[\mathbf{x}\right]^n$, and $\epsilon > 0$.

Local monotonicity The problem of local negative monotonicity of a Lyapunov candidate-function can be reduced to semi-algebraic set-inclusion, namely,

$$\mathbf{s} \vdash \Phi \subseteq_\Sigma \Omega_{\mathfrak{V},\mathfrak{f},\epsilon}, \tag{I.32}$$

where Φ is given by (intersection of) polynomial inequalities, and searching for a suitable Lyapunov-function is likewise implemented as SOS feasibility problem, given that Φ is defined independently from $\mathfrak{V}$. This is in particular useful for local stability analysis (without any statement about the region of attraction) of a polynomial system, or global stability analysis of switching systems (Papachristodoulou and Prajna 2009, p. 1037).

If we want to find the *largest* level set of a given $\mathfrak{V}$ which is invariant, however, we have to relax (I.32) to the quasi-convex problem

$$\max \lambda \quad \mathfrak{s} \vdash \Omega_{\mathfrak{V} \leq \lambda} \subseteq_\Sigma \Omega_{\mathfrak{V},\mathfrak{f},\epsilon}. \tag{I.33}$$

The estimation of the region of attraction is commonly formulated as to find a Lyapunov function where the invariant set is as large as possible. This immediately raises the question: *When is the invariant set $\Omega_{\mathfrak{V}_1 \leq \lambda_1}$ larger than $\Omega_{\mathfrak{V}_2 \leq \lambda_2}$, or even larger as any other invariant set?* In Section I.3 we have already seen that the order defined by "$\subseteq$" is not total and that the largest invariant set is the one that includes any other; yet testing every Lyapunov candidate-function and any invariant set for inclusion surely is a tedious task. Instead, we are going to associate the size of an invariant set with an inscribing body, such as an ellipsoid, $\mathcal{E}$ of given shape $\mathfrak{p}$. The pseudo-radius ρ such that $\mathcal{E}$ inscribes $\Omega_{\mathfrak{V} \leq \lambda}$ can then be estimated as quasi-convex problem

$$\max \rho \quad \mathfrak{s}' \vdash \Omega_{\mathfrak{p} \leq \rho} \subseteq_\Sigma \Omega_{\mathfrak{V} \leq \lambda}. \tag{I.34}$$

Thus, we formulate the region-of-attraction estimation as the optimization problem (Topcu et al. 2008, p. 2670)

$$\max_{\substack{\mathfrak{V} \in \mathbb{R}[\mathbf{x}] \\ \rho, \lambda > 0}} \rho \quad \begin{cases} \mathfrak{V} - \epsilon \|\mathbf{x}\|_2^2 \in \Sigma[\mathbf{x}] \\ \mathfrak{s} \vdash \Omega_{\mathfrak{V} \leq \lambda} \subseteq_\Sigma \Omega_{\mathfrak{V}, \mathfrak{f}, \epsilon} \\ \mathfrak{s}' \vdash \Omega_{\mathfrak{p} \leq \rho} \subseteq_\Sigma \Omega_{\mathfrak{V} \leq \lambda} \end{cases} \tag{I.35}$$

for given $\mathfrak{p}$, $\mathfrak{f}$, and $\epsilon > 0$ small.[18] However, we cannot solve Eq. (I.35) directly as sum-of-squares problem, not even as quasi-convex problem, as it includes a polynomial term bilinear in $\mathfrak{V}$ and $\mathfrak{s}$. In order to address the problem of bilinearity, we will apply a bisection strategy that separates (I.35) in three distinctive steps, each involving a quasi-convex optimisation or feasibility problem. This procedure, typically called "$\mathfrak{V}$-$\mathfrak{s}$-iteration," is composed of the steps:

1. Find the largest invariant set of given a Lyapunov candidate-function $\mathfrak{V}$,

$$\lambda^* =_{\text{def}} \max \lambda \quad \mathfrak{s} \vdash \Omega_{\mathfrak{V} \leq \lambda} \subseteq_\Sigma \Omega_{\mathfrak{V}, \mathfrak{f}, \epsilon}, \tag{I.36}$$

   where $\mathfrak{s} \in \Sigma[\mathbf{x}]$ certifies that $\Omega_{\mathfrak{V} \leq \lambda^*}$ is an invariant set of $\mathfrak{f}$;

2. Find the largest ellipsoid $\mathcal{E}$ of given shape $\mathfrak{p}$ that inscribes this invariant set,

$$\rho^* =_{\text{def}} \max \rho \quad \mathfrak{s}' \vdash \Omega_{\mathfrak{p} \leq \rho} \subseteq_\Sigma \Omega_{\mathfrak{V} \leq \lambda^*}, \tag{I.37}$$

   where $\mathfrak{s}' \in \Sigma[\mathbf{x}]$ certifies that $\Omega_{\mathfrak{p} \leq \rho^*}$ lies within the stable levet-set;

3. Find a polynomial Lyapunov function of given degree that is positive definite and subject to the results and certificates of the two preceding steps,

$$\mathfrak{V}^* =_{\text{def}} \arg \quad \begin{cases} \mathfrak{V} - \epsilon \|\mathbf{x}\|_2^2 \in \Sigma[\mathbf{x}] \\ \mathfrak{s} \vdash \Omega_{\mathfrak{V} \leq \lambda^*} \subseteq_\Sigma \Omega_{\mathfrak{V}, \mathfrak{f}, \epsilon} \\ \mathfrak{s}' \vdash \Omega_{\mathfrak{p} \leq \rho^*} \subseteq_\Sigma \Omega_{\mathfrak{V} \leq \lambda^*} \end{cases} \tag{I.38}$$

[18] The ϵ-terms enforcing positive-definiteness and negative monotonicity of $\mathfrak{V}$ are not necessarily equal, nor do they have to be quadratic. Any two positive definite polynomials $\mathfrak{l}_1, \mathfrak{l}_2$ do the job (see also Topcu et al. 2008, p. 2670).

where $\mathfrak{s}, \mathfrak{s}'$, hold fixed, certify that $\Omega_{\mathfrak{V}^* \leq \lambda^*}$ is indeed both invariant and inscribed by $\mathcal{E}$.

The result of the last step, $\mathfrak{V}^*$, can subsequently be used as candidate for the first step and the procedure is repeated until, e.g., the estimated region of attraction is of adequate size, the pseudo-radius of the ellipsoid $\mathcal{E}$ is non-increasing, or a certain number of iterations is exceeded.

It is worth noting that the last step of the $\mathfrak{V}$-$\mathfrak{s}$-iteration does not necessarily lead to a further increase of the estimated region of attraction; indeed, the previous Lyapunov function-candidate does already solve Eq. (I.38). In practice however, due to trivia of the underlying solvers, the last step usually returns a different $\mathfrak{V}^*$ that allows for an enlarged invariant set (Chakraborty et al. 2011a, p. 340).

The $\mathfrak{V}$-$\mathfrak{s}$-iteration as presented here is by far the only strategy for a region-of-attraction estimation using sum-of-squares polynomials. Topcu et al. 2008, for example, used simulation data to a priori estimate the stable region of a given system and obtain a convex set of Lyapunov candidate-functions. The problem of unfortunate selected ellipsoidal shapes was addressed by Khodadadi et al. 2014, who proposed an adaptation step to update and improve the "direction" of the subsequent search. Other authors removed the necessity of an ellipsoidal shape function and the quasi-convex optimisation steps entirely, simply restricting the result of the feasibility step to have an invariant 1-level set that includes the previous estimate in its interior (Zheng et al. 2018). The quasi-convex optimisation problems in Eqs. (I.36) and (I.37) may also be replaced by further bisection, namely by sum-of-squares optimisation problems in $\lambda, \rho > 0$ for given $\mathfrak{s}, \mathfrak{s}'$ and feasibility problems in $\mathfrak{s}, \mathfrak{s}' \in \Sigma[\mathbf{x}]$ for given λ, ρ, respectively. While this may reduce the computation time, it inevitably results in further sub-optimality of the resulting region-of-attraction estimate.

Chapter 3

Piecewise Modeling of Aircraft Dynamics

This chapter is an exact copy of:

> Torbjørn Cunis et al. (2019). "Piecewise Polynomial Modeling for Control and Analysis of Aircraft Dynamics beyond Stall". In: *Journal of Guidance, Control, and Dynamics* 42.4, pp. 949–957. DOI: 10.2514/1.G003618. (published online December 2018)

in the authors' accepted version.

Synopsis

We will show that, beyond stall, simple polynomial models of the aircraft dynamics which are available in the literature, fail to represent full-envelope aerodynamics accurately. Functional analysis methods such as bifurcation analysis and sum-of-squares programming, however, are computationally heavy for advanced fitting methods such as multi-variate splines. We therefore propose a new method of fitting polynomial piecewise for low and high angles of attack (i.e., beyond stall). This chapter presents the theoretical background of piecewise polynomial fitting using linear least-square optimisation. We further illustrate how to apply continuation analysis and sum-of-squares region of attraction analysis for this kind of piecewise systems and present preliminary results for the GTM longitudinal equations of motion. This proves the proposed piecewise modeling technique to be both accurate in fitting the full-envelope aerodynamic coefficients and trim conditions of the GTM as well as applicable to functional analysis. Therefore, we will continue in using *piecewise polynomial modeling* for the aircraft dynamics in all subsequent chapters of this thesis. Details on the implementation can be found in Appendix A; the piecewise polynomial aircraft model is detailed in Appendix B.1.

Statement of Contribution Torbjørn Cunis developed and implemented the presented modeling and analysis. Jean-Philippe Condomines contributed to the introduction. Both Jean-Philippe Condomines and Laurent Burlion provided supervision and feedback during the initial submission and following revisions until final acceptance.

Piecewise Polynomial Modeling for Control and Analysis of Aircraft Dynamics beyond Stall

Torbjørn Cunis* and Laurent Burlion†
ONERA – The French Aerospace Lab, Centre Midi-Pyrénées, Toulouse, 31055, France

Jean-Philippe Condomines‡
French Civil Aviation School, Toulouse, 31055, France

Nomenclature

α_0 = Low-angle of attack boundary (°);

ρ = Pseudo-radius ($\rho \in \mathbb{R}$);

$\varphi(\cdot)$ = Boundary condition function ($\varphi\colon \mathbb{R}^m \to \mathbb{R}$);

Σ = Positive-definite shape factor ($\Sigma \in \mathbb{R}^{n\times n}$);

Ω_φ = Boundary curve set ($\Omega_\phi \subset \mathbb{R}^m$);

$C_{\mathrm{l,m,n}}$ = Aerodynamic coefficients of moments in body axes (·);

$C_{\mathrm{X,Y,Z}}$ = Aerodynamic coefficients of forces in body axes (·);

$\mathbf{C}$ = Objective matrix ($\mathbf{C} \in \mathbb{R}^{k\times r}$);

$\mathbf{d}$ = Vector of measurements ($\mathbf{d} \in \mathbb{R}^k$);

$\mathbf{f}(\cdot)$ = Non-linear, open-loop system dynamics ($\mathbf{f}\colon (\mathbf{X}, \cdot) \mapsto \dot{\mathbf{X}}$);

$g(\cdot), h(\cdot)$ = Positive-semi-definite Lagrange multiplier ($g, h\colon \mathbb{R}^n \to \mathbb{R}_{\geq 0}$);

k = Number of measurements;

m = Number of variables;

n = Number of states; system degree; polynomial degree;

$\mathbf{q}$ = Vector of coefficients ($\mathbf{q} \in \mathbb{R}^r$);

r = Number of coefficients;

*Doctoral Researcher, Department of Information Processing and Systems, e-mail: torbjoern.cunis@onera.fr; associated researcher with the French Civil Aviation School, Drones Research Group; AIAA Student Member.
†Research Scientist, Department of Information Processing and Systems, e-mail: laurent.burlion@onera.fr.
‡Assistant Professor, Drones Research Group, e-mail: jean-philippe.condomines@enac.fr.

$\mathbf{X}^*, \boldsymbol{\mu}^*$ = States and parameters at trim condition;

$(\cdot)^{post}$ = Domain of high angle of attack;

$(\cdot)^{pre}$ = Domain of low angle of attack;

$\mathcal{X}$ = State space ($\mathcal{X} \subseteq \mathbb{R}^n$);

$\partial\mathcal{X}$ = Set boundary of $\mathcal{X}$.

I. Introduction

Full-envelope aircraft models require extensive effort to represent the aerodynamic coefficients well in the entire region of the envelope as flight dynamics beyond stall are highly non-linear and often unstable [1, 2]. With upset recovery approaches found in the literature being model-based ([3–5], and references herein) there is a clear need for reliable full-envelope models of flight dynamics. NASA's *Generic Transport Model* (GTM) has contributed significantly to analysis and control approaches of civil and unmanned aircraft over the entire flight envelope (see, e.g., [6, 7]). Representing a 5.5 % down-scaled typical aerial transport vehicle, the GTM provides exhaustive, full-envelope aerodynamic data from wind-tunnel studies [8] and its open-source aerodynamic model for MATLAB/Simulink [9] has given access for development of modeling, analysis, and control methods to the aerospace community. An overview of research studies on longitudinal trim conditions, regions of attraction, and upset situations can be found in [2, 5, 10, 11]. However, analytical representations proposed for the full-envelope aerodynamics are still insufficient for non-linear analysis and control design [12]. Therefore, improved methods for accurate modeling are imperative, in particular when developing robust and powerful advanced control strategies for upset recovery. Subsequently, model feedback designs based on full-envelope aerodynamic models will grant full authority and control efficiency for stability and performances in unmanned aircraft (UA) [13].

Polynomial models of the aerodynamic coefficients have provided a constructive method to define and evaluate models based on analytical computation due to their continuous and differentiable nature. Despite the fact that polynomial models have been published recently [10, 11], none of the results represent the aerodynamic coefficients well in the entire region of the envelope [12]. Indeed, at the stall angle of attack, the laminar flow around the wings in the pre-stall region changes to turbulent flow and remains so in post-stall. This significant change of the flow dynamics motivates a piecewise model of the pre-stall and post-stall dynamics instead.

Piecewise regression theory can be dated to the 1970s; first research focused on regression of a few polynomial functions piecewise over the observations. However, the estimation of suitable switching surfaces

or *joints* for the piecewise functions usually adds computational difficulty and load [14–17]. Later, *multivariate splines* were introduced [18, 19]; using simplices and baryocentric coordinates for the base, the so-called B-splines bear the advantage of generalized continuity, dimensional flexibility, and efficient evaluation as well as a stable local basis [20]. Recently, a further approach combining splines with fuzzy logic has been presented in [21].

While splines today present a powerful yet complex tool for accurate and smooth interpolation, they lack an underlying physical model justifying the partition. Moreover, for functional analysis of trim conditions and stable sets, as in [10, 11], splines weren't used but polynomials. Motivated by the practical problems encountered with mini-UAs flight control and guidance, civil aircraft fault detection and isolation, and upset recovery, we aim to derive a simple yet powerful aerodynamic model still suitable for functional analysis. A novel approach for piecewise polynomial modeling aerodynamic coefficients, the `pwpfit` toolbox for MATLAB, was recently proposed in [22]. Here, we have proven feasibility of fitting both a piecewise polynomial model and its joint surface using *linear least-square* (LSQ) optimization techniques. While this approach is limited to a single joint without differential continuity, the switch in the dynamics is motivated by the change from laminar to turbulent flow at stall and the resulting model is found to fit the full-envelope aerodynamics well.

This article focuses on the recent research detailing the theoretical aspects in the sequel and their application to functional analysis. The main contributions of this paper are therefore: to address (in §II) a concise bibliographical review of the polynomial based-methods used for full-envelope identification; to introduce (in §III) a novel and generic formulation of the piecewise polynomial fitting method which approximates a piecewise polynomial function and its joint; to provide (in §IV) a six-degrees-of-freedom model of an aircraft and its aerodynamic coefficients, accounting for both pre-stall and post-stall characteristics by piecewise identification; and finally to demonstrate and assess the extension of functional analysis tools for the piecewise polynomial model (in §V).

II. State of the Art

A. Polynomial regression

Polynomial regression is a general approach similar to linear curve regression, where a polynomial function f is to be found in order to approximate best a set of measured data points. Here, the coefficients of f are subject to the optimality problem of minimal sum of squared residuals of f with respect to the measurements (*goodness of fit*, GoF). The formulation of optimal coefficients as a linear least-square problem dates back to Legendre (1805) and Gauss (1809); a first application can be found by Gergonne in 1815 [23]. It has been shown that on average, the residuals of such an optimal polynomial vanish and their deviation is

minimized [24]. Furthermore, polynomial functions are defined by basic mathematical operations of addition and multiplication and thus provide by their nature smoothness to infinite differentiation. Recent polynomial models of the full-envelope aerodynamic coefficients of the GTM have been presented in [10, 11].

B. Multi-variate splines

Splines are piecewise sequences of polynomial functions, where each polynomial is active only in the respective partition. These partitions are chosen before fitting instead of being subject of the fit. The polynomials sub-functions are computed such that at the boundaries of the selected partitions the overall spline function is smooth to a certain degree of continuity. Thus, spline functions show characteristics of both lookup tables and polynomials, as noted by de Visser et al. [18, p. 3]:

> Effectively, spline functions [...] combine the global nonlinear modeling capability of lookup tables with the analytic, continuous nature of polynomials.

While for a single-variable spline function, the boundaries equal point-wise joints, the partitions of multi-variate splines can be more complex. In addition to simple rectangles (or rather rectangular polytopes), triangular partitions have recently proposed by [20]. However, the high accuracy of splines in terms of their residuals is opposed by their computational costs for further analytical investigation. Multi-variate splines have been used in, among others, [18, 19] in order to model full-envelope aerodynamics.

III. Methodology

In vector notation, optimal coefficients for piecewise polynomial fits are expressed as linear least-squares. We introduce a polynomial notation by the vectors of monomials and coefficients and thus reduce the goodness of fit to a function of the latter. The joint will be given by the scalar field $\varphi(\cdot)$ in the variables of the model and the scalar bound x_0; here, we assume φ to be linear matrix inequality and x_0 will be determined by the fitting. The resulting model then has a single joint with value continuity, i.e., the model is not differentiable at the joint. For models in several variables and outputs, such as the aerodynamic coefficients, it is desirable to have further constraints to the fit enforced. We will add those desired properties of the piecewise fit as constraint matrices.

Definition 1 A *linear least-square* (LSQ) problem is given as the optimization problem

$$\mathrm{lsq}(\mathbf{C}, \mathbf{d}, \mathbf{A}, \mathbf{0}) = \arg\min_{\mathbf{q} \in \Omega_{\mathbf{A}}} \|\mathbf{C}\mathbf{q} - \mathbf{d}\|_2^2 \,. \tag{1}$$

with $\mathbf{q} \in \mathbb{R}^r$, $\mathbf{C} \in \mathbb{R}^{k \times r}$, $\mathbf{d} \in \mathbb{R}^k$, and $\Omega_{\mathbf{A}} = \{\mathbf{q} \,|\mathbf{A}\mathbf{q} = \mathbf{0}\}$ for a constraint matrix $\mathbf{A}$.

A. Polynomials

A *monomial of degree* n is a single product of powers where the exponents add up to the total degree n, without any scalar coefficient. We notate a monomial of $\mathbf{x} = (x_1, \ldots, x_m)$ in degrees $\mathbf{n} = (n_1, \ldots, n_m)$ as

$$\mathbf{x}^{\mathbf{n}} = x_1^{n_1} \ldots x_m^{n_m}, \tag{2}$$

where $\mathbf{x}^{\mathbf{n}}$ has the total degree $n = \|\mathbf{n}\|_1 = n_1 + \cdots + n_m$.

Definition 2 $\boldsymbol{\mathcal{P}}_n(\mathbf{x})$ is the *vector of monomials* $\mathbf{x}^{\boldsymbol{\nu}}$ in variables $\mathbf{x} = (x_1, \ldots, x_m)$ with degrees $\boldsymbol{\nu} \in \mathbb{N}^m$ and total degrees $\|\boldsymbol{\nu}\|_1 \leq n$; and the number of elements in $\boldsymbol{\mathcal{P}}_n(\mathbf{x})$ is denoted by $\mathfrak{r}[n]$, i.e., $\boldsymbol{\mathcal{P}}_n \in \mathbb{R}\,[\mathbf{x}]^{\mathfrak{r}[n]}$.

By this notation, a polynomial f is expressed as scalar product of its monomials and coefficients,

$$f(\mathbf{x}) = \langle \boldsymbol{\mathcal{P}}_n(\mathbf{x}), \mathbf{q} \rangle \tag{3}$$

with the *vector of coefficients* $\mathbf{q} \in \mathbb{R}^{\mathfrak{r}[n]}$.

B. Piecewise polynomial fitting

Consider the k observations $(\mathbf{x}_i, z_i)_i$ given as sequences over $i \in [1, k]$:

$$z_i = \gamma(\mathbf{x}_i) + \epsilon_i, \tag{4}$$

where $(\mathbf{x}_i, z_i, \epsilon_i)_{1 \leq i \leq k} \subset \mathbb{R}^m \times \mathbb{R} \times \mathbb{R}$ and $\gamma(\cdot)$ and $(\epsilon_i)_i$ are an unknown function and measurement error, respectively; we will find coefficients $\mathbf{q}_1, \mathbf{q}_2$ as well as a scalar $x_0 \in \mathbb{R}$ such that

$$f : \mathbf{x} \longmapsto \begin{cases} \langle \boldsymbol{\mathcal{P}}_n(\mathbf{x}), \mathbf{q}_1 \rangle & \text{if } \varphi(\mathbf{x}) \leq x_0; \\ \\ \langle \boldsymbol{\mathcal{P}}_n(\mathbf{x}), \mathbf{q}_2 \rangle & \text{else;} \end{cases}$$

with $\varphi : \mathbb{R}^m \to \mathbb{R}$ minimizes the sum of squared residuals

$$\mathrm{GoF}(f) =_{\mathrm{def}} \sum_{i=1}^{k} |f(\mathbf{x}_i) - z_i|^2 \tag{5}$$

for an $n > 0$. We note the sub-polynomials of f by $f_{1,2} : \mathcal{X}_{1,2} \to \mathbb{R}, \mathbf{x} \mapsto \langle \boldsymbol{\mathcal{P}}_n(\mathbf{x}), \mathbf{q}_{1,2} \rangle$ with $\mathcal{X}_1 \cap \mathcal{X}_2 = \varnothing$ and call $\mathcal{X}_1 \cup \mathcal{X}_2$ the *entire domain of* f. The *joint* of f is given by $\Omega_\varphi =_{\mathrm{def}} \partial\mathcal{X}_1 \cap \partial\mathcal{X}_2 = \{\mathbf{x} \,|\varphi(\mathbf{x}) = x_0\}$; if $\varphi(\cdot)$ is a linear matrix inequality, the boundary is convex. Re-writing the goodness of fit using matrix calculus, we reduce the cost functional to a cost function and polynomial data fitting to a linear least-square problem.

The cost functional for f can be evaluated piecewise to

$$\mathrm{GoF}(f) = \sum_{\mathbf{x}_i \in X_1} |f_1(\mathbf{x}_i) - z_i|^2 + \sum_{\mathbf{x}_i \in X_2} |f_2(\mathbf{x}_i) - z_i|^2 \tag{6}$$

with $X_1 = \{\mathbf{x}_1, \ldots, \mathbf{x}_{i'}\}$, $X_2 = \{\mathbf{x}_{i'+1}, \ldots, \mathbf{x}_k\}$ chosen a priori. As f_1, f_2 are scalar products, we re-write (6) to the cost function

$$\mathrm{GoF}(\mathbf{q}_1, \mathbf{q}_2) = \|\mathbf{C}_1\mathbf{q}_1 - \mathbf{d}_1\|^2 + \|\mathbf{C}_2\mathbf{q}_2 - \mathbf{d}_2\|^2 \tag{7}$$

where $\mathbf{C}_{1,2}$ are the monomials of $\boldsymbol{\mathcal{P}}_n(\cdot)$ evaluated in the observations of X_1 and X_2, respectively, and $\mathbf{d}_{1,2}$ are the vectors $\mathbf{d}_1 = \begin{bmatrix} z_1 & \cdots & z_{i'} \end{bmatrix}^T$, $\mathbf{d}_2 = \begin{bmatrix} z_{i'+1} & \cdots & z_k \end{bmatrix}^T$. The optimal coefficients are now subject to the unconstrained ($\mathbf{A} = \mathbf{0}$) linear-least square problem

$$\begin{bmatrix} \mathbf{q}_1 \\ \hdashline \mathbf{q}_2 \end{bmatrix} = \arg\min_{\mathbf{q}'} \left\| \left[\begin{array}{c:c} \mathbf{C}_1 & \mathbf{0} \\ \hdashline \mathbf{0} & \mathbf{C}_2 \end{array}\right] \mathbf{q}' - \begin{bmatrix} \mathbf{d}_1 \\ \hdashline \mathbf{d}_2 \end{bmatrix} \right\|_2^2 . \tag{8}$$

Here, continuity of the piecewise defined f over its entire domain holds if

$$\langle \boldsymbol{\mathcal{P}}_n(\mathbf{x}), \mathbf{q}_1 \rangle = \langle \boldsymbol{\mathcal{P}}_n(\mathbf{x}), \mathbf{q}_2 \rangle \tag{9}$$

for all $\mathbf{x} \in \Omega_\varphi$. For single-variate functions, we have value continuity for the identity function $\varphi = \mathrm{id}$ and x_0 is zero of

$$\langle \boldsymbol{\mathcal{P}}_n(x), \mathbf{q}_1 - \mathbf{q}_2 \rangle.$$

In this scheme, the observations still need to be split into X_1 and X_2 initially; however, this leaves the actual joint to be free. As the observations form a discrete set, an optimization approach over $X_{1,2}$ would be fair and just, thus yielding an ideal model. With piecewise polynomial fitting keeping most properties of polynomial regression, it has been proven numerically in [22] that the inaccuracy of a fitted erroneous signal is reduced: given data pairs $(x_i, z_i)_i$ by (4) with $\epsilon \sim \mathcal{N}(0, \sigma)$ and a piecewise fit f, the standard deviation of f to the true values, $\gamma(x) - f(x)$, is smaller than the measurement error σ.

C. Constraint matrices

As the coefficients define a polynomial uniquely, we can restrict the coefficients (i.e., the polynomials) by constraint matrices:

Proposition 1 (Constraint of continuity [22]) *Let* $\varphi(\mathbf{x}) = \mathbf{a}^T\mathbf{x} \leq x_0$ *be a linear matrix inequality (LMI) with* $\mathbf{a}^T = \begin{bmatrix} a_1 & \cdots & a_m \end{bmatrix}$ *and* $a_1 \neq 0$*; a piecewise polynomial function* f *with continuity in* Ω_φ *is subject to the constrained LSQ problem given by the continuity constraint matrix* $\boldsymbol{C}$*, i.e.,*

$$\boldsymbol{C}\begin{bmatrix} \mathbf{q}_1 \\ \\ \mathbf{q}_2 \end{bmatrix} = 0 \iff \forall \mathbf{x} \in \Omega_\varphi. \quad \langle \boldsymbol{\mathcal{P}}_n(\mathbf{x}), \mathbf{q}_1 \rangle = \langle \boldsymbol{\mathcal{P}}_n(\mathbf{x}), \mathbf{q}_2 \rangle. \tag{10}$$

The constraint matrix $\boldsymbol{C}$ is constructed by separation of the constrained variables into $\boldsymbol{\Lambda}_0$ such that

$$\langle \boldsymbol{\mathcal{P}}_n(\mathbf{x}_0), \mathbf{q}_{1,2} \rangle = \langle \boldsymbol{\mathcal{P}}_n(\tilde{\mathbf{x}}), \boldsymbol{\Lambda}_0\mathbf{q}_{1,2} \rangle \tag{11}$$

for all $\mathbf{x}_0 \in \left\{ \mathbf{x} \middle| \mathbf{a}^T\mathbf{x} = x_0 \right\}$, where $\tilde{\mathbf{x}}$ are the remaining free variables; we then have that

$$\langle \boldsymbol{\mathcal{P}}_n(\tilde{\mathbf{x}}), \boldsymbol{\Lambda}_0\mathbf{q}_1 \rangle = \langle \boldsymbol{\mathcal{P}}_n(\tilde{\mathbf{x}}), \boldsymbol{\Lambda}_0\mathbf{q}_2 \rangle$$

for all $\tilde{\mathbf{x}} \in \mathbb{R}^{m-1}$ if and only if $\boldsymbol{\Lambda}_0\mathbf{q}_1 = \boldsymbol{\Lambda}_0\mathbf{q}_2$ and hence, Equation (10) holds for $\boldsymbol{C} = \begin{bmatrix} \boldsymbol{\Lambda}_0 & -\boldsymbol{\Lambda}_0 \end{bmatrix}$.

Due to measurement errors or modelling flaws, a polynomial fitting may have relations that either do not exist or shall not be modeled; e.g., for a symmetric aircraft aligned to the flow, there is no side-force—regardless its angle of attack. In this case, it is desirable to constrain the resulting polynomial to be zero (or constant) for certain parameters $\tilde{\mathbf{x}}' = \left(x_{j+1}, \cdots, x_m\right)$:

Proposition 2 (Zero constraint [22]) *Let* $\mathbf{x}' = \left(x_1, \ldots, x_j\right)$ *for* $j > 0$*; a polynomial* $f = \langle \boldsymbol{\mathcal{P}}_n(\mathbf{x}), \mathbf{q} \rangle$ *with*

$$\forall \mathbf{x}' \in \mathbb{R}^j. \quad \langle \boldsymbol{\mathcal{P}}_n\left(\mathbf{x}', \mathbf{0}_{m-j}\right), \mathbf{q} \rangle = 0 \tag{12}$$

and $\mathbf{0}_{m-j} \in \{0\}^{m-j}$ *is subject to the constrained LSQ problem given by the zero constraint matrix* $\boldsymbol{\mathcal{Z}}$*.*

D. Implementation

The approach of piecewise polynomial fitting has two major modes, namely either the joint condition is a result of fitting or the joint is chosen a priori; that is, without or with a given constraint of continuity, respectively. The main steps for both modes are illustrated by the flow chart in Fig. 1, given the split sets of parameters, $X_1 = \{\mathbf{x}_1, \ldots, \mathbf{x}_{i'}\}, X_2 = \{\mathbf{x}_{i'+1}, \ldots, \mathbf{x}_k\}$ and the corresponding observations $Z = \{z_1, \ldots, z_k\}$. Preliminary to the implementation of objective and constraints matrices, we have the computation of the monomials in $\mathbf{x}$. While the order of monomials is arbitrary for fitting, we introduce here the following convention: for $\boldsymbol{\nu}, \boldsymbol{\mu} \in \mathbb{N}^m$, the monomial $\mathbf{x}^{\boldsymbol{\nu}}$ precedes $\mathbf{x}^{\boldsymbol{\mu}}$ as element of $\boldsymbol{\mathcal{P}}_n(\mathbf{x})$ if and only if $\|\boldsymbol{\nu}\|_1 < \|\boldsymbol{\mu}\|_1$ or the first non-zero element of $(\boldsymbol{\nu} - \boldsymbol{\mu})$ is positive and $\|\boldsymbol{\nu}\|_1 = \|\boldsymbol{\mu}\|_1$. In consequence, the vector of monomials breaks up into blocks of monomials $\mathbf{x}^{\mathbf{n}}$ of equal total degree $\|\mathbf{n}\|_1 = N$, denoted by $\mathbf{p}_N \in \mathbb{R}\,[\mathbf{x}]^{\mathrm{r}[N]}$, and $N \in [0; n]$ ascending. The vector of monomials can be computed recursively for a given $\mathbf{x} \in \mathbb{R}^m$ by [22, Alg. 1]. The objective matrices $\mathbf{C}_1, \mathbf{C}_2, \mathbf{d}$ of Eq. (7) can directly be computed with the elements of X_1, X_2, and Z. Without constraints, the output coefficients $\mathbf{q}_1, \mathbf{q}_2$ are subject to the unconstrained LSQ problem of (8).

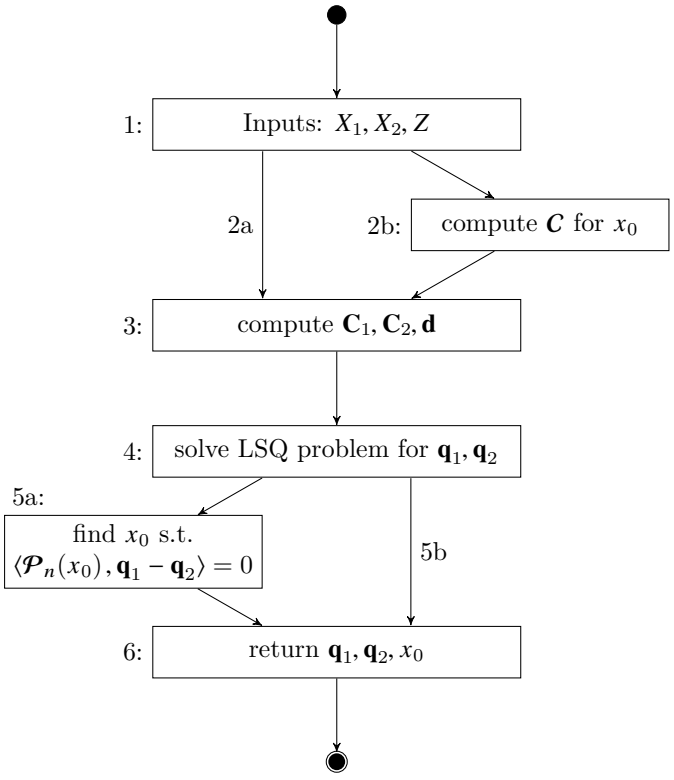

Fig. 1 Flow chart for the piecewise polynomial fitting approach: a) without continuity constraint; b) with continuity constraint in x_0.

With the definition $\mathcal{P}_n = \begin{bmatrix} \mathbf{p}_0(\mathbf{x}) & \cdots & \mathbf{p}_N(\mathbf{x}) \end{bmatrix}$, the continuity constraint matrix $\boldsymbol{C}$ is derived from (11) by linear separation of each block. If the linear matrix inequality $\mathbf{a}^T\mathbf{x} \leq x_0$ of Proposition 1 is given with a single non-zero element of $\mathbf{a}$ – suppose, $a_1 \neq 0$ –, separation of the assigned variable $x_1 \equiv x_0$ yields

$$\mathbf{p}_N(x_0, \tilde{\mathbf{x}}) = \boldsymbol{\lambda}_N(x_0)^T \, \mathbf{p}_N(\tilde{\mathbf{x}})$$

with $\tilde{\mathbf{x}} \in \mathbb{R}^{m-1}$ and $\boldsymbol{\lambda}_N = \operatorname{diag} \mathbf{p}_N(x_0, \mathbf{1}_{m-1})$ for $\mathbf{1}_{m-1} \in \{1\}^{m-1}$. The following algorithm combines $\boldsymbol{\lambda}_0, \boldsymbol{\lambda}_1, \ldots, \boldsymbol{\lambda}_n$ into the matrix $\boldsymbol{\Lambda}_0 \sim$ `Aeq`: [22, Alg. 2]

```
1: one = num2cell(ones(1,m-1));
2: j = 0;
3: for N=0:n
   % let pN:=pN(·); rN:=r[N]
4:    pNx0 = double(pN(x0,one{:}));
5:    Aeq(1:rN,j+(1:rN)) = diag(pNx0);
6:    j = j + rN;
7: end
```

and $\boldsymbol{C} = \begin{bmatrix} \boldsymbol{\Lambda}_0 & -\boldsymbol{\Lambda}_0 \end{bmatrix}$. For $\mathbf{a}^T\mathbf{x} \neq x_1$, there is an invertible $\boldsymbol{\pi} \colon \mathbb{R}^m \to \mathbb{R}^m$ with $\mathbf{a}^T\boldsymbol{\pi}(\mathbf{y}) = y_1$ for $\mathbf{y} = (y_1, \ldots, y_m)$ [22, Lemma 7] and we thus fit polynomials $g_{1,2}$ with continuity constraint in $y_1 \equiv x_0$, resulting in

$$f_1 = \left(g_1 \circ \boldsymbol{\pi}^{-1}\right); \qquad f_2 = \left(g_2 \circ \boldsymbol{\pi}^{-1}\right).$$

The computation of the zero constraint is not illustrated in Fig. 1 but is given, regardless the constraint of continuity, by [22, Alg. 3] and precedes the solution of the LSQ problem. However, if both zero constraint and constraint of continuity are given, we need to ensure full rank of the complete constraint matrix,

$$\begin{bmatrix} \boldsymbol{C} \\ \mathcal{Z} \end{bmatrix} \mathbf{q}' = \mathbf{0}.$$

IV. Piecewise, Full-envelope Aircraft Model

Modeling the aerodynamic coefficients of the GTM piecewise around the stall angle of attack, results in the six-degrees-of-freedom equations of motion

$$\mathbf{f}\colon (\mathbf{X},\mathbf{U}) \longmapsto \dot{\mathbf{X}} = \begin{cases} \mathbf{f}^{pre}(\mathbf{X},\mathbf{U}) & \text{if } \alpha \le \alpha_0; \\ \mathbf{f}^{post}(\mathbf{X},\mathbf{U}) & \text{else;} \end{cases} \tag{13}$$

where $\mathbf{X}$ and $\mathbf{U}$ denote the state and input vectors

$$\mathbf{X} = \begin{bmatrix} V & \alpha & \beta & \mu & \gamma & \chi & p & q & r & \Phi & \Theta & \Psi \end{bmatrix}^T$$

and $\mathbf{U} = \begin{bmatrix} \xi & \eta & \zeta & F \end{bmatrix}^T$. Here, the angles of aerodynamics (α, β), air-path (μ, γ, χ), and attitude (Φ, Θ, Ψ) are defined by the axis systems of ISO 1151-1 (Fig. 2): the *body axis system* $\left(x_f, y_f, z_f\right)$ aligned with the aircraft's fuselage; the *air-path axis system* $\left(x_a, y_a, z_a\right)$ defined by the velocity vector; and the *normal earth-fixed axis system* $\left(x_g, y_g, z_g\right)$. The air speed V is the aircraft's absolute velocity relative to the air and the body rates (p, q, r) are defined around the body axes; as usual, the control inputs are aileron, elevator, and rudder deflections ξ, η, ζ, respectively, and the thrust F.

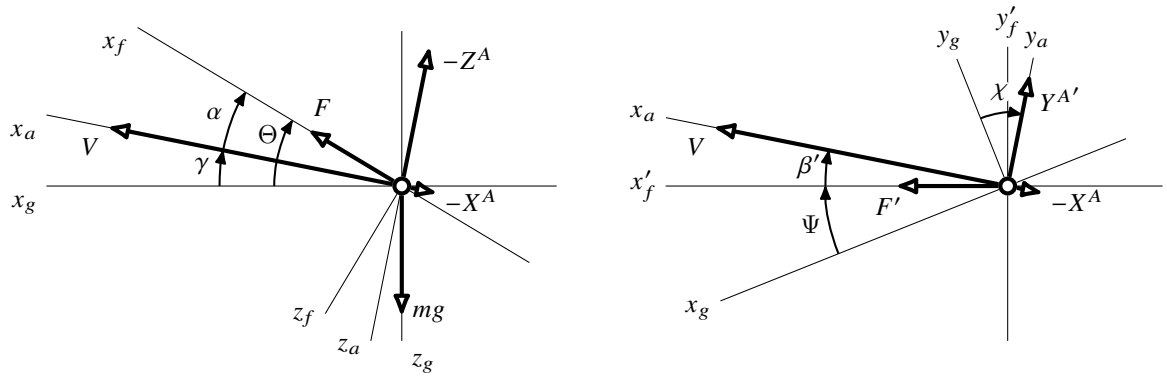

(a) Longitudinal axes ($\beta = \mu = 0$). **(b) Horizontal axes ($\gamma = 0$).**

Fig. 2 Axis systems with angles and vectors (projections into the plane are marked by $'$).

A. Equations of motion

A non-linear system of equations of motion for the six-degrees-of-freedom aircraft model of the GTM has been proposed in [25]. Here, the changes of air speed V, side-slip β, inclination γ, and azimuth χ are subject to lift, drag, thrust, and side-force (given by the aerodynamic force coefficients $C_{\mathrm{X}}, C_{\mathrm{Y}}, C_{\mathrm{Z}}$ and the thrust input F); the changes of angular body rates $\dot{p}, \dot{q}, \dot{r}$ are given by the aerodynamic moment coefficients $C_{\mathrm{l}}, C_{\mathrm{m}}, C_{\mathrm{n}}$; and the changes of attitude Φ, Θ, Ψ are functions of the angular body rates.

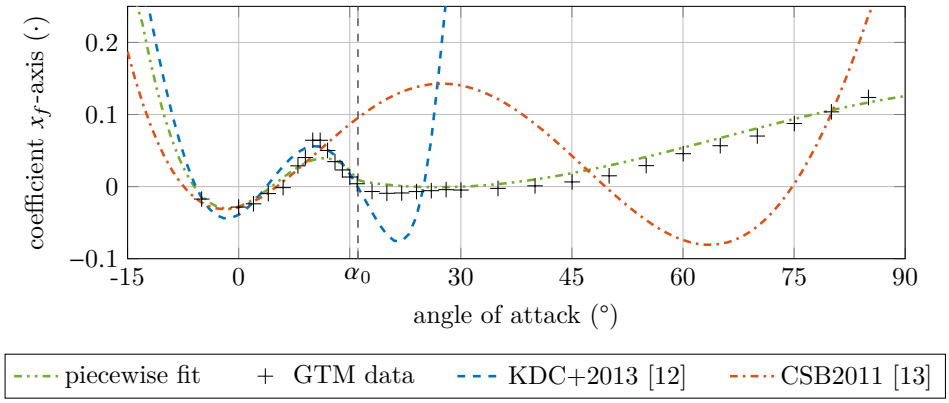

Fig. 3 Comparison of 3rd-order polynomial [10, 11] and piecewise identifications. [12]

B. Aerodynamic coefficients

The aerodynamic coefficients of the GTM are measured by its angle of attack, side-slip angle, surface deflections, and normalized body rates. [9] The measurements are given by the unknown function $\Gamma(\cdot)$:

$$\mathbf{C}_i = \Gamma(\alpha_i, \beta_i, \xi_i, \eta_i, \zeta_i, \hat{p}_i, \hat{q}_i, \hat{r}_i) + \boldsymbol{\epsilon}_i \tag{14}$$

for $i \in [1, k]$ and $\mathbf{C}_i = (C_{\mathrm{X},i}, C_{\mathrm{Y},i}, C_{\mathrm{Z},i}, C_{\mathrm{l},i}, C_{\mathrm{m},i}, C_{\mathrm{n},i})$ with $\boldsymbol{\epsilon}_i$ an unknown measurement error. Here, simple polynomial models are unsuitable to represent the full-envelope aerodynamics (Fig. 3; see also [12]). Instead, we will fit the pre-stall and post-stall dynamics piecewise to $(\mathbf{C}_i)_{1\le i\le k}$ by

$$C_\odot(\alpha, \beta, \dots) = \begin{cases} C_\odot^{pre}(\alpha, \beta, \dots) & \text{if } \alpha \le \alpha_0; \\ C_\odot^{post}(\alpha, \beta, \dots) & \text{else;} \end{cases} \tag{15}$$

and $C_\odot \in \{C_\mathrm{X}, C_\mathrm{Y}, C_\mathrm{Z}, C_\mathrm{l}, C_\mathrm{m}, C_\mathrm{n}\}$ are polynomials in the inputs to (14). Initially, a value for α_0 is found by fitting C_X with respect to the angle of attack only and solve

$$C_{\mathrm{X}\alpha}^{pre}(\alpha) = C_{\mathrm{X}\alpha}^{post}(\alpha),$$

resulting in $\alpha_0 = 16.1110°$. The obtained C_X-model as well as $(\mathbf{C}_i)_{1\le i\le k}$ are shown by Fig. 3. The boundary condition $\alpha \equiv \alpha_0$ then resembles a hyper-plane and for the full envelope, $C_\odot^{pre}$, $C_\odot^{post}$ are chosen to be sums of 3rd-order polynomials

$$C_\odot^\times = C_{\odot\alpha}^\times(\alpha) + C_{\odot\beta}^\times(\alpha, \beta) + C_{\odot\xi}^\times(\alpha, \beta, \xi) + C_{\odot\eta}^\times(\alpha, \beta, \eta) + C_{\odot\zeta}^\times(\alpha, \beta, \zeta) + C_{\odot p}^\times(\alpha, \hat{p}) + C_{\odot q}^\times(\alpha, \hat{q}) + C_{\odot r}^\times(\alpha, \hat{r}) \tag{16}$$

for $\times \in \{pre, post\}$. Continuity of the single terms at the boundary α_0,

$$C^{pre}_{\odot *}(\alpha_0, \dots) = C^{post}_{\odot *}(\alpha_0, \dots) \tag{17}$$

for all $C_{\odot *}$ and inputs, then implies continuity of (15). Lastly, we require the lateral coefficients (C_Y, C_l, C_n) vanish in the symmetric setting, i.e., zero side-slip, no aileron nor rudder deflection ($\beta = \xi = \zeta = 0$), nor out-of-plane body rates ($\hat{p} = \hat{r} = 0$). Fig. 4 shows the piecewise polynomial model of the GTM aerodynamic coefficients for angle of attack with neutral surface deflections ($\xi = \eta = \zeta = 0$) and zero body rates ($p = q = r = 0$). All functions are continuous in the joint α_0 and the lateral coefficients vanish in $\beta \equiv 0$. As only value continuity is ensured here, the obtained model is not continuously differentiable in α_0; a more general spline approach would allow for higher continuity, but comes at the cost of a priori choice of the joint. The full polynomial expressions can be found in the technical report [25].

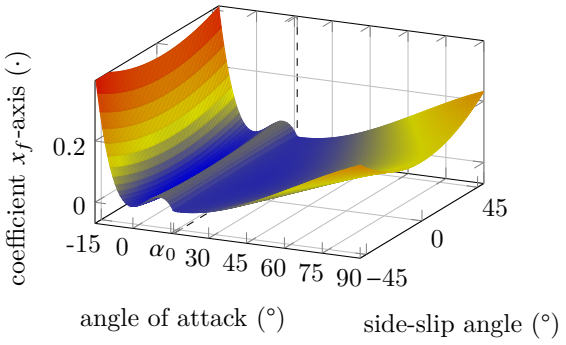

(a) Piecewise model $C_\mathrm{X}(\alpha, \beta)$.

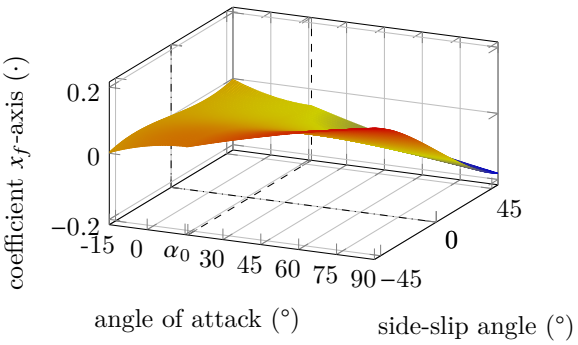

(b) Piecewise model $C_\mathrm{l}(\alpha, \beta)$.

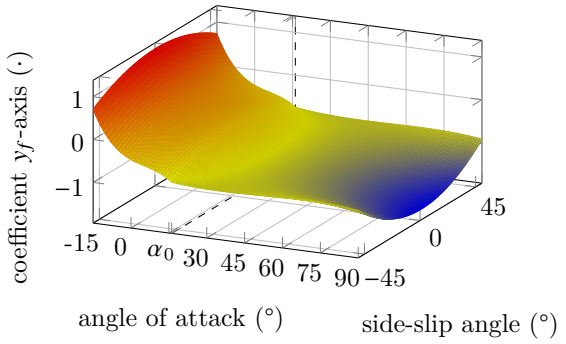

(c) Piecewise model $C_\mathrm{m}(\alpha, \beta)$.

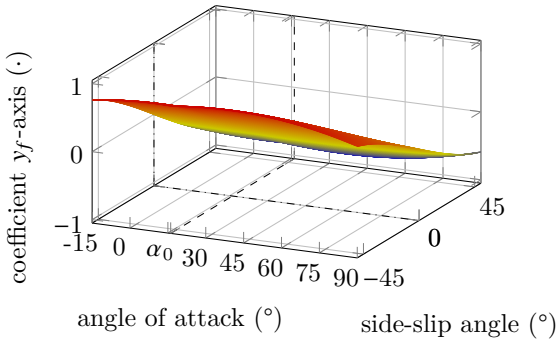

(d) Piecewise model $C_\mathrm{Y}(\alpha, \beta)$.

Fig. 4 (Part 1) Piecewise model of the aerodynamic coefficients in angle of attack and side-slip angle for neutral surface deflections.

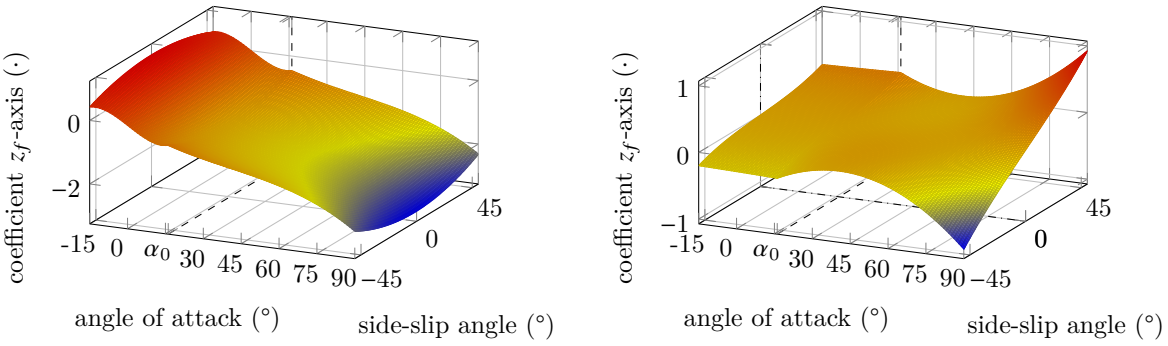

(e) Piecewise model $C_{\mathrm{Z}}(\alpha, \beta)$. **(f) Piecewise model $C_{\mathrm{n}}(\alpha, \beta)$.**

Fig. 4 (Part 2) Piecewise model of the aerodynamic coefficients in angle of attack and side-slip angle for neutral surface deflections.

V. Towards Analysis of Piecewise Models

Functional analysis of full-envelope aerodynamic models, such as continuation of trim conditions and estimation of regions of attraction, provides insight into the dynamical and statical properties of aerial systems in their extended operation range. This section provides adaptations of analysis tools used in the literature for the piecewise defined polynomial equations of motion of §IV despite the discontinuity in the first derivative around stall.

A. Trim condition analysis

The theory of continuation and bifurcation considers the equilibria of a dynamic system

$$\dot{\mathbf{X}} = \mathbf{f}(\mathbf{X}, \mathbf{U}, \boldsymbol{\mu}), \tag{18}$$

where $\boldsymbol{\mu}$ denotes the parameters of the continuation, which may include state variables and control inputs as well as other properties of $\mathbf{f}$ such as system parameters or external influences. By variation of the parameters $\boldsymbol{\mu}$ we can discuss the evolution, in particular creation, vanishing, and changes of stability, of the branches of equilibria $(\mathbf{X}^*, \mathbf{U}^*, \boldsymbol{\mu}^*)$, i.e., $\mathbf{f}(\mathbf{X}^*, \mathbf{U}^*, \boldsymbol{\mu}^*) = \mathbf{0}$, as function of $\boldsymbol{\mu}^*$. Toolboxes like the *Continuation Core and Toolboxes* (COCO) [26] offer computation of continuation and bifurcation of continuous functions. The GTM equations of motion is said to be in a *trim condition* if and only if the airspeed and air-path are constant, i.e., $\dot{V} = \dot{\gamma} = 0$; the side force vanishes, $\dot{\beta} = 0$; the body rates remain unchanged; and roll and pitch angles are constant. The heading is constant for level flight ($\dot{\Psi} = \dot{\chi} = 0$). We now choose the continuation parameters out of airspeed V, inclination γ, bank-angle μ, angle of attack α, side-slip β, the normalized rates $\hat{p}, \hat{q}, \hat{r}$, the surface deflections ζ, η, ξ, and thrust F, leaving the remaining quantities as free variables. We have now the

system of equations of motion in (18) defined piecewise as

$$\mathbf{f}(\mathbf{X},\mathbf{U},\boldsymbol{\mu}) = \begin{cases} \mathbf{f}^{pre}(\mathbf{X},\mathbf{U},\boldsymbol{\mu}) & \text{if } \alpha \leq \alpha_0; \\ \mathbf{f}^{post}(\mathbf{X},\mathbf{U},\boldsymbol{\mu}) & \text{else.} \end{cases} \tag{19}$$

For the partial derivatives of $\mathbf{f}$ are discontinuous in α_0, the COCO toolbox cannot directly compute a continuation of the piecewise system over the entire domain. Instead, we adjust the switching behaviour manually: starting from a low angle of attack, we compute equilibria of $\mathbf{f}^{pre}$ until the boundary condition $\alpha = \alpha_0$ is reached. As continuity holds at the joint,

$$\mathbf{f}^{pre}(\mathbf{X}_0^*,\mathbf{U}_0^*,\boldsymbol{\mu}_0^*) = \mathbf{f}^{post}(\mathbf{X}_0^*,\mathbf{X}_0^*,\boldsymbol{\mu}_0^*) = \mathbf{0}, \tag{20}$$

we can switch here to the dynamics of $\mathbf{f}^{post}$ without any reset and compute the high-angle of attack equilibria starting from $\left(\mathbf{X}_0^*,\mathbf{U}_0^*,\boldsymbol{\mu}_0^*\right)$ until either the limits of the continuation parameter or the boundary again is reached. In the latter case, we switch back to the low-angle of attack dynamics, and so on until finished.

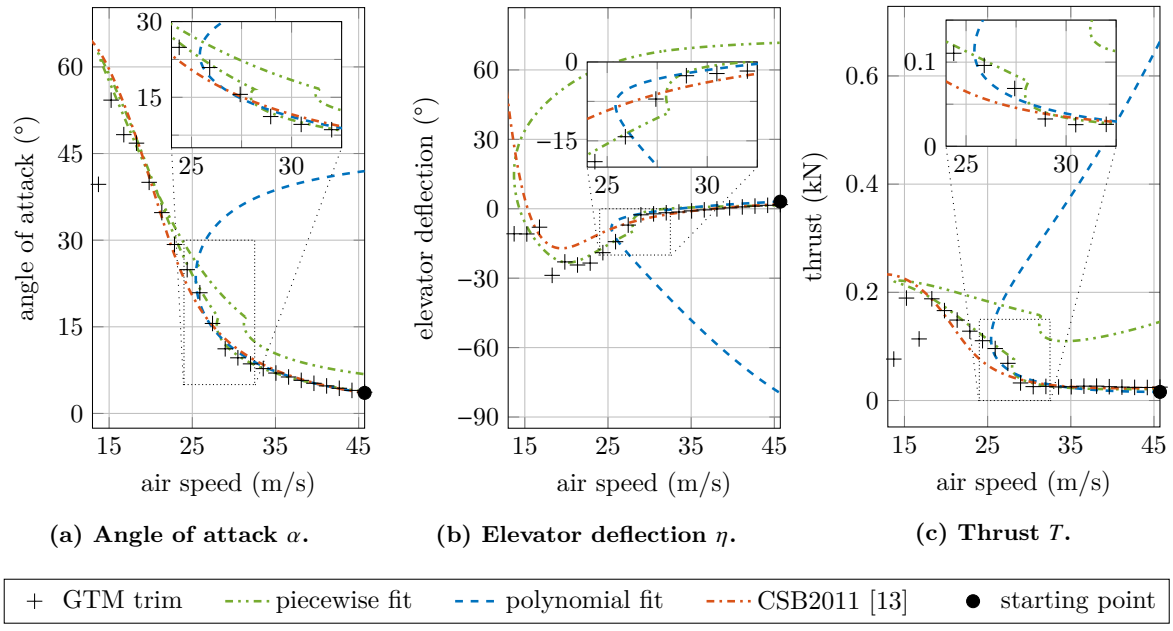

(a) Angle of attack α. **(b) Elevator deflection η.** **(c) Thrust T.**

Fig. 5 Continuation of the longitudinal dynamics of the GTM for polynomial and piecewise defined models of the aerodynamic coefficients.

In Fig. 5, we compare the piecewise continuation of (19) to polynomial models of the aerodynamic coefficients for variation of the air speed and level flight ($\gamma \equiv 0$). The polynomial model of [10] has been replaced by a similar fit. The trim data of the GTM (+) have been obtained by the trim function for the internal interpolation provided in the MATLAB simulation [9]. The first polynomial fit (- - -) shows, similar

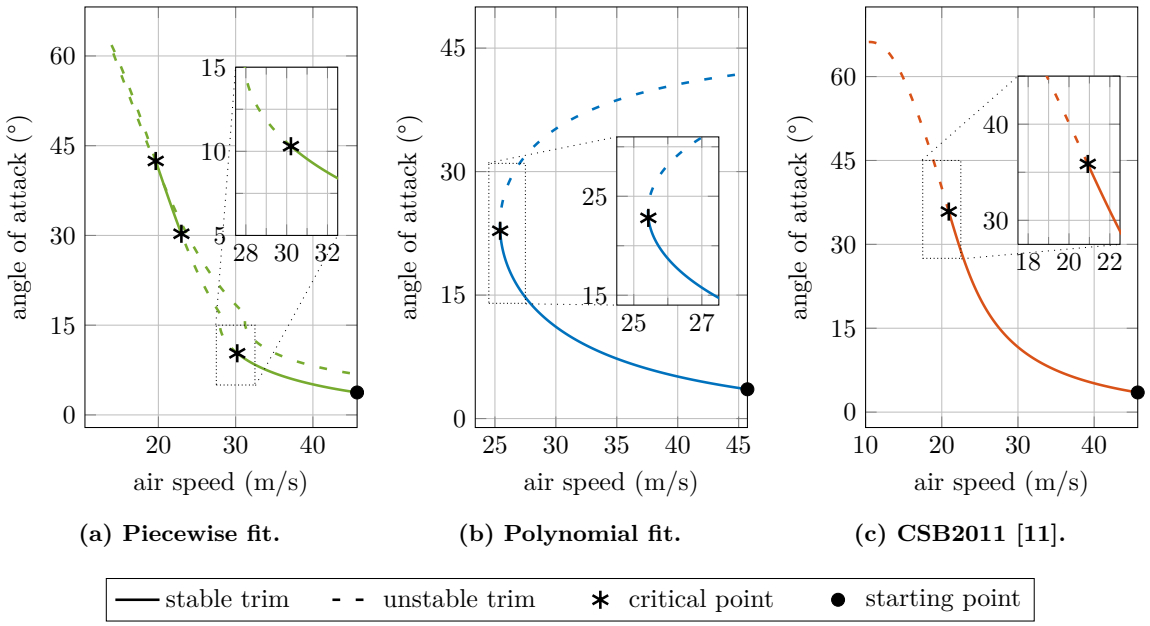

(a) Piecewise fit. **(b) Polynomial fit.** **(c) CSB2011 [11].**

Fig. 6 Stability of the longitudinal dynamics for polynomial and piecewise defined models.

to [10], a high-angle of attack branch for re-increasing air speed, which neither the polynomial fit of [11] (-·-·-) nor the piecewise fit (-·-·-) show. On the other hand, the latter certainly provide a better tracking of the GTM angle of attack, thrust, and elevator deflection values at the varying trim conditions. While for the polynomial fit of [11] the values of elevator deflection diverge to (unrealistic) multiples of 360 degrees with decreasing air speed, the elevator deflection for the piecewise fit converges, allowing a second branch of trim conditions for re-increasing air speed, too, however with far smaller angles of attack here.

We further provide in Fig. 6 information about local stability of the models: the critical point, where the trim condition changes from (locally) stable to unstable, is marked with an asterisk; stable and unstable trim conditions are drawn solid and dashed, respectively. While all three models are stable for low angles of attack and unstable for high angles, the critical points are located differently. The piecewise model shows additionally a section of stable trim conditions along the branch of increasing angles of attack, corresponding to thrust inputs larger than 135 N—i.e., 100 % throttle—and elevator deflections of −19° to −23°. Only the piecewise model has its first critical point located close to the GTM's stall angle of attack (see also Fig. 3).

B. Stable set analysis

When looking for the full-envelope, non-linear behaviour of an aircraft, knowledge about the flight envelope is vitally important for the vehicle's safety. Several characterisations of the flight envelope exist in literature. First and foremost, the desired region of the state-space can be defined by limits on the aircraft states. Within such a strict envelope, one would have the largest control-invariant set (or *safe set*) [27, 28], i.e., the largest set of initial conditions such that, given suitable control input, the aircraft is kept within the flight envelope. Finally, the regions of attraction for each stable trim condition provide a smaller, *stable set* and clearly, the safe set encapsulates the stable sets of the contained trim conditions, where every region of attraction is control-invariant in itself. While the safe set determines the abilities of the aircraft to be controlled, the stable sets highlight the limitations of a chosen controller. The neighbourhood of a trim condition $\mathbf{X}^*$ is called *stable*, denoted by $\mathcal{X}^{\text{stable}}$, if and only if for all initial conditions $\mathbf{X}_0 \in \mathcal{X}^{\text{stable}}$ the system eventually approaches $\mathbf{X}^*$. In order to compute and prove minimal stable sets of aerial vehicles based on Lyapunov function theory, researchers have successfully applied sum-of-squares programming for smooth polynomial models and ellipsoid-shaped sets [11, 29]. Given a shape $\mathcal{P}\colon \mathbf{X} \mapsto \mathbf{X}^T \Sigma \mathbf{X}$, Lyapunov-candidate function $\mathcal{V}$ with $\mathcal{V}(\mathbf{X}) > 0$ for all $\mathbf{X} \neq \mathbf{0}$, and $\mathbf{X}^*$ located in the origin, we have that

$$\mathcal{X}_\rho = \{\mathbf{X} \in \mathcal{X} \,|\, \mathcal{P}(\mathbf{X}) \leq \rho\} \tag{21}$$

with $\rho > 0$ is stable if and only if

$$\dot{\mathcal{V}}(\mathbf{X}) = \nabla \mathcal{V} \mathbf{f}(\mathbf{X}) < 0 \tag{22}$$

for all $\mathbf{X} \in \mathcal{X}_\rho - \{\mathbf{X}^*\}$. Equation (22) holds if there is a positive semi-definite polynomial $h \in \mathbb{R}[\mathbf{X}]$ such that

$$\nabla \mathcal{V} \mathbf{f}(\mathbf{X}) + h(\mathbf{X})\,(\rho - \mathcal{P}(\mathbf{X})) \leq -\epsilon \,\|\mathbf{X}\|_2^2, \tag{23}$$

for $\epsilon > 0$. While this technique requires continuous, polynomial functions to verify stability of a $\mathcal{X}^{\text{stable}}$, we can employ common Lyapunov function theory to compute a stable set for piecewise defined systems.

Theorem 1 ([30]) *Let $(\mathbf{f}_i)_{i \in I}$ be defined in the pair-wise disjunct $(\mathcal{X}_i)_{i \in I}$ and $\mathcal{V}(\mathbf{X}) > 0$ for all $\mathbf{X} \neq \mathbf{0}$; the neighbourhood $\mathcal{X}_\rho$ is stable if for all $i \in I$ and $\mathbf{X} \in \mathcal{X}_\rho \cap \mathcal{X}_i - \{\mathbf{0}\}$*

$$\dot{\mathcal{V}}(\mathbf{X}) = \nabla \mathcal{V} \mathbf{f}_i(\mathbf{X}) < 0. \tag{24}$$

Simply speaking, stability of $\mathcal{X}_\rho$ holds if $\dot{\mathcal{V}}$ with respect to $\mathbf{f}^{pre}$, $\mathbf{f}^{post}$ is negative just for low and high

angles of attack, respectively. Similar to (23), where $h(\mathbf{X})\,(\rho - \mathcal{V}(\cdot))$ compensates for non-negative derivatives outside the stable set, we have with positive semi-definite g_1, g_2

$$g_1(\mathbf{X})\,(\alpha_0 - \alpha) \geq 0 \Longleftrightarrow \alpha \leq \alpha_0 \tag{25}$$

$$g_2(\mathbf{X})\,(\alpha - \alpha_0) > 0 \Longleftrightarrow \alpha > \alpha_0 \tag{26}$$

and hence

$$\begin{cases} \nabla\mathcal{V}\mathbf{f}^{pre}(\mathbf{X}) + h_1(\mathbf{X})\,(\rho - \mathcal{P}(\mathbf{X})) + g_1(\mathbf{X})\,(\alpha_0 - \alpha) \leq -\epsilon\,\|\mathbf{X}\|_2^2, \\ \nabla\mathcal{V}\mathbf{f}^{post}(\mathbf{X}) + h_2(\mathbf{X})\,(\rho - \mathcal{P}(\mathbf{X})) + g_2(\mathbf{X})\,(\alpha - \alpha_0) \leq -\epsilon\,\|\mathbf{X}\|_2^2 \end{cases} \tag{27}$$

for $\epsilon > 0$ implies stability of $\mathcal{X}_\rho$ for the system of (19).

The challenge now is to find a Lyapunov function that grants a largest-possible size ρ for the chosen shape factor Σ. One such approach using sum-of-squares programming is the V-s-iteration, which has been presented in [11] as iteratively-alternating steps:

1) find $\lambda^\diamond = \max \lambda$ such that there is $h'(\cdot)$ positive semi-definite with

$$\nabla\mathcal{V}\mathbf{f}(\mathbf{X}) + h'(\mathbf{X})\,(\lambda - \mathcal{V}(\mathbf{X})) \leq -\epsilon\,\|\mathbf{X}\|_2^2\,;$$

2) find $\rho^\diamond = \max \rho$ such that there is $h_0(\cdot)$ positive semi-definite with

$$(\mathcal{V}(\mathbf{X}) - \lambda^\diamond) + h_0(\mathbf{X})\,(\rho - \mathcal{P}(\mathbf{X})) \leq 0$$

holding $\lambda^\diamond$ of the first step constant;

3) find $\mathcal{V}(\cdot)$ such that

$$\begin{cases} \mathcal{V}(\mathbf{X}) \geq \quad \epsilon\,\|\mathbf{X}\|_2^2, \\ \nabla\mathcal{V}\mathbf{f}(\mathbf{X}) + h'(\mathbf{X})\,(\lambda^\diamond - \mathcal{V}(\mathbf{X})) \leq -\epsilon\,\|\mathbf{X}\|_2^2, \\ (\mathcal{V}(\mathbf{X}) - \lambda^\diamond) + h_0(\mathbf{X})\,(\rho^\diamond - \mathcal{P}(\mathbf{X})) \leq 0, \end{cases}$$

holding $\lambda^\diamond, \rho^\diamond$ as well as $h'(\cdot)$ and $h_0(\cdot)$ of the previous steps constant.

Initially, a crude guess of $\mathcal{V}(\cdot)$ is found here from the linearization of $\mathbf{f}$ around $\mathbf{X}^*$ [11]. The V-s-iteration removes the difficulty to find simultaneously a Lyapunov function and its region of strictly negative time-derivative (*dissipative region*) as well as proving positive multipliers, by distinct steps of sum-of-squares

optimization. First, the dissipative region of $\mathcal{V}(\cdot)$ is determined, i.e., the level set $\mathcal{V}(\mathbf{X}) = \lambda$ such that its derivative is strictly negative within; then, the inscribing ellipsoid $\mathcal{P}(\mathbf{X}) = \rho$, the stable set, is fitted into this level set. The last step attempts to find a feasible Lyapunov function-guess with the prior results witnessing the minimal stable region. Exemplary, we compute a stable set of the piecewise model for the short-period motion,

$$\begin{bmatrix} \dot{\alpha} \\ \dot{q} \end{bmatrix} = \begin{cases} \mathbf{f}_{\mathrm{sp}}^{pre}(\alpha, q, \eta = \eta^*) & \text{if } \alpha \leq \alpha_0; \\ \mathbf{f}_{\mathrm{sp}}^{post}(\alpha, q, \eta = \eta^*) & \text{else;} \end{cases} \tag{28}$$

in the neighbourhood of the trim condition $V^* = 45.7\,\mathrm{m/s}$, $\gamma^* = 0$, $\alpha^* = 3.75°$, $\eta^* = 1.49°$, and $F^* = 21.44\,\mathrm{N}$ with the shape factor

$$\Sigma = \mathrm{diag}(20°,\, 50\,°/\mathrm{s})^{-2}$$

accounting for the physical operation range of the Generic Transport Model at the selected trim condition.

As in [11], the states have thus been scaled by the shape; the non-polynomial operations sin, cos, and $(\cdot)^{-1}$ have been replaced by finite Taylor series expansions; and polynomial terms of 6th order or higher or with coefficients absolute smaller than 10^{-6} were removed. After 94 iterations, we obtain the stable set $\mathcal{X}_{\rho 0} = \{\mathbf{X} \,|\, \mathcal{P}(\mathbf{X}) \leq \rho_0\}$ with

$$\rho_0 = 1.4404 \tag{29}$$

and the dissipative region $\{\mathbf{X} \,|\, \mathcal{V}_0(\mathbf{X}) \leq \lambda_0\} \subseteq \left\{\mathbf{X} \,\middle|\, \dot{\mathcal{V}}_0(\mathbf{X}) < 0\right\}$ of the quartic Lyapunov function $\mathcal{V}_0(\cdot)$ with

$$\lambda_0 = 0.3265. \tag{30}$$

Fig. 7 shows the stable set as well as the dissipative region of the computed common Lyapunov function. For the polynomial short-period model of [11], the stable set $\mathcal{X}_{\rho\mathrm{Pol}}$ and the respective level set of the quartic Lyapunov function $\mathcal{V}_{\mathrm{Pol}}$ have been computed to $\rho_{\mathrm{Pol}} = 1.6785$ and $\lambda_{\mathrm{Pol}} = 0.8522$, respectively, and are too shown by Fig. 7 for comparison. The obtained Lyapunov functions are given by

$$\begin{aligned} \mathcal{V}_0 = {} & 6.5\alpha^4 + 0.37\alpha^3 q + 0.19\alpha^2 q^2 + 0.023\alpha q^3 + 0.0027 q^4 - 0.080\alpha^3 \\ & + 0.000\,44\alpha^2 q + 0.012\alpha q^2 - 0.0067 q^3 + 0.69\alpha^2 - 0.016\alpha q + 0.020 q^2 \end{aligned} \tag{31}$$

and

$$\mathcal{V}_{\mathrm{Pol}} = 20\alpha^4 - 2.8\alpha^3 q + 1.6\alpha^2 q^2 - 0.21\alpha q^3 + 0.029 q^4 + 0.0033\alpha^3 + 0.000\,88\alpha^2 q$$
$$+ 0.000\,13\alpha q^2 - 2.5\times 10^{-6} q^3 + 2.6\times 10^{-5}\alpha^2 + 3.2\times 10^{-7}\alpha q + 1.4\times 10^{-6} q^2$$

It is thus demonstrated that the extension to common Lyapunov functions for the estimation of stable sets for the piecewise polynomial model is feasible using sum-of-squares programming.

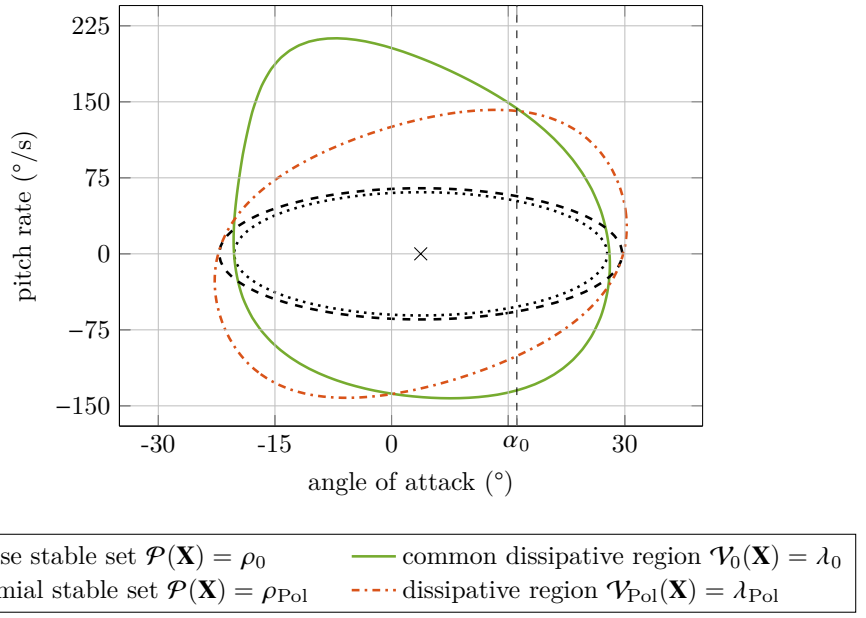

Fig. 7 Stable set of the piecewise short-period model compared to [11].

VI. Conclusion

In-flight loss-of-control remains a severe threat to civil aviation safety. In the presence of highly non-linear, unstable dynamics in upset situations, accurate models of the full-envelope aerodynamics are crucial for successful analysis, protection, and recovery of the aircraft. This note proposes piecewise polynomial fitting of the aerodynamic coefficients with a single non-smooth joint representing the change of dynamics at high angles of attack. This approach yields a model almost as simple as polynomials but with the power of splines to account for complex characteristics. The joint of the piecewise model is justified by the physical properties of the aerial system and has been subject to the fit, too. Without the necessity of a priori choices regarding the fit, we maintain all abilities of polynomial fitting. Given the example of the Generic Transport Model, we have compared the piecewise model of the aerodynamic coefficients to polynomial models available in the literature, proving the accuracy of both piecewise coefficients and trim conditions when measured

against the GTM's raw data. Functional analysis tools such as continuation of equilibria and estimation of safe and stable sets yield invaluable preparations for flight control schemes over the full envelope. We have demonstrated how those tools, typically requiring continuous inputs, can be adapted to piecewise defined systems, retaining crucial information about stability and attraction. Although the extensions apply to all kinds of piecewise models including splines, the problem size grows with the number of cases and, in particular for sum-of-squares programming, computationally unfeasible. The piecewise polynomial model for low and high angles attack, however, provides all three accuracy, regression of measurements, and feasibility of the subsequent analysis.

Funding Sources

This work is funded by ONERA – The French Aerospace Lab, République Française.

References

[1] Goman, M., Zagainov, G., and Khramtsovsky, A., "Application of bifurcation methods to nonlinear flight dynamics problems," *Progress in Aerospace Sciences*, Vol. 33, No. 9–10, 1997, pp. 539–586. doi:10.1016/S0376-0421(97)00001-8.

[2] Gill, S. J., Lowenberg, M. H., Neild, S. A., Krauskopf, B., Puyou, G., and Coetzee, E., "Upset Dynamics of an Airliner Model: A Nonlinear Bifurcation Analysis," *Journal of Aircraft*, Vol. 50, No. 6, 2013, pp. 1832–1842. doi:10.2514/1.C032221.

[3] Chang, B.-C., Kwatny, H. G., Ballouz, E. R., and Hartmann, D. C., "Aircraft Trim Recovery from Highly Nonlinear Upset Conditions," *AIAA Guidance, Navigation, and Control Conference*, San Diego, US-CA, 2016. doi:10.2514/6.2016-0880.

[4] Stepanyan, V., Krishnakumar, K., Kaneshige, J., and Acosta, D., "Stall Recovery Guidance Algorithms Based on Constrained Control Approaches," *AIAA Guidance, Navigation, and Control Conference*, San Diego, US-CA, 2016. doi:10.2514/6.2016-0878.

[5] Engelbrecht, J. A. A., Pauck, S. J., and Peddle, I. K., "A Multi-mode Upset Recovery Flight Control System for Large Transport Aircraft," *AIAA Guidance, Navigation, and Control Conference*, Boston, US-MA, 2013. doi:10.2514/6.2013-5172.

[6] Crespo, L. G., Kenny, S. P., Cox, D. E., and Murri, D. G., "Analysis of Control Strategies for Aircraft Flight Upset Recovery," *AIAA Guidance, Navigation, and Control Conference*, Minneapolis, US-MN, 2012. doi:10.2514/6.2012-5026.

[7] Richards, N. D., Gandhi, N., Bateman, A. J., Klyde, D. H., and Lampton, A. K., "Vehicle Upset Detection and

Recovery for Onboard Guidance and Control," *Journal of Guidance, Control, and Dynamics*, Vol. 40, No. 4, 2017, pp. 920–933. doi:10.2514/1.G001738.

[8] Frink, N. T., Murphy, P. C., Atkins, H. L., Viken, S. A., Petrilli, J. L., Gopalarathnam, A., and Paul, R. C., "Computational Aerodynamic Modeling Tools for Aircraft Loss of Control," *Journal of Guidance, Control, and Dynamics*, Vol. 40, No. 4, 2017, pp. 789–803. doi:10.2514/1.G001736.

[9] "Flight Dynamics Simulation of a Generic Transport Model," , 2016. URL `https://software.nasa.gov/software/LAR-17625-1`.

[10] Kwatny, H. G., Dongmo, J.-E. T., Chang, B.-C., Bajpai, G., Yasar, M., and Belcastro, C., "Nonlinear Analysis of Aircraft Loss of Control," *Journal of Guidance, Control, and Dynamics*, Vol. 36, No. 1, 2013, pp. 149–162. doi:10.2514/1.56948.

[11] Chakraborty, A., Seiler, P., and Balas, G. J., "Nonlinear region of attraction analysis for flight control verification and validation," *Control Engineering Practice*, Vol. 19, No. 4, 2011, pp. 335–345. doi:10.1016/j.conengprac.2010.12.001.

[12] Cunis, T., Burlion, L., and Condomines, J.-P., "Piece-wise Identification and Analysis of the Aerodynamic Coefficients, Trim Conditions, and Safe Sets of the Generic Transport Model," *AIAA Guidance, Navigation, and Control Conference*, Kissimmee, US-FL, 2018. doi:10.2514/6.2018-1114.

[13] Bulka, E., and Nahon, M., "Autonomous control of agile fixed-wing UAVs performing aerobatic maneuvers," *2017 International Conference on Unmanned Aircraft Systems*, Miami, US-FL, 2017, pp. 104–113. doi:10.1109/ICUAS.2017.7991437.

[14] Robison, D. E., "Estimates for the Points of Intersection of Two Polynomial Regressions," *Journal of the American Statistical Association*, Vol. 59, No. 305, 1964, pp. 214–224. doi:10.2307/2282870.

[15] Gallant, A. R., and Fuller, W. A., "Fitting segmented polynomial regression models whose join points have to be estimated," *Journal of the American Statistical Association*, Vol. 68, No. 341, 1973, pp. 144–147. doi:10.2307/2284158.

[16] McGee, V. E., and Carleton, W. T., "Piecewise Regression," *Journal of the American Statistical Association*, Vol. 65, No. 331, 1970, pp. 1109–1124. doi:10.2307/2284278.

[17] Chaudhuri, P., Huang, M.-C., Loh, W.-Y., and Yao, R., "Piecewise-Polynomial Regression Trees," *Statistica Sinica*, Vol. 4, No. 1, 1994, pp. 143–167. URL `http://www.jstor.org/stable/24305278`.

[18] de Visser, C. C., Mulder, J. A., and Chu, Q. P., "A Multidimensional Spline-Based Global Nonlinear Aerodynamic Model for the Cessna Citation II," *AIAA Atmospheric Flight Mechanics Conference*, Toronto, CA, 2010. doi:10.2514/6.2010-7950.

[19] Tol, H. J., de Visser, C. C., Sun, L. G., van Kampen, E., and Chu, Q. P., "Multivariate Spline-Based Adaptive Control of High-Performance Aircraft with Aerodynamic Uncertainties," *Journal of Guidance, Control, and Dynamics*, Vol. 39, No. 4, 2016, pp. 781–800. doi:10.2514/1.G001079.

[20] de Visser, C. C., Chu, Q. P., and Mulder, J. A., "A new approach to linear regression with multivariate splines," *Automatica*, Vol. 45, No. 12, 2009, pp. 2903–2909. doi:10.1016/j.automatica.2009.09.017.

[21] Brandon, J. M., and Morelli, E. A., "Real-Time Onboard Global Nonlinear Aerodynamic Modeling from Flight Data," *Journal of Aircraft*, Vol. 53, No. 5, 2016, pp. 1261–1297. doi:10.2514/1.C033133.

[22] Cunis, T., "The pwpfit Toolbox for Polynomial and Piece-wise Polynomial Data Fitting," *18th IFAC Symposium on System Identification*, Stockholm, SE, 2018. doi:10.1016/j.ifacol.2018.09.204.

[23] Stigler, S. M., "Gergonne's 1815 paper on the design and analysis of polynomial regression experiments," *Historia Mathematica*, Vol. 1, 1974, pp. 431–439. doi:10.1016/0315-0860(74)90033-0.

[24] Smith, K., "On the Standard Deviations of Adjusted and Interpolated Values of an Observed Polynomial Function and its Constants and the Guidance they give Towards a Proper Choice of the Distribution of Observations," *Biometrika*, Vol. 12, No. 1/2, 1918. doi:10.2307/2331929.

[25] Cunis, T., Burlion, L., and Condomines, J.-P., "Piecewise Polynomial Model of the Aerodynamic Coefficients of the Generic Transport Model and its Equations of Motion," Tech. rep., ONERA – The French Aerospace Lab; French Civil Aviation School, Toulouse, FR, 2018. URL `https://hal.archives-ouvertes.fr/hal-01808649`.

[26] Dankowicz, H., and Schilder, F., *Recipes for Continuation*, Computational Science & Engineering, Society for Industrial and Applied Mathematics, Philadelphia, US-PA, 2013. doi:10.1137/1.9781611972573.

[27] Lygeros, J., "On reachability and minimum cost optimal control," *Automatica*, Vol. 40, No. 6, 2004, pp. 917–927. doi:10.1016/j.automatica.2004.01.012.

[28] Nabi, H. N., Lombaerts, T., Zhang, Y., van Kampen, E., Chu, Q. P., and de Visser, C. C., "Effects of Structural Failure on the Safe Flight Envelope of Aircraft," *Journal of Guidance, Control, and Dynamics*, Vol. 41, No. 6, 2018, pp. 1257–1275. doi:10.2514/1.G003184.

[29] Tedrake, R., Manchester, I. R., Tobenkin, M., and Roberts, J. W., "LQR-trees: Feedback Motion Planning via Sums-of-Squares Verification," *The International Journal of Robotics Research*, Vol. 29, No. 8, 2010, pp. 1038–1052. doi:10.1177/0278364910369189.

[30] Johansson, M., and Rantzer, A., "Computation of piecewise quadratic Lyapunov functions for hybrid systems," *IEEE Transactions on Automatic Control*, Vol. 43, No. 4, 1998, pp. 555–559. doi:10.1109/9.664157.

Chapter 4

Dynamic Stability Analysis in Deep-stall

This chapter corresponds to:

> Torbjørn Cunis, Jean-Philippe Condomines, Laurent Burlion, and Anders la Cour-Harbo (2019). "Dynamic Stability Analysis of Aircraft Flight in Deep Stall". In: *Journal of Aircraft*. DOI: 10.2514/1.C035455

in the author's accepted version.

Synopsis

In this chapter, we establish the nonlinear model of Cumulus One, based on piecewise-defined aerodynamic coefficients, that lays the foundation for further control synthesis and analysis in Chapters 6 and 7. Unlike for the Generic Transport Model in the previous chapter, there are no wind-tunnel data available for modeling but we initially base our model on the results of a static continuous fluid dynamics (CFD) simulation. We will thoroughly investigate the longitudinal dynamics using a continuation analysis and, to this extent, shortly review the basics of piecewise polynomial modeling and bifurcation theory. The piecewise polynomial aircraft model is detailed in Appendix B.2. We will further introduce the concept of a *blending function* that smoothens differentiability gap of the piecewise polynomial model and thus facilitates the use of nonlinear solvers for continuation and optimisation.

However, due to the lack of dynamic coefficients, the preliminary model does not represent the aircraft's stable flight in deep-stall which has been demonstrated in flight tests. We therefore discuss two alternative models for the impact of non-zero pitch rate onto the aerodynamic pitch-moment coefficient. Here, we make use of flight test data recorded for deep-stall transition manoeuvres initiated by a specified step in the elevator deflection. Combining bifurcation analysis and nonlinear parameter optimisation, we identify optimal parameters for the two dynamic models. Obtaining good results for both models, in the remainder of the thesis we will utilise what we call a *linear pitch-damping coefficient*, namely, the additional pitch moment is given by $M_q = -C_{\mathrm{M}q}q$ where $C_{\mathrm{M}q} = \hat{\kappa}_{\dot{q}q}$ is the optimal linear damping parameter derived in this chapter.

A six-degrees-of-freedom bifurcation analysis as well as the discussion of descent modes conclude the chapter and complete the previous insights from flight tests.

Statement of Contribution Torbjørn Cunis designed and analysed the nonlinear aircraft model, proposed and discussed different pitch-damping models, performed the parameter optimisation, and performed the final analysis in six degrees of freedom. Jean-Philippe Condomines contributed to the introduction and assisted with the discussion in the frequency domain. Laurent Burlion recommended the parameter optimisation. Anders la Cour-Harbo provided general feedback and established the cooperation with Sky-Watch A/S, who collected and distributed data of flight tests and CFD simulations.

Dynamic Stability Analysis of Aircraft Flight in Deep Stall

Torbjørn Cunis*
ONERA – The French Aerospace Lab, Centre Midi-Pyrénées, Toulouse, 31055, France

Jean-Philippe Condomines†
ENAC, Université de Toulouse, Toulouse, 31055, France

Laurent Burlion‡
Rutgers, The State University of New Jersey, Piscataway, NJ 08854, USA

Anders la Cour-Harbo§
Aalborg University, Aalborg East, 9220, Denmark

Beyond aerodynamic stall, analysis of aircraft flight requires models accurately representing nonlinearities and instabilities. Previous bifurcation analysis studies therefore had a priori knowledge of the aircraft dynamics including dynamic damping. Yet unlike airliners, extensive wind-tunnel tests and high-fidelity models are rarely available for small unmanned aircraft. Instead, continuous fluid dynamic simulations may provide basic insights into the aerodynamics, however limited to static conditions. In this paper, we present bifurcation analysis as a tool to discuss the effects of unidentified pitch-damping dynamics during deep-stall transition that allows us to develop a nonlinear pitch-damping model for a small unmanned aircraft. Preliminary studying the static case, we extend the model based on deep-stall flight data and predict dynamics and stability. As a result, we investigate the deep-stall modes of the extended model in full-envelope.

Nomenclature

α	Angle of attack (rad);
α_0	Low-angle of attack boundary ($\alpha_0 = 16.2949°$);
γ_A	Flight-path angle relative to air (rad);

*Doctoral Researcher, Department of Information Processing and Systems, e-mail: torbjoern.cunis@onera.fr; associated researcher with the ENAC Drones Research Group; AIAA Student Member.
†Assistant Professor, Drones Research Group, e-mail: jean-philippe.condomines@enac.fr
‡Assistant Professor, Department of Mechanical & Aerospace Engineering, e-mail: laurent.burlion@rutgers.edu
§Associate Professor, Department of Electronic Systems, e-mail: alc@es.aau.dk.

η	Elevator deflection (rad), negative if leading to positive pitch moment;
Θ	Pitch angle (rad);
κ_{pr}, κ_q	Parameters of (linear) roll-yaw and pitch damping $(\cdot)$;
$\kappa_{\dot{q}q}$	Parameter of linear damping model $(\cdot)$;
$\lambda_{\alpha q}$	Parameter of model of induced angle of attack $(\cdot)$;
ξ, ζ	Aileron and rudder deflections (rad), negative if leading to positive moments;
Φ	Bank angle (rad);
C_{m}	Aerodynamic coefficient moment body y_f-axis $(\cdot)$;
C_{D}	Aerodynamic drag coefficient $(\cdot)$, parallel to airstream;
C_{L}	Aerodynamic lift coefficient $(\cdot)$, perpendicular to airstream;
$\mathbf{D}$	Drag force (N), pointing towards negative air-path x_{a}-axis;
$\mathbf{F}$	Thrust force (N), pointing towards positive body x_{f}-axis;
k	Number of measurements;
$\mathbf{L}$	Lift force (N), pointing towards negative air-path z_{a}-axis;
p, r	Roll and yaw rates (rad);
q	Pitch rate (rad/s);
$\mathbf{X}^*, \eta^*$	State vector and elevator deflection at trim condition;
$V_{\mathrm{A}}, \mathbf{V}_{\mathrm{A}}$	Aircraft speed and velocity *relative to air* ($V_{\mathrm{A}} = \|\mathbf{V}_{\mathrm{A}}\|_2$, m/s);
$(\cdot)^{post}$	Domain of high angle of attack;
$(\cdot)^{pre}$	Domain of low angle of attack;
$x_{\mathrm{a}}, y_{\mathrm{a}}, z_{\mathrm{a}}$	Air-path axis system;
$x_{\mathrm{f}}, y_{\mathrm{f}}, z_{\mathrm{f}}$	Body axis system;
$x_{\mathrm{g}}, y_{\mathrm{g}}, z_{\mathrm{g}}$	Normal earth-fixed axis system;

I. Introduction

Analysis of aircraft dynamics is nowadays retrieved from discussion of aerodynamic models by means of systems theory, occasionally combined with high-fidelity Monte-Carlo simulations. The underlying aerodynamic model is based on physical models of the vehicle dynamics that include a description of the causes of motion (the external forces experienced by the aircraft). In the context of the flight dynamics of aerial vehicles, these forces include aerodynamic loads, gravitational forces, and propulsion. The models are typically parametric and requires an initial identification phase before operation [1]. Hence, they heavily rely on our a priori knowledge. The knowledge model needs to be as representative as possible for the aircraft physics, such that it can be used to simulate the aircraft dynamics.

Literature review

In the normal flight regime, where the aerodynamic coefficients are fairly linear, and for small perturbations from the trim condition, linear analysis methods apply, such as the Nyquist stability criterion or Bode plots and margins [2]. For flights at high angles of attack as in deep-stall, beyond the bounds of the linear approximation, linear approaches fail [3]. With the aircraft dynamics being highly non-linear and mostly unstable here [4], disparate methods have been applied for analysis: Bifurcation analysis is rooted on mathematical continuation and bifurcation theory to compute trim conditions, critical (bifurcation) points, and periodical orbits of the non-linear aircraft dynamics [5–8]. Recoverable or safe sets are determined by means of reachability [9, 10], control-invariance [11], and regions of local attraction [12, 13]. Modeling dynamic systems by means of state representations, whether linear or non-linear, gives us access to a direct formulation of the underlying physics of the process [1].

An understanding of the aerodynamics of the aircraft is usually gained by performing tests on the aircraft or a scaled replica in a wind tunnel. Among the aircraft studied in a wind tunnel, including almost every commercial type as well as many experimental designs, NASA's generic transport model stands out for its extensively studied aerodynamics [14, 15] and wide recognition in the literature [5, 12, 16–20]. Establishing a satisfactory model is rarely straightforward, and ensuring that it is sufficiently representative of every aspect of the operational behaviour of the true vehicle can be extremely challenging. Today, constant improvements in experimental technology and processing power have enabled us to develop increasingly reliable and accurate forecasting knowledge models. Modern computer programs allow numerical derivation of aerodynamics based on the aircraft's geometry only, additionally—or alternatively—to classical wind tunnel experiments. Computational fluid dynamics (CFD) simulates aerodynamic forces and moments acting on the body in static condition; CFD offers simulations of wide ranges of incidence angles and surface deflections, just as if placed in a real wind tunnel [cf. 21, and references herein], but while the injection of body rates is possible, too,

these computations are highly expensive. In a different approach, the AVL program takes advantage of an extended vortex lattice model to linearise the aerodynamics around a specified trim point [22]. AVL includes dynamic coefficients, but is limited to linearised predictions. In any case, an advanced aerodynamics model demands significant investment of time and funding that should be carefully considered before a modeling approach is adopted by an unmanned aircraft development project with "low-cost" constraints.

Main contributions

In this study, we aim to develop a non-linear flight dynamics model in order to study the deep-stall transition behaviour of an unmanned aircraft with an extended flight envelope. For this purpose, we present bifurcation analysis as a tool to discuss the effects of pitch-damping, which has been unknown here, onto stability and dynamics of the aircraft in deep stall. In previous work analyzing and discussing bifurcations of nonlinear aircraft models, knowledge of the dynamic behaviour of the aircraft was considered a priori. Without these information in the begin of our study, we incorporate models of aerodynamic damping into the analysis while critically assessing the model response against observations from test flights. We further propose and evaluate different approaches for dynamic models.

We consider the Cumulus One, a commercially developed, small-size unmanned aircraft. It is designed to land in a stable, near vertical descent in deep-stall in order to accomodate landing where most other fixed wing aircraft cannot; therefore, its elevator is capable of exceptionally large deflection angles and the wings are set in a dihedral manner to enhance lateral stability. For the purpose of deep-stall analysis and control, CFD simulations resulted in static data covering large incidence angles and surface deflections. These computations took ca. 3 h per configuration.* Further simulations of the aircraft's unsteady dynamics would have resulted in additional computations of about 10 h per configuration and each value of the rotational speed.† Instead, Cumulus One has performed several experimental flights demonstrating the deep-stall descents, including flights with the elevator fixed at various, large deflections. With the available full-envelope modeling data as well as in-flight measurements at high angles of attack, the Cumulus One provides an advantageous testbed for the derivation and discussion of non-linear analysis approaches for low-cost aircraft. However, since the CFD data does not include dynamic behaviour, the effects of body rates to dynamics and stability at high angles of attack need to be modeled separately. We therefore will study the effect of longitudinal pitch damping during the transition into deep-stall and subsequently extend the flight dynamics model in order to predict static and dynamic stability. The extended model then enables the assessment of deep-stall modes on

*Dasam, V. K., private communication (February 2018); here, "configuration" means a static aircraft with angle of attack, side-slip angle, and control surfaces fixed to the selected values (Intel Xeon E5, 28 cores, 64 GB).

†Dasam, V. K., private communication (March 2018): 1 s of simulation equates to roughly 5 h of computation; simulating the aircraft pitching up from −10° to 70° at a speed of 2 rad/s and back to −10° at −1 rad/s then takes around 2 s to be simulated. Faster rotation reduces the simulation time, indeed, but initial trials indicate the need of smaller time steps here, too.

the basis of real flight data gathered from experiments performed on the Cumulus One.

Outline

In the following section, we briefly introduce the Cumulus One aircraft as well as the flight data used in this study, derive a longitudinal aerodynamic model of Cumulus One from well-known equations of motion, and provide an algebraic representation of its aerodynamic coefficients by a smoothened piecewise interpolation of the discrete CFD data points. The subsequent sections are organised as follows: In section III, we investigate the existence and stability of longitudinal trim conditions by bifurcation analysis of the static model. By extension of the original model, we introduce in section IV two different approaches to take into account pitch damping in terms of the pitch rate and each an unkown model parameter. We thus will be able to describe the dynamic behaviour around trim conditions; in particular, we discuss the influence of the model parameters and find optimal values by differential parameter optimization. In section V at last, we study the developed model in a six-degrees-of-freedom trim analysis investigating post-stall and deep-stall flight.

Fig. 1 Digital rendering of Cumulus One ready for flight. [23]

II. Piecewise Aircraft Model

In this section, we present the aircraft that we study and provide the longitudinal equations of motions based on the aerodynamics. We further discuss different fitting methods for the aerodynamic coefficients in order to attain a closed functional expression of the equations of motion suitable for continuation analysis over the full flight envelope.

A. The Cumulus One

The Cumulus One (Fig. 1) is a fully autonomous, 1.65 m-wingspan, unmanned aircraft carried by the Danish company SkyWatch for agricultural mapping, surveillance, and reconnaissance. Instead of landing gear, it is equipped with shock-absorbing foam at its belly and intended to land vertically descending by a deliberate deep-stall manoeuvre. In this manoeuvre, with steeper flight paths the drag of the wings becomes

the dominant component to counteract the gravitational force, leading to a stable trim condition, and the horizontal distance covered during the landing is minimised. For the purpose of stable deep-stall flight, the elevator is designed to exceed the usual range and reach deflections of up to −60°. In the flight experiments considered in this study, the transition to deep-stall is initiated in level flight by a step in the elevator deflection. At the same time, the throttle is reduced to zero. The aircraft responds by pitching up, reduces forward velocity to near zero, and, in consequence, stalls. In stall, the aircraft accelerates vertically downwards and the pitch angle decreases rapidly, until the system settles in a stable deep-stall trim condition with a small, negative pitch angle. During test flights, the descent is aborted after several seconds by setting the flight configuration to take-off mode, which is basically full throttle and an elevator setting for a gentle climb. The transition from deep-stall to post-take-off climb condition takes less than 2 second. The aircraft subsequently climbs to cruising altitude, ready for a new deep-stall. This procedure has been repeated for various deep-stall elevator deflections.

Table 1 Parameters of Cumulus One.

flight mass[‡]	m	1.55	kg
wing span	b	1.66	m
mean chord	c_A	0.174	m
wing area	S	0.277	m^2
air density[§]	ϱ	1.25	kg/m^3
gravitational constant	g	9.81	m/s^2

Fig. 2 shows pitch angle and elevator deflection during initiation, descent, and recovery of an example deep-stall descent manoeuvre. The parameters of the Cumulus One and its environment used in this study are given by Tab. 1.

B. Aerodynamic modeling

Due to its dihedral wings, the Cumulus One is considered to be laterally stable. We therefore initially neglect the lateral dynamics for the analysis of stability and, consequently, assume the side-slip angle β to vanish. In deep-stall flight and transition, the aircraft is further unthrottled, i.e., the thrust force is zero ($\mathbf{F} = 0$). We will refer to the international standard *body axis system* ($x_\mathrm{f}, y_\mathrm{f}, z_\mathrm{f}$), *air-path axis system* ($x_\mathrm{a}, y_\mathrm{a}, z_\mathrm{a}$), and *earth-fixed axis system* ($x_\mathrm{g}, y_\mathrm{g}, z_\mathrm{g}$); respectively defined by the aircraft's fuselage, velocity with respect to air ($\mathbf{V}_\mathrm{A}$), and the ground [24]. Here, lift and drag forces are defined along the air-path axes and denoted $\mathbf{L}$ and $\mathbf{D}$; angle of attack α, flight-path angle γ_A, and pitch angle Θ are given by rotations between the axis systems. (Fig. 3.) If not stated otherwise, all variables are in SI-units, i.e., m, m/s, rad, rad/s, kg,

[‡]Total mass at take-off, including payload

[§]During the flight experiment, air density has been $\varrho = 1.156\,\mathrm{kg/m^3}$.

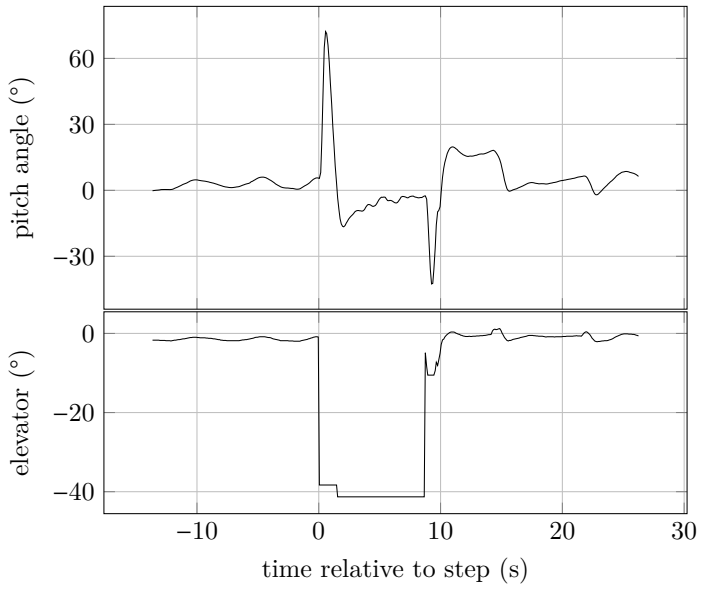

Fig. 2 Aborted deep-stall manoeuvre, initiated in level-flight by a step in the elevator deflection command to $\eta_{t=0} \approx -38°$, then trimmed at $\eta_{t \geq t_0} \approx -41°$.

etc.; angles are however given in degrees where convenient.

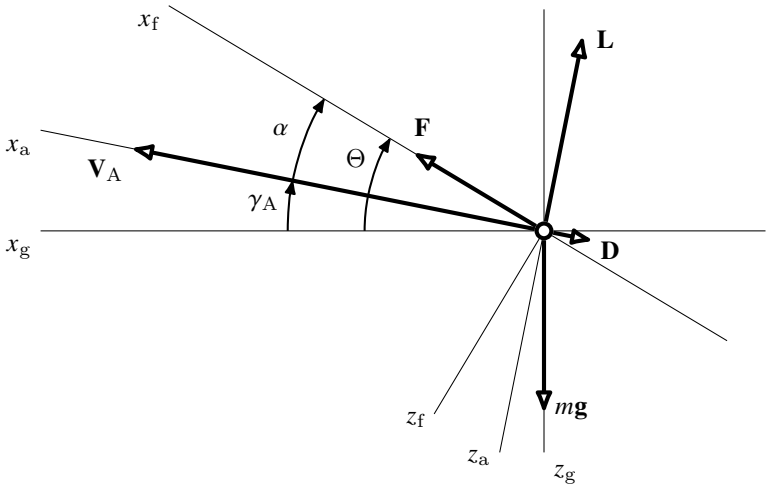

Fig. 3 Longitudinal axes with angles and vectors for $\beta = 0$.

C. Longitudinal equations of motion

The longitudinal equations of motion without thrust are given as non-linear 4-state, ordinary differential equations [12, 16, 25]:

$$m\dot{V}_\mathrm{A} = -\frac{1}{2}\varrho V_\mathrm{A}^2 S C_\mathrm{D}(\alpha,\eta) - g\sin\gamma_\mathrm{A}; \tag{1}$$

$$mV_\mathrm{A}\dot{\gamma}_\mathrm{A} = \frac{1}{2}\varrho V_\mathrm{A}^2 S C_\mathrm{L}(\alpha,\eta) - g\cos\gamma_\mathrm{A}; \tag{2}$$

$$I_y\dot{q} = \frac{1}{2}\varrho V_\mathrm{A}^2 S c_\mathrm{A} C_\mathrm{m}(\alpha,\eta)\,; \tag{3}$$

$$\dot{\Theta} = q; \tag{4}$$

with the pitch angle

$$\Theta = \gamma_\mathrm{A} + \alpha \tag{5}$$

and the air speed V_A as norm of the velocity vector relative to air. Then, C_L, C_D, C_m are dimensionless coefficients connected to lift force, drag force, and pitching moment. The elevator deflection η is, by convention, negative when causing a positive pitching moment.

The aerodynamic coefficients of the body, wing, and surfaces of Cumulus have been simulated at selected angles of attack and elevator deflections using static computational fluid dynamics (CFD) and are given to

$$(\alpha_i, \eta_i, C_{\mathrm{L},i}, C_{\mathrm{D},i}, C_{\mathrm{m},i})_{1\le i\le k} \subset \mathbb{R}^5, \tag{6}$$

where k denotes the number of combinations in α and η at which the CFD simulation was evaluated. Note that we do not further model the effects of the pitch rate q to aerodynamic coefficients due to a lack of dynamic data from CFD. Local stability is obtained by placing the centre of gravity before the aerodynamic centre [2, 26]. It is well known that the pitch rate does not affect the trim conditions, but indeed their stability, and we shall encounter this in the subsequent sections.

D. Polynomial aerodynamic coefficients

Polynomial models benefit from their infinite-differentiable nature and have therefore been used to model full-envelope aerodynamic coefficients [12, 16]. Fitting a polynomial function to discrete data points or measurements is straight-forward and often provided by scientific computation softwares. We find optimal

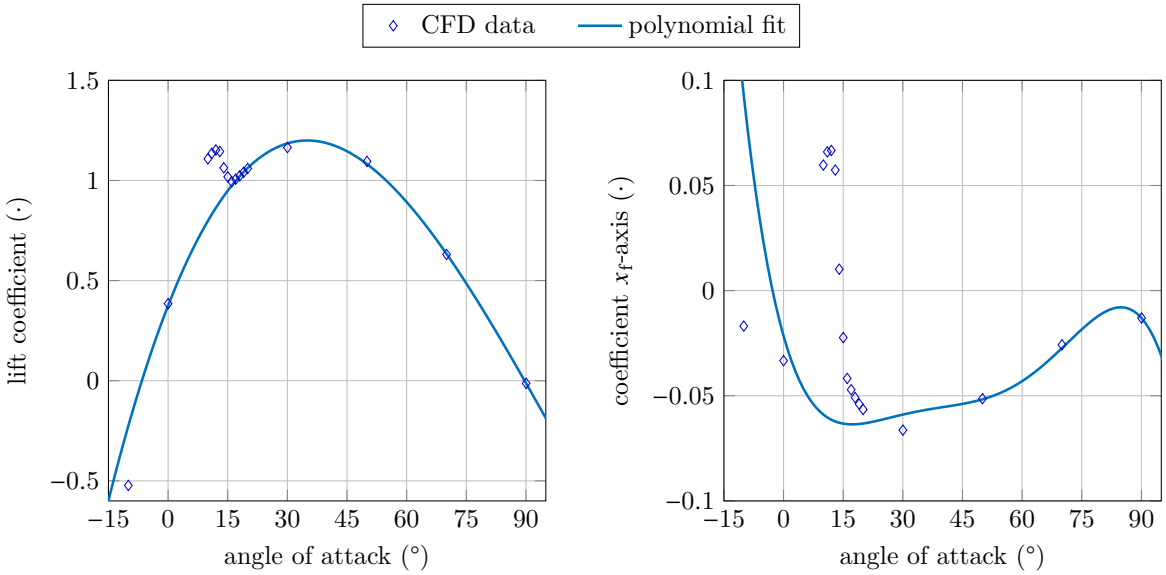

(a) Aerodynamic C_{L} coefficient. **(b) Aerodynamic C_{X} coefficient.**

Fig. 4 Polynomial model of aerodynamic coefficients.

polynomials Γ of finite degrees for the CFD data in (6) by solving the functional minimization problem

$$\Gamma_{\mathrm{opt}} = \arg\min_{\Gamma} \sum_{i=0}^{k} w_i \left| \Gamma(\alpha_i) - C_{\odot,i} \right|^2, \tag{7}$$

where k is again the number of data points from CFD, $C_{\odot,i}$ are the simulated, aerodynamic coefficients at angle of attack α_i, and $w_i > 0$ is a positive weight associated with the data. A solution to (7) can be obtained by least-squares optimization [27].

In order to prevent overfitting for the data points in the normal flight regime, where CFD simulations have been performed in steps in the angle of attack of 1°, we introduce the weights [28]

$$w_i = \begin{cases} 0.1 & \text{if } \alpha_i \leq 20°; \\ 1 & \text{else.} \end{cases}$$

The resulting, 3rd-order polynomial model is shown in Fig. 4. While the polynomial roughly fits the CFD data for the lift coefficient (Fig. 4a), it fails to represent the aerodynamics in the body axis system as demonstrated in Fig. 4b. An extensive discussion of polynomial aerodynamic models can be found in Cunis et al. [29].

E. Piecewise polynomial aerodynamic coefficients

To overcome the limits of polynomial models, Cunis et al. [29, 30] proposed to fit polynomial segments *piecewise* both for low and high angles of attack as the aerodynamics are significantly altered by the stall of the wings. Here, a pair of polynomial functions virtually accounting for the dynamics before and after stall are obtained. The resulting model is continuous over the entire domain but not necessarily differentiable in its joint. Such piecewise optimal polynomial functions are obtained as simultaneous solution to

$$\left(\Gamma_{\text{opt}}^{pre}, \Gamma_{\text{opt}}^{post}\right) = \arg\min_{\Gamma_{1,2}} \sum_{i \in \mathcal{I}_1} w_i \left|\Gamma_1(\alpha_i) - C_{\circledcirc,i}\right|^2 + \sum_{i \in \mathcal{I}_2} w_i \left|\Gamma_2(\alpha_i) - C_{\circledcirc,i}\right|^2, \tag{8}$$

where $\mathcal{I}_{1,2}$ are the indices of low and high angle of attack data, respectively, chosen a priori. The resulting piecewise model is given as

$$\Gamma_{\text{pw}}(\alpha, \cdots) = \begin{cases} \Gamma_{\text{opt}}^{pre}(\alpha, \cdots) & \text{if } \alpha \leq \alpha_0; \\ \\ \Gamma_{\text{opt}}^{post}(\alpha, \cdots) & \text{else;} \end{cases} \tag{9}$$

with $\Gamma_{\text{opt}}^{pre}(\alpha_0, \cdot) \equiv \Gamma_{\text{opt}}^{post}(\alpha_0, \cdot)$ and α_0 is found as joint of the C_{X} coefficient. The `pwpfit` toolbox then ensures that all coefficient models are continuous in the same angle of attack α_0 [31].

Fig. 5 shows the piecewise model and their polynomial segments. Defined as piecewise polynomials, we are able to account for the full-envelope characteristics both of the lift and drag coefficients as well as the coefficients in body axes. The pitch-moment coefficient C_{m} is modeled likewise [32].

F. Blending function for the piecewise model

Numerical tools, such as the Newton method, which utilise the local gradient, fail at the discontinuity of the partial first derivative of (9) in α. Instead, we are blending the polynomial segments into each other using the Heaviside step function:

$$\Gamma_{\mathcal{H}}(\alpha, \cdots) = \mathcal{H}(\alpha - \alpha_0)\, \Gamma_{\text{opt}}^{pre}(\alpha, \cdots) + (1 - \mathcal{H}(\alpha - \alpha_0))\, \Gamma_{\text{opt}}^{post}(\alpha, \cdots)\,. \tag{10}$$

A smooth, analytic approximation for $\mathcal{H}(\cdot)$ is found in the *logistic function*,

$$\mathcal{H}_\epsilon(t) = \frac{1}{1 + e^{-2t/\epsilon}}, \tag{11}$$

which has $\mathcal{H}_\epsilon(0) = \frac{1}{2}$, $\mathcal{H}_\epsilon(t \to -\infty) = 0$, $\mathcal{H}_\epsilon(t \to +\infty) = 1$ for $\epsilon > 0$. Naturally, it is desirable to have the logistic parameter ϵ as small as possible in order to increase steepness; on the other hand, we need ϵ to be

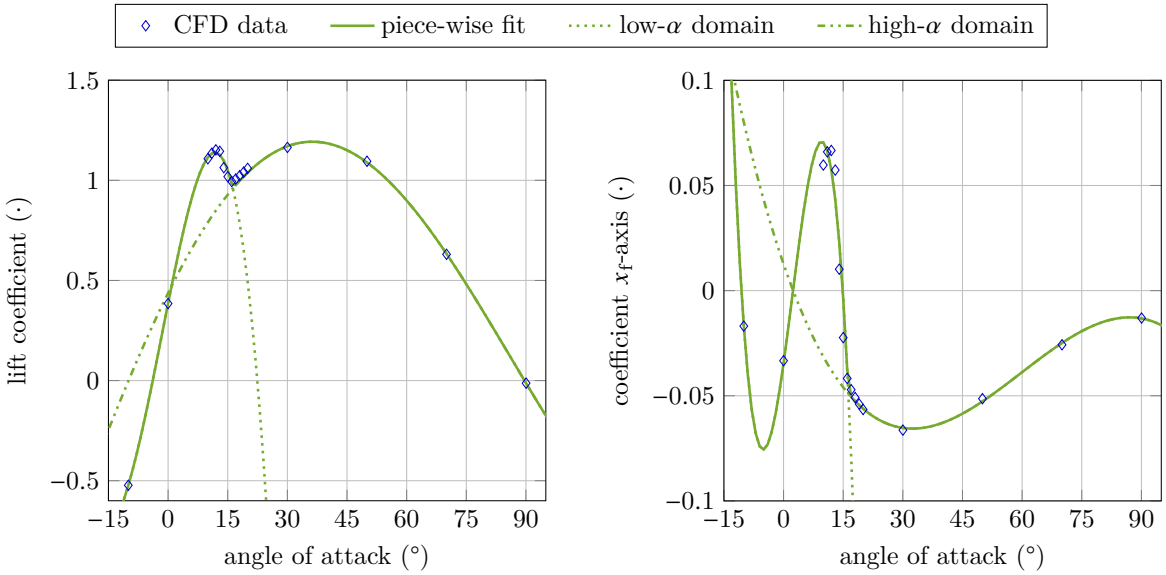

(a) Aerodynamic C_L coefficient. **(b) Aerodynamic C_X coefficient.**

Fig. 5 Piecewise model of aerodynamic coefficients with polynomial segments.

sufficiently large to suit a numerical method. We then have that $\mathcal{H}_\epsilon$ under-approximates the Heaviside step by no more than $\delta > 0$ outside the interval $(-\tau; \tau)$ if and only if

$$\epsilon < \frac{2\tau}{\ln(\delta^{-1} - 1)}.$$

Fig. 6 shows the blended piecewise model around the joint α_0. The polynomial segments are blended into each other by $\mathcal{H}_\epsilon$ with $\epsilon = \pi/36$.

III. Static Bifurcation Analysis

Aircraft trim conditions provide an initial insight into nonlinear aerodynamics. Unlike linear systems, nonlinear dynamics may exhibit multiple of those equilibria and knowledge about their existence and stability is essential to any development of flight control laws. In this section, we conduct a preliminary study of longitudinal trim conditions without further assumption about damping. As zero rate is imperative for trim, damping effects will affect stability but not existence and location of the trim conditions. Existence, branching, and stability of equilibria is the domain of *continuation and bifurcation theory*, which we are going to present first. We then discuss the longitudinal trim conditions and initial stability results before introducing damping models in the subsequent sections.

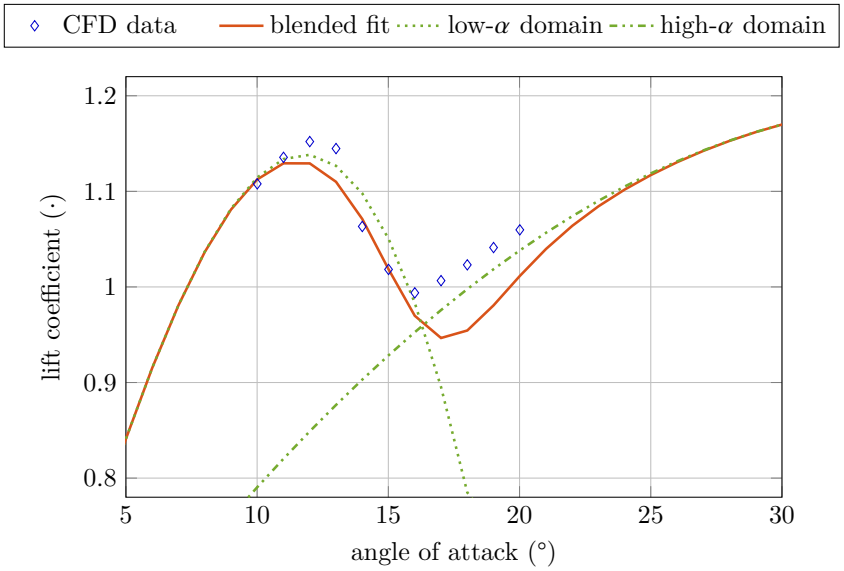

Fig. 6 Blended piecewise polynomial model of the aerodynamic lift coefficients for $\epsilon = \pi/36$.

A. Theory of bifurcation

The equations of motion of section B are written as 4-state ordinary differential equations

$$\mathbf{f}(\mathbf{X}, \eta) = \begin{bmatrix} \dot{V}_\mathrm{A} \\ \dot{\gamma}_\mathrm{A} \\ \dot{q} \\ \dot{\Theta} - \dot{\gamma}_\mathrm{A} \end{bmatrix} \tag{12}$$

with states $\mathbf{X}^T = \begin{bmatrix} V_\mathrm{A} & \gamma_\mathrm{A} & q & \alpha \end{bmatrix}$ and input η. The system is in an equilibrium or *trim condition* if and only if $\mathbf{f}(\mathbf{X}, \eta) = \mathbf{0}$. Here, (4) directly implies $q = 0$ as necessary precondition for trim. Stability of an equilibrium $(\mathbf{X}^*, \eta^*)$ in its close neighbourhood is locally determined by the Jacobian matrix $\mathbf{J}^* = \frac{\partial \mathbf{f}}{\partial \mathbf{X}}(\mathbf{X}^*, \eta^*)$; namely, $(\mathbf{X}^*, \eta^*)$ is locally asymptotically stable if and only if all eigenvalues of $\mathbf{J}^*$ have strictly negative real part, and unstable otherwise [33]. If, for some parameter η^*, an eigenvalue of the Jacobian at the corresponding trim condition $(\mathbf{X}^*, \eta^*)$ crosses zero and the trim condition changes stability, we have a critical or *bifurcation* point (BP). Well-known bifurcations are *saddle-node*, *pitch-fork*, and *transcritical* as well as, for systems of second order or higher, *Andronov-Hopf bifurcations* the latter are characterised by a family of periodic orbits emanating around the critical point. [34]

With the elevator deflection as single parameter,[¶] bifurcation analysis is a result of a continuation method,

[¶]The elevator deflection is chosen as continuation parameter similar to previous studies [5, 18]; being a control input, this choice further allows a quick connection between bifurcation analysis and in-flight measurements.

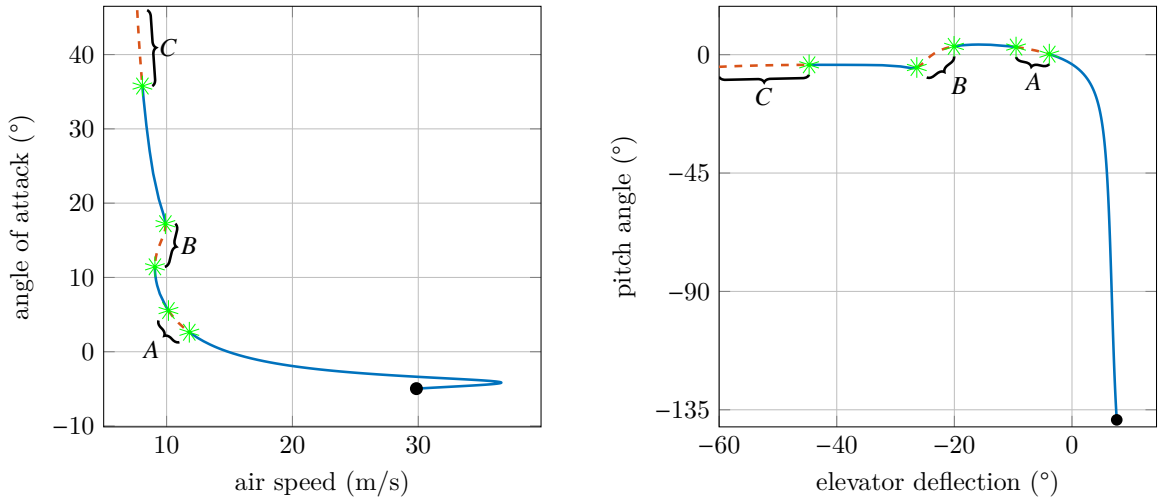

(a) Angle of attack α over air speed V. **(b) Pitch angle Θ over elevator deflection η.**

Fig. 7 Trim conditions of unthrottled longitudinal motion with the unstable regimes (A, B, C) of equilibria dashed (- - -); Hopf bifurcations marked by ✳; starting point marked by ● .

where the four equalities of $\mathbf{f}(\mathbf{X}, \eta^*) = \mathbf{0}$ are solved for small changes in η^*; stability of each trim condition is determined by its Jacobian, $\mathbf{J}^*$, and we have the necessary condition $|\mathbf{J}^*| = 0$ for a bifurcation point [16]. Continuation and bifurcation of a given system can be computed using toolboxes such as COCO [35], MATCONT [36], or the Dynamical Systems Toolbox [37]. In this section, we analyse the trim conditions of longitudinal flight and their eigenvalues for the equations of motion of section B. By comparison of the model with the flight experiment data and introduction of appropriate pitch damping models, we shall later extend the model to cover the dynamics of deep-stall transitioning flight.

B. Stability of longitudinal trim conditions

The longitudinal trim conditions of unthrottled flight (F = 0) along the range of the elevator have been computed using the *Continuation Core and Toolboxes* [COCO, 38] for MATLAB and are shown in Fig. 7. For normal deflections (ca. $-3° \leq \eta \leq 3°$), the trim conditions resemble a stable, moderate descent with air speeds between 12 m/s and 18 m/s and path inclination angles above −10°. With negative deflections, the angle of attack increases while the air speed decreases – a well-known behaviour in aeronautics – until the additional lift decreases: the aircraft stalls (Fig. 7a). Yet, the branch of trim conditions is continued into a deep-stall descent of the almost levelled aircraft (Fig. 7b). At larger, positive deflections instead, the trim conditions indicate a steep dive nose-down. The regimes of unstable trim conditions in level flight, after stall, and in deep-stall are marked by A, B, and C, respectively.

Classically, the longitudinal motion is divided into the short-period oscillation, involving angle of attack

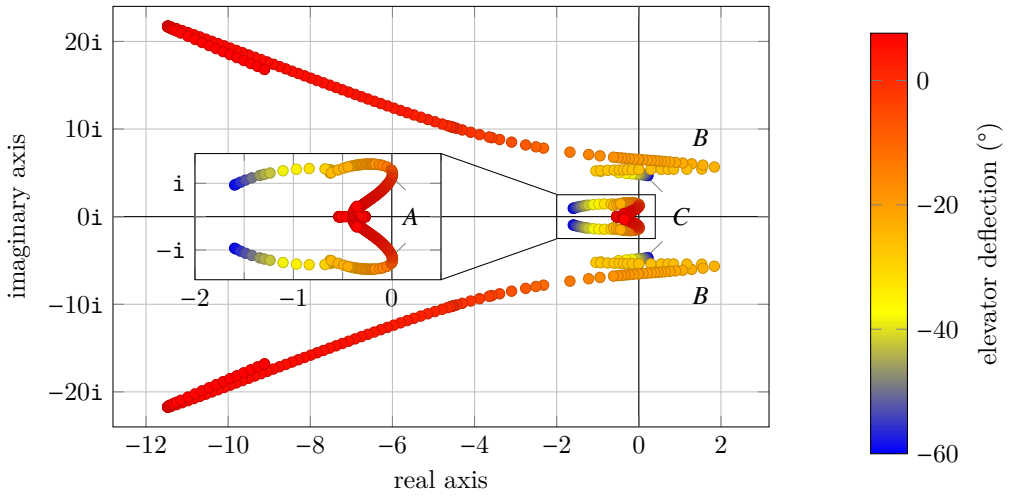

Fig. 8 Eigenvalues of longitudinal motion for varying elevator deflections; eigenvalues in the right half-plane (A, B, C) correspond to unstable trim conditions.

and pitch rate, and the long-period phugoid oscillation of airspeed and flight-path angle [2]. Consequently, we expect two pairs of complex-conjugated eigenvalues. Fig. 8 illustrates the eigenvalues of (12) in the complex plane for the continuation of elevator deflections: The eigenvalues of the phugoid mode are distinguished by small real and imaginary parts, showing the characteristic under-damped and slow motion, while the short period eigenvalues indicate the damped but fast oscillation. When one pair of eigenvalues enters the right half-plane, the longitudinal motion turns unstable and a Hopf bifurcation occurs.

IV. Analysis of Dynamic Models

With the pitch rate not being taken into account by the static CFD simulation, the analysis above has revealed that the model is insufficiently damped to be stable in deep-stall transition, while the flight experiments suggest stable equilibria here. Instead, we need to separately add damping effects to the aerodynamics. We will present two alternative models of pitch damping, each depending on a single, unknown parameter, and discuss stability and time responses for variations in these parameters. Finally, we obtain a quantitative model by optimization against the set of measured step responses.

A. Pitch damping models

Unsteady aerodynamics for stark changes of the aircraft's orientation relative to the air stream affect the damping of the aircraft. In order to describe the effects of a non-zero q to the pitch motion, we provide and compare the two models described in the following. The first model will consist of a simple linear damping term in the pitch-moment equation, that constitutes a steady modeling approach. The second modeling approach takes into account the effective change of the angle of attack due to the rotation of the wings and

thus can be considered as quasi-steady. To fully represent unsteady dynamics, one would need to include either the derivatives of pitch rate and angle of attack or a sequence of their former values over time; this is left for future work. The models discussed here will be of the form $\dot{q} = g(\mathbf{X}, \eta, \cdot)$ with a single, unknown parameter for each model.

Linear damping model A simple model of the pitch damping effects is given by the extension of (3) with a damping term linear in q,

$$\dot{q} = \frac{1}{2}\varrho V_{\mathrm{A}}^2 S c_{\mathrm{A}} I_y^{-1} C_{\mathrm{m}}(\alpha, \eta) - \kappa_{\dot{q}q} q, \tag{13}$$

where $\kappa_{\dot{q}q} > 0$ is the equivalent to linear dampers in classical mechanics.

Model of induced angle of attack More physically inspired, we can model the changes in the angle of attack induced by the non-zero pitch rate. Namely, angle of attack and side-slip angle are calculated as [24]

$$\sin\alpha = \frac{w_{\mathrm{A}}}{\sqrt{u_{\mathrm{A}}^2 + w_{\mathrm{A}}^2}}; \qquad \sin\beta = \frac{v_{\mathrm{A}}}{V_{\mathrm{A}}}; \tag{14}$$

where u_{A}, v_{A}, and w_{A} are the components of the air-path velocity vector in the body axis system. With the side-slip angle being neglected, *i.e.*, the lateral component v_{A} is much smaller than V_{A}, Eq. (14) simplifies to

$$\sin\alpha = \frac{w_{\mathrm{A}}}{V_{\mathrm{A}}}. \tag{15}$$

A non-zero pitch rate leads to a vertical motion of the wing as well as the horizontal tail, proportional to q,

$$\bar{V}_q \sim q, \tag{16}$$

where the proportionality is positive if the aerodynamic center of the aircraft is located behind the aircraft's center of gravity. (That is, the aircraft is stable [26].) Introducing the induced angle of attack $\tilde{\alpha} = \alpha + \Delta\tilde{\alpha}$ and noting $\tilde{w}_{\mathrm{A}} = w_{\mathrm{A}} + \bar{V}_q$, we have

$$\sin\tilde{\alpha} = \frac{w_{\mathrm{A}}}{V_{\mathrm{A}}} + \frac{\bar{V}_q}{V_{\mathrm{A}}}. \tag{17}$$

Trigonometric identity yields

$$\sin(\alpha + \Delta\tilde{\alpha}) = \sin\alpha\cos\Delta\tilde{\alpha} + \cos\alpha\sin\Delta\tilde{\alpha}$$

and with (15) and small changes $\Delta\tilde{\alpha}$ we conclude in

$$\Delta\tilde{\alpha} \approx \lambda' \left(\cos\alpha\right)^{-1} \frac{q}{V_\mathrm{A}}, \tag{18}$$

where λ' is the (unknown) constant of proportionality between $\bar{V}_q$ and q. Using the notation of the normalized pitch rate $\hat{q} = qc_\mathrm{A}/V_\mathrm{A}$, insertion into (3) gives us

$$\dot{q} = \frac{1}{2}\varrho V_\mathrm{A}^2 S c_\mathrm{A} I_y^{-1} C_\mathrm{m}\Big(\alpha + \lambda_{\alpha q}\left(\cos\alpha\right)^{-1}\hat{q}, \eta\Big) \tag{19}$$

with $\lambda_{\alpha q} = \lambda'/c_\mathrm{A} > 0$ for stable aircraft. Here, for $\hat{q}, \eta = const.$ the curve of $C_\mathrm{m}(\alpha, \cdot)$ is shifted to $C_\mathrm{m}(\tilde{\alpha}, \cdot)$ by $\Delta\tilde{\alpha}$. With $C_\mathrm{m}(\tilde{\alpha}, \cdot)$ monotonically decreasing in $\tilde{\alpha}$, a positive pitch-rate decreases the pitch moment ($\alpha \leq \tilde{\alpha} \Rightarrow C_\mathrm{m}(\alpha, \cdot) \geq C_\mathrm{m}(\tilde{\alpha}, \cdot)$; and vice-versa), effectively damping the motion. For an unstable aircraft where the wing's aerodynamic center is located *before* the center of gravity [26], $C_\mathrm{m}(\tilde{\alpha}, \cdot)$ *increases* in $\tilde{\alpha}$; with $\lambda_{\alpha q} < 0$ then, the pitch moment is again decreased by a positive pitch-rate resulting in a dissipative system.

B. Change of stability due to pitch damping

Both the linear damping model (13) and the model of induced angle of attack (19) rely on the choice of suitable parameters $\kappa_{\dot{q}q}, \lambda_{\alpha q} > 0$, which are not easily determined. We therefore provide an analysis of trim conditions, stability, and eigenvalues as well as dynamics system responses for variation of those parameters.

The change in $\kappa_{\dot{q}q}$ or $\lambda_{\alpha q}$ does not affect the existence or location of longitudinal trim conditions, as $q = 0$ has been identified as necessary precondition for trim. However, the occurrence of Hopf bifurcations (and thus the size of unstable regimes) alters for non-zero damping parameters: Fig. 9 shows the respective values of the damping parameters $\kappa_{q\dot{q}}, \lambda_{\alpha q}$, for each of the two damping models, such that the trim condition for the elevator deflection η undergoes a Hopf bifurcation. As result, the regimes of unstable trim conditions within the range of the elevator deflections shrink and eventually vanish for increasing values of the damping parameters. In the regimes A and C, the damping models (13) and (19) are similar in terms of Hopf bifurcations for increasing parameters $\kappa_{\dot{q}q}$ and $\lambda_{\alpha q}$, respectively. Only in regime B larger values of $\lambda_{\alpha q}$ would be necessary to fully stabilise the dynamics with (19) in this regime. For negative damping the unstable regimes are enlarged.

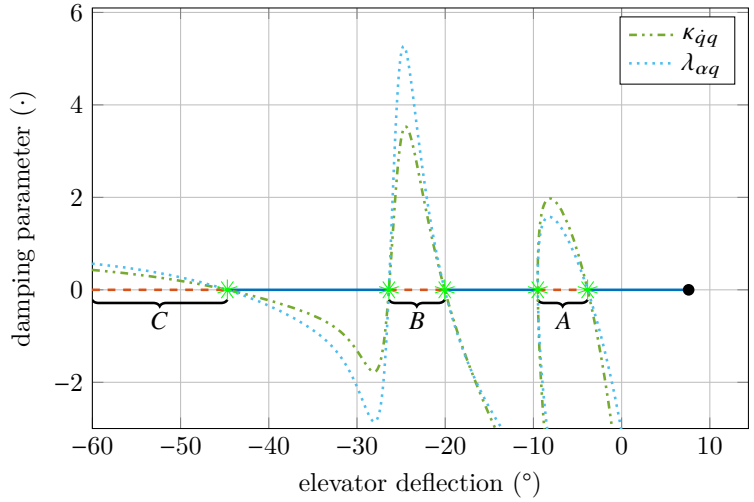

Fig. 9 Occurrences of Hopf bifurcations at elevator deflection η for continuation of the model parameters.

We shall discuss the effects of the damping coefficient for each of the unstable regimes:

***A*: Instability in level-flight** In the undamped model ($\kappa_{\dot{q}q} = \lambda_{\alpha q} = 0$), the eigenvalues of the phugoid mode enter the right half-plane in level flight and the trim conditions are unstable for elevator deflections around $\eta = -8°$ (marked with *A* in Fig. 7 and 8). From continuation of Hopf bifurcations for the pitch damping coefficient in Fig. 9, we learn that this instability vanishes for damping coefficients of approximately $\kappa_{\dot{q}q} \geq 2$ and $\lambda_{\alpha q} \geq 1.6$. Fig. 10 shows step responses to elevator deflections from $\eta_{t<0} = 0°$ to $\eta_{t\geq 0} = -8°$ and damping coefficients $\kappa_{\dot{q}q}, \lambda_{\alpha q} \in [0; 5]$: with eigenvalues close to zero, both unstable and stable conditions respond slowly to the step input.

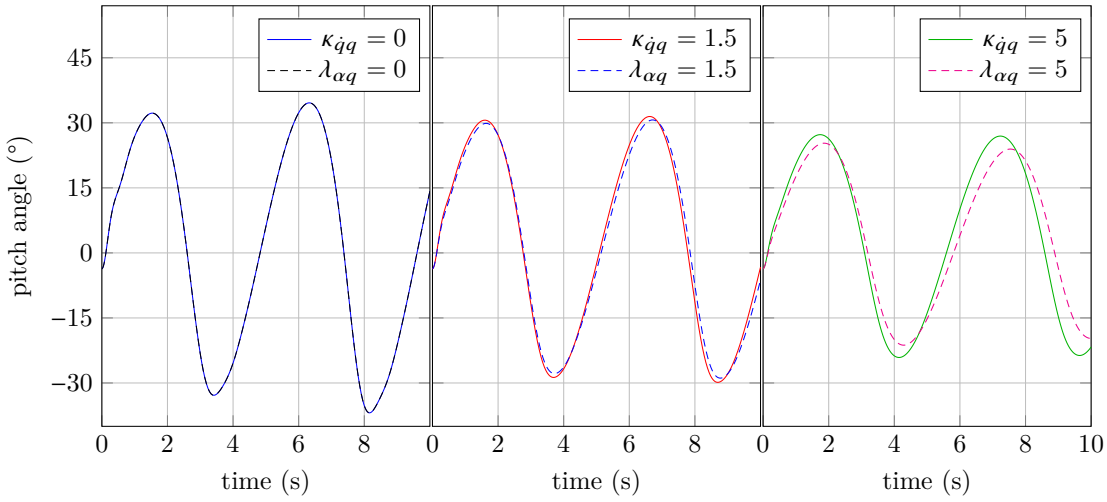

Fig. 10 Step responses for $\eta_{t\geq 0} = -8°$ and increasing pitch damping coefficients.

***B*: Instability in post-stall** At stall, flight dynamics often turn unstable leading to various upset situations for conventional aircraft [5]. The Cumulus model, too, has a regime of unstable trim conditions after stall (Fig. 7, marked with *B*), i.e., for elevator deflections around $\eta = -24°$, that vanishes for pitch damping coefficients of approximately $\kappa_{\dot{q}q} \geq 3.5$ and $\lambda_{\alpha q} \geq 5.3$ (Fig. 9). If the elevator is deflected to this region the system responds to this step with superposed oscillations that are smoothen for larger damping coefficients (Fig. 11; here, values of $\kappa_{\dot{q}q}, \lambda_{\alpha q} \geq 5$ are sufficient for stability of the trim condition). Again, the unstable modes diverge slowly.

***C*: Instability in deep-stall** The instability in deep-stall is the first to vanish for increasing pitch damping coefficient but is in fact pushed towards larger, infeasible elevator deflections (Fig. 9, marked with *C*). Yet when unstable, an elevator step leads to an immediate divergence (see Fig. 12 for elevator deflection $\eta_{t\geq 0} = -50°$ with $\kappa_{\dot{q}q} = \lambda_{\alpha q} = 0$). Larger damping coefficients lead to a fast convergence in the deep-stall

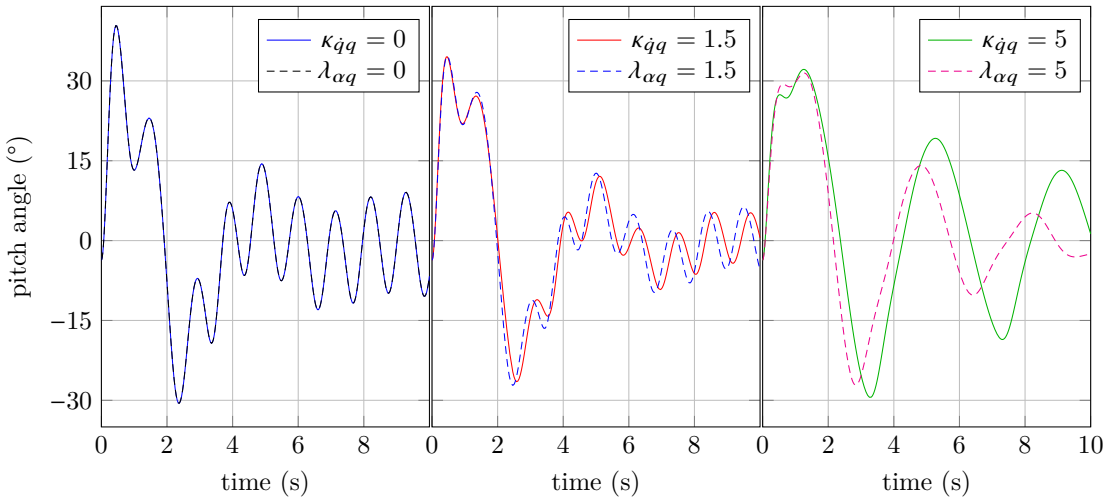

Fig. 11 Step responses for $\eta_{t\geq 0} = -24°$ and increasing pitch damping coefficients.

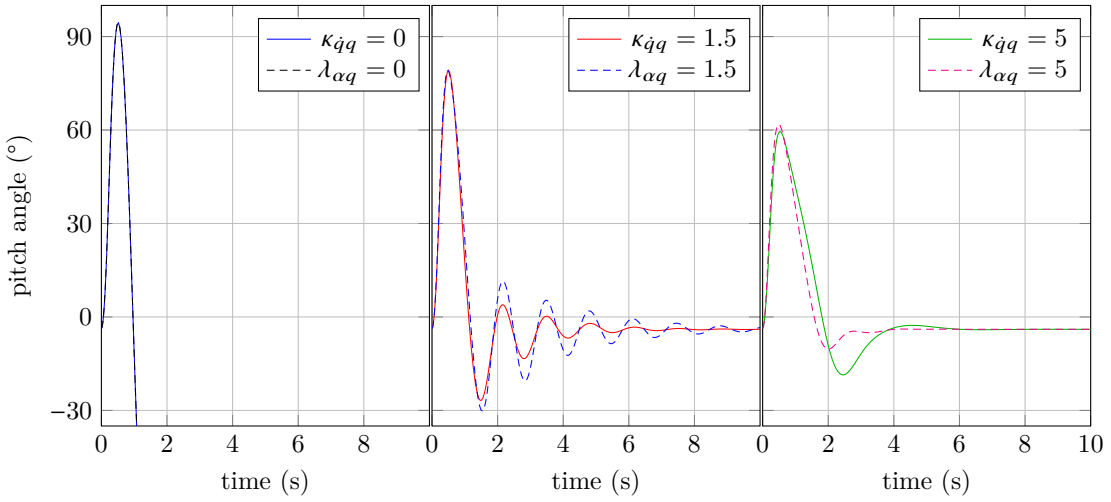

Fig. 12 Step responses for $\eta_{t\geq 0} = -50°$ and increasing pitch damping coefficients.

trim condition (Fig. 12 for $\kappa_{\dot{q}q}, \lambda_{\alpha q} > 0$). Note that the Cumulus One is known to be stable in deep-stall from flight experiments.

In these regimes, the pitch damping of the original model seems insufficient to represent stable modes in deep-stall. In addition to the trim conditions being unstable for large elevator deflections (regime *C* in Fig. 7), the undamped system does not represent the deep-stall transition behaviour of the flight experiments as illustrated by Fig. 13 for an elevator deflection of $\eta_{t\geq 0} = -38°$ (a mathematically stable trim condition for $\kappa_{\dot{q}q} = \lambda_{\alpha q} = 0$); here, the aircraft state does not approach the equilibrium smoothly but rather yields an almost-constant oscillation—opposite to a positive pitch damping coefficient—that converges rather slowly. In flight, we have experienced a smooth transition to deep-stall for this elevator deflection.

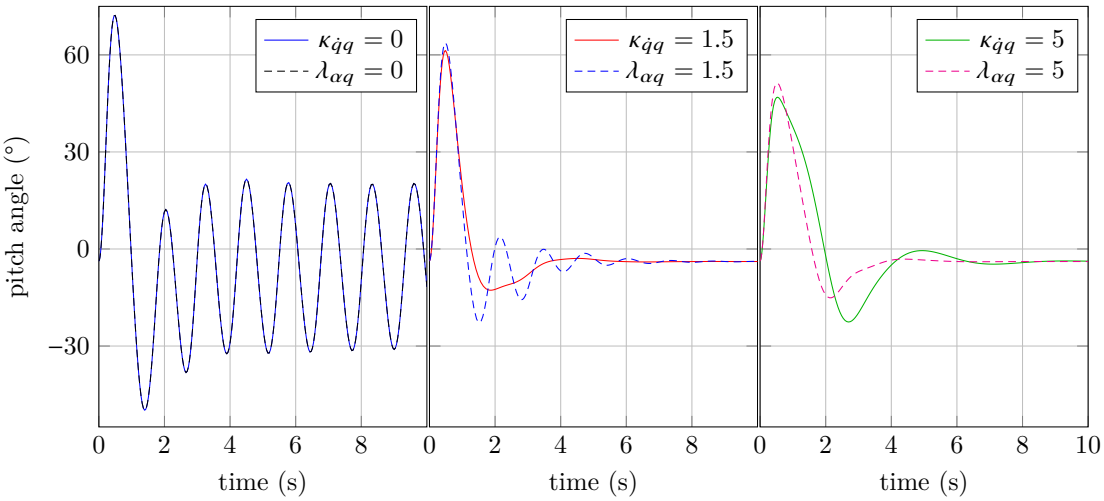

Fig. 13 Step responses for $\eta_{t\geq 0} = -38°$ and increasing pitch damping coefficients.

Fig. 14 now shows the location of eigenvalues for $\eta = -38°$ and increasing pitch damping coefficients: For $\kappa_{\dot{q}q}, \lambda_{\alpha q}$ small, the pair of eigenvalues of the short-period oscillation are close to the imaginary axis, representing the underdamped dynamics obtained in the previous figure. For larger values, this pair of eigenvalues moves deeper into the left half-plane, while the eigenvalues of the Phugoid oscillation move towards the imaginary axis but do not come close. The imaginary parts of all four eigenvalues are marginally affected by the pitch damping coefficient.

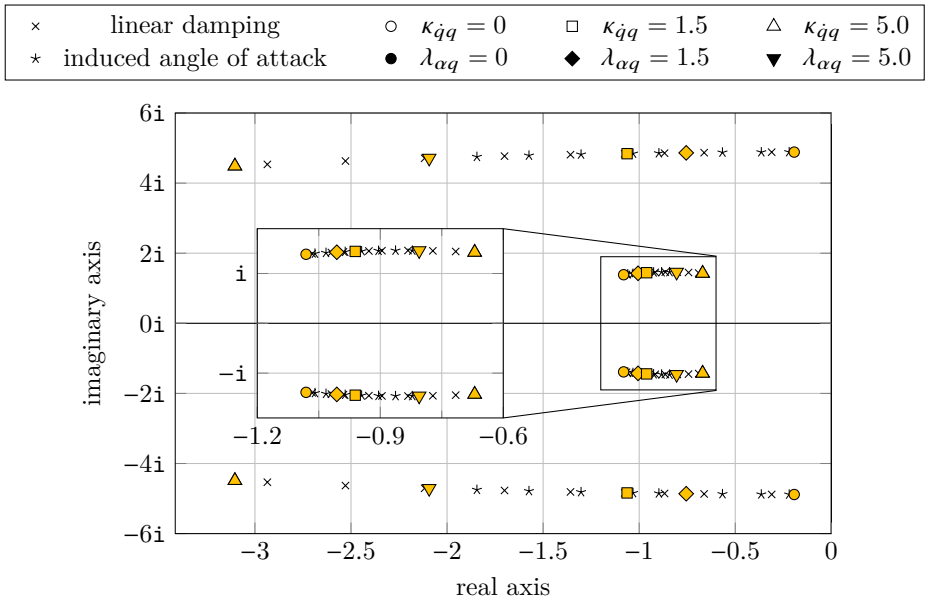

Fig. 14 Eigenvalues of longitudinal motion for $\eta = -38°$ and varying pitch damping coefficients.

C. Optimal model parameters

The static bifurcation analysis suggested the introduction of a pitch damping model; a further study of eigenvalues in this section has revealed the necessity of a sufficiently large damping parameter, in order to ensure both static and dynamic stability of the deep-stall transition. However, neither provide an actual guess of the parameter and indeed, the pitch damping behaviour is an unknown system property. A qualitative comparison of the model to the in-flight measurements can result in a rough estimate, but more accurate values are determined by optimization of the system output with respect to the recorded flight data. Different methods are commonly used for parameter estimation, one of the most notably being the maximum-likelihood method, [39], but without covariance matrix of the measurements, we will rely instead on a simple differentially-constrained optimization of the time-wise $\mathcal{L}_2$ error norm in order to compare and evaluate the proposed damping models. Here, we are going to find optimal values for parameters of both pitch damping models and for each test flight data set separately. The distribution of optimal parameters over the different (commanded) elevator deflections then will allow us to discriminate between the two proposed modeling approaches. As noted previously, this is not meant to be an identification of the real system and rather an attempt to fit the model as close as possible [compare 40, p. 29] and thus assess the proposed models. With the angle of attack and air speed not measured directly during flight, we use the recorded pitch angle during the initiation of the deep stall manoeuvre as reference for the step response of the equations of motion to fit the damping parameter and initial states for each step [39].

For optimal parameters of the pitch damping model, we solve the following differentially-constrained, quadratic optimization problem:

$$\begin{aligned} I_{\text{opt}} &= \min_{k_q, \mathbf{x}_0, \delta_t} \int_0^T \left(\alpha(t) + \gamma_{\text{A}}(t) - \Theta_{\text{meas}}(t+\delta_t)\right)^2 \mathrm{d}t \\ \text{such that} \quad & \dot{\mathbf{x}}(t) = \mathbf{f}\Big(\mathbf{x}(t), \eta_{t\geq 0}, k_q\Big) \quad \text{for } 0 \leq t \leq T \end{aligned} \tag{20}$$

where Θ_{meas} is the measured pitch angle in flight and δ_t is the time difference between recorded actuator command of the autopilot and the deflection of the elevator (time delay and actuator phase lag). The unknown parameter k_q, in lieu of the parameters $\kappa_{\dot{q}q}$ and $\lambda_{\alpha q}$ of the linear damping model and the model of induced angle of attack, respectively, is then subject to the optimization. Further free parameters are the initial state $\mathbf{x}(0) = \mathbf{x}_0$ as well as the time difference δ_t. Introducing discrete operators, a numerical solution

to (20) is computed by MATLAB's `fmincon` function solving for $\boldsymbol{\Xi} \in \mathbb{R}^n \times \mathbb{R}^2$ minimizing $I(t_i, \boldsymbol{\Xi}) \in \mathbb{R}$, where

$$I(t_i, \boldsymbol{\Xi}) = \sum_i \left(\alpha_i + \gamma_{\mathrm{A}\,i} - \tilde{\Theta}(t_i + \delta_t)\right)^2 \tag{21}$$

$$\text{where } \forall 1 \leq i \leq N \quad \frac{\Delta}{\Delta t}\mathbf{x}_i - \mathbf{f}\left(\mathbf{x}_{i-1}, \eta_{t\geq 0}, k_q\right) = 0 \tag{22}$$

with

$$\boldsymbol{\Xi} = \begin{bmatrix} \mathbf{x}_0 & \delta_t & k_q \end{bmatrix}^T. \tag{23}$$

Here, the measured pitch angle has been cubically interpolated to $\tilde{\Theta}(\cdot)$ to yield continuity; the sequence $(\mathbf{x}_i, t_i)_{1\leq i\leq N}$ is found using `ode45` with parameter k_q and $(t_i)_i \subset [0, T]$. Table 2 presents the optimal values for $\kappa_{\dot{q}q}$ and $\lambda_{\alpha q}$ as well as for the time difference δ_t of the linear damping model and model of induced angle of attack, respectively, using MATLAB's `active-set` algorithm and starting from $\kappa_0 = \lambda_0 = 5$, $\delta_{t0} = 0$. A comparison of in-flight measurement and optimal fits, both as sequences with respect to time t and their corresponding frequency spectra, is examplary shown in Fig. 15 for the first data set.

Table 2 Optimal pitch damping parameters with data set #10 marked as outlier of the linear damping model.

Step	Data set	linear		induced	
		$\kappa_{\dot{q}q}$	δ_t / s	$\lambda_{\alpha q}$	δ_t / s
$\eta_{t\geq 0} = -38°$	1	1.240 27	0.079 14	1.584 49	0.097 56
	2	1.228 23	0.066 49	1.974 05	0.058 30
$\eta_{t\geq 0} = -41°$	3	1.966 33	0.046 97	2.473 11	0.046 32
	4	1.749 47	0.054 18	1.673 27	0.086 02
$\eta_{t\geq 0} = -44°$	5	2.091 83	0.019 37	2.870 59	0.044 86
	6	1.945 78	0.074 54	1.749 74	0.099 34
$\eta_{t\geq 0} = -47°$	7	2.384 01	0.030 50	2.254 81	0.086 21
	8	2.173 74	0.032 21	2.776 14	0.066 09
$\eta_{t\geq 0} = -50°$	9	2.239 84	0.033 21	2.414 70	0.084 21
	10	(3.558 45)	0.027 53	2.652 45	0.100 00
$\eta_{t\geq 0} = -53°$	11	2.317 44	0.041 97	2.291 33	0.086 83
	12	2.227 98	0.043 16	2.299 87	0.092 94

Upon a large elevator deflection one gets a stark response of the aircraft, yielding high angles of attack and pitch rates. If the pitch damping is not as simply linear as initially modeled but rather dependent on further parameters, we expect the optimal damping coefficient $\kappa_{\dot{q}q}$ of the linear model to be some function of the elevator deflection. Indeed, Table 2 clearly shows an increasing optimal linear coefficient as the elevator deflections decrease along the data sets. The optimal parameter of the model of induced angle of attack,

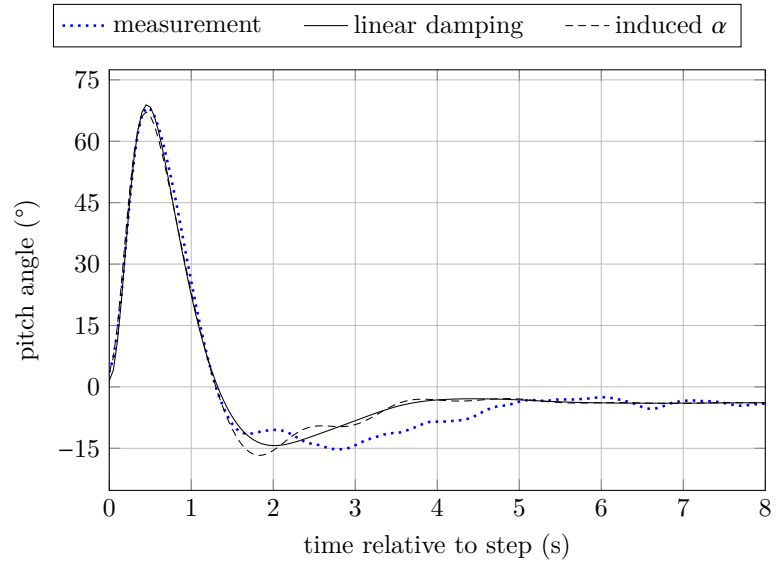

(a) Time domain.

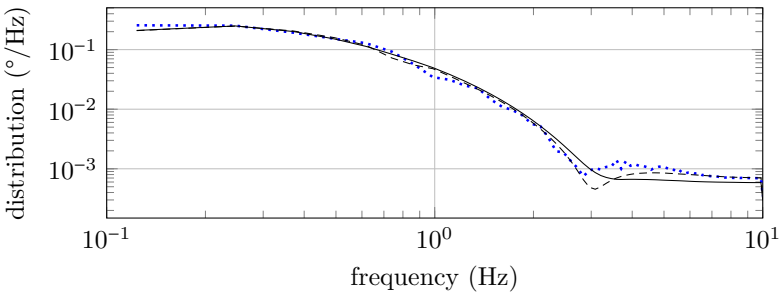

(b) Frequency domain.

Fig. 15 Optimal model fit for data set #1 **($\eta_{t\geq 0} = -38°$; $\kappa_{\dot{q}q} = 1.240\,27$; $\lambda_{\alpha q} = 1.584\,49$).**

although slightly increasing, seems to be less dependent on the elevator deflection; however, this model is more sensitive to external parameters and shows a lot of variation within the data set of equal steps in the deflection.

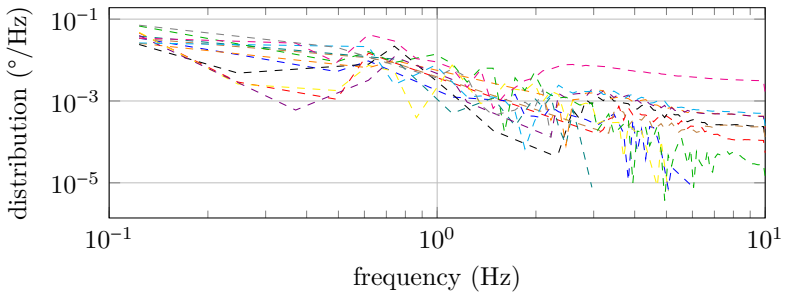

(a) Optimal models.

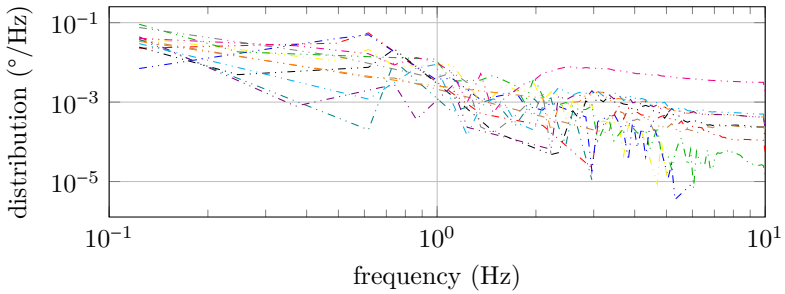

(b) Averaged models.

Fig. 16 Frequency spectra for the errors of optimal and averaged linear damping models.

Removing the outlying dataset #10 for the linear damping model, we result in estimates for the pitch damping parameters as means of the optimal parameters with their 1σ-confidence intervals:

$$\hat{\kappa}_{\dot{q}q} = 1.960\,45 \pm 0.402\,34 \tag{24}$$

$$\hat{\lambda}_{\alpha q} = 2.251\,21 \pm 0.427\,14. \tag{25}$$

We are now going to investigate how the effectiveness of the models to capture the deep-stall transition dynamics changes if the optimal parameter values are changed for the averaged parameters. Figs. 16 and 17 compare, for the linear damping model and the model of induced angle of attack, respectively, the frequency spectra of the errors between optimal models from Tab. 2 and the respective data sets with the errors of the averaged models ($\hat{\kappa}_{\dot{q}q}$ and $\hat{\lambda}_{\alpha q}$). For the linear damping model, the errors are compatible except for frequencies around approximately 0.6 Hz. The optimal model and averaged model of induced angle of attack similarly show an increased disparity for frequencies in the range of approximately 0.6 Hz to 0.75 Hz, although less so than for the linear damping. Neither the linear damping model and the model of induced angle of attack show large disparities in the errors for higher frequencies (2 Hz and beyond), where wind gusts and turbulences disturb the flight.

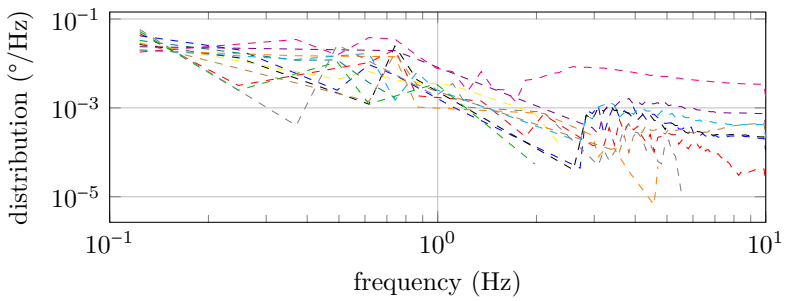

(a) Optimal models.

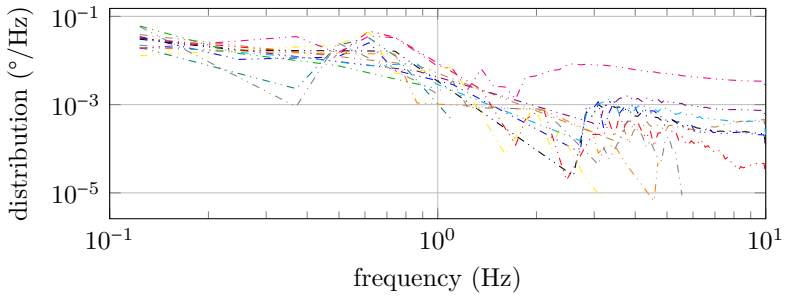

(b) Averaged models.

Fig. 17 Frequency spectra for the errors of optimal and averaged models of induced angle of attack.

The two kinds of pitch damping models that we proposed in this section, a constant gain on the pitch rate q and a shifting of the pitch-moment coefficient by the normalized rate $\hat{q}$, have shown similar properties in terms of stability and dynamics of the deep-stall transition as well as for the extraction of optimal parameters. Other approaches are reasonable, such as constant gain on the normalized rate or a pitch-moment derivative $C_{\mathrm{m}\hat{q}} = \frac{\partial C_{\mathrm{m}}}{\partial \hat{q}}$ thus providing dependency on the air speed, as well as the stability derivative $C_{\mathrm{m}\dot{\alpha}} = \frac{\partial C_{\mathrm{m}}\,\mathrm{d}t}{\partial\,\mathrm{d}\alpha}$ contributing for the horizontal tail [41]; however, a further study of these is omitted here for the similar nature of the proposed models does not suggest additional insights and the obtained results satisfy our needs.

In the subsequent study of six-degrees-of-freedom dynamics, we will therefore rely on the optimal linear model. The model of induced angle of attack, yet more elaborate, does not provide a constructive method to incorporate damping of the lateral rotations.

V. Transition to Deep-stall Flight

For conventional aircraft, aerodynamic stall of the wings almost inevitably leads to a departure of the vehicle. In consequence, the aircraft often enters a spiral or oscillatory spin motion which are fatal without appropriate recovery. An extensive study of post-stall modes has been provided for the Generic Transport Model by Gill et al. [5]. The GTM in particular is characterised by a “preference” to depart to the left

rather than to the right when stalling due to its slightly asymmetric aerodynamics. Cumulus One, on the contrary, is supposed to enter a deep-stall descent mode that is both longitudinally and laterally stable. This stable transition to deep-stall flight can be evaluated in a six-degrees-of-freedom bifurcation analysis. The CFD simulation was performed on a full-body assembly model of the aircraft which was assumed to be symmetric-by-design;[‖] slight asymmetries in the obtained lateral aerodynamic coefficients might therefore be due to numerical inaccuracies.

Here, we extend the longitudinal equations of motion of (1)–(4) and (13) to eight differential equations for the states

$$\mathbf{X}_{6\mathrm{dof}} = \left[\begin{array}{ccc:ccc:cc} u_\mathrm{A} & v_\mathrm{A} & w_\mathrm{A} & p & q & r & \Phi & \Theta \end{array}\right]^T \tag{26}$$

with the components of air velocity, $\mathbf{V}_\mathrm{A} = \begin{bmatrix} u_\mathrm{A} & v_\mathrm{A} & w_\mathrm{A} \end{bmatrix}^T$, and angular rates, $\boldsymbol{\omega} = \begin{bmatrix} p & q & r \end{bmatrix}^T$, defined in body axes; bank and pitch angles, Φ and Θ, respectively, in earth-fixed axes; as well as the inputs

$$\mathbf{U}_{6\mathrm{dof}} = \begin{bmatrix} \xi & \eta & \zeta \end{bmatrix}^T . \tag{27}$$

The deflections of elevator, η, ailerons, ξ, and rudder, ζ, are again negative when causing positive moments. (All variables as defined in ISO 1151-1 [24].)

The equations of motion are then given as

$$\dot{\mathbf{V}}_\mathrm{A} = \frac{1}{2}\rho V_\mathrm{A}^2 S m^{-1} \begin{bmatrix} C_\mathrm{X}(\alpha,\beta,\xi,\eta,\zeta) \\ C_\mathrm{Y}(\alpha,\beta,\xi,\eta,\zeta) \\ C_\mathrm{Z}(\alpha,\beta,\xi,\eta,\zeta) \end{bmatrix} - g \begin{bmatrix} \sin\Theta \\ \sin\Phi\cos\Theta \\ \cos\Phi\cos\Theta \end{bmatrix} - \boldsymbol{\omega} \times \mathbf{V}_\mathrm{A}; \tag{28}$$

$$\mathbf{I}\dot{\boldsymbol{\omega}} = \frac{1}{2}\rho V_\mathrm{A}^2 S \begin{bmatrix} b\, C_\mathrm{l}(\alpha,\beta,\xi,\eta,\zeta) \\ c\, C_\mathrm{m}(\alpha,\beta,\xi,\eta,\zeta) \\ b\, C_\mathrm{n}(\alpha,\beta,\xi,\eta,\zeta) \end{bmatrix} - \boldsymbol{\omega} \times \mathbf{I}\boldsymbol{\omega} - \mathbf{K}\mathbf{I}\boldsymbol{\omega}; \tag{29}$$

$$\begin{bmatrix} \dot{\Phi} \\ \dot{\Theta} \end{bmatrix} = \begin{bmatrix} 1 & \sin\Phi\tan\Theta & \cos\Phi\tan\Theta \\ 0 & \cos\Phi & -\sin\Phi \end{bmatrix} \boldsymbol{\omega}; \tag{30}$$

where $\tan\alpha = w_\mathrm{A}/u_\mathrm{A}$, $\sin\beta = v_\mathrm{A}/V_\mathrm{A}$, and $V_\mathrm{A} = \sqrt{u_\mathrm{A}^2 + v_\mathrm{A}^2 + w_\mathrm{A}^2}$. The linear damping is modeled with the

[‖] Dasam, V. K. and Holst, J., private communication (August 2019).

parameters $\mathbf{K} = \mathrm{diag}\big(\kappa_{pr}, \kappa_q, \kappa_{pr}\big)$. The aircraft's heading and its rate of change are not considered here.

Note that, for this simple demonstration of a bifurcation analysis, we use a coupled roll-yaw damping parameter κ_{pr}, since without reliable flight data for an identification of the lateral damping the observation of independent parameters κ_p, κ_r is feasible. With the physical origins of roll and yaw damping differing considerable, additional tests to obtain separate lateral damping models in future use are strongly recommended. As for the longitudinal motion, stability of the aircraft depends on the choice of the damping parameters and the underdamped system ($\kappa_{pr} = 0$) is in fact unstable for most parts of the normal flight range. A continuation of the occurring Hopf bifurcations reveals this dependency (Fig. 18): The pitch motion exhibits a pair of Hopf bifurcations in the post-stall domain, that were already encountered in the analysis of the longitudinal dynamics. For increasing pitch damping parameter κ_q, the Hopf bifurcation vanishes (note that the continuation of the pitch damping parameter has been set up around the optimal parameter; therefore, the longitudinal dynamics exhibit only a single pair). As for the longitudinal dynamics, trim conditions between are unstable. A third Hopf bifurcation exists at a positive elevator deflection governing the overall stability. With increasing roll-yaw damping parameter κ_{pr} this Hopf bifurcations moves towards neutral elevator but from $\kappa_{pr} > 1$, a corresponding Hopf bifurcation appears for $\eta = -60°$. If κ_{pr} is chosen sufficiently large, the pair of Hopf bifurcations, too, disappears. It should be noted, however, that roll damping in general does not have a stabilizing effect over the full envelope of bank angles. In order to maintain a stable system within the considered envelope, the damping parameters are chosen as

$$\mathbf{K} = \mathrm{diag}(2.5, 1.96, 2.5)\,. \tag{31}$$

With these damping parameters, then, we can perform a six-degrees-of-freedom bifurcation analysis starting from the elevator-neutral trim condition

$$\mathbf{X}^*_{\mathrm{6dof}} = \left[\begin{array}{ccc:ccc:cc} 14.09\,\mathrm{m/s} & <0.01\,\mathrm{m/s} & 0.12\,\mathrm{m/s} & 0.01\,°/\mathrm{s} & <0.01\,°/\mathrm{s} & 0.17\,°/\mathrm{s} & <0.01° & -3.64° \end{array}\right]^T$$

and

$$\mathbf{U}^*_{\mathrm{6dof}} = \Big[0.03° \quad -0.00° \quad 2.34°\Big]^T\,.$$

Note that the roll/yaw rates are non-zero at trim due to a slightly positive bank angle.

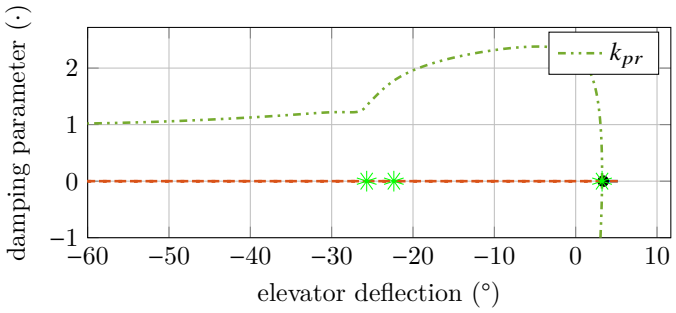

(a) Roll-yaw damping for $\kappa_q = 1.96$.

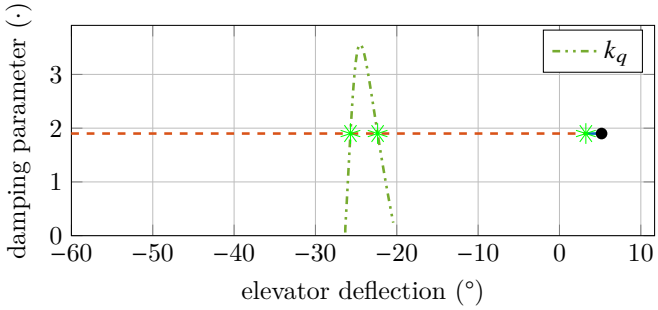

(b) Pitch damping for $\kappa_{pr} = 0$.

Fig. 18 Occurrences of Hopf bifurcations of the six-degrees-of-freedom motion for continuation of the model parameters.

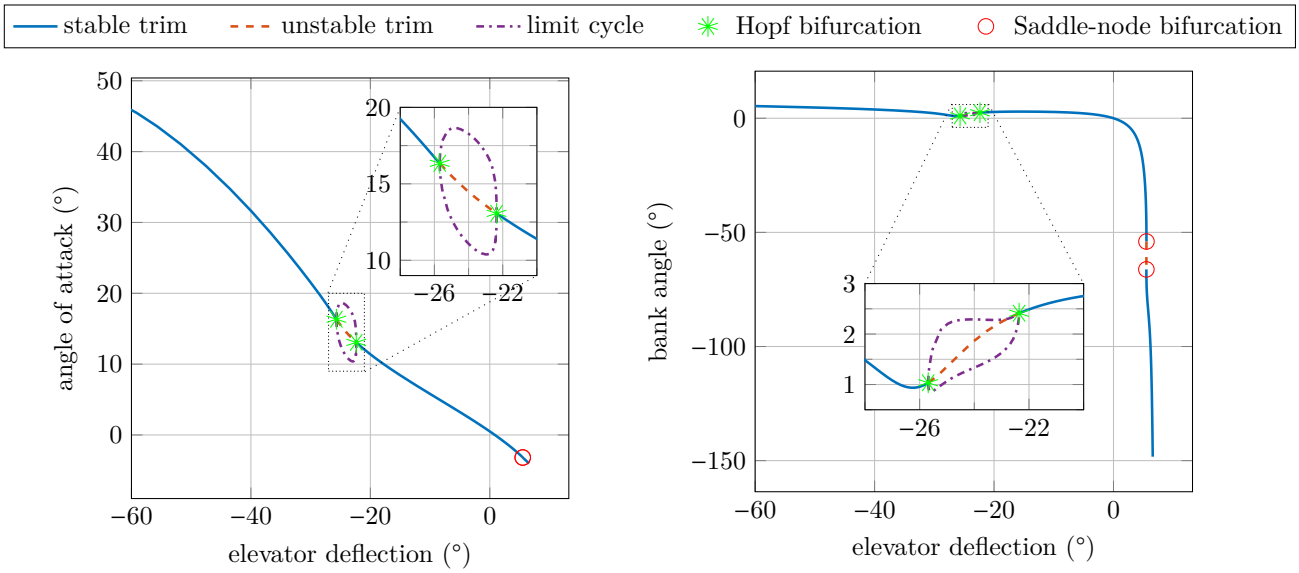

(a) Angle of attack α.

(b) Bank angle Φ.

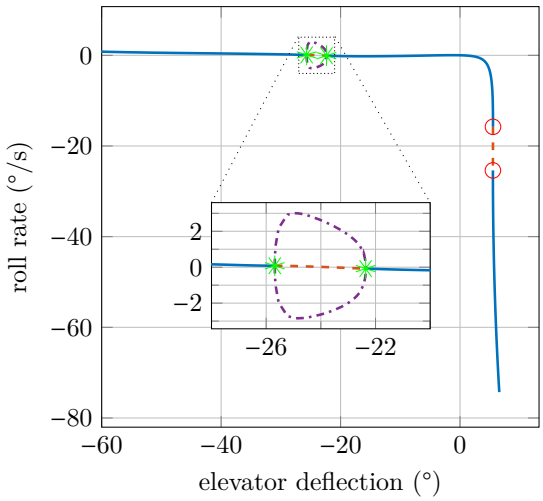

(c) Roll rate p.

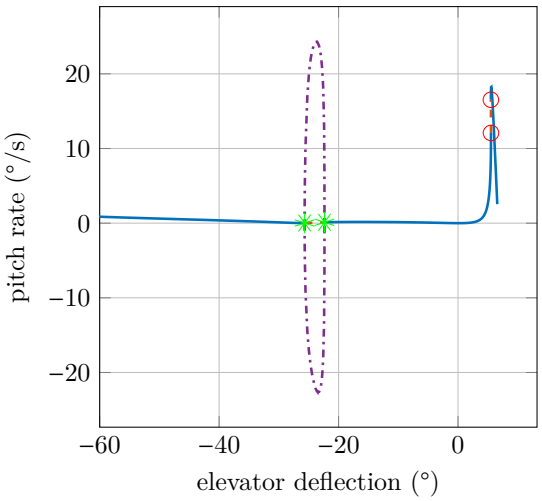

(d) Pitch rate q.

Fig. 19 Six-degrees-of-freedom trim conditions for continuation of the elevator deflection η.

Trim conditions of both longitudinal and lateral motion, as computed by COCO [38], are shown in Fig. 19. Due to a minor dependency of the aircraft's lateral asymmetry, the bank angle at trim deviates from neutral for increase angle of attack. On the other hand, the steep descent for positive elevator deflections involves increasing bank angles and therefore constant change of the heading. The previously encountered Hopf bifurcations around stall bear a family of limit cycles, shown enlarged in the insets, that in fact mainly affects the longitudinal motion (compare Figs. 19a and 19b). A pair of saddle-node bifurcations—a single real eigenvalue crossing the imaginary axis—between $-54°$ and $-66°$ bank angle reveal a branch of unstable trim conditions for constant angle of attack of approximately $-3.2°$. Fig. 20 illustrates the deep-stall and steep descent modes encountered at each end of the bifurcation. Note that the aircraft is drawn scaled with respect to longitude and latitude but in equal time steps; both trajectories are depicted for 10 s. The steep descent, when compared to the deep-stall mode, establishes a significantly larger descent rate in fast and tight downward helix. This circular trajectory must not be confused with a spiral motion, where the aircraft additionally exhibits rotations around its body axes. Instead, the turn is a result of lateral asymmetries of the polynomial model. Our bifurcation analysis has not found any spin or spiral modes, although we would expect some; due to the stability of the aircraft in deep-stall, branches of such limit cycles involving the lateral axis are disconnected from the main branch of longitudinal trim conditions and therefore difficult to find using continuation techniques. The analysis shows, however, that the Cumulus aircraft does not depart at stall, only develops a periodic orbit of longitudinal motion, before settling to a stable deep-stall trim condition.

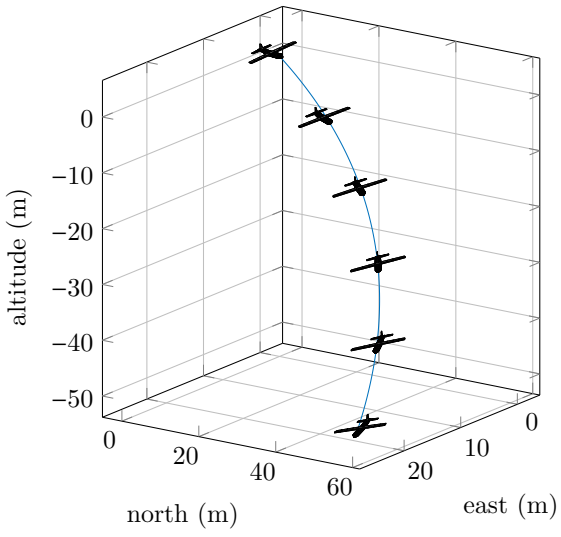

(a) Trajectory for $\eta = -40°$.

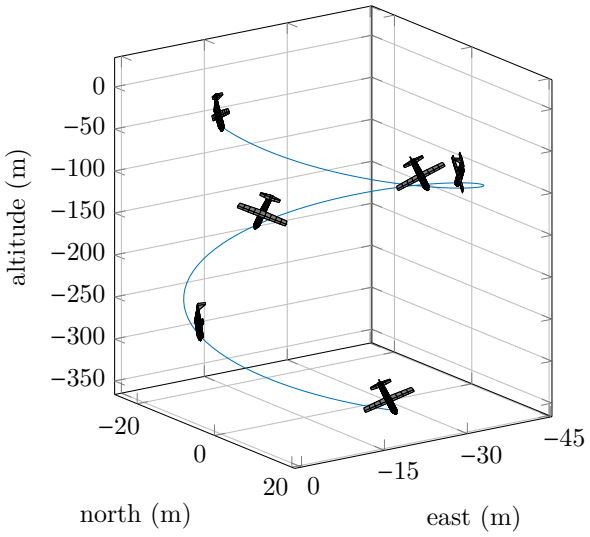

(b) Trajectory for $\eta = 5.6°$.

Fig. 20 Comparison of descent modes: (a) deep-stall descent; (b) steep descent.

VI. Conclusion

In this article, we developed a nonlinear model of a small unmanned aircraft in order to represent deep-stall transition dynamics from static CFD data. For this purpose, we proposed pitch-damping models and demonstrated the use of bifurcation analysis to discuss its effects compared to the initially static model and flight experiments. Starting with a model of longitudinal equations of motion by a blended, piecewise polynomial fit of the aerodynamic coefficients from static CFD, a continuation analysis was able to predict trim conditions. However, we found the stability of deep-stall flight deduced from the model to be inconsistent with the flight experiments and hence proposed alternative extensions to the initial model, both including a single unknown damping parameter. While larger parameters indeed led to increased stability of both models, we could not induce an isolated damping model only by the change of stability. On the other hand, we were able to provide estimations for the coefficients by optimal model fitting and thus also provided a measure for the reliability of the propose damping models. Both models seem to be simple and suitable for further analysis. We have finally provided an extensive, six-degrees-of-freedom bifurcation analysis to investigate the extended model and discussed stability in the aircraft's different modes of post-stall and deep-stall flight.

Funding Sources

This work was funded by the AutoDescent project (HTF 56-2014-3) as well as by ONERA – The French Aerospace Lab, République Française.

Acknowledgments

The authors remain grateful to Sky-Watch for the provision of test flight data and CFD simulations. *Luminita C. Totu* and *Tobias Leth* at Aalborg University further provided valuable discussions and feedback.

References

[1] Klein, V., and Morelli, E. A., *Aircraft System Identification: Theory and Practice*, AIAA Education Series, American Institute of Aeronautics and Astronautics, Reston, US-VA, 2006. doi:10.1017/S0001924000087194.

[2] Brockhaus, R., Alles, W., and Luckner, R., *Flugregelung*, 3rd ed., Springer, Berlin, DE, 2011. doi:10.1007/978-3-642-01443-7.

[3] Chakraborty, A., Seiler, P., and Balas, G. J., "Susceptibility of F/A-18 Flight Controllers to the Falling-leaf Mode: Linear Analysis," *Journal of Guidance, Control, and Dynamics*, Vol. 34, No. 1, 2011, pp. 57–72. doi:10.2514/1.50674.

[4] Chambers, J. R., and Grafton, S. B., "Aerodynamic Characteristics of Airplanes at High Angles of Attack,"

NASA technical memorandum NASA/TM-74097, Langley Research Center, Hampton, US-VA, 1977. URL https://ntrs.nasa.gov/search.jsp?R=19780005068.

[5] Gill, S. J., Lowenberg, M. H., Neild, S. A., Krauskopf, B., Puyou, G., and Coetzee, E., "Upset Dynamics of an Airliner Model: A Nonlinear Bifurcation Analysis," *Journal of Aircraft*, Vol. 50, No. 6, 2013, pp. 1832–1842. doi:10.2514/1.C032221.

[6] Jahnke, C. C., "Application of Dynamical Systems Theory to Nonlinear Aircraft Dynamics," Phd thesis, California Institute of Technology, Pasadena, US-CA, 1990. URL http://resolver.caltech.edu/CaltechETD:etd-05092007-134504.

[7] Goman, M. G., Zagainov, G. I., and Khramtsovsky, A. V., "Application of bifurcation methods to nonlinear flight dynamics problems," *Progress in Aerospace Sciences*, Vol. 33, No. 9–10, 1997, pp. 539–586. doi:10.1016/S0376-0421(97)00001-8.

[8] Caroll, J. V., and Mehra, R. K., "Bifurcation Analysis of Nonlinear Aircraft Dynamics," *Journal of Guidance, Control, and Dynamics*, Vol. 5, No. 5, 1982, pp. 529–536. doi:10.2514/3.56198.

[9] Lombaerts, T. J. J., Schuet, S. R., Wheeler, K. R., Acosta, D. M., and Kaneshige, J. T., "Safe maneuvering envelope estimation based on a physical approach," *AIAA Guidance, Navigation, and Control Conference*, Boston, US-MA, 2013. doi:10.2514/6.2013-4618.

[10] McDonough, K., and Kolmanovsky, I., "Fast Computable Recoverable Sets and Their Use for Aircraft Loss-of-Control Handling," *Journal of Guidance, Control, and Dynamics*, Vol. 40, No. 4, 2017, pp. 934–947. doi:10.2514/G001747.

[11] Lygeros, J., "On reachability and minimum cost optimal control," *Automatica*, Vol. 40, No. 6, 2004, pp. 917–927. doi:10.1016/j.automatica.2004.01.012.

[12] Chakraborty, A., Seiler, P., and Balas, G. J., "Nonlinear region of attraction analysis for flight control verification and validation," *Control Engineering Practice*, Vol. 19, No. 4, 2011, pp. 335–345. doi:10.1016/j.conengprac.2010.12.001.

[13] Chakraborty, A., Seiler, P., and Balas, G. J., "Susceptibility of F/A-18 Flight Controllers to the Falling-leaf Mode: Nonlinear Analysis," *Journal of Guidance, Control, and Dynamics*, Vol. 34, No. 2, 2011, pp. 73–85. doi:10.2514/1.50675.

[14] Foster, J. V., Cunningham, K., Fremaux, C. M., Shah, G. H., and Stewart, E. C., "Dynamics Modeling and Simulation of Large Transport Airplanes in Upset Conditions," *AIAA Guidance, Navigation, and Control Conference and Exhibit*, San Francisco, US-CA, 2005. doi:10.2514/6.2005-5933.

[15] Jordan, T. L., Foster, J. V., Bailey, R. M., and Belcastro, C. M., "AirSTAR: A UAV Platform for Flight Dynamics and Control System Testing," *AIAA Aerodynamics Measurement Technology and Ground Testing Conference*, San Francisco, US-CA, 2006. doi:10.2514/6.2006-3307.

[16] Kwatny, H. G., Dongmo, J.-E. T., Chang, B.-C., Bajpai, G., Yasar, M., and Belcastro, C., "Nonlinear Analysis of Aircraft Loss of Control," *Journal of Guidance, Control, and Dynamics*, Vol. 36, No. 1, 2013, pp. 149–162. doi:10.2514/1.56948.

[17] McDonough, K., Kolmanovsky, I., and Atkins, E., "Recoverable sets of initial conditions and their use for aircraft flight planning after a loss of control event," *AIAA Guidance, Navigation, and Control Conference*, National Harbor, US-MD, 2014. doi:10.2514/6.2014-0786.

[18] Engelbrecht, J. A. A., Pauck, S. J., and Peddle, I. K., "A Multi-mode Upset Recovery Flight Control System for Large Transport Aircraft," *AIAA Guidance, Navigation, and Control Conference*, Boston, US-MA, 2013. doi:10.2514/6.2013-5172.

[19] Crespo, L. G., Kenny, S. P., Cox, D. E., and Murri, D. G., "Analysis of Control Strategies for Aircraft Flight Upset Recovery," *AIAA Guidance, Navigation, and Control Conference*, Minneapolis, US-MN, 2012. doi:10.2514/6.2012-5026.

[20] Stepanyan, V., Krishnakumar, K., Kaneshige, J., and Acosta, D., "Stall Recovery Guidance Algorithms Based on Constrained Control Approaches," *AIAA Guidance, Navigation, and Control Conference*, San Diego, US-CA, 2016. doi:10.2514/6.2016-0878.

[21] Kuzmin, D., "A Guide to Numerical Methods for Transport Equations," Book draft, Friedrich-Alexander University, Erlangen/Nürnberg, DE, 2010. URL `http://www.mathematik.uni-dortmund.de/~kuzmin/Transport.pdf`.

[22] Drela, M., and Youngren, H., "AVL 3.36," Software user guide, Massachusetts Institute of Technology, Cambridge, US-MA, 2017. URL `http://web.mit.edu/drela/Public/web/avl/avl_doc.txt`.

[23] "The Cumulus v1 UAV," , 2017. URL `http://sky-watch.com/products/cumulus/`.

[24] ISO 1151-1, *Flight dynamics – Concepts, quantities and symbols – Part 1: Aircraft motion relative to the air*, 4^{th} ed., ISO 1151-1:1988, International Organization for Standarization, Genève, CH, 1988.

[25] Chang, B.-C., Kwatny, H. G., Ballouz, E. R., and Hartmann, D. C., "Aircraft Trim Recovery from Highly Nonlinear Upset Conditions," *AIAA Guidance, Navigation, and Control Conference*, San Diego, US-CA, 2016. doi:10.2514/6.2016-0880.

[26] Phillips, W. F., *Mechanics of Flight*, 2^{nd} ed., John Wiley & Sons, Hoboken, US-NJ, 2010.

[27] Lawson, C. L., and Hanson, R. J., *Solving Least Squares Problems*, Classics in Applied Mathematics, Society for Industrial and Applied Mathematics, 1995. doi:10.1137/1.9781611971217.

[28] Cunis, T., Leth, T., Totu, L. C., and la Cour-Harbo, A., "Identification of Thrust, Lift, and Drag for Deep-stall Flight Data of a Fixed-wing Unmanned Aircraft," *2018 International Conference on Unmanned Aircraft Systems*, Dallas, US-TX, 2018, pp. 531–538. doi:10.1109/ICUAS.2018.8453340.

[29] Cunis, T., Burlion, L., and Condomines, J.-P., "Piece-wise Identification and Analysis of the Aerodynamic Coefficients, Trim Conditions, and Safe Sets of the Generic Transport Model," *AIAA Guidance, Navigation, and Control Conference*, Kissimmee, US-FL, 2018. doi:10.2514/6.2018-1114.

[30] Cunis, T., Burlion, L., and Condomines, J.-P., "Piecewise Polynomial Modeling for Control and Analysis of Aircraft Dynamics beyond Stall," *Journal of Guidance, Control, and Dynamics*, Vol. 42, No. 4, 2019, pp. 949–957. doi:10.2514/1.G003618.

[31] Cunis, T., "The `pwpfit` Toolbox for Polynomial and Piece-wise Polynomial Data Fitting," *18th IFAC Symposium on System Identification*, Stockholm, SE, 2018, pp. 682–687. doi:10.1016/j.ifacol.2018.09.204.

[32] Cunis, T., and la Cour-Harbo, A., "Piecewise Polynomial Model of the Aerodynamic Coefficients of the *Cumulus One* Unmanned Aircraft," Tech. Rep. `hal-02280789`, Sky-Watch A/S, Støvring, DK, 2019. URL `https://hal-enac.archives-ouvertes.fr/hal-02280789`.

[33] Slotine, J.-J. E., and Li, W., *Applied Nonlinear Control*, Prentice-Hall, Upper Saddle River, US-NJ, 1991.

[34] Kuznetsov, Y. A., *Elements of Applied Bifurcation Theory*, 2nd ed., No. 112 in Applied Mathematical Sciences, Springer, Berlin, DE, 1998. doi:10.1007/978-1-4757-3978-7.

[35] Dankowicz, H., and Schilder, F., *Recipes for Continuation*, Computational Science & Engineering, Society for Industrial and Applied Mathematics, Philadelphia, US-PA, 2013. doi:10.1137/1.9781611972573.

[36] Dhooge, A., Govaerts, W., Kuznetsov, Y. A., Meijer, H. G. E., and Sautois, B., "New features of the software MatCont for bifurcation analysis of dynamical systems," *Mathematical and Computer Modelling of Dynamical Systems*, Vol. 14, No. 2, 2008, pp. 147–175. doi:10.1080/13873950701742754.

[37] Coetzee, E., Krauskopf, B., and Lowenberg, M. H., "The Dynamical Systems Toolbox: Integrating AUTO into MATLAB," *16th US National Congress on Theoretical and Applied Mechanics*, State College, US-PA, 2010.

[38] Dankowicz, H., and Schilder, F., "Continuation Core and Toolboxes (COCO)," , 2016. URL `https://sourceforge.net/projects/cocotools/`.

[39] Jategaonkar, R. V., *Flight Vehicle System Identification: A Time Domain Methodology*, No. 216 in Progress in Astronautics and Aeronautics, American Institute of Aeronautics and Astronautics, Reston, US-VA, 2006. doi:10.1017/S0001924000011015.

[40] Graichen, K., "Feedforward Control Design for Finite-Time Transition Problems of Nonlinear Systems," Phd thesis, University of Stuttgart, Stuttgart, DE, 2006. doi:10.18419/opus-4093.

[41] Nelson, R. C., *Flight Stability and Automatic Control*, 2nd ed., McGraw-Hill, Boston, US-MA, 1998.

Chapter 5

Local Stability Analysis for Splines

This chapter corresponds to:

> Torbjørn Cunis, Jean-Philippe Condomines, and Laurent Burlion (2019a). "Local stability analysis for large polynomial spline systems". In: Revision under review for *Automatica*

in the author's revised version, edited for format.

Synopsis

From the algebraic point of view, the piecewise polynomial models of the previous chapters are splines with a single knot in α_0, and thus constitute a switching system. Unlike switching systems commonly considered in the literature for stability analysis, however, the boundary between the two polynomial segments (i.e., between the two subsystems) for a normal flight trim condition does not cross the boundary. Therefore, an invariant set of the trim condition might include states of both the low and high angles of attack regimes (as in Fig. 3.7), or be contained in the low angle of attack regime exclusively. As the estimated region of attraction grows in the course of the $\mathcal{V}$-s-iteration, evaluating the invariance as polynomial or piecewise problem can affect the computation time significantly. This chapter provides the theoretical background for the stable set analysis in Chapter 3 and further extends the bespoken idea for arbitrarily defined polynomial splines systems. Improving the efficiency of spline analysis, it enables the application of this thesis's results to more accurate aerodynamic models in future work. We will elaborate that thought in Chapter 9.

Statement of Contribution Torbjørn Cunis devised and implemented the proposed algorithm, proved its correctness, and estimated the asymptotic run time. Jean-Philippe Condomines assisted with the wording of the article. Laurent Burlion provided feedback both for theoretical and engineering aspects.

Nomenclature

n	Number of states;
Φ	Subset of the state-space ($\Phi \subset \mathbb{R}^n$);
$\Omega_{q \leq a}$	Polynomial surface ($\Omega_{q \leq a} = \{x \in \mathbb{R}^n \,|\, q(x) \leq a\}$) with $q \in \mathbb{R}[x]$ and $a \in \mathbb{R}$;
$\partial\mathcal{A}$	Boundary of a set $\mathcal{A} \subset \mathbb{R}^n$;
$\text{int}\mathcal{A}$	Interior of a set $\mathcal{A} \subset \mathbb{R}^n$;
$\text{cl}\mathcal{A}$	Closure of a set $\mathcal{A} \subset \mathbb{R}^n$;
$\Sigma[x]$	Polynomial sum-of-squares cone ($\Sigma[x] \subset \mathbb{R}[x]$);
$\mathbb{R}[x]$	Set of polynomials in $x \in \mathbb{R}^n$ with real-valued coefficients;

Local stability analysis for large polynomial spline systems ⋆

Torbjørn Cunis [a,b], Jean-Philippe Condomines [b], Laurent Burlion [c]

[a] *ONERA – The French Aerospace Lab, 2 avenue Edouard Belin, 31055 Toulouse, France*

[b] *ENAC, Université de Toulouse, 7 avenue Edouard Belin, 31055 Toulouse, France*

[c] *Rutgers, The State University of New Jersey, 98 Brett Road, Piscataway, NJ 08854, USA*

Abstract

Polynomial switching systems such as multivariate splines provide accurate fitting while retaining an algebraic representation and offering arbitrary degrees of smoothness; yet, application of sum-of-squares techniques for local stability analysis is computationally demanding for a large number of subdomains. This communiqué presents an algorithm for region of attraction estimation that is confined to those subdomains actually covered by the estimate, thereby significantly reducing computation time. Correctness of the results is subsequently proven and the run time is approximated in terms of the number of total and covered subdomains. Application to longitudinal aircraft motion concludes the study.

Key words: Nonlinear analysis; stability analysis; switching functions; polynomial methods; Lyapunov function.

1 Introduction

Recently, several works on polynomial fitting have been led and provide a constructive method for determining models based on analytical computation due to their continuous and differentiable nature. Computing the exact region

⋆ This paper was not presented at any IFAC meeting. Corresponding author T. Cunis.

Email addresses: tcunis@umich.edu (Torbjørn Cunis), jean-philippe.condomines@enac.fr (Jean-Philippe Condomines), laurent.burlion@rutgers.edu (Laurent Burlion).

of attraction for this kind of nonlinear dynamics is very hard if not impossible. Therefore, researchers have focused on determining polynomial Lyapunov functions for polynomial systems building upon sum-of-squares [1–3] including extensions to rational and composite Lyapunov-functions [4–6]. However, when polynomials are unsuitable to represent system dynamics, piecewise defined polynomials such as splines [7] provide more tractable models, requiring extended effort when determining local stability: it is well known for example, that stability of the subsystems does not guarantee stability of the entire system [8]. Therefore, approximation techniques have been developed for the estimation of the region of attraction of piecewise systems. Early work was limited to a priori given, multiple quadratic Lyapunov functions [9] and could only provide very rough estimates of the region of attraction. In [10] though, analysis of polynomial fuzzy models is considered employing again composite Lyapunov functions; taking each the point-wise extremum, this approach provides directly a continuous function. It is worth noting that this might come at the cost of a large number of decision variables and that there are no relaxations with respect to the respectively active subdomains. [11] proposes a further approach using multiple Lyapunov functions for switching hybrid systems with polyhedral subdomains which share a boundary in the origin. Sum-of-squares complexity was discussed [12]; where subdomains are considered for stability, the complexity increases with the number of bounding constraints.

The present paper focuses on a new formulation of the region of attraction estimation for large piecewise systems of local polynomial dynamics and polynomial domains, such as switching systems and multivariate splines, within the sum-of-squares framework. We present preliminary results and extend previous work to switching systems (in Sec. 2). The main result, an algorithm for splines, is discussed in Sec. 3, and is applied to an engineering example in Sec. 4. The appendix illustrates an extension to multiple Lyapunov functions. For the implementation of the constraints, in particular the polynomial containment problem (Lemma 1), we rely on the semidefinite programming techniques of [1, 13]. A concise discussion of the $\mathcal{V}$-s-iteration is given in [14].

2 Preliminaries

Consider the autonomous system $\dot{x} = f(x)$ given by the $k \in \mathbb{N}$ ordinary differential equations

$$\dot{x} = f_i(x)\,, \qquad \text{if } x \in \Phi_i \tag{1}$$

for $1 \leq i \leq k$, where $x \in \mathbb{R}^n$, $f_i \in \mathbb{R}[x]^n$, and $\Phi_1, \ldots, \Phi_k$ are intersections of polynomial inequalities $\Omega_{\varphi \leq x_0} =_{\text{def}} \{x \in \mathbb{R}^n \,|\, \varphi(x) \leq x_0\}$ with $\varphi \in \mathbb{R}[x]$,

$x_0 \in \mathbb{R}^n$, forming a set partition of $\mathbb{R}^m$. [1]

Notation The interior, boundary, and closure of $\mathcal{A} \subseteq \mathbb{R}^m$ are notated by $\text{int}\mathcal{A}$, $\partial\mathcal{A}$, and $\text{cl}\mathcal{A}$, respectively. $\mathcal{A}^* =_{\text{def}} \mathcal{A} - \{0\}$. The set of sum-of-squares polynomials is notated by $\Sigma[x]$.

Assumptions $f(0) = 0$, i.e., the origin is a stationary point of f.

Lemma 1 *Let $p, q_1, \ldots, q_k \in \mathbb{R}[x]$; we have*

$$\Omega_{q_1 \leq 0} \cap \cdots \cap \Omega_{q_k \leq 0} \subseteq \Omega_{p \leq 0}$$

if there exist $s_1, \ldots, s_k \in \Sigma[x]$ such that $\sum_{i=1}^k s_i q_i - p \in \Sigma[x]$.

Lemma 1 is an explicit formulation of [1, Lemma 2]. We then write with $\mathbf{s} = (s_1, \ldots, s_k)$,

$$\mathbf{s} \vdash \bigcap_i \Omega_{q_i \leq 0} \subseteq_\Sigma \Omega_{p \leq 0} \tag{2}$$

and say "$\mathbf{s}$ proves" the inclusion. We also say that "q_i, p solve" the inclusion.

Problem 2 *Let $p \in \Sigma[x]$; solve the optimisation*

$$\begin{aligned} \max_{\substack{\beta^\diamond, \gamma^\diamond \in \mathbb{R} \\ \mathcal{V} \in \mathbb{R}[x]}} \beta^\diamond \quad & \text{such that} \\ & \Omega_{p \leq \beta^\diamond} \subseteq \Omega_{\mathcal{V} \leq \gamma^\diamond} && (3) \\ & \Omega^*_{\mathcal{V} \leq \gamma^\diamond} \subseteq \{x \,|\, \nabla\mathcal{V}(x)\, f(x) < 0\} && (4) \end{aligned}$$

with $\mathcal{V}(\cdot)$ positive definite [2] and $\mathcal{V}(x) = 0$.

If $(\mathcal{V}, \beta^\diamond, \gamma^\diamond)$ solve Problem 2 for p, then $\Omega_{\mathcal{V} \leq \gamma^\diamond}$ is an invariant subset of the region of attraction [1, Lemma 1] and admits the largest inscribing region $\Omega_{p \leq \beta^\diamond}$. Simultaneously searching for an optimal function $\mathcal{V}(\cdot)$ while proving invariance of $\Omega_{\mathcal{V} \leq \gamma^\diamond}$ involves bilinear terms. If the degree of $\mathcal{V} \in \mathbb{R}[x]$ is restricted and $f \in \mathbb{R}[x]$, the $\mathcal{V}$-s-iteration [1, 14] solves Problem 2 by alternating-iteratively searching for $\mathcal{V}$, $\gamma^\diamond$, and $\beta^\diamond$ maximal such that s_1, s_2 prove (3) and (4).

Remark 3 *The sum-of-squares formulation is limited to nonnegativity; we thus make use of that $p(x) < 0$ if $p(x) \leq -\epsilon\,|x|_2^2$ for $p \in \mathbb{R}[x]$, $x \neq 0$, and $\epsilon > 0$.*

[1] $\mathcal{A}_1, \ldots, \mathcal{A}_k$ form a *set partition* of a body $\mathbb{K}$ if and only if they are pairwise interior-disjunct and $\bigcup_i \mathcal{A}_i = \mathbb{K}$.

[2] A continuous function φ is said to be *positive definite* (p.d.) if $\varphi(\cdot) > 0$ everywhere except the origin and $\varphi(0) = 0$.

We write $\Omega_{\mathcal{V},f,\epsilon} =_{\text{def}} \left\{ x \,\middle|\, \nabla\mathcal{V} f(x) \leq -\epsilon x^T x \right\}$ for $\mathcal{V} \in \mathbb{R}[x]$, $f \in \mathbb{R}[x]^m$, and $\epsilon > 0$.

If there exists a single function $\mathcal{V} : \mathbb{R}^m \to \mathbb{R}$ p.d. such that $\nabla\mathcal{V} f_i(x) < 0$ for all $x \in \mathcal{A}^*$ and all $1 \leq i \leq k$, then $\mathcal{A}$ is also invariant for the piecewise system and $\mathcal{V}$ is a Lyapunov function of the switching dynamics. However, this requirement is unnecessary strict when it comes to the subsystems that are *not* active [8]; indeed, the following suffices:

Corollary 4 *Let $\mathcal{V}\colon \mathbb{R}^m \to \mathbb{R}$ be continuous p.d. with $\mathcal{V}(0) = 0$ and $\mathcal{A} = \Omega_{\mathcal{V}\leq\alpha}$ for some $\alpha \in \mathbb{R}$; if*

$$\forall x \in \mathcal{A}^*. \quad (x \in \Phi_i \Rightarrow \nabla\mathcal{V} f_i(x) < 0) \tag{5}$$

for all $1 \leq i < j \leq k$, then $\mathcal{A} = \bigcup_i (\mathcal{A} \cap \Phi_i)$ is invariant.

Lemma 1 encodes (5) into a polynomial sum-of-squares problem, recalling Φ_i is an intersection of polynomial inequalities. Now, $\bigcup_i (\Omega_{\mathcal{V}\leq\gamma^\diamond} \cap \Phi_i)$ is invariant if

$$\mathbf{s}_{2,i} \vdash \Omega^*_{\mathcal{V}\leq\gamma_i} \cap \Phi_i \subseteq_\Sigma \Omega_{\mathcal{V},f_i,\epsilon}, \tag{6}$$

$\mathbf{s}_{2,i} \subset \Sigma[x]$, for all $1 \leq i \leq k$ and $\gamma^\diamond = \min\{\gamma_1, \ldots, \gamma_k\}$.

Remark 5 *The idea of Corollary 4, and of the paper, can be extended to piecewise defined functions*

$$\mathcal{V}(x) = \mathcal{V}_i(x)\,, \qquad \text{if } x \in \Phi_i,$$

for $1 \leq i \leq k$. We further illustrate this in the appendix.

3 Spline systems

While we have not taken further assumptions on the Φ_i, in the present literature the invariant set is commonly assumed to cover all domains.[3] For large spline systems with bounded domains and only local stability, each subdomain taken into account whilst not part of the invariant set adds an inactive boundary to the computational load. We therefore present an adapted algorithm to efficiently compute a region of attraction estimation for spline systems.

Definition 6 *A* spline system *is a triple $\mathcal{SP} = \left(\mathcal{I}, f_{(\cdot)}, \mathcal{E}\right)$, where $\mathcal{I} \subset \mathbb{N}$ are the domains, $f : \mathcal{I} \times \mathbb{R}^m$ are the piecewise nonlinear dynamics, and $\mathcal{E} : \mathcal{I} \times \mathcal{I} \to$*

[3] Either by looking for global stability [15] or choosing boundaries crossing the origin [9, 11].

$\{\mathbb{R}^m \to \mathbb{R}\}$ *is the weighted switching relation, where the dynamics switch from* f_i *to* f_j *with* $i, j \in \mathcal{I}$ *for* $x \in \mathbb{R}^m$ *if and only if* $h_{ij} = \mathcal{E}(i,j)$ *is defined and* $h_{ij}(x) > 0$. [4]

We define some further notation: for $i \in \mathcal{I}$, let $\mathrm{adj}[i] =_{\mathrm{def}} \{j \,|\, h_{ij} = \mathcal{E}(i,j) \text{ is defined}\}$ be the set of adjacent domains of Φ_i, that is, $\Phi_i = \bigcap_{j \in \mathrm{adj}[i]} \{x \,|\, h_{ij}(x) \leq 0\}$; $\mathcal{V}_K(\cdot)$ denotes the function-candidate in the K-th iteration and $I_K \subset \mathcal{I}$ will denote the set of domains covered by the invariant set $\Omega_{\mathcal{V}_K \leq \gamma^\diamond}$; for $i' \in \mathcal{I}$, $\mathrm{dist}_K[i']$ is the distance of $\Phi_{i'}$ with respect to $\mathcal{V}_K$, defined as

$$\mathrm{dist}_K[i'] = \sup\{\gamma \,|\, \Omega_{\mathcal{V}_K \leq \gamma} \cap \Phi_{i'} = \varnothing\}\,; \tag{7}$$

at last, we extend $\mathrm{adj}[\cdot]$ to $2^{\mathcal{I}}$ with $\mathrm{adj}[I] =_{\mathrm{def}} \bigcup_{i \in I} \mathrm{adj}\,[i] - I$ for $I \subset \mathcal{I}$.

With this notation, we can state Algorithm 1 computing the optimal estimate $\Omega_{\mathcal{V} \leq \gamma^\diamond}$ for a spline structure: If, for any iteration K, the invariant set $\Omega_{\mathcal{V}_K \leq \gamma^\diamond}$ is contained in the subdomains I_K, it suffices to check invariance only of these subdomains and with respect to the boundaries in between, instead of proving Eq. (6) for *all* $i \in \mathcal{I}$. Now, in order to examine whether an $i' \in \mathcal{I}$ is covered by the optimal invariant set of $\mathcal{V}_K$, we preliminary compute the invariant set for some $I' \subset \mathcal{I} - \{i'\}$ and evaluate the distance of i'; only if i' is "closer" than the boundary of the preliminary invariant set, $i' \in I_K$.

The algorithm consists of three cascaded loops; the outer **for** loop over K of the basic $\mathcal{V}$-s-iteration ("K-iteration"), an inner **repeat-until** loop determining I_K ("I_K-loop"), and inner-most **for** loops over the elements of I_K. While the restriction to I_K in line 8 reduces the problem size, the I_K-loop itself adds to the run time. On the other hand, if $\mathcal{V}_K$ and $\mathrm{adj}[i] \cap I_K$ remain unchanged, Eq. $(*_i)$ yields the same value γ_i; that is, after each i_{next} added to I_K, it suffices to re-execute line 8 for any $i \in I_K \cap \mathrm{adj}[i_{\mathrm{next}}]$. We refer to the thus modified algorithm as Algorithm 1b.

Proposition 7 *After each repetition of the* K*-iteration in Algorithm 1(b), the following hold:*

(1) $\Omega_{\mathcal{V}_K \leq \gamma^\diamond} \subset \bigcup_{i \in I_K} \Phi_i$*;*
(2) $\Omega_{\mathcal{V}_K \leq \gamma^\diamond}$ *is invariant.*

PROOF. After each iteration of the I_K-loop, we have that

$$\forall i \in I_K \quad \Omega^*_{\mathcal{V}_K \leq \gamma_{\mathrm{pre}}} \cap \Phi_i \subseteq \{x \,|\, \nabla \mathcal{V} f_i(x) < 0\}\,; \tag{8}$$

[4] For a spline structure to behave like a spline, we tacitly understand that $\mathcal{E}(\cdot,\cdot)$ is irreflexive as well as symmetric with $h_{ij} = \mathcal{E}(i,j) = -h_{ji}$ if defined for $i, j \in \mathcal{I}$.

Algorithm 1 Estimate invariant set $\Omega_{\mathcal{V}\le\gamma^\diamond} \subset \bigcup_{i\in I}\Phi_i$ with $I = I_{K_{\max}}$ and $\mathcal{V} = \mathcal{V}_{K_{\max}}$.

1: **for** $K = 1$ to $K_{\max}$
2: **if** $K > 1$ **then**
3: find $\mathcal{V}_K$ p.d. solving

$$s_1 \vdash \Omega_{p\le\beta^\diamond} \subseteq_\Sigma \Omega_{\mathcal{V}_K\le\gamma^\diamond} \tag{††}$$

$$\forall i \in I_K.\ \mathbf{s}_{2,i} \vdash \Omega_{\mathcal{V}_K\le\gamma_i} \cap \bigcap_{j\in \mathrm{adj}[i]\cap I_K} \Omega_{h_{ij}\le 0} \subseteq_\Sigma \Omega_{\mathcal{V}_K, f_{i,\epsilon}} \tag{**}$$

4: **end**
5: $I_K := I_{K-1}$
6: **repeat**
7: **for** $i \in I_K$
8: find $\gamma_i := \max_{\gamma\ge 0}\gamma$ s.t. $\mathbf{s}_{2,i} \subset \Sigma[x]$ solves

$$\mathbf{s}_{2,i} \vdash \Omega_{\mathcal{V}_K\le\gamma} \cap \bigcap_{j\in \mathrm{adj}[i]\cap I_K} \Omega_{h_{ij}\le 0} \subseteq_\Sigma \Omega_{\mathcal{V}_K, f_{i,\epsilon}} \tag{$*_i$}$$

9: **end**
10: $\gamma_{\mathrm{pre}} := \min\{\gamma_i \mid i \in I_K\}$
11: **for** $i' \in \mathrm{adj}[I_K]$
12: compute $\mathrm{dist}_K[i']$ as

$$\min_{\substack{\gamma\ge 0, x \\ \mathcal{V}_K(x)=\gamma}} \gamma \text{ s.t. } \bigwedge_{j\in\mathrm{adj}[i']} h_{i'j}(x) \le 0 \tag{$\ddagger_{i'}$}$$

13: **end**
14: $\gamma_{\min} := \min_{i'\in\mathrm{adj}[I_K]} \mathrm{dist}_K[i']$
15: **if** $\gamma_{\mathrm{pre}} \ge \gamma_{\min}$ **then**
16: $i_{\mathrm{next}} := \arg\min_{i'\in\mathrm{adj}[I_K]} \mathrm{dist}_K[i']$
17: $I_K := I_K \cup \{i_{\mathrm{next}}\}$
18: **end**
19: **until** $I_K = \mathcal{I}$ or $\gamma_{\mathrm{pre}} < \gamma_{\min}$
20: $\gamma^\diamond := \gamma_{\mathrm{pre}}$
21: **for** $i \in I_K$
22: find $\beta^\diamond := \max_{\beta\ge 0}$ s.t. $s_1 \in \Sigma[x]$ solves

$$s_1 \vdash \Omega_{p\le\beta} \subseteq_\Sigma \Omega_{\mathcal{V}_K\le\gamma^\diamond} \tag{†}$$

23: **end**
24: **end**

as $\Phi_i \subseteq \bigcap_{j\in I} \Omega_{h_{ij}\leq 0}$ for any $I \subset \mathrm{adj}[i]$, $\mathrm{adj}[i] \cap I_K \subset \mathrm{adj}[i]$, $\gamma_{\mathrm{pre}} \leq \gamma_i$, and $\mathbf{s}_{2,i}$ proves $(*_i)$,[5] for all $i \in I_K$; and

$$\Omega_{\mathcal{V}_K \leq \gamma_{\min}} \subset \bigcup_{i\in I_K} \Phi_i; \tag{9}$$

as $\gamma_{\min} \leq \mathrm{dist}_K[i']$ for $i' \notin I_K$ and $(\ddagger_{i'})$ implies (7). Since $\gamma_{\mathrm{pre}} < \gamma_{\min}$ for termination of the I_K-loop, (9) implies $\Omega_{\mathcal{V}_K \leq \gamma^\diamond} \subset \bigcup_{i\in I_K} \Phi_i$ with $\gamma^\diamond = \gamma_{\mathrm{pre}}$. Thus, $\Omega_{\mathcal{V}_K \leq \gamma^\diamond} \cap \Phi_i = \varnothing$ for all $i \in \mathcal{I} - I_K$ [6] and therefore, $\Omega_{\mathcal{V}_K \leq \gamma^\diamond} = \bigcup_{i\in\mathcal{I}} (\Omega_{\mathcal{V}_K \leq \gamma^\diamond} \cap \Phi_i)$ is invariant by Corollary 4 for (8) holds. □

As all loops are limited by either the number of elements in $\mathcal{I}$ or $K_{\max}$, Algorithm 1b terminates and $\Omega_{\mathcal{V} \leq \gamma^\diamond}$ is an invariant set of the given spline system. Initially, we have $I_0 = \{i \in \mathcal{I} \,|\, 0 \in \Phi_i\}$, and, assuming a singleton $I_0 = \{i_0\}$, $\mathcal{V}_1 = x^T P x$ as solution to the polynomial Lyapunov equation for f_{i_0}.[7]

Asymptotic run time estimation In order to compare the run time of the proposed approach for splines to the basic approach of the previous section, we count the total number of executions of line 8 and the number of decision variables $\mathbf{s}_{2,i}$ involved each time.[8] Here, we assume that the spline structure $\mathcal{SP}$ has k subdomains; every domain has (in average) M adjacent cells; the resulting invariant set covers R subdomains; and the number of iterations is chosen as $K_{\max} = R$. Consider now the following, distinct cases: in the *worst case*, the initial invariant set $\Omega_{\mathcal{V}_1 \leq \gamma^\diamond}$ covers all R subdomains; whereas in the *average case*, $\Omega_{\mathcal{V}_K \leq \gamma^\diamond}$ grows in each repetition of the K-iteration into one further subdomain i_{next}. In both cases, I_0 is taken as singleton.
Clearly, the asymptotic run time of the basic approach in both cases is equivalent to $T_M^{\mathrm{basic}}(k) = R\,k(M+1)$. Algorithm 1b, in the worst case, repeats line 8 in the first iteration for R times, afterwards once each iteration: proving $(*_i)$ requires a single decision variable the first time $(\mathrm{adj}[i_0] \cap \{i_0\} = \varnothing)$ and m^*+1 decision variables from there on, where m^* is the number of adjacent domains of i in I_1 and each repetition of the I_K-loop adds one i_{next}; in the following $R-1$ iterations, line 8 is executed R times each with $M+1$ decision variables;

[5] Using $\mathcal{A}_1 \cap \mathcal{A}_2 \subseteq \mathcal{A}'_1 \cap \mathcal{A}'_2$ for $\mathcal{A}_{1,2} \subseteq \mathcal{A}'_{1,2}$.
[6] Assuming that $\mathrm{int}\Phi_{i,j}$ are disjunct if $i \neq j$.
[7] If I_0 is *not* a singleton, P can be found as solution to

$$A_i^T P + P A_i < \sum_{j\in \mathrm{adj}[i]\cap I_0} h_{ij}(x) \;\forall i \in I_0$$

with $A_i = \partial f_i / \partial x$.
[8] Line 8, being inside of all three loops, is the major difficulty if line 12 is efficiently computed using MATLAB's `fmincon` or a similar numerical method.

that is,

$$T_M^{\text{worst}}(R) = 1 + R \sum_{m^*=1}^{M} (m^* + 1) + (R - 1)\, R\, (M + 1)\,.$$

In the average case, Algorithm 1b executes line 8 once in every iteration for each of the r^* domains in I_K with $m^* \leq M$ decision variables; additionally, since $I_{K+1} = I_K \cup \{i_{\text{next}}\}$, line 8 is executed for every adjacent subdomain of i_{next} in I_K (i.e., at most M times) with $m^* + 1$ decision variables; that is,

$$T_M^{\text{avg}}(R) = 1 + \sum_{r^*=2}^{R} r^*\,(M + 1) + R \sum_{m^*=1}^{M} (m^* + 1)\,.$$

If $M = 3$ ($M = 4$),[9] the worst-case asymptotic run time is less than T_M^{basic} for $R < 0.987\,k$ ($R < 0.981\,k$) and the average-case is less than $\frac{1}{2}T_M^{\text{basic}}$ for $R < 0.944\,k$ ($R < 0.933\,k$).

4 Application example

The short-period motion of a transport aircraft might be given as autonomous system

$$\dot{x}_1 = x_2 \tag{10}$$
$$\dot{x}_2 = f_{\text{M}}(x_1, x_2)\,, \tag{11}$$

where x_1 is the angle of attack, x_2 is the pitch rate, and $f_{\text{M}}(\cdot)$ is a 3rd-order piecewise polynomial model of the aerodynamic pitch coefficient defined as 5-by-5 rectangular spline (boundaries depicted in Fig. 1) with $f_{\text{M}}(0, 0) = 0$.[10] After scaling the system to $\tilde{x} = \mathbf{D}x$ with $\mathbf{D} \in \mathbb{R}^{2\times 2}$, we compute the invariant set of the origin using Algorithm 1b. Such a problem has been discussed in [14] for a polynomial model and in [17] for a once-piecewise polynomial model.

[9] $M = 3$ and $M = 4$ are tantamount to planar systems with triangular and rectangular domains, respectively.
[10] See [16] for details.

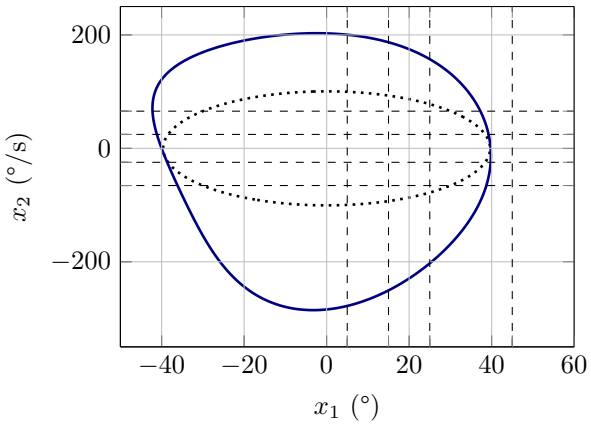

Fig. 1. Invariant set after $K_{\text{fin}} = 124$ iterations for aircraft short-period motion (solid: invariant set $\Omega_{\mathcal{V}_K \leq \gamma^\diamond}$; dotted: inscribing ellipsoid $\Omega_{p \leq \beta^\diamond}$; dashed: subdomain boundaries).

Algorithm 1b finds the optimal invariant set shown in Fig. 1, covering 20 of 25 domains, after 124 repetitions of the K-iteration and a run time equivalent of $T = 10\,098$. The basic approach runs the same number of repetitions with a run time equivalent of $T^{\text{basic}} = 13\,020$. In each repetition of the K-iteration, line 8 is executed multiple times subject to both the elements already in I_{K-1} and those added to I_K during the inner I_K-loop. The number of linear matrix inequality (LMI) variables to solve the sum-of-squares problems $(*_i)$ then varies with the number of elements in $\text{adj}[i] \cap I_K$. Table 1 gives details of the computations, including the number of LMI variables in $(*_i)$ *averaged* for each repetition K, comparing Algorithm 1b and the basic approach. [11]

Table 1
Details of the application example: number of elements in $I_K \subseteq \mathcal{I}$; run time equivalent; number of executions of line 8; and average number of LMI variables.

	Alg. 1b				basic			
K	$\#I_K$	T_K	#l8	LMI	$\#I_K$	T_K	#l8	LMI
1	12	86	28	208	25	105	25	250
2	12	44	12	356	25	105	25	378
3	13	56	15	359	25	105	25	378
4	14	60	16	360	25	105	25	378
5	15	65	17	363	25	105	25	378
6	20	111	29	365	25	105	25	378
7	20	86	20	374	25	105	25	378
⋮	⋮	⋮	⋮	⋮	⋮	⋮	⋮	⋮
K_{fin}	20	86	20	374	25	105	25	378

[11] The basic approach corresponds to Alg. 1 with $I_K \equiv \mathcal{I}$.

5 Conclusion

Extensions of sum-of-squares techniques such as the $\mathcal{V}$-s-iteration for piecewise polynomial systems quickly grow infeasible for large systems, which spline models embody. In this article, we therefore presented an adapted algorithm for splines, relaxing the problem to the subdomains that are actually covered by the region of attraction estimate. We have proven correctness of our approach and demonstrated a *worst case* run time superior to the basic approach for regions of attractions spanning more than 90 % of the subdomains of a regular planar spline system. While this ratio will shrink for higher dimensions, so does the number of subdomains increase.

Acknowledgements

The implementation of Algorithm 1 utilises the `SOSOPT` / `SOSAnalysis` toolboxes of the University of Minnesota.

References

[1] Ufuk Topcu, Andrew Packard, and Peter Seiler. Local stability analysis using simulations and sum-of-squares programming. *Automatica*, 44(10):2669–2675, 2008. doi: 10.1016/j.automatica.2008.03.010.

[2] Ufuk Topcu, Andrew K. Packard, Peter Seiler, and Gary J. Balas. Robust Region-of-Attraction Estimation. *IEEE Transactions on Automatic Control*, 55 (1):137–142, jan 2010. doi: 10.1109/TAC.2009.2033751.

[3] Larissa Khodadadi, Behzad Samadi, and Hamid Khaloozadeh. Estimation of region of attraction for polynomial nonlinear systems: A numerical method. *ISA Transactions*, 53(1):25–32, 2014. doi: 10.1016/j.isatra.2013.08.005.

[4] Giorgio Valmorbida and James Anderson. Region of attraction estimation using invariant sets and rational Lyapunov functions. *Automatica*, 75:37–45, 2017. doi: 10.1016/j.automatica.2016.09.003.

[5] Weehong Tan and Andrew Packard. Stability region analysis using polynomial and composite polynomial Lyapunov functions and sum-of-squares programming. *IEEE Transactions on Automatic Control*, 53(2):565–571, 2008. doi: 10.1109/TAC.2007.914221.

[6] Graziano Chesi. Rational Lyapunov functions for estimating and controlling the robust domain of attraction. *Automatica*, 49(4):1051–1057, 2013. doi: 10.1016/j.automatica.2013.01.032.

[7] Coen C. de Visser, Q. P. Chu, and J. A. Mulder. A new approach to linear regression with multivariate splines. *Automatica*, 45(12):2903–2909, 2009. doi: 10.1016/j.automatica.2009.09.017.

[8] Mikael Johansson and Anders Rantzer. Computation of piecewise quadratic Lyapunov functions for hybrid systems. *IEEE Transactions on Automatic Control*, 43(4):555–559, 1998. doi: 10.1109/9.664157.

[9] F. Amato, R. Ambrosino, G. De Tommasi, and A. Merola. Estimation of the domain of attraction for a class of hybrid systems. *Nonlinear Analysis: Hybrid Systems*, 5(3):573–582, 2011. doi: 10.1016/j.nahs.2010.12.005.

[10] Ying-Jen Chen, Motoyasu Tanaka, Kazuo Tanaka, and Hua O. Wang. Stability Analysis and Region-of-Attraction Estimation Using Piecewise Polynomial Lyapunov Functions: Polynomial Fuzzy Model Approach. *IEEE Transactions on Fuzzy Systems*, 23(4):1314–1322, 2015. doi: 10.1109/TFUZZ.2014.2347993.

[11] Xiuliang Zheng, Zhikun She, Junjie Lu, and Meilun Li. Computing multiple Lyapunov-like functions for inner estimates of domains of attraction of switched hybrid systems. *International Journal of Robust and Nonlinear Control*, 2018. doi: 10.1002/rnc.4280.

[12] Graziano Chesi. On the Complexity of SOS Programming and Applications in Control Systems. *Asian Journal of Control*, 20(5):2005–2013, 2018. doi: 10.1002/asjc.1684.

[13] Pablo A. Parillo. Semidefinite programming relaxations for semialgebraic problems. *Mathematical Programming, Series B*, 96(2):293–320, 2003. doi: 10.1007/s10107-003-0387-5.

[14] Abhijit Chakraborty, Peter Seiler, and Gary J. Balas. Nonlinear region of attraction analysis for flight control verification and validation. *Control Engineering Practice*, 19(4):335–345, 2011. doi: 10.1016/j.conengprac.2010.12.001.

[15] Antonis Papachristodoulou and Stephen Prajna. Robust Stability Analysis of Nonlinear Hybrid Systems. *IEEE Transactions on Automatic Control*, 54(5):1035–1041, 2009. doi: 10.1109/TAC.2009.2017155.

[16] Torbjørn Cunis, Laurent Burlion, and Jean-Philippe Condomines. Piecewise Polynomial Model of the Aerodynamic Coefficients of the Generic Transport Model and its Equations of Motion. Technical Report `hal-01808649`, ONERA – The French Aerospace Lab; French Civil Aviation School, Toulouse, FR, 2018. URL https://hal.archives-ouvertes.fr/hal-01808649. Appendix A with Eq. (104): $f_{\mathrm{M}}(\cdot) = \dot{q}$ for the trim condition $V_{\mathrm{A}} = 77.17\,\mathrm{m\,s^{-1}}$, $\gamma_{\mathrm{A}} = 0$, $q = 0$, $\alpha = 3.65°$, and $\eta = 2.14°$, $F = 29.81\,\mathrm{N}$.

[17] Torbjørn Cunis, Laurent Burlion, and Jean-Philippe Condomines. Piecewise Polynomial Modeling for Control and Analysis of Aircraft Dynamics beyond Stall. *Journal of Guidance, Control, and Dynamics*, 42(4):949–957, 2019. doi: 10.2514/1.G003618.

A Appendix

The proposed algorithm can be modified for multiple Lyapunov functions:

Corollary 8 *Let $\mathcal{V}_i : \mathbb{R}^m \to \mathbb{R}$ be continuous p.d. with $\mathcal{V}_i(0) = 0$ and $\mathcal{A}_i = \Omega_{\mathcal{V}_i \leq \alpha}$ for all $1 \leq i \leq k$ and some $\alpha \in \mathbb{R}$; if*

$$\forall x \in \mathcal{A}_i^*. \quad (x \in \Phi_i \Rightarrow \nabla \mathcal{V}_i f_i(x) < 0) \tag{A.1}$$
$$\forall x \in \partial\Phi_i \cap \partial\Phi_j. \quad \mathcal{V}_i(x) = \mathcal{V}_j(x) \tag{A.2}$$

for all $1 \leq i < j \leq k$, then $\mathcal{A} = \bigcup_i (\mathcal{A}_i \cap \Phi_i)$ is invariant.

Then, Eq. (3) holds if

$$s_{1,i} \vdash \Omega_{p \leq \beta_i} \subseteq_\Sigma \Omega_{\mathcal{V}_i \leq \gamma^\diamond}, \tag{A.3}$$

$s_{1,i} \in \Sigma[x]$, for all $1 \leq i \leq k$ and $\beta^\diamond = \min\{\beta_1, \ldots, \beta_k\}$.

The continuity condition (A.2) cannot be represented by sum-of-squares immediately. Papachristodoulou and Prajna [15] suggested to add an equality constraint for each polynomial boundary, however leading to increased conservativeness for large systems.

Proposition 9 *Eq.* (A.2) *holds if and only if*

$$\forall x \in \mathrm{cl}\Phi_i \cap \mathrm{cl}\Phi_j. \quad \mathcal{V}_i(x) \leq \mathcal{V}_j(x) \tag{A.4}$$

for Φ_i, Φ_j pairwise disjunct.

PROOF. Follows directly from $\mathrm{cl}\Phi_i \cap \mathrm{cl}\Phi_j = (\partial\Phi_i \cap \partial\Phi_j) \cup (\mathrm{int}\Phi_i \cap \mathrm{int}\Phi_j)$ with $\mathrm{int}\Phi_i \cap \mathrm{int}\Phi_j = \varnothing$ and $(v_i \leq v_j) \wedge (v_j \leq v_i) \Leftrightarrow v_i = v_j$. □

In line 3 of Algorithm 1(b), Eq. (A.4) holds for $\mathcal{V}_i, \mathcal{V}_j \in \mathbb{R}[x]$ p.d. if

$$\mathbf{r}_{ij} \vdash \bigcap_{a \in \mathrm{adj}[i] \cap I_K} \Omega_{h_{ia} \leq 0} \cap \bigcap_{b \in \mathrm{adj}[j] \cap I_K} \Omega_{h_{jb} \leq 0} \subseteq_\Sigma \Omega_{\mathcal{V}_i \leq \mathcal{V}_j} \tag{A.5}$$

with $\mathbf{r}_{ij} \subset \Sigma[x]$ and $i \in I_K$, $j \in \mathrm{adj}[i] \cap I_K$.

Now, when adding a subdomain i_{next} to the current I_K (line 17), we search for $\mathcal{V}_{i_{\mathrm{next}}} \in \mathbb{R}[x]$ p.d. such that (A.5) holds for $i = i_{\mathrm{next}}$ and all $j \in \mathrm{adj}[i_{\mathrm{next}}] \cap I_K$.

Remark 10 *Instead of* (A.3)*, we might require*

$$s_{1,i} \vdash \Omega_{p \leq \beta^\diamond} \subseteq_\Sigma \Omega_{\mathcal{V}_i \leq \gamma^\diamond} \tag{A.6}$$

for all $1 \leq i \leq k$ *when searching for* $\mathcal{V}_1, \ldots, \mathcal{V}_k$.

Eq. (A.6) imposes a less strict constraint on those $\mathcal{V}_i$ with $\beta_i > \beta^\diamond$.

Part II

Upset Recovery Control

Upset Recovery Control

The nonlinear equations of motion of an aircraft surely belong to the most difficult problems of control engineering (cf. Brockhaus et al. 2011, pp. 30–34; and Philippe et al. 2011, p. 11). Several independent states describe the translational and rotational velocities coupled, amongst others, by the (unknown) aerodynamic coefficients. Time-varying effects such as fuel consumption, uncertain models, and various disturbances as well as state and input constraints further add to the difficulty. It is for that reason that, of all control approaches theoreticians have thought of almost everyone has or will be dedicated to the problem of flight control.

Until today, flight control systems are organised in a hierarchical manner (Brockhaus et al. 2011, p. 46). It would be too easy though to dismiss this as reluctance of flight control engineers when confronted with novel technologies; in fact, the hierarchical structure accommodates for the need of certification through third-body agencies (Bates and Postlethwaite 2002). Nevertheless, several advanced techniques have been developed in recent years that solve nonlinear and robust flight control problems in a single loop. To name a few, Sieberling et al. (2010) introduced *incremental dynamic inversion*, which is comparatively robust against model errors and disturbances but sensitive to time delays in measurements; Lombaerts et al. (2010) proposed to use *pseudo control hedging* as a method to prevent control saturation and violation of the safe flight envelope; and Ure and Inalhan (2012) reported a sliding-mode control framework for acrobatic flight of unmanned aircraft.

Engelbrecht and Engelbrecht (2016) further employed dynamic as well as sequential quadratic programming techniques to obtain altitude-minimal trajectories for open-loop recovery from an inverted-bank upset condition. The idea of solving the nonlinear optimal problem in feedback loop for a control input (as in Schuet, Lombaerts, Kaneshige, et al. 2017, for pilot guidance) is called *model-predictive control* (MPC). Today, MPC is widely applied in aeronautics (see Eren et al. 2017 for a state of the art). In particular, for its ability to accommodate for input constraints MPC is widely applied in fault-tolerant control schemes (such as Joosten et al. 2010; de Almeida and Leißling 2010; Maciejowski and Yang 2015; Ferranti et al. 2018). With a mature theory of closed-loop stability and robustness, MPC is well-suited to our need for *certifiable* upset recovery control under constraints and optimality measures.

Sum-of-squares programming, too, can be applied for a control synthesis that implicitly grants stability. Ataei-Esfahani and Wang (2007), for the example of flight control, employed sum-of-squares programming and Rantzer's dual-Lyapunov theorem (Rantzer 2001, p. 162) in order to synthesize a linear feedback for the slow-dynamics of a hypersonic aircraft with global stability. For this purpose, the aircraft dynamics are modeled by bilinear aerodynamic coefficients.

Part Outline This part studies the synthesis and verification of control approaches for upset recovery. It is organised as follows: The initial technical background chapter

serves as an introduction into nonlinear control theory with focus on optimal and model-predictive control. Chapter 6 applies the sum-of-squares programming technique in order to verify stable recovery from deep-stall conditions. In Chapter 7, we formulate altitude-minimal recovery as model-predictive control problem and proof stability of the control scheme. Chapter 8 concludes the part by extending model-predictive control to recovery from spiral and spin events.

Nonlinear Control

The purpose of designing a control law, whether based on the current states and outputs of a system ("feedback control") or not ("feed-forward control"), is augmenting the system in order to achieve a desired controlled behaviour. Common goals are to enhance the performance or stability of the underlying system; to ensure that the system remains within a certain set of states; to recover a desired state after a disturbance of the system; or to make the system follow a given reference trajectory. Roughly speaking, there are about as many control approaches as there are classes of control systems – illustrated in Fig. II.1 – and some approaches classically designed for linear systems can be extended to nonlinear systems. A deep study of linear control approaches would be beyond the scope of this chapter, but it should be noted that approaches such as pole placement or optimal linear control synthesis are well applied locally in the neighbourhood of an equilibrium.

For nonlinear systems such as polynomial, rational, or switching systems, the linear concept of *controllability* can be extended to the notion of flatness. Here, a system is said to be *flat* if there is a (virtual) output which is uniquely described by the system's states, inputs, and history of inputs, and which in turn determines states and inputs for all times (Abel 2013, p. 412). While the existence of such a *flat output* is sufficient for controllability, there are further necessary conditions for a system to be flat (Rigeros 2015, pp. 85–86). If the system under consideration is not flat, a "flat-like" control law can still be synthesized solving a boundary-value problem (Graichen 2006, pp. 14–20) or a set of differential algebraic equations (Seifried and Blajer 2013, p. 116). Related to the concept of flatness is the idea of *feedback linearisation*, where a nonlinear system is transformed in such a way that an equivalent linear system is found,[1] for which then a linear control law can be designed (Slotine and Li 1991, pp. 236–241; see also Isidori 2013, p. 370, and references herein). The process of input-state linearisation is also known as *nonlinear dynamic inversion* (cf., e.g., Sieberling et al. 2010, pp.1733–1734).

Control of nonlinear systems is especially challenging in the presence of bifurcations as well as input and state constraints. The field of control that aims to influence how and where a bifurcation occurs is called *bifurcation control* (see, e.g., Alonso et al. 2003, for an introduction). Various control approaches further address state and input constraints, such as augmenting the reference signal by pseudo-control hedging (Johnson 2000, pp. 15–18) or reference-governor schemes (Nicotra and Garone 2018, p. 91). A more direct method is found in nonlinear optimal control, where the control signal is subject to minimising a given cost function amid state and input constraints (Abel 2013, p. 344). Itself a method of feed-forward control design, solving the optimisation problem repetitively and with respect to the current state leads to the idea of *model-predictive control* (MPC).

[1] Therefore, this approach is also called *exact linearisation* in contrast to the "inexact" linearisation of the Taylor series.

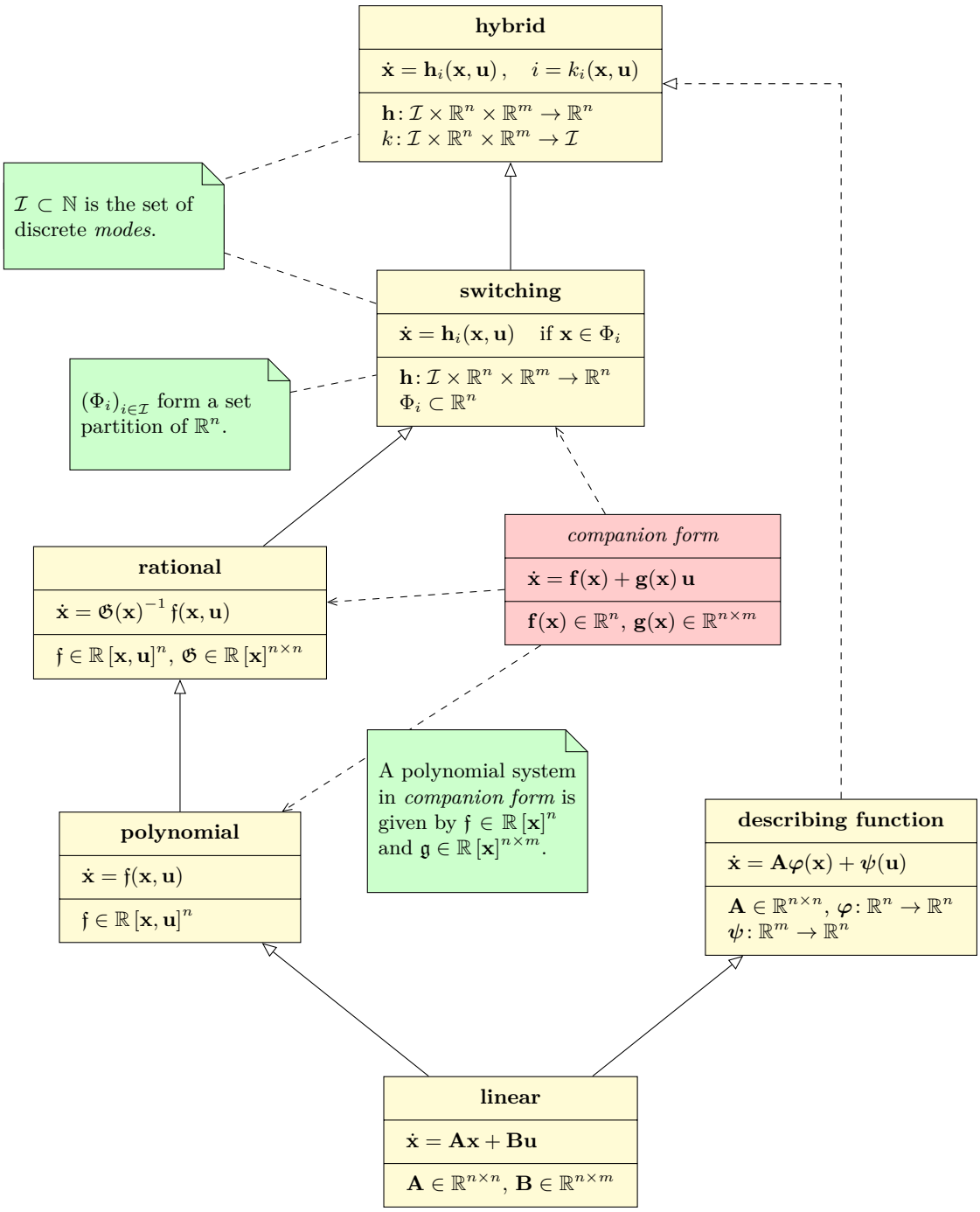

Figure II.1: Overview of linear and nonlinear control system classes and their relationship (non-exhaustive).

The remainder of this chapter is concerned with the formulation of optimal control problems and, subsequently, model-predictive control techniques. In particular, we introduce the concepts of tracking and economic MPC and explain their differences for the analysis of stability and robustness. Prior to that, we revisit the *companion form* for control-affine systems, which is utilised in various control design approaches.

Trajectories under control input

We consider from now on control systems in form of the extended differential equation

$$\dot{\mathbf{x}}(t) = \mathbf{f}(\mathbf{x}(t)\,, \mathbf{u}(\cdot)) \tag{II.1}$$

with $\mathbf{f}\colon \mathcal{X} \times \mathcal{U} \to \mathbb{R}^n$ and $\mathcal{U} \subseteq \mathbb{R}^p$. The input signal $\mathbf{u}(\cdot) \in \mathcal{U}$ is commonly interpreted as constant, known input (compare the bifurcation parameter of Section I.2); time-varying control input; time-varying, unknown disturbance signal; or a constant or time-varying but unknown uncertainty. If the input signal is represented by the parametrised curve $\mathbf{u}: \mathbb{R} \to \mathcal{U}$, the system is time-variant and, if also Lipschitz-continuous, has a unique solution $\mathbf{x}^{\mathbf{u}}\colon \mathbb{R} \to \mathcal{X}$ for the initial solution $\mathbf{x}^{\mathbf{u}}(t_0) = \mathbf{x}_0$. We then call $\mathbf{x}^{\mathbf{u}}(\cdot)$ the solution of $\mathbf{f}$ starting in $\mathbf{x}_0$ *under the control input* $\mathbf{u}(\cdot)$.

The *companion form*: control-affine systems

For the design of control laws by input-state linearisation or nonlinear dynamic inversion, but also the control synthesis using sum-of-squares programming, it is necessary that the considered system is affine in its control inputs. This notion is equivalent to the so-called companion form of a polynomial or rational system:

$$\dot{\mathbf{x}} = \mathbf{f}'(\mathbf{x}, \mathbf{u}) = \mathbf{f}(\mathbf{x}) + \mathbf{g}(\mathbf{x})\,\mathbf{u} \tag{II.2}$$

where the control input $\mathbf{u}$ enters linearly via the matrix-valued field $\mathbf{g}(\cdot)$ and the system is only nonlinear in its state variables. Slotine and Li (1991, p. 236) notes that the companion form can be derived by a substitution of variables from a system of the form

$$\dot{\mathbf{x}} = \mathbf{f}(\mathbf{x}) + \mathbf{g}(\mathbf{x})\, w(\mathbf{u} + \boldsymbol{\phi}(\mathbf{x}))\,, \tag{II.3}$$

where $w\colon \mathbb{R}^m \to \mathbb{R}^n$ is invertible and $\boldsymbol{\phi}(\mathbf{x}) \in \mathbb{R}^m$.

In general, the companion form can be derived by augmenting a non-affine system with integrating input dynamics:

$$\begin{bmatrix} \dot{\mathbf{x}} \\ \dot{\mathbf{x}}_u \end{bmatrix} = \begin{bmatrix} \mathbf{f}'(\mathbf{x}, \mathbf{x}_u) \\ \mathbf{0}_m \end{bmatrix} + \begin{bmatrix} \mathbf{0}_n \\ \mathbf{1}_m \end{bmatrix} d\mathbf{u}, \tag{II.4}$$

where $\mathbf{x}_u$ denotes the inputs-turned-states and $d\mathbf{u}$, their desired change. While this can be applied to any nonlinear system that is not control-affine, it also results in non-hyperbolic eigenvalues representing the input dynamics.

II.1 Optimal Control Problems

Optimal control problems can be formulated in different ways, for linear and nonlinear systems, in continuous or discrete time, with an infinite or finite horizon, subject to constraints or not. All share that we seek to find a pair of trajectories of states $\hat{\mathbf{x}}\colon (\cdot) \to \mathcal{X}$ and inputs $\hat{\mathbf{u}}\colon (\cdot) \to \mathcal{X}$, where $\mathcal{X} \subseteq \mathbb{R}^n$ denotes, again, the state-space and $\mathcal{U} \subseteq \mathbb{R}^m$ is the set of *admissible* inputs, that minimises a *cost function*[2] $\mathcal{J}\colon (\cdot, \cdot) \to \mathbb{R}$. We will consider first that the optimal control problems are solved once, prior execution of the control law ("offline"), whereas the next section is dedicated to iterative ("online") solutions.

The unconstrained, continous-time, infinite-horizon control problem for a linear system with initial condition $\mathbf{x}_0$ is commonly written as

$$\min_{\substack{\mathbf{x}(\cdot)\in\{\mathbb{R}\to\mathbb{R}^n\}\\ \mathbf{u}(\cdot)\in\{\mathbb{R}\to\mathbb{R}^m\}}} \mathcal{J}(\mathbf{x}(\cdot)\,, \mathbf{u}(\cdot)) = \int_0^\infty \|\mathbf{x}(t)\|_{\mathbf{Q}}^2 + \|\mathbf{u}(t)\|_{\mathbf{R}}^2 \,\mathrm{d}t \tag{II.5}$$

such that $\dot{\mathbf{x}}(t) = \mathbf{A}\mathbf{x}(\mathbf{x}) + \mathbf{B}\mathbf{u}(t)$ for all $t \geq 0$ and $\mathbf{x}(0) = \mathbf{x}_0$. Here, $\|\mathbf{x}\|_{\mathbf{Q}}^2$ and $\|\mathbf{u}\|_{\mathbf{R}}^2$ denote the weighted quadratic errors of states and inputs, $\mathbf{x}^T\mathbf{Q}\,\mathbf{x}$ and $\mathbf{u}^T\mathbf{R}\,\mathbf{u}$ respectively, for some weight matrices $\mathbf{Q} \in \mathbb{R}^{n\times n}, \mathbf{R} \in \mathbb{R}^{m\times m}$. If one chooses a *structured* control input of the form $\mathbf{u}\colon t \mapsto \mathbf{K}\,\mathbf{x}(t)$ with the feedback gain matrix $\mathbf{K} \in \mathbb{R}^{m\times n}$ as decision variable, Eq. (II.5) resembles just the common *linear quadratic regulator* problem with the well-known solution $\hat{\mathbf{K}} = -\mathbf{R}^{-1}\mathbf{B}^T\mathbf{P}$ and $\mathcal{J}(\hat{\mathbf{x}}, \hat{\mathbf{u}}) = \|\mathbf{x}_0\|_{\mathbf{P}}$, where $\mathbf{P}$ denotes the unique solution of the algebraic Riccati equation (Skogestad and Postlethwaite 2005, p. 376).

Introducing nonlinear dynamics or constraints – or both – into the cost equation imposes a greater challenge. Without further assumptions about the structure of $\mathbf{u}(\cdot)$, the infinite horizon results into an infinite-dimensional, generally intractable optimisation problem (Kouvaritakis and Cannon 2016, p. 18). Instead, one often relies on a finite-horizon approximation of the cost function. Denote

$$\mathcal{J}_T(\mathbf{x}(\cdot)\,, \mathbf{u}(\cdot)) = \int_0^T \ell(\mathbf{x}(t)\,, \mathbf{u}(t))\,\mathrm{d}t \tag{II.6}$$

for $T \in \mathbb{R}_{\geq 0}$, $\mathbf{x}\colon [0, T] \to \mathcal{X}, \mathbf{u}\colon [0, T] \to \mathcal{U}$, and an arbitrary stage cost $\ell\colon \mathcal{X} \times \mathcal{U} \to \mathbb{R}$; we obtain the cost of (II.5) as special case $\lim_{T\to\infty} \mathcal{J}_T$. We will now attempt to minimise the combined cost $\mathcal{J}_T(\mathbf{x}(\cdot)\,, \mathbf{u}(\cdot)) + \ell_\infty(\mathbf{x}(T))$, where the *terminal penalty* $\ell_\infty : \mathcal{X} \to \mathbb{R}$ accounts for the omitted terms of $t \in [T, \infty)$ (Jadbabaie et al. 2001, p. 778). The terminal penalty commonly represents the suboptimal cost of a local controller taking over at time T (*dual-mode paradigm*, Kouvaritakis and Cannon 2016, p. 19).

In order to further relax the optimisation problem, we consider the discrete system

$$\mathbf{x}_{k+1} = \mathbf{f}^+(\mathbf{x}_k, \mathbf{u}_k)\,, \tag{II.7}$$

where the vector field $\mathbf{f}^+\colon \mathbb{R}^n \times \mathbb{R}^m = \mathbb{R}^n$ is chosen in such a matter that

$$\mathbf{x}_k = \mathbf{x}(k\tau) \tag{II.8}$$

[2] Or functional, as the case may be.

for all $k \in \{0, \dots, N\}$ if $\mathbf{x}(\cdot)$ is the trajectory of the continuous system $\mathbf{f}(\cdot, \cdot)$ under the *zero-order hold* control input $\mathbf{u}(\cdot)$ given by

$$\mathbf{u} \colon t \mapsto \begin{cases} \mathbf{u}_0 & \text{if } t < \tau \\ \mathbf{u}_k & \text{if } k\tau \leq t < (k+1)\,\tau \\ \mathbf{u}_N & \text{if } N\tau \leq t \end{cases} \tag{II.9}$$

and starting in $\mathbf{x}(t = 0) = \mathbf{x}_{k=0}$. Interpreting $\tau \in \mathbb{R}_{\geq 0}$ as *sample time*, $N \in \mathbb{N}$ as discrete horizon, and k as discrete samples, we have that, in other words, $\mathbf{f}^+$ and $\mathbf{f}$ coincide periodically at the sampling time points $t_k = k\tau$ (Grüne and Pannek 2017, p. 17). While the existence of an equivalent discrete system can be proven,[3] one will often rely on a numerical approximation in absence of an algebraic notation (Grüne and Pannek 2017, pp. 20 and 22).

With Eqs. (II.6) and (II.7), we obtain the constrained, discrete-time, finite-horizon control problem for a system $\mathbf{f}^+(\cdot, \cdot)$ with initial condition $\mathbf{x}_0$ and nonlinear constraints $(g_i \colon \mathbb{R}_{\geq 0} \times \mathcal{X} \times \mathcal{U} \to \mathbb{R})_{i \in I}$, where $I \subset \mathbb{N}$ is finite, as

$$\min_{\substack{\mathbf{x}_{(\cdot)} \in \mathcal{X}^N \\ \mathbf{u}_{(\cdot)} \in \mathcal{U}^N}} \mathcal{J}_N\Big(\mathbf{x}_{(\cdot)}, \mathbf{u}_{(\cdot)}\Big) = \ell_\infty(\mathbf{x}_N) + \sum_{k=1}^{N-1} \ell(\mathbf{x}_k, \mathbf{u}_k) \tag{II.10}$$

such that $\mathbf{x}_{k+1} = \mathbf{f}^+(\mathbf{x}_k, \mathbf{u}_k)$ for all $k \in \{0, \cdots, N-1\}$ and $g_i(k, \mathbf{x}_k, \mathbf{u}_k) \geq 0$ for all $k \in \{0, \dots, N\}$ and $i \in I$. Solved in open loop with a terminal constraint $\mathbf{x}_N = \mathbf{x}_f$, Eq. (II.10) constitutes an optimal variant to the boundary value problems of Graichen (2006, pp. 73 and following). However, it also serves as an entry point for the model-predictive control paradigm of the next section, where the open-loop, finite-horizon optimisation will be solved iteratively.

II.2 Model-Predictive Control

The fundamental idea behind model-predictive control (MPC) is to solve the optimal control problem iteratively for the most recent state measurement $\mathbf{x}(t_0)$, usually but not necessarily with as same a period as the sampling time of the underlying discrete model, and only take the first element(s) of the optimal control sequence. Thus, the terminal time step $t_0 + N\tau$ is perpetually pushed back ("receding horizon") and the terminal state $\mathbf{x}_N$ with its suboptimal local controller is never reached. While being computationally demanding, the model-predictive control scheme constitutes in fact a feedback control law; if $\hat{\mathbf{x}}_{(\cdot)}, \hat{\mathbf{u}}_{(\cdot)}$ denote the arguments of the optimal solution of the open-loop problem of Eq. (II.10) with initial condition $\mathbf{x}_0 = \mathbf{x}(t_0)$, the model-predictive control feedback is given as

$$\mathbf{u}_{\mathrm{MPC}}(t) = \boldsymbol{\mu}_N(\mathbf{x}_0) = \hat{\mathbf{u}}[1] \tag{II.11}$$

[3] Note that neither the choice of $(t_k)_{0 \leq k \leq N}$ as periodic sample times, nor that of $\mathbf{u}(\cdot)$ as zero-order hold is necessary for this result. For a complete introduction into sampled-data systems, refer to Grüne and Pannek 2017, Chap. 2.2.

for $t \in [t_0, t_0 + \tau)$, where $\hat{\mathbf{u}}[i]$ denotes the i-th element of $\hat{\mathbf{u}}_{(\cdot)}$.

We are naturally interested in the set of initial conditions $\mathbf{x}_0 \in \mathcal{X}$ whence the MPC-feedback is able to drive the system to a stable solution – in other words, we would like determine the region of attraction. Necessary for a stabilising control is the plain existence of a solution to the open-loop problem, that is, the *feasibility* of the optimisation. We denote the set of initial conditions which elicit a feasible optimisation problem as

$$\mathcal{X}_N = \left\{ \mathbf{x}_0 \in \mathcal{X} \,\middle|\, \exists \mathbf{u}_{(\cdot)} \in \mathcal{U}^N. \quad \left(\mathbf{x}_0, \mathbf{u}_{(\cdot)}\right) \in \mathcal{Z}_N \right\}, \tag{II.12}$$

where $\mathcal{Z}_N$ is the set of *admissible solutions*, that is,

$$\mathcal{Z}_N = \left\{ \left(\mathbf{x}, \mathbf{u}_{(\cdot)}\right) \in \mathcal{X} \times \mathcal{U}^N \,\middle|\, \textstyle\bigwedge_{i \in I} g_i(k, \mathbf{x}^{\mathbf{u}}_k, \mathbf{u}_k) \geq 0 \text{ for all } 0 \leq k \leq N \right\} \tag{II.13}$$

if $\mathbf{x}^{\mathbf{u}}_{(\cdot)}$ denotes the trajectory under control inputs $\mathbf{u}_{(\cdot)}$ and starting in $\mathbf{x}_0$. However, feasibility for an initial condition $\mathbf{x}(t_0) = \mathbf{x}_0$ does not guarantee that any future state $\mathbf{x}(t)$, $t > t_0$, under MPC-feedback grants a feasible problem (Grüne and Pannek 2017, p. 178) or leads to a desired region of attraction. We will conclude this section reviewing the conditions for the stage cost ℓ, terminal penalty ℓ_∞, and constraints $g_i(\cdot)$ such that the feasible initial conditions $\mathcal{X}_N$ are not only forward-invariant[4] but also lead to stable operation.

In the following, we assume that the constraints $g_i(k, \cdot)$ either hold independently of $k \in \{0, \ldots, N\}$ (in which case we may omit the first argument) or are only active in the last time step N, and

$$g_i(N, \mathbf{x}, \mathbf{u}) \geq 0 \quad \Longrightarrow \quad g_i(\mathbf{x}, \mathbf{u}) \geq 0 \tag{II.14}$$

for all $i \in I$. The set of admissible state-input pairs is then denoted

$$\mathcal{Z} = \left\{ (\mathbf{x}, \mathbf{u}) \in \mathcal{X} \times \mathcal{U} \,\middle|\, \textstyle\bigwedge_{i \in I} g_i(\mathbf{x}, \mathbf{u}) \geq 0 \right\}. \tag{II.15}$$

For further convenience, we write the set of states that satisfy the *terminal* constraint as

$$\mathcal{X}_f = \left\{ \mathbf{x}_N \in \mathcal{X} \,\middle|\, \exists \mathbf{u} \in \mathcal{U}. \textstyle\bigwedge_{i \in I} g_i(N, \mathbf{x}_N, \mathbf{u}) \geq 0 \right\}. \tag{II.16}$$

Then, $\mathcal{X}_N$ constitutes nothing else than set of states $\mathbf{x}_0$ that can be recovered into $\mathcal{X}_f$ without violating any state and input constraints. The terminal set is commonly chosen to contain a stationary solution $\mathbf{x}_f$, including the singular set $\{\mathbf{x}_f\}$, which grants an optimal steady-state operation.

Remark The use of a 'stability-related' (Alamir 2017, p. 288) terminal set $\mathcal{X}_f$ as well as penalty ℓ_∞ is common in the literature to ensure asymptotically stable closed-loop operation, yet it restricts the feasible set, requires long predictions horizons, and thus lead to increased computation times (ibid.). Recent work proved stability of *unconstrained* MPC schemes under conditions such as suboptimality (Reble and Allgöwer 2012, p. 1815) or contraction (Alamir 2017, p. 290). These are beyond the scope of this thesis.

[4] A set $\mathcal{A} \subset \mathcal{X}$ is *forward-invariant* (under feedback $\boldsymbol{\mu}(\cdot)$) if and only if $\mathbf{x} \in \mathcal{A} \Rightarrow \mathbf{f}^+(\mathbf{x}, \boldsymbol{\mu}(\mathbf{x})) \in \mathcal{A}$.

II.2.1 Tracking and economic stage cost

We have not further considered the structure nor properties of the stage cost function ℓ, although we may have thought of a weighted cost similar to that of Eq. (II.5). In order to further formalise this idea, we introduce now the *tracking MPC* (also "standard" MPC) stage cost

$$\ell_{\mathrm{T}} \colon (\mathbf{x}, \mathbf{u}) \mapsto \|\mathbf{x} - \mathbf{x}_f\|_{\mathbf{Q}}^2 + \|\mathbf{u} - \mathbf{u}_f\|_{\mathbf{R}}^2 \tag{II.17}$$

for a target stationary solution $(\mathbf{x}_f, \mathbf{u}_f)$ and positive-definite weights $\mathbf{Q} \in \mathbb{S}_n, \mathbf{R} \in \mathbb{S}_m$. Then, ℓ_{T} has an unique minimum in $(\mathbf{x}_f, \mathbf{u}_f)$, namely, $\min_{\mathbf{x},\mathbf{u}} \ell_{\mathrm{T}}(\mathbf{x}, \mathbf{u}) = \ell_{\mathrm{T}}(\mathbf{x}_f, \mathbf{u}_f) = 0$. In consequence, the MPC feedback will drive the system towards the target point – as far as possible amid the constraints – in its attempt to minimise the cost function. The tracking MPC stage cost formulation is not necessarily limited to stationary solutions but can indeed be extended to an arbitrary reference trajectory $\mathbf{x}_{\mathrm{ref}}(\cdot)$ under the control inputs $\mathbf{u}_{\mathrm{ref}}(\cdot)$ if the stage cost is chosen to be time-varying (Grüne and Pannek 2017, pp. 53 and following). We shall see that, under moderate assumptions on the terminal penalty and constraints, the tracking MPC stage cost almost always yields stable closed-loop dynamics.

Yet, not every measure that might be desirable to optimise can be formulated as positive definite tracking cost. Those cases have first been considered in the field of chemical process engineering, where a process is to be operated under monetary, *economic* aspects and the economically best operation point even is not necessarily a steady state (Ellis et al. 2017, p. 6). In subsequence, the branch of model-predictive control feedback subject to non-definite cost functions is called *economic MPC* and we denote the corresponding ecnomic stage cost by ℓ_{E}. Since the economic cost is not formulated with respect to a chosen reference, the target stationary solution is obsolete. Instead, we have the notion of an *optimal equilibrium* (Grüne and Pannek 2017, p. 222).

Definition II.1. A stationary solution $(\mathbf{x}^*, \mathbf{u}^*) \in \mathcal{Z}$ is *optimal* with respect to the stage cost ℓ_{E} if and only if

$$\ell_{\mathrm{E}}(\mathbf{x}^*, \mathbf{u}^*) \leq \ell_{\mathrm{E}}(\mathbf{x}, \mathbf{u}) \tag{II.18}$$

for all admissible stationary solutions $(\mathbf{x}, \mathbf{u}) \in \mathcal{Z}$, i.e., $\mathbf{f}^+(\mathbf{x}, \mathbf{u}) = \mathbf{x}$ (in continuous time, $\mathbf{f}(\mathbf{x}, \mathbf{u}) = 0$). Then, the *optimal cost* is $\ell^* = \ell_{\mathrm{E}}(\mathbf{x}^*, \mathbf{u}^*)$.[5]

While the existence of at least one optimal equilibrium can be proven under the assumption of continuity and compact $\mathcal{Z}$ (Grüne and Pannek 2017, Lemma 8.4), its uniqueness is not guaranteed. Moreover, there might be a non-stationary solution such as a periodic orbit that provides a better performance *in average*. This is formulated in the concept of *optimal operation at steady-state* (Ellis et al. 2017, p. 61); namely, we

[5]The optimal cost is not necessarily zero, and could be as well positive as negative. We can, however, always adapt the stage cost such that $\ell^* = 0$ without losing generality.

have an asymptotic average economic performance of

$$\limsup_{N\to\infty} \frac{1}{N} \sum_{k=1}^{N} \ell_{\mathrm{E}}(\mathbf{x}_k, \mathbf{u}_k) \geq \ell^* \tag{II.19}$$

for any trajectory $\mathbf{x}_{(\cdot)}$ under control input $\mathbf{u}_{(\cdot)}$ where $(\mathbf{x}_k, \mathbf{u}_k) \in \mathcal{Z}$ for all $k \geq 0$. Indeed, if we consider stability of a system under economic model-predictive control as whether the optimal equilibrium is stable – in the sense of the bespoken definitions – for any recoverable initial condition, there must not be any other stationary or periodic solution with matching performance. Determining whether a given system is optimally operated at steady-state or not, however, turns out to be a challenging task for many practical systems.

II.2.2 Stability of model-predictive control

With the optimisation problem solved numerically in feedback loop to the control system, the closed-loop model-predictive control system constitutes in fact a hybrid system. Even if the control system itself is considered in discrete-time, the model-predictive control loop has no closed algebraic representation. These aspects render proving stability of model-predictive control strategies difficult. The natural methodology here is Lyapunov's stability theory (Theorem I.6) for a complex nonlinear system. We will consider stability as the existence of a "quasi-global" asymptotic stable equilibrium, that is, any initial condition that can be recovered (as defined by $\mathcal{X}_N$) will be recovered.

Problem II.2. Let $(\mathbf{x}^*, \mathbf{u}^*) \in \mathcal{Z}$ be an admissible stationary solution of the system $\mathbf{f}^+$ and $\boldsymbol{\mu}\colon \mathcal{X}_N \to \mathcal{U}$, a model-predictive control feedback with horizon $N \in \mathbb{N}$; find a Lyapunov candidate-function $\mathcal{V}\colon \mathcal{X} \to \mathbb{R}$ with respect to $\mathbf{x}^*$ such that

$$\mathcal{V} \circ \mathbf{f}^+(\mathbf{x}, \boldsymbol{\mu}_N(\mathbf{x})) - \mathcal{V}(\mathbf{x}) \leq -\rho(|\mathbf{x} - \mathbf{x}^*|) \tag{II.20}$$

for all $\mathbf{x} \in \mathcal{X}_N$ and with $\rho(\cdot)$ continuous, positive definite.

Stability of the infinite-horizon problem does not imply stability of the finite horizon, predictive control scheme without further assumptions (Jadbabaie et al. 2001, p. 778). Even though the second, local mode is technically never reached by the receding-horizon optimal feedback, it is commonly taken that a local controller κ_f is present and the cost of the latter mode is represented by the terminal penalty.

Assumption II.3. Let $\ell, \ell_\infty\colon \mathcal{X} \to \mathbb{R}$ be stage cost and terminal penalty, respectively, and $\mathcal{X}_f \subset \mathcal{X}$ be the terminal region; there is a local control law $\boldsymbol{\kappa}_f\colon \mathcal{X} \to \mathcal{U}$ such that

$$\ell_\infty \circ \mathbf{f}^+(\mathbf{x}, \boldsymbol{\kappa}_f(\mathbf{x})) - \ell_\infty(\mathbf{x}) \leq -\ell(\mathbf{x}, \kappa_f(\mathbf{x})) \tag{II.21}$$

and $\mathbf{f}^+(\mathbf{x}, \kappa_f(\mathbf{x})) \in \mathcal{X}_f$ for all $\mathbf{x} \in \mathcal{X}_f$.

We will further assume tacitly that $\mathbf{f}^+(\cdot,\cdot)$, $\ell(\cdot)$, and $\ell_\infty(\cdot)$ are continuous, as well as that $\mathcal{X}$, $\mathcal{X}_f$, and $\mathcal{U}$ are compact (hence, $\mathcal{Z}$ is compact). The following, classical theorem provides sufficient conditions for closed-loop stability (cf. Jäschke et al. 2014, p. 1261; Rawlings et al. 2017, p. 114).

Theorem II.4. *Let $(\mathbf{x}^*,\mathbf{u}^*)\in\mathcal{Z}$ be an admissible stationary solution, $\ell\colon\mathcal{Z}\to\mathbb{R}, \ell_\infty\colon\mathcal{X}\to\mathbb{R}$ be stage cost and terminal penalty, respectively, with $\ell(\mathbf{x}^*,\mathbf{u}^*)=\ell_\infty(\mathbf{x}^*)=0$ and $\mathcal{X}_f\subset\mathcal{X}$ be a terminal region with $\mathbf{x}^*\in\mathcal{X}_f$; if there are functions $\alpha_1,\alpha_2\in\mathcal{K}_\infty$ such that*

$$\begin{aligned}\alpha_1(|\mathbf{x}-\mathbf{x}^*|)&\leq\ell(\mathbf{x},\mathbf{u})\\ \ell_\infty(\mathbf{x}_f)&\leq\alpha_2(|\mathbf{x}_f-\mathbf{x}^*|)\end{aligned}\tag{II.22}$$

for all $(\mathbf{x},\mathbf{u})\in\mathcal{Z}$ where $\mathbf{x}\in\mathcal{X}_N$ and $\mathbf{x}_f\in\mathcal{X}_f$, and ℓ_∞ is positive definite in $\mathcal{X}_f$, then $(\mathbf{x}^*,\mathbf{u}^*)$ is asymptotically stable under model-predictive control feedback $\boldsymbol{\mu}_N$ with region of attraction $\mathcal{X}_N$. ◁

For a proof, the optimal value function $\mathcal{J}_N^0:\mathbf{x}_0\mapsto\hat{\mathcal{J}}_N$, where $\hat{\mathcal{J}}_N$ is the optimal value of (II.7) with initial condition $\mathbf{x}_0$, is demonstrated to be a Lyapunov function in $\mathcal{X}_N$ with respect to $\mathbf{x}^*$ (Rawlings et al. 2017, pp. 115–119). In the special case that the terminal set constitutes the singleton $\mathcal{X}_f=\{\mathbf{x}^*\}$, boundedness of $\mathcal{J}_N^0$ from above is not established by (II.22); instead, we introduce the assumption of *weak controllability* (Rawlings et al. 2017, p. 116; cited after Diehl et al. 2011, p. 704).

Assumption II.5. Let $(\mathbf{x}^*,\mathbf{u}^*)\in\mathcal{Z}$ be an admissible stationary solution; there exists a function $\gamma\in\mathcal{K}_\infty$ such that

$$\sum_{k=1}^{N}|\mathbf{u}_k-\mathbf{u}^*|\leq\gamma(|\mathbf{x}-\mathbf{x}^*|)\tag{II.23}$$

with $\left(\mathbf{x},\mathbf{u}_{(\cdot)}\right)\in\mathcal{Z}_N$ for all $\mathbf{x}\in\mathcal{X}_N$.

The lower bound in Eq. (II.22) implies necessarily that the stage cost is positive definite, which is the case for the tracking cost but not the more general economic cost. All is not lost though, for stability of an economic MPC feedback scheme might still hold (Angeli et al. 2012, p. 1617) and an alternative Lyapunov function can be formulated under certain requirements on the system $\mathbf{f}^+$ and the economic cost ℓ_E. Different approaches have been proposed hitherto, and these share the notion of *rotated* cost

$$\bar{\ell}(\mathbf{x},\mathbf{u})=_\mathrm{def}\ell(\mathbf{x},\mathbf{u})+\Lambda(\mathbf{x})-\Lambda\circ\mathbf{f}^+(\mathbf{x},\mathbf{u})-\ell^*\tag{II.24}$$

$$\bar{\ell}_\infty(\mathbf{x})=_\mathrm{def}\ell_\infty(\mathbf{x})\ +\Lambda(\mathbf{x})-\Lambda(\mathbf{x}^*)-\ell_\infty(\mathbf{x}^*)\tag{II.25}$$

for a suitable function $\Lambda\colon\mathcal{X}\to\mathbb{R}$ such that the auxiliary optimal control problem

$$\bar{\mathcal{J}}_N^0(\mathbf{x}_0)=_\mathrm{def}\min_{\mathbf{u}_{(\cdot)}\,|\,(\mathbf{x}_0,\mathbf{u})\in\mathcal{Z}_N}\bar{\ell}_\infty(\mathbf{x}_N^\mathbf{u})+\sum_{k=1}^{N-1}\bar{\ell}(\mathbf{x}_k^\mathbf{u},\mathbf{u}_k)\,,\tag{II.26}$$

where $\mathbf{x}^{\mathbf{u}}_{(\cdot)}$ denotes the trajectory under control inputs $\mathbf{u}_{(\cdot)}$ and starting in $\mathbf{x}_0$, has as same the optimal argument $\hat{\mathbf{u}}_{(\cdot)}$ as Eq. (II.10) and $\bar{\mathcal{J}}^0_N(\cdot)$ constitutes a Lyapunov function with respect to $\mathbf{x}^*$ (Jäschke et al. 2014, p. 1263; Amrit et al. 2011, p. 180).

The first to establish a Lyapunov function for economic model-predictive control were Diehl et al. (2011), who assumed strong duality of the steady-state problem. Namely, if there exist $\boldsymbol{\lambda} \in \mathbb{R}^n$ and $\alpha \in \mathcal{K}_\infty$ such that $(\mathbf{x}^*, \mathbf{u}^*)$ is the unique pair satisfying

$$\ell(\mathbf{x}^*, \mathbf{u}^*) + \alpha(|\mathbf{x} - \mathbf{x}^*|) \leq \ell(\mathbf{x}, \mathbf{u}) + \langle \boldsymbol{\lambda},\, \mathbf{x} - \mathbf{f}^+(\mathbf{x}, \mathbf{u}) \rangle \tag{II.27}$$

for all $(\mathbf{x}, \mathbf{u}) \in \mathcal{Z}$ and $\mathcal{X}_f = \{\mathbf{x}^*\}$, then the rotated optimal value function $\bar{\mathcal{J}}^0_N$ with $\Lambda : \mathbf{x} \mapsto \langle \boldsymbol{\lambda}, \mathbf{x} \rangle$ can be proven to be a Lyapunov function. (Diehl et al. 2011, p. 704). The condition of strong duality was subsequently relaxed to the more general concept of *strict dissipativity* (Amrit et al. 2011, p. 179; Angeli et al. 2012, p. 1618) with respect to $\varsigma_\ell(\mathbf{x}, \mathbf{u}) =_{\text{def}} \ell(\mathbf{x}, \mathbf{u}) - \ell^*$.

Definition II.6. Let $(\mathbf{x}^*, \mathbf{u}^*) \in \mathcal{Z}$ be the optimal stationary solution of the system $\mathbf{f}^+$ and $\varsigma \colon \mathcal{Z} \to \mathbb{R}$ be a supply rate; $\mathbf{f}^+$ is called *strictly dissipative* with respect to $\varsigma(\cdot)$ if and only if there exists a *storage function* $\Lambda : \mathcal{X} \to \mathbb{R}$ and positive definite $\rho : \mathbb{R}_{\geq 0} \to \mathbb{R}_{\geq 0}$ such that

$$\Lambda \circ \mathbf{f}(\mathbf{x}, \mathbf{u}) - \Lambda(\mathbf{x}) \leq -\rho(|\mathbf{x} - \mathbf{x}^*|) + \varsigma(\mathbf{x}, \mathbf{u}) \tag{II.28}$$

for all $(\mathbf{x}, \mathbf{u}) \in \mathcal{Z}$.

Strict dissipativity with respect to $\varsigma_\ell(\cdot)$ follows from strong duality, whereas strong duality follows from *strong convexity* of the rotated stage cost $\bar{\ell}$ given that $\Lambda(\cdot)$ is linear (Jäschke et al. 2014, p. 1263). We can thus summarise the results for closed-loop stability of economic model-predictive control as follows:

Theorem II.7. *Let $\ell : \mathcal{Z} \to \mathbb{R}, \ell_\infty : \mathcal{X} \to \mathbb{R}$ be stage cost and terminal penalty, respectively, $(\mathbf{x}^*, \mathbf{u}^*) \in \mathcal{Z}$ be an optimal stationary solution of the system $\mathbf{f}^+$, and $\mathcal{X}_f \subset \mathcal{X}$ be a terminal region with $\mathbf{x}^* \in \mathcal{X}_f$; if one of the following hold:*

1. *There is a linear $\Lambda : \mathcal{X} \to \mathbb{R}$ such that the rotated stage cost $\bar{\ell}$ is strongly convex;*
2. *There is a $\boldsymbol{\lambda} \in \mathbb{R}^n$ satisfying the assumption of strong duality for ℓ and $\mathbf{f}^+$ as given above;*
3. *The system $\mathbf{f}^+$ is strictly dissipative with respect to the supply rate $\varsigma_\ell : (\mathbf{x}, \mathbf{u}) \mapsto \ell(\mathbf{x}, \mathbf{u}) - \ell^*$;*

then $(\mathbf{x}^*, \mathbf{u}^*)$ is asymptotically stable under model-predictive feedback $\boldsymbol{\mu}_N$ with region of attraction $\mathcal{X}_N$. ◁

See Amrit et al. (2011, pp. 180 and 181, with Assumption II.3) and Angeli et al. (2012, pp. 1619 and 1620, with Assumption II.5) for a proof.

Regularisation for unstable steady-state operation

Angeli et al. (2012) and Jäschke et al. (2014) considered the situation that a chosen, purely economic stage cost ℓ_{E} does *not* result in a optimal operation at steady-state which is stable; therefore, both proposed augmenting the stage cost by a positive definite penalty term in order to ensure strict dissipativity (Angeli et al. 2012, p. 1620) and strong convexity (Jäschke et al. 2014, p. 1263), respectively. The *regularized* economic stage cost is thus given as[6]

$$\ell_{\mathrm{R}} \colon \mathbf{z} \mapsto \ell_{\mathrm{E}}(\mathbf{z}) + \tfrac{1}{2} \left\| \mathbf{z} - \mathbf{z}^* \right\|_{\mathbf{Q}}^2 \tag{II.29}$$

for all $\mathbf{z} =_{\mathrm{def}} (\mathbf{x}, \mathbf{u}) \in \mathcal{Z}$, where $\mathbf{Q} \in \mathbb{S}_{n+m}$ is a nonnegative, matrix-valued regularisation weight and $\mathbf{z}^* =_{\mathrm{def}} (\mathbf{x}^*, \mathbf{u}^*) \in \mathcal{Z}$ is the desired stationary solution.

Jäschke et al. (2014) selected the linear function $\Lambda(\mathbf{x}) = \langle \boldsymbol{\lambda}, \mathbf{x} \rangle$ such that

$$\nabla_{\mathbf{z}} \ell_{\mathrm{E}}(\mathbf{z}^*) + \nabla_{\mathbf{z}} \Big(\mathbf{x} - \mathbf{f}^+(\mathbf{x}, \mathbf{u}) \Big)(\mathbf{z}^*)\, \boldsymbol{\lambda} + \sum_{i \in I} \nabla_{\mathbf{z}} g_i(\mathbf{z}^*)\, \eta_i = 0 \tag{II.30}$$

with $\eta_i \geq 0$ for all $i \in I$ and $\sum_{i \in I} \eta_i g_i(\mathbf{z}^*)$, where $\nabla_{\mathbf{z}} \phi(\mathbf{z}^*)$ denotes the gradient of a function $\phi(\cdot)$ with respect to $\mathbf{z}$ evaluated in $\mathbf{z}^*$. Here, $\boldsymbol{\lambda}$ and $(\eta_i)_{i \in I}$ are the unique Lagrange multipliers of the *Karush-Kuhn-Tucker condition* (cf. Grüne and Pannek 2017, p. 388) for the optimal steady-state problem "$\min_{(\mathbf{x},\mathbf{u}) \in \mathcal{Z}} \ell_{\mathrm{E}}(\mathbf{x}, \mathbf{u})$ such that $\mathbf{x} = \mathbf{f}^+(\mathbf{x}, \mathbf{u})$." The *rotated* regularised stage cost function $\bar{\ell}_{\mathrm{R}}$ then has a global minimum in $\mathbf{z}^*$ if the second-order condition

$$\nabla_{\mathbf{z}}^2 \bar{\ell}_{\mathrm{R}}(\mathbf{z}) = \nabla_{\mathbf{z}}^2 \ell_{\mathrm{E}}(\mathbf{z}) - \sum_{i=1}^{n} \nabla_{\mathbf{z}}^2 f_i^+(\mathbf{z}) + \mathbf{Q} \succ 0 \tag{II.31}$$

holds for all $\mathbf{z} \in \mathcal{Z}$ (Jäschke et al. 2014, p. 1263), where $\nabla_{\mathbf{z}}^2 \phi(\mathbf{z})$ denotes the Hessian matrix of $\phi(\cdot)$ with respect to $\mathbf{z}$ and f_i^+ denotes the i-th component of $\mathbf{f}^+(\cdot, \cdot)$. That is, $\bar{\ell}_{\mathrm{R}}(\cdot)$ is strongly convex. In order to ensure positivity of the Hessian matrix, one may select a diagonal weight $\mathbf{Q} = \mathrm{diag}(q_1, \cdots, q_{n+m}) \succeq 0$ by exploiting the lower bound of the Gershgorin circle theorem for matrix eigenvalues (Jäschke et al. 2014, p. 1264), namely that a quadratic matrix $\mathbf{A}$ with elements $A_{i,j} \in \mathbb{R}$ is positive definite[7] if the lower bound

$$0 < A_{i,i} - \sum_{i \neq j} |A_{i,j}| \tag{II.32}$$

holds for all diagonal entries $A_{i,i}$. Now, if $\mathbf{A}$ denotes the matrix-valued function $\mathbf{z} \mapsto \nabla_{\mathbf{z}}^2 \ell_{\mathrm{E}}(\mathbf{z}) - \sum_{i=1}^{n} \nabla_{\mathbf{z}}^2 f_i^+(\mathbf{z})$ with elements $A_{i,j}(\mathbf{z}) \in \mathbb{R}$, choosing

$$q_i > \max_{\mathbf{z} \in \mathcal{Z}} \quad \sum_{i \neq j} |A_{i,j}(\mathbf{z})| - A_{i,i}(\mathbf{z}) \tag{II.33}$$

[6] Cited after Jäschke et al. (2014); note that Angeli et al. (2012) maintained a more general formulation allowing for a positive definite function $\alpha \colon \mathcal{Z} \to \mathbb{R}_{\geq 0}$.

[7] Recall that $\mathbf{A}$ is positive definite if and only if all eigenvalues are positive.

for $q_1, \ldots, q_{n+m}$ implies strong convexity of the rotated stage cost and thus stability of the regularised economic MPC feedback.

Note that Gershgorin's circle theorem tends to result in highly conservative estimates for the eigenvalues (DeVille 2016, p. 1). Moreover, strong convexity of the stage cost is not necessary for closed-loop stability. Therefore, the regularisation weights $\mathbf{Q}$ obtained by the procedure above are likely to be unnecessarily large, thus over-penalising the original, economic cost. Later work of Yu and Biegler (2019) hence addressed the identification of so-called *critical states* in order to reduce the overall regularisation penalty (Yu and Biegler 2019, pp. 47–49 and 51). Furthermore, in order to facilitate the selection of regularisation weights for strong convexity by the Gershgorin bound, the procedure above is restricted to the use of the Lagrange multiplier $\boldsymbol{\lambda}$ for duality. The regularisation scheme of Angeli et al. (2012), on the other hand, allows for arbitrary linear or continuous functions $\Lambda(\cdot)$, yet the proposed search for the weakest lower bound is computationally demanding.

Chapter 6

Sum-of-squares Control Synthesis

This chapter corresponds to:

> Torbjørn Cunis, Jean-Philippe Condomines, and Laurent Burlion (2019b). "Sum-of-squares Flight Control Synthesis for Deep-stall Recovery". In: Revision under review for *Journal of Guidance, Control, and Dynamics*

in the author's revised version.

Synopsis

So far, sum-of-squares (SOS) programming has been used to analyse the region of attraction of a given flight control approach. Now we are going to augment the bespoken approaches of the previous chapters to synthesise new linear and polynomial feedback laws. Estimating the region of attraction also under control input constraints, we can thus verify stable recovery as backwards reachability problem for upset conditions. Here, the choice of an ellipsoid as parameter of the SOS iteration turns out to be both crucial and challenging. Instead, we will directly utilise a given deep-stall flight condition and ensure its reachability. The derived control feedback grants stable recovery by design. This chapter constitutes a further demonstration of the usability of sum-of-squares programming techniques for flight control synthesis and verification in the view of LOC-I prevention and upset recovery.

Statement of Contribution Torbjørn Cunis implemented the sum-of-squares algorithms for control analysis and synthesis as well as developed the backwards-reachability scheme for deep-stall recovery. Jean-Philippe Condomines contributed to the wording of the manuscript. Laurent Burlion provided guidance and feedback throughout the drafting.

Sum-of-squares Flight Control Synthesis for Deep-stall Recovery

Torbjørn Cunis*
ONERA – The French Aerospace Lab, Centre Midi-Pyrénées, Toulouse, 31055, France

Jean-Philippe Condomines†
ENAC, Université de Toulouse, Toulouse, 31055, France

Laurent Burlion‡
Rutgers, The State University of New Jersey, Piscataway, NJ 08854, USA

In lieu of extensive Monte-Carlo simulations for flight control verification, sum-of-squares programming techniques provide an algebraic approach to the problem of nonlinear control synthesis and analysis. However, their reliance on polynomial models has hitherto limited the applicability to aeronautical control problems. Taking advantage of recently proposed piecewise polynomial models, this paper revisits sum-of-squares techniques for recovery of an aircraft from deep-stall conditions using a realistic yet tractable aerodynamic model. Local stability analysis of classical controllers is presented as well as synthesis of polynomial feedback laws with the objective of enlarging their nonlinear region of attraction. A newly developed synthesis algorithm for backwards-reachability facilitates the design of recovery control laws, ensuring stable recovery by design. The paper's results motivate future research in aeronautical sum-of-squares applications.

Nomenclature

α	Angle of attack (rad);
α_0	Low-angle of attack boundary ($\alpha_0 = 16.2949°$);
γ_A	Flight-path angle relative to air (rad);
η	Elevator deflection (rad), negative if leading to positive pitch moment;
ϑ	Signed distance ratio ($\vartheta \in \mathbb{R}$);

*Now with the University of Michigan, Ann Arbor, Michigan 48109, USA, e-mail: tcunis@umich.edu; Member AIAA.
†Assistant Professor, Drones Research Group, e-mail: jean-philippe.condomines@enac.fr
‡Assistant Professor, Department of Mechanical & Aerospace Engineering, e-mail: laurent.burlion@rutgers.edu

λ	Level set ($\lambda \in \mathbb{R}_+$);
ρ	Pseudo-radius ($\rho \in \mathbb{R}_+$);
$\varphi(\cdot)$	Boundary condition function ($\varphi\colon \mathbb{R}^m \to \mathbb{R}$);
$d\eta$	Change of elevator deflection (rad/s);
$\mathbf{K}$	Feedback control law ($\mathbf{K}\colon \mathbb{R}^n \to \mathbb{R}^p$);
n	Number of states; system degree;
p	Number of inputs;
P	Positive-definite, polynomial shape function ($P\colon \mathbb{R}^n \to \mathbb{R}_{\geq 0}, P \in \mathbb{R}[\mathbf{x}]$);
q	Pitch rate (rad/s);
V_A	Aircraft speed relative to air (m/s), positive along x_a-axis;
$\mathbf{x}^*, \eta^*$	State vector and elevator deflection at trim condition;
$\tilde{\mathbf{x}}, \tilde{\eta}$	Scaled state vector and elevator deflection;
$(\cdot)^{post}$	Domain of high angle of attack;
$(\cdot)^{pre}$	Domain of low angle of attack;
$\mathcal{E}$	(Quasi)-Ellipsoidal set ($\mathcal{E} = \{\mathbf{x} \,\vert\, P(\mathbf{x}) \leq \rho\}$) with shape function P and pseudo-radius ρ;
$\Sigma[\mathbf{x}]$	Polynomial sum-of-squares cone ($\Sigma[\mathbf{x}] \subset \mathbb{R}[\mathbf{x}]$);
$\mathbb{R}[\mathbf{x}]$	Set of polynomials in $\mathbf{x}$ with real-valued coefficients;

I. Introduction

Prediction and prevention of inflight loss-of-control (LOC-I) commonly requires prior knowledge of the aircraft's dynamics using a reliable and representative aerodynamic model. However, establishing a satisfactory model is rarely straightforward, and ensuring sufficient representation of every aspect of the operational envelope of the true vehicle is extremely challenging. Indeed, dynamics beyond the nominal flight envelope are highly nonlinear and often unstable. Flight control certification for commercial airliners therefore relies today on simple but extensive and cumbersome Monte-Carlo simulations of high-fidelity models [1] in order to analyse the viable subset of the flight envelope, which demands significant investment of time and computational power. Yet, more sophisticated tools based on nonlinear stability theory have

been applied in the literature. Mathematical continuation and bifurcation analysis establishes trim conditions and periodic orbits as well as their stability [2, 3]; however, attraction or reachability of a stable solution cannot be determined quantitatively using the continuation methodology. Reachability analysis, on the other hand, numerically evolves reachable subsets of the state-space over time, identifying possible violations of predefined constraints [4, 5]. An alternative formulation of the reachability problem is the algebraic notion of controlled invariant sets, or *safe sets* [6, 7]. Defined as the largest set such that the aircraft can be kept within the state constraints subject to control input limitations, the safe set determines bounds for prevention and recoverability from LOC-I events. The idea of a safe set as defined by the existence of an admissible control sequences is thus contrasted by the set of converging state trajectories subject to an a priori specified control law, namely, the region of attraction of the closed-loop system.

Determining the region of attraction of a given system up to a desired accuracy is, in general, a non-trivial task [8]. Recently, Lyapunov stability theory and LaSalle's later extension have been turned into a systematic analysis approach employing sum-of-squares (SOS) programming techniques [9, 10]. Relaxed to semi-definite problems [11], SOS provides global stability proofs [12] as well as provable under-estimates for the region of attraction of systems defined by polynomial dynamics [13]. Those methods for stability analysis can further extended for synthesis of control feedback laws ensuring or enlarging a region of attraction subject to input constraints [14, 15].

Sum-of-squares techniques have been exploited to analyze the short-period motion of an F/A-18 aircraft model [16]. A special iteration technique, called $\mathcal{V}$-*s-iteration*, was applied to estimate the region of attraction of the longitudinal motion of the Generic Transport Model [17]. In [18], this technique was employed to validate a revised control law for the F/A-18 "falling-leaf" mode. It is worth noting that this work used a reduced six-state polynomial aircraft model that was derived by sampling the equations of motion rather than the aerodynamic coefficients. Despite SOS techniques being a powerful tool to generate Lyapunov functions for suitable models, few work on SOS for aircraft dynamics has been published since. Simple polynomials are often unsuitable to fit full-envelope aerodynamics accurately, whereas advanced modeling techniques, such as multivariate splines [19], are computationally heavy to analyse using SOS. Simple piecewise-defined models, as proposed by the authors in [20], have the potential of bridging this gap, since they both describe accurately aircraft dynamics in the domains of low and high angles of attack while only slightly increasing the computational load for sum-of-squares programming.

In this article, we synthesize controllers for and verify deep-stall recovery of a small unmanned aircraft using SOS programming and a piecewise polynomial model. The choice of aircraft, a fixed-wing capable of stable deep-stall transition, descent, and recovery [21], allows us to isolate longitudinal dynamics. Continuing our work in [20], we present an extended $\mathcal{V}$-s-iteration for piecewise-defined aircraft dynamics in order to

obtain feedback control laws subject to state and inputs constraints. While we initially rely on common polynomial surfaces to govern the estimate (cf. [13, 14, 17, 18]), we later replace it by a single deep-stall condition. We thus provide a systematic analysis by SOS beyond polynomial aircraft models. The present paper is organised as follows: In Section II, we introduce the aircraft, its piecewise polynomial model and recall the basics of SOS analysis. Section III analyzes stable recovery of a linear-quadratic regulator and synthesizes polynomial controllers subject to an enlarged region of attraction. Section IV concludes the article by a revised formulation of control synthesis specifically for deep-stall recovery.

Note on *polynomial surfaces* For sum-of-squares analysis and control synthesis, we make use of geometric objects defined by polynomial functions on the state-space, i.e., $\mathcal{E} = \{\mathbf{x}\,|, P(\mathbf{x}) \leq \rho\}$ for some polynomial P in $\mathbf{x}$ and $\rho > 0$. The most common examples are ellipsoids (in three dimensions) and the related hyper-ellipsoidal surfaces, which are governed by quadratic functions $P = \mathbf{x}^T\mathbf{Q}\mathbf{x}$ with positive-definite matrix $\mathbf{Q}$. For simplicity, we call both ellipsoids and hyper-ellipsoids *ellipsoidal* surfaces. The concept of (hyper)-ellipsoids can be further extended to positive polynomial surfaces of order larger than two, of which we will refer as *quasi-ellipsoids*.

II. Methodology

We consider an autonomous, 1.65 m-wingspan, unmanned aircraft that, instead of landing gear, is intended to land vertically descending by a deliberate deep-stall manoeuvre. In this manoeuvre, the drag of the wings counteract the gravitational force, leading to a stable trim condition, and the horizontal distance covered during the landing is minimised. For the purpose of stable deep-stall flight, the elevator is designed to exceed the usual range and reach deflections of up to $-60°$. The parameters of the aircraft used in this study are given by Tab. 1.

Table 1 Parameters of the aircraft.

flight mass	m	1.55	kg
wing span	b	1.66	m
mean chord	c_a	0.174	m
wing area	S	0.277	m^2
air density	ϱ	1.25	$\mathrm{kg/m}^3$
gravitational constant	g	9.81	$\mathrm{m/s}^2$

The aircraft is considered to be laterally stable due to its dihedral wings. We therefore neglect the lateral dynamics for the analysis of stability and, consequently, assume the side-slip angle β to vanish. In deep-stall flight and transition, the aircraft is further unthrottled, i.e., the thrust force is zero ($\mathbf{F} = 0$).

We will refer mainly to the international standard *air-path axis system* $(x_\mathrm{a}, y_\mathrm{a}, z_\mathrm{a})$ oriented along the

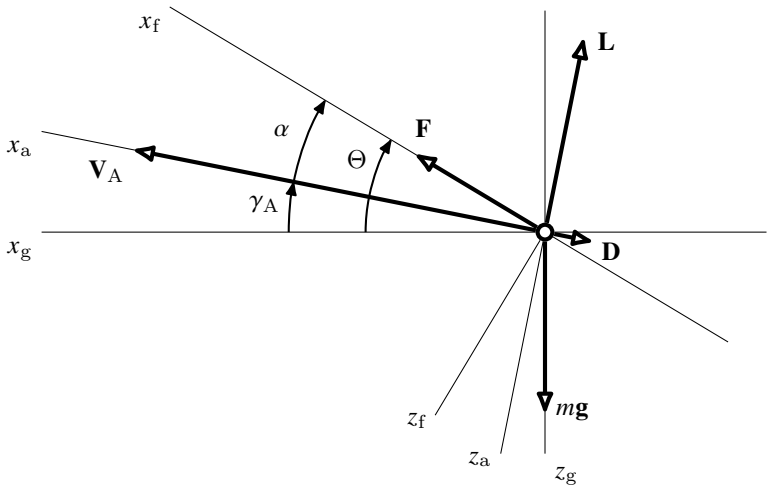

Fig. 1 Longitudinal axes with angles and vectors for $\beta = 0$.

aircraft's velocity vector with respect to air ($\mathbf{V}_\mathrm{A}$) [22]. Lift and drag forces are defined along these axes and denoted **L** and **D**; angle of attack α, flight-path angle γ_A, and pitch angle Θ are given by rotations into *body axis system* $(x_\mathrm{f}, y_\mathrm{f}, z_\mathrm{f})$ as well as *earth-fixed axis system* $(x_\mathrm{g}, y_\mathrm{g}, z_\mathrm{g})$, defined by the aircraft's fuselage and the ground, and between. (Fig. 1). If not stated otherwise, all variables are in SI-units; angles are however given in degrees where convenient.

A polynomial $g \in \mathbb{R}[\mathbf{x}]$ is a *sum of squares* (SOS) if $g = \sum_i g_i(\mathbf{x})^2$ for some $(g_i)_i \subset \mathbb{R}[\mathbf{x}]$; the set of sum-of-squares polynomials is denoted by $\Sigma[\mathbf{x}]$. It can be proven that $g \in \Sigma[\mathbf{x}]$ if and only if there is a positive semidefinite matrix $\mathbf{M}$ such that $g = \mathbf{z}^T \mathbf{M} \mathbf{z}$, where $\mathbf{z}$ is a vector of monomials in $\mathbf{x}$ [10]. This relation reduces the problem of finding SOS polynomials to semidefinite programming [11], given that the objective is linear in the SOS variables. However, the problem of a single decision variable entering bilinearly into the objective, although bilinear problems are generally $\mathcal{NP}$-hard, can efficiently be solved as quasi-convex SOS program [10]. Notwithstanding that any SOS polynomial is positive semidefinite, the opposite does not hold.

A. Equations of motion

The longitudinal equations of motion without thrust are given as nonlinear 4-state, ordinary differential equations [17, 23, 24]:

$$\dot{V}_\mathrm{A} = -\frac{1}{2}\varrho V_\mathrm{A}^2 S m^{-1} C_\mathrm{D}(\alpha,\eta) - g\sin\gamma_\mathrm{A}; \tag{1}$$

$$V_\mathrm{A}\,\dot{\gamma}_\mathrm{A} = \frac{1}{2}\varrho V_\mathrm{A}^2 S m^{-1} C_\mathrm{L}(\alpha,\eta) - g\cos\gamma_\mathrm{A}; \tag{2}$$

$$I_y\dot{q} = \frac{1}{2}\varrho V_\mathrm{A}^2 S c_\mathrm{a} C_\mathrm{m}(\alpha,\eta) - k_{\dot{q}q} q; \tag{3}$$

$$\dot{\Theta} = q; \tag{4}$$

with the pitch angle

$$\Theta = \gamma_\mathrm{A} + \alpha \tag{5}$$

and the air speed V_A as norm of the velocity vector relative to air. Then, C_L, C_D, C_m are dimensionless coefficients connected to lift force, drag force, and pitching moment. The elevator deflection η is, by convention, negative when causing a positive pitching moment. The linear damping coefficient $k_{\dot{q}q}$ accounts for non-static aerodynamics (see [21]).

The aerodynamic coefficients of the body, wing, and surfaces have been modeled by piecewise polynomial functions

$$C_\odot(\alpha,\cdots) = \begin{cases} C_\odot^{pre}(\alpha,\cdots) & \text{if } \alpha \le \alpha_0; \\ C_\odot^{post}(\alpha,\cdots) & \text{else;} \end{cases} \tag{6}$$

with $C_\odot^{pre}(\alpha_0,\cdot) \equiv C_\odot^{post}(\alpha_0,\cdot)$ and $\alpha_0 = 16.2949°$. Fig. 2 shows the piecewise model and their polynomial segments. Defined as piecewise polynomials, we are able to account for full-envelope characteristics both of the lift and drag coefficients as well as the coefficients in body axes [20]. The resulting models are continuous over the entire domain but not necessarily differentiable in its joint. The pitch-moment coefficient C_m is modeled likewise. The full aircraft model is detailed in [25].

B. Region of attraction estimation

In the following, we develop a region of attraction estimation for piecewise polynomial systems under constrained control inputs using SOS programming and extend this framework to find a control law that enlarges the region of attraction of the controlled system. In order to resolve the resulting bilinear terms, we

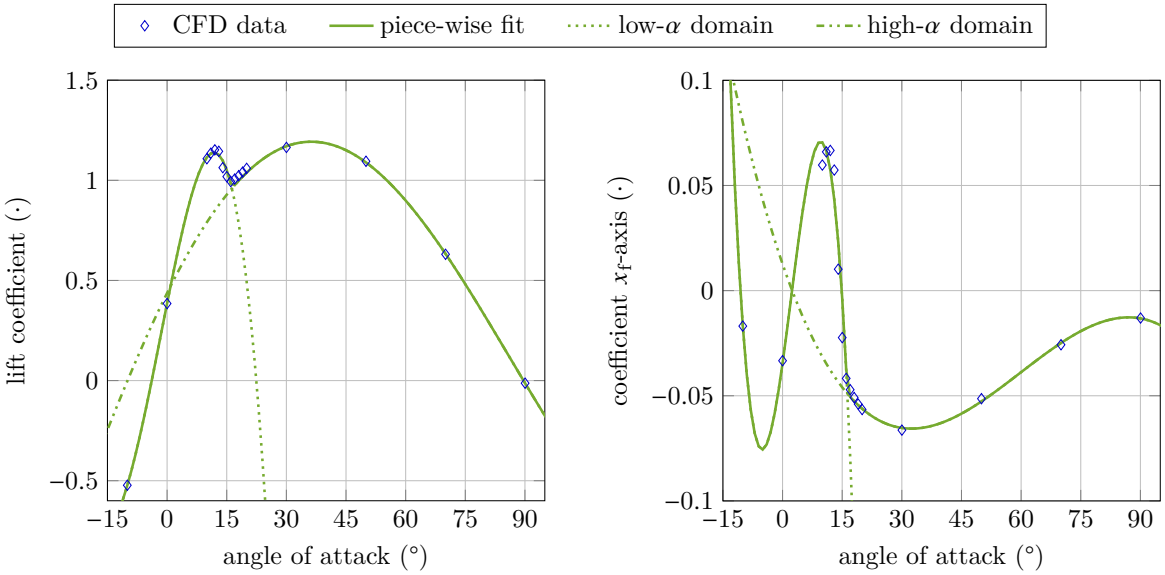

(a) Aerodynamic C_{L} coefficient. **(b) Aerodynamic C_{X} coefficient.**

Fig. 2 Piecewise model of aerodynamic coefficients with polynomial segments [21].

will make use of the $\mathcal{V}$-s-iteration [17].

Let a piecewise polynomial system be defined as

$$\mathbf{f}(\mathbf{x},\mathbf{u}) = \begin{cases} \mathbf{f}_1(\mathbf{x},\mathbf{u}) & \text{if } \varphi(\mathbf{x}) \leq 0; \\ \mathbf{f}_2(\mathbf{x},\mathbf{u}) & \text{else;} \end{cases} \tag{7}$$

with state vector $\mathbf{x} \in \mathcal{X} \subset \mathbb{R}^n$, input vector $\mathbf{u} \in \mathcal{U} \subset \mathbb{R}^p$, submodels $\mathbf{f}_1, \mathbf{f}_2 \in \mathbb{R}[\mathbf{x},\mathbf{u}]^n$and boundary $\varphi \in \mathbb{R}[\mathbf{x}]$; assume further $\mathbf{f}(\mathbf{x}^*,\mathbf{u}^*) = 0$. The equilibrium $(\mathbf{x}^*,\mathbf{u}^*)$ is stable if there exists a non-empty set of initial conditions such that the trajectories converge, the *region of attraction* $\mathcal{R}$, and $\mathcal{R}$ contains $\mathbf{x}^*$ in its interior. Now, $\Omega_\lambda = \{\mathbf{x} \,|\, \mathcal{V}(\mathbf{x}) \leq \lambda\}$ is an invariant subset of $\mathcal{R}$ if, for $\mathcal{V} : \mathcal{X} \to \mathbb{R}$ continuous and positive definite, $\mathcal{V}(0) = 0$, and $\lambda \in \mathbb{R}_+$,

$$\forall \mathbf{x} \in \Omega_\lambda. \quad \nabla\mathcal{V}\mathbf{f}(\mathbf{x},\mathbf{u}^*) < 0 \tag{8}$$

and Ω_λ is bounded [8]. Moreover, we call Ω_λ *invariant under control* $\mathbf{K}(\cdot)$ if Ω_λ is an invariant set of the closed-loop system $\mathbf{f}_{\mathbf{K}} : \mathbf{x} \mapsto \mathbf{f}(\mathbf{x},\mathbf{K}(\mathbf{x}))$ for some control law $\mathbf{u} = \mathbf{K}(\mathbf{x})$ and $\mathbf{K}(\mathbf{x}) \in \mathcal{U}$ for all $\mathbf{x} \in \Omega_\lambda$.

As Lyapunov functions are non-unique, alternative $\mathcal{V}(\cdot)$ give rise to different estimates of the region of attraction. For comparison of the size of an invariant subset, the $\mathcal{V}$-s-iteration introduces a surface $\mathcal{E}_\rho = \{\mathbf{x} \,|\, P(\mathbf{x}) \leq \rho\}$ with $P \in \mathbb{R}[\mathbf{x}]$ positive (quadratic) chosen as parameter of the estimation [13]. The

estimation of a maximal invariant subset of the region of attraction is then subject to the optimisation problem

$$\max_{\substack{\mathcal{V},\in\mathbb{R}[\mathbf{x}]\\ \lambda>0}} \rho > 0 \quad \text{s.t. (8) and } \mathcal{E}_\rho \subset \Omega_\lambda.$$

as well as $\mathcal{V}(\mathbf{x}) > 0$ if $\mathbf{x} \neq 0$ and $\mathcal{V}(0) = 0$.

1. Piecewise region of attraction

Recall that Ω_λ bounded is an invariant subset of $\mathcal{R}$ under control $\mathbf{K}$ if $\mathcal{V}(\cdot)$ is a continuous and positive definite function and $\nabla\mathcal{V}\mathbf{f}_{\mathbf{K}i}(x) < 0$ for any $\mathbf{x} \in \Omega_\lambda$ and $i \in \{1, 2\}$ such that $\mathbf{f}_{\mathbf{K}i}$ is active. For $\mathcal{V}_{1,2} \in \mathbb{R}[\mathbf{x}]$, we have the sufficient SOS constraint [20] (see also [13, Lemma 10])

$$\mathcal{V}_{1,2}(\mathbf{x}) - l_a \in \Sigma[\mathbf{x}] \tag{9}$$

$$-\nabla\mathcal{V}_1\mathbf{f}_{\mathbf{K}1} - l_b + (\mathcal{V}_1 - \lambda)\, s_{1,\lambda} + \varphi\, s_{1,\varphi} \in \Sigma[\mathbf{x}] \tag{10}$$

$$-\nabla\mathcal{V}_2\mathbf{f}_{\mathbf{K}2} - l_b + (\mathcal{V}_2 - \lambda)\, s_{2,\lambda} + \varphi\, s_{2,\varphi} \in \Sigma[\mathbf{x}], \tag{11}$$

where $s_{i,\lambda}, s_{i,\varphi} \in \Sigma[\mathbf{x}]$, $i \in \{1, 2\}$ relax negativity of $\nabla\mathcal{V}_i\mathbf{f}_i$ to the respective partitions defined by Ω_λ and $\varphi(\cdot)$ and $l_{a,b} \in \mathbb{R}[\mathbf{x}]$ are positive definite terms [13], e.g., $l_a = l_b = \epsilon\mathbf{x}^T\mathbf{x}$ with some small $\epsilon > 0$. As $\mathcal{V}(\cdot)$ is defined piecewise itself—i.e., $\mathcal{V}(\mathbf{x}) = \mathcal{V}_1(\mathbf{x})$ if $\varphi(\mathbf{x}) \leq 0$; $\mathcal{V}(\mathbf{x}) = \mathcal{V}_2(\mathbf{x})$ else;—, we ensure continuity along the boundary $\varphi \equiv 0$ by the additional SOS constraint

$$-\mathcal{V}_1 + \mathcal{V}_2 + \varphi\, s_{\varphi,1} - \varphi\, s_{-\varphi,1} \in \Sigma[\mathbf{x}] \tag{12}$$

$$-\mathcal{V}_2 + \mathcal{V}_1 + \varphi\, s_{\varphi,2} - \varphi\, s_{-\varphi,2} \in \Sigma[\mathbf{x}], \tag{13}$$

where $s_{\varphi,i}, s_{-\varphi,i} \in \Sigma[\mathbf{x}]$ with $i \in \{1, 2\}$ enforce that both $\mathcal{V}_1(\mathbf{x}) \leq \mathcal{V}_2(\mathbf{x})$ and $\mathcal{V}_2(\mathbf{x}) \leq \mathcal{V}_1(\mathbf{x})$ if $\varphi(\mathbf{x}) = 0$.

2. Invariant sets under control

The definition (7) and subsequent constraints (9)–(11), as is easy to see, apply equally to closed-loop controlled systems $\mathbf{f}_{\mathbf{K}}$ where $\mathbf{K}(\cdot)$ is linear or polynomial in $\mathbf{x}$. This alone, however, is insufficient for invariance under control as we have defined it above. We might now assume $\mathcal{U}$ to be defined as conjunction $\mathcal{U} = \{\mathbf{u} \,|\, p_1(\mathbf{u}) \leq 0, \ldots, p_m(\mathbf{u}) \leq 0\}$ with $\left(p_j\right)_{1\leq j\leq m} \subset \mathbb{R}[\mathbf{u}]$; if furthermore $\mathbf{K} \in \mathbb{R}[\mathbf{x}]^p$, we can state a necessary

SOS constraint for invariance of Ω_{λ} under control $\mathbf{K}$ as

$$-\left(p_j \circ \mathbf{K}\right) + (\mathcal{V} - \lambda)\, s_{j,\lambda'} \in \Sigma\,[\mathbf{x}], \tag{14}$$

where $\left(p_j \circ \mathbf{K}\right)(\mathbf{x}) = p_j(\mathbf{K}(\mathbf{x}))$, with $s_{j,\lambda'} \in \Sigma\,[\mathbf{x}]$ for all $1 \leq j \leq m$. The constraints (9)–(11) and (14), in fact, hold independently of each other and can be evaluated separately. As the subset-relation "$\subseteq$" on the level sets $\Omega_{(\cdot)}$ constitutes a total order, $\Omega_{\lambda_{\mathbf{K}}}$ with $\lambda_{\mathbf{K}} = \min\{\lambda, \lambda'\}$ is an invariant subset of the region of attraction of $\mathbf{f}_{\mathbf{K}}(\cdot)$ under control $\mathbf{K}$.

3. $\mathcal{V}$-s-iteration

The ellipsoid $\mathcal{E}_{\rho}$ can be fitted inside the invariant Ω_{λ} if

$$-(\mathcal{V}_i - \lambda) + (P - \rho)\, s_{i,P} \in \Sigma\,[\mathbf{x}] \tag{15}$$

with $s_{i,P} \in \Sigma\,[\mathbf{x}]$ for $i \in \{1, 2\}$.

Note that we require $\mathcal{V}_{1,2}$ to be of some fixed degree. However, some constraints involve bilinear terms of the form $\mathcal{V}_i\, s_{(\cdot)}$ once $\mathcal{V}_{1,2}$ become decision variables. The $\mathcal{V}$-s-iteration uses a bisection approach of iteratively-alternating steps; a detailed discussion of the basic $\mathcal{V}$-s-iteration has been given by Chakraborty et al. [17]. We extend here the approach in order to incorporate control input constraints for a $\mathbf{K}(\cdot)$ given a priori and, later on, synthesize an optimal control feedback:

1a) Find λ° maximal such that (10)–(11) hold for $\mathcal{V}_{1,2}$ fixed;

1b) Find λ^{*} maximal such that (14) holds for $\mathcal{V}_{1,2}$ fixed;

2) Find ρ° maximal such that (15) holds for $\mathcal{V}_{1,2}$ and $\lambda^{\dagger} = \min\{\lambda^{\circ}, \lambda^{*}\}$ fixed;

3) Find $\mathcal{V}_1, \mathcal{V}_2 \in \mathbb{R}\,[\mathbf{x}]$ of fixed degree such that (9)–(15) hold for ρ° and $\lambda^{\dagger}$ fixed.

The purpose of $\mathcal{E}_{\rho}$ here is twofold: first, to quantify the size of the provable invariant subset Ω_{λ} for each iteration; and second, to prevent the last step from yielding a smaller estimate than hitherto achieved.

C. Control synthesis

Until now, we have considered the control law to be given and fixed. Yet, we can further adapt our approach to find a suitable $\mathbf{K}$ in the attempt to enlarge the (estimated) region of attraction within the bounds imposed by the control input constrains. As the SOS constraints must be linear in the prospective control function, we require the control system to be in the *companion form* affine in $\mathbf{u}$, viz. $\dot{\mathbf{x}} = \mathbf{f}_{\mathbf{x}}(\mathbf{x}) + \mathbf{f}_{\mathbf{u}}(\mathbf{x})\,\mathbf{u}$ with $\mathbf{f}_{\mathbf{x}} \in \mathbb{R}\,[\mathbf{x}]^n, \mathbf{f}_{\mathbf{u}} \in \mathbb{R}\,[\mathbf{x}]^{n \times p}$, such that $\mathbf{f}_{\mathbf{K}}(\mathbf{x}) = \mathbf{f}_{\mathbf{x}}(\mathbf{x}) + \mathbf{f}_{\mathbf{u}}(\mathbf{x})\,\mathbf{K}(\mathbf{x})$. The input constraints $\left(p_j\right)_j$, too, must be

linear in $\mathbf{u}$, $p_j(\mathbf{u}) = \mathbf{p}_j^T \mathbf{u}$ with $\mathbf{p}_j \in \mathbb{R}^p$, and $\mathbf{K}$ guarantees control-invariance of $\Omega_{\mathcal{V}'}$ if

$$-\mathbf{p}_j^T \mathbf{K} + (\mathcal{V} - \lambda')\, s_{j,\mathcal{V}'} \in \Sigma[\mathbf{x}] \tag{16}$$

with $s_{j,\mathcal{V}'} \in \Sigma[\mathbf{x}]$ for all j.

Then, in order to circumvent bilinearities, we execute again steps 1) and 2) for $\mathbf{K}$ fixed and incorporate a supplementary second-to-last step

3a) Find $\mathbf{K} \in \mathbb{R}[\mathbf{x}]$ of fixed degree such that (10)–(11) and (16) hold for $\mathcal{V}_{1,2}$ as well as $\rho^\diamond$ and $\lambda^\dagger$ fixed.

The old and new last step is once more computed for $\mathbf{K}$ fixed. The thus augmented iteration is performed by Algorithm 1.

D. Preliminary stability analysis

In [21], we have applied bifurcation theory as well as optimization techniques in order to derive the linear pitch-damping model in Eq. (3). We have thus identified an optimal coefficient $C_{\mathrm{m}q} \approx 1.96$. In consequence, Fig. 3 shows the location and stability of longitudinal trim conditions (note that the choice of $C_{\mathrm{m}q}$ does not affect the location of stationary solutions as $q = 0$ is a necessary conditions for trim), parametrized by the elevator deflection η. The black dot in Fig. 3 indicates the largest deflection, $\eta = 6.5°$, for which the aircraft enters a steep, nose-down descent; the minimal elevator deflection is $-60°$. Shortly after stall, the aircraft encounters an unstable regime of stationary solutions with a family of limit cycles (*Hopf bifurcation*).

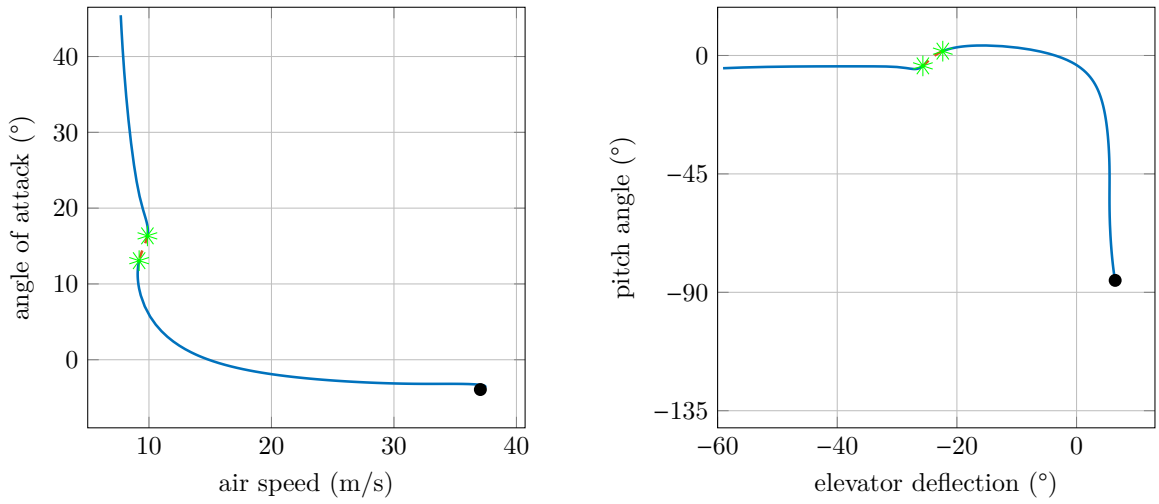

(a) Angle of attack α over air speed V. **(b) Pitch angle Θ over elevator deflection η.**

Fig. 3 Trim conditions of longitudinal motion with unstable regimes dashed [21].

Algorithm 1 Extended $\mathcal{V}$-s-iteration for control synthesis under state and input constraints.

1: **for** $N = 1$ to $N_{\max}$
2: **if** $N > 1$ **then**
3: find $\mathbf{K}_N \in \mathbb{R}[\mathbf{x}]$ s.t. for all $j \in [1, m]$, $i \in \{1, 2\}$,

$$\begin{aligned} -\mathbf{p}_j^T \mathbf{K}_N + \left(\mathcal{V}_{N,i} - \lambda^\dagger\right) s_{ij,\lambda'} &\in \Sigma[\mathbf{x}] \\ -\nabla \mathcal{V}_{N,i} \mathbf{f}_{\mathbf{K}_N i} - l_b + \left(\mathcal{V}_{N,i} - \lambda^\dagger\right) s_{i,\lambda} + \varphi\, s_{i,\varphi} &\in \Sigma[\mathbf{x}] \end{aligned}$$

4: find $\mathcal{V}_{N,1}, \mathcal{V}_{N,2} \in \mathbb{R}[\mathbf{x}]$ s.t. $s_{\varphi,i}, s_{-\varphi,i} \in \Sigma[\mathbf{x}]$ and for all $j \in [1, m]$, $i \in \{1, 2\}$,

$$\begin{aligned} \mathcal{V}_{N,i}(\mathbf{x}) - l_a &\in \Sigma[\mathbf{x}] \\ -\left(\mathcal{V}_{N,i} - \lambda^\dagger\right) + (P - \rho^\diamond)\, s_{i,P} &\in \Sigma[\mathbf{x}] \\ -\nabla \mathcal{V}_{N,i} \mathbf{f}_{\mathbf{K}_N i} - l_b + \left(\mathcal{V}_{N,i} - \lambda^\dagger\right) s_{i,\lambda} + \varphi\, s_{i,\varphi} &\in \Sigma[\mathbf{x}] \\ -\mathbf{p}_j^T \mathbf{K}_N + \left(\mathcal{V}_{N,i} - \lambda^\dagger\right) s_{ij,\lambda'} &\in \Sigma[\mathbf{x}] \\ -\mathcal{V}_{N,i} + \mathcal{V}_{N,3-i} + \varphi\, s_{\varphi,i} - \varphi\, s_{-\varphi,i} &\in \Sigma[\mathbf{x}] \end{aligned}$$

5: **end**
6: **for** $i \in \{1, 2\}$
7: find $\lambda_i^\diamond := \max_{\lambda \geq 0} \lambda$ s.t. $s_{i,\lambda}, s_{i,\varphi} \in \Sigma[x]$ and

$$-\nabla \mathcal{V}_{N,i} \mathbf{f}_{\mathbf{K}_N i} - l_b + (\mathcal{V}_{N,i} - \lambda)\, s_{i,\lambda} + \varphi\, s_{i,\varphi} \in \Sigma[\mathbf{x}]$$

8: find $\lambda_i^* := \max_{\lambda' \geq 0} \lambda'$ s.t. $s_{ij,\lambda'} \in \Sigma[\mathbf{x}]$ and for all $j \in [1, m]$,

$$-\mathbf{p}_j^T \mathbf{K}_N + (\mathcal{V}_{N,i} - \lambda')\, s_{ij,\lambda'} \in \Sigma[\mathbf{x}]$$

9: **end**
10: $\lambda^\dagger := \min\left\{\lambda_1^\diamond, \lambda_2^\diamond, \lambda_1^*, \lambda_2^*\right\}$
11: **for** $i \in \{1, 2\}$
12: find $\rho_i := \max_{\rho \geq 0}$ s.t. $s_{i,P} \in \Sigma[x]$ and

$$-\left(\mathcal{V}_{N,i} - \lambda^\dagger\right) + (P - \rho)\, s_{i,P} \in \Sigma[\mathbf{x}]$$

13: **end**
14: $\rho^\diamond = \min\{\rho_1, \rho_2\}$
15: **end**

III. Region of Attraction at Trim Point

Where classical control synthesis relies upon linearized models, the region of attraction estimation provides knowledge about the limitations of the chosen control implementation. Unlike the safe set [see, e.g., 6, 7], that provides an exploratory study in order to estimate the abilities of the aircraft to be controlled, we must study a region of attraction in the context of a given controller and the respective trim condition [20]. For the latter we choose a low-inclination gliding descent trim at $\eta^*_{\text{glide}} = -5°$ (see Appendix A).

In this section, we investigate the capability of different controllers to stably recover the aircraft from a deep-stall trim condition. We first consider a linear quadratic regulator, which could have been derived by classical control techniques. Later on however, we apply the SOS tools in order to derive a polynomial control law that improves stability and recovery of the vehicle. For both analysis and control synthesis, we scale the state vector $\mathbf{x}^T = \begin{bmatrix} V_\text{A} & \gamma_\text{A} & q & \alpha \end{bmatrix}$ by $\text{diag}(10\,\text{m/s}, 45°, 150\,°/\text{s}, 45°)^{-1}$ and the input η, by $(80°)^{-1}$, in order to normalize states and inputs. The scaled variables are henceforth denoted by $\tilde{\mathbf{x}}$, $\tilde{\eta}$, etc. The viable (unscaled) elevator inputs are given to $\mathcal{U} = [-60°; +20°]$ and represent the physical limits of the aircraft elevator. We further approximate the non-polynomial functions (sine, cosine, inverse) by Taylor series expansions and truncate high-order polynomial terms (Appendix A) in order to facilitate the resulting SOS problems [17].

The aircraft longitudinal motion is commonly divided into *short-period* dynamics involving pitch rate and angle of attack as well as the long-period *phugoid* oscillation of airspeed and flight-path angle and often discussed separately, as-if uncoupled. When discussing the region of attraction, we take into account the full, coupled 4-state model of Eqs. (1)–(4) but display the estimates as projections into either phugoid V_A-γ_A plane or short-period α-q plane. Details for all SOS computations are given in Appendix B.

A. Analysis of the Linear Quadratic Regulator

A further but more advanced element of the classical linear toolbox is the renown *linear quadratic regulator* (LQR). Here, we minimize the quadratic cost function $\tilde{J} = \int_0^\infty \tilde{\mathbf{x}}(t)^T\, \tilde{\mathbf{Q}}\, \tilde{\mathbf{x}}(t) + \tilde{R}\, \tilde{\eta}(t)^2\, \mathrm{d}t$ taking into account the linearized dynamics $\tilde{\mathbf{f}}(\tilde{\mathbf{x}}^* + \delta\tilde{\mathbf{x}}, \tilde{\eta}^* + \delta\tilde{\eta}) \approx \tilde{\mathbf{A}}\delta\tilde{\mathbf{x}} + \tilde{\mathbf{b}}\delta\tilde{\eta}$ in order to find a linear feedback. We obtain the optimal cost-to-go for an initial condition $\tilde{\mathbf{x}}_0 = \tilde{\mathbf{x}}(0)$ as $\tilde{J}_\text{opt} = \tilde{\mathbf{x}}_0^T \tilde{\mathbf{S}}\, \tilde{\mathbf{x}}_0$, where $\tilde{\mathbf{S}}$ denotes the solution to the general Riccati equation with $\left(\tilde{\mathbf{A}}, \tilde{\mathbf{b}}, \tilde{\mathbf{Q}}, \tilde{R}\right)$ and the LQR feedback is given as $\tilde{\eta} = \tilde{\mathbf{K}}_\text{LQR} = -\left[\tilde{R}^{-1}\tilde{\mathbf{b}}^T \tilde{\mathbf{S}}\right] \tilde{\mathbf{x}}$. For weights $\tilde{\mathbf{Q}} = \mathbb{I}_{4\times4}$, $\tilde{R} = 10$, the LQR feedback is synthesized to

$$\tilde{\mathbf{K}}_\text{LQR} = -0.1163\tilde{V}_\text{A} + 0.3881\tilde{\gamma}_\text{A} + 0.2412\tilde{q} + 0.0007\tilde{\alpha}. \tag{17}$$

The control-invariant estimate of the region of attraction for $\tilde{\mathbf{K}}_\text{LQR}$ is presented in Fig. 4 with the ellipsoidal shape $\mathcal{E}$ governed by $\tilde{P} = 4\tilde{V}_\text{A}^2 + 4\tilde{\gamma}_\text{A}^2 + \tilde{q}^2 + \tilde{\alpha}^2$. Again, $\mathcal{E}$ and the control inputs returned by the LQR

feedback are illustrated in Fig. 4, too.

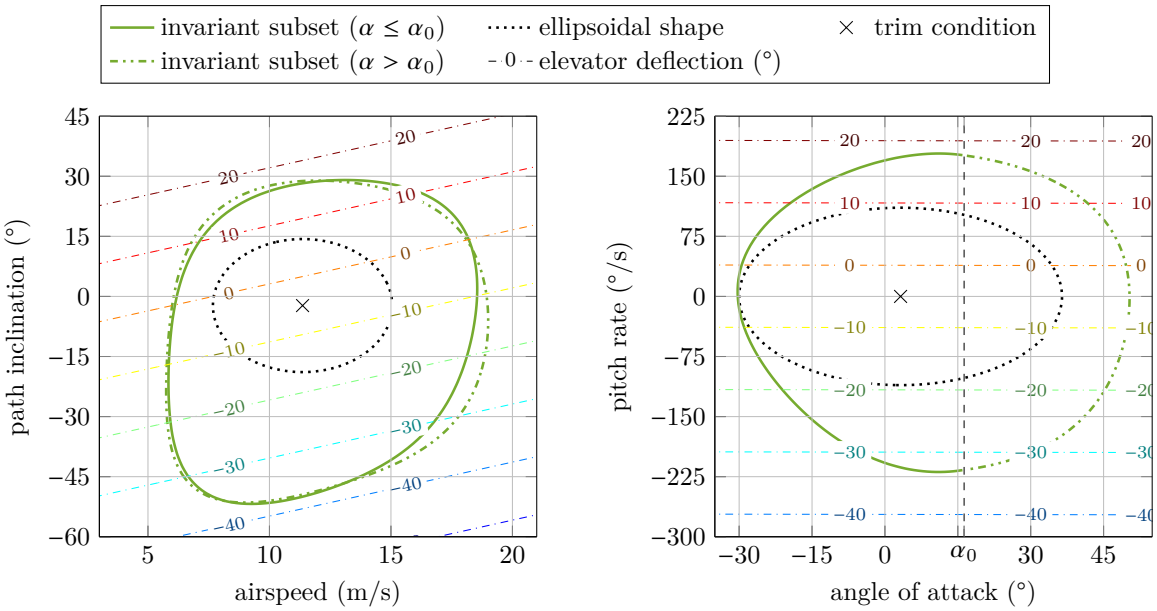

(a) Projection into phugoid plane. **(b) Projection into short-period plane.**

Fig. 4 Estimated control-invariant region of attraction of the linear quadratic regulator.

Even after descaling, the LQR gain on the angle of attack is significantly smaller, diminishing its contribution to the overall control feedback. With the additional gains on airspeed and path inclination, the estimated region of attraction contains the aircraft's high-angle of attack conditions in the lower-left corner of the phugoid plane. Consequently, the depicted LQR feedback is able to stably recover from deep-stall.

B. Synthesis of polynomial control laws

Until now, we have considered the control input to be determined by an *a priori* obtained state feedback law, which might have been designed by any means of control engineering. Synthesis of such a control law is subject to various objectives including desired closed-loop dynamics, disturbance rejection, and optimal reference tracking. From this section on, we treat the feedback law as decision variables of sum-of-squares analysis rather than as part of the initial problem formulation. Thus, the feedback control is synthesized with the aim of enlarging the region of attraction, again quantified by the size of the ellipsoidal shape $\mathcal{E}$. In the following, we subsequently derive a linear feedback similar to laws discussed in the previous section, a polynomial feedback, and piecewise feedback comparable to gain-scheduling control approaches. Further details can be found in Appendix B.

In order to reformulate the dynamics of section II into the companion form, we take the elevator deflection

η to be a state and introduce the rate of the actuator, $d\eta$, as new input:

$$\begin{bmatrix} \dot{\mathbf{x}} \\ \dot{\eta} \end{bmatrix} = \begin{bmatrix} \mathbf{f}_{\mathrm{EOM}}(\mathbf{x}, \eta) \\ 0 \end{bmatrix} + \begin{bmatrix} 0 \\ 1 \end{bmatrix} d\eta, \tag{18}$$

where $\mathbf{f}_{\mathrm{EOM}}$ are the system dynamics of the previous sections. The thus extended state vector is denoted by $\mathbf{x}_\eta$ and scaled by $\mathrm{diag}(10\,\mathrm{m/s}, 45°, 150\,°/\mathrm{s}, 45°, 20°)^{-1}$; the new input $d\eta$ is scaled by $(100\,°/\mathrm{s})^{-1}$. The viable (unscaled) actuator rate inputs are constrained to $|d\eta| \leq 200\,°/\mathrm{s}$ in order to ensure realistic actuator dynamics.

The role of the ellipsoid $\mathcal{E}$, and in particular the polynomial P governing its shape, for control synthesis deserves a further discussion. In the last step of the extended $\mathcal{V}$-s-iteration that is employed for both analysis and control synthesis, the ellipsoid $\{\mathbf{x} \,|\, P(\mathbf{x}) \leq \rho^\diamond\}$ serves as lower bound for the region of attraction estimate, both in size and shape. Recall further that each estimate $\{\mathbf{x} \,|\, \mathcal{V}(\mathbf{x}) \leq \lambda^\diamond\}$ is itself invariant; if the feedback law is chosen prior analysis, as in the preceding section, all invariant sets of the aircraft are predetermined by the closed-loop system dynamics. That is, we "find" a certain invariant set by guessing a Lyapunov function and computing its largest stable level set. With the feedback law being a decision variable of the control synthesis now, the selection of a control feedback actively "shapes" the resulting invariant set. In consequence, we expect the estimated region of attraction to follow the chosen ellipsoidal shape more closely and therefore, we must carefully select its shape.

We will initially choose a polynomial P of second order that results in an ellipsoid which is rotated with respect to the normal vector of the phugoid plane, in order to enhance recovery from deep-stall trim conditions, where air speed is exceptionally low and the path inclination is oriented steeply downwards. As the elevator deflection constitutes a state of Eq. (18), the constraints $\eta \in [-60°; 20°]$ form asymmetric boundaries. Hence, to ensure recovery from deep-stall trim of conditions of largely negative elevator deflections is challenging. We will therefore employ an asymmetrically defined quasi-ellipsoidal shape governed by a fourth-order polynomial.

1. Linear feedback control

We start with synthesizing a linear feedback law $d\eta = \mathbf{K}_{\mathrm{lin}} = \mathbf{G}\,\mathbf{x}$, where $\mathbf{G} \in \mathbb{R}^{5\times5}$ is a decision variable of the sum-of-squares program. Fig. 5 shows the estimated region of attraction for the synthesized linear control feedback. The ellipsoidal shape $\mathcal{E}$ is governed by

$$\tilde{P} = 220\tilde{V}_{\mathrm{A}}^2 - 360\tilde{V}_{\mathrm{A}}\tilde{\gamma}_{\mathrm{A}} + 100\tilde{\alpha}^2 + 25\tilde{\eta}^2 + 220\tilde{\gamma}_{\mathrm{A}}^2 + 100\tilde{q}^2$$

and rotated with respect to the phugoid plane. The synthesized linear feedback law is illustrated in Fig. 5 as contour plots with respect to states and elevator deflection.

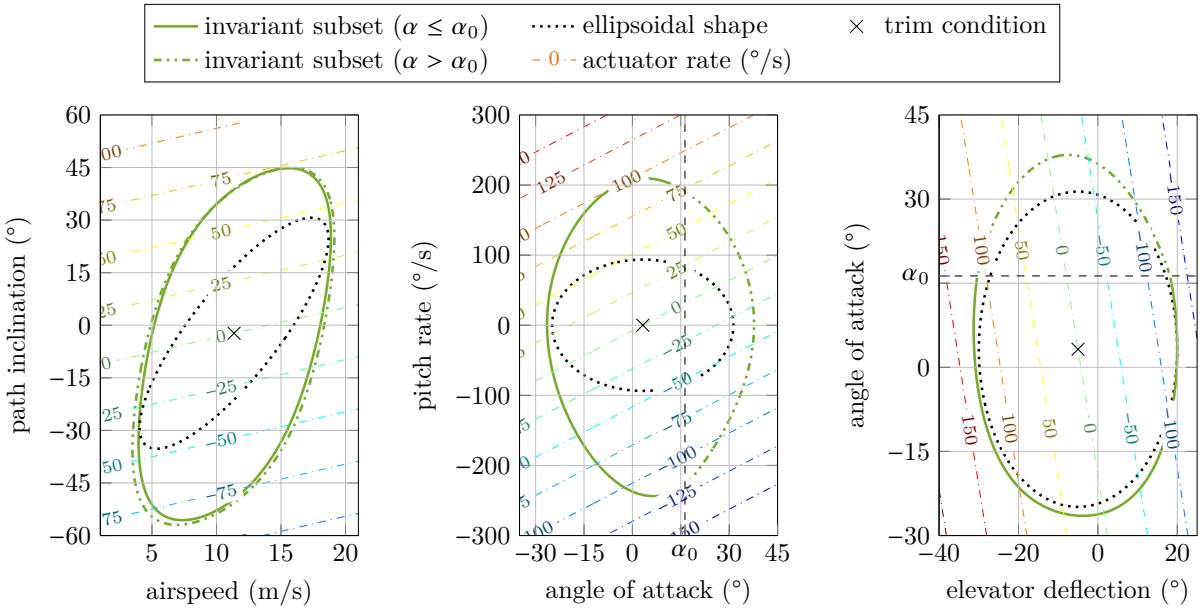

(a) Phugoid plane. **(b) Short-period plane.** **(c) Elevator-input plane.**

Fig. 5 Region of attraction of the synthesized linear control feedback matrix.

The synthesized linear feedback maintains a region of attracting that contains initial conditions of a wide range of airspeed, path inclination, and angle of attack. In phugoid and short-period plane, the invariant set only loosely follows the ellipsoidal shape, leading to an enlarged region of attraction. However, the ellipsoidal shape starkly affects the elevator deflection, as the dynamics of the actuator are decoupled, and the upper bound constraints both positive and negative deflections. Thus, negative elevator deflections observed in deep-stall flight are not contained by the estimated region of attraction of this linear feedback controller.

2. Polynomial feedback control

Indeed, sum-of-squares control synthesis benefits from its ability to synthesized polynomial feedback laws which are not represented by linear matrices. Whereas the Lyapunov function-candidate is conveniently represented by a polynomial without linear coefficients and of even degree to facilitate positivity of the Lyapunov function, it seems reasonable to have a polynomial feedback law without constant terms and of odd degree. Here, we choose a polynomial $d\eta = \mathbf{K}_{\text{poly}}$ with linear, quadratic, and cubic terms. Furthermore, to maintain a region of attraction including large negative elevator deflections, we select an asymmetric quasi-ellipsoidal shape $\mathcal{E}$ that is governed by $\tilde{P}_{\text{poly}}$ given in Appendix C. The estimated region of attraction for the synthesized third-order control feedback is shown in Fig. 6.

The differences between third-order (cubic) and first-order (linear) feedback laws can well be obtained from the isolines, that is, the contour lines of equal actuator rate inputs. Not only decreases the distance

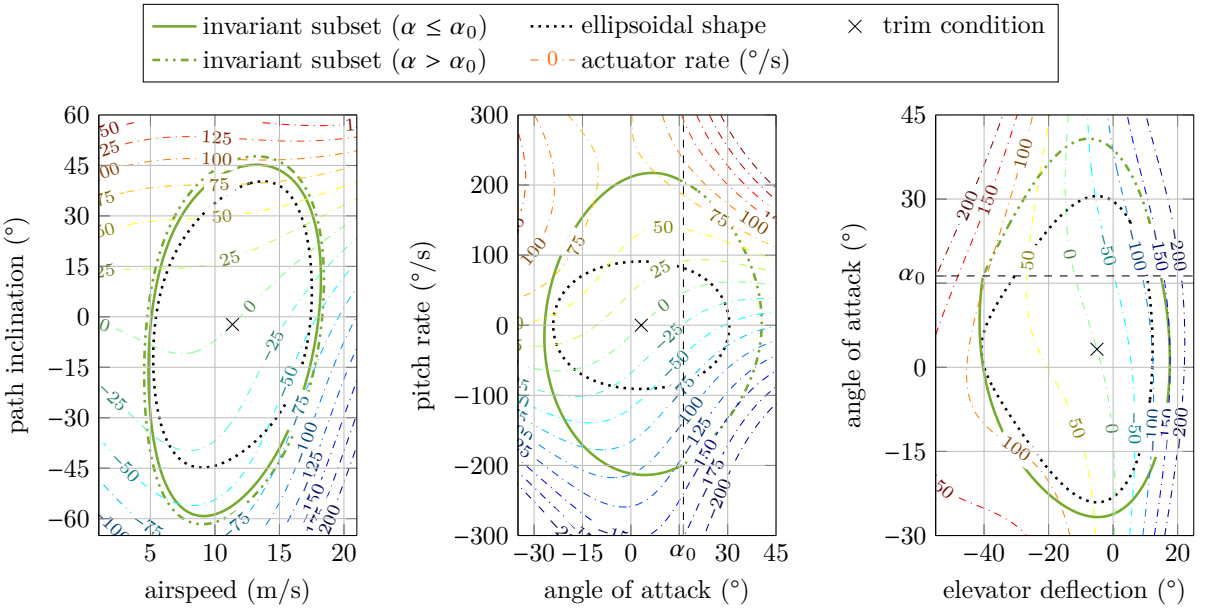

(a) Phugoid plane. **(b) Short-period plane.** **(c) Elevator-input plane.**

Fig. 6 Region of attraction of the synthesized polynomial control feedback law.

between two isolines with increasing distance from the trim condition, their course varies starkly between different sections of the state-space. Moreover, the invariant set seems to be "embedded" into the contour lines of equal feedback.

The asymmetric quasi-ellipsoid pushes the boundary of the invariant set towards larger negative elevator deflections, without violating the upper constraint. However, deep-stall trim conditions with their angles of attack of $\geq 30°$ are not contained by the estimated region of attraction.

3. Piecewise feedback control

It seems desirable to have alternative control laws for high and low angles of attack in order to adapt for changed dynamics beyond stall. With the aerodynamic model defined piecewise, it is convenient to synthesize a piecewise polynomial control law for the same regions, that is,

$$d\eta = \mathbf{K}_{\text{pw}}(\mathbf{x}) = \begin{cases} \mathbf{K}^{pre} & \text{if } \alpha \leq \alpha_0; \\ \mathbf{K}^{post} & \text{else;} \end{cases} \tag{19}$$

where $\mathbf{K}^{pre}, \mathbf{K}^{post}$ are third-order polynomials in $\mathbf{x}$. Note that we don't require a boundary condition, as we command a change of deflection, but could enforce equality of $\mathbf{K}^{pre}$ and $\mathbf{K}^{post}$ along $\alpha \equiv \alpha_0$ similar to (12)–(13). When synthesizing polynomial feedbacks for a control-invariant region of attraction spanning both

low and high angles of attack, both must not violate state and input constraints within their respective domains. Fig. 7 shows the estimated region of attraction for the synthesized piecewise third-order control feedback. The ellipsoidal shape $\mathcal{E}$ is extended towards the section of high angles of attack and large negative elevator deflections and therefore governed by $\tilde{P}_{\text{pw}}$ detailed in Appendix C. For the sake of legibility of the phugoid-plane projection, we only show the contour lines of equal control feedback for the low angle of attack law.

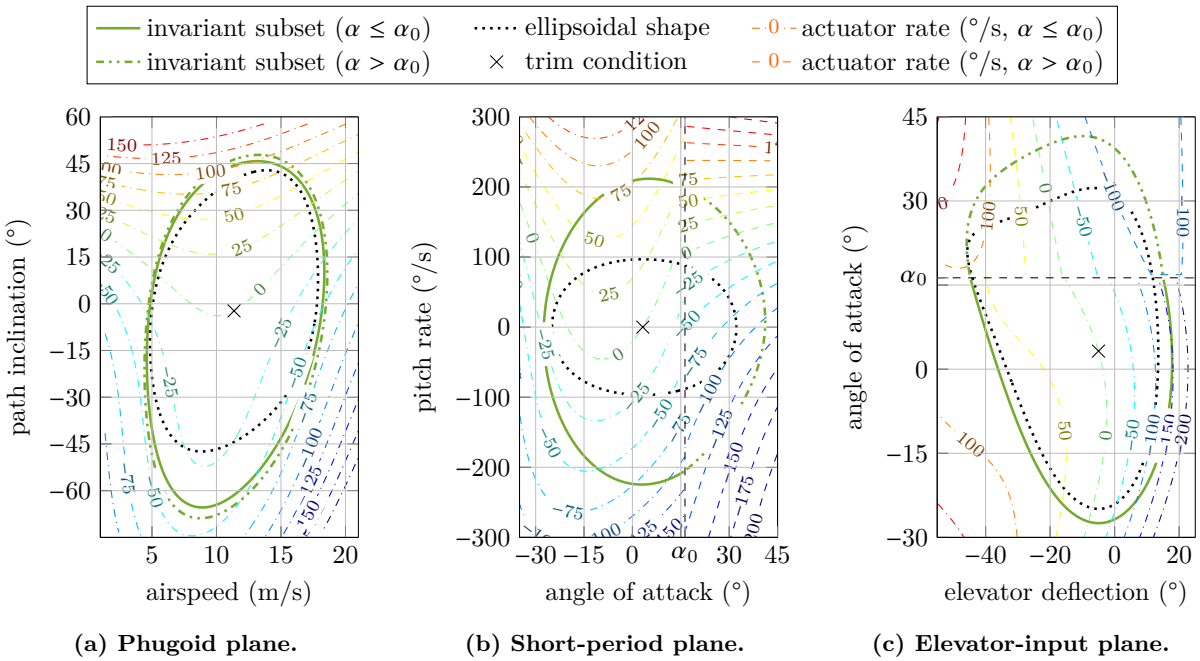

(a) Phugoid plane. **(b) Short-period plane.** **(c) Elevator-input plane.**

Fig. 7 Region of attraction of the synthesized piecewise polynomial control feedback law.

C. Discussion

We employed the sum-of-squares framework in order to synthesize linear, polynomial, and piecewise polynomial control feedback laws that, by design, grant an enlarged region of attraction subject to constraints on the deflection and rate of change of the elevator. Here, as discussed in the beginning, the choice of its shape P turns out to be crucial for the shape of the resulting provable invariant set and thus the synthesized feedback law. Alternative iteration approaches which remove the necessity of a shape function by a set-inclusion constraint of the estimates likewise lack the directional information to effectively synthesize a control feedback that enlarges the region of attraction towards the desired states. On the other hand, during the iteration the surface $\mathcal{E}_\rho$ and the input constraints form lower and upper bounds, respectively, for the computation of a new feedback law $\mathbf{K}$. As the deflection constraint has been particularly asymmetric (−60° to 20°), we made use of increasingly complicated, asymmetrically shaped quasi-elliposidal surfaces. Thus we were able to

synthesize feedback laws for recovery from flight condition at increasingly steep descents at low airspeeds without violating the elevator deflection constraint. However, if the generated invariant sets do not contain the deep-stall flight conditions (which is the case), this is rather due to the choice of P as parameter of the $\mathcal{V}$-s-iteration then to the form of the control feedback. Despite a large number of iterations, when these bounds finally converge and the iteration terminates (see Table 2 in Appendix B), we have not succeeded in reaching the deep-stall flight conditions with the resulting set invariant under the synthesized control. In the next section, we will therefore propose an alternative algorithm that directly formulates the SOS control synthesis as reachability problem.

Sum-of-squares programming is notoriously limited by the size of the resulting matrices for the semidefinite problems, which in turn is a function of both the number of state variables and polynomial degree and scales badly [26]. A further partitioning of the state-space into piecewise defined polynomials could help reduce the necessary polynomial degree to accurately represent aircraft dynamics, thus also the underlying matrix size, but increases the number of decision variables in Eq. (10) and must be subject to a careful trade-off.

IV. Deep-stall Recovery

Reachability of deep-stall trim conditions via SOS control synthesis, as the previous section revealed, remains subject of a careful selection of the ellipsoidal shape $\mathcal{E}$. Defining a polynomial surface, in particular in higher dimensions and larger-than-quadratic order, is a nontrivial task (see also Appendix C for a sum-of-squares procedure for quasi-ellipsoids based on a selection of points). On the other hand, deep-stall recovery is often formulated as finite-horizon problem, namely, as part of a multi-mode paradigm where the flight controller switches to a local feedback after recovery. In this section, we modify the control synthesis into a simplified backwards reachability scheme, where the ellipsoidal shape is replaced by a target state whence recovery is to be ensured. An alternative approach for a finite-horizon backwards reachability analysis was presented in [27]; here, the ellipsoidal shape is replaced by a constraint enforcing that each prior estimate is nested in the next. However, this approach lacks any directional information for enlarging the closed-loop reachable set under the control law to be synthesized. We further provide a numerical comparison of deep-stall recovery by all presented feedback laws in the time domain.

A. Backwards reachability control synthesis

Denote the target state by $\mathbf{x}_1$ and the distance vector from the nominal trim by $\bar{\mathbf{x}} = \mathbf{x}_1 - \mathbf{x}^*$. The target state can be *recovered* into the nominal trim condition by a control feedback $\mathbf{K}$ (i.e., $\mathbf{x}_1$ is backwards reachable from $\mathbf{x}^*$), if there is a function $\mathcal{V}(\cdot)$ and level set λ such that Ω_λ is a control-invariant region of attraction estimate (cf. Eqs. (10)–(14)) and $\mathbf{x}_1 \in \Omega_\lambda$, that is, $\mathcal{V}(\bar{\mathbf{x}}) \leq \lambda$. Obtaining such $\mathbf{K}$, $\mathcal{V}(\cdot)$, and λ requires again

bisection: Given $\mathcal{V}(\cdot)$ and λ such that (10)–(14) hold, we define the *degree of reachability* $\vartheta^\diamond$ as the maximal distance ratio ϑ such that

$$\mathcal{V}(\vartheta\bar{\mathbf{x}}) \leq \lambda \tag{20}$$

and observe that $\mathbf{x}_1$ can be recovered if $\vartheta^\diamond \geq 1$. For robustness, it might be desirable to have $\mathbf{x}_1$ well inside the interior of Ω_λ, that is, the degree of reachability is strictly larger than one or even satisfies a chosen margin. The $\mathcal{V}$-s-iteration for backwards reachability is then formulated as follows:

1) Find λ°, λ^* maximal such that (10)–(11) as well as (14) hold for $\mathcal{V}$ and $\mathbf{K}$ fixed;
2) Find $\vartheta^\diamond$ maximal such that (20) holds for $\mathcal{V}$ and $\mathbf{K}$ as well as $\lambda' = \min\{\lambda^\circ, \lambda^*\}$ fixed;
3a) Find $\mathbf{K} \in \mathbb{R}[\mathbf{x}]$ of fixed degree such that (10)–(11) and (16) hold for $\mathcal{V}$ as well as $\vartheta^\diamond$ and λ' fixed;
3b) Find $\mathcal{V} \in \mathbb{R}[\mathbf{x}]$ of fixed degree such that (9)–(14) and (20) hold for $\mathbf{K}$ as well as $\vartheta^\diamond$ and λ' fixed.

Instead of $\mathcal{E}_\rho$ before, the degree of reachability $\vartheta^\diamond$ ensures that, in the last step, the region of attraction estimate grows towards the target state $\mathbf{x}_1$, that is, the degree of reachability increases. The thus modified V-s-iteration is performed by Algorithm 2. Note that, unlike finite-horizon reachability the obtained feedback law $\mathbf{K}$ stabilizes the target trim condition *beyond* recovery, too. Line 11 of Algorithm 2 cannot be solved as the sum-of-squares problem (20) is not linear in ϑ in general, but is efficiently obtained using a nonlinear solver such as MATLAB's `fmincon`.

We choose now one of the stable deep-stall trim conditions as target state, namely, that at $\eta_1 = -40°$ (see Appendix A). Again, states and inputs are scaled to $\tilde{\mathbf{x}}$, $\tilde{d\eta}$, etc. and subject to state and input constraints. For the sake of a demonstration here, we choose a single function-candidate $\mathcal{V}(\cdot)$ as well as a linear control feedback. Fig. 8 illustrates the estimated region of attraction, a five-dimensional surface, as slices projected into the phugoid plane; for this purpose, we assign the free parameters as $\alpha = t\bar{\alpha}$, $q = t\bar{q}$, and $\eta = t\bar{\eta}$ and use the ratio t for the out-of-plane drawing axis.

With a terminal degree of reachability of $\vartheta^\diamond = 1.3027$, the synthesized feedback law robustly recovers the aircraft from the deep-stall target into nominal flight. Note that the invariant subset is shaped mainly around the trajectory from $\mathbf{x}_1$ to $\mathbf{x}^*$, as this has been the objective, rather than growing as large as possible. This is further illustrated in Fig. 9, which depicts the estimated regions of attraction in the course of the 39 iterations. With increasing iterations, the region of attraction estimate it stretched towards the target flight condition $\mathbf{x}_1$ until contained ($\vartheta^\diamond \geq 1$).

Algorithm 2 Modified $\mathcal{V}$-s-iteration for backwards reachability of target $\bar{\mathbf{x}} = \mathbf{x}_1 - \mathbf{x}^*$.

1: **for** $N = 1$ to $N_{\max}$
2: **if** $N > 1$ **then**
3: find $\mathbf{K}_N \in \mathbb{R}[\mathbf{x}]$ s.t. for all $j \in [1, m]$, $i \in \{1, 2\}$,

$$-\mathbf{p}_j^T \mathbf{K}_N + \left(\mathcal{V}_N - \lambda^\dagger\right) s_{j,\lambda'} \in \Sigma[\mathbf{x}]$$
$$-\nabla \mathcal{V}_N \mathbf{f}_{\mathbf{K}_N i} - l_b + \left(\mathcal{V}_N - \lambda^\dagger\right) s_{i,\lambda} + \varphi\, s_{i,\varphi} \in \Sigma[\mathbf{x}]$$

4: find $\mathcal{V}_N \in \mathbb{R}[\mathbf{x}]$ s.t. for all $j \in [1, m]$, $i \in \{1, 2\}$,

$$\mathcal{V}_N(\mathbf{x}) - l_a \in \Sigma[\mathbf{x}]$$
$$-\nabla \mathcal{V}_N \mathbf{f}_{\mathbf{K}_N i} - l_b + \left(\mathcal{V}_N - \lambda^\dagger\right) s_{i,\lambda} + \varphi\, s_{i,\varphi} \in \Sigma[\mathbf{x}]$$
$$-\mathbf{p}_j^T \mathbf{K}_N + \left(\mathcal{V}_N - \lambda^\dagger\right) s_{ij,\lambda'} \in \Sigma[\mathbf{x}]$$
$$\mathcal{V}_N(\vartheta^\diamond \bar{\mathbf{x}}) \leq \lambda^\dagger$$

5: **end**
6: **for** $i \in \{1, 2\}$
7: find $\lambda_i^\diamond := \max_{\lambda \geq 0} \lambda$ s.t. $s_{i,\lambda}, s_{i,\varphi} \in \Sigma[x]$ and

$$-\nabla \mathcal{V}_N \mathbf{f}_{\mathbf{K}_N i} - l_b + (\mathcal{V}_N - \lambda)\, s_{i,\lambda} + \varphi\, s_{i,\varphi} \in \Sigma[\mathbf{x}]$$

8: **end**
9: find $\lambda^* := \max_{\lambda' \geq 0} \lambda'$ s.t. $s_{j,\lambda'} \in \Sigma[\mathbf{x}]$ and for all $j \in [1, m]$,

$$-\mathbf{p}_j^T \mathbf{K}_N + (\mathcal{V}_N - \lambda')\, s_{j,\lambda'} \in \Sigma[\mathbf{x}]$$

10: $\lambda^\dagger := \min\left\{\lambda_1^\diamond, \lambda_2^\diamond, \lambda^*\right\}$
11: find $\vartheta^\diamond := \max_{\vartheta \geq 0}$ s.t.

$$\mathcal{V}_N(\vartheta \bar{\mathbf{x}}) \leq \lambda^\dagger$$

12: **end**

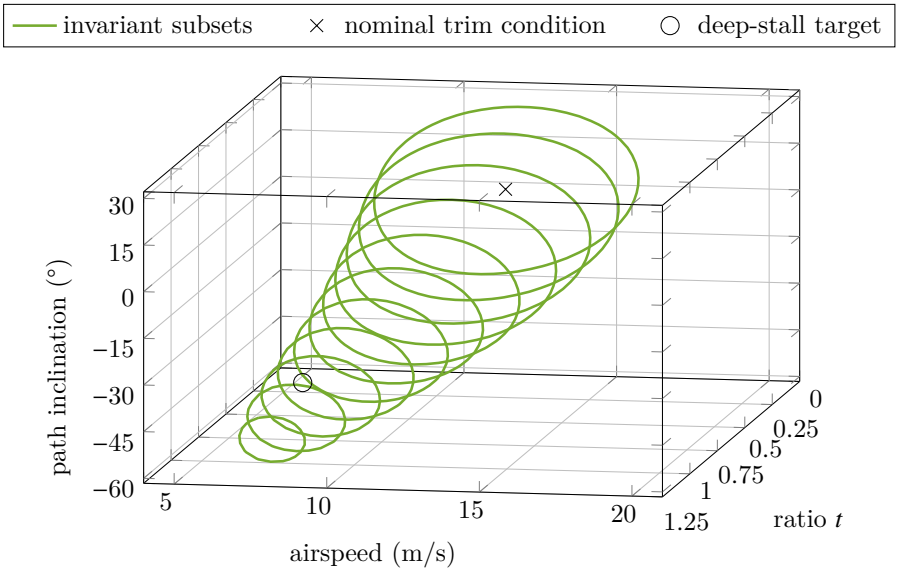

Fig. 8 Region of attraction of a linear control feedback law, synthesized by backwards reachability of the deep-stall target.

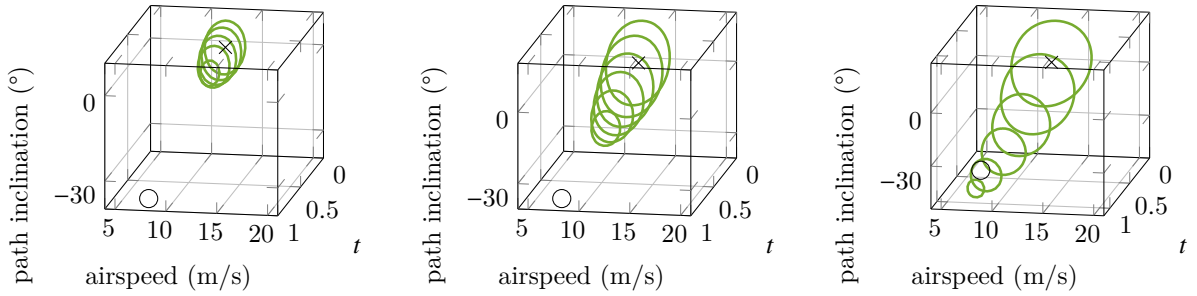

(a) 5 iterations ($\vartheta_5^\diamond = 0.2179$). **(b) 15 iterations ($\vartheta_{15}^\diamond = 0.5486$).** **(c) 25 iterations ($\vartheta_{25}^\diamond = 1.1841$).**

Fig. 9 Region of attraction estimates during iteration of the backwards-reachability control synthesis.

B. Numerical comparison

We consider recovery from the deep-stall trim condition $\mathbf{x}_1$, given in Appendix A, and simulate the closed-loop behaviour for the feedback laws discussed in this study. Fig. 10 compares recovery under control synthesized for reachability to the previous synthesized linear, polynomial, and piecewise polynomial feedback laws as well as to the LQR feedback. In addition, the closed-loop response with a single-rate damping law, $\tilde{\eta} = \tilde{k}_{\eta q}\tilde{q}$, where $\tilde{k}_{\eta q} = 1$ is a positive, proportional gain on the (scaled) pitch rate. All trajectories have been computed against the non-polynomial longitudinal equations of motion given in Eqs. (1)–(4) rather than the polynomial approximations employed for the SOS iterations.

The LQR controller, as bespoken in Section III, recovers stably and fast; the pitch-damper (in dashed) too is eventually recovering though delayed and with large oscillations. As for the control laws of Section B,

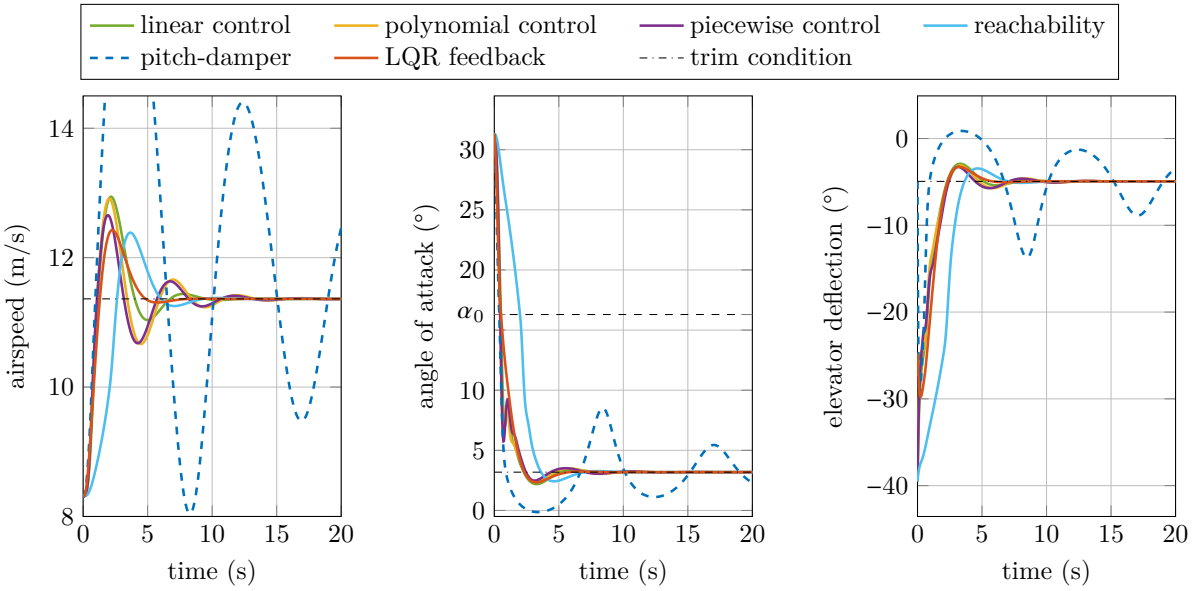

(a) Airspeed V_A. **(b) Angle of attack α.** **(c) Elevator deflection η.**

Fig. 10 Comparison of time responses starting in $\mathbf{x}_1$.

the objective of synthesis has been an enlarged region of attraction rather than closed-loop performance; consequently, the recovery is performed rather slow and with considerable overshoot (in particular for the polynomial and piecewise polynomial feedback laws). The control law synthesized for reachability of the deep-stall condition also leads to a slow but straight recovery. An extended SOS control synthesis improving performance measures in addition to enlarging the region of attraction and/or ensuring backwards reachability could be achieved by further maximizing a exponential stability gain in Eqs. (10) and (10).

In Fig. 11, we detail trajectories starting in various deep-stall flight conditions in the phugoid plane and additionally show projections of the respective region of attraction estimates. The response for the trim condition $\mathbf{x}_1$ is drawn in solid; the other responses (in dashed) have been computed for non-trim conditions given in Appendix A. In addition, for each trajectory the point it enters the region of attraction estimate is marked by a black square (due to the projection into the phugoid plane, these points might not necessarily appear inside the ellipsoid). For the feedback law synthesized by backwards reachability, further out-of-plane slices of the estimated region of attraction are projected into the phugoid plane as well. Except for one trajectory of the LQR feedback (drawn dotted), all controllers are able to recover from each deep-stall condition into the gliding trim condition. However, for the high-inclination conditions $\mathbf{x}_6$ and $\mathbf{x}_7$ this has partially led to saturations of the elevator deflection and its rate of change. Therefore, even though the saturation has not prevented recovery, these conditions could not have been included in any region of attraction estimate subject to the imposed constraints in the methodology presented in this paper. In

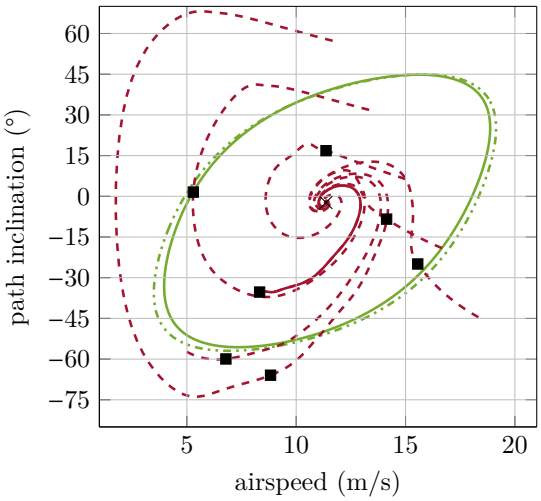

(a) Linear control law.

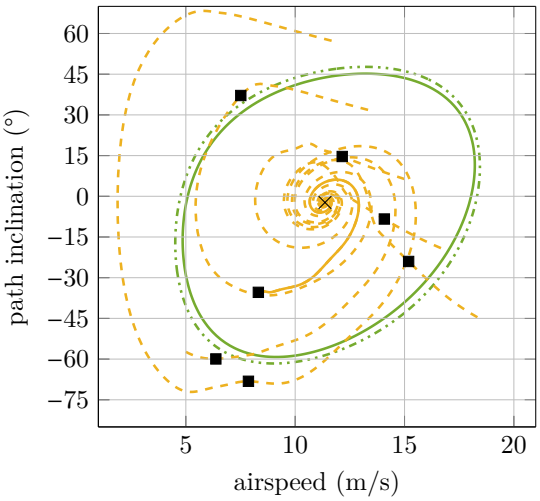

(b) Polynomial control law.

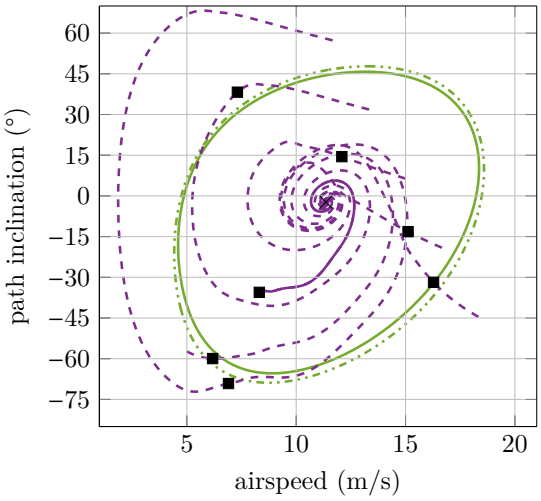

(c) Piecewise control law.

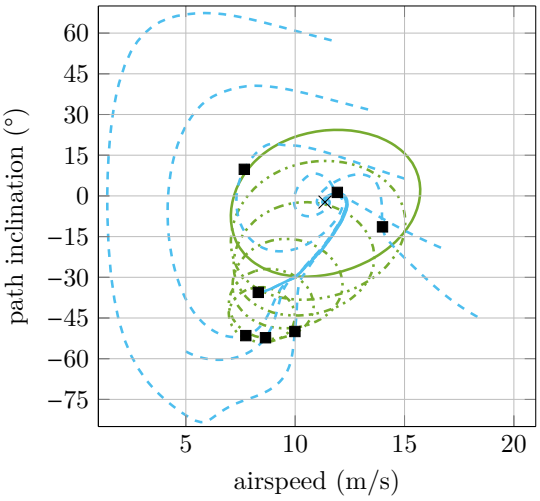

(d) Reachability-synthesis law.

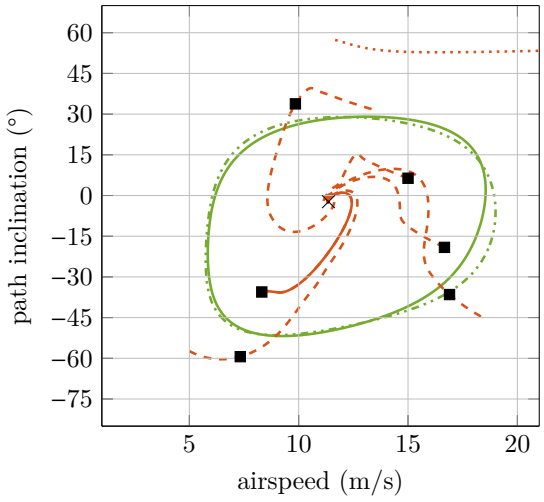

(e) LQR feedback law.

Fig. 11 Time responses and region of attraction estimates in the phugoid plane.

the other cases, the fact that stable recovery trajectories lie outside the estimates highlights the inevitable conservatism of any sum-of-squares analysis approach.

V. Conclusion

Sum-of-squares techniques provide exact certificates for stability and the region of attraction, but the application to accurate, full-envelope aircraft models such as multivariate splines is computationally demanding. Simple piecewise polynomial models, on the other hand, accommodate the aerodynamic coefficients well in both domains of low and high angles of attack, while only moderately increasing the costs of sum-of-squares analysis. In this note, we have applied sum-of-squares techniques to a fixed-wing aircraft model in order to verify stable recovery from deep-stall. As an intermediate result, we verified that a classical LQR feedback law onto the elevator deflection is sufficient for recovery without violation of input constraints. We then further extended the sum-of-squares analysis for control synthesis, using the actuator rate instead of deflection. Here, the choice of an ellipsoidal shape function for the sum-of-squares program turned out to be crucial, yet a selection was challenged by asymmetric constraints on the elevator deflection. Despite all three of the synthesized linear, polynomial, and piecewise polynomial feedback laws could not be verified to recover the aircraft from its deep-stall trim conditions, this does not imply no such control feedback exist. Concluding our study, we proposed a reformulated sum-of-squares control synthesis based on backwards-reachability of a target trim condition without the necessity of an ellipsoidal shape. Indeed, a simple linear control feedback could thus be verified to recover the aircraft. We therefore held sum-of-squares programming combined with piecewise polynomial models a powerful tool for aircraft analysis and verification.

Appendix

We provide details of the polynomial aircraft model, the sum-of-squares computations, and the computation of quasi-ellipsoidal surfaces using SOS programming.

A. Details on the polynomial aircraft model

The low-angle of attack trim condition $\mathbf{x}^*$ for gliding descent in Section III is given by

$$V_{\mathrm{A}}^* = 11.3631\,\mathrm{m/s}, \quad \gamma_{\mathrm{A}}^* = -2.2834°, \quad q^* = 0\,°/\mathrm{s}, \quad \alpha^* = 3.2240°, \quad \eta^* = -5°,$$

and the deep-stall target trim condition $\mathbf{x}_1$ in Section IV, by

$$V_{\mathrm{A}1} = 8.3131\,\mathrm{m/s}, \quad \gamma_{\mathrm{A}1} = -35.5372°, \quad q_1 = 0\,°/\mathrm{s}, \quad \alpha_1 = 31.6781°, \quad \eta_1 = -40°.$$

The additional deep-stall conditions are given by

$$
\begin{aligned}
&V_{\mathrm{A}\,2} = 5.0000\,\mathrm{m/s}, \quad \gamma_{\mathrm{A}\,2} = -57.2958°, \quad q_2 = 0\,°/\mathrm{s}, \quad \alpha_2 = 29.8081°, \quad \eta_2 = -38°;\\
&V_{\mathrm{A}\,3} = 18.3333\,\mathrm{m/s}, \quad \gamma_{\mathrm{A}\,3} = -44.5634°, \quad q_3 = 0\,°/\mathrm{s}, \quad \alpha_3 = 32.5836°, \quad \eta_3 = -41°;\\
&V_{\mathrm{A}\,4} = 16.6667\,\mathrm{m/s}, \quad \gamma_{\mathrm{A}\,4} = -19.0986°, \quad q_4 = 0\,°/\mathrm{s}, \quad \alpha_4 = 35.1836°, \quad \eta_4 = -44°;\\
&V_{\mathrm{A}\,5} = 15\,\mathrm{m/s}, \quad \gamma_{\mathrm{A}\,5} = 6.3662°, \quad q_5 = 0\,°/\mathrm{s}, \quad \alpha_5 = 37.6092°, \quad \eta_5 = -47°;\\
&V_{\mathrm{A}\,6} = 13.3333\,\mathrm{m/s}, \quad \gamma_{\mathrm{A}\,6} = 31.8310°, \quad q_6 = 0\,°/\mathrm{s}, \quad \alpha_6 = 39.8574°, \quad \eta_6 = -50°;\\
&V_{\mathrm{A}\,7} = 11.6667\,\mathrm{m/s}, \quad \gamma_{\mathrm{A}\,7} = 57.2958°, \quad q_7 = 0\,°/\mathrm{s}, \quad \alpha_7 = 41.9214°, \quad \eta_7 = -53°.
\end{aligned}
$$

The piecewise model of Eqs. (1)–(4) is not immediately suitable for sum-of-squares analysis. The non-polynomial sine and cosine functions in γ_{A} and α are therefore approximated by 5th-order and 4th-order Taylor series expansions,

$$
\sin a \approx a - \frac{a^3}{3!} + \frac{a^5}{5!}; \qquad \cos a \approx 1 - \frac{a^2}{2} + \frac{a^4}{4!};
$$

respectively, which have an error of less than ± 0.02 for $\gamma_{\mathrm{A}}, \alpha \in]-90°; +90°[$. The inversion of V_{A} in Eq. (2) is likewise replaced by

$$
a^{-1} \approx a_0^{-1} - a_0^{-2}(a - a_0) + 2a_0^{-3}(a - a_0)^2 - 3!a_0^{-4}(a - a_0)^3,
$$

where a_0 denotes the airspeed in trim. This approximation is less accurate, however, the resulting piecewise polynomial seems to be conservative, that is, it diverges rather than the nonlinear model.

The uncontrolled piecewise polynomial model with the polynomial approximations above is of order 13. In order to ease the complexity of the SOS computation, we have removed any polynomial term of 6th order or higher or with coefficients absolutely smaller than 10^{-6}.

B. Details on the SOS computations

We provide details about the sum-of-squares computations, polynomial degrees of the problems, and the decision variables involved, respectively. Table 2 details the results of the different SOS computations in Sections III and IV in terms of the pseudo-radii $\rho^\diamond$ of the ellipsoidal shapes $\mathcal{E}_\rho$ and degree of reachability $\vartheta^\diamond$, respectively, as well as the level sets for invariance and invariance under control, $\lambda^\diamond$ and λ^*. The number of involved states is further given as well as the number of repetitions of the (extended) $\mathcal{V}$-s-iteration and

Table 2 Results of SOS computations.

(a) Stability analysis (Intel Core i7, 3 GHz, 16 GB).

Section	n	$\rho^\diamond$	$\lambda^\diamond$	λ^*	Iterations	Time	
Sec. III.A	4	54.5349	1.0513	1.0513	135	3.8295	h

(b) Control synthesis (Intel Core E5, 3 GHz, 16 GB).

Section		n	$\rho^\diamond$	$\lambda^\diamond$	λ^*	Iterations	Time	
	1		39.0320	38.7939	38.5986	109	36.4526	h
Sec. III.B	*2*	5	251.9531	35.3516	38.6230	70	18.4957	h
	3		295.6543	17.7979	19.1650	73	21.1351	h

(c) Deep-stall recovery (Intel Core i7, 3 GHz, 16 GB).

Section	n	$\vartheta^\diamond$	$\lambda^\diamond$	λ^*	Iterations	Time	
Sec. IV	5	1.3027	57.5684	99.9023	29	4.5832	h

Table 3 Polynomial degrees of SOS problems.

Section		$\mathbf{f}$	$\mathbf{K}$	$\mathbf{f_K}$	$\mathcal{V}_{1,2}$	$l_{a,b}$	P	p_η
Sec. III.A		5	1	5	4	2	2	2
	1		1					
Sec. III.B	*2*	5	3	5	4	2	2	2
	3		3					
Sec. IV		5	1	5	4	2	–	2

Table 4 Polynomial degrees of SOS multipliers.

Section		$s_{i,\lambda}$	$s_{i,\varphi}$	$s_{\varphi,i}$	$s_{-\varphi,i}$	$s_{i,P}$	$s_{\eta,\lambda'}$
Sec. III.A		2	2	2	2	1	1
	1						
Sec. III.B	*2*	2	2	2	2	1	1
	3						
Sec. IV		2	2	2	2	–	1

the total computation time. Table 3 reports the polynomial degrees of control system, Lyapunov functions, positive terms $l_{a,b}$, ellipsoidal shape functions, and constraints. In addition, Table 4 gives the chosen degrees for the sum-of-squares multipliers in Eqs. (9)–(16).

C. Computing quasi-ellipsoids with SOS

If the cartesian dimensions, that is, number of variables, or the desired polynomial order of a quasi-ellipsoid grow, so does the number of independent coefficients. Thus, selecting an ellipsoidal manually becomes increasingly difficult. In order to obtain the asymmetric shapes in Sections III.B-2 and III.B-3, we have solved the following sum-of-squares problem given a sequence of points $\mathbf{x}_1^\circ, \ldots, \mathbf{x}_k^\circ \in \mathbb{R}^n$, $k \in \mathbb{N}$ finite: find $P \in \mathbb{R}[\mathbf{x}]$ such that P is positive-definite and

$$P(\mathbf{x}_i^\circ) = 1 \tag{21}$$

for all $1 \leq i \leq k$. As the degree of P is predefined, the equality constraints in (21) are linear in the decision variables (the coefficients of P).

The 4th-order, asymmetric shape functions $\tilde{P}_{\text{poly}}$ and $\tilde{P}_{\text{pw}}$ are thus derived to (coefficients are subject to rounding; coefficients $< 10^{-3}$ are omitted):

$$\begin{aligned}
\tilde{P}_{\text{poly}} = {} & 5.37\times10^{2}\tilde{V}_{\text{A}}^{4} - 2.90\times10^{1}\tilde{V}_{\text{A}}^{3}\tilde{\gamma}_{\text{A}} - 1.48\times10^{-3}\tilde{V}_{\text{A}}^{3}\tilde{q} + 5.42\times10^{2}\tilde{V}_{\text{A}}^{2}\tilde{\alpha}^{2} + 2.41\times10^{2}\tilde{V}_{\text{A}}^{2}\tilde{\eta}^{2} \\
& + 4.11\times10^{2}\tilde{V}_{\text{A}}^{2}\tilde{\gamma}_{\text{A}}^{2} + 5.42\times10^{2}\tilde{V}_{\text{A}}^{2}\tilde{q}^{2} - 2.51\times10^{-3}\tilde{V}_{\text{A}}\tilde{\alpha}^{2}\tilde{\eta} - 2.84\times10^{-3}\tilde{V}_{\text{A}}\tilde{\alpha}\tilde{q}^{2} - 2.61\times10^{2}\tilde{V}_{\text{A}}\tilde{\gamma}_{\text{A}}^{3} \\
& + 1.09\times10^{-3}\tilde{V}_{\text{A}}\tilde{\gamma}_{\text{A}}\tilde{q}^{2} + 5.00\times10^{2}\tilde{\alpha}^{4} - 1.33\times10^{-3}\tilde{\alpha}^{3}\tilde{\gamma}_{\text{A}} - 2.65\times10^{-3}\tilde{\alpha}^{3}\tilde{q} + 2.41\times10^{2}\tilde{\alpha}^{2}\tilde{\eta}^{2} \\
& - 1.89\times10^{-3}\tilde{\alpha}^{2}\tilde{\eta}\tilde{\gamma}_{\text{A}} + 5.42\times10^{2}\tilde{\alpha}^{2}\tilde{\gamma}_{\text{A}}^{2} - 1.93\times10^{-3}\tilde{\alpha}^{2}\tilde{\gamma}_{\text{A}}\tilde{q} + 5.42\times10^{2}\tilde{\alpha}^{2}\tilde{q}^{2} + 2.04\times10^{1}\tilde{\eta}^{4} \\
& + 2.41\times10^{2}\tilde{\eta}^{2}\tilde{\gamma}_{\text{A}}^{2} + 2.41\times10^{2}\tilde{\eta}^{2}\tilde{q}^{2} + 1.35\times10^{-3}\tilde{\eta}\tilde{\gamma}_{\text{A}}\tilde{q}^{2} + 1.38\times10^{-3}\tilde{\eta}\tilde{q}^{3} + 1.50\times10^{2}\tilde{\gamma}_{\text{A}}^{4} \\
& + 5.42\times10^{2}\tilde{\gamma}_{\text{A}}^{2}\tilde{q}^{2} - 2.46\times10^{-3}\tilde{\gamma}_{\text{A}}\tilde{q}^{3} + 5.00\times10^{2}\tilde{q}^{4} - 4.93\times10^{-3}\tilde{\alpha}^{2}\tilde{\eta} - 2.34\times10^{-3}\tilde{\alpha}\tilde{q}^{2} \\
& + 1.17\times10^{2}\tilde{\eta}^{3} + 5.04\times10^{2}\tilde{V}_{\text{A}}^{2} - 2.24\times10^{2}\tilde{V}_{\text{A}}\tilde{\gamma}_{\text{A}} + 5.00\times10^{2}\tilde{\alpha}^{2} + 6.63\times10^{-3}\tilde{\alpha}\tilde{q} \\
& + 2.23\times10^{2}\tilde{\eta}^{2} + 2.06\times10^{2}\tilde{\gamma}_{\text{A}}^{2} + 5.00\times10^{2}\tilde{q}^{2};
\end{aligned}$$

$$\begin{aligned}
\tilde{P}_{\text{pw}} = {} & 5.41\times10^{2}\tilde{V}_{\text{A}}^{4} - 2.93\times10^{1}\tilde{V}_{\text{A}}^{3}\tilde{\gamma}_{\text{A}} - 1.21\times10^{-3}\tilde{V}_{\text{A}}^{3}\tilde{q} + 5.46\times10^{2}\tilde{V}_{\text{A}}^{2}\tilde{\alpha}^{2} + 2.07\times10^{-3}\tilde{V}_{\text{A}}^{2}\tilde{\alpha}\tilde{q} \\
& + 2.43\times10^{2}\tilde{V}_{\text{A}}^{2}\tilde{\eta}^{2} - 1.44\times10^{-3}\tilde{V}_{\text{A}}^{2}\tilde{\eta}\tilde{q} + 4.15\times10^{2}\tilde{V}_{\text{A}}^{2}\tilde{\gamma}_{\text{A}}^{2} + 1.69\times10^{-3}\tilde{V}_{\text{A}}^{2}\tilde{\gamma}_{\text{A}}\tilde{q} + 5.46\times10^{2}\tilde{V}_{\text{A}}^{2}\tilde{q}^{2} \\
& - 1.12\times10^{-3}\tilde{V}_{\text{A}}\tilde{\alpha}^{2}\tilde{q} - 2.02\times10^{-3}\tilde{V}_{\text{A}}\tilde{\alpha}\tilde{\eta}\tilde{q} + 1.32\times10^{-3}\tilde{V}_{\text{A}}\tilde{\alpha}\tilde{\gamma}_{\text{A}}^{2} - 2.63\times10^{2}\tilde{V}_{\text{A}}\tilde{\gamma}_{\text{A}}^{3} - 2.86\times10^{-3}\tilde{V}_{\text{A}}\tilde{\gamma}_{\text{A}}\tilde{q}^{2} \\
& - 1.33\times10^{-3}\tilde{V}_{\text{A}}\tilde{q}^{3} + 5.24\times10^{2}\tilde{\alpha}^{4} + 1.51\times10^{1}\tilde{\alpha}^{3}\tilde{\eta} + 1.10\times10^{-3}\tilde{\alpha}^{3}\tilde{\gamma}_{\text{A}} + 1.11\times10^{-3}\tilde{\alpha}^{3}\tilde{q}
\end{aligned}$$

$$
\begin{aligned}
&+ 1.91 \times 10^{2} \tilde{\alpha}^{2} \tilde{\eta}^{2} + 1.05 \times 10^{-3} \tilde{\alpha}^{2} \tilde{\eta} \tilde{\gamma}_{\mathrm{A}} + 5.46 \times 10^{2} \tilde{\alpha}^{2} \tilde{\gamma}_{\mathrm{A}}^{2} + 4.00 \times 10^{-3} \tilde{\alpha}^{2} \tilde{\gamma}_{\mathrm{A}} \tilde{q} + 5.46 \times 10^{2} \tilde{\alpha}^{2} \tilde{q}^{2} \\
&+ 7.84 \times 10^{1} \tilde{\alpha} \tilde{\eta}^{3} - 1.58 \times 10^{-3} \tilde{\alpha} \tilde{\eta} \tilde{q}^{2} - 1.32 \times 10^{-3} \tilde{\alpha} \tilde{\gamma}_{\mathrm{A}}^{2} \tilde{q} + 1.05 \times 10^{-3} \tilde{\alpha} \tilde{\gamma}_{\mathrm{A}} \tilde{q}^{2} + 2.89 \times 10^{1} \tilde{\eta}^{4} \\
&+ 2.43 \times 10^{2} \tilde{\eta}^{2} \tilde{\gamma}_{\mathrm{A}}^{2} + 2.43 \times 10^{2} \tilde{\eta}^{2} \tilde{q}^{2} - 2.17 \times 10^{-3} \tilde{\eta} \tilde{q}^{3} + 1.51 \times 10^{2} \tilde{\gamma}_{\mathrm{A}}^{4} + 5.46 \times 10^{2} \tilde{\gamma}_{\mathrm{A}}^{2} \tilde{q}^{2} \\
&+ 3.83 \times 10^{-3} \tilde{\gamma}_{\mathrm{A}} \tilde{q}^{3} + 5.00 \times 10^{2} \tilde{q}^{4} + 1.69 \times 10^{-3} \tilde{V}_{\mathrm{A}} \tilde{\alpha} \tilde{\eta} - 1.86 \times 10^{-3} \tilde{V}_{\mathrm{A}} \tilde{\gamma}_{\mathrm{A}} \tilde{q} - 1.15 \times 10^{-3} \tilde{V}_{\mathrm{A}} \tilde{q}^{2} \\
&- 4.61 \times 10^{1} \tilde{\alpha}^{3} + 3.65 \times 10^{1} \tilde{\alpha}^{2} \tilde{\eta} + 1.58 \times 10^{-3} \tilde{\alpha}^{2} \tilde{\gamma}_{\mathrm{A}} + 2.24 \times 10^{-3} \tilde{\alpha}^{2} \tilde{q} - 8.84 \times 10^{1} \tilde{\alpha} \tilde{\eta}^{2} \\
&+ 1.57 \times 10^{-3} \tilde{\alpha} \tilde{q}^{2} + 1.06 \times 10^{2} \tilde{\eta}^{3} + 1.07 \times 10^{-3} \tilde{\gamma}_{\mathrm{A}} \tilde{q}^{2} + 5.08 \times 10^{2} \tilde{V}_{\mathrm{A}}^{2} - 2.27 \times 10^{2} \tilde{V}_{\mathrm{A}} \tilde{\gamma}_{\mathrm{A}} \\
&+ 1.19 \times 10^{-3} \tilde{V}_{\mathrm{A}} \tilde{q} + 5.22 \times 10^{2} \tilde{\alpha}^{2} + 2.25 \times 10^{1} \tilde{\alpha} \tilde{\eta} + 2.21 \times 10^{2} \tilde{\eta}^{2} + 2.05 \times 10^{2} \tilde{\gamma}_{\mathrm{A}}^{2} \\
&+ 1.06 \times 10^{-3} \tilde{\gamma}_{\mathrm{A}} \tilde{q} + 5.00 \times 10^{2} \tilde{q}^{2};
\end{aligned}
$$

shape functions are defined in scaled variables.

Funding Sources

This work was funded by ONERA – The French Aerospace Lab, République Française.

References

[1] Philippe, C., "Verification, Validation, and Certification of Aerospace Control Systems," *The Impact of Control Technology*, edited by T. Samad and A. M. Annaswamy, IEEE Control Systems Society, New York, US-NY, 2011, Chap. 4, pp. 205–206. URL `http://www.ieeecss.org/general/impact-control-technology`.

[2] Goman, M. G., Zagainov, G. I., and Khramtsovsky, A. V., "Application of bifurcation methods to nonlinear flight dynamics problems," *Progress in Aerospace Sciences*, Vol. 33, No. 9–10, 1997, pp. 539–586. doi:10.1016/S0376-0421(97)00001-8.

[3] Gill, S. J., Lowenberg, M. H., Neild, S. A., Krauskopf, B., Puyou, G., and Coetzee, E., "Upset Dynamics of an Airliner Model: A Nonlinear Bifurcation Analysis," *Journal of Aircraft*, Vol. 50, No. 6, 2013, pp. 1832–1842. doi:10.2514/1.C032221.

[4] McDonough, K., Kolmanovsky, I., and Atkins, E., "Recoverable sets of initial conditions and their use for aircraft flight planning after a loss of control event," *AIAA Guidance, Navigation, and Control Conference*, National Harbor, US-MD, 2014. doi:10.2514/6.2014-0786.

[5] McDonough, K., and Kolmanovsky, I., "Fast Computable Recoverable Sets and Their Use for Aircraft Loss-of-Control Handling," *Journal of Guidance, Control, and Dynamics*, Vol. 40, No. 4, 2017, pp. 934–947. doi:10.2514/G001747.

[6] Lygeros, J., "On reachability and minimum cost optimal control," *Automatica*, Vol. 40, No. 6, 2004, pp. 917–927. doi:10.1016/j.automatica.2004.01.012.

[7] Nabi, H. N., Lombaerts, T. J. J., Zhang, Y., van Kampen, E., Chu, Q. P., and de Visser, C. C., "Effects of Structural Failure on the Safe Flight Envelope of Aircraft," *Journal of Guidance, Control, and Dynamics*, Vol. 41, No. 6, 2018, pp. 1257–1275. doi:10.2514/1.G003184.

[8] Genesio, R., Tartaglia, M., and Vicino, A., "On the Estimation of Asymptotic Stability Regions: State of the Art and New Proposals," *IEEE Transactions on Automatic Control*, Vol. 30, No. 8, 1985, pp. 747–755. doi:10.1109/TAC.1985.1104057.

[9] Tan, W., "Nonlinear Control Analysis and Synthesis using Sum-of-Squares Programming," Phd thesis, University of California, Berkeley, Berkeley, US-CA, 2006.

[10] Seiler, P., and Balas, G. J., "Quasiconvex sum-of-squares programming," *49th IEEE Conference on Decision and Control*, Atlanta, US-GA, 2010, pp. 3337–3342. doi:10.1109/CDC.2010.5717672.

[11] Parillo, P. A., "Semidefinite programming relaxations for semialgebraic problems," *Mathematical Programming, Series B*, Vol. 96, No. 2, 2003, pp. 293–320. doi:10.1007/s10107-003-0387-5.

[12] Papachristodoulou, A., and Prajna, S., "Robust Stability Analysis of Nonlinear Hybrid Systems," *IEEE Transactions on Automatic Control*, Vol. 54, No. 5, 2009, pp. 1035–1041. doi:10.1109/TAC.2009.2017155.

[13] Topcu, U., Packard, A., and Seiler, P., "Local stability analysis using simulations and sum-of-squares programming," *Automatica*, Vol. 44, No. 10, 2008, pp. 2669–2675. doi:10.1016/j.automatica.2008.03.010.

[14] Jarvis-Wloszek, Z., Feeley, R., Tan, W., Sun, K., and Packard, A., "Some Controls Applications of Sum of Squares Programming," *Proceedings of the IEEE Conference on Decision and Control*, Vol. 5, Maui, US-HI, 2003, pp. 4676–4681. doi:10.1109/CDC.2003.1272309.

[15] Majumdar, A., Ahmadi, A. A., and Tedrake, R., "Control Design Along Trajectories via Sum of Squares Optimization," *2013 IEEE International Conference on Robotics and Automation*, Karlsruhe, DE, 2013, pp. 4039–4046. doi:10.1109/ICRA.2013.6631149.

[16] Anderson, J., and Papachristodoulou, A., "Robust nonlinear stability and performance analysis of an F/A-18 aircraft model using sum of squares programming," *International Journal of Robust and Nonlinear Control*, Vol. 23, 2012, pp. 1099–1114. doi:10.1002/rnc.2928.

[17] Chakraborty, A., Seiler, P., and Balas, G. J., "Nonlinear region of attraction analysis for flight control verification and validation," *Control Engineering Practice*, Vol. 19, No. 4, 2011, pp. 335–345. doi:10.1016/j.conengprac.2010.12.001.

[18] Chakraborty, A., Seiler, P., and Balas, G. J., "Susceptibility of F/A-18 Flight Controllers to the Falling-leaf Mode: Nonlinear Analysis," *Journal of Guidance, Control, and Dynamics*, Vol. 34, No. 2, 2011, pp. 73–85. doi:10.2514/1.50675.

[19] Tol, H. J., de Visser, C. C., Sun, L. G., van Kampen, E., and Chu, Q. P., "Multivariate Spline-Based Adaptive Control of High-Performance Aircraft with Aerodynamic Uncertainties," *Journal of Guidance, Control, and Dynamics*, Vol. 39, No. 4, 2016, pp. 781–800. doi:10.2514/1.G001079.

[20] Cunis, T., Burlion, L., and Condomines, J.-P., "Piecewise Polynomial Modeling for Control and Analysis of Aircraft Dynamics beyond Stall," *Journal of Guidance, Control, and Dynamics*, Vol. 42, No. 4, 2019, pp. 949–957. doi:10.2514/1.G003618.

[21] Cunis, T., Condomines, J.-P., Burlion, L., and la Cour-Harbo, A., "Dynamic Stability Analysis of Aircraft Flight in Deep Stall," *Journal of Aircraft*, 2019. doi:10.2514/1.C035455.

[22] ISO 1151-1, *Flight dynamics – Concepts, quantities and symbols – Part 1: Aircraft motion relative to the air*, 4$^{\text{th}}$ ed., International Organization for Standarization, Genève, CH, 1988.

[23] Chang, B.-C., Kwatny, H. G., Ballouz, E. R., and Hartmann, D. C., "Aircraft Trim Recovery from Highly Nonlinear Upset Conditions," *AIAA Guidance, Navigation, and Control Conference*, San Diego, US-CA, 2016. doi:10.2514/6.2016-0880.

[24] Kwatny, H. G., Dongmo, J.-E. T., Chang, B.-C., Bajpai, G., Yasar, M., and Belcastro, C., "Nonlinear Analysis of Aircraft Loss of Control," *Journal of Guidance, Control, and Dynamics*, Vol. 36, No. 1, 2013, pp. 149–162. doi:10.2514/1.56948.

[25] Cunis, T., and la Cour-Harbo, A., "Piecewise Polynomial Model of the Aerodynamic Coefficients of the *Cumulus One* Unmanned Aircraft," Tech. Rep. `hal-02280789`, Sky-Watch A/S, Støvring, DK, 2019. URL `https://archives-ouvertes.fr/hal-02280789`.

[26] Chesi, G., "On the Complexity of SOS Programming and Applications in Control Systems," *Asian Journal of Control*, Vol. 20, No. 5, 2018, pp. 2005–2013. doi:10.1002/asjc.1684.

[27] Yin, H., Packard, A., Arcak, M., and Seiler, P., "Finite horizon backward reachability analysis and control synthesis for uncertain nonlinear systems," *Proceedings of the American Control Conference*, Philadelphia, US-PA, 2019, pp. 5020–5026. doi:10.23919/ACC.2019.8814444.

Chapter 7

Economic Deep-stall Recovery

This chapter corresponds to:

> Torbjørn Cunis, Dominic Liao-McPherson, et al. (2019). "Economic Model-Predictive Control Strategies for Aircraft Deep-stall Recovery with Stability Guarantees". In: *58th IEEE Conference on Decision and Control* (to be presented). Nice, FR

in the authors' finally submitted version, edited for layouting.

Synopsis

Versatile control feedback amid nonlinear dynamics and strict input constraints as well as a mature stability theory makes the use of model-predictive control for upset recovery advantageous. Several publications considered upset trajectories that minimised the loss of altitude (LOA) during the recovery. However, these studies did not take into account the implications of the LOA-minimal formulation for closed-loop stability. Indeed, if no thrust is applied, the aircraft can only acquire a descending trim condition; nevertheless, this does not rule out transient flight conditions with positive ascend. Therefore, the LOA objective function is not positive-definite as necessary in Theorem II.4 for closed-loop stability of tracking MPC. In this chapter, we formulate the problem of LOA-minimising receding-horizon optimal control for longitudinal recovery from deep-stall as the economic MPC problem it actually is. Proving stability of EMPC, as we have seen, requires dissipativity (or a similar notion, cf. Theorem II.7) and is a nontrivial task. Employing sum-of-squares programming techniques for the piecewise polynomial model, in addition to estimating a region of attraction of a level-flight trim condition, allows us to ensure dissipativity of the aircraft dynamics. Thus, we are able to ensure stable recovery under the objective of minimal altitude-loss.

Statement of Contribution Torbjørn Cunis implemented the MPC synthesis and simulation, analysed the region of attraction, and developed the sum-of-squares regularisation procedure. Dominic Liao-McPherson contributed to the wording of the manuscript and assisted with practical and theoretical aspects of model-predictive control. Jean-Philippe Condomines, Laurent Burlion, and Ilya Kolmanovsky provided feedback and review.

Nomenclature

α	Angle of attack (rad);
α_0	Low-angle of attack boundary ($\alpha_0 = 16.2949°$);
γ	Flight-path angle relative to air (rad);
η	Elevator deflection (rad), negative if leading to positive pitch moment;
$\dot{\eta}$	Rate of elevator deflection (rad/s);
$\kappa(\cdot)$	Control feedback law ($\kappa\colon \mathbb{R}^n \to \mathbb{R}^m$);
$f^N(\cdot, \mathbf{u})$	Iterative system evaluation ($f^N = f(\cdot, u_N) \circ \cdots \circ f(\cdot, u_1)$) for $\mathbf{u} \in \mathcal{U}^N$;
F	Thrust force (N), positive along x_f-axis;
$\ell(\cdot)$	MPC stage cost function ($\ell\, \mathbb{R}^n \times \mathbb{R}^m \to \mathbb{R}$);
m	Number of inputs;
n	Number of states;
N	Horizon length ($N \in \mathbb{N}$);
q	Pitch rate (rad/s);
Q	Symmetric weight matrix ($Q \succeq 0$);
Q_x, Q_u	Positive weight matrices for states and inputs ($Q_u \in \mathbb{R}^{m\times m}, Q_x \in \mathbb{R}^{n\times n}$);
V	Aircraft speed relative to air (m/s), positive along x_a-axis;
x_f, u_f	States and inputs at *target* trim condition;
$x_\mathrm{lvl}, u_\mathrm{lvl}$	States and inputs at *level-flight* trim condition;
z_g	Vertical position in earth-fixed reference system (m); negative altitude;
$(\cdot)^{post}$	Domain of high angle of attack;
$(\cdot)^{pre}$	Domain of low angle of attack;
$\mathcal{U}$	Viable control inputs ($\mathcal{U} \subset \mathbb{R}^m$);
$\mathcal{X}$	Viable state-space ($\mathcal{X} \subset \mathbb{R}^n$);
$\mathcal{X}_N$	Set of feasible initial conditions ($\mathcal{X}_N \subseteq \mathcal{X}$) with horizon N;
$\Sigma\,[x]$	Polynomial sum-of-squares cone ($\Sigma\,[x] \subset \mathbb{R}\,[x]$);
$\mathbb{R}\,[x]$	Set of polynomials in $x \in \mathbb{R}^n$ with real-valued coefficients;

Economic Model-Predictive Control Strategies for Aircraft Deep-stall Recovery with Stability Guarantees*

Torbjørn Cunis,[1] Dominic Liao-McPherson,[2] Jean-Philippe Condomines,[3]
Laurent Burlion,[4] and Ilya Kolmanovsky[2]

Abstract

Aircraft upset recovery requires aggressive control actions to handle highly nonlinear aircraft dynamics and critical state and input constraints. Model predictive control is a promising approach for returning the aircraft to the nominal flight envelope, even in the presence of altered dynamics or actuator limits; however, proving stability of such strategies requires careful algebraic or semi-algebraic analysis of both the system and the proposed control scheme, which can be challenging for realistic control systems. This paper develops economic model predictive strategies for recovery of a fixed-wing aircraft from deep-stall. We provide rigorous stability proofs using sum-of-squares programming and compare several economic, nonlinear, and linear model predictive controllers.

I. Introduction

Aircraft upset incidents remain a severe cause of fatalities in civil aviation [1] and this has motivated research into upset and loss of control recovery [2–6]. Upset recovery has been approached with various control techniques including adaptive control [7], machine learning [8], and model predictive control (MPC) [9, 10]. MPC, in particular, is promising since it can handle nonlinearities, actuator saturation, and state constraints. It also tends to have a provably large closed-loop region of attraction.

In this paper, we propose a loss of altitude (LOA) minimizing economic model predictive control (EMPC) strategy for deep-stall recovery which we compare to linear and nonlinear tracking type MPC controllers. LOA is an important performance metric for upset recovery maneuvers and it can be exploited to enlarge the operational envelope during and after the maneuver, particularly at low altitudes [11, 12]. The EMPC framework, see, e.g., [13] for an overview, allows for direct minimization of the LOA. We consider a 1.6 kg fixed-wing unmanned aircraft capable of stable deep-stall descent [14, 15], which allows us to isolate the longitudinal aerodynamics.

*Partly supported by ONERA, University of Michigan Advanced Research Computing, and NSF Award No. CMMI 1562209.

[1]TC was with the Department of Information Processing and Systems, ONERA – The French Aerospace Lab, 31055 Toulouse, France, and the ENAC Drones Research Group; TC is now with the University of Michigan, tcunis@umich.edu.

[2]DL and IK are with the Department of Aerospace Engineering, University of Michigan, Ann Arbor, Michigan 48109, USA, {dliaomcp,ilya}@umich.edu.

[3]JC is with the Drones Research Group, ENAC, Université de Toulouse, jean-philippe.condomines@enac.fr.

[4]LB is with Rutgers, The State University of New Jersey, New Brunswick, New Jersey, USA, laurent.burlion@rutgers.edu.

MPC has been applied to a variety of aerospace systems [16]. In [9], MPC is employed to generate guidance trajectories for recovery of a piloted aircraft from a high-pitch upset. EMPC has been extensively studied in the context of process control [13]; however, comparatively few aerospace applications have been reported in the literature [16]. LOA minimizing EMPC was considered in [10] for automatic recovery from a high-bank condition. However, closed-loop stability of the proposed MPC recovery scheme was not proven in either [9] or [10].

Closed-loop stability of an EMPC controller can be guaranteed if the dynamics and stage cost jointly satisfy an appropriate dissipativity condition both with [17] and without [18] terminal constraints. When dissipativity does not hold (or cannot be proven), regularization terms can be added to ensure closed-loop stability [19]. For nonlinear systems proving these conditions is nontrivial. However, advances in semi-definite relaxations [20] have led to a surge of sum-of-squares (SOS) programming techniques [21, 22] which have been used to compute stability certificates for continuous [23, 24] and discrete [25, 26] systems as well as proving dissipativity properties [27, 28]. Further, an SOS-based stability analysis for general MPC strategies is presented in [29]. However, computational issues and the restriction of SOS programming to polynomial functions conflict with the need for accurate aerodynamic models.

Our contributions are fourfold: (i) We design an LOA minimizing EMPC controller using a piecewise polynomial model of the aircraft dynamics that is suitable for both accurate control and application of SOS techniques; (ii) we illustrate how SOS techniques can be applied to systems with piecewise dynamics in order to rigorously prove the stability of our EMPC controller; (iii) we propose an adaptive regularization scheme using SOS to determine minimal regularization gains that ensure dissipativity; (iv) we provide a comparison between linear, nonlinear, and economic MPC for LOA-minimal recovery. In this work, we restrict ourselves to terminal state constraints.

The layout of the paper is as follows: In II, we discuss the upset recovery problem. In III, we recall the theories of EMPC and SOS programming; we then provide the optimal control formulation in IV. In V, we show using SOS programming that the synthesized closed-loop system satisfies the conditions for asymptotic stability. Finally, VI compares different MPC strategies.

Notation: Real-valued variables and functions are designated in italic, finite sequences in bold, polynomials in Fraktur. $\mathbf{x}[i]$ is the i-th element of a sequence $\mathbf{x}$. $\bar{x}$ is the difference between x and a reference x^*. $\mathbb{R}[x]$ is the set of polynomials with real coefficients. For a function p (polynomial $\mathfrak{p}$) and $a \in \mathbb{R}$, denote $\Omega_{p\leq a} = \{x \,|\, p(x) \leq a\}$ and $\mathcal{O}_{p=a} = \{x \,|\, p(x) = a\}$. Superscripts ^{pre} and ^{post} denote low and high-angle of attack dynamics.

II. Problem Formulation

In the context of aviation, the term *upset* can be used to describe a variety of abnormal situations. In a technical sense, an upset can be understood as an undesired yet often attractive mode of the nonlinear dynamics that shows significantly altered steady-state responses and usually immediately precedes wing stall

and departure of the aircraft (e.g., deep-stall flight, gyroscopic spins, or spirals). Input saturation, inversion and tight state constraints make designing recovery approaches challenging.

In this paper, we develop an MPC strategy to minimize loss-of-altitude using only the elevator η, i.e., thrust $F = 0$, in accordance with governmental procedures for manual recovery [30]. LOA is a crucial metric for both collision avoidance and operating envelope recovery post stabilization [11, 12]. We will adopt the convention that the aircraft has recovered when it returns to a stable trim condition within the region of attraction of a nominal flight controller which subsequently reinstates level flight.

We consider only the longitudinal aircraft dynamics, which are given by

$$m\dot{V} = F\cos\alpha - (\bar{q}C_{\mathrm{D}}(\alpha,\eta) + mg\sin\gamma)\,, \tag{1a}$$

$$mV\dot{\gamma} = F\sin\alpha + (\bar{q}C_{\mathrm{L}}(\alpha,\eta) - mg\cos\gamma)\,, \tag{1b}$$

$$\dot{\Theta} = q, \tag{1c}$$

$$I_y\dot{q} = (c_{\mathrm{A}}\bar{q}C_{\mathrm{m}}(\alpha,\eta) - C_{\mathrm{M}q}q)\,, \tag{1d}$$

with airspeed V, inclination γ, pitch rate q, angle of attack α, pitch angle $\Theta = \gamma + \alpha$, and elevator deflection η, where $\bar{q} = \frac{1}{2}\varrho SV^2$ and $C_{\mathrm{M}q} > 0$ is a linear damping parameter. The aircraft's descent rate is then

$$\dot{z}_{\mathrm{g}} = -V\sin\gamma. \tag{2a}$$

The aerodynamic coefficients $C_{\mathrm{L}}, C_{\mathrm{D}}, C_{\mathrm{m}}$ are given as continuous piecewise polynomial models

$$C_{\odot}(\alpha,\eta) = \begin{cases} \mathfrak{C}^{pre} & \text{if } \alpha \le \alpha_0; \\ \mathfrak{C}^{post} & \text{else;} \end{cases} \tag{3}$$

with $\alpha_0 = 16.29°$ and $\mathfrak{C}^{pre}, \mathfrak{C}^{post} \in \mathbb{R}[\alpha,\eta]$. The polynomials and remaining parameters are provided in [31].

The elevator deflection is physically restricted to values between $-60°$ to $20°$. In this work, we treat the elevator rate $\dot{\eta}$, rather than the deflection, as a control input, the state is thus $x = (V,\ \gamma,\ q,\ \alpha,\ \eta)$ and the control input is $u = (\dot{\eta}, F)$. The underlying aerodynamic models are defined on the following regions of the state-space $\mathcal{X} = [5\,\mathrm{m/s}; 30\,\mathrm{m/s}] \times [-60°; +60°] \times [-150\,°/\mathrm{s}; +150\,°/\mathrm{s}] \times [-10°; +75°] \times [-60°; +20°]$. The control inputs are restricted to $\mathcal{U} = [-200\,°/\mathrm{s}; +200\,°/\mathrm{s}] \times \mathbb{R}_{\ge 0}$;

III. Methodology

Consider a nonlinear system which represents (1),

$$\dot{x} = f(x,u)\,, \tag{4}$$

subject to the constraints $x \in \mathcal{X} \subseteq \mathbb{R}^n$, $u \in \mathcal{U} \subseteq \mathbb{R}^m$, and its discrete time representation

$$x^+ = f^+(x,u) = x + \tau\, f(x,u) \tag{5}$$

with sampling period $\tau > 0$. For some $\mathbf{u} \in \mathcal{U}^N$ and $x_1 = x$, write $x_{N+1} = f^N(x,\mathbf{u})$; let $\mathcal{Z} = \mathcal{X} \times \mathcal{U}$ and denote the set of trim conditions as $\mathcal{Z}^{\mathrm{trim}} = \{(x,u) \in \mathcal{Z} \,|\, x = f^+(x,u)\}$.

Definition 1: A set $\mathcal{X}' \subset \mathcal{X}$ is called a *stable set* for $x_0 \in \mathcal{X}'$ and $\kappa\colon \mathcal{X}' \to \mathcal{U}$ if and only if

$$f_\kappa^N(x) \in \mathcal{X}', \tag{6a}$$

$$|x_0 - f_\kappa^\infty(x)| \to 0, \tag{6b}$$

with $f_\kappa^+ = f^+(\cdot, \kappa(\cdot))$ for all $x \in \mathcal{X}'$ and $N > 0$. The *region of attraction* $\mathcal{R}$ then is the largest* stable set. The stable sets of (4) can be characterized using Lyapunov's stability theory:

Theorem 1: [32] Let $\mathcal{V}(\cdot)$ be positive-definite with $\mathcal{V}(0) = 0$ and $\lambda > 0$; if

$$\nabla \mathcal{V} \cdot (f_\kappa(x) - x^*) < 0 \tag{7}$$

for all $x \neq x^*$ with $\mathcal{V}(\bar{x}) \leq \lambda$, then $\Omega_{\mathcal{V} \leq \lambda}$ is a stable set for $f_\kappa(x^*) = 0$. $\lhd$

Stability of (4) follows under some mild conditions [33].

A. Model predictive control

The model-predictive feedback law is defined by the solution of the following OCP:

Given a measured state $x_0 \in \mathcal{X}$ and target $(x_f, u_f) \in \mathcal{Z}^{trim}$; solve the constrained nonlinear program

$$\min_{\mathbf{x},\mathbf{u}} \quad \sum_{i=1}^{N-1} \ell(x_i, u_i)\,, \tag{8a}$$

$$x_{i+1} = f^+(x_i, u_i), \quad i = 0, \ldots, N-1, \tag{8b}$$

$$x_N = x_f, \quad \mathbf{x} \in \mathcal{X}^N, \quad \mathbf{u} \in \mathcal{U}^N \tag{8c}$$

Here, $\ell\colon \mathcal{Z} \to \mathbb{R}$ is called the *stage cost*. The MPC feedback law is then

$$u(t) = \hat{\mathbf{u}}[1](x(t)) \tag{9}$$

where $(\hat{\mathbf{x}}, \hat{\mathbf{u}})$ is a minimizer of (8) with $x_0 = x(t)$. The set of recoverable conditions is further defined as

$$\begin{aligned} \mathcal{Z}_N = \big\{ (x_0, \mathbf{u}) \in \mathcal{X} \times \mathcal{U}^N \,\big|\, & f^N(x_0, \mathbf{u}) = x_f \text{ and} \\ & \forall k \leq N.\, f^k\big(x_0, \mathbf{u}^k\big) \in \mathcal{X} \big\}\,, \end{aligned} \tag{10}$$

where $\mathbf{u}^k$ are the first k elements of $\mathbf{u}$, and $\mathcal{X}_N$ denotes the projection of $\mathcal{Z}_N$ onto $\mathcal{X}$. We assume that [17]:

Assumption 1: $\mathcal{Z}$ is compact, ℓ and f^+ are continuous and $\mathcal{X}_N$ contains x_f in its interior.

The following Theorem provides sufficient conditions for closed-loop stability of EMPC.

Theorem 2: [17] Let $(x_f, u_f) \in \mathcal{Z}^{\text{trim}}$ satisfy:†

1) f^+ is strictly dissipative with respect to (w.r.t.) the supply rate‡ $\varsigma_\ell\colon (x, u) \mapsto \ell(x, u) - \ell(x_f, u_f)$;

*In the sense of $\mathcal{X}' \subseteq \mathcal{R}$ for any stable set $\mathcal{X}'$.

†Assumption 2 of [17] is fulfilled if f^+ is locally controllable in an open environment of x_f.

‡We write hereafter "dissipative w.r.t. the cost ℓ."

2) $\ell(x_f, u_f) \leq \ell(x, u)$ for all $(x, u) \in \mathcal{Z}^{\text{trim}}$;

then x_f is an asymptotically stable equilibrium of (5), (9) with region of attraction $\mathcal{X}_N$ as defined above. $\lhd$

Recall that:

Definition 2: The control system (5) is called *strictly dissipative* w.r.t. a supply rate $\varsigma\colon \mathcal{Z} \to \mathbb{R}$ if and only if there exists a storage function $\Lambda\colon \mathcal{X} \to \mathbb{R}$ such that

$$\Lambda\left(x^+\right) - \Lambda(x) \leq -\rho(x - x_f) + \varsigma(x, u) \tag{11}$$

for a $\rho\colon \mathcal{X} \to \mathbb{R}_{\geq 0}$ positive definite[§] and all $(x, u) \in \mathcal{Z}$.

Note that unlike conventional MPC, ℓ may not necessarily be positive definite around the target equilibrium.

B. Sum-of-squares programming

We make extensive use of sum-of-squares (SOS) programming to prove dissipativity and to estimate the region of attraction of the nominal controller. A polynomial $\mathfrak{f} \in \mathbb{R}[x]$ is a sum of squares, $\mathfrak{f} = \sum_i \mathfrak{f}_i^2$ with $(\mathfrak{f}_i)_i \subset \mathbb{R}[x]$, if and only if $\mathfrak{f} = \mathfrak{z}(x)^T Q \mathfrak{z}(x)$, where $Q \succeq 0$ and $\mathfrak{z}$ is a vector of monomials in x [22]; the set of sum-of-squares polynomials is denoted $\Sigma[x]$. This equivalence reduces the problem "$\mathfrak{f} \in \Sigma[x]$" to a semi-definite programming problem [20]. Since sum-of-squares polynomials are non-negative, the following lemma can be proven.

Lemma 1: [23] Let $\mathfrak{f}, \mathfrak{g}_1, \ldots, \mathfrak{g}_k, \mathfrak{h} \in \mathbb{R}[x]$; we have

$$\bigcap_i \Omega_{\mathfrak{g}_i \leq 0} \cap \mathcal{O}_{\mathfrak{h}=0} \subseteq \Omega_{\mathfrak{f} \leq 0}. \tag{12}$$

if $\sum_i \mathfrak{s}_i \mathfrak{g}_i + \mathfrak{p}\mathfrak{h} - \mathfrak{f} \in \Sigma[x]$ for $\mathfrak{s}_1, \ldots, \mathfrak{s}_k \in \Sigma[x]$ and $\mathfrak{p} \in \mathbb{R}[x]$. $\lhd$

If the sufficient condition holds, we write $(\mathbf{s}, \mathfrak{h}) \vdash \bigcap_i \Omega_{\mathfrak{g}_i \leq 0} \cap \mathcal{O}_{\mathfrak{h}=0} \subseteq_\Sigma \Omega_{\mathfrak{f} \leq 0}$ with $\mathbf{s} = (\mathfrak{s}_1, \ldots, \mathfrak{s}_k)$, saying that $(\mathbf{s}, \mathfrak{h})$ *proves* the set inclusion.

IV. Controller Design

In this section, we devise an EMPC strategy for LOA minimal recovery and a corresponding regularization scheme to ensure dissipativity. No thrust is applied during recovery and we consider only the elevator rate as an input, i.e., $u = \dot{\eta}$. In level flight a nominal flight controller κ_{lvl} stabilizes the aircraft. Thus, the nominal trim condition is unattainable for the elevator-only recovery strategy; instead, we choose a target steady-state (x_f, u_f) for EMPC that is contained in the interior of the control-invariant nominal stable set, viz.

$$x_f = (10.8\,\text{m/s},\ -2.28°,\ 0\,°/\text{s},\ 4.15°,\ -6.80°)\,, \tag{13a}$$

$$u_f = 0\,°/\text{s}, \tag{13b}$$

[§]A continuous function ϕ is said to be *positive definite* (p.d.) if $\phi(\cdot) > 0$ everywhere except at the origin and $\phi(0) = 0$.

the unique gliding trim condition with minimal descend speed [15]. We want the EMPC controller to minimize the positive loss-of-altitude, $\Delta z_\mathrm{g} = z_{\mathrm{g}N} - z_{\mathrm{g}0}$, which corresponds to the altitude-loss stage cost

$$\ell_\Delta(x) = z_\mathrm{g}^+ - z_\mathrm{g} = -\tau V \sin\gamma. \tag{14}$$

We denote by ℓ_Δ^* the steady-state loss of altitude, which satisfies $\ell_\Delta^* = \ell_\Delta(x_f, u_f) \leq \ell_\Delta(x,u)$ for all $(x,u) \in \mathcal{Z}^\mathrm{trim}$. Without propulsion, the aircraft descends in steady-state in order to convert potential into kinetic energy and $\ell_\Delta^* > 0$. However, (14) is not positive definite on $\mathcal{Z}$; the loss of altitude becomes negative (i.e., the aircraft ascends) for any positive inclination γ. To ensure that the dissipativity condition in Theorem 2 holds we add quadratic regularization terms to the stage cost:

$$\ell_R(x,u) = \ell_\Delta(x) + \tfrac{1}{2}\left\|x - x_f\right\|_{Q_x}^2 + \tfrac{1}{2}\left\|u - u_f\right\|_{Q_u}^2, \tag{15}$$

where $Q_x \in \mathbb{R}^{n\times n}, Q_u \in \mathbb{R}^{m\times m}$ are positive diagonal matrices. In the next section we illustrate how to determine minimal gains Q_x and Q_u which ensure dissipativity.

We also investigate the performance of a nonlinear tracking MPC controller which uses the stage cost

$$\ell_T(x,u) = \tfrac{1}{2}\left\|x - x_f\right\|_{Q_x}^2 + \tfrac{1}{2}\left\|u - u_f\right\|_{Q_u}^2; \tag{16}$$

where Q_x and Q_u are positive definite weighting matrices. The stability of the tracking NMPC can be established using [33, Theorem 5.5]. All controllers enforce the box constraints $(x,u) \in \mathcal{X} \times \mathcal{U}$.

V. Analysis

As our main result, we use SOS programming to synthesize a suitable storage-candidate function $\mathfrak{L}$ and regularization gains satisfying the conditions of Theorem 2. We further estimate the region of attraction of the nominal level-flight trim condition to ensure that the target steady-state for recovery lies within reach of the nominal flight controller. In order to transform the nonlinear aircraft dynamics model (1)–(2) into a piecewise polynomial form, we replace sine and cosine by their 3rd-order Taylor polynomials, providing sufficient accuracy within the chosen ranges of γ and α. Likewise, within the stable neighbourhood the inversion V^{-1} is well approximated by a 5th-order Taylor polynomial. The resulting polynomial functions are denoted by $\mathfrak{f}_V$, $\mathfrak{f}_\gamma$, etc. and $x^+ = \mathfrak{f}^{pre}$ ($\dot{x} = \mathfrak{f}^{pre}$) if $\alpha \leq \alpha_0$, $x^+ = \mathfrak{f}^{post}$ ($\dot{x} = \mathfrak{f}^{post}$) else. For tractability, any terms of $\mathfrak{f}^{pre}, \mathfrak{f}^{post}$ with degree larger than 5 or coefficients smaller than 10^{-6} are removed with negligible loss of accuracy. The cost supply rate is likewise approximated by $\mathfrak{S}_\ell \in \mathbb{R}[x,u]$.

A. Dissipativity & Regularization

To prove that the EMPC feedback law is stabilizing, the system dynamics must be strictly dissipative w.r.t. the stage cost ℓ. Proving this condition requires a suitable storage function $\Lambda : \mathcal{X} \to \mathbb{R}$ satisfying (11). With an analytical search for Λ being intractable in general, a polynomial storage function *proving dissipativity* can be synthesized by solving a sum-of-squares feasibility problem. However, it is often unknown a-priori if there exists a sum-of-squares polynomial storage function of a given degree which proves dissipativity of the

dynamics w.r.t. the chosen stage cost. This can be remedied with a regularization. It has been established in [19] that if the gains $Q = \mathrm{diag}(Q_x, Q_u)$ in (15) are chosen sufficiently large, then the dynamics are dissipative w.r.t. the stage cost. There, the authors propose a procedure based on Gershgorin's circle theorem which is computationally simple but prone to conservative (large) regularization gains.

Instead, we propose to use min-trace SOS programming to search simultaneously for a polynomial storage-candidate $\mathfrak{L}$ and diagonal gains Q that directly prove the dissipativity condition (11), by solving the problem

$$\min_{\substack{Q\succeq 0\\ \mathbf{s}_1,\mathbf{s}_2\subset\Sigma[z]\\ \mathfrak{L}\in\mathbb{R}[x]}} \quad \mathrm{tr}(Q) \quad \text{s.t.} \begin{cases} \mathbf{s}_1 \vdash \mathcal{Z}\cap\Omega_{\alpha\le\alpha_0} \subseteq_\Sigma \Omega^{pre}_{\mathfrak{L},Q} \\ \mathbf{s}_2 \vdash \mathcal{Z}\cap\Omega_{\alpha\ge\alpha_0} \subseteq_\Sigma \Omega^{post}_{\mathfrak{L},Q} \end{cases} \tag{17}$$

where $\Omega^{(\cdot)}_{\mathfrak{L},Q}$ denotes the set of all $z\in\mathbb{R}^{m+n}$ where

$$\mathfrak{L}\circ \mathfrak{f}^{(\cdot)}(z) - \mathfrak{L}(z) - \mathfrak{S}_\ell(z) \le \tfrac{1}{2}\left\|z - z_f\right\|^2_Q - \epsilon\left\|\bar{x}\right\|_2^2 \tag{18}$$

for some small $\epsilon > 0$ and $x^+ = \mathfrak{f}^{(\cdot)} \in \{\mathfrak{f}^{pre}, \mathfrak{f}^{post}\}$. This approach is guaranteed to have a feasible solution, allows the choice of $\mathfrak{L}$ as a polynomial of arbitrary order, while ensuring that $Q \to 0$ if the system is dissipative and $\mathfrak{L}$ is a polynomial of suitable order.

For a linear storage-candidate, solving Eq. (17) yields

$$Q_1 = \mathrm{diag}(0.0014,\, 0.39,\, \tilde{\epsilon}_1,\, \tilde{\epsilon}_2,\, \tilde{\epsilon}_3,\, \tilde{\epsilon}_4)\,, \tag{19}$$

where $\tilde{\epsilon}_i < \epsilon$. For a quadratic storage however, we get regularization gains $Q_2 \prec \epsilon\,\mathbb{I}_5$, indicating that the discrete aircraft system is *almost* dissipative.

B. Nominal region of attraction

The MPC recovery controllers do not use thrust; we rely on a nominal flight controller κ_{lvl} to return the aircraft to steady level flight. To ensure safety we switch from the MPC to the nominal control law only once the system state is within the region of attraction of κ_{lvl}. As an example we choose the *nominal flight* trim condition

$$x_{\mathrm{lvl}} = (13\,\mathrm{m/s},\, 0°,\, 0\,°/\mathrm{s},\, 1.35°,\, -1.51°)\,, \tag{20a}$$

$$u_{\mathrm{lvl}} = (0\,°/\mathrm{s},\, 0.835\,\mathrm{N})\,, \tag{20b}$$

with κ_{lvl} given as continuous LQR feedback for the linearized dynamics around $(x_{\mathrm{lvl}}, u_{\mathrm{lvl}})$. The controlled dynamics are given by $\dot{x} = \mathfrak{f}^{(\cdot)}_\kappa$.

Using a polynomial Lyapunov-candidate function $\mathfrak{V}\in\mathbb{R}[x]$, we can reformulate (7) into a sum-of-squares optimization problem in order to estimate the region of attraction of $(x_{\mathrm{lvl}}, u_{\mathrm{lvl}})$ in nominal flight. An arbitrarily chosen ellipsoidal shape function $\mathfrak{p}$ is used to determine the size of the stable set. As sum-of-squares are limited to non-negativity, we use the relaxed condition

$$\nabla\mathfrak{V}\cdot\mathfrak{f}^{(\cdot)}_\kappa(x) \le -\epsilon\left\|\bar{x}\right\|_2^2 \tag{21}$$

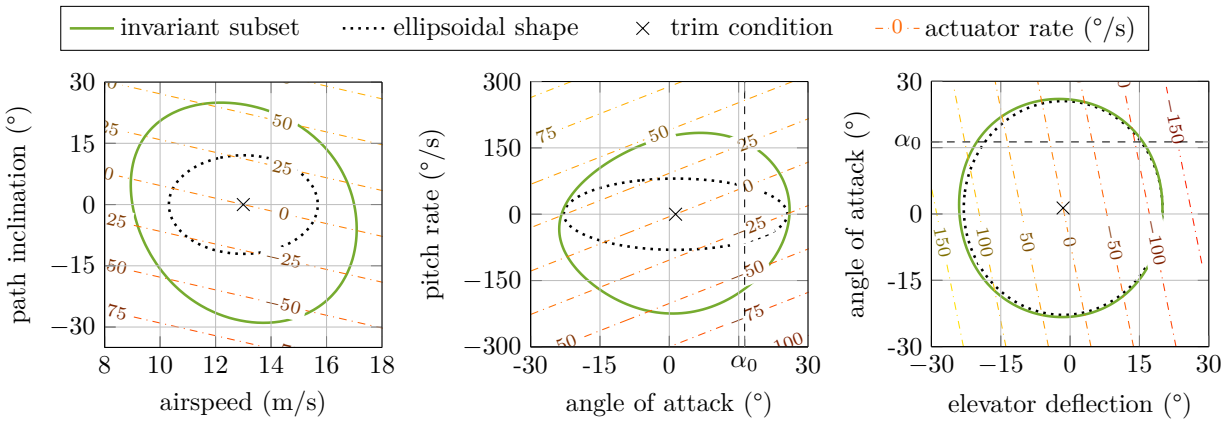

Fig. 1: Provable stable set under nominal LQR control inputs.

with $\epsilon > 0$ small; let $\Omega_{\mathfrak{V}}^{(\cdot)}$ denote the set of states x such that (21) holds for $\dot{x} = \mathfrak{f}_\kappa^{(\cdot)} \in \{\mathfrak{f}_\kappa^{pre}, \mathfrak{f}_\kappa^{post}\}$. The optimization problem is then given as

$$\max_{\substack{\lambda,\rho>0 \\ \mathfrak{s}_0\in\Sigma[x] \\ \mathbf{s}_1,\mathbf{s}_2\subset\Sigma[x] \\ \mathfrak{V}\text{ p.d.}}} \lambda \quad \text{s.t.} \quad \begin{cases} \mathfrak{s}_0 \vdash \Omega_{\mathfrak{p}\le\rho} \subseteq_\Sigma \Omega_{\mathfrak{V}\le\lambda} \\ \mathbf{s}_1 \vdash \Omega_{\mathfrak{V}\le\lambda} \cap \Omega_{\alpha\le\alpha_0} \subseteq_\Sigma \Omega_{\mathfrak{V}}^{pre} \\ \mathbf{s}_2 \vdash \Omega_{\mathfrak{V}\le\lambda} \cap \Omega_{\alpha\ge\alpha_0} \subseteq_\Sigma \Omega_{\mathfrak{V}}^{post} \end{cases} \tag{22}$$

which is a bilinear program. We therefore employ the iterative bisection strategy described in [23, 24].

After 49 iterations, the provable stable set in Fig. 1 is obtained with $\lambda^* = 0.6859$ and $\rho^* = 28.8696$; $\mathfrak{p}$ is given in the appendix. A larger ROA may be computable using multiple Lyapunov function-candidates $\mathcal{V}^{pre}, \mathcal{V}^{post}$.

VI. Numerical Results

We placed an NMPC controller (NMPC, ℓ_T), a linear MPC (LMPC) controller[¶], an EMPC controller with regularization gains Q_1 (r-EMPC, ℓ_R) and the un-regularized EMPC controller (EMPC, ℓ_Δ) in closed-loop with the nonlinear model. The regularization gains Q_2 are small enough that the closed-loop traces of r-EMPC using Q_2 were indistinguishable from un-regularized EMPC. All MPC simulations utilize Euler integration with a sampling rate $\tau = 50\,\text{ms}$, horizon length $N = 120$, and simulation time $T = 20\,\text{s}$. The optimal control problem (8) was solved using `Ipopt` [34]. Further details of the computations are given in the appendix (Tab. I). The initial condition was $(8.26\,\text{m/s}, -36.4°, 0\,°/\text{s}, 32.6°, -41°)$.

Fig. 2 shows the closed-loop trajectories for all four strategies; only LMPC fails to recover the aircraft due to elevator inversion in deep-stall. Of the remaining three, pure EMPC provides the most aggressive

[¶]The LMPC controller was designed using the same stage cost and constraints as the NMPC controller but using (5) linearized about the target equilibrium as the prediction model.

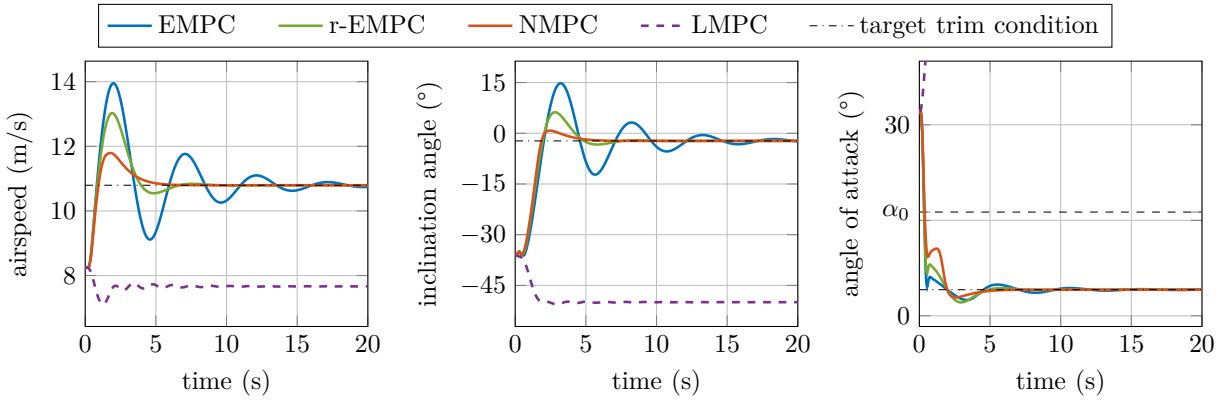

Fig. 2: Economic and tracking MPC for deep-stall recovery in airspeed V, inclination γ, and angle of attack α.

approach, partially regaining height by ascent, leading to a slower transition back to normal flight, whereas the regularization gains cause r-EMPC to transition faster. Both economic strategies noticeably overshoot[‖] the target airspeed and path inclination in order to regain altitude.

Recall that the MPC controllers guide the aircraft to a stable gliding conditions and a nominal flight controller is used to resume level flight. The nominal controller takes over if the state enters its ROA, which was estimated in Section V, (but not earlier than 5 s into the recovery). The resulting recovery trajectories are shown in Fig. 3. The tracking NMPC recovery shows by far the largest LOA (8.4 m), while non-regularized and regularized EMPC are similar (7.5 m and 7.4 m), with r-EMPC encountering a slightly reduced LOA due to the later switching point of the non-regularized scheme.

VII. Conclusion

Economic MPC is a promising tool for LOA-minimal recovery of an aircraft from upset conditions; however, providing certifiable guarantees of closed-loop stability is nontrivial. In this paper, we applied polynomial SOS programming to a piecewise longitudinal aerodynamics model to prove stability of a deep-stall recovery EMPC strategy, proposed an SOS based regularization scheme that computes minimal regularization gains needed to ensure dissipativity and illustrated that the gains approach zero as the order of the storage function-candidate is increased. To guarantee stability for all (admissible) states, even very small gains help to avoid undesirable closed-loop behaviour such as periodic oscillations.

Finally, we presented a numerical comparison of different MPC strategies for recovery of nominal flight. Our investigations revealed EMPC offers significant performance advantages compared nonlinear tracking MPC and that regularized EMPC is also compatible with recovery of level flight. Future work includes reduction of computation and application to NASA's GTM.

[‖]Overshoot is acceptable in this application except during very low-altitude flight.

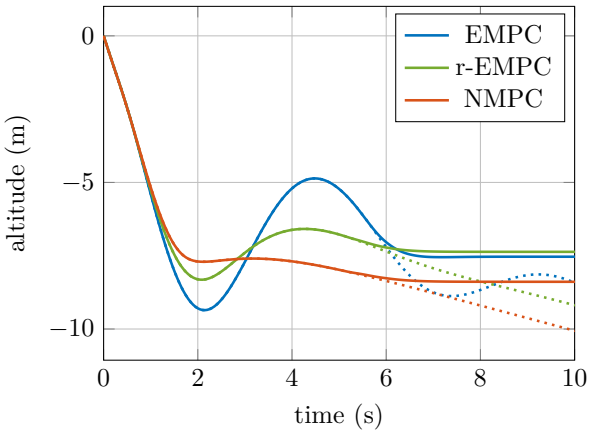

Fig. 3: Upset recovery strategies with switching to nominal control. The full MPC trajectories are shown dotted.

Appendix

The aircraft states and inputs, were scaled by $d_V = 10\,\mathrm{m/s}$, $d_\gamma = 45°$, $d_q = 150\,°/\mathrm{s}$, $d_\alpha = 45°$, $d_\eta = 80°$, $d_{d\eta} = 100\,°/\mathrm{s}$, and $d_F = 25\,\mathrm{N}$. The gains for linear and nonlinear tracking MPC were $Q_x = \mathbb{I}_5$ and $Q_{d\eta} = 0.010$ and for nominal LQR feedback, $Q_x = \mathbb{I}_5$ and $Q_u = \mathbb{I}_2$ (all gains with respect to the scaled states and inputs).

Eq. (17) for Q_2 has been solved on a single node of the University of Michigan HPC cluster in 3 h (Intel Xeon E5, 2.4 GHz, 44 GB). The ellipsoidal shape for Eq. (22) is defined as $\mathfrak{p} = \left(d_x^{-1}x\right)^T \mathrm{diag}(0.50, 0.50, 1, 1, 0.50)\left(d_x^{-1}x\right)$; the computation took 6.0 h on a personal computer (Intel Core i7, 3 GHz, 16 GB). All SOS problems were constructed and solved by `sosopt/SeDuMi`. As the piecewise model is not differentiable in α_0 due to Eq. (3), we approximate the aerodynamics by $\mathcal{H}(\alpha - \alpha_0)\,\mathcal{C}^{pre} + (1 - \mathcal{H}(\alpha - \alpha_0))\,\mathcal{C}^{post}$, where $\mathcal{H}(\alpha) = \frac{1}{1+e^{-2\alpha/\mu}}$, and Problem 8 is solved while iteratively decreasing μ. Further details of the simulations are given in Tab. I. The implemented controllers are not yet real-time capable and need efforts to optimize their computational footprint.

TABLE I: Simulation details & results. Computation time accuracy ±10 ms (Intel Core i7, 3 GHz, 16 GB).

	EMPC	r-EMPC	NMPC
average time OCP	1.74 s	0.768 s	0.674 s
comp. time (MPC)	951 s	503 s	486 s
comp. time (to level)	522 s	362 s	309 s
optimal cost ($k=1$)	4.76	6.65	9.89
residual norm	$<3\times10^{-5}$	$<1\times10^{-5}$	$<9\times10^{-4}$

References

[1] *Loss of Control In-Flight Accident Analysis Report, 2010–2014.* Montreal, CA: International Air Transport Association, 2015.

[2] M. H. Smaili, J. Breeman, T. J. J. Lombaerts, J. A. Mulder, Q. P. Chu, and O. Stroosma, "Intelligent Flight Control Systems Evaluation for Loss-of-Control Recovery and Prevention," *J. Guid. Control Dynam.*, vol. 40, no. 4, pp. 890–904, 2016.

[3] N. D. Richards, N. Gandhi, A. J. Bateman, D. H. Klyde, and A. K. Lampton, "Vehicle Upset Detection and Recovery for Onboard Guidance and Control," *J. Guid. Control Dynam.*, vol. 40, no. 4, pp. 920–933, 2017.

[4] R. C. Allen, H. G. Kwatny, and G. Bajpai, "Safe Set Protection and Restoration for Unimpaired and Impaired Aircraft," in *AIAA Guidance, Navigation, and Control Conf.*, Minneapolis, US-MN, 2012.

[5] P. Di Donato, S. Balachandran, K. McDonough, E. Atkins, and I. Kolmanovsky, "Envelope-aware Flight Management for Loss of Control Prevention given Rudder Jam," *J. Guid. Control Dynam.*, vol. 40, pp. 1027–1041, 2017.

[6] B.-C. Chang, H. G. Kwatny, E. R. Ballouz, and D. C. Hartmann, "Aircraft Trim Recovery from Highly Nonlinear Upset Conditions," in *AIAA Guidance, Navigation, and Control Conf.*, San Diego, US-CA, 2016.

[7] H. J. Tol, C. C. de Visser, L. G. Sun, E. van Kampen, and Q. P. Chu, "Multivariate Spline-Based Adaptive Control of High-Performance Aircraft with Aerodynamic Uncertainties," *J. Guid. Control Dynam.*, vol. 39, no. 4, pp. 781–800, 2016.

[8] D. Kim, G. Oh, Y. Seo, and Y. Kim, "Reinforcement Learning-Based Optimal Flat Spin Recovery for Unmanned Aerial Vehicle," *J. Guid. Control Dynam.*, vol. 40, no. 4, pp. 1076–1084, 2016.

[9] S. Schuet, T. Lombaerts, J. Kaneshige, K. H. Shish, and V. Stepanyan, "Stall Recovery Guidance Using Fast Model Predictive Control," in *AIAA Guidance, Navigation, and Control Conf.*, Grapevine, US-TX, 2017.

[10] J. J. Engelbrecht and J. A. Engelbrecht, "Optimal Attitude and Flight Vector Recovery for Large Transport Aircraft using Sequential Quadratic Programming," in *2016 Pattern Recognition Association of South Africa and Robotics and Mechatronics International Conf.*, Stellenbosch, SA, 2016.

[11] D. Sparks and D. Moerder, "Optimal Aircraft Control Upset Recovery With and Without Component Failures," in *Proc. of the American Control Conf.*, Anchorage, US-AK, 2002, pp. 3644–3649.

[12] R. Bunge and I. Kroo, "Automatic Spin Recovery with Minimal Altitude Loss," in *2018 AIAA Guidance, Navigation, and Control Conf.*, Kissimmee, US-FL, 2018.

[13] M. Ellis, J. Liu, and P. D. Christofides, *Economic Model Predictive Control.* Basel, CH: Springer, 2017.

[14] T. Cunis, T. Leth, L. C. Totu, and A. la Cour-Harbo, "Identification of Thrust, Lift, and Drag for Deep-stall Flight Data of a Fixed-wing Unmanned Aircraft," in *2018 Int. Conf. on Unmanned Aircraft Systems*, Dallas, US-TX, 2018.

[15] T. Cunis, J.-P. Condomines, L. Burlion, and A. la Cour-Harbo, "Dynamic Stability Analysis of Aircraft Flight in Deep-stall," Under review for *J. Aircraft*, 2019.

[16] U. Eren, A. Prach, B. B. Koçer, S. V. Raković, E. Kayacan, and B. Açıkmeşe, "Model Predictive Control in Aerospace Systems: Current State and Opportunities," *J. Guid. Control Dynam.*, vol. 40, no. 7, pp. 1541–1566, 2017.

[17] D. Angeli, R. Amrit, and J. B. Rawlings, "On Average Performance and Stability of Economic Model Predictive Control," *IEEE Trans. Automat. Contr.*, vol. 57, no. 7, pp. 1615–1626, 2012.

[18] M. Zanon and T. Faulwasser, "Economic MPC without terminal constraints: Gradient-correcting end penalties enforce asymptotic stability," *J. of Process Contr.*, vol. 63, pp. 1–14, 2018.

[19] J. Jäschke, X. Yang, and L. T. Biegler, "Fast economic model predictive control based on NLP-sensitivities," *J. Process Contr.*, vol. 24, no. 8, pp. 1260–1272, 2014.

[20] P. A. Parillo, "Semidefinite programming relaxations for semialgebraic problems," *Math. Program. B*, vol. 96, no. 2, pp. 293–320, 2003.

[21] W. Tan, "Nonlinear Control Analysis and Synthesis using Sum-of-Squares Programming," PhD thesis, UC Berkeley, Berkeley, US-CA, 2006.

[22] P. Seiler and G. J. Balas, "Quasiconvex sum-of-squares programming," in *49th IEEE Conf. on Decision and Control*, Atlanta, US-GA, 2010, pp. 3337–3342.

[23] U. Topcu, A. Packard, and P. Seiler, "Local stability analysis using simulations and sum-of-squares programming," *Automatica*, vol. 44, no. 10, pp. 2669–2675, 2008.

[24] A. Chakraborty, P. Seiler, and G. J. Balas, "Nonlinear region of attraction analysis for flight control verification and validation," *Control Eng. Pract.*, vol. 19, no. 4, pp. 335–345, 2011.

[25] A. A. Ahmadi and P. A. Parrilo, "Non-monotonic Lyapunov functions for stability of discrete time nonlinear and switched systems," in *47th IEEE Conf. on Decision and Control*, 2008, pp. 614–621.

[26] G. Chesi, "Establishing robust stability of discrete-time systems with time-varying uncertainty: The Gram-SOS approach," *Automatica*, vol. 50, no. 11, pp. 2813–2821, 2014.

[27] C. Ebenbauer and F. Allgöwer, "Analysis and design of polynomial control systems using dissipation inequalities and sum of squares," *Comp. Chem. Eng.*, vol. 30, pp. 1590–1602, 2006.

[28] T. Faulwasser, M. Korda, C. N. Jones, and D. Bonvin, "Turnpike and dissipativity properties in dynamic real-time optimization and economic MPC," in *53rd IEEE Conf. on Decision and Control*, Los Angeles, US-CA, 2014, pp. 2734–2739.

[29] M. Korda and C. N. Jones, "Automatica Stability and performance verification of optimization-based," *Automatica*, vol. 78, pp. 34–45, 2017.

[30] "Airplane Flying Handbook," Flight Standards Service, Washington, US-DC, FAA handbook FAA-H-8083-3B, 2016.

[31] T. Cunis and A. la Cour-Harbo, "Piecewise Polynomial Model of the Aerodynamic Coefficients of the *Cumulus One* Unmanned Aircraft," Sky-Watch A/S, Støvring, DK, Tech. Rep. `hal-02280789`. [Online]. Available: https://hal-enac.archives-ouvertes.fr/hal-02280789

[32] J. P. La Salle, "Some Extensions of Liapunov's Second Method," *IRE Trans. Circuit Theory*, vol. CT-7, pp. 520–527, dec 1960.

[33] L. Grüne and J. Pannek, *Nonlinear Model Predictive Control: Theory and Algorithms*, 2nd ed. Basel, CH: Springer, 2017.

[34] A. Wächter and L. T. Biegler, "On the implementation of an interior-point filter line-search algorithm for large-scale nonlinear programming," *Math. Program. A*, vol. 106, pp. 25–57, 2006.

Chapter 8

Model-Predictive Spiral and Spin Recovery

Model-predictive control, due to its optimality formulation, is indeed powerful for systems with allocation problems[1] or multiple, inter-coupled inputs and outputs. This makes MPC well suited for the problem of upset recovery in the full six degrees of freedom, where all three ailerons, elevator, and rudder are to be controlled within their physical limits. We therefore prepare in this chapter an MPC scheme for recovery from spiral and spin upset conditions and demonstrate its ability for six-degrees-of-freedom recovery using the GTM's high-fidelity simulation as "real" system and the piecewise polynomial aerodynamics as imperfect prediction model. This draws the arch back from the system theoretic approaches, such as MPC with its theory of stability, towards control of real physical systems and high-fidelity models. A full analysis of the (nominal) control setting, as presented in the previous chapter for the longitudinal motion, within the present study is not computationally tractable and must remain future work; so does the dissipativity analysis for EMPC stability. This chapter concludes the control part of the dissertation.

In the following, we will refer to the piecewise polynomial equations of motion of Chapter 3 as *model*; and of the high-fidelity simulation (NASA 2016) as *simulation*.

Nomenclature

α, β	Angle of attack and side-slip angle (rad);
Θ, Φ	Pitch and bank angle (rad);
ζ	Rudder deflection (rad), negative if leading to positive yaw moment;
η	Elevator deflection (rad), negative if leading to positive pitch moment;
ξ	Aileron deflection (rad), negative if leading to positive roll moment;
$\ell(\cdot)$	NMPC stage cost function ($\ell\colon \mathbb{R}^{n+m} \times \mathbb{R}^m \to \mathbb{R}$);
m	Number of actuators ($m = 3$);
n	Number of equation-of-motion states ($n = 8$);
N	Horizon length ($N \in \mathbb{N}$);
p, q, r	Components of body rate $\boldsymbol{\omega}$ (rad/s);
$\mathbf{Q}, \mathbf{R}$	Positive weight matrices for states and inputs ($\mathbf{Q} \in \mathbb{S}_{n+m}, \mathbf{R} \in \mathbb{S}_m$);

[1] *Allocation*: Assignment of several, partially redundant control inputs in order to achieve a single control task, e.g., tracking a reference pitch angle. This is a particular problem for agile and highly nonlinear fighter jets, some of which have more than 12 independent control surfaces (e.g., Proctor 2019).

t	Simulation time (s);
t_0	Time (s) at which the optimal control problem is solved;
V_A	Aircraft speed relative to air (m/s), positive along x_a-axis;
u, v, w	Components of aircraft velocity $\mathbf{V}_\mathrm{A}$ relative to air (m/s);
$\mathbf{x}_\delta, \mathbf{u}_\delta$	States and inputs of the actuator dynamics;
$\mathbf{x}_\mathrm{e8}$	States of the eight-parameter equations of motion;
$\mathbf{x}_f, \mathbf{u}_f$	States and inputs at *target* trim condition;
$\mathcal{X}$	Viable state-space of the eight-parameter equations of motion ($\mathcal{X} \subset \mathbb{R}^n$);
$\mathcal{X}_\eta$	Viable state-space of the elevator ($\mathcal{X}_\eta \subset \mathbb{R}$);
$\mathcal{X}_\xi$	Viable state-space of the ailerons ($\mathcal{X}_\xi \subset \mathbb{R}$);
$\mathcal{X}_\zeta$	Viable state-space of the rudder ($\mathcal{X}_\zeta \subset \mathbb{R}$);
$\mathcal{X}_\delta$	Viable state-space of the actuator dynamics ($\mathcal{X}_\delta = \mathcal{X}_\xi \times \mathcal{X}_\eta \times \mathcal{X}_\zeta$);
$\mathcal{U}_\delta$	Viable control inputs of the actuator dynamics ($\mathcal{U}_\delta \subset \mathbb{R}^m$);

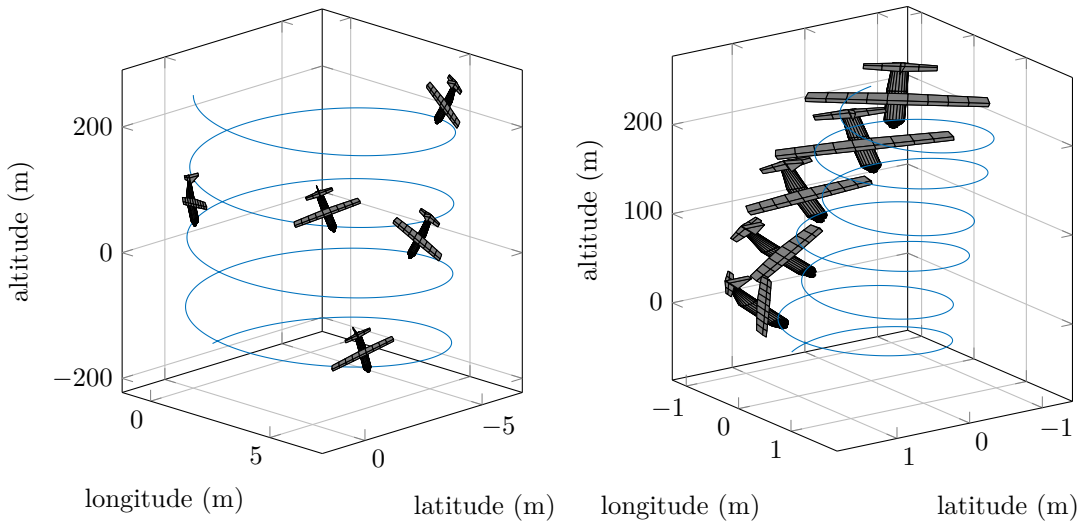

(a) Steep spiral ($\eta = -30°$, $\zeta = 0°$). (b) Oscillatory spin ($\eta = -24°$, $\zeta = -10°$).

Figure 8.1: Flight paths for spiral and oscillatory spin modes of the GTM (aircraft to scale).

8.1 Problem Setting

Spiral and spin both are three-dimensional rotary motions, that is, they involve revolutions around more than one of the aircraft body axes. Hence, recovery requires coordinate effort of multiple, independent control inputs. Gill et al. (2013) identified dynamic regimes with rotary motion of the GTM, including regimes of steep spirals (Gill et al. 2013, p. 1837, cf. Fig. 2.2a) and oscillatory spins of period one and three

(Gill et al. 2013, pp. 1838 and following, cf. Fig. 2.2b) which are partially stable and attractive. In this chapter, we consider recovery from each a steep spiral and period-one oscillatory spin initial condition. Fig. 8.1 illustrates these flight conditions.[2] Here, the steep spiral mode is entered for an elevator deflection $\eta = -30°$ and neutral rudder; the oscillatory spin mode, for an elevator and rudder deflections $\eta = -24°$ and $\zeta = -10°$.[3] Unlike oscillatory spin, the spiral motion is characterised by constant (non-zero) body rates; only the heading changes as result of the steep spiral. Therefore, the spiral is technically[4] a trim condition of aircraft flight. The oscillatory spin, in contrast, is in fact a periodic motion involving all three airspeed and aerodynamic angles, body rates, and attitude. The (approximate) periodicity of the chosen oscillatory spin condition is illustrated in Fig. 8.2. Again, we consider recovery approaches of the unthrottled aircraft ($F = 0$) in order not to further model the engines of the GTM and to follow the means of the previous chapters. This is in agreement with the FAA procedures (FAA 2016, Chapter 4, pp. 15 and 23).

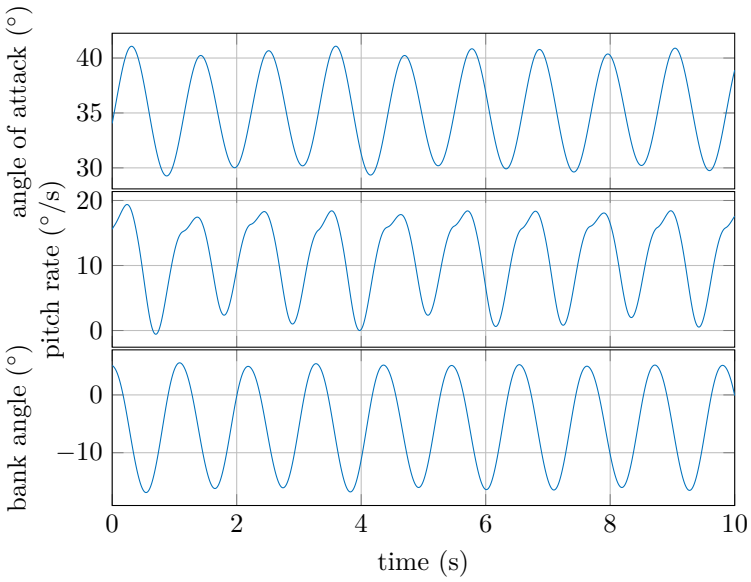

Figure 8.2: Periodic motion in oscillatory spin mode ($\eta = -24°$, $\zeta = -10°$).

In the GTM simulation, the surface actuators are represented by first-order linear dynamics with restricted range and speed. These dynamics can be written as

$$\dot{\delta}(t) = 2\pi f \left(\delta_{\text{cmd}} - \delta(t)\right) \tag{8.1}$$

[2] In the figure, the aircraft drawing is roughly to scale and its orientation represents the aircraft attitude. The aircraft are depicted first at $t = 1.495\,\text{s}$ and subsequently with a period of $\Delta t = 1.75\,\text{s}$.

[3] The present GTM simulation appears to be rather sturdy with respect to spin; without a significant rudder deflection, the aircraft spin will eventually steady into a spiral (see Gill et al. 2013, pp. 1839–1841, for a discussion of the effects of rudder onto spiral and spin modes).

[4] Also *practically*; yet, why would one want to trim their aircraft into a steep spiral?

with $f = 5\,\mathrm{Hz}$ for $\delta \in \{\xi, \eta, \zeta\}$. Deflections are limited to $\xi \in \mathcal{X}_\xi = [-20°; +20°]$, $\eta \in \mathcal{X}_\eta = [-30°; +20°]$, and $\zeta \in \mathcal{X}_\zeta = [-30°; +30°]$. The actuator speed is limited to $\left|\dot{\delta}(t)\right| \leq \dot{\delta}_{\max} = 300\,°/\mathrm{s}$ for all surfaces. The piecewise polynomial model is defined on the following regions of the state-space $\mathcal{X}$, namely, $\mathbf{V}_\mathrm{A} \in [-100\,\mathrm{m/s}; +100\,\mathrm{m/s}]^3$; $\boldsymbol{\omega} \in [-300\,°/\mathrm{s}; +300\,°/\mathrm{s}]^3$; $\Phi \in [-90°; +90°]$; $\Theta \in [-85\,°/\mathrm{s}; +75\,°/\mathrm{s}]$.[5]

8.2 Controller Design

We are going to synthesise a tracking model-predictive control (NMPC) strategy in order to recover the aircraft from an upset condition to an unthrottled, normal flight trim condition with low descent speed, viz.[6]

$$\begin{aligned} V_f = 35.9\,\mathrm{m/s}, \quad \alpha_f = 6.42°, \qquad \Phi_f = -0.037°, \quad \Theta_f = 0.238°, \\ \xi_f = -0.893°, \quad \eta_f = -1.71°, \qquad \zeta_f < 0.005°, \end{aligned} \tag{8.2}$$

and $\beta_f = 0\,°/\mathrm{s}$, $\boldsymbol{\omega}_f = 0\,°/\mathrm{s}$, as well as $\dot{\Psi}_f = 0\,°/\mathrm{s}$. To this extent, we take into account the discrete nonlinear dynamics

$$\mathbf{x}_{8\mathrm{e}}^+ = \mathbf{x}_{8\mathrm{e}} + \tau\,\mathbf{f}_{8\mathrm{e}}(\mathbf{x}_{8\mathrm{e}}, \mathbf{x}_\delta)\,, \tag{8.3}$$

$$\mathbf{x}_\delta^+ = \mathbf{x}_\delta + \tau\,\mathbf{u}_\delta, \tag{8.4}$$

where $\mathbf{f}_{8\mathrm{e}}(\cdot,\cdot)$ denotes the continuous, eight-parameter nonlinear equations of motions of Eqs. (2.3)–(2.9), not taking into account the change of heading $\dot{\Psi}$, and (2.20) with

$$\begin{aligned} \mathbf{x}_{8\mathrm{e}}^T &= \left[\begin{array}{ccc:ccc:cc} u & v & w & p & q & r & \Phi & \Theta \end{array}\right] \in \mathcal{X}, \\ \mathbf{x}_\delta^T &= \begin{bmatrix} \xi & \eta & \zeta \end{bmatrix} \in \mathcal{X}_\xi \times \mathcal{X}_\eta \times \mathcal{X}_\zeta = \mathcal{X}_\delta, \\ \mathbf{u}_\delta^T &= \begin{bmatrix} \dot{\xi} & \dot{\eta} & \dot{\zeta} \end{bmatrix} \in \mathcal{U}_\delta, \end{aligned}$$

and $F = 0$. For the model, we use the (desired) actuator rates $\dot{\xi}, \dot{\eta}, \dot{\zeta}$ as inputs and have the sampling period $\tau = 50\,\mathrm{ms}$. The set of admissible state-input pairs is then $\mathcal{Z} = \mathcal{X} \times \mathcal{X}_\delta \times \mathcal{U}_\delta$. Note that, although we do not model the actuator dynamics of (8.1) in order to cut down the a priori knowledge, we limit the actuator rates such that $\left|2\pi f\,(\delta^+ - \delta(t))\right| \leq \dot{\delta}_{\max}$ for all $t \in [0; \tau)$; i.e.,

$$\mathcal{U}_\delta = \left[-\frac{\dot{\delta}_{\max}}{2\pi f \tau}; +\frac{\dot{\delta}_{\max}}{2\pi f \tau}\right]^3.$$

Finally, we denote the combined state vector by

$$\mathbf{x} = \begin{bmatrix} \mathbf{x}_{8\mathrm{e}} \\ \hdashline \mathbf{x}_\delta \end{bmatrix},$$

the discrete system by $\mathbf{x}^+ = \mathbf{f}^+(\mathbf{x}, \mathbf{u}_\delta)$, and the steady-state control inputs are $\mathbf{u}_{\delta f} = 0\,°/\mathrm{s}$.

[5] Recall $\mathbf{V}_\mathrm{A}^T = \begin{bmatrix} u & v & w \end{bmatrix}$ and $\boldsymbol{\omega}^T = \begin{bmatrix} p & q & r \end{bmatrix}$.

[6] The subscript $\mathbf{x}_f$ for the target steady-state is not to be confused with the body-axis system, $(\cdot)_\mathrm{f}$.

8.2.1 Tracking-control cost function

For the model-predictive control feedback $\boldsymbol{\mu}_N(\cdot)$, we solve the finite-horizon optimal control problem (II.10) with finite horizon $N = 120$, initial state $\mathbf{x}_0 = \mathbf{x}(t)$, terminal state constaint $\mathcal{X}_f = \{\mathbf{x}_f\}$, and tracking stage cost

$$\ell(\mathbf{x}, \mathbf{u}_\delta) = \frac{1}{2} \left\|\mathbf{x} - \mathbf{x}_f\right\|_{\mathbf{Q}} + \frac{1}{2} \left\|\mathbf{u}_\delta\right\|_{\mathbf{R}} \tag{8.5}$$

with positive-definite weights $\mathbf{Q} \in \mathbb{S}_{11}, \mathbf{R} \in \mathbb{S}_3$. After scaling of states and inputs, we choose the weights $\tilde{\mathbf{Q}} = \mathbb{I}_{11}$ and $\tilde{\mathbf{R}}_3 = \mathbb{I}/100$; the scaling matrices are given in the end of this chapter. Recall, the control feedback $\boldsymbol{\mu}_N(\mathbf{x}(t)) = \hat{\mathbf{u}}_1$ is subject to the optimal solution

$$\left(\hat{\mathbf{x}}_{(\cdot)}, \hat{\mathbf{u}}_{(\cdot)}\right) = \arg\max_{\mathbf{x}_{(\cdot)}, \mathbf{u}_{(\cdot)}} \sum_{k=1}^{N-1} \ell(\mathbf{x}_k, \mathbf{u}_k) \qquad \text{s.t. } \mathbf{x}_{k+1} = \mathbf{f}^+(\mathbf{x}_k, \mathbf{u}_k) \tag{8.6}$$

with $\mathbf{x}_k \in \mathcal{X} \times \mathcal{X}_\delta$, $\mathbf{u}_k \in \mathcal{U}_\delta$ for all $k \in \{0, \ldots, N\}$ and $\mathbf{x}_N = \mathbf{x}_f$. Furthermore, the tracking cost function in (8.5) is positive-definite. Asymptotic stability of the nominal closed-loop dynamics hence follows by Theorem II.4 under the assumption of weak controllability (Assumption II.5).

8.2.2 Nominal closed-loop response

Evaluating the closed-loop behaviour of the nominal model provides first insights into the offered upset recovery strategies. Fig. 8.3 therefore shows the nominal recovery trajectories for the initial steep spiral and oscillatory spin conditions. Here, air speed V_A and angle of attack α have been calculated afterwards based on the velocity components in the body axis system.

The nominal aircraft model can be said to be fully recovered both from steep spiral and oscillatory spin after 15 s. Furthermore, as it is seen often in the literature, the speed of the aircraft is initially increased in both manoeuvres to gain lift. For spin recovery with its initially low airspeed and high angle of attack (compared to the spiral initial condition as well as the target steady-state), the angle of attack too is increased first before driven down and held roughly constant below 15° until the bank angle is recovered (ca 3 s to 5 s into the manoeuvres). After the bank angle is level, the angle of attack is reduced well under the trim value and the desired longitudinal flight condition is subsequently attained. Perhaps counter-intuitively, the bank angle during recovery from oscillatory spin, although initially positive (i.e., banking to star board), is driven beyond −30° (towards port) before recovered. We will observe this behaviour also in the high-fidelity simulation. At the lowest bank angle, the angle of attack of both manoeuvres is lowered to a temporary minimum and it is only after that point in time that the air speed is increased.

∾

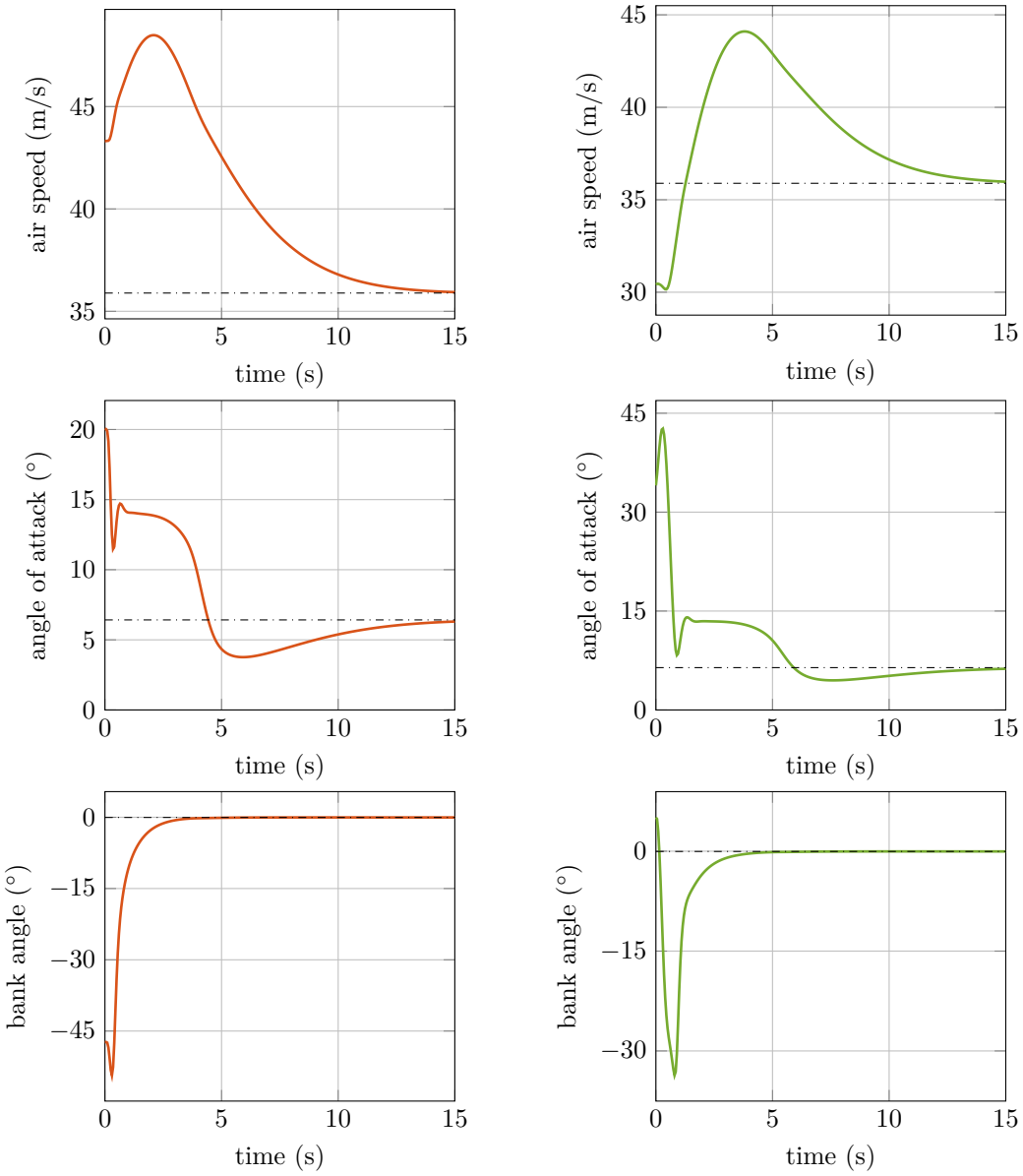

(a) Recovery from steep spiral.

(b) Recovery from oscillatory spin.

Figure 8.3: Nominal NMPC strategies for recovery from steep spiral and oscillatory spin upsets.

8.3 Simulation Results

We are now going to simulate the tracking-control MPC strategy, with the nominal piecewise polynomial model for prediction, embedded into the high-fidelity GTM simulation. The Simulink instance of the latter uses a fixed-step `ode3` solver operating at a frequency of 200 Hz, 10 times faster than the discrete prediction model ($\tau^{-1} = 20\,\text{Hz}$). The optimal control problem is still solved at the lower frequency of 20 Hz and the control input is subsequently hold constant in between. The optimal control inputs, the actuator rates returned by $\boldsymbol{\mu}_N(\cdot)$, are converted into the deflection commands as

$$\delta_{\text{cmd}}(t) = \delta(t_0) + \tau\,\dot{\delta}_{\boldsymbol{\mu}} \tag{8.7}$$

for all $t \in [t_0; t_0 + \tau)$ if $\dot{\delta}_{\boldsymbol{\mu}}$ is the MPC feedback for $\mathbf{x}(t_0)$. As the time constant of (8.1) is smaller than τ, the actuators will not reach the commanded deflection within one period of the MPC feedback. This adds to disparity between the nominal model and simulation. Furthermore, the simulation computes the dynamic coefficients using the hybrid Kalviste method (Murch and Foster 2007, p. 4), whereas the piecewise polynomial model directly evaluates the aerodynamic coefficients for the normalised body rates $\hat{p}, \hat{q}, \hat{r}$.

The simulation has been given a "head start," that is, the model-predictive controller engages first for $t = \tau$.

8.3.1 Recovery from steep spiral

Fig. 8.5 shows the aircraft states during simulated recovery from the steep spiral upset condition. Air speed and and aerodynamic angles were calculated post-simulation based on the components of the velocity vector in the body axis system. The figure further details the state values predicted by MPC for the next step, i.e., $\hat{\mathbf{x}}(t) = \hat{\mathbf{x}}_1$ for $t \in [t_0; t_0 + \tau)$ if $\hat{\mathbf{x}}_{(\cdot)}$ is the optimal trajectory for $\mathbf{x}(t_0)$. Here, commanded and one-step ahead predicted actuator deflections are equal. A bit surprising, the simulation recovers faster than the nominal model but in a similar manner. Again, the bank angle is recovered first with a medium angle of attack of about 15°. After 4 s, similar to the nominal system response, the aircraft is levelled and the longitudinal flight condition is restored by reducing angle of attack and air speed.

Fig. 8.4 further details the aircraft's flight path and attitude during recovery. Note that the depiction of the aircraft is enlarged here for convenience. We observe that, due to the quick recovery of the bank angle, the spiral recovery constitutes an almost straight manoeuvre without further change of the heading despite the initial rotatory flight condition.

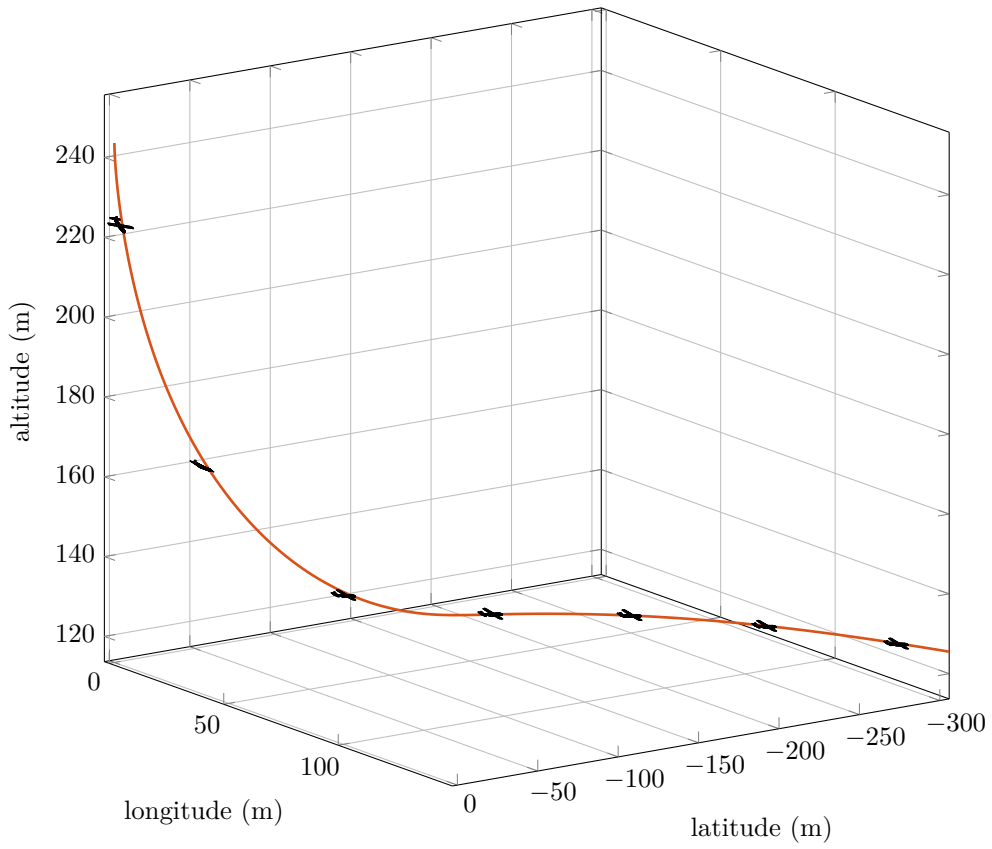

Figure 8.4: Flight path of NMPC recovery from steep spiral upset (aircraft *not* to scale).

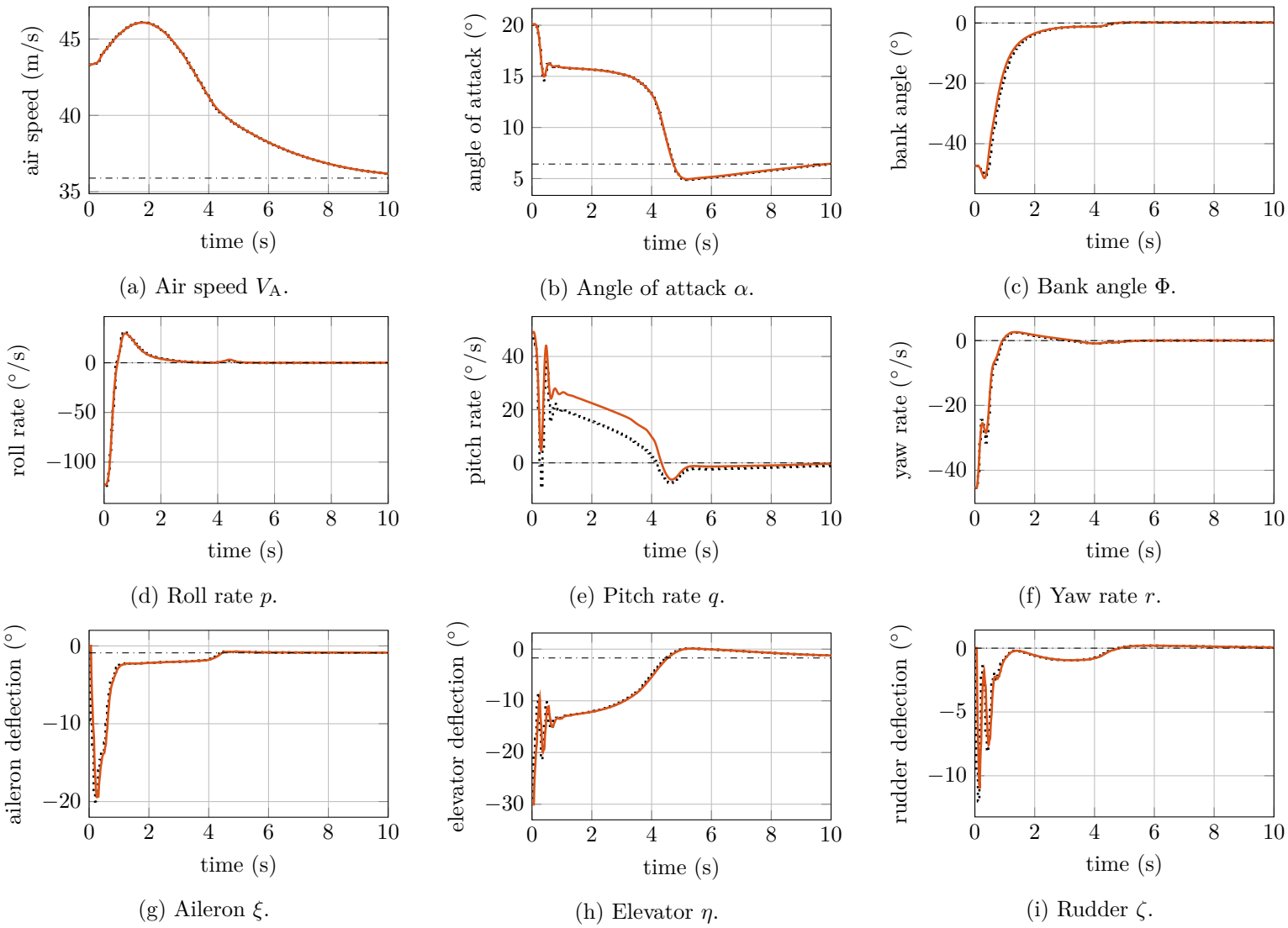

(a) Air speed V_A.

(b) Angle of attack α.

(c) Bank angle Φ.

(d) Roll rate p.

(e) Pitch rate q.

(f) Yaw rate r.

(g) Aileron ξ.

(h) Elevator η.

(i) Rudder ζ.

Figure 8.5: Simulated NMPC recovery for steep spiral upset. Simulation in solid (——), one-step prediction dotted (·····).

8.3.2 Recovery from oscillatory spin

As depicted in Fig. 8.7, for oscillatory spin, too, the simulated recovery is faster than the nominal model but otherwise behaves similar. It should be noted here that, due to the delayed engagement of the MPC feedback only after one period τ and the fact that the oscillatory spin constitutes a periodic motion, the first state of the simulated NMPC recovery has been slightly evolved compared to the initial condition of the aircraft simulation, which has coincided with the initial condition for the nominal NMPC recovery. During early restoration of the bank angle, the aileron operates at this lower limit for almost 400 ms but is moved to a near-neutral position soon after. When the aircraft restores its angle of attack, after the lateral motion has been kept close to the trim condition for some time, however, we observe a spike in the lateral motion initiated by a sharp deflection of ailerons and rudder. It is only afterwards that, together with the angle of attack, the lateral motion is fully restored. Yet, this aberration does not seem to have much impact on the flight path of oscillatory spin recovery, as Fig. 8.6 shows. The flight path further reveals a quick recovery of the lateral spin motion.

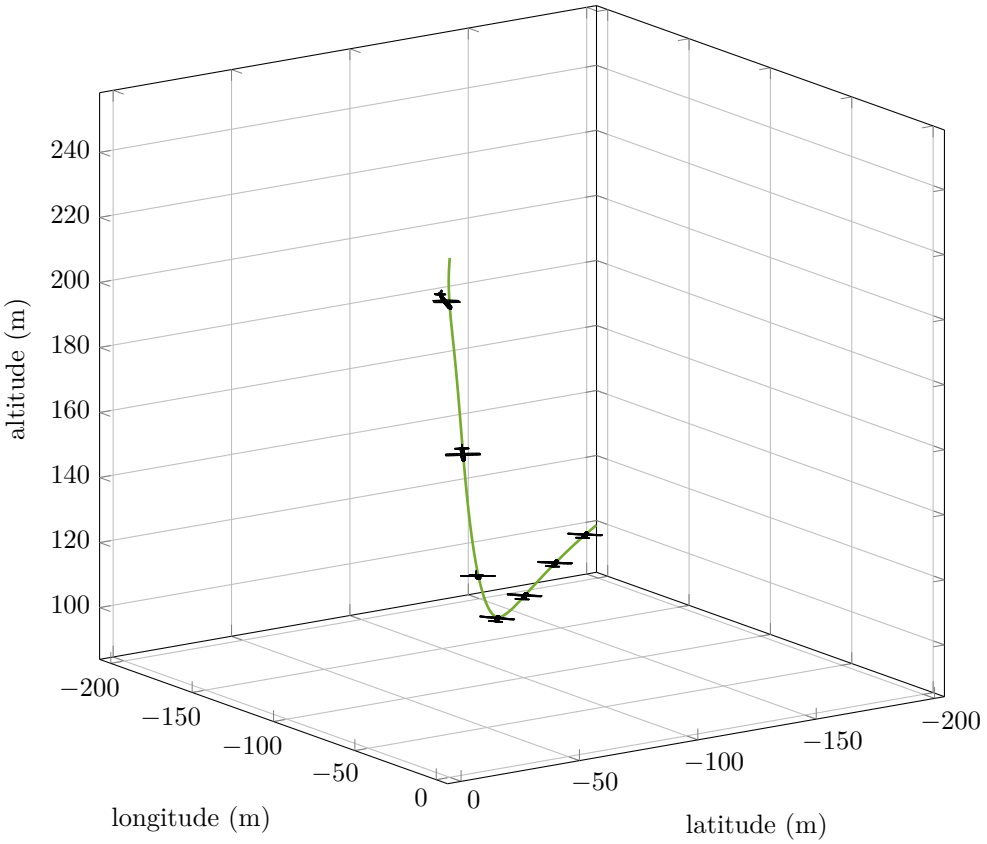

Figure 8.6: Flight path of NMPC recovery from oscillatory spin upset (aircraft *not* to scale).

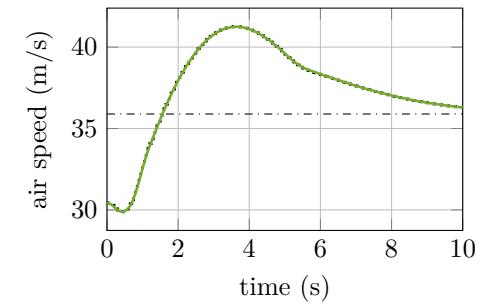

(a) Air speed V_A.

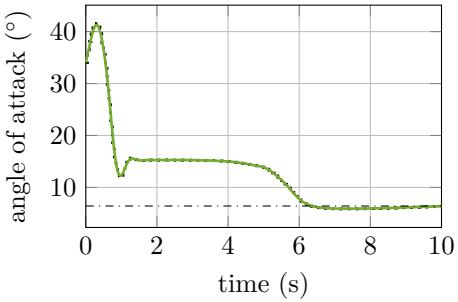

(b) Angle of attack α.

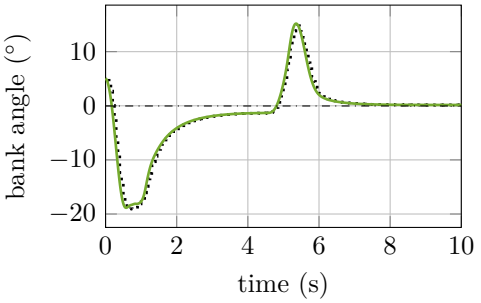

(c) Bank angle Φ.

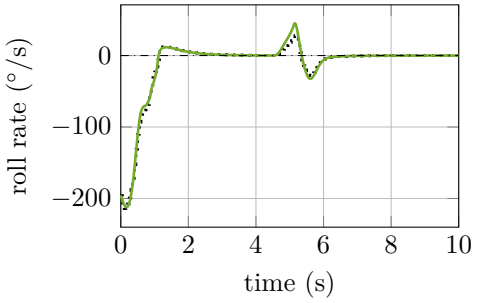

(d) Roll rate p.

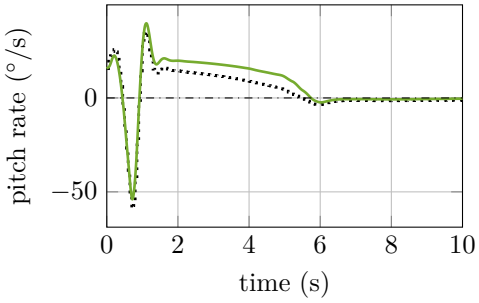

(e) Pitch rate q.

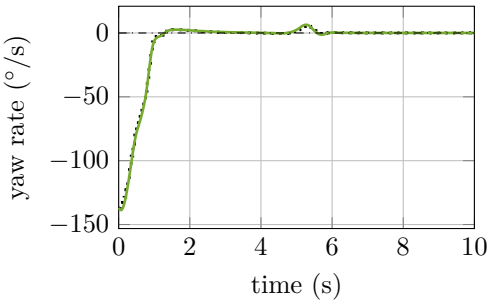

(f) Yaw rate r.

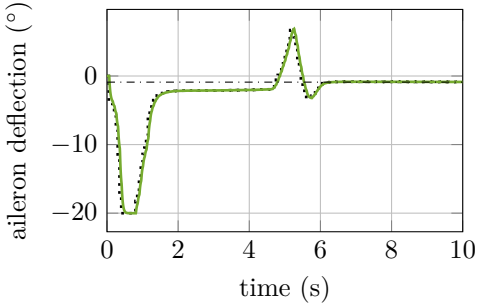

(g) Aileron ξ.

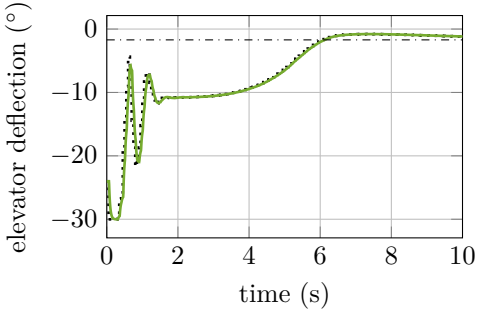

(h) Elevator η.

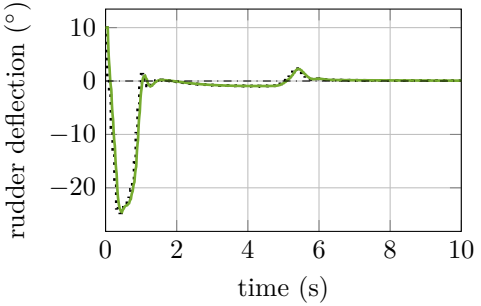

(i) Rudder ζ.

Figure 8.7: Simulated NMPC recovery for oscillatory spin upset. Simulation in solid (——), one-step prediction dotted (·····).

8.3.3 Discussion

Overall, the piecewise polynomial model has well predicted the one-step ahead future aircraft states during recovery from steep spiral and oscillatory spin. During both manoeuvres, however, we observe a stark disparity between the predicted and actual pitch rates while the bank angle is recovered. Here, angle of attack and elevator deflection both are roughly constant with $\alpha = 15°$ and $\eta = -10°$. Comparison of look-up table data and polynomial model for the pitch-moment coefficient C_m, in Fig. 8.8, reveals a highly inaccurate model for these conditions. It is worth noting that polynomials of higher degrees could improve model and thus prediction.

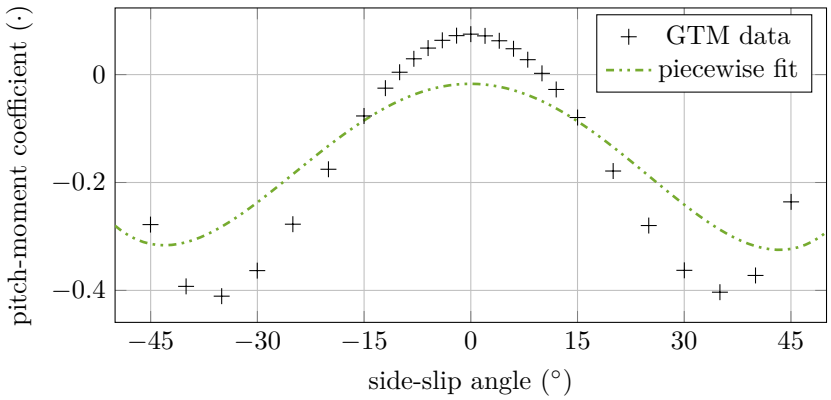

Figure 8.8: Piecewise polynomial C_m model over β for $\alpha = 15°$, $\eta = -10°$.

It might be interesting to further compare the optimising tracking MPC (NMPC) recovery strategies to switching control approaches such as presented by Engelbrecht et al. (2013) or Yildiz et al. (2019). In fact, the NMPC recovery reveals some sequential elements for the recovery of angle of attack and side-slip, reduction of roll and yaw rate, as well as bank angle restoration.[7] First, angle of attack and side-slip[8] are reduced – yet not recovered – and the body rates are regulated. Only after restoration of the bank angle angle of attack and side-slip, too, are fully recovered. In that, the NMPC recovery contrasts the approach of Engelbrecht et al. which emphasised the recovery of aerodynamic angles over attitude (Engelbrecht et al. 2013, pp. 4 and 13–15). The work of Yildiz et al., on the other hand, focused on the regulation of body rates first before recovering all three angle of attack, side-slip angle, and bank angle (Yildiz et al. 2019, pp. 11 and 12). As in the switching approaches, the NMPC recovery restores air speed last.

[7] We omit pitch angle and rate from this discussion, since both are tightly coupled to the reduction and recovery of the angle of attack.

[8] The side-slip angle is not shown in Figs. 8.5 and 8.7.

8.4 Concluding Remarks

The lower recovery time of the simulation compared to the nominal model indicates that the aircraft is, in fact, rather well-behaving in terms of spiral and spin upsets. Indeed, previous analysis revealed that reduction of the angle of attack suffices for spiral recovery (Gill et al. 2013, p. 1836) and neutral position of the rudder leads to the relaxation of oscillatory spin into a spiral motion (see footnote 3 above). Nevertheless, the use of MPC seems to be advantageous for optimal recovery trajectories. Further application of economic MPC for optimal recovery, which comes with an increased computation time (cf. Tab. 7.1), as well as algebraic analysis of the six-degrees-of-freedom dynamics remain future work. The presented, successful recovery of the high-fidelity GTM simulation shows that the piecewise model is as well sufficiently accurate, as the mode-predictive control approach robust against uncertainties, in order to recovery the aircraft despite the immanent model disparity. Of course, this demonstration is not a conclusive verification of necessary robustness, which thus remains for future work. Beyond Monte-Carlo simulations, the natural theoretic entry point for the discussion of robustness is the notion of input-to-state stability (e.g., Limon et al. 2009, p. 6).

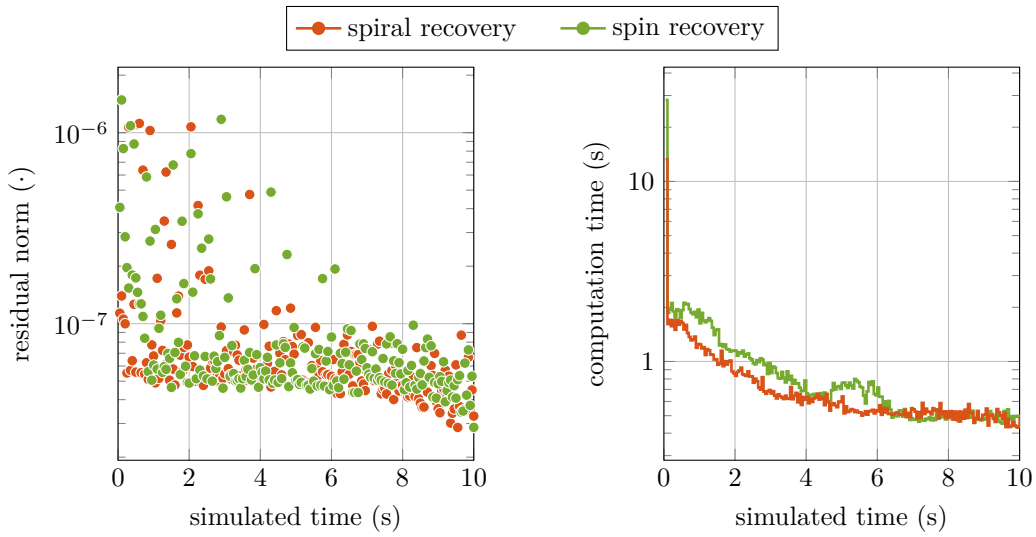

(a) Residual norm $\|\mathbf{F}_{\mathrm{NR}}\|$.

(b) Computation time T_{CPU}.

Figure 8.9: Details of the NMPC simulation. Computation time accuracy ±10 ms (Intel Core i7, 3 GHz, 16 GB).

We further discuss details of simulation and model:

Simulation details We have solved the optimal control problem in Eq. (8.6) using the nonlinear interior-point solver `Ipopt` (Wächter and Biegler 2006). Here, the functions necessary to solve the problem, such as the objective function $\mathcal{J}_N(\cdot,\cdot)$ of (II.10) as well as its gradient vector and Hessian matrix, were compiled into MATLAB's binary `mex`

file format in order to increase evaluation speed. The computed optimal trajectories $\hat{\mathbf{x}}'_{(\cdot)}, \hat{\mathbf{u}}'_{(\cdot)}$ of $\mathbf{x}(t_0)$ for a time t_0 are subsequently used as initial guess for $\mathbf{x}(t_0 + \tau)$. Thus, we are able to reduce the time for computing the optimal control feedback below 1 s in average; only the first optimal control problem, for which no proper initial guess exists, requires between 10 s and 30 s (Fig. 8.9). Further reduction of the computation times is imperative for future work integrating model-predictive recovery strategies into real aircraft systems, in particular if economic MPC is to be used for altitude-minimal recovery.

Model details The singular non-differentiable point of the piecewise polynomial aerodynamic models (namely, at α_0) were again smoothened by the Heaviside step function $\mathcal{H}(\alpha) = \frac{1}{1+e^{-2\alpha/\nu}}$ and the parameter ν has been reduced from $\frac{\pi}{36}$ for the first iteration down to $\frac{\pi}{576}$ for the fifth and all following iterations. States and inputs of the discrete nonlinear dynamics are scaled by

$$\begin{aligned}
\mathbf{D}_{\mathbf{x}_{8\mathrm{e}}} &= \mathrm{diag}(40\,\mathrm{m/s}, 25\,\mathrm{m/s}, 35\,\mathrm{m/s}, 50\,^\circ\mathrm{/s}, 100\,^\circ\mathrm{/s}, 50\,^\circ\mathrm{/s}, 30^\circ, 45^\circ)\,, \\
\mathbf{D}_{\mathbf{x}_\delta} &= \mathrm{diag}(15^\circ, 20^\circ, 25^\circ)\,, \\
\mathbf{D}_{\mathbf{u}_\delta} &= \mathrm{diag}(150\,^\circ\mathrm{/s}, 150\,^\circ\mathrm{/s}, 150\,^\circ\mathrm{/s})\,,
\end{aligned}$$

respectively.

A lemma for weak controllability

In Chapters 7 and 8 we have made, without further justification, the assumption of weak controllability in order to proof stability of model-predictive feedback control with a singular terminal state constraint $\mathcal{X}_f = \{\mathbf{x}_f\}$ (cf. Theorem II.4 and Assumption II.5). We will see now that this assumption was indeed reasonable. Namely, we shall proof that local controllability around $\mathbf{x}_f$ within a non-singular set satisfying the input constraints implies *weak controllability*.

Lemma. *Let $(\mathbf{x}^*, \mathbf{u}^*) \in \mathcal{Z}$ be an admissible stationary solution of the system $\mathbf{f}^+$ and $N \in \mathbb{N}_+$; if there are a set $\mathcal{X}_E \subset \mathcal{X}$ that contains $\mathbf{x}^*$ in its interior, a local control law $\boldsymbol{\kappa}_f \colon \mathcal{X} \to \mathcal{U}$, and a function $\alpha \in \mathcal{K}_\infty$ such that for all $\mathbf{x} \in \mathcal{X}_E$ there is a trajectory $\check{\mathbf{x}}_{(\cdot)}$ with $\check{\mathbf{x}}_0 = \mathbf{x}$, $\check{\mathbf{x}}_N = \mathbf{x}^*$, and for all $k \in \{0, \dots, N-1\}$*

$$\check{\mathbf{x}}_{k+1} = \mathbf{f}^+(\check{\mathbf{x}}_k, \boldsymbol{\kappa}_f(\check{\mathbf{x}}_k))\,, \tag{8.8}$$

$$(\check{\mathbf{x}}_k, \boldsymbol{\kappa}_f(\check{\mathbf{x}}_k)) \in \mathcal{Z}, \tag{8.9}$$

$$|\boldsymbol{\kappa}_f(\check{\mathbf{x}}_k) - \mathbf{u}^*| \leq N^{-1}\alpha(|\mathbf{x} - \mathbf{x}^*|) \tag{8.10}$$

then $(\mathbf{x}^*, \mathbf{u}^*)$ and $\mathcal{X}_N$ satisfy Assumption II.5.

For simplicity, we assume without loss of generality that $\mathbf{x}^* = 0$, $\mathbf{u}^* = 0$. Assumption II.5 now reads that, for each $\mathbf{x} \in \mathcal{X}_N$,

$$\sum_{k=1}^{N} |\mathbf{u}_k| \leq \gamma(|\mathbf{x}|)\,,$$

where $\mathbf{u}_{(\cdot)} \in \mathcal{U}^N$ is a control sequence that drives $\check{\mathbf{x}}_0 = \mathbf{x}$ to $\check{\mathbf{x}}_N = \mathbf{x}_f$ and $\gamma \in \mathcal{K}_\infty$ is a function independent of the choice of $\mathbf{x}$. To construct such a function $\gamma(\cdot)$ making use of $\boldsymbol{\kappa}_f$, $\mathcal{X}_E$, and $\alpha(\cdot)$ will proof our lemma. To this extent, we choose a positive number $A_0 > 0$ satisfying

$$|\mathbf{x}| \leq A_0 \Rightarrow \mathbf{x} \in \mathcal{X}_E. \tag{8.11}$$

Proof. Let $\boldsymbol{\kappa}_f$, $\mathcal{X}_E$, and $\alpha(\cdot)$ satisfy the sufficient condition and denote $\bar{u} = \max_{\mathbf{u} \in \mathcal{U}} |\mathbf{u}|$. We define $\gamma(\cdot)$ piecewise as

$$\gamma \colon y \mapsto \alpha(y) + N\bar{u} \cdot \begin{cases} y/A_0 & \text{if } 0 \leq y < A_0, \\ 1 & \text{if } y \geq A_0. \end{cases}$$

Since $\alpha \in \mathcal{K}_\infty$, $\gamma(\cdot)$ is indeed continuous, strongly monotonic increasing, radially unbounded, and $\gamma(0) = 0$; that is, $\gamma \in \mathcal{K}_\infty$, too. Furthermore, if $|\mathbf{x}| \geq A_0$, we have immediately $\sum_{k=1}^{N} |\mathbf{u}_k| \leq N\bar{u} \leq \gamma(|\mathbf{x}|)$ for any $\mathbf{u}_{(\cdot)}$ with $\left(\mathbf{x}, \mathbf{u}_{(\cdot)}\right) \in \mathcal{Z}_N$. On the other hand, for any $|\mathbf{x}| < A_0$ (i.e., $\mathbf{x} \in \mathcal{X}_E$) there is a trajectory $\check{\mathbf{x}}_{(\cdot)}$ as above such that

$$\sum_{k=1}^{N} |\boldsymbol{\kappa}_f(\check{\mathbf{x}}_k)| \leq \alpha(|\mathbf{x}|) \leq \gamma(|\mathbf{x}|) \tag{8.12}$$

and $(\check{\mathbf{x}}_k, \boldsymbol{\kappa}_f(\check{\mathbf{x}}_k)) \in \mathcal{Z}$ for all $k \in \{0, \dots, N\}$. Hence, Assumption II.5 holds. □

We conclude our brief discussion with some remarks. First, for the existence of $\bar{u}$ we made use of the compactness of $\mathcal{U}$.[9] The accumulated control expenses then are trivially bounded by $N\bar{u}$; the difficulty here is to drive the system into the target condition in *finite* time while the necessary control inputs *diminish* when approaching steady-state. With an argument similar to our reasoning for local stability, the system $\mathbf{f}^+$ behaves in a small environment $\mathcal{E}$ around the stationary solution $(\mathbf{x}^*, \mathbf{u}^*)$ similar to the linearisation $\Delta\mathbf{x}^+ = \mathbf{A}\Delta\mathbf{x} + \mathbf{B}\Delta\mathbf{u}$, where $\Delta\mathbf{x} = \mathbf{x} - \mathbf{x}^*$ and $\Delta\mathbf{u} = \mathbf{u} - \mathbf{u}^*$. If now the linear system is controllable, namely, the linear equalities (Abel 2013, p. ?)

$$-\mathbf{A}^n (\mathbf{x} - \mathbf{x}^*) = \underbrace{\begin{bmatrix}\mathbf{B} & \mathbf{AB} & \cdots & \mathbf{A}^{n-1}\mathbf{B}\end{bmatrix}}_{=_{\text{def}}\boldsymbol{\mathcal{C}}} \begin{bmatrix}\Delta\mathbf{u}_{n-1} \\ \vdots \\ \Delta\mathbf{u}_0\end{bmatrix}, \tag{8.13}$$

where n is the number of states, have a unique solution $\Delta\check{\mathbf{u}}_{(\cdot)}$ for any $\mathbf{x} \in \mathcal{E}$, we say $\mathbf{f}^+$ is *locally controllable in* $\mathcal{E}$. In this case, the controllability matrix $\boldsymbol{\mathcal{C}}$ has full rank and the control sequence $\mathbf{u}_{(\cdot)}$ to drive $\mathbf{f}^+$ in n steps from $\mathbf{x} \in \mathcal{E}$ to $\mathbf{x}^*$ is subject to the mapping $\mathbf{u}^* - \boldsymbol{\mathcal{C}}^{-1}\mathbf{A}^n (\mathbf{x} - \mathbf{x}^*) + g(\mathbf{x} - \mathbf{x}^*)$ with the so-called "high-order function" g (Chen and Narendra 2004, Theorem 3, p. 665).[10] Thus, if $(\mathbf{x}^*, \mathbf{u}^*)$ is contained in the interior of $\mathcal{Z}$ and $N \geq n$, we can choose $\mathcal{X}' \subseteq \mathcal{E}$ such that $\mathbf{u}_k \in \mathcal{U}$ for all $k \in \{0, \ldots, n, \ldots, N\}$ and $\mathbf{x} \in \mathcal{X}'$;[11] furthermore, the input cost $\sum_{k=1}^{N} |\mathbf{u}_k - \mathbf{u}^*|$ is bounded by a $\mathcal{K}_\infty$-function $\alpha(|\mathbf{x} - \mathbf{x}^*|)$. That is, local controllability implies weak controllability.

In this study, both the longitudinal equations of motion of Cumulus as well as the six-degrees-of-freedom equations of motion of the GTM were locally controllable around the chosen normal-flight trim conditions. Hence, we were right to assume weak controllability for stability of the synthesised model-predictive feedback.

[9] This is a classic assumption in MPC theory (Section II.2); in Chapters 7 and 8 we have therefore defined $\mathcal{U}$ by closed and bounded intervals.

[10] Chen and Narendra (2004, p. 664) define a *high-order function* $g(\cdot)$ to be continuous, $g(\mathbf{0}) = \mathbf{0}$, and

$$\frac{\partial g}{\partial \mathbf{x}}(\mathbf{0}) = \mathbf{0}.$$

In this case, $|g(\cdot)|$ can be locally bounded by a $\mathcal{K}_\infty$ function.

[11] Note that $\mathbf{u}_k = \mathbf{u}^*$ for $n \leq k \leq N$.

Chapter 9

Conclusions

Upset flight conditions are characterised by highly nonlinear aerodynamics and unstable or undesired attractive equilibria. Upset aircraft are prone to accidents due to *in-flight loss-of-control* which, albeit rare, contribute most to fatal accidents in civil aviation. For this reasons, in-flight loss-of-control constitutes a severe threat to both manned and unmanned aviation and recovery from upset flight conditions is highly imperative. However, recovery approaches are challenged by uncertain aerodynamic models for upset flight dynamics, nonlinear traits, and state and input constraints. In this thesis, we have hence recalled, applied, and extended methods to recover an aircraft from an upset condition into its normal flight envelope. For application, we have considered the well-known Generic Transport Model (GTM) as well as a smaller unmanned aircraft named *Cumulus One* which is capable of stable flight in deep-stall trim conditions. These aircraft differ not only in the lateral stability post stall, but in their modeling premises: while the GTM comes with extensive aerodynamic data from wind-tunnel and flight tests, for Cumulus One we were limited to CFD simulations.

Following a review of the extensive literature on upset prediction, prevention, and recovery, we have initially presented a new modeling technique for piecewise polynomial models of the aerodynamic coefficients. We have then used this technique to create a model of the GTM based on the provided windtunnel and flight test data and have compared equilibria of the piecewise model to trim conditions of the GTM simulation. We have also demonstrated the use of a previously presented sum-of-squares programming techniques to estimate the region of attraction of the piecewise short-period motion. Moreover, we have investigated the deep-stall dynamics of Cumulus One in order to derive a piecewise polynomial model of its aerodynamics, too. Here, we were limited to data of static continuous fluid dynamics simulations. We have thus proposed further models of the dynamic derivatives and elaborately discussed the implied behaviour during transition into deep-stall, eventually optimising the model parameters against recorded flight data of deep-stall transitions.

Stability of deep-stall recovery has been verified using sum-of-squares programming to estimate the region of attraction of the normal flight condition under local control feedback. We have further extended the sum-of-squares methodology in order to synthesise feedback laws which enlarge the region of attraction towards deep-stall flight conditions, thus certifying stable recovery by control design, and proposed a backwards-reachability scheme that facilitates the representation of deep-stall flight. Based on our initial ideas for piecewise sum-of-squares analysis of the GTM's region of attraction, we have proposed an improved algorithm for stability analysis of multivariate spline systems.

Where upset recovery is subject to measures of optimality, iterative solutions of optimal control problems led to model-predictive control (MPC). Here, we formulated the problem of minimising the loss-of-altitude during recovery within the economic MPC framework. Using sum-of-squares, we were able to prove dissipativity of the control system and thus stability of the designed MPC feedback. Despite a regularisation penalty necessary to ensure dissipativity, this strategy has been advantageous when compared to linear and nonlinear tracking MPC strategies. Finally, we have applied MPC to recover an aircraft from steep spiral and oscillatory spin conditions, which we have demonstrated within the high-fidelity GTM simulation, using the piecewise polynomial aerodynamics as uncertain prediction model. As sum-of-squares do not scale well with an increasing number of state variables, we could not simply expand the EMPC scheme but resorted to tracking MPC here.

We shall conclude the dissertation discussing the results, drawing connections in between, and indicating future work. Finally, we summarise its major contributions.

9.1 Discussion

In this thesis, we have examined in deep different techniques for modeling, analysis, and control of aircraft upset dynamics and recovery of a vehicle into its normal flight envelope. Hereby, the vehicle was assumed to operate fully autonomous and the flight control system to have exclusive authority over the control surfaces. This setting is opposed by the, in the literature considering commercial aviation more common, case of recovery by the pilots while guided by the flight computer. Stability analysis of guided recovery approaches might be performed by means of this thesis with the pilot activity in feed-back loop, yet in this case the actions and reactions of the pilots, in particular their possibly imperfect and delayed behaviour, must be taken into further account. Such an approach, for example, has been followed by Richards et al. (2017), who provided a separate pilot model (Richards et al. 2017, pp. 921 and 922). It should be noted though, that modeling pilot behaviour as part of a prediction model for MPC recovery guidance might lead to an attempted inversion of this dynamics in the optimised recovery strategies.

Piecewise modeling techniques

Essentially constituting a simple spline model with single knot, the piecewise polynomial modeling technique presented in Chapter 3 turned out to be a tractable method and well-suited to improve the accuracy of polynomial-based aerodynamic models while keeping the cost of analysis such as sum-of-squares programming affordable. Yet, further improvements are thinkable that do not change the underlying structure of the model definition. Namely, so far we have modeled the aerodynamics piecewise along a

hyperplane through α_0 and orthogonal to the angle of attack-axis,

$$C_{\odot}(\alpha,\ldots) = \begin{cases} C_{\odot}^{pre}(\alpha,\ldots) & \text{if } \alpha \leq \alpha_0, \\ C_{\odot}^{post}(\alpha,\ldots) & \text{if } \alpha > \alpha_0, \end{cases}$$

and argued that the change of dynamics around the stall angle of attack suggests a piecewise model. This choice of a switching surface facilitated both the derivation of α_0 as free parameter of the C_{L}-over-α model[1] and the further implementation of equality constraints in α_0. The argument of switching dynamics, however, does not rely on a planar switching surface and indeed, one would imagine the stall angle of attack (and thus a change of dynamics) to depend on further parameters such as side-slip angle or elevator deflection. The following, piecewise model would be able to provide a better fitting while still obeying the structure of piecewise polynomial model with single switching surface:

$$C_{\odot}(\alpha,\beta,\ldots) = \begin{cases} C_{\odot}^{pre}(\alpha,\beta,\ldots) & \text{if } \varphi(\alpha,\beta) \leq 0, \\ C_{\odot}^{post}(\alpha,\beta,\ldots) & \text{if } \varphi(\alpha,\beta) > 0, \end{cases} \tag{9.1}$$

where $\varphi(\cdot)$ is a strongly monotonous, polynomial function in α and β. On the other hand, obtaining a suitable φ as well as ensuring continuity along this surface for all (sub)-models is unlike more difficult. The computation of such an advanced model might even require the application of further preprocessing steps such as classification of the identification data as in, e.g., Scampicchio et al. (2018), or the use of neural networks. The necessity of continuity of all piecewise coefficient models along a chosen surface $\varphi(\cdot) \equiv 0$ further requires a careful selection of the polynomial fitting method.

Where computation time and resource consumption is not a major concern but model accuracy, multivariate splines such as proposed by de Visser et al. (2009) provide a powerful alternative to simple piecewise polynomial models. We hold that all applications of this thesis can be augmented for multivariate spline models using the ideas of Chapter 5. Given the fact that stability certificates are to be computed only once, it can be envisaged to have a control approach designed based on simple piecewise polynomial model for speed yet eventually certified against a spline model for accuracy. The further potential of *adaptive* spline models (cf. Tol et al. 2016) is especially promising for model-based predictive control strategies. Moreover, an extended local analysis of hybrid (polynomial) systems allows for certification of recently published, state-based switching recovery control strategies (such as Engelbrecht 2016; Yildiz et al. 2019). To this extend, the spline system definition of Section 5.3 can be modified to allow for unilateral switching surfaces.

Sum-of-squares stability analysis

Local stability analysis and region of attraction estimation using sum-of-squares programming have been extensively discussed within this and previous studies, usually founded in Lyapunov's stability theory and La Salle's subsequent theory of invariant

[1] Or C_{X}-over-α with forces in the body axis system.

sets. The latter stated that the level set of a Lyapunov-candidate function, $\mathcal{V}(\cdot) \equiv \gamma$ for some $\gamma > 0$, bounded an invariant subset of the region of attraction if $\dot{\mathcal{V}}(\mathbf{x})$ is negative definite for all $\mathbf{x}$ where $\mathcal{V}(\mathbf{x}) \leq \gamma$. We have encoded this constraint as the SOS problem

$$\mathfrak{s} \vdash \left\{ \mathbf{x} \,\middle|\, \mathcal{V}(\mathbf{x}) \leq \gamma \right\} \subseteq_\Sigma \left\{ \mathbf{x} \,\middle|\, \dot{\mathcal{V}}(\mathbf{x}) \leq -\epsilon \left\| \mathbf{x} \right\|_2^2 \right\} \tag{9.2}$$

or, equivalently,

$$\mathfrak{s} \ (\mathcal{V} - \gamma) - \dot{\mathcal{V}} - \epsilon \left\| \mathbf{x} \right\|_2^2 \in \Sigma \left[\mathbf{x} \right] \tag{9.3}$$

with $\mathfrak{s} \in \Sigma \left[\mathbf{x} \right]$ and $\epsilon > 0$ making use of the Positivstellensatz.
A further, interesting insight can now be gained by looking at Zubov's equation with the formulation above in mind: Recall that $\mathcal{V}(\cdot) \equiv \gamma$ bounds the *true* region of attraction if

$$\dot{\mathcal{V}}(\mathbf{x}) + \epsilon \left\| \mathbf{x} \right\|_2^2 = -\mathfrak{s}(\mathbf{x}) \ (\gamma - \mathcal{V}(\mathbf{x})) \tag{9.4}$$

for all $\mathbf{x} \in \mathcal{X}$, replacing the positive definite multiplier of Eq. (I.20) by $\mathfrak{s} \in \Sigma \left[\mathbf{x} \right]$ and $\epsilon > 0$. Similarly, we might require

$$\left.\begin{array}{r} \dot{\mathcal{V}} + \epsilon \left\| \mathbf{x} \right\|_2^2 + \mathfrak{s}_+ \ (\gamma - \mathcal{V}) \\ -\dot{\mathcal{V}} - \epsilon \left\| \mathbf{x} \right\|_2^2 + \mathfrak{s}_- \ (\mathcal{V} - \gamma) \end{array}\right\} \in \Sigma \left[\mathbf{x} \right] \tag{9.5}$$

with $\mathfrak{s}_+, \mathfrak{s}_- \in \Sigma \left[\mathbf{x} \right]$. This, however, is nothing else than to say that $\dot{\mathcal{V}}(\cdot)$ is positive definite in the interior of $\mathcal{V}(\cdot) \equiv \gamma$ but negative in the exterior. With a small relaxation, we can extend the thought to the approximation of inner and outer bounds of the region of attraction, viz.

$$\mathfrak{s}_- \vdash \left\{ \mathbf{x} \,\middle|\, \mathcal{V}(\mathbf{x}) \leq \gamma_1 \right\} \subseteq_\Sigma \left\{ \mathbf{x} \,\middle|\, \dot{\mathcal{V}}(\mathbf{x}) \leq -\epsilon \left\| \mathbf{x} \right\|_2^2 \right\} \tag{9.6}$$

$$\mathfrak{s}_+ \vdash \left\{ \mathbf{x} \,\middle|\, \mathcal{V}(\mathbf{x}) \geq \gamma_2 \right\} \subseteq_\Sigma \left\{ \mathbf{x} \,\middle|\, \dot{\mathcal{V}}(\mathbf{x}) \geq +\epsilon \left\| \mathbf{x} \right\|_2^2 \right\} \tag{9.7}$$

for $0 < \gamma_1 \leq \gamma_2$. Here, Eq. (9.6) is just equivalent to the invariant set of La Salle's; however, it might be more challenging to find a Lyapunov-candidate function that fulfils (9.7), too.

In particular, the region of attraction estimation is powerful to investigate local stability of a passive or controlled aircraft around a given flight condition. With an aircraft being capable to fly at several, possibly continuous trim conditions (compare the bifurcation diagrams in Chapters 3 and 4), this is only a small aspect of the general flight control system. Future research should therefore focus on the dependency and change of the region of attraction on variation of one or multiple parameters: Consider, for the sake of an example, a family of equilibria $(\mathbf{x}_\mu, \mu)$ for a scalar parameter $\mu \in \mathbb{R}$ such that for $\mu^* = 0$, the equilibrium in $\mathbf{x}_0^*$ turns from stable ($\mu < 0$) into unstable ($\mu > 0$); that is, the right-hand side region of attraction $\mathcal{R}_{\mu>0}$ is singular. It is tempting now to assume that for $\mu < 0$, the region of attraction shrinks towards $\mathcal{R}_{\mu\to-0}$; yet, the simple case of a linear system which is either globally stable ($\mathcal{R} = \mathcal{X}$) or not ($\mathcal{R} = \{\mathbf{x}^*\}$)

demonstrates that this cannot be true in general. A possible approach towards the analysis of regions of attraction along a family of trim conditions lies in parametrised polynomial function $\mathcal{V} \in \mathbb{R}[\mathbf{x}, \mu]$ such that $\mathcal{V}(\cdot, \mu)$ is a Lyapunov-candidate function for all (viable) parameters μ. Such functions were considered by, e.g., Papachristodoulou and Prajna (2009) for global robust stability, but the conservativeness of the approach might be challenging. On the other hand, the analysis of region of attraction estimates along the trim conditions seems crucial for further acceptance of sum-of-squares methods for aeronautical control certification.

Model-predictive control considerations

In Chapters 7 and 8, we have bespoken stability of the presented MPC strategies in terms of the set of feasible initial conditions $\mathcal{X}_N$. We have not further considered this set, which gives rise to the closed-loop region of attraction and indeed depends on the horizon length N as well as on the final set $\mathcal{X}_f$, but we can relate it to the safe set discussed by, amongst others, Kwatny et al. (2013). Consider the structural envelope $\mathcal{C} \subset \mathcal{X}$; the operational safe set is defined in infinite discrete time as $\mathcal{X}^{\text{safe}} = \left\{ \mathbf{x} \,\middle|\, \exists \mathbf{u}_{(\cdot)} \subset \mathcal{U}. \forall k. \mathbf{f}^k(\mathbf{x}, \mathbf{u}_{1\cdots k}) \in \mathcal{C} \right\}$ for dynamics $\mathbf{x}^+ = \mathbf{f}(\mathbf{x}, \mathbf{u})$.[2] If, as it is commonly assumed, the final set $\mathcal{X}_f$ itself is a forward-invariant subset of $\mathcal{C}$, we have the following set inclusions:[3]

$$\mathcal{X}_f = \mathcal{X}_0 \subseteq \mathcal{X}_1 \subseteq \cdots \subseteq \mathcal{X}_N \subseteq \mathcal{X}_{N+1} \subseteq \cdots \subseteq \mathcal{X}^{\text{safe}}. \tag{9.8}$$

Here, two questions are of particular interest. First, whether there exist a horizon length N^* such that $\mathcal{X}_{N^*+1} \subseteq \mathcal{X}_{N^*}$; in this case, increasing the horizon length beyond N^* does not further enlarge the region of attraction. And second, whether the final inclusion is in fact strict, $\mathcal{X}_{N\to\infty} \subsetneq \mathcal{X}^{\text{safe}}$; that is, whether there are conditions from which the aircraft can be kept within the operational envelope albeit not recovered for any horizon length. A particular difficulty in the determination of $\mathcal{X}_N$ is the simultaneous problem of *viability* in $\mathcal{C}$ and *reachability* of $\mathcal{X}_f$. Lygeros (2004) introduced the sets of viable, invariant, and reachable states, of which the safe set is a special case, and which are given in discrete time as (based on Lygeros 2004, p. 919)

$$\begin{aligned}
\operatorname{Vib}_N \mathcal{K} &= \left\{ \mathbf{x} \,\middle|\, \exists \mathbf{u}_{(\cdot)} \in \mathcal{U}^N. \forall k \leq N. \quad \mathbf{f}^k(\mathbf{x}, \mathbf{u}_{1\cdots k}) \in \mathcal{K} \right\}, \\
\operatorname{Inv}_N \mathcal{K} &= \left\{ \mathbf{x} \,\middle|\, \forall \mathbf{u}_{(\cdot)} \in \mathcal{U}^N. \forall k \leq N. \quad \mathbf{f}^k(\mathbf{x}, \mathbf{u}_{1\cdots k}) \in \mathcal{K} \right\}, \\
\operatorname{Rec}_N \mathcal{K} &= \left\{ \mathbf{x} \,\middle|\, \exists \mathbf{u}_{(\cdot)} \in \mathcal{U}^N. \exists k \leq N. \quad \mathbf{f}^k(\mathbf{x}, \mathbf{u}_{1\cdots k}) \in \mathcal{K} \right\},
\end{aligned}$$

for some $\mathcal{K} \subset \mathcal{X}$ and $N \geq 0$.[4] Clearly, we have $\mathcal{X}_N \subseteq \operatorname{Rec}_N \mathcal{X}_f$ by definition, yet it does follow immediately that the reaching trajectory also is viable in $\mathcal{C}$. The feasible initial

[2] The $\mathbf{f}^k$-notation was defined in Chapter 7 as $\mathbf{f}^k = \mathbf{f} \circ \cdots \circ \mathbf{f}$.

[3] Recall the definition

$$\mathcal{X}_N = \left\{ \mathbf{x} \,\middle|\, \exists \mathbf{u}_{(\cdot)} \in \mathcal{U}^N. \mathbf{f}^N(\mathbf{x}, \mathbf{u}_{1\cdots N}) \in \mathcal{X}_f \wedge \forall k < N. \mathbf{f}^k(\mathbf{x}, \mathbf{u}_{1\cdots k}) \in \mathcal{C} \right\}$$

for any horizon length $N \geq 0$.

[4] Note that $\mathcal{X} - \operatorname{Rec}_N \mathcal{K} = \operatorname{Inv}_N(\mathcal{X} - \mathcal{K})$ and $\operatorname{Vib}_{N\to\infty} \mathcal{C} = \mathcal{X}^{\text{safe}}$.

conditions are then subject to the lower and upper bounds

$$\mathrm{Rec}_N\,\mathcal{X}_f \cap \mathrm{Inv}_N\,\mathcal{C} \quad \subseteq \quad \mathcal{X}_N \quad \subseteq \quad \mathrm{Rec}_N\,\mathcal{X}_f \cap \mathrm{Vib}_N\,\mathcal{C}, \tag{9.9}$$

although these approximations are likely to be rather vague. Further research should focus on the estimation of $\mathcal{X}_N$ for MPC recovery schemes in order to certify stable operation over the desired upset envelopes.

A further challenge for upset recovery by model-predictive control has turned out to be the computation time necessary to solve the optimal control problem online and in feedback-loop. Foregoing improved solver algorithms and computational power of the flight computer systems, possible solutions are to update the optimal recovery trajectories at a lower frequency (that is, further prediction states and inputs are used for control feedback) or even to compute the full trajectory off-board, ensuring robust tracking by simpler onboard feedback designs.

9.2 Summary

For the past decades, in-flight loss-of-control has remained a severe threat to the safety of aircraft and aerial operations as well as crew and passengers alike. In response, an extensive literature for upset prediction, prevention, and recovery was established. Most of these developments can be divided into experiments with (piloted) aircraft training devices, application of control engineering to high-fidelity models, and advances motivated in system theory. However, these strategies lacked a common, holistic approach. Moreover, the need for verification of the proposed strategies has not been resolved yet, in particular with an increasing number of unmanned and autonomous vehicles to enter the airspaces in near future. This thesis has aimed towards the inclusion of system theoretic approaches for realistic models and thorough verification of their stability.

A piecewise polynomial modeling technique was proposed as simple alternative to multi-variate splines. The established model of the Generic Transport Model turned out to accurately represent the full-envelope aerodynamic coefficients and well predicted a wide range of trim conditions. Yet, the aircraft model was accessible for functional analysis tools such as bifurcation theory and sum-of-squares programming. Moreover, we established an equations-of-motion model for the unmanned aircraft *Cumulus One* based on static continuous fluid dynamics data and we elaborately discussed dynamics and stability during its transition into stable deep-stall flight, as demonstrated in recorded flight tests. Thus, we eliminated the need of extensive wind-tunnel studies, as commonly used to study the dynamics of airliners, which might be not attainable in the scope of small aircraft projects. These two piecewise polynomial aircraft models laid the fundament for the further application of analysis and control methodologies.

Early applications of sum-of-squares programming for investigations of aircraft stability or robustness relied on polynomial models of limited accuracy. The development of a simple yet accurate polynomial-based model motivated further application of sum-of-squares programming for analysis and control of aircraft flight. Thus, we applied the initial framework for Lyapunov-based region-of-attraction estimation to verify stable

recovery from deep stall. An extension of this approach allowed the synthesis of feedback laws which by design ensure stable recovery. The proposed backwards-reachability scheme removed the necessity of a high-dimensional ellipsoidal (or quasi-ellipsoidal) surfaces, of which the specification is nontrivial problem, and replaced it by a single target flight state such as a deep-stall trim condition. Furthermore, we illustrated initial ideas for the efficient application of sum-of-squares programming for Lyapunov-based stability analysis of splines, thus enabling the extension of this thesis' results to highly accurate large-scale models.

Model-predictive control strategies for upset recovery have been promising for their ability to deal with nonlinearities and input constraints of upset conditions as well as for the introduction of optimality measures. Reformulating the problem of upset recovery minimising the loss of altitude as economic MPC strategy, we rigorously proved its stability by computing a minimal regularisation weight using sum-of-squares. Despite the regularisation, the proposed strategy successfully increased the outcoming altitude of the aircraft after recovery from deep stall. We further demonstrated the power of nonlinear tracking MPC for the recovery from steep spiral and oscillatory spin flight modes against the GTM high-fidelity simulation. This also showed the accuracy of the piecewise polynomial model for prediction.

Future work envisages the application of sum-of-squares programming techniques, based on piecewise polynomial or even spline models, for the verification of advanced flight control techniques and upset recovery approaches. The application of sum-of-squares analysis to the six-degrees-of-freedom flight dynamics, which would also enable future verification of EMPC recovery schemes minimising the loss of altitude, continues to be challenging yet highly incentive. With its manifold contributions, this thesis constitutes a first step stone of holistic approaches that combine realistic models, functional analysis for verification, advanced control techniques, and high-fidelity aircraft simulations in order to tackle the problems of in-flight loss-of-control and upset recovery.

Acronyms

AVL Advanced Vortex Lattice method. 79–112

BP Bifurcation Point. 35–37, 79–112
HB Andronov-Hopf bifurcation (*Hopf-bifurcation*) point. 36, 38, 79–112
SN Saddle-node bifurcation point. 36, 38, 39, 79–112

CAST Commercial Aviation Safety Team. 1, 2, 7
CFD Continuous Fluid Dynamics. 77–112, 145–170, 201, 206
COCO Continuation Core and Toolboxes for MATLAB. 55–76, 79–112

FAA Federal Aviation Administration, United States of America. 1, 11, 187

GoF Goodness of Fit. 55–76, 239–255
GTM Generic Transport Model. 3, 4, 11–14, 19–22, 25, 26, 53–197, 200–202, 206, 207, 239–255, 257–269, 275–282

IATA International Air Transport Association. 1
ICAO International Civil Aviation Organization (*Organisation de l'aviation civile internationale*). 1, 2, 7
ISO International Organization for Standardization (*Organisation internationale de normalisation*). 1

LMI Linear Matrix Inequality. 55–76, 239–255
LOA Loss of Altitude. 171, 173–184, 202, 207
LOC-I In-flight Loss-of-control. 1, 2, 7, 9, 10, 143, 145–170, 201, 206, 207
LQR Linear Quadratic Regulator. 11, 13, 134, 145–170
LSQ Linear Least Square. 53, 55–76, 239–255

MPC Model-Predictive Control. 129, 131, 133, 135–139, 171–185, 191–197, 199, 202, 203, 205–207, 275
EMPC Economic (nonlinear) Model-Predictive Control. 137–140, 171, 173–185, 197, 198, 202, 207
r-EMPC Regularised Economic Model-Predictive Control. 141, 142, 173–184
LMPC Linear (tracking) Model-Predictive Control. 173–184
NMPC Nonlinear (tracking) Model-Predictive Control. 137, 139, 171, 173–185, 188–198, 202, 207, 275, 277, 284

NASA National Aeronautics and Space Administration, United States of America. 2, 3, 14, 15, 20, 55–76, 275
NP Nondeterministic Polynomial time complexity. 45, 145–170

List of Figures

List of Tables

Bibliography

Abel, Dirk (2013). *Umdruck zur Vorlesung Regelungstechnik und Ergänzugen (Höhere Regelungstechnik)*. 4th ed. Aachen, DE: Verlagshaus Mainz.

Ahmadi, Amir Ali, Georgina Hall, Antonis Papachristodoulou, James Saunderson, and Yang Zheng (2017). "Improving Efficiency and Scalability of Sum of Squares Optimization : Recent Advances and Limitations". In: *56th IEEE Conference on Decision and Control*. Melbourne, AU, pp. 453–462. DOI: 10.1109/CDC.2017.8263706.

Ahmadi, Amir Ali and Anirudha Majumdar (2018). "DSOS and SDSOS Optimization: More Tractable Alternatives to Sum of Squares and Semidefinite Optimization". In: To appear in *SIAM Journal on Applied Algebraic Geometry*. DOI: arXiv:1706.02586v3. arXiv: 1706.02586.

Ahmadi, Amir Ali and Pablo A. Parrilo (2008). "Non-monotonic Lyapunov functions for stability of discrete time nonlinear and switched systems". In: *47th IEEE Conference on Decision and Control*, pp. 614–621. DOI: 10.1109/CDC.2008.4739402.

Akcal, Ugur, Batuhan Hostas, Nazim K. Ure, and Gokhan Inalhan (2018). "Recoverability Envelope Analysis of Nonlinear Control Laws for Agile Maneuvering Aircraft". In: *2018 AIAA Guidance, Navigation, and Control Conference*. Kissimmee, US-FL: American Institute of Aeronautics and Astronautics. DOI: 10.2514/6.2018-1865.

Alamir, Mazen (2017). "Contraction-based nonlinear model predictive control formulation without stability-related terminal constraints". In: *Automatica* 75, pp. 288–292. DOI: 10.1016/j.automatica.2016.09.045.

Allen, Robert C., Harry G. Kwatny, and Gaurav Bajpai (2012). "Safe Set Protection and Restoration for Unimpaired and Impaired Aircraft". In: *AIAA Guidance, Navigation, and Control Conference*. Minneapolis, US-MN. DOI: 10.2514/6.2012-4822.

de Almeida, Fabio A. and Dirk Leißling (2010). "Fault-Tolerant Model Predictive Control with Flight-Test Results". In: *Journal of Guidance, Control, and Dynamics* 33.2, pp. 363–375. DOI: 10.2514/1.46108.

Alonso, Diego M., Daniel W. Berns, Eduardo E. Paolini, and Jorge L. Moiola (2003). "Bifurcation Control in Feedback Systems". In: *Bifurcation Control. Theory and Applications*. Ed. by Guanrong Chen, David J. Hill, and Xinghuo Yu. Berlin, DE: Springer. Chap. 10, pp. 205–228. DOI: 10.1007/978-3-540-44925-6_10.

Amato, F., R. Ambrosino, G. De Tommasi, and A. Merola (2011). "Estimation of the domain of attraction for a class of hybrid systems". In: *Nonlinear Analysis: Hybrid Systems* 5.3, pp. 573–582. DOI: 10.1016/j.nahs.2010.12.005.

Amrit, Rishi, James B. Rawlings, and David Angeli (2011). "Economic optimization using model predictive control with a terminal cost". In: *Annual Reviews in Control* 35.2, pp. 178–186. DOI: 10.1016/j.arcontrol.2011.10.011.

Anderson, James and Antonis Papachristodoulou (2012). "Robust nonlinear stability and performance analysis of an F/A-18 aircraft model using sum of squares programming". In: *International Journal of Robust and Nonlinear Control* 23, pp. 1099–1114. DOI: 10.1002/rnc.2928.

Andersson, Joel A. E., Joris Gillis, Greg Horn, James B. Rawlings, and Moritz Diehl (2018). "CasADi – A software framework for nonlinear optimization and optimal control". In: *Mathematical Programming Computation,* In Press.

Andersson, Joel, Joris Gillis, and Moritz Diehl (2018). *User Documentation for CasADi v3.4.5*. Software documentation.

Angeli, David, Rishi Amrit, and James B. Rawlings (2012). "On Average Performance and Stability of Economic Model Predictive Control". In: *IEEE Transactions on Automatic Control* 57.7, pp. 1615–1626. DOI: 10.1109/TAC.2011.2179349.

Åström, Karl Johan and Richard M. Murray (2008). *Feedback Systems: An Introduction for Scientists and Engineers*. Princeton, US-NJ: Princeton University Press. ISBN: 978-0-691-13576-2.

Ataei-Esfahani, Armin and Qian Wang (2007). "Nonlinear control design of a hypersonic aircraft using sum-of-squares method". In: *Proceedings of the 2007 American Control Conference*. New York, US-NY, pp. 5278–5283. DOI: 10.1007/978-3-642-25992-0_48.

Bates, Declan and Ian Postlethwaite (2002). *Robust Multivariable Control of Aerospace Systems*. Control and Simulation. Delft, NL: Delft University Press.

Belcastro, Christine M., John V. Foster, Gautam H. Shah, Irene M. Gregory, David E. Cox, Dennis A. Crider, Loren Groff, Richard L. Newman, and David H. Klyde (2017). "Aircraft Loss of Control Problem Analysis and Research Toward a Holistic Solution". In: *Journal of Guidance, Control, and Dynamics* 40.4, pp. 733–775. DOI: 10.2514/1.G002815.

Blanchini, F. (1999). "Set invariance in control". In: *Automatica* 35, pp. 1747–1767. DOI: 10.1016/S0005-1098(99)00113-2.

Boeing (2001). *Statistical Summary of Commercial Jet Airplane Accidents, Worldwide Operations, 1959–2000*. Tech. rep. Seattle, US-WA: Aviation Safety, Boeing Commercial Airplanes.

Boeing (2008). *Statistical Summary of Commercial Jet Airplane Accidents, Worldwide Operations, 1959–2007*. Tech. rep. Seattle, US-WA: Aviation Safety, Boeing Commercial Airplanes.

Boeing (2016). *Statistical Summary of Commercial Jet Airplane Accidents, Worldwide Operations, 1959–2015*. Tech. rep. Seattle, US-WA: Aviation Safety, Boeing Commercial Airplanes.

Brandon, Jay M. and Eugene A. Morelli (2016). "Real-Time Onboard Global Nonlinear Aerodynamic Modeling from Flight Data". In: *Journal of Aircraft* 53.5, pp. 1261–1297. DOI: 10.2514/1.C033133.

Branicky, Michael S. (1998). "Multiple Lyapunov functions and other analysis tools for switched and hybrid systems". In: *IEEE Transactions on Automatic Control* 43.4, pp. 475–482. DOI: 10.1109/9.664150.

Brockhaus, Rudolf, Wolfgang Alles, and Robert Luckner (2011). *Flugregelung*. 3rd rev. ed. Berlin, DE: Springer. DOI: 10.1007/978-3-642-01443-7.

Bulka, E. and M. Nahon (2017). "Autonomous control of agile fixed-wing UAVs performing aerobatic maneuvers". In: *2017 International Conference on Unmanned Aircraft Systems*. Miami, US-FL, pp. 104–113. DOI: 10.1109/ICUAS.2017.7991437.

Bunge, Roberto A. (2017). "Automatic Spin Detection and Recovery for Small Aircraft". PhD thesis. Stanford, US-CA: Stanford University.

Bunge, Roberto A. and Ilan M. Kroo (2018). "Automatic Spin Recovery with Minimal Altitude Loss". In: *2018 AIAA Guidance, Navigation, and Control Conference*. Kissimmee, US-FL. DOI: 10.2514/6.2018-1866.

Burcham Jr, Frank W., John J. Burken, Trindel A. Maine, and C. Gordon Fullerton (1997). *Development and Flight Test of an Emergency Flight Control System Using Only Engine Thrust on an MD-11 Transport Airplane*. NASA technical publication NASA/TP-97-206217. Edwards, US-CA: Dryden Flight Research Center. URL: https://ntrs.nasa.gov/search.jsp?R=19980210483.

Burcham Jr, Frank W., Richard Stevens, Ronald Broderick, and Kerry Wilson (2009). "Manual Throttles-Only Control Effectiveness for Emergency Flight Control of Transport Aircraft". In: *9th AIAA Aviation Technology, Integration, and Operations Conference*. Hilton Head Island, US-SC. DOI: 10.2514/6.2009-7088.

Carbaugh, Dave, Larry Rockliff, and Bob Vandel, eds. (2008). *Airplane Upset Recovery Training Aid*. 2nd rev. ed. Alexandria, US-VA: Flight Safety Foundation (et al.)

Caroll, James V. and Raman K. Mehra (1982). "Bifurcation Analysis of Nonlinear Aircraft Dynamics". In: *Journal of Guidance, Control, and Dynamics* 5.5, pp. 529–536. DOI: 10.2514/3.56198.

Chakraborty, Abhijit, Peter Seiler, and Gary J. Balas (2011a). "Nonlinear region of attraction analysis for flight control verification and validation". In: *Control Engineering Practice* 19.4, pp. 335–345. DOI: 10.1016/j.conengprac.2010.12.001.

Chakraborty, Abhijit, Peter Seiler, and Gary J. Balas (2011b). "Susceptibility of F/A-18 Flight Controllers to the Falling-leaf Mode: Linear Analysis". In: *Journal of Guidance, Control, and Dynamics* 34.1, pp. 57–72. DOI: 10.2514/1.50674.

Chakraborty, Abhijit, Peter Seiler, and Gary J. Balas (2011c). "Susceptibility of F/A-18 Flight Controllers to the Falling-leaf Mode: Nonlinear Analysis". In: *Journal of Guidance, Control, and Dynamics* 34.2, pp. 73–85. DOI: 10.2514/1.50675.

Chambers, J. R. and S. B. Grafton (1977). *Aerodynamic Characteristics of Airplanes at High Angles of Attack*. NASA technical memorandum NASA/TM-74097. Hampton, US-VA: Langley Research Center. URL: https://ntrs.nasa.gov/search.jsp?R=19780005068.

Chang, Bor-Chin, Harry G. Kwatny, Elie R. Ballouz, and David C. Hartmann (2016). "Aircraft Trim Recovery from Highly Nonlinear Upset Conditions". In: *AIAA Guidance, Navigation, and Control Conference*. San Diego, US-CA. DOI: 10.2514/6.2016-0880.

Chaudhuri, Probal, Min-Ching Huang, Wei-Yin Loh, and Ruji Yao (1994). "Piecewise-Polynomial Regression Trees". In: *Statistica Sinica* 4.1, pp. 143–167. URL: http://www.jstor.org/stable/24305278.

Chen, Guanrong, Jorge L. Moiola, and Hua O. Wang (2000). "Bifurcation Control: Theories, Methods, and Applications". In: *International Journal of Bifurcation and Chaos* 10.03, pp. 511–548. DOI: 10.1142/S0218127400000360.

Chen, Lingji and Kumpati S. Narendra (2004). "Identification and Control of a Nonlinear Discrete-Time System Based on its Linearization :" in: *IEEE Transactions on Neural Networks* 15.3, pp. 663–673. DOI: 10.1109/TNN.2004.826206.

Chen, Ying-Jen, Motoyasu Tanaka, Kazuo Tanaka, and Hua O. Wang (2015). "Stability Analysis and Region-of-Attraction Estimation Using Piecewise Polynomial Lyapunov Functions: Polynomial Fuzzy Model Approach". In: *IEEE Transactions on Fuzzy Systems* 23.4, pp. 1314–1322. DOI: 10.1109/TFUZZ.2014.2347993.

Chesi, Graziano (2013). "Rational Lyapunov functions for estimating and controlling the robust domain of attraction". In: *Automatica* 49.4, pp. 1051–1057. DOI: 10.1016/j.automatica.2013.01.032.

Chesi, Graziano (2014). "Establishing robust stability of discrete-time systems with time-varying uncertainty: The Gram-SOS approach". In: *Automatica* 50.11, pp. 2813–2821. DOI: 10.1016/j.automatica.2014.10.007.

Chesi, Graziano (2018). "On the Complexity of SOS Programming and Applications in Control Systems". In: *Asian Journal of Control* 20.5, pp. 2005–2013. DOI: 10.1002/asjc.1684.

Choi, M. D., T. Y. Lam, and B. Reznick (1995). "Sums of Squares of Real Polynomials". In: *Proceedings of Symposia in Pure Mathematics* 58.2, pp. 103–126.

Coetzee, Etienne, Bernd Krauskopf, and Mark H. Lowenberg (2010). "The Dynamical Systems Toolbox: Integrating AUTO into MATLAB". In: *16th US National Congress on Theoretical and Applied Mechanics*. State College, US-PA.

Corey, Stephens, Olivier Ferrante, Kyle Olsen, and Vivek Sood (2008). "Standardizing International Taxonomies". In: *ISASI Forum* 41.1, pp. 8–13. ISSN: 1088-8128.

Crawford, John David (1991). "Introduction to bifurcation theory". In: *Reviews of Modern Physics* 63.4, pp. 991–1037. DOI: 10.1103/RevModPhys.63.991.

Crespo, Luis G., Sean P. Kenny, David E. Cox, and Daniel G. Murri (2012). "Analysis of Control Strategies for Aircraft Flight Upset Recovery". In: *AIAA Guidance, Navigation, and Control Conference*. Minneapolis, US-MN. DOI: 10.2514/6.2012-5026.

Cunis, Torbjørn (2018). "The `pwpfit` Toolbox for Polynomial and Piece-wise Polynomial Data Fitting". In: *18th IFAC Symposium on System Identification*. Stockholm, SE, pp. 682–687. DOI: 10.1016/j.ifacol.2018.09.204.

Cunis, Torbjørn and Elgiz Baskaya (2018). "Performance of Unmanned Aircrafts in the Event of Loss-of-control". In: *10th International Micro Air Vehicle Conference and Competition*. Melbourne, AU.

Cunis, Torbjørn and Murat Bronz (2017). "EDURA: an Evolvable Demonstrator for Upset Recovery Approaches with a 3D-printed Launcher". In: *9th International Micro Air Vehicle Conference and Competition*. Toulouse, FR.

Cunis, Torbjørn, Laurent Burlion, and Jean-Philippe Condomines (2017). "Non-linear Analysis and Control Proposal for In-flight Loss-of-control". In: *20th IFAC World Congress, preprints*. Toulouse, FR, pp. 10681–10685.

Cunis, Torbjørn, Laurent Burlion, and Jean-Philippe Condomines (2018a). "Piece-wise Identification and Analysis of the Aerodynamic Coefficients, Trim Conditions, and Safe Sets of the Generic Transport Model". In: *AIAA Guidance, Navigation, and Control Conference*. Kissimmee, US-FL. DOI: 10.2514/6.2018-1114.

Cunis, Torbjørn, Laurent Burlion, and Jean-Philippe Condomines (2018b). *Piecewise Polynomial Model of the Aerodynamic Coefficients of the Generic Transport Model and its Equations of Motion*. Tech. rep. hal-01808649, version 3. Toulouse, FR: ONERA – The French Aerospace Lab; French Civil Aviation School. URL: https://archives-ouvertes.fr/hal-01808649v3.

Cunis, Torbjørn, Laurent Burlion, and Jean-Philippe Condomines (2019). "Piecewise Polynomial Modeling for Control and Analysis of Aircraft Dynamics beyond Stall". In: *Journal of Guidance, Control, and Dynamics* 42.4, pp. 949–957. DOI: 10.2514/1.G003618.

Cunis, Torbjørn, Jean-Philippe Condomines, and Laurent Burlion (2017). "Full-envelope, Six-Degrees-of-Freedom Trim Analysis of Unmanned Aerial Systems based on Piecewise Polynomial Aerodynamic Coefficients". In: *4th Workshop on Research, Education, and Development of Unmanned Aerial Systems*. Linköping, SE, pp. 108–113. DOI: 10.1109/RED-UAS.2017.8101652.

Cunis, Torbjørn, Jean-Philippe Condomines, and Laurent Burlion (2019a). "Local stability analysis for large polynomial spline systems". In: Revision under review for *Automatica*.

Cunis, Torbjørn, Jean-Philippe Condomines, and Laurent Burlion (2019b). "Sum-of-squares Flight Control Synthesis for Deep-stall Recovery". In: Revision under review for *Journal of Guidance, Control, and Dynamics*.

Cunis, Torbjørn, Jean-Philippe Condomines, Laurent Burlion, and Anders la Cour-Harbo (2019). "Dynamic Stability Analysis of Aircraft Flight in Deep Stall". In: *Journal of Aircraft*. DOI: 10.2514/1.C035455.

Cunis, Torbjørn and Anders la Cour-Harbo (2019). *Piecewise Polynomial Model of the Aerodynamic Coefficients of the* Cumulus One *Unmanned Aircraft*. Tech. rep. hal-02280789. Støvring, DK: Sky-Watch A/S. URL: https://archives-ouvertes.fr/hal-02280789.

Cunis, Torbjørn and Sarah Gluschitz (2018). "Talking Aviation Safety: How to make airplanes safer". In: *EuroScience Open Forum*. Toulouse, FR.

Cunis, Torbjørn, Tobias Leth, Luminita C. Totu, and Anders la Cour-Harbo (2018). "Identification of Thrust, Lift, and Drag for Deep-stall Flight Data of a Fixed-wing Unmanned Aircraft". In: *2018 International Conference on Unmanned Aircraft Systems*. Dallas, US-TX, pp. 531–538. DOI: 10.1109/ICUAS.2018.8453340.

Cunis, Torbjørn, Dominic Liao-McPherson, Jean-Philippe Condomines, Laurent Burlion, and Ilya Kolmanovsky (2019). "Economic Model-Predictive Control Strategies for Aircraft Deep-stall Recovery with Stability Guarantees". In: *58th IEEE Conference on Decision and Control* (to be presented). Nice, FR.

Cunningham, Kevin, David E. Cox, Daniel G. Murri, and Stephen E. Riddick (2011). "A Piloted Evaluation of Damage Accommodating Flight Control Using a Remotely

Piloted Vehicle". In: *AIAA Guidance, Navigation, and Control Conference*. Portland, US-OR. DOI: 10.2514/6.2011-6451.

Dankowicz, Harry and Frank Schilder (2013). *Recipes for Continuation*. Computational Science & Engineering. Philadelphia, US-PA: Society for Industrial and Applied Mathematics. DOI: 10.1137/1.9781611972573.

Dankowicz, Harry and Frank Schilder (2016). *Continuation Core and Toolboxes (COCO)*. Urbana, US-IL. URL: https://sourceforge.net/projects/cocotools/.

De Schutter, Bart, W. P. M. H. Heemels, Jan Lunze, and C. Prieur (2009). "Survey of modeling, analysis, and control of hybrid systems". In: *Handbook of Hybrid Systems Control: Theory, Tools, Applications*. Ed. by Jan Lunze and Françoise Lamnabhi-Lagarrigue. Cambridge, GB: Cambridge University Press, pp. 31–55.

DeVille, Lee (2016). *Optimizing Gershgorin for Symmetric Matrices*. Preprint. arXiv: 1605.07239.

Dhooge, A., W. Govaerts, Yu A. Kuznetsov, H. G. E. Meijer, and B. Sautois (2008). "New features of the software MatCont for bifurcation analysis of dynamical systems". In: *Mathematical and Computer Modelling of Dynamical Systems* 14.2, pp. 147–175. DOI: 10.1080/13873950701742754.

Di Donato, Pedro F. A., Sweewarman Balachandran, Kevin McDonough, Ella Atkins, and Ilya Kolmanovsky (2017). "Envelope-aware Flight Management for Loss of Control Prevention given Rudder Jam". In: *Journal of Guidance, Control, and Dynamics* 40, pp. 1027–1041. DOI: 10.2514/1.G000252.

Diehl, Moritz, Rishi Amrit, and James B. Rawlings (2011). "A Lyapunov function for economic optimizing model predictive control". In: *IEEE Transactions on Automatic Control* 56.3, pp. 703–707. DOI: 10.1109/TAC.2010.2101291.

Dongmo, Jean-Etienne Temgoua (2010). "Aircraft loss-of-control prevention and recovery: a hybrid control strategy". PhD thesis. Philadelphia, US-PA: Drexel University.

Drela, Mark and Harold Youngren (2017). *AVL 3.36*. Software User Guide. Cambridge, US-MA: Massachusetts Institute of Technology. URL: http://web.mit.edu/drela/Public/web/avl/avl_doc.txt.

Ebenbauer, Christian and Frank Allgöwer (2006). "Analysis and design of polynomial control systems using dissipation inequalities and sum of squares". In: *Computers and Chemical Engineering* 30, pp. 1590–1602. DOI: 10.1016/j.compchemeng.2006.05.014.

Ellis, Matthew, Jinfeng Liu, and Panagiotis D. Christofides (2017). *Economic Model Predictive Control: Theory, Formulations and Chemical Process Applications*. Basel, CH: Springer. ISBN: 9783319411071.

Endsley, Mica R. (2017). "From Here to Autonomy: Lessons Learned From Human-Automation Research". In: *Human Factors* 59.1, pp. 5–27. DOI: 10.1177/0018720816681350.

Engelbrecht, Jacobus A. A. (2016). "Automatic Flight Envelope Recovery for Large Transport Aircraft". PhD thesis. Matieland, ZA: University of Stellenbosch.

Engelbrecht, Jacobus A. A., Simon J. Pauck, and Iain K. Peddle (2013). "A Multimode Upset Recovery Flight Control System for Large Transport Aircraft". In: *AIAA*

Guidance, Navigation, and Control Conference. Boston, US-MA. DOI: 10.2514/6.2013-5172.

Engelbrecht, Johannes J. K. and Jacobus A. A. Engelbrecht (2016). "Optimal attitude and flight vector recovery for large transport aircraft using sequential quadratic programming". In: *2016 Pattern Recognition Association of South Africa and Robotics and Mechatronics International Conference*. Stellenbosch, SA. DOI: 10.1109/RoboMech.2016.7813153.

Eren, Utku, Anna Prach, Başaran Bahadır Koçer, Saša V. Raković, Erdal Kayacan, and Behçet Açıkmeşe (2017). "Model Predictive Control in Aerospace Systems: Current State and Opportunities". In: *Journal of Guidance, Control, and Dynamics* 40.7, pp. 1541–1566. DOI: 10.2514/1.G002507.

FAA (2016). *Airplane Flying Handbook*. FAA handbook FAA-H-8083-3B. Washington, US-DC: Flight Standards Service.

Faulwasser, Timm, Milan Korda, Colin N. Jones, and Dominique Bonvin (2014). "Turnpike and dissipativity properties in dynamic real-time optimization and economic MPC". In: *53rd IEEE Conference on Decision and Control*. Los Angeles, US-CA, pp. 2734–2739. DOI: 10.1109/CDC.2014.7039808.

Ferranti, L., Y. Wan, and T. Keviczky (2018). "Fault-tolerant reference generation for model predictive control with active diagnosis of elevator jamming faults". In: *International Journal of Robust and Nonlinear Control*. DOI: 10.1002/rnc.4063.

Foster, John V., Kevin Cunningham, Charles M. Fremaux, Gautam H. Shah, and Eric C. Stewart (2005). "Dynamics Modeling and Simulation of Large Transport Airplanes in Upset Conditions". In: *AIAA Guidance, Navigation, and Control Conference and Exhibit*. San Francisco, US-CA. DOI: 10.2514/6.2005-5933.

Frink, Neal T., Patrick C. Murphy, Harold L. Atkins, Sally A. Viken, Justin L. Petrilli, Ashok Gopalarathnam, and Ryan C. Paul (2017). "Computational Aerodynamic Modeling Tools for Aircraft Loss of Control". In: *Journal of Guidance, Control, and Dynamics* 40.4, pp. 789–803. DOI: 10.2514/1.G001736.

Gallant, A. R. and Wayne A. Fuller (1973). "Fitting segmented polynomial regression models whose join points have to be estimated". In: *Journal of the American Statistical Association* 68.341, pp. 144–147. DOI: 10.2307/2284158.

Genesio, Roberto, Michele Tartaglia, and Antonio Vicino (1985). "On the Estimation of Asymptotic Stability Regions: State of the Art and New Proposals". In: *IEEE Transactions on Automatic Control* 30.8, pp. 747–755. DOI: 10.1109/TAC.1985.1104057.

Gill, Stephen J., Mark H. Lowenberg, Simon A. Neild, Bernd Krauskopf, Guilhem Puyou, and Etienne Coetzee (2013). "Upset Dynamics of an Airliner Model: A Nonlinear Bifurcation Analysis". In: *Journal of Aircraft* 50.6, pp. 1832–1842. DOI: 10.2514/1.C032221.

Golub, Gene H. (1982). *Numerical Methods for Solving Least Squares Problems*. Final report ARO 16037.9-MA. Research Triangle Park, US-NC: U.S. Army Research Office.

Goman, M. G., G. I. Zagainov, and A. V. Khramtsovsky (1997). "Application of bifurcation methods to nonlinear flight dynamics problems". In: *Progress in Aerospace Sciences* 33.9–10, pp. 539–586. DOI: 10.1016/S0376-0421(97)00001-8.

Graichen, Knut (2006). "Feedforward Control Design for Finite-Time Transition Problems of Nonlinear Systems". PhD thesis. Stuttgart, DE: University of Stuttgart. DOI: 10.18419/opus-4093.

Gratton, G. B., R. I. Hoff, A. Rahman, C. Harbour, S. Williams, and M. Bromfield (2014). "Evaluating a set of stall recovery actions for single engine light aeroplanes". In: *The Aeronautical Journal* 118.1203, pp. 461–484. DOI: 10.1017/S0001924000009313.

Gregory, Irene, Enric Xargay, Chengyu Cao, and Naira Hovakimyan (2011). "Flight Test of $\mathcal{L}_1$ Adaptive Control Law: Offset Landings and Large Flight Envelope Modeling Work". In: *AIAA Guidance, Navigation, and Control Conference*. Portland, US-OR. DOI: 10.2514/6.2010-8015.

Grossman, Robert L., Anil Nerode, Anders Peter Ravn, and Hans Rischel, eds. (1993). *Hybrid Systems*. Berlin, DE: Springer. ISBN: 3-540-57318-6.

Grüne, Lars and Jürgen Pannek (2017). *Nonlinear Model Predictive Control: Theory and Algorithms*. 2nd ed. Basel, CH: Springer. ISBN: 9783319460239.

Harris, Don (2007). "A human-centred design agenda for the development of single crew operated commercial aircraft". In: *Aircraft Engineering and Aerospace Technology* 79.5, pp. 518–526. DOI: 10.1108/00022660710780650.

Haskell, Karen H. and Richard J. Hanson (1981). "An Algorithm for Linear Least Squares Problems with Equality and Nonnegativity Constraints". In: *Mathematical Programming* 21.1, pp. 98–118. DOI: 10.1007/BF01584232.

IATA (2015). *Loss of Control In-Flight Accident Analysis Report, 2010–2014*. Montreal, CA: International Air Transport Association. ISBN: 978-92-9252-775-4.

IATA (2015). *Unstable Approaches: Risk Mitigation Policies, Procedures and Best Practices*. Montreal, CA: International Air Transport Association. ISBN: 978-92-9252-804-1.

ICAO (2011). *Unmanned Aircraft Systems (UAS)*. Circular 328. Montreal, CA: International Civil Aviation Organization.

ICAO (2013). *Accident/Incident Data Reporting taxonomy – Occurence category*. Data Definition Standard. Montreal, CA: International Civil Aviation Organization.

IPOPT (2016). *Introduction to* IPOPT*: A tutorial for downloading, installing, and using* IPOPT. Software documentation Revision 2617. Maintained by Stefan Vigerske and Andreas Wächter. URL: https://www.coin-or.org/Ipopt/documentation/.

Isidori, Alberto (2013). "The zero dynamics of a nonlinear system: From the origin to the latest progresses of a long successful story". In: *European Journal of Control* 19.5, pp. 369–378. DOI: 10.1016/j.ejcon.2013.05.014.

ISO 1151-1 (1988). *Flight dynamics – Concepts, quantities and symbols – Part 1: Aircraft motion relative to the air*. 4th ed. ISO 1151-1:1988. Genève, CH: International Organization for Standarization.

Jadbabaie, Ali, Jie Yu, and John Hauser (2001). "Unconstrained Receding-Horizon Control of Nonlinear Systems". In: *IEEE Transactions on Automatic Control* 46.5, pp. 776–783. DOI: 10.1109/9.920800.

Jahnke, Craig C. (1990). "Application of Dynamical Systems Theory to Nonlinear Aircraft Dynamics". PhD thesis. Pasadena, US-CA: California Institute of Technology. URL: http://resolver.caltech.edu/CaltechETD:etd-05092007-134504.

Jarvis-Wloszek, Zachary, Ryan Feeley, Weehong Tan, Kunpeng Sun, and Andrew Packard (2003). "Some Controls Applications of Sum of Squares Programming". In: *Proceedings of the IEEE Conference on Decision and Control*. Vol. 5. Maui, US-HI, pp. 4676–4681. DOI: 10.1109/CDC.2003.1272309.

Jäschke, Johannes, Xue Yang, and Lorenz T. Biegler (2014). "Fast economic model predictive control based on NLP-sensitivities". In: *Journal of Process Control* 24.8, pp. 1260–1272. DOI: 10.1016/j.jprocont.2014.04.009.

Jategaonkar, Ravindra V. (2006). *Flight Vehicle System Identification: A Time Domain Methodology*. Progress in Astronautics and Aeronautics 216. Reston, US-VA: American Institute of Aeronautics and Astronautics. DOI: 10.1017/S0001924000011015.

Johansson, Mikael and Anders Rantzer (1998). "Computation of piecewise quadratic Lyapunov functions for hybrid systems". In: *IEEE Transactions on Automatic Control* 43.4, pp. 555–559. DOI: 10.1109/9.664157.

Johnson, Eric N. (2000). "Limited Authority Adaptive Flight Control". PhD thesis. Atlanta, US-GA: Georgia Institute of Technology.

Joosten, D. A., T. J. J. van den Boom, and M. Verhaegen (2010). "Fault-Tolerant Control through a Synthesis of Model-Predictive Control and Nonlinear Inversion". In: *RECOVER: A Benchmark for Integrated Fault Tolerant Flight Control Evaluation*. Ed. by Christopher Edwards, Thomas J. J. Lombaerts, and Hafid Smaili. Berlin, DE: Springer, pp. 319–336.

Jordan, Thomas L., John V. Foster, Roger M. Bailey, and Christine M. Belcastro (2006). "AirSTAR: A UAV Platform for Flight Dynamics and Control System Testing". In: *AIAA Aerodynamics Measurement Technology and Ground Testing Conference*. San Francisco, US-CA. DOI: 10.2514/6.2006-3307.

Jordan, Thomas L., William Langford, Christine M Belcastro, J.V. Foster, Gautam Shah, Gregory Howland, and Reggie Kidd (2004). "Development of a Dynamically Scaled Generic Transport Model Testbed for Flight Research Experiments". In: *AUVSI's Unmanned Systems North America 2004 Symposium and Exhibition*. Anaheim, US-CA: Association for Unmanned Vehicle Systems International. URL: https://ntrs.nasa.gov/search.jsp?R=20040085988.

Kariya, Takeaki and Hiroshi Kurata (2004). *Generalized Least Squares*. Wiley Series in Probability and Statistics. Chichester, GB: John Wiley & Sons.

Kheirandishfard, Mohsen, Fariba Zohrizadeh, and Ramtin Madani (2018). "Convex Relaxation of Bilinear Matrix Inequalities Part I: Theoretical Results". In: *57th IEEE Conference on Decision and Control*. Miami Beach, US-FL, pp. 67–74. DOI: 10.1109/CDC.2018.8619567.

Khodadadi, Larissa, Behzad Samadi, and Hamid Khaloozadeh (2014). "Estimation of region of attraction for polynomial nonlinear systems: A numerical method". In: *ISA Transactions* 53.1, pp. 25–32. DOI: 10.1016/j.isatra.2013.08.005.

Kim, Donghae, Gyeongtaek Oh, Yongjun Seo, and Youdan Kim (2016). "Reinforcement Learning-Based Optimal Flat Spin Recovery for Unmanned Aerial Vehicle". In: *Journal of Guidance, Control, and Dynamics* 40.4, pp. 1076–1084. DOI: 10.2514/1.G001739.

Klein, Vladislav and Eugene A. Morelli (2006). *Aircraft System Identification: Theory and Practice*. AIAA Education Series. Reston, US-VA: American Institute of Aeronautics and Astronautics, p. 484. DOI: 10.1017/S0001924000087194.

Korda, Milan and Colin N. Jones (2017). "Stability and performance verification of optimization-based controllers". In: *Automatica* 78, pp. 34–45. DOI: 10.1016/j.automatica.2016.12.008.

Kouvaritakis, Basil and Mark Cannon (2016). *Model Predictive Control: Classical, Robust and Stochastic*. Basel, CH: Springer. DOI: 10.1007/978-0-85729-398-5.

Kuzmin, Dmitri (2010). *A Guide to Numerical Methods for Transport Equations*. Book Draft. Erlangen/Nürnberg, DE: Friedrich-Alexander University. URL: http://www.mathematik.uni-dortmund.de/~kuzmin/Transport.pdf.

Kuznetsov, Yuri A. (1998). *Elements of Applied Bifurcation Theory*. 2nd ed. Applied Mathematical Sciences 112. Berlin, DE: Springer. DOI: 10.1007/978-1-4757-3978-7.

Kwatny, Harry G., Bor-Chin Chang, and Shiu-Ping Wang (2003). "Static Bifurcation in Mechanical Control Systems". In: *Bifurcation Control. Theory and Applications*. Ed. by Guanrong Cheng, David J. Hill, and Xinghuo Yu. Lecture Notes in Control and Information Sciences. Berlin, DE: Springer. Chap. 4, pp. 67–81. DOI: 10.1007/978-3-540-44925-6_4.

Kwatny, Harry G., Jean-Etienne Temgoua Dongmo, Bor-Chin Chang, Gaurav Bajpai, Murat Yasar, and Christine Belcastro (2013). "Nonlinear Analysis of Aircraft Loss of Control". In: *Journal of Guidance, Control, and Dynamics* 36.1, pp. 149–162. DOI: 10.2514/1.56948.

La Salle, J. P. (1960). "Some Extensions of Liapunov's Second Method". In: *IRE Transactions on Circuit Theory* CT-7.4, pp. 520–527. DOI: 10.1109/TCT.1960.1086720.

Lawson, Charles L. and Richard J. Hanson (1995). *Solving Least Squares Problems*. Classics in Applied Mathematics. Society for Industrial and Applied Mathematics. DOI: 10.1137/1.9781611971217.

Limon, D., T. Alamo, D. M. Raimondo, D. Muñoz De La Peña, J. M. Bravo, A. Ferramosca, and E. F. Camacho (2009). "Input-to-state stability: A unifying framework for robust model predictive control". In: *Nonlinear Model Predictive Control*. Ed. by Lalo Magni, Davide Martino Raimondo, and Frank Allgöwer. Lecture Notes in Control and Information Sciences 384. Berlin, DE: Springer, pp. 1–26. DOI: 10.1007/978-3-642-01094-1-1.

Linse, Dennis J. and Robert F. Stengel (1993). "Identification of Aerodynamic Coefficients Using Computational Neural Networks". In: *Journal of Guidance, Control, and Dynamics* 16.6, pp. 1018–1025. DOI: 10.2514/3.21122.

Lombaerts, Thomas J. J., G. H. N. Looye, Q. P. Chu, and J. A. Mulder (2010). "Pseudo Control Hedging and its Application for Safe Flight Envelope Protection". In: *AIAA Guidance, Navigation, and Control Conference*. Toronto, CA. DOI: 10.2514/6.2010-8280.

Lombaerts, Thomas J. J., Stefan R. Schuet, John Kaneshige, Kimberlee H. Shish, and Vahram Stepanyan (2017). "Stall Recovery Guidance Using an Energy Based Algorithm". In: *AIAA Guidance, Navigation, and Control Conference*. Grapevine, US-TX. DOI: 10.2514/6.2017-1021.

Lombaerts, Thomas J. J., Stefan R. Schuet, Vahram Stepanyan, John Kaneshige, Gordon Hardy, Kimberlee H. Shish, and Peter Robinson (2018). "Piloted Simulator Evaluation Results of Flight Physics Based Stall Recovery Guidance". In: *2018 AIAA Guidance, Navigation, and Control Conference*. Kissimmee, US-FL: American Institute of Aeronautics and Astronautics. DOI: 10.2514/6.2018-0383.

Lombaerts, Thomas J. J., Stefan R. Schuet, Kevin R. Wheeler, Diana M. Acosta, and John T. Kaneshige (2013). "Safe maneuvering envelope estimation based on a physical approach". In: *AIAA Guidance, Navigation, and Control Conference*. Boston, US-MA. DOI: 10.2514/6.2013-4618.

Lu, Ping, John L. Crassidis, Craig A. Kluever, et al., eds. (2017). *Special Issue on Aircraft Loss of Control*. Vol. 40. Journal of Guidance, Control, and Dynamics 4, pp. 733–1084. URL: https://arc.aiaa.org/toc/jgcd/40/4.

Lunze, Jan and Françoise Lamnabhi-Lagarrigue, eds. (2009). *Handbook of Hybrid Systems Control: Theory, Tools, Applications*. Cambridge, GB: Cambridge University Press. ISBN: 978-0-521-76505-3.

Lygeros, John (2004). "On reachability and minimum cost optimal control". In: *Automatica* 40.6, pp. 917–927. DOI: 10.1016/j.automatica.2004.01.012.

Maciejowski, Jan M. and Xiaoke Yang (2015). "Fault tolerant control using Gaussian processes and model predictive control". In: *International Journal of Applied Mathematics and Computer Science* 25, pp. 133–148. DOI: 10.1109/SysTol.2013.6693820.

Majumdar, Anirudha, Amir Ali Ahmadi, and Russ Tedrake (2013). "Control Design Along Trajectories via Sum of Squares Optimization". In: *2013 IEEE International Conference on Robotics and Automation*. Karlsruhe, DE, pp. 4039–4046. DOI: 10.1109/ICRA.2013.6631149. arXiv: arXiv:1210.0888v1.

Malisoff, Michael and Frédéric Mazenc (2009). "Review of Lyapunov Functions". In: *Constructions of Strict Lyapunov Functions*. Communications and Control Engineering. London, GB: Springer. Chap. 2, pp. 25–57. DOI: 10.1007/978-1-84882-535-2_2.

Marcos, Andres, Declan G. Bates, and Ian Postlethwaite (2007). "Nonlinear Symbolic LFT Tools for Modelling, Analysis and Design". In: *Nonlinear Analysis and Synthesis Techniques for Aircraft Control*. Ed. by Declan Bates and Martin Hagström. Berlin, DE: Springer. Chap. 5, pp. 69–92. DOI: 10.1007/978-3-540-73719-3.

Marshall, Curtis J., Blake Roberts, and Michael W. Grenn (2018). "Context-Driven Autonomy for Enhanced System Resilience in Emergent Operating Environments". In: *IEEE Systems Journal*, pp. 1–12. DOI: 10.1109/JSYST.2018.2881111.

McDonough, Kevin and Ilya Kolmanovsky (2017). "Fast Computable Recoverable Sets and Their Use for Aircraft Loss-of-Control Handling". In: *Journal of Guidance, Control, and Dynamics* 40.4, pp. 934–947. DOI: 10.2514/G001747.

McDonough, Kevin, Ilya Kolmanovsky, and Ella Atkins (2014). "Recoverable sets of initial conditions and their use for aircraft flight planning after a loss of control event". In: *AIAA Guidance, Navigation, and Control Conference*. National Harbor, US-MD. DOI: 10.2514/6.2014-0786.

McGee, Victor E. and Willard T. Carleton (1970). "Piecewise Regression". In: *Journal of the American Statistical Association* 65.331, pp. 1109–1124. DOI: 10.2307/2284278.

Motzkin, Theodore S. (1967). "The arithmetic-geometric inequality". In: *Symposium on Inequalities*. Air Force Academy, US-CO, pp. 205–224.

Murch, Austin M. and John V. Foster (2007). "Recent NASA Research on Aerodynamic Modeling of Post-Stall and Spin Dynamics of Large Transport Airplanes". In: *45th AIAA Aerospace Sciences Meeting and Exhibit*. Reno, US-NV: American Institute of Aeronautics and Astronautics. DOI: 10.2514/6.2007-463.

Nabi, H. N., Thomas J. J. Lombaerts, Y. Zhang, E. van Kampen, Q. P. Chu, and Coen C. de Visser (2018). "Effects of Structural Failure on the Safe Flight Envelope of Aircraft". In: *Journal of Guidance, Control, and Dynamics* 41.6, pp. 1257–1275. DOI: 10.2514/1.G003184.

NASA (2016). *Flight Dynamics Simulation of a Generic Transport Model*. Online resource. Hampton, US-VA. URL: https://software.nasa.gov/software/LAR-17625-1.

Nelson, Robert C. (1998). *Flight Stability and Automatic Control*. 2nd ed. Boston, US-MA: McGraw-Hill. ISBN: 0070462739.

Nicotra, Marco M. and Emanuele Garone (2018). "The Explicit Reference Governor: A General Framework for the Closed-Form Control of Constrained Nonlinear Systems". In: *IEEE Control Systems* 38.4, pp. 89–107. DOI: 10.1109/MCS.2018.2830081.

Nooij, S. A. E., M. Wentink, H. Smaili, L. Zaichik, and E. L. Groen (2016). "Motion Simulation of Transport Aircraft in Extended Envelopes : Test Pilot Assessment". In: *Journal of Guidance, Control, and Dynamics*. DOI: 10.2514/1.G001790.

Papachristodoulou, Antonis and Stephen Prajna (2009). "Robust Stability Analysis of Nonlinear Hybrid Systems". In: *IEEE Transactions on Automatic Control* 54.5, pp. 1035–1041. DOI: 10.1109/TAC.2009.2017155.

Parillo, Pablo A. (2003). "Semidefinite programming relaxations for semialgebraic problems". In: *Mathematical Programming, Series B* 96.2, pp. 293–320. DOI: 10.1007/s10107-003-0387-5.

Parks, P. C. (1992). "A. M. Lyapunov's stability theory—100 years on". In: *IMA Journal of Mathematical Control & Information* 9.4, pp. 275–303. DOI: 10.1093/imamci/9.4.275.

Permenter, Frank and Pablo A. Parrilo (2014). "Basis selection for SOS programs via facial reduction and polyhedral approximations". In: *53rd IEEE Conference on Decision and Control*. Los Angeles, US-CA, pp. 6615–6620. DOI: 10.1109/CDC.2014.7040427.

Philippe, Christian (2011). "Verification, Validation, and Certification of Aerospace Control Systems". In: *The Impact of Control Technology*. Ed. by T. Samad and A. M. Annaswamy. New York, US-NY: IEEE Control Systems Society. Chap. 4, pp. 205–206. URL: http://www.ieeecss.org/general/impact-control-technology.

Philippe, Christian, Anuradha Annaswamy, Gary Balas, Johann Bals, Sanjay Garg, and Alexander Knoll (2011). "Aerospace Control". In: *The Impact of Control Technology*. Ed. by T. Samad and A. M. Annaswamy. New York, US-NY: IEEE Control Systems Society. Chap. 1, pp. 9–20. URL: http://www.ieeecss.org/general/impact-control-technology.

Phillips, Warren F. (2010). *Mechanics of Flight*. 2nd ed. Hoboken, US-NJ: John Wiley & Sons.

Proctor, Christopher (2019). "Model Predictive Control Synthesis for the Innovative Control Effector Tailless Fighter Aircraft". Master's thesis. Kalamazoo, US-MI: Western Michigan University. URL: https://scholarworks.wmich.edu/masters_theses/4304.

Putinar, Mihai (1993). "Positive Polynomials on Compact Semi-algebraic sets". In: *Indiana University Mathematics Journal* 42.3, pp. 969–984. URL: https://www.jstor.org/stable/24897130.

Rantzer, Anders (2001). "A dual to Lyapunov's stability theorem". In: *Systems and Control Letters* 42.3, pp. 161–168. DOI: 10.1016/S0167-6911(00)00087-6.

Rao, Arjun H., Daniel V. Uhlig, and Michael S. Selig (2012). "Glide and Powered Flight Characteristics of Micro Air Vehicles from Experimental Measurements". In: *AIAA Applied Aerodynamics Conference*. New Orleans, US-LA. DOI: 10.2514/6.2012-2768.

Rawlings, James B., David Q. Mayne, and Moritz Diehl (2017). *Model Predictive Control: Theory, Computation, and Design*. 2nd ed. Santa Barbara, US-CA: Nob Hill. DOI: 10.1002/9783527645206.ch16.

Reble, Marcus and Frank Allgöwer (2012). "Unconstrained model predictive control and suboptimality estimates for nonlinear continuous-time systems". In: *Automatica* 48.8, pp. 1812–1817. DOI: 10.1016/j.automatica.2012.05.067.

Richards, Nathan D., Neha Gandhi, Alec J. Bateman, David H. Klyde, and Amanda K. Lampton (2017). "Vehicle Upset Detection and Recovery for Onboard Guidance and Control". In: *Journal of Guidance, Control, and Dynamics* 40.4, pp. 920–933. DOI: 10.2514/1.G001738.

Richards, Nathan D., Neha Gandhi, Alec J. Bateman, David H. Klyde, Philip C. Schulze, and Christine M. Belcastro (2018). "Piloted Flight Test Evaluation of Robust Upset-Recovery Guidance". In: *2018 AIAA Guidance, Navigation, and Control Conference*. Kissimmee, US-FL: American Institute of Aeronautics and Astronautics. DOI: 10.2514/6.2018-1864.

Rigeros, Gerasimos (2015). "Differential Flatness Theory and Flatness-Based Control". In: *Nonlinear Control and Filtering Using Differential Flatness Approaches*. Zurich, CH: Springer. Chap. 2, pp. 47–102. DOI: 10.1007/978-3-319-16420-5.

Robison, D. E. (1964). "Estimates for the Points of Intersection of Two Polynomial Regressions". In: *Journal of the American Statistical Association* 59.305, pp. 214–224. DOI: 10.2307/2282870.

Rozgonyi, Szabolcs, Katalin M. Hangos, and Gábor Szederkényi (2010). "Determining the domain of attraction of hybrid non-linear systems using maximal Lyapunov functions". In: *Kybernetika* 46.1, pp. 19–37. URL: https://eudml.org/doc/37706.

Scampicchio, Anna, Alberto Giaretta, and Gianluigi Pillonetto (2018). "Nonlinear Hybrid Systems Identification using Kernel-Based Techniques". In: *18th IFAC Symposium on System Identification*. Stockholm, SE, pp. 269–274. DOI: 10.1016/j.ifacol.2018.09.146.

Schuet, Stefan R., Thomas J. J. Lombaerts, Diana Acosta, John Kaneshige, Kevin Wheeler, and Kimberlee Shish (2017). "Autonomous Flight Envelope Estimation for Loss-of-Control Prevention". In: *Journal of Guidance, Control, and Dynamics* 40.4. DOI: 10.2514/1.G001729.

Schuet, Stefan R., Thomas J. J. Lombaerts, John Kaneshige, Kimberlee H. Shish, and Vahram Stepanyan (2017). "Stall Recovery Guidance Using Fast Model Predictive Control". In: *AIAA Guidance, Navigation, and Control Conference*. Grapevine, US-TX. DOI: 10.2514/6.2017-1513.

Schuet, Stefan R., Thomas J. J. Lombaerts, Vahram Stepanyan, John Kaneshige, Kimberlee Shish, Peter Robinson, and Gordon H. Hardy (2017). *Vertical Motion Simulator Experiment on Stall Recovery Guidance*. NASA technical publication NASA/TP-2017-219733. Mofett Field, US-CA: Ames Research Center.

Seifried, R. and W. Blajer (2013). "Analysis of servo-constraint problems for underactuated multibody systems". In: *Mechanical Sciences* 4.1, pp. 113–129. DOI: 10.5194/ms-4-113-2013.

Seiler, Peter and Gary J. Balas (2010). "Quasiconvex sum-of-squares programming". In: *49th IEEE Conference on Decision and Control*. Atlanta, US-GA, pp. 3337–3342. DOI: 10.1109/CDC.2010.5717672.

Selig, Michael S (2010). "Modeling Full-Envelope Aerodynamics of Small UAVs in Real-time". In: *AIAA Atmospheric Flight Mechanics Conference*. Toronto, CA, pp. 1–35. DOI: 10.2514/6.2010-7635.

Sieberling, S., Q. P. Chu, and J. A. Mulder (2010). "Robust Flight Control Using Incremental Nonlinear Dynamic Inversion and Angular Acceleration Prediction Inversion and Angular Acceleration Prediction". In: *Journal of Guidance, Control, and Dynamics* 33.6, pp. 1732–1742. DOI: 10.2514/1.49978.

Skogestad, Sigurd and Ian Postlethwaite (2005). *Multivariable Feedback Control: Analysis and Design*. 2 ed. Chichester, GB: John Wiley & Sons. DOI: 978-0-470-01167-6. arXiv: 0470011688.

Sky-Watch (2017). *The Cumulus v1 UAV*. URL: http://sky-watch.com/products/cumulus/ (visited on 02/06/2018).

Slotine, Jean-Jacques E. and Weiping Li (1991). *Applied Nonlinear Control*. Upper Saddle River, US-NJ: Prentice-Hall. ISBN: 0-13-040890-5.

Smaili, M. H., J. Breeman, Thomas J. J. Lombaerts, J. A. Mulder, Q. P. Chu, and O. Stroosma (2016). "Intelligent Flight Control Systems Evaluation for Loss-of-Control Recovery and Prevention". In: *Journal of Guidance, Control, and Dynamics* 40.4, pp. 890–904. DOI: 10.2514/1.G001756.

Smaili, M. H., W. F. J. A. Rouwhorst, and P. Frost (2017). "Conceptual Design and Evaluation of Upset-Recovery Systems for Civil Transport Aircraft". In: *Journal of Aircraft* 55.3, pp. 947–964. DOI: 10.2514/1.C034422.

Smith, Kirstine (1918). "On the Standard Deviations of Adjusted and Interpolated Values of an Observed Polynomial Function and its Constants and the Guidance they give Towards a Proper Choice of the Distribution of Observations". In: *Biometrika* 12.1/2. DOI: 10.2307/2331929.

Sparks, D. W. and D. D. Moerder (2002). "Optimal aircraft control upset recovery with and without component failures". In: *Proceedings of the American Control Conference*. Anchorage, US-AK, pp. 3644–3649. DOI: 10.1109/ACC.2002.1024494.

Stengle, Gilbert (1974). "A Nullstellensatz and a Positivstellensatz in Semialgebraic Geometry". In: *Mathematische Annalen* 207.2, pp. 87–97. DOI: 10.1007/BF01362149.

Stepanyan, Vahram, Kalmanje Krishnakumar, Greg Dorais, Scott Reardon, Jonathan Barlow, Amanda K Lampton, and Gordon Hardy (2017). "Loss-of-Control Mitigation via Predictive Cuing". In: *Journal of Guidance, Control, and Dynamics* 40.4. DOI: 10.2514/1.G001731.

Stepanyan, Vahram, Kalmanje Krishnakumar, John Kaneshige, and Diana Acosta (2016). "Stall Recovery Guidance Algorithms Based on Constrained Control Approaches". In: *AIAA Guidance, Navigation, and Control Conference*. San Diego, US-CA. DOI: 10.2514/6.2016-0878.

Stigler, Stephen M. (1974). "Gergonne's 1815 paper on the design and analysis of polynomial regression experiments". In: *Historia Mathematica* 1, pp. 431–439. DOI: 10.1016/0315-0860(74)90033-0.

Swihart, Donald E., Arthur F. Barfield, Edward M. Griffin, Richard C. Lehmann, Shawn C. Whitcomb, Billie Flynn, Mark A. Skoog, and Kevin E. Processor (2011). "Automatic Ground Collision Avoidance System Design, Integration, & Flight Test". In: *IEEE Aerospace and Electronic Systems Magazine* 26, pp. 4–11. DOI: 10.1109/MAES.2011.5871385.

Tan, Weehong (2006). "Nonlinear Control Analysis and Synthesis using Sum-of-Squares Programming". PhD thesis. Berkeley, US-CA: University of California, Berkeley. ISBN: 9780542826740.

Tan, Weehong and Andrew Packard (2008). "Stability region analysis using polynomial and composite polynomial Lyapunov functions and sum-of-squares programming". In: *IEEE Transactions on Automatic Control* 53.2, pp. 565–571. DOI: 10.1109/TAC.2007.914221.

Tedrake, Russ, Ian R. Manchester, Mark Tobenkin, and John W. Roberts (2010). "LQR-trees: Feedback Motion Planning via Sums-of-Squares Verification". In: *The International Journal of Robotics Research* 29.8, pp. 1038–1052. DOI: 10.1177/0278364910369189.

Tekles, Nikolas, June Chongvisal, Enric Xargay, Ronald Choe, Donald A. Talleur, Naira Hovakimyan, and Christine M. Belcastro (2017). "Design of a Flight Envelope Protection System for NASA's Transport Class Model". In: *Journal of Guidance, Control, and Dynamics* 40.4. DOI: 10.2514/1.G001728.

Toker, Onur and Hitay Özbay (1995). "On the NP-hardness of solving Bilinear Matrix Inequalities and simultaneous stabilization with static output feedback". In: *Proceedings of the 1995 American Control Conference*. Seattle, US-WA, pp. 2525–2526. DOI: 10.1109/ACC.1995.532300.

Tol, H. J., Coen C. de Visser, L. G. Sun, E. van Kampen, and Q. P. Chu (2016). "Multivariate Spline-Based Adaptive Control of High-Performance Aircraft with Aerodynamic Uncertainties". In: *Journal of Guidance, Control, and Dynamics* 39.4, pp. 781–800. DOI: 10.2514/1.G001079.

Topcu, Ufuk, Andrew K. Packard, Peter Seiler, and Gary J. Balas (2010). "Robust Region-of-Attraction Estimation". In: *IEEE Transactions on Automatic Control* 55.1, pp. 137–142. DOI: 10.1109/TAC.2009.2033751.

Topcu, Ufuk, Andrew Packard, and Peter Seiler (2008). "Local stability analysis using simulations and sum-of-squares programming". In: *Automatica* 44.10, pp. 2669–2675. DOI: 10.1016/j.automatica.2008.03.010.

Ure, N. Kemal and Gokhan Inalhan (2012). "Autonomous control of unmanned combat air vehicles: Design of a multimodal control and flight planning framework for agile maneuvering". In: *IEEE Control Systems Magazine* 32.5, pp. 74–95. DOI: 10.1109/MCS.2012.2205532.

Urnes Sr, James M. (2012). "Flight Control for Multi-engine UAV Aircraft using Propulsion Control". In: *AIAA Infotech@Aerospace*. Garden Grove, US-CA. DOI: 10.2514/6.2012-2570.

Valmorbida, Giorgio and James Anderson (2017). "Region of attraction estimation using invariant sets and rational Lyapunov functions". In: *Automatica* 75, pp. 37–45. DOI: 10.1016/j.automatica.2016.09.003.

Vandenberghe, Lieven and Stephen Boyd (1996). "Semidefinite Programming". In: *SIAM Review* 38.1, pp. 49–95. DOI: 10.1137/1038003.

Vannelli, A. and M. Vidyasagar (1985). "Maximal Lyapunov Functions and Domains of Attraction for Autonomous Nonlinear Systems". In: *Automatica* 21.1, pp. 69–80. DOI: 10.1016/0005-1098(85)90099-8.

de Visser, Coen C., Q. P. Chu, and J. A. Mulder (2009). "A new approach to linear regression with multivariate splines". In: *Automatica* 45.12, pp. 2903–2909. DOI: 10.1016/j.automatica.2009.09.017.

de Visser, Coen C., J. A. Mulder, and Q. P. Chu (2010). "A Multidimensional Spline-Based Global Nonlinear Aerodynamic Model for the Cessna Citation II". In: *AIAA*

Atmospheric Flight Mechanics Conference. Toronto, CA. DOI: 10.2514/6.2010-7950.

Wächter, Andreas and Lorenz T. Biegler (2006). "On the implementation of an interior-point filter line-search algorithm for large-scale nonlinear programming". In: *Mathematical Programming, Series A* 106, pp. 25–57. DOI: 10.1007/s10107-004-0559-y.

Wilborn, James and John V. Foster (2004). "Defining Commercial Transport Loss-of-Control: A Quantitative Approach". In: *AIAA Atmospheric Flight Mechanics Conference and Exhibit*. August, pp. 1–11. DOI: 10.2514/6.2004-4811.

Xargay, Enric, Naira Hovakimyan, and Chengyu Cao (2010). "$\mathcal{L}_1$ adaptive controller for multi-input multi-output systems in the presence of nonlinear unmatched uncertainties". In: *IEEE American Control Conference*. Baltimore, US-MD, pp. 874–879. DOI: 10.1109/ACC.2010.5530686.

Yildiz, Anil, M. Ugur Akcal, Batuhan Hostas, and N. Kemal Ure (2019). "Switching Control Architecture with Parametric Optimization for Aircraft Upset Recovery". In: *Journal of Guidance, Control, and Dynamics*. DOI: 10.2514/1.G004180.

Yin, He, Andrew Packard, Murat Arcak, and Peter Seiler (2019). "Finite horizon backward reachability analysis and control synthesis for uncertain nonlinear systems". In: *Proceedings of the American Control Conference*. Philadelphia, US-PA, pp. 5020–5026. DOI: 10.23919/ACC.2019.8814444. arXiv: 1810.00313.

Yu, Mingzhao and Lorenz T. Biegler (2019). "A reduced regularization strategy for economic NMPC". In: *Journal of Process Control* 73, pp. 46–57. DOI: 10.1016/j.jprocont.2018.11.001.

Yu, Pei (2003). "Bifurcation Dynamics in Control Systems". In: *Bifurcation Control. Theory and Applications*. Ed. by Guanrong Chen, David J. Hill, and Xinghuo Yu. Berlin, DE: Springer. Chap. 6, pp. 99–126. DOI: 10.1007/978-3-540-44925-6_6.

Zanon, Mario and Timm Faulwasser (2018). "Economic MPC without terminal constraints: Gradient-correcting end penalties enforce asymptotic stability". In: *Journal of Process Control* 63, pp. 1–14. DOI: 10.1016/j.jprocont.2017.12.005.

Zhao, Yue (2016). "Automatic Prevention and Recovery of Aircraft Loss-of-Control by a Hybrid Control Approach". PhD thesis. Athens, US-OH: Ohio University.

Zheng, Xiuliang, Zhikun She, Junjie Lu, and Meilun Li (2018). "Computing multiple Lyapunov-like functions for inner estimates of domains of attraction of switched hybrid systems". In: *International Journal of Robust and Nonlinear Control*. DOI: 10.1002/rnc.4280.

Zubov, V I (1964). *Methods of A. M. Lyapunov and their Application*. Groningen, NL: P. Noordhoff.

Appendix

Appendix A

The `pwpfit` Toolbox

This appendix chapter corresponds to:

> Torbjørn Cunis (2018). "The `pwpfit` Toolbox for Polynomial and Piece-wise Polynomial Data Fitting". In: *18th IFAC Symposium on System Identification*. Stockholm, SE, pp. 682–687. DOI: `10.1016/j.ifacol.2018.09.204`

in the author's finally submitted version.

Synopsis

The `pwpfit` toolbox has been developed in order to compute the piecewise polynomial models of Chapters 3 and 4. This appendix details the mathematical background as well as the implementation beyond the initial presentation in Chapter 3. Furthermore, we discuss aspects of the fitting method such as computation time and sensitivity to measurement noise. Note that for demonstration purposes only, the piecewise polynomial aerodynamics model has been derived as single polynomials in all inputs,

$$C_{\odot}(\alpha, \beta, \xi, \eta, \zeta, \ldots)$$

Due to the disadvantages of this strategy both in computation time and fitting accuracy, the models finally used in this thesis are sums of polynomials

$$C_{\odot\alpha}(\alpha) + C_{\odot\beta}(\alpha, \beta) + C_{\odot\xi}(\alpha, \beta, \xi) + C_{\odot\eta}(\alpha, \beta, \eta) + C_{\odot\zeta}(\alpha, \beta, \zeta) + \cdots ,$$

as bespoken in Section A.7 and given in Appendix B.1 and B.2.

The `pwpfit` Toolbox for Polynomial and Piece-wise Polynomial Data Fitting

Torbjørn Cunis [a,b]

[a] *Department of Information Processing and Systems, ONERA – The French Aerospace Lab, Centre Midi-Pyrénées, 31055 Toulouse, France*
(e-mail: torbjoern.cunis@onera.fr)

[b] *Drones Research Group, French Civil Aviation School, 31055 Toulouse, France*
(e-mail: torbjoern.cunis@recherche.enac.fr)

Abstract

Several techniques have been proposed for piecewise regression as extension to standard polynomial data fitting, either selecting the joints a priori or adding computational load for optimal joints. The `pwpfit` [1] toolbox provides piecewise polynomial fitting without pre-selection of joints using linear-least square (LSQ) optimization only. Additional constraints are realised as constraint matrices for the LSQ problem. We give an application example for the multi-variable aerodynamic coefficients of the general transport model in pre-stall and post-stall.

Key words: Grey Box Modeling; Toolboxes; Mechanical and Aerospace; Multivariable System Identification; Nonlinear System Identification; Hybrid System Identification.

1 Introduction

Polynomial data fitting names a branch of approaches dedicated to the problem of optimal coefficients for a polynomial function f, such that f approximates the measured data points, usually called "observations". A common solution consists of minimising the sum of squared residuals of f with respect to the observations using *linear least-square* (LSQ) techniques (Kariya and Kurata, 2004). Several methods exist to solve LSQ problems (Golub, 1982; Lawson and Hanson, 1995). Compared to modern tools, polynomials benefit from fast and simple evaluation.

[1] Published under LGPL-2.1: https://github.com/pwpfit.

However, a single polynomial function might not be suitable to describe the observed characteristics. Early approaches included regression of a few polynomial functions *piecewise* over the observations; in order to find suitable switching surfaces (*joints*) for the piecewise functions, these approaches used maximum-likelihood or Newton-Gauss methods (Robison, 1964; Gallant and Fuller, 1973), hierarchical clustering (McGee and Carleton, 1970), or regressions trees (Chaudhuri et al., 1994). Later, *multivariate splines* were introduced fitting sequences of polynomial functions over fine grids, which are rectangular (Klein and Morelli, 2006) or triangular (de Visser et al., 2009) partitions of the observations. Here, the knots of the grids, *i.e.* the joints of the piecewise functions, are chosen prior, and are not a subject of, the fit. Both piecewise regression and multivariate splines ensure the fitted piecewise functions to be continuous or even smooth at their joints.

While splines today present a powerful yet complex tool for accurate and smooth interpolation, they lack of an underlying physical model justifying the partition. [2] The problem of finding appropriate joints remains open.
In this paper, we introduce the `pwpfit` [1] toolbox for MATLAB, which uses standard LSQ techniques while leaving the joint as parameter of optimization. The interface of the toolbox, on the other hand, resembles that of MATLAB's well-known `fit` function. [3] Following a study of the theoretical and implementation details, we discuss exemplary the fitting of piecewise aerodynamic coefficients for the model of a typical airliner.

2 Preliminaries

A *monomial of degree* n is a single product of powers where the exponents add up to the total degree n, without any scalar coefficient. We introduce the vector notation for a monomial $\mathbf{x} = (x_1, \ldots, x_m)$ in degrees $\mathbf{n} = (n_1, \ldots, n_m)$,

$$\mathbf{x}^{\mathbf{n}} = x_1^{n_1} \ldots x_m^{n_m}, \tag{1}$$

with the total degree $n = \|\mathbf{n}\|_1 = n_1 + \cdots + n_m$.

2.1 Monomials & Polynomials

Definition 1 *$\boldsymbol{\mathcal{P}}_n(\mathbf{x})$ is the vector of monomials $\mathbf{x}^{\boldsymbol{\nu}}$ in variables $\mathbf{x} = (x_1, \ldots, x_m)$ with degrees $\boldsymbol{\nu} \in \mathbb{N}^m$ and total degrees $\|\boldsymbol{\nu}\|_1 \leq n$; and the number of elements*

[2] MATLAB's *smoothing spline* option for the built-in curve fitting function, for example, uses by default the observation points itself.
[3] https://mathworks.com/help/curvefit/fit.html

in $\boldsymbol{\mathcal{P}}_n(\mathbf{x})$ *is denoted by* $\mathfrak{r}[n]$*, i.e.* $\boldsymbol{\mathcal{P}}_n \in \mathbb{R}\left[\mathbf{x}\right]^{\mathfrak{r}[n]}$.

While the order of monomials in $\boldsymbol{\mathcal{P}}_n(\mathbf{x})$ is arbitrary, we choose to have $\mathbf{x}^{\boldsymbol{\mu}}$ before $\mathbf{x}^{\boldsymbol{\nu}}$ if and only if $\|\boldsymbol{\mu}\|_1 < \|\boldsymbol{\nu}\|_1$ or $\boldsymbol{\mu}$ is reverse-lexicographically before $\boldsymbol{\nu}$ if $\|\boldsymbol{\mu}\|_1 = \|\boldsymbol{\nu}\|_1$.
Defining the auxiliary vector $\mathbf{p}_N$ of monomials $\mathbf{x}^{\boldsymbol{\nu}}$ with $\|\boldsymbol{\nu}\|_1 = N$, recursively over the number of variables m as

$$\mathbf{p}_N(\mathbf{x}) = \begin{cases} x_1^N & \text{if } m = 1; \\ \left[x_1^N \;\; x_1^{N-1}\mathbf{p}_1(\tilde{\mathbf{x}})^T \;\cdots\; \mathbf{p}_N(\tilde{\mathbf{x}})^T\right]^T & \text{else} \end{cases} \tag{2}$$

with $\tilde{\mathbf{x}} = (x_2, \ldots, x_m)$ for $m > 1$, we can write

$$\boldsymbol{\mathcal{P}}_n(\mathbf{x}) = \left[1 \;\; \mathbf{p}_1(\mathbf{x})^T \;\; \cdots \;\; \mathbf{p}_n(\mathbf{x})^T\right]^T. \tag{3}$$

By this notation, a polynomial f is expressed as scalar product of its monomials and coefficients,

$$f(\mathbf{x}) = \left\langle \boldsymbol{\mathcal{P}}_n(\mathbf{x}), \mathbf{q} \right\rangle \tag{4}$$

with the *vector of coefficients* $\mathbf{q}^T = \left[b_1 \;\cdots\; b_{\mathfrak{r}[n]}\right]$.

2.2 Polynomial fitting

The observations $(\mathbf{x}_i, z_i)$ are conveniently given as sequences over $i \in [1, k]$:

Problem 2 *Consider the* k *observations*

$$z_i = \gamma(\mathbf{x}_i) + \epsilon_i, \tag{5}$$

where $(\mathbf{x}_i, z_i, \epsilon_i)_{1 \le i \le k} \subset \mathbb{R}^m \times \mathbb{R} \times \mathbb{R}$ *and* $\gamma(\cdot)$ *and* $(\epsilon_i)_i$ *are an unknown function and measurement error, respectively; find coefficients for* $f = \left\langle \boldsymbol{\mathcal{P}}_n(\mathbf{x}), \mathbf{q} \right\rangle$ *minimizing the goodness of fit (GoF)*

$$\mathrm{GoF}(f) \stackrel{def}{=} \sum_{i=1}^{k} |f(\mathbf{x}_i) - z_i|^2 \tag{6}$$

for an $n > 0$.

Re-writing the goodness of fit using matrix calculus, we reduce the cost functional to a cost function and polynomial data fitting to a linear least-square problem.

Definition 3 *A linear least-square (LSQ) problem is given as the optimization problem*

$$\operatorname{lsq}(\mathbf{C},\mathbf{d}) = \arg\min_{\mathbf{q}} \|\mathbf{C}\mathbf{q}-\mathbf{d}\|_2^2 \tag{7}$$

with $\mathbf{q}\in\mathbb{R}^r$, $\mathbf{C}\in\mathbb{R}^{k\times r}$, *and* $\mathbf{d}\in\mathbb{R}^k$.

We have the residuals in vector notation as

$$\mathbf{e} = \underbrace{\begin{bmatrix} \boldsymbol{\mathcal{P}}_n(x_{1,1},\ldots,x_{1,m})^T \\ \vdots \\ \boldsymbol{\mathcal{P}}_n(x_{k,1},\ldots,x_{k,m})^T \end{bmatrix}}_{\stackrel{\text{def}}{=}\mathbf{K}} \mathbf{q} - \underbrace{\begin{bmatrix} z_1 \\ \vdots \\ z_k \end{bmatrix}}_{\stackrel{\text{def}}{=}\boldsymbol{\kappa}} \tag{8}$$

and the goodness of fit

$$\operatorname{GoF}(\mathbf{q}) = \|\mathbf{e}\|_2^2 . \tag{9}$$

The coefficients of the optimal fit $\langle \boldsymbol{\mathcal{P}}_n(\mathbf{x}), \mathbf{q}_0\rangle$ now are subject to the linear-least square problem

$$\mathbf{q}_0 = \arg\min_{\mathbf{q}} \|\mathbf{K}\mathbf{q}-\boldsymbol{\kappa}\|_2^2 . \tag{10}$$

3 Piecewise fitting

Problem 4 *Take the observations of Problem 2; find coefficients* $\mathbf{q}_1,\mathbf{q}_2$ *such that*

$$f:\mathbf{x}\longmapsto \begin{cases} \langle \boldsymbol{\mathcal{P}}_n(\mathbf{x}), \mathbf{q}_1\rangle \text{ if } \varphi(\mathbf{x}) \le x_0; \\ \langle \boldsymbol{\mathcal{P}}_n(\mathbf{x}), \mathbf{q}_2\rangle \text{ else} \end{cases}$$

with $\varphi\colon\mathbb{R}^m\to\mathbb{R}$ *and* $x_0\in\mathbb{R}$ *minimizes the goodness of fit of* (6).[4]

We note the sub-polynomials of f by $f_{1,2}\colon \mathcal{X}_{1,2}\to\mathbb{R}, \mathbf{x}\mapsto\langle \boldsymbol{\mathcal{P}}_n(\mathbf{x}), \mathbf{q}_{1,2}\rangle$ and call $\mathcal{X}_1\cup\mathcal{X}_2$ the *entire domain of* f. The *joint* of f is given as $\Omega_\varphi \stackrel{\text{def}}{=} \mathcal{X}_1\cap\mathcal{X}_2 = \{\mathbf{x}\,|\varphi(\mathbf{x})=x_0\}$.

The cost functional for f can be evaluated piecewise to

$$\operatorname{GoF}(f) = \sum_{\mathbf{x}_i\in X_1} |f_1(\mathbf{x}_i)-z_i|^2 + \sum_{\mathbf{x}_i\in X_2} |f_2(\mathbf{x}_i)-z_i|^2, \tag{11}$$

[4] While solutions for multiple pieces can be derived, we focus on a single joint here.

where $X_1 = \{\mathbf{x}_1, \ldots, \mathbf{x}_{i'}\}$, $X_2 = \{\mathbf{x}_{i'+1}, \ldots, \mathbf{x}_k\}$ are initial guesses of the subdomains.

We then have the residuals as $\mathbf{e}_{1,2} = \mathbf{K}_{1,2}\,\mathbf{q}_{1,2} - \boldsymbol{\kappa}_{1,2}$ with

$$\mathbf{K}_1 = \begin{bmatrix} \boldsymbol{\mathcal{P}}_n(\mathbf{x}_1)^T \\ \vdots \\ \boldsymbol{\mathcal{P}}_n(\mathbf{x}_{i'})^T \end{bmatrix}, \qquad \boldsymbol{\kappa}_1 = \begin{bmatrix} z_1 \\ \vdots \\ z_{i'} \end{bmatrix}; \tag{12}$$

$$\mathbf{K}_2 = \begin{bmatrix} \boldsymbol{\mathcal{P}}_n(\mathbf{x}_{i'+1})^T \\ \vdots \\ \boldsymbol{\mathcal{P}}_n(\mathbf{x}_k)^T \end{bmatrix}, \quad \boldsymbol{\kappa}_2 = \begin{bmatrix} z_{i'+1} \\ \vdots \\ z_k \end{bmatrix}; \tag{13}$$

and

$$\mathrm{GoF}(f) = \|\mathbf{e}_1\|_2^2 + \|\mathbf{e}_2\|_2^2 = \left\| \left[\mathbf{e}_1^T \,\vdots\, \mathbf{e}_2^T \right] \right\|_2^2. \tag{14}$$

Again, we reduce piecewise fitting to the linear least-square problem

$$\begin{bmatrix} \mathbf{q}_1 \\ \hdashline \mathbf{q}_2 \end{bmatrix} = \arg\min_{\mathbf{q}'} \left\| \left[\begin{array}{c:c} \mathbf{K}_1 & \mathbf{0} \\ \hdashline \mathbf{0} & \mathbf{K}_2 \end{array}\right] \mathbf{q}' - \begin{bmatrix} \boldsymbol{\kappa}_1 \\ \hdashline \boldsymbol{\kappa}_2 \end{bmatrix} \right\|_2^2 \tag{15}$$

with the *objective matrix* $\mathbf{K} \overset{\text{def}}{=} \mathrm{diag}(\mathbf{K}_1, \mathbf{K}_2)$.

Continuity of the piecewise defined f over its entire domain holds if

$$\forall \mathbf{x} \in \Omega_\varphi. \quad \langle \boldsymbol{\mathcal{P}}_n(\mathbf{x}), \mathbf{q}_1 \rangle = \langle \boldsymbol{\mathcal{P}}_n(\mathbf{x}), \mathbf{q}_2 \rangle. \tag{16}$$

For single-variable functions, we have continuity for the identity function $\varphi = \mathrm{id}$ and x_0 is zero of

$$\langle \boldsymbol{\mathcal{P}}_n(x), \mathbf{q}_1 - \mathbf{q}_2 \rangle.$$

In the multivariate case, computing φ is generally hard.

4 Constraints

To impose constraints on the coefficients (and thus the polynomials), we recall the *constrained* linear least-square problem (Haskell and Hanson, 1981)

$$\operatorname{lsq}(\mathbf{C}, \mathbf{d}, \mathbf{A}, \mathbf{0}) = \arg\min_{\mathbf{q} \in \Omega_{\mathbf{A}}} \|\mathbf{C}\mathbf{q} - \mathbf{d}\|_2^2 . \tag{17}$$

with $\Omega_{\mathbf{A}} = \{\mathbf{q} \,|\mathbf{A}\mathbf{q} = \mathbf{0}\}$.

Lemma 5 *Let $f_{1,2} = \langle \boldsymbol{\mathcal{P}}_n(\mathbf{x}) \,, \mathbf{q}_{1,2} \rangle$ be polynomials; we have $f_1(\mathbf{x}) = f_2(\mathbf{x})$ for all $\mathbf{x} \in \mathbb{R}^{\mathfrak{r}[n]}$ if and only if $\mathbf{q}_1 = \mathbf{q}_2$.*

In case of multiple variables or outputs, one may have x_0 for the single-variable, single-output case and ensure continuity in x_0 for all other variables and outputs.

Proposition 6 (Constraint of continuity) *Let*

$$\varphi(\mathbf{x}) = \mathbf{a}^T \mathbf{x} \leq x_0 \tag{18}$$

be a linear matrix inequality (LMI) with $\mathbf{a}^T = \begin{bmatrix} a_1 & \cdots & a_m \end{bmatrix}$ and $a_1 \neq 0$; a piecewise polynomial function f with continuity in Ω_ϕ is subject to the constrained LSQ problem with continuity constraint matrix $\boldsymbol{\mathcal{C}}$.

PROOF. We can simplify (18) to $\varphi(\mathbf{x}) = x_1 \leq x_0$ w.l.o.g.:

Lemma 7 *Let $\varphi \colon \mathbf{x} \mapsto \mathbf{a}^T \mathbf{x}$ with $a_1 \neq 0$; there is a linear, invertible $\boldsymbol{\pi}$ such that*

$$(\varphi \circ \boldsymbol{\pi}) \colon \mathbf{y} \longmapsto y_1 \tag{19}$$

with $\mathbf{y} = (y_1, \ldots, y_m)$.

For $\varphi(\mathbf{x}) \neq x_1$, we thus fit polynomials $g_{1,2}$ to $(\boldsymbol{\pi}\mathbf{x}_i, z_i)_i$ such that $g_{1,2}$ join in $(\varphi \circ \boldsymbol{\pi})(\mathbf{y}) = x_0$ and find $f_{1,2}$ as

$$f_1 = \left(g_1 \circ \boldsymbol{\pi}^{-1}\right); \qquad f_2 = \left(g_2 \circ \boldsymbol{\pi}^{-1}\right). \tag{20}$$

We now have continuity if

$$\forall \mathbf{x} \in \Omega_{x_0}. \quad \langle \boldsymbol{\mathcal{P}}_n(\mathbf{x}) \,, \mathbf{q}_1 \rangle = \langle \boldsymbol{\mathcal{P}}_n(\mathbf{x}) \,, \mathbf{q}_2 \rangle \tag{21}$$

with $\Omega_{x_0} = \{\mathbf{x} \,| x_1 = x_0 \}$; hence

$$\forall \tilde{\mathbf{x}} \in \mathbb{R}^{m-1}. \quad \langle \boldsymbol{\mathcal{P}}_n(x_0, \tilde{\mathbf{x}}) \,, \mathbf{q}_1 \rangle = \langle \boldsymbol{\mathcal{P}}_n(x_0, \tilde{\mathbf{x}}) \,, \mathbf{q}_2 \rangle. \tag{22}$$

Separation of the assigned variable $x_1 \equiv x_0$ as $\mathbf{\Lambda}_0^T$ yields

$$\begin{aligned}\langle \boldsymbol{\mathcal{P}}_n(x_0, \tilde{\mathbf{x}}) \, , \mathbf{q}_{1,2} \rangle &= \langle \mathbf{\Lambda}_0^T \boldsymbol{\mathcal{P}}_n(\tilde{\mathbf{x}}) \, , \mathbf{q}_{1,2} \rangle \\ &= \langle \boldsymbol{\mathcal{P}}_n(\tilde{\mathbf{x}}) \, , \mathbf{\Lambda}_0 \mathbf{q}_{1,2} \rangle \end{aligned} \tag{23}$$

with

$$\mathbf{\Lambda}_0 = \left[\begin{array}{c|c|c|c} 1 & x_0 & & x_0^n \\ \hline & \operatorname{diag} \mathbf{p}_1(\mathbf{1}_{m-1}) & \cdots & x_0^{n-1} \operatorname{diag} \mathbf{p}_1(\mathbf{1}_{m-1}) \\ \hline & & & \ddots \\ & & & \operatorname{diag} \mathbf{p}_n(\mathbf{1}_{m-1}) \end{array}\right], \tag{24}$$

where $\mathbf{1}_{m-1} \in \{1\}^{m-1}$. By Lemma 5, we have that

$$\langle \boldsymbol{\mathcal{P}}_n(\tilde{\mathbf{x}}) \, , \mathbf{\Lambda}_0 \mathbf{q}_1 \rangle = \langle \boldsymbol{\mathcal{P}}_n(\tilde{\mathbf{x}}) \, , \mathbf{\Lambda}_0 \mathbf{q}_2 \rangle \tag{25}$$

for all $\tilde{\mathbf{x}} \in \mathbb{R}^{m-1}$ if and only if $\mathbf{\Lambda}_0 \mathbf{q}_1 = \mathbf{\Lambda}_0 \mathbf{q}_2$. Hence, the constraint of continuity is written as

$$\left[\begin{array}{c|c} \mathbf{\Lambda}_0 & -\mathbf{\Lambda}_0 \end{array}\right] \left[\begin{array}{c} \mathbf{q}_1 \\ \hline \mathbf{q}_2 \end{array}\right] = \mathbf{0} \tag{26}$$

and $\boldsymbol{\mathcal{C}} = \Big[\mathbf{\Lambda}_0 \; -\mathbf{\Lambda}_0\Big]$.

Due to measurement errors or modelling flaws, a polynomial fitting may have relations that shall not be modeled;[5] in this case, it is desirable to constrain the resulting polynomial to be zero (or constant) for certain parameters $\tilde{\mathbf{x}}^* = (x_{j+1}, \cdots, x_m)$:

Proposition 8 (Zero constraint) *Let* $\mathbf{x}^* = (x_1, \ldots, x_j)$ *for* $j > 0$*; a polynomial* $f = \langle \boldsymbol{\mathcal{P}}_n(\mathbf{x}) \, , \mathbf{q} \rangle$ *with*

$$\forall \mathbf{x}^* \in \mathbb{R}^j. \quad \langle \boldsymbol{\mathcal{P}}_n(\mathbf{x}^*, \mathbf{0}_{m-j}) \, , \mathbf{q} \rangle = 0 \tag{27}$$

with $\mathbf{0}_{m-j} \in \{0\}^{m-j}$ *is subject to the zero constraint matrix* $\boldsymbol{\mathcal{Z}}$*.*

PROOF. Separating the assigned parameters $\tilde{\mathbf{x}}^* = \mathbf{0}_{m-j}$ as $\mathbf{V}_0^T$ and applying

[5] E.g., for a symmetric aircraft aligned to the flow, there is no side-force—regardless its angle of attack.

Lemma 5, we have that

$$\langle \boldsymbol{\mathcal{P}}_n(\mathbf{x}^*)\,, \mathbf{V}_0\mathbf{q}\rangle = 0 \tag{28}$$

for all $\mathbf{x}^* \in \mathbb{R}^j$ if and only if $\mathbf{V}_0\mathbf{q} = \mathbf{0}$.

Using $\mathbf{V}' = \operatorname{diag}\big(v_1, \ldots, v_{\mathfrak{r}[n]}\big)$ where $v_i = 1$ if the i-th element of $\boldsymbol{\mathcal{P}}_n(\mathbf{1}_j, \mathbf{0}_{m-j})$ is non-zero, $v_i = 0$ otherwise, $\mathbf{V}_0$ is obtained by removing the all-zero rows of $\mathbf{V}'$, thus ensuring full rank.

For piecewise polynomial fitting with zero constraint, take

$$\boldsymbol{\mathcal{Z}} = \left[\begin{array}{c|c} \mathbf{V}_0 & \mathbf{0} \\ \hline \mathbf{0} & \mathbf{V}_0 \end{array}\right]. \tag{29}$$

If both zero constraint and constraint of continuity are given, we need to ensure full rank of the complete constraint matrix:

$$\begin{bmatrix} \boldsymbol{\mathcal{C}} \\ \boldsymbol{\mathcal{Z}} \end{bmatrix} \mathbf{q}' = \left[\begin{array}{c|c} \boldsymbol{\Lambda}_0 & -\boldsymbol{\Lambda}_0 \\ \mathbf{V}_0 & \mathbf{0} \\ \mathbf{0} & \mathbf{V}_0 \end{array}\right] \begin{bmatrix} \mathbf{q}_1 \\ \hline \mathbf{q}_2 \end{bmatrix} = \mathbf{0}.$$

5 Implementation

The `pwpfit` toolbox is implemented in MATLAB using the *Optimization toolbox*[6] for linear least-square solving and *Symbolic math toolbox*[7] for representation of the vector of monomials.

As MATLAB is rather slow on arrays of variable length, we use a statically allocated array to generate the vector of monomials $\boldsymbol{\mathcal{P}}_n$ in m variables. Applying a recursive sub-routine (Alg. 1) to write the auxiliary $\mathbf{p}_N(\mathbf{x})$ at the `l`-th(and following) positions of `P`, the vector of monomials is then computed as *symbolic expression* `P` of parameters `X:=x` according to (3).

The length of `P`, *i.e.* the number of monomials in $\boldsymbol{\mathcal{P}}_n(\mathbf{x})$, is given as sum of multicombinations

$$\mathfrak{r}[n] = \sum_{N=1}^{n} \binom{m+N-1}{N-1} = \binom{m+n}{n}. \tag{30}$$

[6] https://mathworks.com/help/optim

[7] https://mathworks.com/help/symbolic

Algorithm 1. Recursive algorithm for $\mathbf{p}_N(\mathbf{x})$.

```
function [P,l] = MONOMIAL(P,l,X,m,n,X0=1)
    if m == 1 then
        P(l) = X0*X^n;
        l = l+1;
    else
        for j = 0:n
            X0 = X0*X(1)^(n-j));
            [P,l] = ...
            MONOMIAL(P,l,X(2:end),m-1,j,X0);
        end
    end
end
```

Alg. 2 illustrates the computation of the left-hand side of the continuity constraint matrix, $\mathbf{\Lambda}_0$, for $\varphi(\mathbf{x}) = x_1 \leq x_0$, using the auxiliary vectors $\mathbf{p}_N(x_0, \mathbf{1}_{m-1})$ in degrees $N \in [0, n]$ with $\mathbf{1}_{m-1} \sim$ `one`.

Algorithm 2. Code-snippet for $\mathbf{\Lambda}_0 \sim$ `Aeq` in x_0.

```
one = num2cell(ones(1,m-1));
j = 0;
for N=0:n
  % let pN:=p_N(·); rN:=r[N]
    pNx0 = double(pN(x0,one{:}));
    Aeq(1:rN,j+(1:rN)) = diag(pNx0);
    j = j + rN;
end
```

Given a vector `y0` whose i-th component is zero if and only if the fitted polynomials are zero in the parameter x_i, Alg. 3 yields the zero separation matrix $\mathbf{V}_0$. Here, we make direct use of MATLAB's logical indexing for matrices in order to remove the all-zero rows of the square matrix $\mathbf{V}'$.

Algorithm 3. Code-snippet for $\mathbf{V}_0 \sim$ `Azero`.

```
  % let p:=P_n(·); r:=r[n]
Azero = eye(r);
Y = num2cell(y0);
pY = double(p(Y{:}));
Azero(pY==0,:) = [];
```

The constrained linear least-square problem is solved by the `lsqlin` function of the Optimization toolbox. As `lsqlin` requires a linear inequality constraint,

$$\mathbf{A}\mathbf{q} \leq b,$$

we assign $\mathbf{A} = \begin{bmatrix} 1 \cdots 1 \end{bmatrix}$ and $b = 10^4$.

If no continuity constraints are given, the joint x_0 of a single-variable function with $\varphi = \mathrm{id}$ is found using a non-linear function solver. [8] The resulting coefficients and their joint are returned as `pwfitobject`, which provides interfaces for plotting and exporting the obtained piecewise function and the polynomial sub-functions.

The auxiliary functions `prepareHyperSurfaceData` and `LMI2single` are provided to prepare tabular data for fitting [9] and to simplify an LMI constraint of continuity (Lemma 7), respectively.

6 Aerodynamic identification

The aerodynamic coefficients of an aircraft are subject to, amongst others, its angle of attack, side-slip angle, the deflection of ailerons, elevator, and rudder, as well as the body rates. Measurements for various inputs, e.g. of the NASA Generic Transport Model (GTM, Jordan et al., 2006), are usually performed in the wind-tunnel:

Example 9 (GTM [10]) *The observations of the aerodynamic coefficients of the GTM are given by the unknown function* $\Gamma(\cdot)$ *to*

$$\hat{\mathbf{C}} = \Gamma\left(\hat{\alpha}, \hat{\beta}, \hat{\xi}, \hat{\eta}, \hat{\zeta}\right) + \boldsymbol{\epsilon} \tag{31}$$

for the observed inputs $\hat{\alpha} \in A$, $\hat{\beta} \in B$, $\hat{\xi} \in \Xi$, $\hat{\eta} \in H$, *and* $\hat{\zeta} \in Z$ *with* $\hat{\mathbf{C}} = \left(\hat{C}_\mathrm{X}, \hat{C}_\mathrm{Y}, \hat{C}_\mathrm{Z}, \hat{C}_\mathrm{l}, \hat{C}_\mathrm{m}, \hat{C}_\mathrm{n}\right)$ *and* $\boldsymbol{\epsilon}$ *an unknown measurement error.*

For polynomial and piecewise polynomial fitting, observations in (31) have to be transformed to tabular data

$$(\mathbf{C}_i)_{1\leq i\leq k} = \Gamma(A \times B \times \Xi \times H \times Z) + (\boldsymbol{\epsilon}_i)_{1\leq i\leq k} \tag{32}$$

with $\mathbf{C}_i = (C_{\mathrm{X},i}, C_{\mathrm{Y},i}, C_{\mathrm{Z},i}, C_{\mathrm{l},i}, C_{\mathrm{m},i}, C_{\mathrm{n},i})$ and

$$k = |A \times B \times \Xi \times H \times Z| \,. \tag{33}$$

Here, simple polynomials models seem unsuitable to represent the full-envelope aerodynamics (Fig. 1; see also Cunis et al., 2018). At the stall angle of attack, the laminar flow around the wings of the pre-stall region changes to turbulent

[8] https://mathworks.com/help/optim/ug/fsolve.html
[9] Extending MATLAB's functions `prepareCurveData` and `prepareSurfaceData`.
[10] https://software.nasa.gov/software/LAR-17625-1

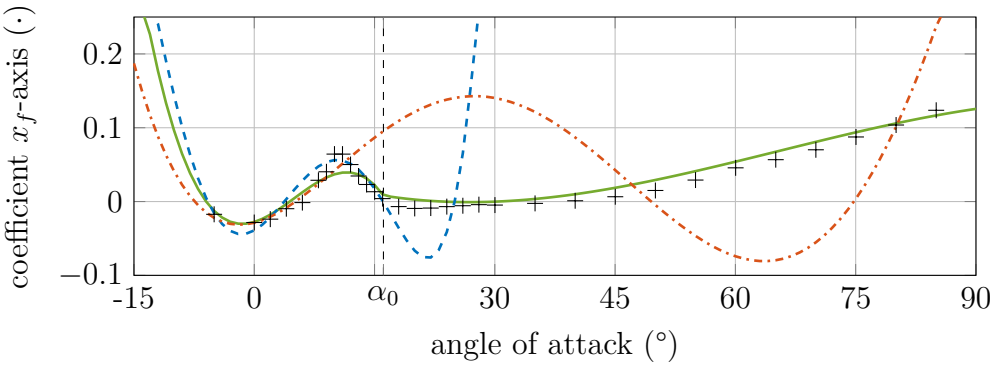

Fig. 1. Observed coefficients $\hat{C}_X(\hat{\alpha})$ (+) and comparison of 3rd-order polynomial (- - -, -·-·-) and piecewise (——) identifications. (Cunis et al., 2018)

flow and remains so in post-stall. This significant change of the flow dynamics motivates a piecewise fitting of the pre-stall and post-stall dynamics: [11]

$$C_{\odot}(\alpha,\beta,\xi,\eta,\zeta) = \begin{cases} C_{\odot}^{pre}(\alpha,\beta,\xi,\eta,\zeta) & \text{if } \alpha \leq \alpha_0 \\ C_{\odot}^{post}(\alpha,\beta,\xi,\eta,\zeta) & \text{else} \end{cases}$$

where $C_{\odot} \in \{C_{\mathrm{X}}, C_{\mathrm{Y}}, C_{\mathrm{Z}}, C_{\mathrm{l}}, C_{\mathrm{m}}, C_{\mathrm{n}}\}$ are 6-dimensional polynomials. Initially, $\alpha_0 = 16.11°$ is found by fitting $C_{\mathrm{X}\alpha}$ with respect to the angle of attack only, resulting in

$$C_{\mathrm{X}\alpha}^{pre}(\alpha_0) = C_{\mathrm{X}\alpha}^{post}(\alpha_0)\,,$$

which is the boundary angle of attack. The boundary condition $\alpha \equiv \alpha_0$ then resembles a 5-dimensional hyper-plane.

We now have continuity of the coefficient functions over their entire domain if

$$C_{\odot}^{pre}(\alpha_0,\cdots) \equiv C_{\odot}^{post}(\alpha_0,\cdots)\,.$$

At last, we require the lateral coefficients (C_{Y}, C_{l}, C_{n}) to vanish in the symmetric setting, *i.e.* zero side-slip, no aileron nor rudder deflection ($\beta = \xi = \zeta = 0$).

The obtained, piecewise polynomial models for the C_{X} and C_{Y} coefficients are exemplary shown in Fig. 2 for angle of attack and side-slip angle with neutral surface deflections ($\xi = \eta = \zeta = 0$). Besides, the residuals

$$e_{\mathrm{X}} = C_{\mathrm{X}}\left(\hat{\alpha},\hat{\beta}\right) - \hat{C}_{\mathrm{X}}$$
$$e_{\mathrm{Y}} = C_{\mathrm{Y}}\left(\hat{\alpha},\hat{\beta}\right) - \hat{C}_{\mathrm{Y}}$$

are given for $\left(\hat{\alpha},\hat{\beta}\right) \in A \times B$.

[11] A script for MATLAB can be found in the `demo` folder.

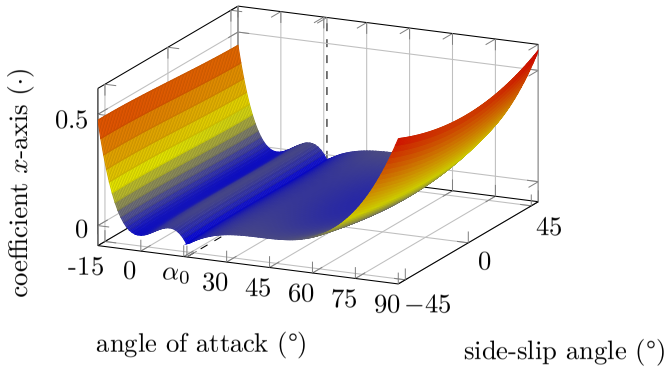

(a) Piecewise model $C_{\mathrm{X}}(\alpha, \beta)$.

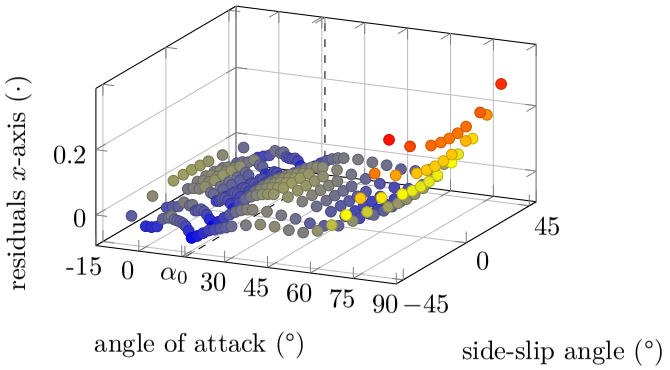

(b) Residuals of $C_{\mathrm{X}}(\alpha, \beta)$.

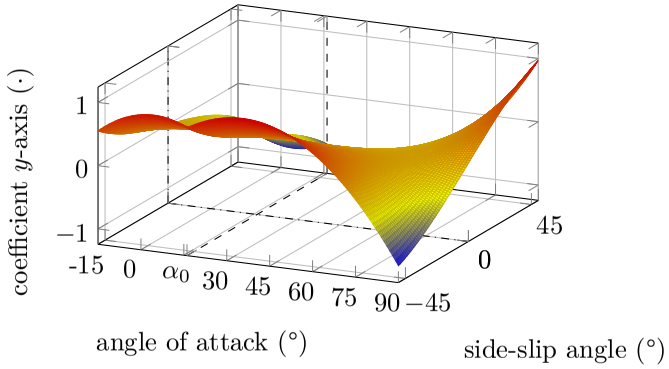

(c) Piecewise model $C_{\mathrm{Y}}(\alpha, \beta)$.

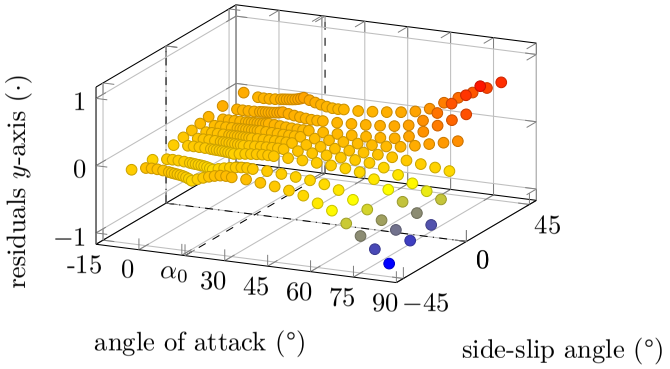

(d) Residuals of $C_{\mathrm{Y}}(\alpha, \beta)$.

Fig. 2. Piecewise model of the C_{X} and C_{Y} coefficients of the Generic Transport Model in angle of attack α and side-slip angle β, and their residuals; for surface deflections $\xi = \eta = \zeta = 0$. Both models are continuous in the joint $\alpha \equiv \alpha_0$ and the lateral C_{Y} model vanishes in $\beta \equiv 0$.

A six-degrees-of-freedom trim analysis of the GTM with piecewise polynomial, aerodynamic coefficients has been presented in (Cunis et al., 2017).

7 Note on computation time

When fitting polynomials of high dimension to large data sets, the computation of a single polynomial in all variables usually takes a considerably long time. In Tab. 1 we compare the computation time for objective matrix, constraint matrices, and the solution of the resulting LSQ problem for all six coefficients of Example 9.
Here, the objective matrix $\mathbf{K}$ takes by far the most time; by (15), the size of $\mathbf{K}$ resolves to

$$2k \times \mathfrak{r}[n] \tag{34}$$

and both k (33) and $\mathfrak{r}[n]$ (30) grow exponentially with the number of variables m. The size of $\boldsymbol{\mathcal{C}}$ and $\boldsymbol{\mathcal{Z}}$, too, grow with m but are independent of k. [12]

Table 1
Time consumption for fit of multi-variate polynomials $C_\odot(\alpha, \beta, \xi, \eta, \zeta)$: computation time for objective matrix $\mathbf{K}$, continuity constraint matrix $\boldsymbol{\mathcal{C}}$, zero constraint matrix $\boldsymbol{\mathcal{Z}}$, and solving the LSQ problem. All values in seconds with accuracy ± 10 ms (Intel Core i7, 3 GHz, 16 GB).

		$\mathbf{K}$	$\boldsymbol{\mathcal{C}}$	$\boldsymbol{\mathcal{Z}}$	lsq
C_X	$(\alpha, \beta, \xi, \eta, \zeta)$	2058.39	0.84	—	2.60
C_Y	$(\alpha, \beta, \xi, \eta, \zeta)$	2100.64	0.59	—	2.62
C_m	$(\alpha, \beta, \xi, \eta, \zeta)$	2100.22	0.59	—	2.62
C_Y	$(\alpha, \beta, \xi, \eta, \zeta)$	2102.25	0.60	<0.01	1.71
C_l	$(\alpha, \beta, \xi, \eta, \zeta)$	2109.07	0.63	<0.01	1.65
C_n	$(\alpha, \beta, \xi, \eta, \zeta)$	2102.38	0.59	0.01	1.54

Rather than single, high-dimensional polynomials, it may be more appropriate to sequentially fit sums of polynomial terms lower dimensions, for sub-sets of the variables:

$$\begin{aligned} C_\odot = C_{\odot\alpha}(\alpha) + C_{\odot\beta}(\alpha, \beta) + C_{\odot\xi}(\alpha, \beta, \xi) \\ + C_{\odot\eta}(\alpha, \beta, \eta) + C_{\odot\zeta}(\alpha, \beta, \zeta) \end{aligned} \tag{35}$$

[12] In addition, the computation of $\boldsymbol{\mathcal{Z}}$ by MATLAB's logical indexing is obviously very efficient.

with $m \leq 3$. In this case, continuity of each term in α_0 implies continuity of $C_\odot$ over its entire domain. Tab. 2 shows the reduced computation time for the sequential fit of C_X.

Table 2
Time consumption for sequential fit of polynomial sum $C_\mathrm{X} = C_{\mathrm{X}\alpha} + C_{\mathrm{X}\beta} + C_{\mathrm{X}\xi} + C_{\mathrm{X}\eta} + C_{\mathrm{X}\zeta}$: computation time for objective matrix $\mathbf{K}$, continuity constraint matrix $\boldsymbol{\mathcal{C}}$, and solving the LSQ problem. All values in seconds with accuracy ± 10 ms (Intel Core i7, 3 GHz, 16 GB).

		$\mathbf{K}$	$\boldsymbol{\mathcal{C}}$	lsq
$C_{\mathrm{X}\alpha}$	(α)	0.16	—	0.04
$C_{\mathrm{X}\beta}$	(α, β)	4.89	0.16	0.15
$C_{\mathrm{X}\xi}$	(α, β, ξ)	39.06	0.25	0.10
$C_{\mathrm{X}\eta}$	(α, β, η)	31.34	0.20	0.11
$C_{\mathrm{X}\zeta}$	(α, β, ζ)	36.49	0.20	0.04
C_X	$(\alpha, \beta, \xi, \eta, \zeta)$	111.94	0.81	0.44

8 Sensitivity analysis

In order to study the sensitivity of piecewise fitting, we take the GTM coefficients data of Example 9 as "true" values ($\epsilon \equiv 0$) and add a white noise ν_X:

$$C_\mathrm{X}^\dagger = \Gamma_X(\hat{\alpha}) + \nu_X \tag{36}$$

and ν_X is normally distributed with deviation $\sigma_X \stackrel{\mathrm{def}}{=} 0.01$. We then compute a batch of piecewise fits

$$\Big(C_\mathrm{X}^{\{j\}}(\alpha)\Big)_j$$

for 10 000 noise samples; a family of obtained curves is shown in Fig. 3.

The joints $\alpha_0^{\{j\}}$ have a sample mean $\overline{\alpha}_0 = 16.11°$ and deviation $\sigma_\alpha = 0.51°$. The error of fit with respect to the "true" values has a sample standard deviation

$$\sigma\Big(C^{\{j\}}(\hat{\alpha}) - \Gamma_X(\hat{\alpha})\Big) < \sigma_X$$

for all observations $\hat{\alpha}$. That is, piecewise polynomial fitting is able to reduce the error with respect to the erroneous signal.

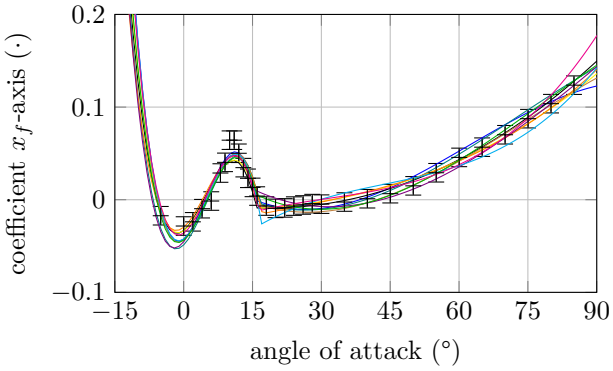

Fig. 3. Piecewise fits of erroneous coefficients ($\sigma_X = 0.01$).

9 Conclusion

With the rise of multivariate splines, prior research to piecewise polynomial regression has been abandoned. However, by pre-selection of the knots, spline fitting does not take into the underlying model; in fact, it thus over-estimates the observations. On the other hand, the estimation of the "true" switching points of a piecewise physical system usually adds computational difficulty and load.

In this paper, we have presented an approach of piecewise polynomial fitting using the LSQ optimization technique in order to fit both polynomial models and the joint point. The `pwpfit` toolbox for MATLAB provides functions for polynomial and piecewise polynomial data fitting under continuity and zero constraints. We demonstrated our approach by fitting piecewise polynomial models of the aerodynamic coefficients of an airliner model; here, we argued that simple polynomial models are unsuitable for the full-envelope dynamics while the dynamical changes at the stall point prompt the application of piecewise regression. By simulation of the sensitivity to random noise samples, we proved that piecewise polynomial fitting improves the estimation of an erroneous signal.

References

Chaudhuri, P., Huang, M.C., Loh, W.Y., and Yao, R. (1994). Piecewise-Polynomial Regression Trees. *Statistica Sinica*, 4(1), 143–167.

Cunis, T., Burlion, L., and Condomines, J.P. (2018). Piece-wise Identification and Analysis of the Aerodynamic Coefficients, Trim Conditions, and Safe Sets of the Generic Transport Model. In *AIAA Guidance, Navigation, and Control Conference*. Kissimmee, US-FL.

Cunis, T., Condomines, J.P., and Burlion, L. (2017). Full-envelope, Six-Degrees-of-Freedom Trim Analysis of Unmanned Aerial Systems based on Piece-wise Polynomial Aerodynamic Coefficients. In *4th Workshop on Research, Education, and Development of Unmanned Aerial Systems*. Linköping, SE.

de Visser, C.C., Chu, Q.P., and Mulder, J.A. (2009). A new approach to linear regression with multivariate splines. *Automatica*, 45(12), 2903–2909.

Gallant, A.R. and Fuller, W.A. (1973). Fitting segmented polynomial regression models whose join points have to be estimated. *Journal of the American Statistical Association*, 68(341), 144–147.

Golub, G.H. (1982). Numerical Methods for Solving Least Squares Problems. Technical report, U.S. Army Research Office.

Haskell, K.H. and Hanson, R.J. (1981). An Algorithm for Linear Least Squares Problems with Equality and Nonnegativity Constraints. *Mathematical Programming*, 21, 98–118.

Jordan, T.L., Foster, J.V., Bailey, R.M., and Belcastro, C.M. (2006). AirSTAR: A UAV Platform for Flight Dynamics and Control System Testing. In *AIAA Aerodynamics Measurement Technology and Ground Testing Conference*. San Francisco, US-CA.

Kariya, T. and Kurata, H. (2004). *Generalized Least Squares*. Wiley Series in Probability and Statistics. John Wiley & Sons, Chichester, GB.

Klein, V. and Morelli, E.A. (2006). *Aircraft System Identification: Theory and Practice*. American Institute of Aeronautics and Astronautics, Reston, US-VA.

Lawson, C.L. and Hanson, R.J. (1995). *Solving Least Squares Problems*. Society for Industrial and Applied Mathematics.

McGee, V.E. and Carleton, W.T. (1970). Piecewise Regression. *Journal of the American Statistical Association*, 65(331), 1109–1124.

Robison, D.E. (1964). Estimates for the Points of Intersection of Two Polynomial Regressions. *Journal of the American Statistical Association*, 59(305), 214–224.

Appendix: Proofs

PROOF. [Lemma 5] *By reduction to:*

$$\langle \boldsymbol{\mathcal{P}}_n(\mathbf{x}) \, , \mathbf{q}_1 - \mathbf{q}_2 \rangle \equiv 0 \Longleftrightarrow \mathbf{q_1} - \mathbf{q_2} = 0$$

where $\langle \boldsymbol{\mathcal{P}}_n(\mathbf{x}) \, , \mathbf{q}_1 - \mathbf{q}_2 \rangle$ is the zero polynomial.

PROOF. [Lemma 7] *By construction:*

$$\boldsymbol{\pi}^{-1} = \begin{bmatrix} a_1 & a_2 & \cdots & a_m \\ & 1 & & \\ & & \ddots & \\ & & & 1 \end{bmatrix};$$

$\boldsymbol{\pi}^{-1}$ is invertible as $|\boldsymbol{\pi}^{-1}| = a_1$ and $\varphi(\mathbf{x}) = y_1 \Leftrightarrow \mathbf{x} = \boldsymbol{\pi}\mathbf{y}$.

Appendix B

Aerodynamic Models

This appendix chapter details the piecewise polynomial models for the aerodynamic coefficients of the Generic Transport Model (GTM) and Cumulus One. The polynomial models of its sections B.1 and B.2 are part of the technical reports

> Torbjørn Cunis et al. (2018b). *Piecewise Polynomial Model of the Aerodynamic Coefficients of the Generic Transport Model and its Equations of Motion.* Tech. rep. `hal-01808649`, version 3. Toulouse, FR: ONERA – The French Aerospace Lab; French Civil Aviation School. URL: `https://archives-ouvertes.fr/hal-01808649v3`;

and

> Torbjørn Cunis and Anders la Cour-Harbo (2019). *Piecewise Polynomial Model of the Aerodynamic Coefficients of the* Cumulus One *Unmanned Aircraft.* Tech. rep. `hal-02280789`. Støvring, DK: Sky-Watch A/S. URL: `https://archives-ouvertes.fr/hal-02280789`;

respectively.

Preliminaries

If not stated otherwise, all variables are in SI units. We will refer to the following axis systems of ISO 1151-1: the *body axis system* $(x_\mathrm{f}, y_\mathrm{f}, z_\mathrm{f})$ aligned with the aircraft's fuselage; the *air-path axis system* $(x_\mathrm{a}, y_\mathrm{a}, z_\mathrm{a})$ defined by the velocity vector $\mathbf{V}_\mathrm{A}$; and the *normal earth-fixed axis system* $(x_\mathrm{g}, y_\mathrm{g}, z_\mathrm{g})$. The orientation of the body axes with respect to the normal earth-fixed system is given by the attitude angles Φ, Θ, Ψ and to the air-path system by angle of attack α and side-slip β; the orientation of the air-path axes to the normal earth-fixed system is given by azimuth χ_A, inclination γ_A, and bank-angle μ_A. (Fig. B.1.)

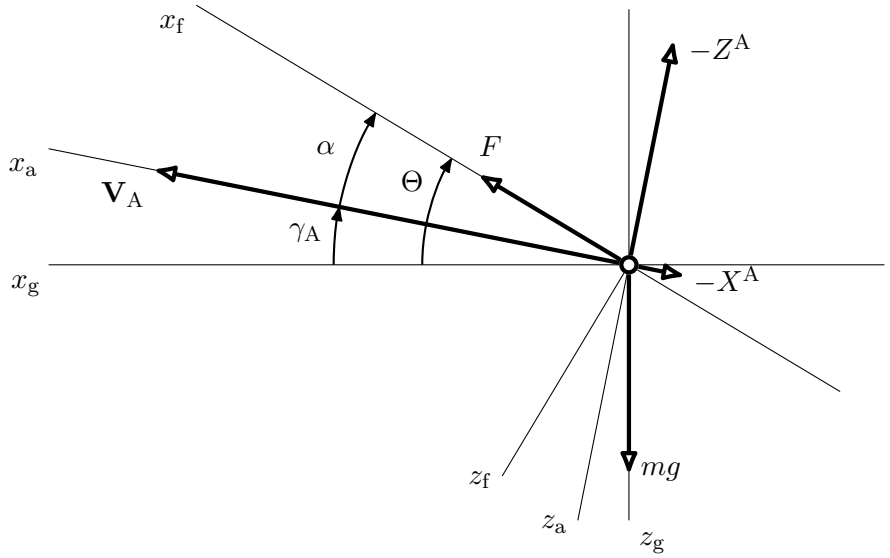

(a) Longitudinal axes ($\beta = \mu_\mathrm{A} = 0$).

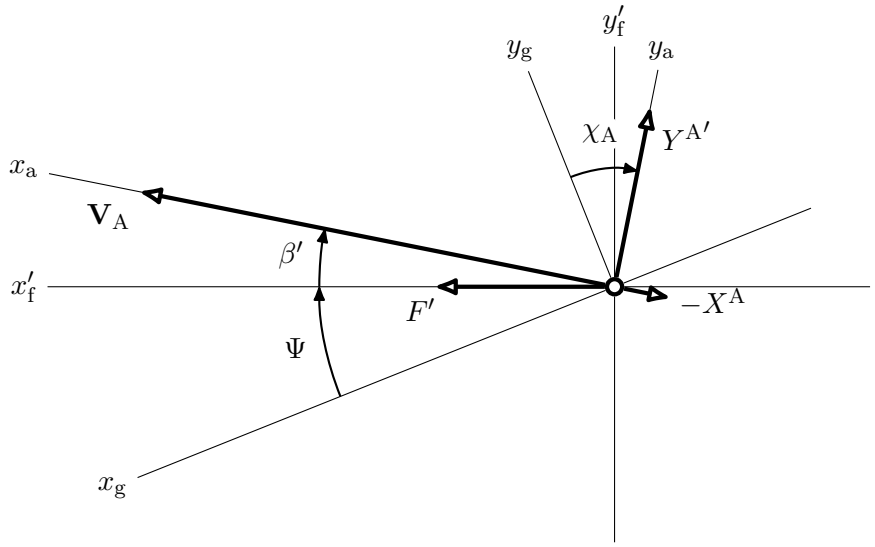

(b) Horizontal axes ($\gamma_\mathrm{A} = 0$).

Figure B.1: Axis systems with angles and vectors, following Brockhaus et al. (2011, Figures 2.7 and 2.8, p. 66). Projections into the drawing plane are marked by $'$.

B.1 Generic Transport Model

The piece-wise polynomial models of the aerodynamic coefficients are given

$$C_\odot(\alpha,\beta,\xi,\eta,\zeta,\hat{p},\hat{q},\hat{r}) = \begin{cases} C_\odot^{pre}(\alpha,\beta,\dots) & \text{if } \alpha \le \alpha_0, \\ C_\odot^{post}(\alpha,\beta,\dots) & \text{else,} \end{cases} \tag{B-1.1}$$

where $C_\odot \in \{C_\mathrm{X}, C_\mathrm{Y}, C_\mathrm{Z}, C_\mathrm{l}, C_\mathrm{m}, C_\mathrm{n}\}$ are polynomials in angle of attack α, side-slip β, surface deflections ξ, η, ζ, and normalized body rates $\hat{p}, \hat{q}, \hat{r}$; and the boundary is found at

$$\alpha_0 = 1.611 \times 10^{1\circ}. \tag{B-1.2}$$

The polynomials in low and high angle of attack, $C_\odot^{pre}$, $C_\odot^{post}$, are sums

$$\begin{aligned} C_\odot^{pre} = {} & C_{\odot\alpha}^{pre}(\alpha) + C_{\odot\beta}^{pre}(\alpha,\beta) + C_{\odot\xi}^{pre}(\alpha,\beta,\xi) + C_{\odot\eta}^{pre}(\alpha,\beta,\eta) + C_{\odot\zeta}^{pre}(\alpha,\beta,\zeta) \\ & + C_{\odot p}^{pre}(\alpha,\hat{p}) + C_{\odot q}^{pre}(\alpha,\hat{q}) + C_{\odot r}^{pre}(\alpha,\hat{r})\,; \end{aligned} \tag{B-1.3}$$

$$\begin{aligned} C_\odot^{post} = {} & C_{\odot\alpha}^{post}(\alpha) + C_{\odot\beta}^{post}(\alpha,\beta) + C_{\odot\xi}^{post}(\alpha,\beta,\xi) + C_{\odot\eta}^{post}(\alpha,\beta,\eta) + C_{\odot\zeta}^{post}(\alpha,\beta,\zeta) \\ & + C_{\odot p}^{post}(\alpha,\hat{p}) + C_{\odot q}^{post}(\alpha,\hat{q}) + C_{\odot r}^{post}(\alpha,\hat{r})\,. \end{aligned} \tag{B-1.4}$$

In the following subsections, we present the polynomial terms obtained using the `pwpfit` toolbox. Coefficients of absolute value $< 10^{-2}$ have been omitted for readability.

B.1.1 Domain of low angle of attack

Polynomials in angle of attack:

$$C_{\mathrm{X}\alpha}^{pre} = -3.873 \times 10^{-2} + 2.436 \times 10^{-1}\alpha + 4.452\alpha^2 - 1.739 \times 10^{1}\alpha^3; \tag{B-1.5}$$

$$C_{\mathrm{Z}\alpha}^{pre} = -1.674 \times 10^{-2} - 5.241\alpha - 1.866\alpha^2 + 2.847 \times 10^{1}\alpha^3; \tag{B-1.6}$$

$$C_{\mathrm{m}\alpha}^{pre} = 1.192 \times 10^{-1} - 1.465\alpha + 8.129\alpha^2 - 3.198 \times 10^{1}\alpha^3; \tag{B-1.7}$$

$C_{\mathrm{Y}\alpha}^{pre}$, $C_{\mathrm{l}\alpha}^{pre}$, $C_{\mathrm{n}\alpha}^{pre}$ are zero by definition.

Polynomials in angle of attack and side-slip:

$$\begin{aligned} C_{\mathrm{X}\beta}^{pre} = {} & 1.167 \times 10^{-2} + 1.270 \times 10^{-2}\alpha - 2.049\alpha^2 + 2.727 \times 10^{-2}\alpha\beta + 6.619 \times 10^{-2}\beta^2 \\ & + 9.808\alpha^3 + 2.490 \times 10^{-1}\alpha^2\beta - 5.723 \times 10^{-1}\alpha\beta^2 - 1.065 \times 10^{1}\alpha^4 - 1.178\alpha^3\beta \\ & + 1.936\alpha^2\beta^2 - 4.259 \times 10^{-2}\beta^4; \end{aligned} \tag{B-1.8}$$

$$\begin{aligned} C_{\mathrm{Y}\beta}^{pre} = {} & -1.024\beta + 2.190 \times 10^{-1}\alpha\beta - 3.066 \times 10^{-1}\alpha^2\beta + 6.970 \times 10^{-2}\beta^3 + 4.667\alpha^3\beta \\ & - 1.062\alpha\beta^3; \end{aligned} \tag{B-1.9}$$

Polynomials in angle of attack and side-slip (ct'd):

$$C_{\mathrm{Z}\beta}^{pre} = -3.530 \times 10^{-2} - 1.815 \times 10^{-2}\alpha + 2.911\alpha^2 + 2.392 \times 10^{-2}\beta^2 - 6.328\alpha^3 - 9.822 \times 10^{-2}\alpha^2\beta + 4.018\alpha\beta^2 - 8.805\alpha^4 + 3.280 \times 10^{-1}\alpha^3\beta - 8.609\alpha^2\beta^2 + 1.649 \times 10^{-1}\beta^4; \quad \text{(B-1.10)}$$

$$C_{\mathrm{l}\beta}^{pre} = -1.438 \times 10^{-1}\beta + 1.768 \times 10^{-1}\alpha\beta + 5.193 \times 10^{-2}\alpha^2\beta + 2.029 \times 10^{-1}\beta^3 + 3.495\alpha^3\beta - 1.113\alpha\beta^3; \quad \text{(B-1.11)}$$

$$C_{\mathrm{m}\beta}^{pre} = 6.781 \times 10^{-2} - 2.047 \times 10^{-1}\alpha - 9.113\alpha^2 + 2.062 \times 10^{-2}\alpha\beta - 1.396\beta^2 + 5.492 \times 10^{1}\alpha^3 + 1.698 \times 10^{-1}\alpha^2\beta - 1.633\alpha\beta^2 - 8.362 \times 10^{1}\alpha^4 - 9.896 \times 10^{-1}\alpha^3\beta + 1.176 \times 10^{1}\alpha^2\beta^2 - 2.705 \times 10^{-2}\alpha\beta^3 + 1.164\beta^4; \quad \text{(B-1.12)}$$

$$C_{\mathrm{n}\beta}^{pre} = 2.279 \times 10^{-1}\beta - 2.278 \times 10^{-1}\alpha\beta - 2.297 \times 10^{-1}\beta^3 - 1.697\alpha^3\beta + 5.385 \times 10^{-1}\alpha\beta^3. \quad \text{(B-1.13)}$$

Polynomials in angle of attack, side-slip, and aileron deflections:

$$C_{\mathrm{X}\xi}^{pre} = 3.259 \times 10^{-2}\alpha - 2.617 \times 10^{-1}\alpha^2 + 4.191 \times 10^{-2}\beta^2 + 1.406 \times 10^{-2}\beta\xi + 1.355 \times 10^{-1}\xi^2 + 1.195\alpha^3 + 9.401 \times 10^{-2}\alpha^2\beta - 1.475 \times 10^{-1}\alpha\beta^2 + 1.610 \times 10^{-2}\alpha\beta\xi - 1.289 \times 10^{-1}\alpha\xi^2 - 2.732\alpha^4 - 3.076 \times 10^{-1}\alpha^3\beta + 9.928 \times 10^{-1}\alpha^2\beta^2 - 5.747 \times 10^{-1}\alpha^2\beta\xi + 1.614 \times 10^{-1}\alpha^2\xi^2 - 1.105 \times 10^{-1}\beta^4 - 4.821 \times 10^{-2}\beta^2\xi^2 - 1.241 \times 10^{-2}\beta\xi^3 - 4.992 \times 10^{-1}\xi^4; \quad \text{(B-1.14)}$$

$$C_{\mathrm{Y}\xi}^{pre} = 8.019 \times 10^{-2}\beta - 2.155 \times 10^{-2}\xi - 1.925\alpha\beta - 3.586 \times 10^{-2}\alpha\xi + 5.012 \times 10^{-1}\alpha^2\beta + 2.295 \times 10^{-1}\alpha^2\xi - 2.054 \times 10^{-2}\beta^3 - 2.441 \times 10^{-1}\beta\xi^2 - 1.469\alpha^3\beta - 7.512 \times 10^{-1}\alpha^3\xi + 3.189\alpha\beta^3 + 5.135\alpha\beta\xi^2 + 2.269 \times 10^{-1}\alpha\xi^3; \quad \text{(B-1.15)}$$

$$C_{\mathrm{Z}\xi}^{pre} = -3.007 \times 10^{-2}\alpha - 3.219 \times 10^{-1}\alpha^2 - 3.316 \times 10^{-2}\beta^2 - 1.395 \times 10^{-1}\beta\xi + 2.880 \times 10^{-2}\xi^2 + 3.097\alpha^3 + 9.414 \times 10^{-2}\alpha^2\beta - 3.276 \times 10^{-1}\alpha\beta^2 + 3.851 \times 10^{-1}\alpha\beta\xi - 2.473 \times 10^{-1}\alpha\xi^2 - 5.289\alpha^4 - 3.080 \times 10^{-1}\alpha^3\beta + 1.422 \times 10^{-1}\alpha^2\beta^2 + 1.690 \times 10^{-1}\alpha^2\beta\xi - 7.951 \times 10^{-1}\alpha^2\xi^2 + 1.092 \times 10^{-1}\beta^4 + 2.744 \times 10^{-2}\beta^3\xi - 5.842 \times 10^{-2}\beta^2\xi^2 + 1.970 \times 10^{-1}\beta\xi^3 + 1.180 \times 10^{-1}\xi^4; \quad \text{(B-1.16)}$$

Polynomials in angle of attack, side-slip, and aileron deflections (ct'd):

$$\begin{aligned}C_{\mathrm{l}\xi}^{pre} &= 2.091\times10^{-2}\beta - 7.928\times10^{-2}\xi - 1.577\times10^{-1}\alpha\beta + 4.597\times10^{-2}\alpha\xi \\ &+ 1.493\times10^{-1}\alpha^2\beta + 6.975\times10^{-1}\alpha^2\xi - 6.616\times10^{-2}\beta^3 + 2.718\times10^{-2}\beta^2\xi \\ &- 3.594\times10^{-2}\beta\xi^2 + 6.936\times10^{-2}\xi^3 - 5.085\times10^{-1}\alpha^3\beta - 1.316\alpha^3\xi \\ &+ 3.379\times10^{-1}\alpha\beta^3 + 1.641\times10^{-2}\alpha\beta^2\xi + 4.531\times10^{-1}\alpha\beta\xi^2 - 1.387\times10^{-1}\alpha\xi^3; \end{aligned} \tag{B-1.17}$$

$$\begin{aligned}C_{\mathrm{m}\xi}^{pre} &= -3.941\times10^{-2} + 5.900\times10^{-2}\alpha + 1.630\times10^{-1}\alpha^2 + 4.007\times10^{-1}\beta^2 \\ &- 1.319\times10^{-2}\beta\xi - 5.638\times10^{-1}\xi^2 + 2.568\alpha^3 + 9.425\times10^{-2}\alpha^2\beta \\ &- 1.548\alpha\beta^2 + 6.836\times10^{-2}\alpha\beta\xi - 4.389\times10^{-1}\alpha\xi^2 - 4.594\alpha^4 - 3.084\times10^{-1}\alpha^3\beta \\ &- 1.295\alpha^2\beta^2 - 4.795\times10^{-2}\alpha^2\beta\xi + 3.560\times10^{-1}\alpha^2\xi^2 + 8.456\times10^{-2}\beta^4 \\ &+ 8.246\times10^{-2}\beta^3\xi + 8.406\times10^{-2}\beta^2\xi^2 + 3.826\times10^{-2}\beta\xi^3 + 2.201\xi^4; \end{aligned} \tag{B-1.18}$$

$$\begin{aligned}C_{\mathrm{n}\xi}^{pre} &= -2.486\times10^{-1}\alpha\beta + 1.367\times10^{-2}\alpha\xi + 4.109\times10^{-2}\alpha^2\beta + 5.253\times10^{-2}\alpha^2\xi \\ &+ 2.860\times10^{-2}\beta^3 - 1.716\times10^{-2}\beta\xi^2 + 1.565\times10^{-2}\xi^3 + 3.371\times10^{-1}\alpha^3\beta \\ &+ 4.834\times10^{-2}\alpha^3\xi + 3.373\times10^{-1}\alpha\beta^3 + 4.935\times10^{-2}\alpha\beta^2\xi + 6.904\times10^{-1}\alpha\beta\xi^2 \\ &- 1.224\times10^{-1}\alpha\xi^3. \end{aligned} \tag{B-1.19}$$

Polynomials in angle of attack, side-slip, and elevator deflections:

$$\begin{aligned}C_{\mathrm{X}\eta}^{pre} &= -3.562\times10^{-2}\alpha - 2.917\times10^{-1}\alpha^2 + 1.480\times10^{-1}\alpha\eta - 1.017\times10^{-1}\eta^2 + 1.173\alpha^3 \\ &- 4.111\times10^{-1}\alpha^2\eta + 3.333\times10^{-2}\alpha\beta^2 - 1.113\times10^{-2}\alpha\beta\eta + 1.050\times10^{-1}\alpha\eta^2 \\ &- 3.584\times10^{-2}\eta^3; \end{aligned} \tag{B-1.20}$$

$$C_{\mathrm{Y}\eta}^{pre} = -2.666\times10^{-1}\beta + 1.036\alpha\beta - 3.141\alpha^2\beta + 5.318\times10^{-1}\beta^3; \tag{B-1.21}$$

$$\begin{aligned}C_{\mathrm{Z}\eta}^{pre} &= 4.072\times10^{-2}\alpha - 1.635\times10^{-2}\beta - 5.261\times10^{-1}\eta + 2.051\times10^{-1}\alpha^2 \\ &+ 7.380\times10^{-2}\alpha\beta + 5.000\times10^{-2}\alpha\eta - 1.185\times10^{-2}\beta^2 - 1.770\alpha^3 \\ &- 6.003\times10^{-2}\alpha^2\beta + 8.150\times10^{-1}\alpha^2\eta + 3.060\times10^{-1}\alpha\beta^2 - 2.759\times10^{-2}\alpha\beta\eta \\ &+ 1.808\times10^{-1}\alpha\eta^2 + 2.965\times10^{-1}\beta^2\eta + 1.207\times10^{-2}\beta\eta^2 + 6.445\times10^{-1}\eta^3; \end{aligned} \tag{B-1.22}$$

$$C_{\mathrm{l}\eta}^{pre} = -1.224\times10^{-2}\beta + 5.692\times10^{-2}\alpha\beta - 2.864\times10^{-1}\alpha^2\beta + 4.670\times10^{-2}\beta^3; \tag{B-1.23}$$

Polynomials in angle of attack, side-slip, and elevator deflections (ct'd):

$$\begin{aligned}C_{\mathrm{m}\eta}^{pre} &= 2.816\times10^{-2} + 3.174\times10^{-2}\alpha - 5.357\times10^{-2}\beta - 1.851\eta - 1.719\times10^{-1}\alpha^2 \\ &+ 2.062\times10^{-1}\alpha\beta - 1.716\times10^{-1}\alpha\eta - 1.994\times10^{-1}\beta^2 + 2.626\times10^{-2}\beta\eta \\ &- 1.733\times10^{-1}\eta^2 - 2.999\times10^{-1}\alpha^3 - 6.794\times10^{-2}\alpha^2\beta + 5.136\alpha^2\eta \\ &+ 8.162\times10^{-1}\alpha\beta^2 - 2.269\times10^{-2}\alpha\beta\eta + 8.973\times10^{-1}\alpha\eta^2 + 6.933\times10^{-1}\beta^2\eta \\ &+ 1.107\times10^{-1}\beta\eta^2 + 1.324\eta^3; \end{aligned} \tag{B-1.24}$$

$$C_{\mathrm{n}\eta}^{pre} = -5.721\times10^{-2}\beta + 1.419\times10^{-1}\alpha\beta - 3.441\times10^{-1}\alpha^2\beta + 1.099\times10^{-1}\beta^3. \tag{B-1.25}$$

Polynomials in angle of attack, side-slip, and rudder deflections:

$$\begin{aligned}C_{\mathrm{X}\zeta}^{pre} &= -1.087\times10^{-2} + 2.617\times10^{-2}\alpha + 3.514\times10^{-1}\alpha^2 + 2.213\times10^{-2}\beta^2 \\ &+ 9.083\times10^{-2}\beta\zeta - 2.731\alpha^3 - 4.230\times10^{-2}\alpha\beta^2 - 3.962\times10^{-2}\alpha\beta\zeta \\ &+ 1.321\times10^{-2}\alpha\zeta^2 + 6.059\alpha^4 + 5.290\times10^{-2}\alpha^2\beta^2 + 2.449\times10^{-1}\alpha^2\beta\zeta \\ &- 2.110\times10^{-1}\alpha^2\zeta^2 - 1.102\times10^{-2}\beta^4 - 4.228\times10^{-2}\beta^2\zeta^2 - 1.300\times10^{-1}\beta\zeta^3 \\ &- 5.581\times10^{-2}\zeta^4; \end{aligned} \tag{B-1.26}$$

$$\begin{aligned}C_{\mathrm{Y}\zeta}^{pre} &= 1.871\times10^{-1}\beta + 3.080\times10^{-1}\zeta + 8.200\times10^{-1}\alpha\beta - 5.011\times10^{-1}\alpha\zeta \\ &+ 1.596\times10^{-1}\alpha^2\beta + 1.251\alpha^2\zeta - 4.553\times10^{-1}\beta^3 - 2.243\times10^{-1}\beta^2\zeta \\ &+ 1.677\times10^{-1}\beta\zeta^2 - 2.346\times10^{-1}\zeta^3 + 1.401\times10^{1}\alpha^3\beta - 6.802\alpha^3\zeta - 2.757\alpha\beta^3 \\ &+ 3.067\times10^{-1}\alpha\beta^2\zeta - 6.776\times10^{-1}\alpha\beta\zeta^2 + 1.093\alpha\zeta^3; \end{aligned} \tag{B-1.27}$$

$$\begin{aligned}C_{\mathrm{Z}\zeta}^{pre} &= -1.061\times10^{-1}\alpha + 1.635\times10^{-2}\beta + 2.543\times10^{-1}\alpha^2 - 7.380\times10^{-2}\alpha\beta \\ &+ 5.456\times10^{-2}\beta^2 + 5.442\times10^{-2}\beta\zeta + 1.172\times10^{-1}\zeta^2 + 3.459\alpha^3 \\ &+ 6.003\times10^{-2}\alpha^2\beta + 8.863\times10^{-2}\alpha\beta^2 - 3.667\times10^{-1}\alpha\beta\zeta + 6.284\times10^{-2}\alpha\zeta^2 \\ &- 6.397\alpha^4 - 9.843\times10^{-1}\alpha^2\beta^2 + 1.934\alpha^2\beta\zeta - 1.049\alpha^2\zeta^2 - 9.888\times10^{-2}\beta^4 \\ &- 1.397\times10^{-1}\beta^3\zeta - 4.678\times10^{-2}\beta^2\zeta^2 - 4.313\times10^{-2}\beta\zeta^3 - 1.221\times10^{-1}\zeta^4; \end{aligned} \tag{B-1.28}$$

$$\begin{aligned}C_{\mathrm{l}\zeta}^{pre} &= 2.400\times10^{-2}\zeta + 2.695\times10^{-2}\alpha\beta - 2.740\times10^{-2}\alpha\zeta + 1.495\times10^{-1}\alpha^2\beta \\ &+ 6.804\times10^{-2}\alpha^2\zeta - 1.278\times10^{-2}\beta^3 - 2.597\times10^{-2}\beta^2\zeta - 1.680\times10^{-2}\zeta^3 \\ &+ 6.000\times10^{-1}\alpha^3\beta - 2.512\times10^{-1}\alpha^3\zeta - 1.717\times10^{-1}\alpha\beta^3 + 4.621\times10^{-2}\alpha\beta^2\zeta \\ &+ 2.036\times10^{-2}\alpha\beta\zeta^2 + 4.049\times10^{-2}\alpha\zeta^3; \end{aligned} \tag{B-1.29}$$

Polynomials in angle of attack, side-slip, and rudder deflections (ct'd):

$$\begin{aligned}C_{\mathrm{m}\zeta}^{pre} &= -1.559\times10^{-2} - 3.890\times10^{-2}\alpha + 5.357\times10^{-2}\beta + 3.346\times10^{-1}\alpha^2 \\ &\quad - 2.061\times10^{-1}\alpha\beta + 3.233\times10^{-2}\beta^2 - 3.399\times10^{-1}\beta\zeta + 2.982\times10^{-1}\zeta^2 - 7.653\alpha^3 \\ &\quad + 6.794\times10^{-2}\alpha^2\beta + 7.235\times10^{-1}\alpha\beta^2 - 3.538\times10^{-1}\alpha\beta\zeta + 2.117\times10^{-2}\alpha\zeta^2 \\ &\quad + 2.328\times10^{1}\alpha^4 - 1.037\alpha^2\beta^2 + 5.879\times10^{-1}\alpha^2\beta\zeta - 1.013\alpha^2\zeta^2 - 3.110\times10^{-1}\beta^4 \\ &\quad - 3.042\times10^{-1}\beta^3\zeta + 2.127\times10^{-1}\beta^2\zeta^2 + 6.797\times10^{-1}\beta\zeta^3 - 2.471\times10^{-1}\zeta^4;\end{aligned} \tag{B-1.30}$$

$$\begin{aligned}C_{\mathrm{n}\zeta}^{pre} &= 3.962\times10^{-2}\beta - 1.448\times10^{-1}\zeta + 1.089\times10^{-1}\alpha\beta + 3.297\times10^{-2}\alpha\zeta \\ &\quad + 6.064\times10^{-1}\alpha^2\beta - 2.636\times10^{-1}\alpha^2\zeta - 1.082\times10^{-1}\beta^3 + 1.142\times10^{-1}\beta^2\zeta \\ &\quad - 5.237\times10^{-2}\beta\zeta^2 + 8.848\times10^{-2}\zeta^3 - 1.391\alpha^3\beta + 1.698\alpha^3\zeta - 3.869\times10^{-1}\alpha\beta^3 \\ &\quad - 9.788\times10^{-2}\alpha\beta^2\zeta + 7.711\times10^{-2}\alpha\beta\zeta^2 - 8.987\times10^{-2}\alpha\zeta^3.\end{aligned} \tag{B-1.31}$$

Polynomials in angle of attack and normalized body p-rate:

$$\begin{aligned}C_{\mathrm{Y}\hat{p}}^{pre} &= -7.051\times10^{-2}\hat{p} - 1.377\times10^{-1}\alpha\hat{p} - 1.268\times10^{-2}\hat{p}^2 - 8.622\times10^{-1}\alpha^2\hat{p} \\ &\quad + 3.826\times10^{-1}\alpha\hat{p}^2 \ + 1.414\times10^{1}\hat{p}^3;\end{aligned} \tag{B-1.32}$$

$$\begin{aligned}C_{\mathrm{l}\hat{p}}^{pre} &= -2.657\times10^{-1}\hat{p} - 2.469\times10^{-1}\alpha\hat{p} - 1.523\times10^{-2}\hat{p}^2 + 3.159\alpha^2\hat{p} \\ &\quad + 5.397\times10^{-1}\alpha\hat{p}^2 - 2.843\hat{p}^3;\end{aligned} \tag{B-1.33}$$

$$\begin{aligned}C_{\mathrm{n}\hat{p}}^{pre} &= -8.324\times10^{-2}\hat{p} - 4.426\times10^{-2}\alpha\hat{p} - 6.486\times10^{-2}\hat{p}^2 + 1.221\alpha^2\hat{p} \\ &\quad + 7.313\times10^{-2}\alpha\hat{p}^2 + 5.811\hat{p}^3;\end{aligned} \tag{B-1.34}$$

$C_{\mathrm{X}\hat{p}}^{pre}$, $C_{\mathrm{Z}\hat{p}}^{pre}$, $C_{\mathrm{m}\hat{p}}^{pre}$ are zero due to lack of GTM measurement data.

Polynomials in angle of attack and normalized body q-rate:

$$\begin{aligned}C_{\mathrm{X}\hat{q}}^{pre} &= -2.988\times10^{-2}\alpha + 8.513\times10^{-1}\hat{q} + 7.587\times10^{-2}\alpha^2 + 1.243\times10^{1}\alpha\hat{q} \\ &\quad + 5.713\times10^{2}\hat{q}^2 + 1.273\times10^{-1}\alpha^3 + 2.348\times10^{1}\alpha^2\hat{q} + 2.197\times10^{3}\alpha\hat{q}^2 \\ &\quad + 2.529\times10^{3}\hat{q}^3;\end{aligned} \tag{B-1.35}$$

$$\begin{aligned}C_{\mathrm{Z}\hat{q}}^{pre} &= -3.295\times10^{1}\hat{q} - 2.025\times10^{-1}\alpha^2 - 3.215\times10^{1}\alpha\hat{q} + 1.402\times10^{3}\hat{q}^2 \\ &\quad - 2.820\times10^{-1}\alpha^3 - 8.058\times10^{1}\alpha^2\hat{q} + 1.239\times10^{3}\alpha\hat{q}^2 + 2.346\times10^{3}\hat{q}^3;\end{aligned} \tag{B-1.36}$$

Polynomials in angle of attack and normalized body q-rate (ct'd):

$$C_{\mathrm{m}\hat{q}}^{pre} = -2.440 \times 10^{-2} - 3.282 \times 10^{-2}\alpha - 4.238 \times 10^{1}\hat{q} + 4.962 \times 10^{-1}\alpha^2 - 2.991\alpha\hat{q} + 7.650 \times 10^{2}\hat{q}^2 + 9.087 \times 10^{-1}\alpha^3 + 2.959 \times 10^{1}\alpha^2\hat{q} + 2.215 \times 10^{3}\alpha\hat{q}^2 + 2.370 \times 10^{3}\hat{q}^3; \quad \text{(B-1.37)}$$

$C_{\mathrm{Y}\hat{q}}^{pre}$, $C_{\mathrm{l}\hat{q}}^{pre}$, $C_{\mathrm{n}\hat{q}}^{pre}$ are zero due to lack of GTM measurement data.

Polynomials in angle of attack and normalized body r-rate:

$$C_{\mathrm{Y}\hat{r}}^{pre} = 7.481 \times 10^{-1}\hat{r} + 8.649 \times 10^{-1}\alpha\hat{r} + 8.814 \times 10^{-1}\hat{r}^2 + 1.625\alpha^2\hat{r} - 1.485\alpha\hat{r}^2 + 2.662\hat{r}^3; \quad \text{(B-1.38)}$$

$$C_{\mathrm{l}\hat{r}}^{pre} = 1.470 \times 10^{-1}\hat{r} + 7.551 \times 10^{-1}\alpha\hat{r} + 8.625 \times 10^{-1}\alpha^2\hat{r} + 1.246 \times 10^{-1}\alpha\hat{r}^2 - 5.986\hat{r}^3; \quad \text{(B-1.39)}$$

$$C_{\mathrm{n}\hat{r}}^{pre} = -3.366 \times 10^{-1}\hat{r} - 2.491 \times 10^{-1}\alpha\hat{r} - 4.710 \times 10^{-1}\hat{r}^2 - 9.122 \times 10^{-1}\alpha^2\hat{r} + 1.028\alpha\hat{r}^2 + 1.990 \times 10^{1}\hat{r}^3; \quad \text{(B-1.40)}$$

$C_{\mathrm{X}\hat{r}}^{pre}$, $C_{\mathrm{Z}\hat{r}}^{pre}$, $C_{\mathrm{m}\hat{r}}^{pre}$ are zero due to lack of GTM measurement data.

B.1.2 Domain of high angle of attack

Polynomials in angle of attack:

$$C_{\mathrm{X}\alpha}^{post} = 1.884 \times 10^{-2} - 1.304 \times 10^{-1}\alpha + 1.687 \times 10^{-1}\alpha^2 - 2.236 \times 10^{-2}\alpha^3; \quad \text{(B-1.41)}$$

$$C_{\mathrm{Z}\alpha}^{post} = -3.648 \times 10^{-1} - 2.712\alpha + 1.647\alpha^2 - 3.692 \times 10^{-1}\alpha^3; \quad \text{(B-1.42)}$$

$$C_{\mathrm{m}\alpha}^{post} = 2.467 \times 10^{-1} - 2.847\alpha + 2.748\alpha^2 - 1.105\alpha^3; \quad \text{(B-1.43)}$$

$C_{\mathrm{Y}\alpha}^{post}$, $C_{\mathrm{l}\alpha}^{post}$, $C_{\mathrm{n}\alpha}^{post}$ are zero by definition.

Polynomials in angle of attack and side-slip:

$$C_{\mathrm{X}\beta}^{post} = 1.005 \times 10^{-1}\alpha - 2.388 \times 10^{-1}\alpha^2 + 2.516 \times 10^{-2}\beta^2 + 1.987 \times 10^{-1}\alpha^3 + 1.597 \times 10^{-1}\alpha\beta^2 - 1.083 \times 10^{-2}\beta^3 - 5.455 \times 10^{-2}\alpha^4 - 1.480 \times 10^{-1}\alpha^2\beta^2 + 1.008 \times 10^{-2}\alpha\beta^3 - 4.259 \times 10^{-2}\beta^4; \quad \text{(B-1.44)}$$

$$C_{\mathrm{Y}\beta}^{post} = -3.931 \times 10^{-1}\beta - 2.181\alpha\beta + 1.680\alpha^2\beta - 5.908 \times 10^{-1}\beta^3 - 4.016 \times 10^{-1}\alpha^3\beta + 1.287\alpha\beta^3; \quad \text{(B-1.45)}$$

Polynomials in angle of attack and side-slip (ct'd):

$$C_{\mathrm{Z}\beta}^{post} = -3.984 \times 10^{-2} + 1.833 \times 10^{-1}\alpha - 2.681 \times 10^{-1}\alpha^2 + 3.892 \times 10^{-2}\alpha\beta - 2.931 \times 10^{-1}\beta^2 + 1.685 \times 10^{-1}\alpha^3 - 8.820 \times 10^{-2}\alpha^2\beta + 3.329\alpha\beta^2 - 3.904 \times 10^{-2}\alpha^4 + 5.597 \times 10^{-2}\alpha^3\beta - 2.148\alpha^2\beta^2 + 1.649 \times 10^{-1}\beta^4; \quad \text{(B-1.46)}$$

$$C_{\mathrm{l}\beta}^{post} = 7.429 \times 10^{-2}\beta - 3.392 \times 10^{-1}\alpha\beta + 1.114 \times 10^{-1}\alpha^2\beta - 1.420 \times 10^{-1}\beta^3 + 1.134 \times 10^{-1}\alpha\beta^3; \quad \text{(B-1.47)}$$

$$C_{\mathrm{m}\beta}^{post} = 3.566 \times 10^{-1} - 2.954\alpha - 9.610 \times 10^{-2}\beta + 7.802\alpha^2 + 5.097 \times 10^{-1}\alpha\beta - 5.890 \times 10^{-1}\beta^2 - 7.667\alpha^3 - 7.357 \times 10^{-1}\alpha^2\beta - 1.740\alpha\beta^2 + 2.469\alpha^4 + 2.962 \times 10^{-1}\alpha^3\beta + 1.931\alpha^2\beta^2 - 4.029 \times 10^{-2}\alpha\beta^3 + 1.164\beta^4; \quad \text{(B-1.48)}$$

$$C_{\mathrm{n}\beta}^{post} = 1.972 \times 10^{-1}\beta - 1.857 \times 10^{-1}\alpha\beta - 2.858 \times 10^{-1}\alpha^2\beta - 2.377 \times 10^{-1}\beta^3 + 1.598 \times 10^{-1}\alpha^3\beta + 5.671 \times 10^{-1}\alpha\beta^3. \quad \text{(B-1.49)}$$

Polynomials in angle of attack, side-slip, and aileron deflections:

$$C_{\mathrm{X}\xi}^{post} = 7.897 \times 10^{-2} - 6.106 \times 10^{-1}\alpha + 1.476\alpha^2 + 1.348 \times 10^{-1}\beta^2 - 2.540 \times 10^{-2}\beta\xi - 8.348 \times 10^{-2}\xi^2 - 1.489\alpha^3 - 2.532 \times 10^{-1}\alpha\beta^2 - 1.262 \times 10^{-2}\alpha\beta\xi + 8.968 \times 10^{-1}\alpha\xi^2 + 5.305 \times 10^{-1}\alpha^4 + 1.935 \times 10^{-1}\alpha^2\beta^2 + 2.641 \times 10^{-2}\alpha^2\beta\xi - 7.173 \times 10^{-1}\alpha^2\xi^2 - 1.105 \times 10^{-1}\beta^4 - 4.821 \times 10^{-2}\beta^2\xi^2 - 1.241 \times 10^{-2}\beta\xi^3 - 4.992 \times 10^{-1}\xi^4; \quad \text{(B-1.50)}$$

$$C_{\mathrm{Y}\xi}^{post} = -1.486\beta - 5.892 \times 10^{-2}\xi + 4.744\alpha\beta + 1.271 \times 10^{-1}\alpha\xi - 4.548\alpha^2\beta - 9.750 \times 10^{-2}\alpha^2\xi + 2.041\beta^3 + 2.727\beta\xi^2 + 1.205 \times 10^{-1}\xi^3 + 2.605\alpha^3\beta + 3.095 \times 10^{-2}\alpha^3\xi - 4.143\alpha\beta^3 + 1.328 \times 10^{-2}\alpha\beta^2\xi - 5.429\alpha\beta\xi^2 - 1.846 \times 10^{-1}\alpha\xi^3; \quad \text{(B-1.51)}$$

$$C_{\mathrm{Z}\xi}^{post} = 3.850 \times 10^{-2} - 3.322 \times 10^{-1}\alpha + 7.616 \times 10^{-1}\alpha^2 - 4.318 \times 10^{-2}\beta^2 - 2.775 \times 10^{-1}\xi^2 - 4.800 \times 10^{-1}\alpha^3 - 3.257 \times 10^{-1}\alpha\beta^2 - 3.434 \times 10^{-2}\alpha\beta\xi + 6.763 \times 10^{-1}\alpha\xi^2 + 5.426 \times 10^{-2}\alpha^4 + 2.623 \times 10^{-1}\alpha^2\beta^2 - 3.271 \times 10^{-2}\alpha^2\beta\xi - 2.060 \times 10^{-1}\alpha^2\xi^2 + 1.092 \times 10^{-1}\beta^4 + 2.744 \times 10^{-2}\beta^3\xi - 5.842 \times 10^{-2}\beta^2\xi^2 + 1.970 \times 10^{-1}\beta\xi^3 + 1.180 \times 10^{-1}\xi^4; \quad \text{(B-1.52)}$$

Polynomials in angle of attack, side-slip, and aileron deflections (ct'd):

$$\begin{aligned}C_{\mathrm{l}\xi}^{post} &= -1.068\times10^{-1}\beta - 3.470\times10^{-2}\xi + 4.186\times10^{-1}\alpha\beta - 4.155\times10^{-2}\alpha\xi \\ &\quad - 4.999\times10^{-1}\alpha^2\beta + 8.423\times10^{-2}\alpha^2\xi + 8.172\times10^{-2}\beta^3 + 3.547\times10^{-2}\beta^2\xi \\ &\quad + 1.940\times10^{-1}\beta\xi^2 + 3.000\times10^{-2}\xi^3 + 2.530\times10^{-1}\alpha^3\beta - 3.236\times10^{-2}\alpha^3\xi \\ &\quad - 1.880\times10^{-1}\alpha\beta^3 - 1.308\times10^{-2}\alpha\beta^2\xi - 3.645\times10^{-1}\alpha\beta\xi^2; \end{aligned} \tag{B-1.53}$$

$$\begin{aligned}C_{\mathrm{m}\xi}^{post} &= -6.152\times10^{-2} + 6.358\times10^{-1}\alpha - 1.619\alpha^2 - 5.200\times10^{-1}\beta^2 + 5.069\times10^{-2}\beta\xi \\ &\quad - 6.111\times10^{-2}\xi^2 + 1.436\alpha^3 + 1.727\alpha\beta^2 - 2.018\times10^{-1}\alpha\beta\xi - 2.612\alpha\xi^2 \\ &\quad - 4.335\times10^{-1}\alpha^4 - 1.297\alpha^2\beta^2 + 1.048\times10^{-1}\alpha^2\beta\xi + 1.727\alpha^2\xi^2 + 8.456\times10^{-2}\beta^4 \\ &\quad + 8.246\times10^{-2}\beta^3\xi + 8.406\times10^{-2}\beta^2\xi^2 + 3.826\times10^{-2}\beta\xi^3 + 2.201\xi^4; \end{aligned} \tag{B-1.54}$$

$$\begin{aligned}C_{\mathrm{n}\xi}^{post} &= -1.696\times10^{-1}\beta + 1.289\times10^{-2}\xi + 4.582\times10^{-1}\alpha\beta - 3.435\times10^{-2}\alpha\xi \\ &\quad - 2.269\times10^{-1}\alpha^2\beta + 3.699\times10^{-2}\alpha^2\xi + 3.275\times10^{-1}\beta^3 + 1.669\times10^{-2}\beta^2\xi \\ &\quad + 3.967\times10^{-1}\beta\xi^2 - 4.545\times10^{-2}\xi^3 + 1.614\times10^{-1}\alpha^3\beta - 2.100\times10^{-2}\alpha^3\xi \\ &\quad - 7.257\times10^{-1}\alpha\beta^3 - 1.728\times10^{-2}\alpha\beta^2\xi - 7.814\times10^{-1}\alpha\beta\xi^2 + 9.485\times10^{-2}\alpha\xi^3. \end{aligned} \tag{B-1.55}$$

Polynomials in angle of attack, side-slip, and elevator deflections:

$$\begin{aligned}C_{\mathrm{X}\eta}^{post} &= 4.213\times10^{-2} - 2.760\times10^{-1}\alpha - 1.058\times10^{-2}\eta + 5.456\times10^{-1}\alpha^2 \\ &\quad + 6.126\times10^{-2}\alpha\eta + 3.880\times10^{-2}\beta^2 - 6.334\times10^{-2}\eta^2 - 2.930\times10^{-1}\alpha^3 \\ &\quad - 6.328\times10^{-2}\alpha^2\eta - 8.755\times10^{-2}\alpha\beta^2 - 3.154\times10^{-2}\alpha\eta^2 - 3.584\times10^{-2}\eta^3; \end{aligned} \tag{B-1.56}$$

$$C_{\mathrm{Y}\eta}^{post} = -6.083\times10^{-1}\beta + 1.973\alpha\beta - 2.152\alpha^2\beta + 5.318\times10^{-1}\beta^3; \tag{B-1.57}$$

$$\begin{aligned}C_{\mathrm{Z}\eta}^{post} &= -1.001\times10^{-1} + 5.594\times10^{-1}\alpha - 5.939\times10^{-1}\eta - 9.261\times10^{-1}\alpha^2 \\ &\quad + 2.903\times10^{-2}\alpha\beta + 5.851\times10^{-1}\alpha\eta + 1.100\times10^{-1}\beta^2 - 3.519\times10^{-2}\eta^2 \\ &\quad + 4.519\times10^{-1}\alpha^3 - 2.379\times10^{-2}\alpha^2\beta - 2.296\times10^{-1}\alpha^2\eta - 1.273\times10^{-1}\alpha\beta^2 \\ &\quad + 3.189\times10^{-1}\alpha\eta^2 + 2.965\times10^{-1}\beta^2\eta + 1.207\times10^{-2}\beta\eta^2 + 6.445\times10^{-1}\eta^3; \end{aligned} \tag{B-1.58}$$

$$C_{\mathrm{l}\eta}^{post} = -4.916\times10^{-2}\beta + 1.503\times10^{-1}\alpha\beta - 1.517\times10^{-1}\alpha^2\beta + 4.670\times10^{-2}\beta^3; \tag{B-1.59}$$

Polynomials in angle of attack, side-slip, and elevator deflections (ct'd):

$$\begin{aligned} C_{\mathrm{m}\eta}^{post} &= 9.009 \times 10^{-2} - 3.720 \times 10^{-1}\alpha - 1.880\eta + 4.356 \times 10^{-1}\alpha^2 + 1.470\alpha\eta \\ &+ 1.915 \times 10^{-2}\beta\eta - 8.652 \times 10^{-2}\eta^2 - 1.393 \times 10^{-1}\alpha^3 - 3.411 \times 10^{-1}\alpha^2\eta \\ &+ 7.562 \times 10^{-2}\alpha\beta^2 + 5.886 \times 10^{-1}\alpha\eta^2 + 6.933 \times 10^{-1}\beta^2\eta + 1.107 \times 10^{-1}\beta\eta^2 \\ &+ 1.324\eta^3; \end{aligned} \tag{B-1.60}$$

$$C_{\mathrm{n}\eta}^{post} = -6.973 \times 10^{-2}\beta + 1.423 \times 10^{-1}\alpha\beta - 1.871 \times 10^{-1}\alpha^2\beta + 1.099 \times 10^{-1}\beta^3. \tag{B-1.61}$$

Polynomials in angle of attack, side-slip, and rudder deflections:

$$\begin{aligned} C_{\mathrm{X}\zeta}^{post} &= 1.608 \times 10^{-2} - 1.403 \times 10^{-1}\alpha + 4.785 \times 10^{-1}\alpha^2 + 8.168 \times 10^{-2}\beta^2 \\ &+ 2.035 \times 10^{-1}\beta\zeta - 1.219 \times 10^{-1}\zeta^2 - 6.694 \times 10^{-1}\alpha^3 - 3.163 \times 10^{-1}\alpha\beta^2 \\ &- 4.627 \times 10^{-1}\alpha\beta\zeta + 4.562 \times 10^{-1}\alpha\zeta^2 + 2.979 \times 10^{-1}\alpha^4 + 2.740 \times 10^{-1}\alpha^2\beta^2 \\ &+ 3.251 \times 10^{-1}\alpha^2\beta\zeta - 3.071 \times 10^{-1}\alpha^2\zeta^2 - 1.102 \times 10^{-2}\beta^4 - 4.228 \times 10^{-2}\beta^2\zeta^2 \\ &- 1.300 \times 10^{-1}\beta\zeta^3 - 5.581 \times 10^{-2}\zeta^4; \end{aligned} \tag{B-1.62}$$

$$\begin{aligned} C_{\mathrm{Y}\zeta}^{post} &= 3.051\beta - 2.050 \times 10^{-1}\zeta - 1.179 \times 10^{1}\alpha\beta + 1.702\alpha\zeta + 1.445 \times 10^{1}\alpha^2\beta \\ &- 2.320\alpha^2\zeta - 2.302\beta^3 - 2.597 \times 10^{-1}\beta^2\zeta - 1.821 \times 10^{-1}\beta\zeta^2 + 3.527 \times 10^{-1}\zeta^3 \\ &- 6.130\alpha^3\beta + 1.104\alpha^3\zeta + 3.811\alpha\beta^3 + 4.328 \times 10^{-1}\alpha\beta^2\zeta + 5.664 \times 10^{-1}\alpha\beta\zeta^2 \\ &- 9.961 \times 10^{-1}\alpha\zeta^3; \end{aligned} \tag{B-1.63}$$

$$\begin{aligned} C_{\mathrm{Z}\zeta}^{post} &= 2.196 \times 10^{-1} - 1.248\alpha + 2.437\alpha^2 - 2.903 \times 10^{-2}\alpha\beta - 8.348 \times 10^{-2}\beta^2 \\ &+ 1.415 \times 10^{-1}\beta\zeta - 8.089 \times 10^{-2}\zeta^2 - 2.074\alpha^3 + 2.379 \times 10^{-2}\alpha^2\beta \\ &+ 3.447 \times 10^{-1}\alpha\beta^2 - 1.626 \times 10^{-1}\alpha\beta\zeta + 5.912 \times 10^{-1}\alpha\zeta^2 + 6.539 \times 10^{-1}\alpha^4 \\ &- 1.491 \times 10^{-1}\alpha^2\beta^2 + 1.068 \times 10^{-1}\alpha^2\beta\zeta - 4.224 \times 10^{-1}\alpha^2\zeta^2 - 9.888 \times 10^{-2}\beta^4 \\ &- 1.397 \times 10^{-1}\beta^3\zeta - 4.678 \times 10^{-2}\beta^2\zeta^2 - 4.313 \times 10^{-2}\beta\zeta^3 - 1.221 \times 10^{-1}\zeta^4; \end{aligned} \tag{B-1.64}$$

$$\begin{aligned} C_{\mathrm{l}\zeta}^{post} &= 1.292 \times 10^{-1}\beta - 4.707 \times 10^{-1}\alpha\beta + 4.654 \times 10^{-2}\alpha\zeta + 5.459 \times 10^{-1}\alpha^2\beta \\ &- 7.022 \times 10^{-2}\alpha^2\zeta - 9.073 \times 10^{-2}\beta^3 - 1.892 \times 10^{-2}\beta^2\zeta + 1.235 \times 10^{-2}\beta\zeta^2 \\ &- 2.025 \times 10^{-1}\alpha^3\beta + 3.111 \times 10^{-2}\alpha^3\zeta + 1.055 \times 10^{-1}\alpha\beta^3 + 2.116 \times 10^{-2}\alpha\beta^2\zeta \\ &- 1.039 \times 10^{-2}\alpha\beta\zeta^2 - 3.324 \times 10^{-2}\alpha\zeta^3; \end{aligned} \tag{B-1.65}$$

Polynomials in angle of attack, side-slip, and rudder deflections (ct'd):

$$\begin{aligned}C_{\mathrm{m}\zeta}^{post} &= 4.285\times10^{-1} - 3.325\alpha + 8.084\alpha^2 + 2.446\times10^{-1}\beta^2 - 9.740\times10^{-1}\beta\zeta \\ &+ 1.994\times10^{-1}\zeta^2 - 7.822\alpha^3 - 3.630\times10^{-1}\alpha\beta^2 + 2.617\alpha\beta\zeta + 1.495\times10^{-1}\alpha\zeta^2 \\ &+ 2.615\alpha^4 + 1.423\times10^{-1}\alpha^2\beta^2 - 1.957\alpha^2\beta\zeta - 2.199\times10^{-1}\alpha^2\zeta^2 - 3.110\times10^{-1}\beta^4 \\ &- 3.042\times10^{-1}\beta^3\zeta + 2.127\times10^{-1}\beta^2\zeta^2 + 6.797\times10^{-1}\beta\zeta^3 - 2.471\times10^{-1}\zeta^4;\end{aligned} \tag{B-1.66}$$

$$\begin{aligned}C_{\mathrm{n}\zeta}^{post} &= 1.492\times10^{-1}\beta - 1.462\times10^{-1}\zeta - 2.233\times10^{-1}\alpha\beta + 5.470\times10^{-2}\alpha\zeta \\ &+ 1.477\times10^{-2}\alpha^2\beta + 1.840\times10^{-1}\alpha^2\zeta - 3.768\times10^{-1}\beta^3 + 1.760\times10^{-1}\beta^2\zeta \\ &- 3.633\times10^{-2}\beta\zeta^2 + 6.741\times10^{-2}\zeta^3 - 1.341\times10^{-2}\alpha^3\beta - 1.060\times10^{-1}\alpha^3\zeta \\ &+ 5.682\times10^{-1}\alpha\beta^3 - 3.177\times10^{-1}\alpha\beta^2\zeta + 2.005\times10^{-2}\alpha\beta\zeta^2 - 1.492\times10^{-2}\alpha\zeta^3.\end{aligned} \tag{B-1.67}$$

Polynomials in angle of attack and normalized body p-rate:

$$\begin{aligned}C_{\mathrm{Y}\hat{p}}^{post} &= -5.752\times10^{-2}\hat{p} - 5.900\times10^{-1}\alpha\hat{p} + 9.700\times10^{-1}\hat{p}^2 + 5.820\times10^{-1}\alpha^2\hat{p} \\ &- 3.112\alpha\hat{p}^2 + 1.414\times10^{1}\hat{p}^3;\end{aligned} \tag{B-1.68}$$

$$\begin{aligned}C_{\mathrm{l}\hat{p}}^{post} &= 4.360\times10^{-2}\hat{p} - 5.892\times10^{-1}\alpha\hat{p} + 1.330\times10^{-1}\hat{p}^2 + 4.640\times10^{-1}\alpha^2\hat{p} \\ &+ 1.256\times10^{-2}\alpha\hat{p}^2 - 2.843\hat{p}^3;\end{aligned} \tag{B-1.69}$$

$$\begin{aligned}C_{\mathrm{n}\hat{p}}^{post} &= 1.134\times10^{-1}\hat{p} - 5.042\times10^{-1}\alpha\hat{p} - 2.397\times10^{-1}\hat{p}^2 + 3.692\times10^{-1}\alpha^2\hat{p} \\ &+ 6.950\times10^{-1}\alpha\hat{p}^2 + 5.811\hat{p}^3;\end{aligned} \tag{B-1.70}$$

$C_{\mathrm{X}\hat{p}}^{post}$, $C_{\mathrm{Z}\hat{p}}^{post}$, $C_{\mathrm{m}\hat{p}}^{post}$ are zero due to lack of GTM measurement data.

Polynomials in angle of attack and normalized body q-rate:

$$\begin{aligned}C_{\mathrm{X}\hat{q}}^{post} &= 3.365\times10^{-2} - 2.087\times10^{-1}\alpha + 2.296\times10^{1}\hat{q} + 2.462\times10^{-1}\alpha^2 \\ &- 7.636\times10^{1}\alpha\hat{q} + 8.211\times10^{2}\hat{q}^2 - 9.727\times10^{-2}\alpha^3 + 5.965\times10^{1}\alpha^2\hat{q} \\ &+ 1.308\times10^{3}\alpha\hat{q}^2 + 2.529\times10^{3}\hat{q}^3;\end{aligned} \tag{B-1.71}$$

$$\begin{aligned}C_{\mathrm{Z}\hat{q}}^{post} &= 1.480\times10^{-2} - 3.851\times10^{-1}\alpha - 9.123\times10^{1}\hat{q} + 9.776\times10^{-1}\alpha^2 \\ &+ 1.991\times10^{2}\alpha\hat{q} + 1.312\times10^{3}\hat{q}^2 - 6.773\times10^{-1}\alpha^3 - 1.656\times10^{2}\alpha^2\hat{q} \\ &+ 1.558\times10^{3}\alpha\hat{q}^2 + 2.346\times10^{3}\hat{q}^3;\end{aligned} \tag{B-1.72}$$

Polynomials in angle of attack and normalized body q-rate (ct'd):

$$C_{\mathrm{m}\hat{q}}^{post} = 1.277 \times 10^{-1} - 4.700 \times 10^{-1}\alpha - 1.137 \times 10^{1}\hat{q} + 4.318 \times 10^{-1}\alpha^2 - 1.460 \times 10^{2}\alpha\hat{q} + 1.029 \times 10^{3}\hat{q}^2 - 1.729 \times 10^{-1}\alpha^3 + 1.459 \times 10^{2}\alpha^2\hat{q} + 1.275 \times 10^{3}\alpha\hat{q}^2 + 2.370 \times 10^{3}\hat{q}^3; \tag{B-1.73}$$

$C_{\mathrm{Y}\hat{q}}^{post}$, $C_{\mathrm{l}\hat{q}}^{post}$, $C_{\mathrm{n}\hat{q}}^{post}$ are zero due to lack of GTM measurement data.

Polynomials in angle of attack and normalized body r-rate:

$$C_{\mathrm{Y}\hat{r}}^{post} = 3.868\hat{r} - 1.182 \times 10^{1}\alpha\hat{r} + 1.677\hat{r}^2 + 7.267\alpha^2\hat{r} - 4.315\alpha\hat{r}^2 + 2.662\hat{r}^3; \tag{B-1.74}$$

$$C_{\mathrm{l}\hat{r}}^{post} = -1.541 \times 10^{-1}\hat{r} + 3.156\alpha\hat{r} + 1.893 \times 10^{-2}\hat{r}^2 - 3.867\alpha^2\hat{r} + 4.201 \times 10^{-2}\alpha\hat{r}^2 - 5.986\hat{r}^3; \tag{B-1.75}$$

$$C_{\mathrm{n}\hat{r}}^{post} = -6.393 \times 10^{-1}\hat{r} + 7.144 \times 10^{-1}\alpha\hat{r} - 2.392 \times 10^{-1}\hat{r}^2 - 5.096 \times 10^{-1}\alpha^2\hat{r} + 2.033 \times 10^{-1}\alpha\hat{r}^2 + 1.990 \times 10^{1}\hat{r}^3; \tag{B-1.76}$$

$C_{\mathrm{X}\hat{r}}^{post}$, $C_{\mathrm{Z}\hat{r}}^{post}$, $C_{\mathrm{m}\hat{r}}^{post}$ are zero due to lack of GTM measurement data.

B.1.3 MATLAB source code

The source code for the aerodynamic coefficients and the equations of motion can be found at:

`https://github.com/pwpfit/GTMpw`.

B.1.4 Spline-based longitudinal coefficients

This model is used in Chapter 5 as an application example of a spline-based longitudinal aircraft model. It has neither been designed nor evaluated for engineering purposes.

The longitudinal aerodynamic coefficients are obtained as

$$C_{\odot}(\alpha, \eta, \hat{q}) = C_{\odot\alpha}(\alpha) + C_{\odot\eta}(\alpha, \eta) + C_{\odot\hat{q}}(\alpha, \hat{q})\,, \tag{B-1.77}$$

where $C_{\odot} \in \{C_{\mathrm{X}}, C_{\mathrm{Z}}, C_{\mathrm{m}}\}$, $\hat{q} = c_{\mathrm{a}} q / (2V_{\mathrm{A}})$, and

$$C_{\odot\alpha}(\alpha, \eta) = \begin{cases} C_{\odot\alpha}^{(1)} & \text{if } \alpha \in (-\infty; \alpha_1), \\ C_{\odot\alpha}^{(2)} & \text{if } \alpha \in [\alpha_1; \alpha_2), \\ C_{\odot\alpha}^{(3)} & \text{if } \alpha \in [\alpha_2; \alpha_3), \\ C_{\odot\alpha}^{(4)} & \text{if } \alpha \in [\alpha_3; \alpha_3), \\ C_{\odot\alpha}^{(5)} & \text{if } \alpha \in [\alpha_4; \infty); \end{cases} \tag{B-1.78}$$

$$C_{\odot\eta}(\alpha,\eta) = \begin{cases} C_{\odot\eta}^{(1)} & \text{if } \alpha \in (-\infty;\alpha_1), \\ C_{\odot\eta}^{(2)} & \text{if } \alpha \in [\alpha_1;\alpha_2), \\ C_{\odot\eta}^{(3)} & \text{if } \alpha \in [\alpha_2;\alpha_3), \\ C_{\odot\eta}^{(4)} & \text{if } \alpha \in [\alpha_3;\alpha_3), \\ C_{\odot\eta}^{(5)} & \text{if } \alpha \in [\alpha_4;\infty); \end{cases} \tag{B-1.79}$$

$$C_{\odot\hat{q}}(\alpha,\hat{q}) = \begin{cases} C_{\odot\hat{q}}^{(1)} & \text{if } \hat{q} \in (-\infty;\hat{q}_1), \\ C_{\odot\hat{q}}^{(2)} & \text{if } \hat{q} \in [\hat{q}_1;\hat{q}_2), \\ C_{\odot\hat{q}}^{(3)} & \text{if } \hat{q} \in [\hat{q}_2;\hat{q}_3), \\ C_{\odot\hat{q}}^{(4)} & \text{if } \hat{q} \in [\hat{q}_3;\hat{q}_3), \\ C_{\odot\hat{q}}^{(5)} & \text{if } \hat{q} \in [\hat{q}_4;\infty); \end{cases} \tag{B-1.80}$$

with

$$\alpha_1 = 5^\circ, \qquad \alpha_2 = 15^\circ, \qquad \alpha_3 = 25^\circ, \qquad \alpha_4 = 45^\circ; \tag{B-1.81}$$

$$\hat{q}_1 = -0.200^\circ, \qquad \hat{q}_2 = -0.075^\circ, \qquad \hat{q}_3 = 0.075^\circ, \qquad \hat{q}_4 = 0.200^\circ; \tag{B-1.82}$$

and

$$C_{\mathrm{X}\alpha}^{(1)}(\alpha) = -2.459 \times 10^{-2} - 1.835 \times 10^{-3}\alpha + 8.268 \times 10^{-1}\alpha^2; \tag{B-1.83}$$

$$C_{\mathrm{X}\alpha}^{(2)}(\alpha) = -2.039 \times 10^{-1} + 2.778\alpha - 7.493\alpha^2; \tag{B-1.84}$$

$$C_{\mathrm{X}\alpha}^{(3)}(\alpha) = 2.173 \times 10^{-1} - 1.218\alpha + 1.628\alpha^2; \tag{B-1.85}$$

$$C_{\mathrm{X}\alpha}^{(4)}(\alpha) = 2.206 \times 10^{-2} - 1.103 \times 10^{-1}\alpha + 1.143 \times 10^{-1}\alpha^2; \tag{B-1.86}$$

$$C_{\mathrm{X}\alpha}^{(5)}(\alpha) = -5.170 \times 10^{-2} + 2.378 \times 10^{-2}\alpha + 6.318 \times 10^{-2}\alpha^2; \tag{B-1.87}$$

$$C_{\mathrm{Z}\alpha}^{(1)}(\alpha) = -2.815 \times 10^{-2} - 4.949\alpha + 8.370 \times 10^{-1}\alpha^2; \tag{B-1.88}$$

$$C_{\mathrm{Z}\alpha}^{(2)}(\alpha) = 1.546 \times 10^{-1} - 8.239\alpha + 1.454 \times 10^{1}\alpha^2; \tag{B-1.89}$$

$$C_{\mathrm{Z}\alpha}^{(3)}(\alpha) = -8.150 \times 10^{-1} - 2.984 \times 10^{-1}\alpha - 1.648\alpha^2; \tag{B-1.90}$$

$$C^{(4)}_{\mathrm{Z}\alpha}(\alpha) = -4.669 \times 10^{-1} - 2.158\alpha + 7.858 \times 10^{-1}\alpha^2; \quad C^{(5)}_{\mathrm{Z}\alpha}(\alpha) = -1.052 - 9.955 \times 10^{-1}\alpha + 2.537 \times 10^{-1}\alpha^2; \tag{B-1.91}$$

$$C^{(1)}_{\mathrm{m}\alpha}(\alpha) = 1.569 \times 10^{-1} - 1.724\alpha + 1.806\alpha^2 + 1.197 \times 10^{1}\alpha^3; \tag{B-1.92}$$

$$C^{(2)}_{\mathrm{m}\alpha}(\alpha) = 5.646 \times 10^{-1} - 1.042 \times 10^{1}\alpha + 5.928 \times 10^{1}\alpha^2 - 1.183 \times 10^{2}\alpha^3; \tag{B-1.93}$$

$$C^{(3)}_{\mathrm{m}\alpha}(\alpha) = 7.543 - 6.430 \times 10^{1}\alpha + 1.743 \times 10^{2}\alpha^2 - 1.604 \times 10^{2}\alpha^3; \tag{B-1.94}$$

$$C^{(4)}_{\mathrm{m}\alpha}(\alpha) = -8.659 \times 10^{-1} + 1.176\alpha - 1.875\alpha^2 + 6.807 \times 10^{-1}\alpha^3; \tag{B-1.95}$$

$$C^{(5)}_{\mathrm{m}\alpha}(\alpha) = -1.053 + 1.752\alpha - 2.210\alpha^2 + 5.614 \times 10^{-1}\alpha^3; \tag{B-1.96}$$

$$\begin{aligned} C^{(1)}_{\mathrm{X}\eta}(\alpha,\eta) = {} & -9.929 \times 10^{-3}\eta + 1.946 \times 10^{-1}\alpha\eta - 8.214 \times 10^{-2}\eta^2 + 6.278 \times 10^{-1}\alpha^2\eta \\ & + 2.128 \times 10^{-1}\alpha\eta^2 - 3.587 \times 10^{-2}\eta^3; \end{aligned} \tag{B-1.97}$$

$$\begin{aligned} C^{(2)}_{\mathrm{X}\eta}(\alpha,\eta) = {} & 1.140 \times 10^{-2}\eta - 9.478 \times 10^{-3}\alpha\eta - 5.982 \times 10^{-2}\eta^2 + 1.652 \times 10^{-1}\alpha^2\eta \\ & - 4.294 \times 10^{-2}\alpha\eta^2 - 3.587 \times 10^{-2}\eta^3; \end{aligned} \tag{B-1.98}$$

$$\begin{aligned} C^{(3)}_{\mathrm{X}\eta}(\alpha,\eta) = {} & 6.012 \times 10^{-2}\eta - 1.752 \times 10^{-1}\alpha\eta - 4.327 \times 10^{-2}\eta^2 + 8.743 \times 10^{-2}\alpha^2\eta \\ & - 1.062 \times 10^{-1}\alpha\eta^2 - 3.587 \times 10^{-2}\eta^3; \end{aligned} \tag{B-1.99}$$

$$\begin{aligned} C^{(4)}_{\mathrm{X}\eta}(\alpha,\eta) = {} & 2.681 \times 10^{-2}\eta - 7.895 \times 10^{-2}\alpha\eta - 5.634 \times 10^{-2}\eta^2 + 4.179 \times 10^{-2}\alpha^2\eta \\ & - 7.621 \times 10^{-2}\alpha\eta^2 - 3.587 \times 10^{-2}\eta^3; \end{aligned} \tag{B-1.100}$$

$$\begin{aligned} C^{(5)}_{\mathrm{X}\eta}(\alpha,\eta) = {} & -2.814 \times 10^{-1}\eta + 5.861 \times 10^{-1}\alpha\eta - 1.327 \times 10^{-1}\eta^2 - 3.053 \times 10^{-1}\alpha^2\eta \\ & + 2.098 \times 10^{-2}\alpha\eta^2 - 3.587 \times 10^{-2}\eta^3; \end{aligned} \tag{B-1.101}$$

$$\begin{aligned} C^{(1)}_{\mathrm{Z}\eta}(\alpha,\eta) = {} & -5.950 \times 10^{-1}\eta + 5.769 \times 10^{-2}\alpha\eta + 3.917 \times 10^{-2}\eta^2 + 4.460 \times 10^{-2}\alpha^2\eta \\ & + 2.304 \times 10^{-2}\alpha\eta^2 + 1.142\eta^3; \end{aligned} \tag{B-1.102}$$

$$C^{(2)}_{\mathrm{Z}\eta}(\alpha,\eta) = -6.264\times10^{-1}\eta + 4.609\times10^{-1}\alpha\eta + 1.219\times10^{-2}\eta^2 - 4.523\times10^{-1}\alpha^2\eta + 3.323\times10^{-1}\alpha\eta^2 + 1.142\eta^3; \quad \text{(B-1.103)}$$

$$C^{(3)}_{\mathrm{Z}\eta}(\alpha,\eta) = -6.306\times10^{-1}\eta + 2.994\times10^{-1}\alpha\eta + 5.138\times10^{-2}\eta^2 + 2.243\times10^{-1}\alpha^2\eta + 1.826\times10^{-1}\alpha\eta^2 + 1.142\eta^3; \quad \text{(B-1.104)}$$

$$C^{(4)}_{\mathrm{Z}\eta}(\alpha,\eta) = -6.662\times10^{-1}\eta + 5.157\times10^{-1}\alpha\eta - 3.375\times10^{-1}\eta^2 - 8.418\times10^{-2}\alpha^2\eta + 1.074\alpha\eta^2 + 1.142\eta^3; \quad \text{(B-1.105)}$$

$$C^{(5)}_{\mathrm{Z}\eta}(\alpha,\eta) = -1.116\eta + 1.625\alpha\eta + 3.116\times10^{-1}\eta^2 - 7.678\times10^{-1}\alpha^2\eta + 2.473\times10^{-1}\alpha\eta^2 + 1.142\eta^3; \quad \text{(B-1.106)}$$

$$C^{(1)}_{\mathrm{m}\eta}(\alpha,\eta) = -1.879\eta - 4.676\times10^{-2}\alpha\eta - 2.274\times10^{-1}\eta^2 - 8.450\times10^{-1}\alpha^2\eta + 3.783\times10^{-1}\alpha\eta^2 + 1.409\eta^3; \quad \text{(B-1.107)}$$

$$C^{(2)}_{\mathrm{m}\eta}(\alpha,\eta) = -2.006\eta + 1.410\alpha\eta - 2.604\times10^{-1}\eta^2 - 8.072\times10^{-1}\alpha^2\eta + 7.561\times10^{-1}\alpha\eta^2 + 1.409\eta^3; \quad \text{(B-1.108)}$$

$$C^{(3)}_{\mathrm{m}\eta}(\alpha,\eta) = -1.916\eta - 7.109\times10^{-2}\alpha\eta - 7.037\times10^{-1}\eta^2 + 3.530\alpha^2\eta + 2.449\alpha\eta^2 + 1.409\eta^3; \quad \text{(B-1.109)}$$

$$C^{(4)}_{\mathrm{m}\eta}(\alpha,\eta) = -1.612\eta + 7.653\times10^{-1}\alpha\eta + 8.022\times10^{-1}\eta^2 + 1.680\times10^{-2}\alpha^2\eta - 1.002\alpha\eta^2 + 1.409\eta^3; \quad \text{(B-1.110)}$$

$$C^{(5)}_{\mathrm{m}\eta}(\alpha,\eta) = -1.555\eta + 5.348\times10^{-1}\alpha\eta - 7.773\times10^{-1}\eta^2 + 2.185\times10^{-1}\alpha^2\eta + 1.009\alpha\eta^2 + 1.409\eta^3; \quad \text{(B-1.111)}$$

as well as

$$C^{(1)}_{\mathrm{X}\hat{q}}(\alpha,\hat{q}) = -2.944\times10^{-3} - 1.776\hat{q} - 9.511\times10^{-3}\alpha - 2.765\times10^{2}\hat{q}^{(2)} - 2.319\hat{q}\alpha - 5.445\times10^{-3}\alpha^2; \quad \text{(B-1.112)}$$

$$C^{(2)}_{\mathrm{X}\hat{q}}(\alpha,\hat{q}) = 8.254\times10^{-4} + 6.887\times10^{-1}\hat{q} + 3.791\times10^{-3}\alpha + 1.201\times10^{2}\hat{q}^{(2)} + 1.492\hat{q}\alpha - 5.445\times10^{-3}\alpha^2; \quad \text{(B-1.113)}$$

$$C^{(3)}_{\mathrm{X}\hat{q}}(\alpha,\hat{q}) = 1.483\times10^{-3} + 1.338\hat{q} + 2.569\times10^{-3}\alpha + 2.324\times10^{2}\hat{q}^{(2)} + 5.581\times10^{-1}\hat{q}\alpha - 5.445\times10^{-3}\alpha^{2}; \quad \text{(B-1.114)}$$

$$C^{(4)}_{\mathrm{X}\hat{q}}(\alpha,\hat{q}) = 9.025\times10^{-4} + 1.897\hat{q} + 4.214\times10^{-3}\alpha + 1.449\times10^{2}\hat{q}^{(2)} - 6.991\times10^{-1}\hat{q}\alpha - 5.445\times10^{-3}\alpha^{2}; \quad \text{(B-1.115)}$$

$$C^{(5)}_{\mathrm{X}\hat{q}}(\alpha,\hat{q}) = 1.446\times10^{-3} + 2.271\hat{q} - 8.633\times10^{-3}\alpha - 7.040\hat{q}^{(2)} + 2.981\hat{q}\alpha - 5.445\times10^{-3}\alpha^{2}; \quad \text{(B-1.116)}$$

$$C^{(1)}_{\mathrm{Z}\hat{q}}(\alpha,\hat{q}) = -8.248\times10^{-3} - 2.581\times10^{1}\hat{q} + 1.378\times10^{-1}\alpha + 2.806\times10^{3}\hat{q}^{(2)} + 2.216\times10^{1}\hat{q}\alpha + 3.690\times10^{-3}\alpha^{2}; \quad \text{(B-1.117)}$$

$$C^{(2)}_{\mathrm{Z}\hat{q}}(\alpha,\hat{q}) = -9.819\times10^{-3} - 3.215\times10^{1}\hat{q} + 1.877\times10^{-2}\alpha + 1.121\times10^{3}\hat{q}^{(2)} - 1.192\times10^{1}\hat{q}\alpha + 3.690\times10^{-3}\alpha^{2}; \quad \text{(B-1.118)}$$

$$C^{(3)}_{\mathrm{Z}\hat{q}}(\alpha,\hat{q}) = -1.398\times10^{-2} - 3.613\times10^{1}\hat{q} + 2.921\times10^{-2}\alpha + 5.071\times10^{2}\hat{q}^{(2)} - 3.943\hat{q}\alpha + 3.690\times10^{-3}\alpha^{2}; \quad \text{(B-1.119)}$$

$$C^{(4)}_{\mathrm{Z}\hat{q}}(\alpha,\hat{q}) = -9.819\times10^{-3} - 4.011\times10^{1}\hat{q} + 1.877\times10^{-2}\alpha + 1.121\times10^{3}\hat{q}^{(2)} + 4.036\hat{q}\alpha + 3.690\times10^{-3}\alpha^{2}; \quad \text{(B-1.120)}$$

$$C^{(5)}_{\mathrm{Z}\hat{q}}(\alpha,\hat{q}) = -8.248\times10^{-3} - 4.644\times10^{1}\hat{q} + 1.378\times10^{-1}\alpha + 2.806\times10^{3}\hat{q}^{(2)} - 3.005\times10^{1}\hat{q}\alpha + 3.690\times10^{-3}\alpha^{2}; \quad \text{(B-1.121)}$$

$$C^{(1)}_{\mathrm{m}\hat{q}}(\alpha,\hat{q}) = 8.325\times10^{-3} - 4.163\times10^{1}\hat{q} - 1.327\times10^{-2}\alpha + 3.004\times10^{2}\hat{q}^{(2)} - 1.072\times10^{1}\hat{q}\alpha - 8.073\times10^{-2}\alpha^{2}; \quad \text{(B-1.122)}$$

$$C^{(2)}_{\mathrm{m}\hat{q}}(\alpha,\hat{q}) = 9.034\times10^{-3} - 4.027\times10^{1}\hat{q} + 9.180\times10^{-3}\alpha + 6.325\times10^{2}\hat{q}^{(2)} - 4.284\hat{q}\alpha - 8.073\times10^{-2}\alpha^{2}; \quad \text{(B-1.123)}$$

$$C^{(3)}_{\mathrm{m}\hat{q}}(\alpha,\hat{q}) = 8.730\times10^{-3} - 4.045\times10^{1}\hat{q} + 1.195\times10^{-2}\alpha + 6.749\times10^{2}\hat{q}^{(2)} - 2.169\hat{q}\alpha - 8.073\times10^{-2}\alpha^{2}; \quad \text{(B-1.124)}$$

$$C_{\mathrm{m}\hat{q}}^{(4)}(\alpha,\hat{q}) = 8.541\times10^{-3} - 3.992\times10^{1}\hat{q} + 9.362\times10^{-3}\alpha + 3.814\times10^{2}\hat{q}^{(2)} \\ - 1.927\times10^{-1}\hat{q}\alpha - 8.073\times10^{-2}\alpha^{2}; \tag{B-1.125}$$

$$C_{\mathrm{m}\hat{q}}^{(5)}(\alpha,\hat{q}) = -5.290\times10^{-4} - 3.526\times10^{1}\hat{q} + 8.018\times10^{-3}\alpha - 2.086\times10^{2}\hat{q}^{(2)} \\ + 1.922\times10^{-1}\hat{q}\alpha - 8.073\times10^{-2}\alpha^{2}; \tag{B-1.126}$$

B.2 Cumulus One

The piece-wise polynomial models of the aerodynamic coefficients are given

$$C_{\odot}(\alpha,\beta,\xi,\eta,\zeta) = \begin{cases} C_{\odot}^{pre}(\alpha,\beta,\dots) & \text{if } \alpha \leq \alpha_0, \\ C_{\odot}^{post}(\alpha,\beta,\dots) & \text{else,} \end{cases} \tag{B-2.1}$$

where $C_{\odot} \in \{C_{\mathrm{X}}, C_{\mathrm{Y}}, C_{\mathrm{Z}}, C_{\mathrm{l}}, C_{\mathrm{m}}, C_{\mathrm{n}}\}$ are polynomials in angle of attack α, side-slip β, and surface deflections ξ, η, ζ; and the boundary is found at

$$\alpha_0 = 17.949^{\circ}. \tag{B-2.2}$$

The polynomials in low and high angle of attack, $C_{\odot}^{pre}$, $C_{\odot}^{post}$, are sums

$$C_{\odot}^{pre} = C_{\odot\alpha}^{pre}(\alpha) + C_{\odot\xi}(\beta,\xi) + C_{\odot\eta}^{pre}(\alpha,\eta) + C_{\odot\zeta}(\beta,\zeta) \tag{B-2.3}$$

$$C_{\odot}^{post} = C_{\odot\alpha}^{post}(\alpha) + C_{\odot\xi}(\beta,\xi) + C_{\odot\eta}^{post}(\alpha,\eta) + C_{\odot\zeta}(\beta,\zeta)\,. \tag{B-2.4}$$

In the following subsections, we present the polynomial terms obtained using the `pwpfit` toolbox. Coefficients of absolute value $< 10^{-2}$ have been omitted for readability.

B.2.1 Domain of low angle of attack

Polynomials in angle of attack:

$$C_{\mathrm{X}\alpha}^{pre} = -2.566 \times 10^{-2} + 5.722 \times 10^{-1}\alpha + 1.496\alpha^2 - 1.148 \times 10^{1}\alpha^3; \tag{B-2.5}$$

$$C_{\mathrm{Y}\alpha}^{pre} = 5.402 \times 10^{-2} - 2.345 \times 10^{-1}\alpha - 2.001\alpha^2 + 7.054\alpha^3; \tag{B-2.6}$$

$$C_{\mathrm{Z}\alpha}^{pre} = -3.475 \times 10^{-1} - 5.467\alpha + 1.853\alpha^2 + 2.663 \times 10^{1}\alpha^3; \tag{B-2.7}$$

$$C_{\mathrm{l}\alpha}^{pre} = 4.875 \times 10^{-2} - 2.190 \times 10^{-1}\alpha - 2.004\alpha^2 + 7.146\alpha^3; \tag{B-2.8}$$

$$C_{\mathrm{m}\alpha}^{pre} = 6.214 \times 10^{-2} - 1.755\alpha - 3.427\alpha^2 + 1.256 \times 10^{1}\alpha^3; \tag{B-2.9}$$

$$C_{\mathrm{n}\alpha}^{pre} = 4.748 \times 10^{-2} - 2.097 \times 10^{-1}\alpha - 2.016\alpha^2 + 7.171\alpha^3. \tag{B-2.10}$$

Polynomials in angle of attack and elevator deflections:

$$\begin{aligned} C_{\mathrm{X}\eta}^{pre} = {} & 4.327 \times 10^{-2}\eta - 4.458 \times 10^{-1}\alpha\eta + 3.370 \times 10^{-1}\alpha^2\eta - 4.567 \times 10^{-1}\alpha\eta^2 \\ & + 7.331 \times 10^{-2}\eta^3; \end{aligned} \tag{B-2.11}$$

Polynomials in angle of attack and elevator deflections (ct'd):

$$C_{\mathrm{Y}\eta}^{pre} = 1.832 \times 10^{-2}\eta + 7.484 \times 10^{-2}\alpha\eta - 4.384 \times 10^{-1}\alpha^2\eta; \tag{B-2.12}$$

$$C_{\mathrm{Z}\eta}^{pre} = -2.567 \times 10^{-1}\eta + 3.085 \times 10^{-1}\alpha\eta - 5.105 \times 10^{-2}\eta^2 - 7.394 \times 10^{-1}\alpha^2\eta + 6.936 \times 10^{-1}\alpha\eta^2 + 1.337 \times 10^{-1}\eta^3; \tag{B-2.13}$$

$$C_{\mathrm{l}\eta}^{pre} = 1.699 \times 10^{-2}\eta + 8.936 \times 10^{-2}\alpha\eta - 4.564 \times 10^{-1}\alpha^2\eta + 1.571 \times 10^{-2}\alpha\eta^2; \tag{B-2.14}$$

$$C_{\mathrm{m}\eta}^{pre} = -9.028 \times 10^{-1}\eta + 7.437 \times 10^{-1}\alpha\eta - 4.924 \times 10^{-2}\eta^2 - 8.415 \times 10^{-1}\alpha^2\eta + 2.210\alpha\eta^2 + 5.251 \times 10^{-1}\eta^3; \tag{B-2.15}$$

$$C_{\mathrm{n}\eta}^{pre} = 1.532 \times 10^{-2}\eta + 8.758 \times 10^{-2}\alpha\eta - 4.513 \times 10^{-1}\alpha^2\eta + 1.487 \times 10^{-2}\alpha\eta^2. \tag{B-2.16}$$

B.2.2 Domain of high angle of attack

Polynomials in angle of attack:

$$C_{\mathrm{X}\alpha}^{post} = 1.266 \times 10^{-2} - 3.159 \times 10^{-1}\alpha + 3.832 \times 10^{-1}\alpha^2 - 1.226 \times 10^{-1}\alpha^3; \tag{B-2.17}$$

$$C_{\mathrm{Y}\alpha}^{post} = -2.297 \times 10^{-2}\alpha^2 + 1.337 \times 10^{-2}\alpha^3; \tag{B-2.18}$$

$$C_{\mathrm{Z}\alpha}^{post} = -4.179 \times 10^{-1} - 2.345\alpha + 9.586 \times 10^{-1}\alpha^2 - 3.665 \times 10^{-2}\alpha^3; \tag{B-2.19}$$

$$C_{\mathrm{l}\alpha}^{post} = 2.006 \times 10^{-2} - 8.200 \times 10^{-2}\alpha + 1.012 \times 10^{-1}\alpha^2 - 3.515 \times 10^{-2}\alpha^3; \tag{B-2.20}$$

$$C_{\mathrm{m}\alpha}^{post} = -2.552 \times 10^{-1} - 5.131 \times 10^{-1}\alpha - 2.677 \times 10^{-1}\alpha^2 + 1.332 \times 10^{-1}\alpha^3; \tag{B-2.21}$$

$$C_{\mathrm{n}\alpha}^{post} = 1.159 \times 10^{-2} - 3.062 \times 10^{-2}\alpha + 2.727 \times 10^{-2}\alpha^2. \tag{B-2.22}$$

Polynomials in angle of attack and elevator deflections:

$$C_{\mathrm{X}\eta}^{post} = -1.342 \times 10^{-2}\eta - 1.663 \times 10^{-1}\alpha\eta - 1.796 \times 10^{-1}\eta^2 + 2.254 \times 10^{-2}\alpha^2\eta + 9.274 \times 10^{-2}\alpha\eta^2 + 7.331 \times 10^{-2}\eta^3; \tag{B-2.23}$$

$$C_{\mathrm{Z}\eta}^{post} = -2.922 \times 10^{-1}\eta + 1.829 \times 10^{-1}\alpha\eta + 1.277 \times 10^{-1}\eta^2 + 2.284 \times 10^{-2}\alpha^2\eta + 1.229 \times 10^{-1}\alpha\eta^2 + 1.337 \times 10^{-1}\eta^3; \tag{B-2.24}$$

$$C_{\mathrm{m}\eta}^{post} = -9.498 \times 10^{-1}\eta + 6.099 \times 10^{-1}\alpha\eta + 5.093 \times 10^{-1}\eta^2 + 6.456 \times 10^{-2}\alpha^2\eta + 4.264 \times 10^{-1}\alpha\eta^2 + 5.251 \times 10^{-1}\eta^3; \tag{B-2.25}$$

$C_{\mathrm{Y}\eta}^{post}$, $C_{\mathrm{l}\eta}^{post}$, $C_{\mathrm{n}\eta}^{post}$ are approximately zero.

B.2.3 Full-envelope polynomials

Polynomials in side-slip and aileron deflections:

$$C_{X\xi} = 6.557 \times 10^{-2}\beta^2 + 4.214 \times 10^{-2}\beta\xi - 1.493\xi^2 + 4.264 \times 10^{-2}\xi^3 - 1.647 \times 10^{-2}\beta^4 - 2.321 \times 10^{-2}\beta^3\xi + 9.649 \times 10^{-2}\beta^2\xi^2 + 2.859 \times 10^{-2}\beta\xi^3 + 3.084 \times 10^{1}\xi^4; \quad \text{(B-2.26)}$$

$$C_{Y\xi} = -3.697 \times 10^{-1}\beta - 1.570 \times 10^{-1}\xi - 3.231 \times 10^{-2}\beta^2 - 6.137\xi^2 + 7.416 \times 10^{-2}\beta^3 + 1.611 \times 10^{-2}\beta\xi^2 + 2.214\xi^3 + 6.487 \times 10^{-1}\beta^2\xi^2 + 5.323 \times 10^{-2}\beta\xi^3 + 1.456 \times 10^{2}\xi^4; \quad \text{(B-2.27)}$$

$$C_{Z\xi} = 3.411 \times 10^{-1}\beta^2 + 4.141 \times 10^{-1}\beta\xi - 3.717\xi^2 + 4.234 \times 10^{-2}\xi^3 - 9.915 \times 10^{-2}\beta^4 - 1.922 \times 10^{-1}\beta^3\xi + 1.945 \times 10^{-1}\beta^2\xi^2 + 9.909 \times 10^{-1}\beta\xi^3 + 9.856 \times 10^{1}\xi^4; \quad \text{(B-2.28)}$$

$$C_{l\xi} = -5.798 \times 10^{-2}\beta - 3.929 \times 10^{-1}\xi - 2.906 \times 10^{-2}\beta^2 - 5.551\xi^2 + 1.763 \times 10^{-2}\beta^3 + 1.722 \times 10^{-1}\beta^2\xi + 4.557 \times 10^{-1}\xi^3 + 5.835 \times 10^{-1}\beta^2\xi^2 + 5.332 \times 10^{-2}\beta\xi^3 + 1.319 \times 10^{2}\xi^4; \quad \text{(B-2.29)}$$

$$C_{m\xi} = -3.978 \times 10^{-2}\beta^2 + 5.554 \times 10^{-1}\beta\xi - 4.689\xi^2 + 4.229 \times 10^{-2}\xi^3 + 2.585 \times 10^{-2}\beta^4 - 2.309 \times 10^{-1}\beta^3\xi + 4.077 \times 10^{-1}\beta^2\xi^2 - 5.068 \times 10^{-1}\beta\xi^3 + 1.160 \times 10^{2}\xi^4; \quad \text{(B-2.30)}$$

$$C_{n\xi} = 3.686 \times 10^{-2}\beta + 1.392 \times 10^{-2}\xi - 2.828 \times 10^{-2}\beta^2 - 5.410\xi^2 - 1.160 \times 10^{-1}\xi^3 + 5.678 \times 10^{-1}\beta^2\xi^2 + 5.334 \times 10^{-2}\beta\xi^3 + 1.286 \times 10^{2}\xi^4. \quad \text{(B-2.31)}$$

Polynomials side-slip and rudder deflections:

$$C_{X\zeta} = -1.031 \times 10^{-2}\beta\zeta - 7.986 \times 10^{-2}\zeta^2 + 1.086 \times 10^{-2}\beta\zeta^3 + 9.739 \times 10^{-2}\zeta^4; \quad \text{(B-2.32)}$$

$$C_{Y\zeta} = -8.526 \times 10^{-2}\zeta - 2.128 \times 10^{-2}\beta^2 - 3.569 \times 10^{-1}\zeta^2 + 1.049 \times 10^{-2}\beta^2\zeta + 1.924 \times 10^{-2}\beta\zeta^2 + 7.679 \times 10^{-2}\zeta^3 + 5.663 \times 10^{-2}\beta^2\zeta^2 + 5.247 \times 10^{-1}\zeta^4; \quad \text{(B-2.33)}$$

$$C_{Z\zeta} = -2.036 \times 10^{-2}\beta^2 - 1.332 \times 10^{-2}\beta\zeta - 1.743 \times 10^{-1}\zeta^2 + 1.834 \times 10^{-2}\beta^2\zeta^2 + 3.683 \times 10^{-2}\beta\zeta^3 + 2.631 \times 10^{-1}\zeta^4; \quad \text{(B-2.34)}$$

Polynomials side-slip and rudder deflections (ct'd):

$$C_{\mathrm{l}\zeta} = -1.930 \times 10^{-2}\beta^2 - 3.221 \times 10^{-1}\zeta^2 + 5.111 \times 10^{-2}\beta^2\zeta^2 + 4.735 \times 10^{-1}\zeta^4; \tag{B-2.35}$$

$$\begin{aligned} C_{\mathrm{m}\zeta} = &-3.231 \times 10^{-2}\beta^2 - 1.436 \times 10^{-2}\beta\zeta - 2.672 \times 10^{-1}\zeta^2 + 1.241 \times 10^{-2}\beta^3\zeta \\ &+ 1.472 \times 10^{-2}\beta^2\zeta^2 + 1.051 \times 10^{-2}\beta\zeta^3 + 4.193 \times 10^{-1}\zeta^4; \end{aligned} \tag{B-2.36}$$

$$\begin{aligned} C_{\mathrm{n}\zeta} = &\ 2.158 \times 10^{-2}\zeta - 1.882 \times 10^{-2}\beta^2 - 3.137 \times 10^{-1}\zeta^2 - 1.338 \times 10^{-2}\zeta^3 \\ &+ 4.978 \times 10^{-2}\beta^2\zeta^2 + 4.611 \times 10^{-1}\zeta^4. \end{aligned} \tag{B-2.37}$$

B.2.4 Linear pitch-damping model

In Chapters 6 and 7, the pitch-damping behaviour of the longitudinal motion was represented by the linear model

$$I_y M = \bar{q} c_{\mathrm{a}} C_{\mathrm{m}}(\alpha, \eta) - C_{\mathrm{M}q} q \tag{B-2.38}$$

with $C_{\mathrm{M}q} = 1.960$.

Appendix C

Implementation of MPC Recovery

This appendix chapter details the implementation of model-predictive control (MPC) strategies for upset recovery. We discuss the reduction of the optimal control problem (OCP) onto a nonlinear optimisation problem, which is solved using an open-source interior-point solver; review the aircraft simulation of the Generic Transport Model (GTM) provided by NASA; and explain the simulation of tracking MPC (NMPC) recovery within MATLAB/Simulink.

C.1 Solving the Optimal Control Problem

We use the `Ipopt` open-source software package (as detailed in Wächter and Biegler 2006) to iteratively solve the OCP – formulated as general nonlinear optimisation problem – at each step of the MPC feedback.

C.1.1 Nonlinear optimisation with `Ipopt`

`Ipopt` solves the general nonlinear programming problem (cf. Ipopt 2016, p. 3)

$$\min_{\Xi\in\mathbb{R}^{\mathcal{N}}} \quad J(\Xi) \tag{C.1}$$

$$\text{s.t.} \quad \Gamma^{\mathrm{L}} \leq \boldsymbol{\gamma}(\Xi) \leq \Gamma^{\mathrm{U}}, \tag{C.2}$$

$$\Xi^{\mathrm{L}} \leq \quad \Xi \quad \leq \Xi^{\mathrm{U}}, \tag{C.3}$$

where $J\colon \mathbb{R}^{\mathcal{N}} \to \mathbb{R}$ is the objective function; $\Xi = (\xi_1, \ldots, \xi_{\mathcal{N}})$ are real-valued decision variables with lower and upper bounds $\Xi^{\mathrm{L}}, \Xi^{\mathrm{U}} \in (\mathbb{R} \cup \{\pm\infty\})^{\mathcal{N}}$, $\Xi^{\mathrm{L}} \leq \Xi^{\mathrm{U}}$, respectively;[1] and $\boldsymbol{\gamma}\colon \mathbb{R}^{\mathcal{N}} \to \mathbb{R}^{\mathcal{M}}$ are $\mathcal{M}$ nonlinear constraints with $\Gamma^{\mathrm{L}}, \Gamma^{\mathrm{U}} \in (\mathbb{R} \cup \{\pm\infty\})^{\mathcal{M}}$, $\Gamma^{\mathrm{L}} \leq \Gamma^{\mathrm{U}}$.

Easy to see, we can write the nonlinear constraints of (C.2) equivalently as

$$\boldsymbol{\gamma}_{\leq}(\Xi) = \begin{bmatrix} \boldsymbol{\gamma}(\Xi) - \Gamma^{\mathrm{U}} \\ \Gamma^{\mathrm{L}} - \boldsymbol{\gamma}(\Xi) \end{bmatrix} \leq 0 \tag{C.4}$$

and, for convenience, define

$$\boldsymbol{\gamma}_{\leq}(\Xi) =_{\text{def}} \begin{bmatrix} \mathbf{g}_{\leq}(\Xi) \\ \mathbf{g}_{=}(\Xi) \\ -\mathbf{g}_{=}(\Xi) \end{bmatrix} \tag{C.5}$$

[1] The inequality operator "$\leq$" here is to be understood *element-wise* and, in general, $\infty \not\leq \infty$.

with $\mathbf{g}_{\leq}\colon \mathbb{R}^{\mathcal{N}} \to \mathbb{R}^{\mathcal{M}_1}$ and $\mathbf{g}_{=}\colon \mathbb{R}^{\mathcal{N}} \to \mathbb{R}^{\mathcal{M}_2}$, imposing the equality constraints $\mathbf{g}_{=}(\Xi) = 0$.

Of importance for an efficient and successful optimisation are the gradient vector and the Jacobian matrix of $J(\cdot)$ and $\gamma(\cdot)$, respectively, and the Hessian matrix of the Lagrangian $\mathcal{L}(\cdot)$, with respect to Ξ, viz. (IPOPT 2016, p. 27)

$$\operatorname{grad}_J(\Xi) = \left[\frac{\partial J}{\partial \xi_1}(\Xi) \quad \cdots \quad \frac{\partial J}{\partial \xi_{\mathcal{N}}}(\Xi)\right]^T; \tag{C.6}$$

$$\mathbf{J}_{\gamma}(\Xi) = \begin{bmatrix} \frac{\partial \gamma_1}{\partial \xi_1}(\Xi) & \cdots & \frac{\partial \gamma_1}{\partial \xi_{\mathcal{N}}}(\Xi) \\ \vdots & \ddots & \vdots \\ \frac{\partial \gamma_{\mathcal{M}}}{\partial \xi_1}(\Xi) & \cdots & \frac{\partial \gamma_{\mathcal{M}}}{\partial \xi_{\mathcal{N}}}(\Xi) \end{bmatrix}; \tag{C.7}$$

$$\mathbf{H}_{\mathcal{L}}(\Xi, \lambda, \boldsymbol{\mu}) = \begin{bmatrix} \frac{\partial^2 \mathcal{L}}{\partial \xi_1^2}(\cdot) & \cdots & \frac{\partial^2 \mathcal{L}}{\partial \xi_1 \partial \xi_{\mathcal{N}}}(\cdot) \\ \vdots & \ddots & \vdots \\ \frac{\partial^2 \mathcal{L}}{\partial \xi_{\mathcal{N}} \partial \xi_1}(\cdot) & \cdots & \frac{\partial^2 \mathcal{L}}{\partial \xi_{\mathcal{N}}^2}(\cdot) \end{bmatrix}; \tag{C.8}$$

with

$$\mathcal{L}(\Xi, \lambda, \boldsymbol{\mu}) =_{\text{def}} \lambda J(\Xi) + \sum_{i=1}^{\mathcal{M}} \mu_i \gamma_i(\Xi)\,, \tag{C.9}$$

where γ_i, μ_i are the i-th components of $\boldsymbol{\gamma}(\cdot)$ and $\boldsymbol{\mu}$, respectively.

C.1.2 Formulation of the OCP

The open-loop OCPs of Eq. (II.10) and following are formulated as the nonlinear problem with decision variables

$$\Xi = (\mathbf{x}_1, \ldots, \mathbf{x}_N, \mathbf{u}_0, \ldots, \mathbf{u}_{N-1})\,, \tag{C.10}$$

objective function

$$J\colon \Xi \mapsto \ell_{\infty}(\mathbf{x}_N) + \sum_{k=1}^{N-1} \ell(\mathbf{x}_k, \mathbf{u}_k)\,, \tag{C.11}$$

equality constraints

$$\mathbf{g}_{=}\colon \Xi \mapsto \begin{bmatrix} \mathbf{f}^+(\mathbf{x}_0, \mathbf{u}_0) - \mathbf{x}_1 \\ \vdots \\ \mathbf{f}^+(\mathbf{x}_{N-1}, \mathbf{u}_{N-1}) - \mathbf{x}_N \end{bmatrix}, \tag{C.12}$$

and inequality constraints

$$\mathbf{g}_{\leq}\colon \Xi \mapsto \left[\begin{array}{c} g_i(\mathbf{x}_1, \mathbf{u}_1) \\ \vdots \\ g_i(\mathbf{x}_{N-1}, \mathbf{u}_{N-1}) \\ \hdashline g_i(N, \mathbf{x}_N) \end{array}\right]_{i \in I}. \tag{C.13}$$

Where state-space $\mathcal{X}$ and admissible control inputs $\mathcal{U}$ are defined as box constraints $\underline{\mathbf{x}} \leq \mathbf{x} \leq \overline{\mathbf{x}}$ and $\underline{\mathbf{u}} \leq \mathbf{u} \leq \overline{\mathbf{u}}$, respectively, upper and lower bounds of the decision variables are set to

$$\Xi^{\mathrm{L}} = \left[\begin{array}{ccc|ccc} \underline{\mathbf{x}} & \cdots_N & \underline{\mathbf{x}} & \underline{\mathbf{u}} & \cdots_N & \underline{\mathbf{u}} \end{array} \right]^T, \tag{C.14}$$

$$\Xi^{\mathrm{U}} = \left[\begin{array}{ccc|ccc} \overline{\mathbf{x}} & \cdots_N & \overline{\mathbf{x}} & \overline{\mathbf{u}} & \cdots_N & \overline{\mathbf{u}} \end{array} \right]^T, \tag{C.15}$$

where "$a \cdots_n a$" denotes a repetition of a for in total n times.

We have made use of CasADi (Andersson, Gillis, Horn, et al. 2018) in order to construct and evaluate Eqs. (C.11)–(C.13) as well as (C.6)–(C.9) given N, $\ell(\cdot,\cdot)$, $\ell_\infty(\cdot)$, $\mathbf{f}^+(\cdot,\cdot)$, and $g_i(\cdot,\cdot)$ for all $i \in I$ as well as $\underline{\mathbf{x}}, \overline{\mathbf{x}}$ and $\underline{\mathbf{u}}, \overline{\mathbf{u}}$. All problem function instances have been compiled into MATLAB executables (`mex`) for fast, iterative execution (see Andersson, Gillis, and Diehl 2018, p. 42).

C.2 The GTM Simulation

The MATLAB/Simulink model[2] for the Generic Transport Model (NASA 2016) consists of the aircraft simulation block itself ("`GTM_T2`"), a wind and feedback command generator block, and further utility blocks for trimming, linearisation, and logging of the simulation (Fig. C.1).

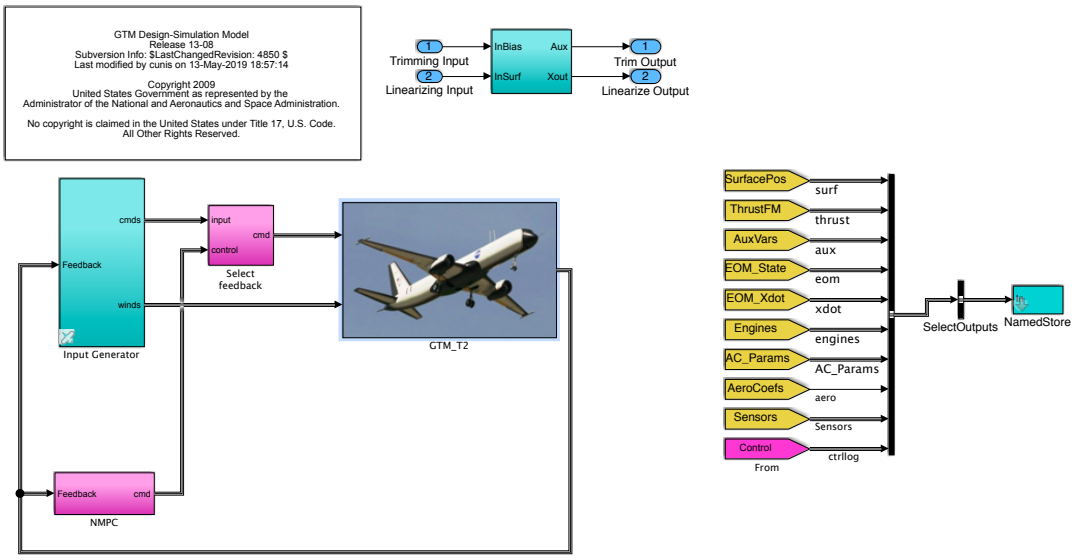

Figure C.1: Overview of the Simulink model with aircraft simulation (centre), feedback (left), and utilities (top & right). The NMPC feedback is also shown (bottom left).

[2]We use "model" here for the MATLAB/Simulink `mdl` file in the sense Mathworks does.

For the simulation, forces and moments of aerodynamics, engines, gravity, and the landing gear, and subsequently the aircraft's equations of motion, are modeled as well as uplink/downlink transport delays, actuators dynamics, and sensors (Fig. C.2).

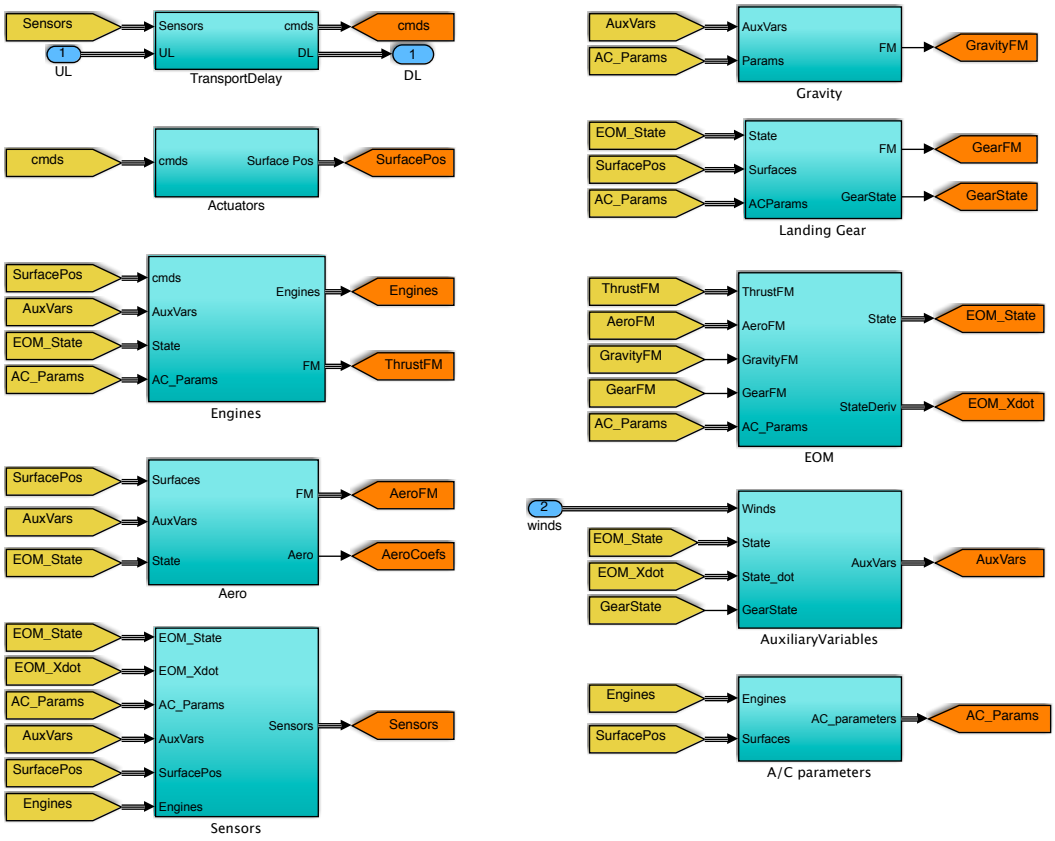

Figure C.2: Overview of the aircraft simulation with blocks for engines (3rd row left), aerodynamics (4th row left), gravity (top row right), landing gear (2nd row right), and equations of motion (3rd row right) as well as delays, actuators, and sensors (respectively top, 2nd, and bottom row left).

C.2.1 Equations of motion

Central part of the simulation are the equations of motion based on forces and moments generated by the aircraft and its components. Main contributor to the aircraft dynamics are the aerodynamic forces and moments divided into basic airframe, control surfaces, dynamics derivatives, and stall-rolling asymmetry (Fig. C.3). The latter has not been used in the upset recovery experiments. Based on the total of forces and moments, the equations of motions are modeled as simple point-mass dynamics of a rigid body (Fig. C.4); note that the input `Forces` consists of both forces and moments.

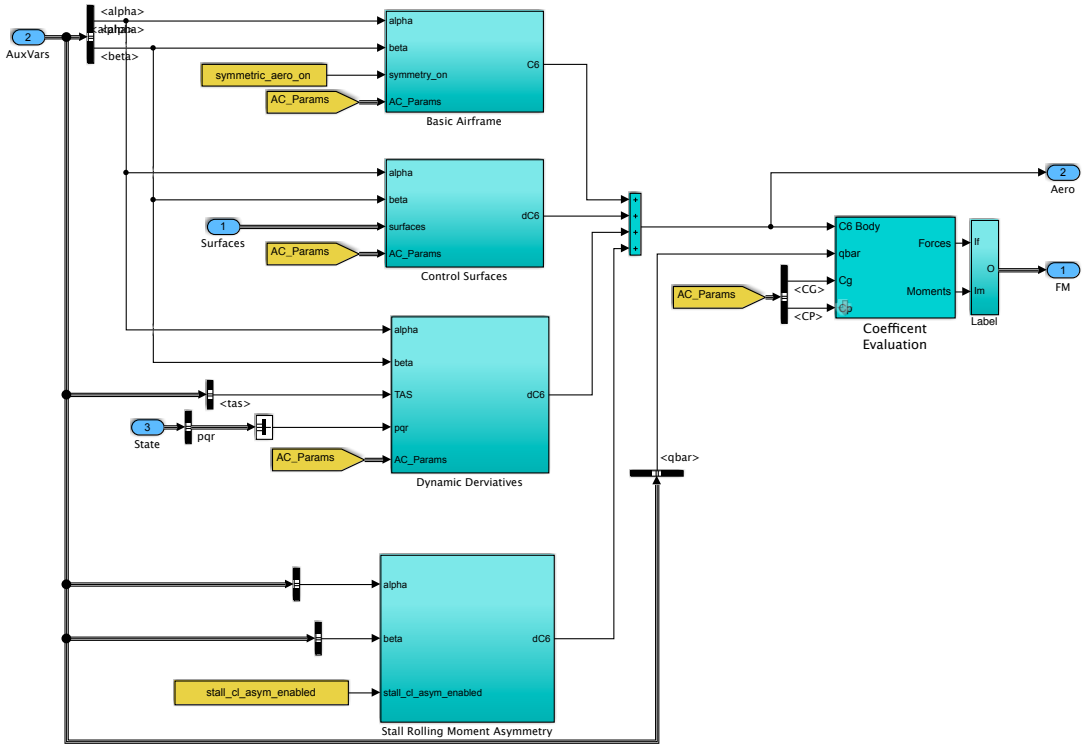

Figure C.3: Simulation of aerodynamics forces and moments generated by the fuselage, control surfaces, dynamic derivatives, and stall-rolling asymmetry (top to bottom).

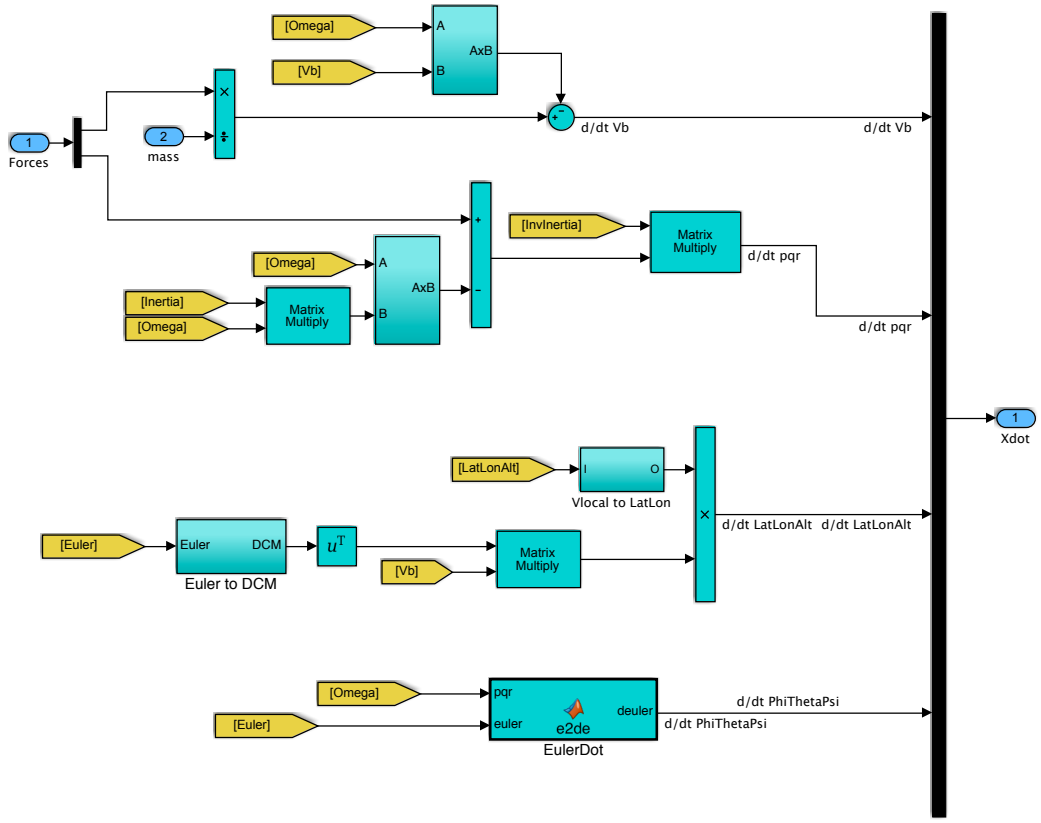

Figure C.4: Point-mass rigid body equations of motion based on forces and moments.

C.2.2 Inputs & Outputs

From the point of view of a feedback controller – human or computer – the outputs of the aircraft simulation are provided as sensor data and subject to a downlink delay; the respective input commands are again delayed in the uplink and then applied to the actuator dynamics, which result in the actual change of the control surfaces. In both directions, the transport delays (Fig. C.5) equate to 15 ms for sensor downlink and for command uplink.[3]

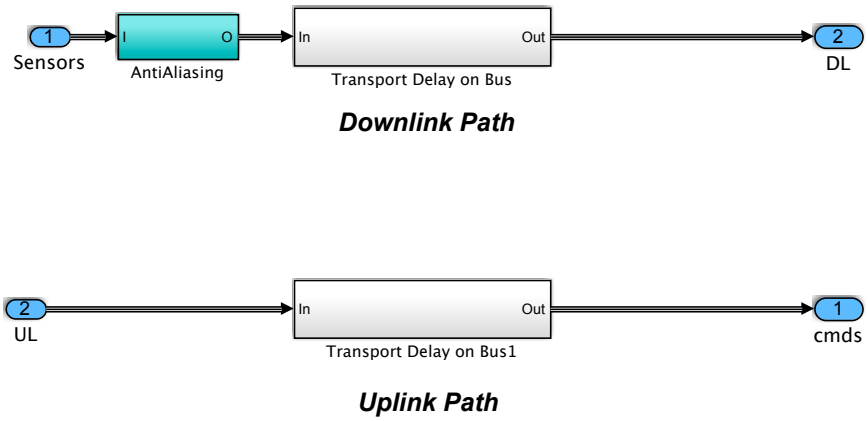

Figure C.5: Uplink and downlink of inputs and outputs with transport delays.

The GTM has a total of 16 independent control surfaces; namely, each inner and outer, left and right elevators; left and right ailerons; upper and lower rudder; each inner and outer, left and right spoiler; as well as each inner and outer, left and right flaps.

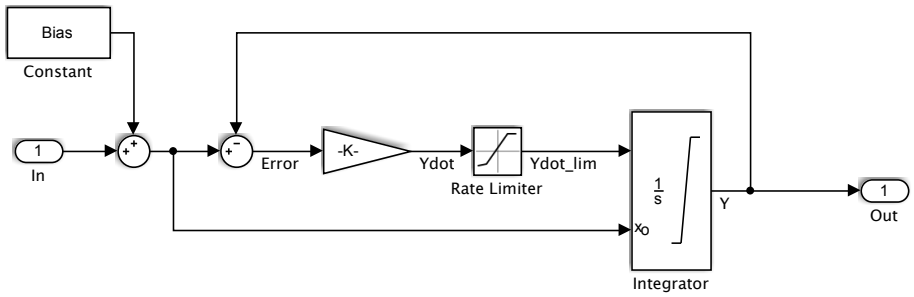

Figure C.6: Actuator dynamics for elevator, aileron, rudder, spoiler, and flaps.

[3]The time delay of the inputs are divided into 5 ms prior actuator dynamics and 10 ms for the surface positions to "take effect."

The dynamics of each surface are independently modeled as first-order linear transfer functions (Fig. C.6, exemplary for the outer left elevator) with individual limits on rates and positions. These control inputs are further completed by gear shift, break, and steering servo of the landing gear (for control on ground) as well as individual throttle commands for the left and right engine.

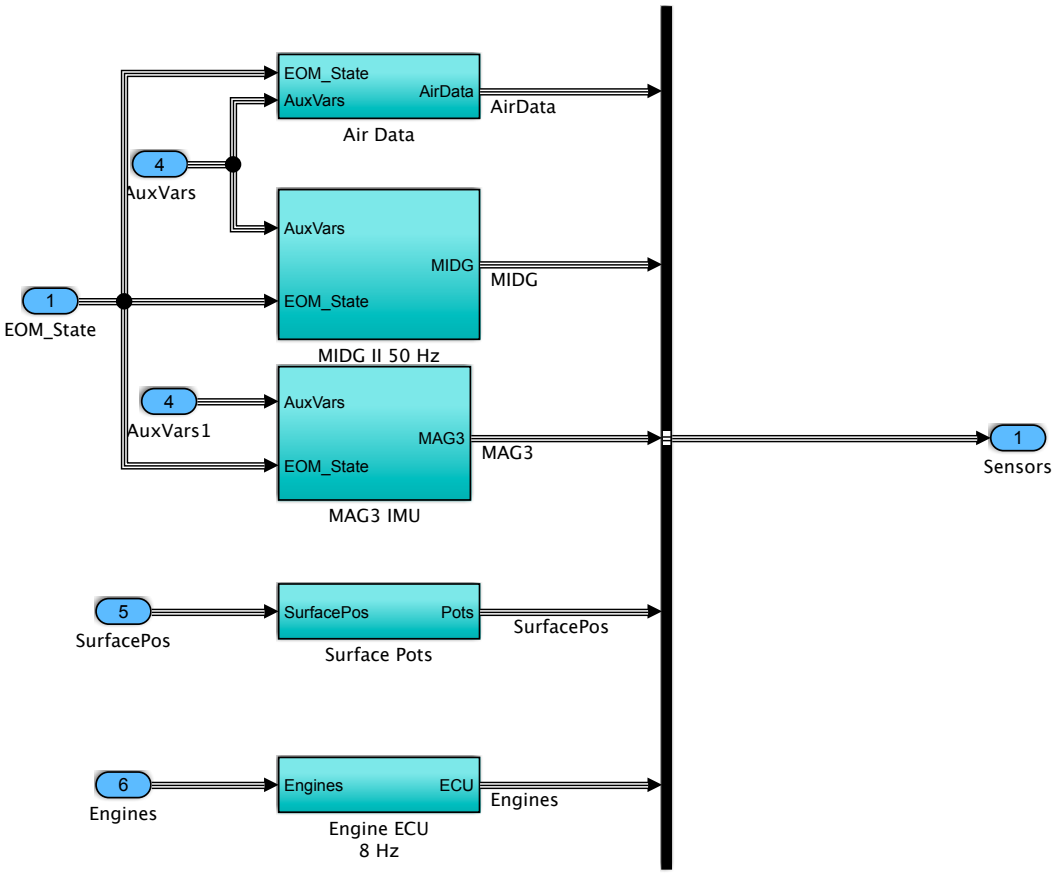

Figure C.7: Sensor data output grouped into aerodynamic data, earth-fixed position, velocity, and orientation ("MIDG"), body rates and accelerations ("MAG3") as well as outputs of the control devices (all top to bottom).

Finally, the sensor outputs are grouped into aerodynamic data (such as angle of attack, side-slip angle, and true airspeed), inertial measurements[4] (position, orientation, velocity) with respect to the earth-fixed axis system, rates and accelerations within the body axis system, and the outputs of the control subsystems, i.e., surface positions and engine data (Fig. C.7).

[4]Subject to an additional time delay of 40 ms.

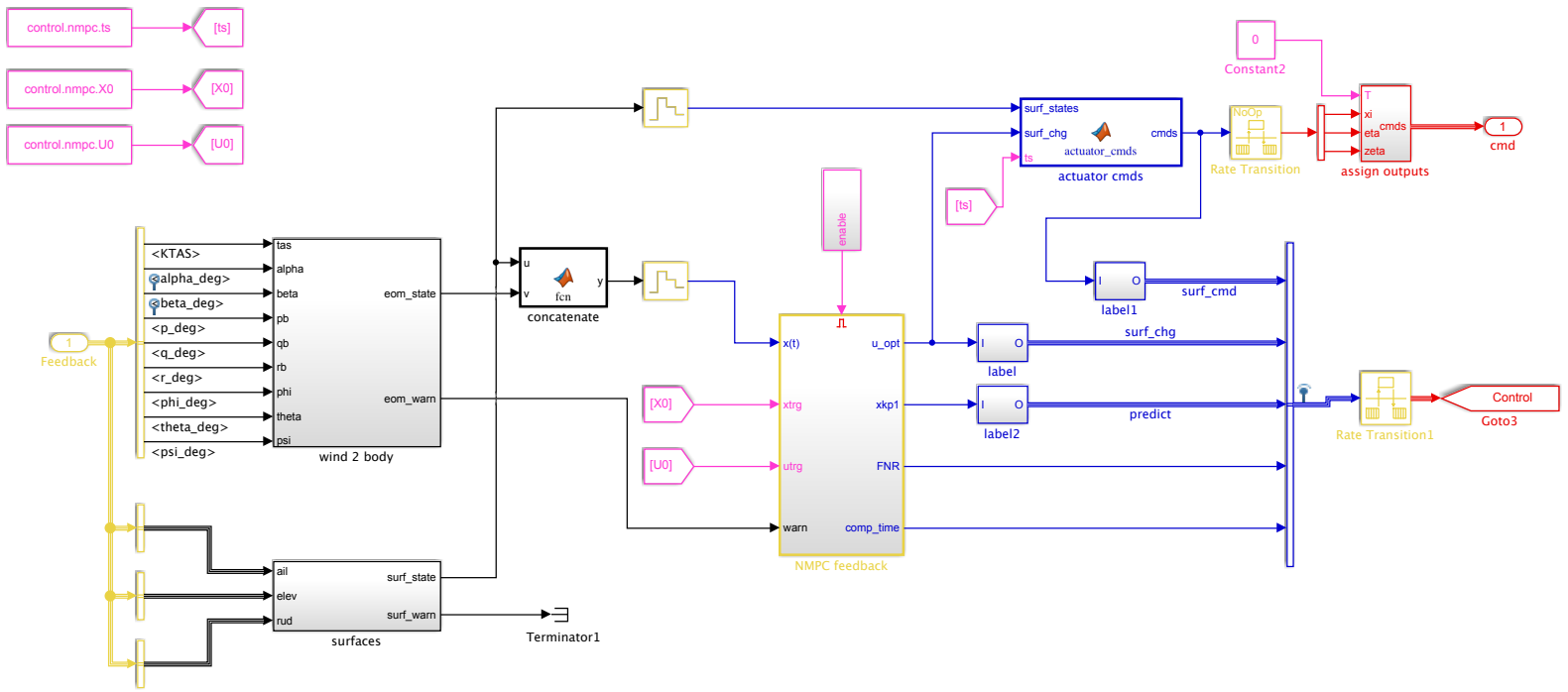

Figure C.8: Overview of the NMPC feedback block with collection of aircraft and control outputs (left), OCP (centre), and control input assignment (top row, centre-right & right). Details of the iteration are fed-through for logging (right).

C.3 MPC Recovery Simulation

The NMPC feedback block subsumes mainly three distinguished elements, namely, collecting aircraft and actuator outputs from the sensor data into the extended NMPC state vector, solving the OCP using `Ipopt`, and computing and assigning the optimal control inputs onto the aircraft actuator commands (Fig. C.8). The target condition and sample time for NMPC are given as constant parameters to the simulation.

Remark The NMPC feedback is evaluated as discrete system with a frequency of 20 Hz, whereas the aircraft simulation is considered continuous – although, in fact, the aircraft equations of motion are solved with a fixed step of 5 ms (200 Hz). In these figures depicting the MATLAB/Simulink elements, the sample time of the signals is color-coded as follows: black, continuous time; red, quasi-continuous (5 ms); blue, NMPC sample time (50 ms); yellow, mixed sample time; and pink, constants.

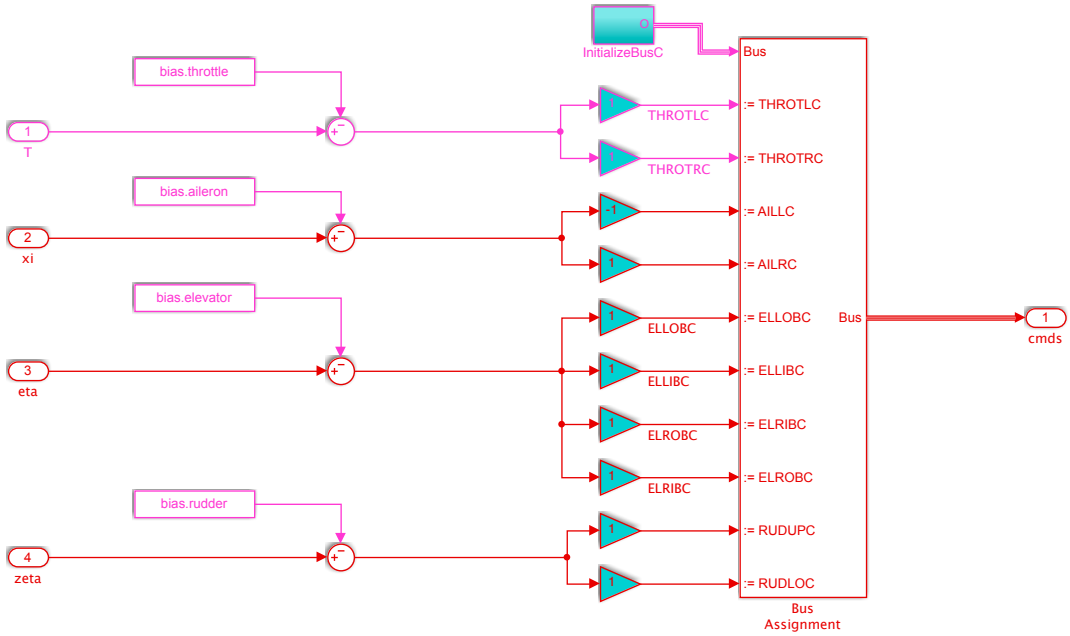

Figure C.9: Assignment of control inputs onto the aircraft actuator commands (throttle was chosen to be constantly zero).

For the NMPC state vector, the velocity vector in air-path axis system (in SI units) is calculated from aerodynamic sensor data (angle of attack, side-slip angle, true airspeed in knots) and angular values are converted from degrees to radians. A warning is issued if the aircraft's state violates the NMPC constraints and render the OCP infeasible. Positions of the individual control surfaces are collected into a single variable

for each ailerons, elevator, and rudder.[5] The OCP is solved within a Simulink `MATLAB Function` block that calls the `Ipopt` nonlinear solver using the pre-compiled MATLAB executables for objectives, constraints, and first and second derivatives. Here, the most recent optimal solution is kept *persistent* in order to benefit from the `Ipopt` warm-start capabilities (IPOPT 2016, p. 58). Finally, the resulting actuator control inputs, based on the surfaces' current positions and optimal changes, are assigned to the individual surface commands (Fig. C.9; note the negative sign of the left aileron command).

[5] As of now, this is done by calculating the respective median. A warning may be issued if the individual surface positions do not coincide.

Abstract Upset flight dynamics are characterised by unstable, highly nonlinear behaviour of the aircraft aerodynamic system. As upsets often lead to in-flight loss-of-control (LOC-I) accidents, it still poses a severe threat to today's commercial aviation. Contributing to almost every second fatality in civil aviation while representing merely 10 % of the total accidents (both fatal and nonfatal), the International Air Transport Association has classified LOC-I as the "highest risk to aviation safety". Considerable effort has been undertaken in response by academics, manufacturers, commercial airlines, and authorities to predict and prevent LOC-I events as well as recover from upset conditions into the nominal flight envelope. As result, researchers from both aeronautical engineering and system theory have made significant contributions towards aviation safety; however, approaches from engineering and theory are rather disparate. This thesis therefore focuses on the application and transfer of system theoretical results to engineering applications.

In particular, we have found simple polynomial models for aircraft dynamics, despite common in the system theoretical literature, failing to represent full-envelope aerodynamics accurately. Advanced fitting methods such as multi-variate splines, on the other hand, are unsuitable for some of the proposed functional analysis methods. Instead, a simple piecewise defined polynomial model proves to be accurate in fitting the aerodynamic coefficients for low and high angles of attack. State-of-the-art bifurcation analysis and analysis based on sum-of-squares programming techniques are extended for this class of models and applied to a piecewise equations of motion of the Generic Transport Model (GTM). In the same spirit, we develop a model for a small, fixed-wing aircraft based on static continuous fluid dynamics (CFD) simulations. In the lack of dynamic coefficients from CFD, we identify a pitch-damping model comparing bifurcation analysis and flight data that predicts well dynamics and stability of deep-stall flight.

Previous developments in sum-of-squares programming have been promising for the certification of nonlinear dynamics and flight control laws, yet their application in aeronautical engineering halted. In combination with piecewise polynomial modeling, we are able to re-apply this technique for analysis in an accurate but computationally feasible manner to verify stable recovery. Subsequently, we synthesise inherently stable linear and polynomial feedback laws for deep-stall recovery. We further extend the estimation of regions of attraction for the piecewise polynomial model towards an improved algorithm for local stability analysis of arbitrary switching systems, such as splines, thus making our work available for future analysis and certification of highly accurate algebraic models.

With highly nonlinear dynamics and critical state and input constraints challenging upset recovery, model-predictive control (MPC) with receding horizon is a powerful approach. MPC further provides a mature stability theory contributing towards the needs for flight control certification. Yet, for realistic control systems careful algebraic or semi-algebraic considerations are necessary in order to rigorously prove closed-loop stability. Employing sum-of-squares programming, we provide a stability proof for a deep-stall recovery strategy minimising the loss of altitude during recovery. We further demonstrate MPC schemes for recovery from spiral and oscillatory spin upsets in an uncertain environment making use of the well-known and freely available high-fidelity GTM desktop simulation.

The results of this thesis are thus promising for future system theoretic approaches in modeling, analysis, and control of aircraft upset dynamics for the development and certification of flight control systems in order to prevent in-flight loss-of-control accidents.

Keywords Nonlinear control; upset recovery; aerodynamics modeling; stability analysis; unmanned aircraft; system theory.

Résumé Le travail effectué au cours de cette thèse tente d'apporter des solutions algorithmiques à la problématique de reprise au décrochage d'un aéronef. A travers de nombreux exemples d'application sur des modèles aérodynamiques, le lecteur pourra appréhender les concepts abstraits présentés dans cette thèse. Alors que la capacité pour un aéronef à revenir à une situation nominale après une sortie du domaine de vol est un élément clé pour les systèmes de transport aérien du futur, les recherches menées dans ce cadre sont encore peu nombreuses. Pourtant, un tel dépassement conduit généralement à une perte de contrôle (dénommée LOC-I), que l'Association du Transport Aérien International (IATA) a classé dans la catégorie des « risques les plus élevés pour l'aviation ».

Dans un premier temps, nous avons montré que les modèles polynomiaux habituellement utilisés en théorie des systèmes ne représentent pas fidèlement l'aérodynamique d'un modèle d'avion sur l'ensemble de son enveloppe de vol. Nous avons donc tout d'abord montré qu'un modèle polynomial par morceaux représente avec exactitude les coefficients aérodynamiques pour les angles d'attaque faibles et élevés. Nous avons alors pu étendre à cette classe de systèmes, des méthodes récentes d'étude de bifurcation et d'analyse de stabilité qui utilisent des techniques de programmation semi-définie basées sur la positivité de polynômes (SOS); nous avons notamment appliqué ces résultats au modèle d'avion de transport générique dénommé GTM. Dans le même esprit, nous avons développé un modèle pour un petit aéronef à voilure fixe basé sur des simulations numériques en mécanique des fluides (CFD). Les coefficients dynamiques n'étant pas déterminés en CFD, nous avons identifié le coefficient d'amortissement du tangage en comparant l'analyse de bifurcation et les données de vol, ce qui nous a permis d'étudier à la fois la dynamique et la stabilité du vol en cas de fort décrochage.

Des résultats antérieurs ont montré que les techniques SOS étaient prometteuses pour la certification des lois de commande pour des systèmes non-linéaires, cependant sans avoir été appliqués à l'ingénierie aéronautique. En adaptant ces techniques aux modèles polynomiaux par morceaux, nous avons montré qu'il est désormais possible de les utiliser d'une manière précise mais réalisable sur le plan calculatoire. Ensuite, nous avons synthétisé des lois de commandes linéaires et polynomiales pour la récupération d'un fort décrochage. En outre, nous sommes désormais en mesure d'estimer des régions d'attraction pour des modèles polynomiaux par morceaux; pour cela, nous avons proposé un algorithme amélioré pour l'analyse de stabilité locale des systèmes à commutation, tels que ceux qui sont définis par des splines, rendant ainsi notre travail disponible pour l'analyse et la certification futures de modèles d'avion très fidèles.

La commande prédictive basée modèle (MPC) s'est avérée être une approche très efficace lorsque la dynamique du système est fortement non linéaire et soumise à des contraintes d'état qui rendent difficile la récupération après le décrochage. Cependant, pour des systèmes réalistes, il est nécessaire de prendre des précautions afin de prouver rigoureusement la stabilité en boucle fermée. En utilisant la technique SOS, nous avons ainsi montré la stabilité d'une stratégie de récupération d'un fort décrochage visant à minimiser la perte d'altitude. Nous avons aussi montré qu'une telle stratégie de commande permet la récupération d'une spirale infernale en utilisant le simulateur GTM.

Les résultats de cette thèse sont donc prometteurs et fournissent de nouvelles approches théoriques pour la modélisation, l'analyse de stabilité et le contrôle de la dynamique des futurs aéronefs ainsi que pour le développement et la certification de systèmes de commande de vol visant a prévenir les accidents dus à la perte de contrôle.

Mots clés Commande non linéaire ; récupération d'un aéronef ; modélisation dynamique ; analyse de stabilité ; pilote automatique ; théorie des systèmes.

Summary

Aircraft upset conditions have, in the past, led to rare but fatal accidents and to this day remain a severe threat to civil aviation. In response, considerable efforts contributed towards the prevention and detection of upset conditions as well as recovery of the aircraft into its desired flight regime. Despite these efforts made, comprehensive strategies including analysis of aircraft dynamics, recovery control, and verification of the implemented control over a large flight envelope have been missing for future aircraft safety.

In this thesis, we apply and extend recently developed tools such as bifurcation theory, sum of squares analysis and control synthesis, and nonlinear model-predictive control, to a set of newly developed piecewise polynomial aircraft models, which provide a trade-off between modeling accuracy and computational complexity. Thus, we contribute to the development as well as certification of safer flight control systems.

Dans le passé, le décrochage d'aéronefs a entraîné des accidents rares mais mortels et reste à ce jour une préoccupation importante pour l'aviation civile. Malgré les efforts déployés pour la prévention et la détection du décrochage ainsi que la récupération de l'avion, des stratégies telles que l'analyse de la dynamique, le contrôle de la récupération au décrochage et la vérification des lois de commande mises en œuvre constituent un chaînon manquant pour la sécurité des avions à venir.

Dans cette thèse, nous appliquons et étendons des outils récents de l'automatique, tels que la théorie de la bifurcation, les programmes de « sum of squares » et le contrôle prédictif modèle non-linéaire aux modèles d'avions polynomiaux par morceaux développés, qui offrent une bonne précision de modélisation et une faible capacité de calcul. Ainsi, nous contribuons au développement et à la certification de systèmes de contrôle de vol plus sûrs.

Sommaire

ONERA — The French Aerospace Lab
7 avenue Edouard Belin

&

ENAC, Université de Toulouse
2 avenue Edouard Belin

•

TOULOUSE